NASA-CP-2376-VOL-9
19860022011

19TH INTERNATIONAL COSMIC RAY CONFERENCE

LA JOLLA, USA AUGUST 11-23, 1985

CONFERENCE PAPERS

INVITED
RAPPORTEUR
HIGHLIGHT
MISCELLANEOUS
VOL. 9

19TH INTERNATIONAL COSMIC RAY CONFERENCE

LA JOLLA, USA AUGUST 11-23, 1985

CONFERENCE PAPERS

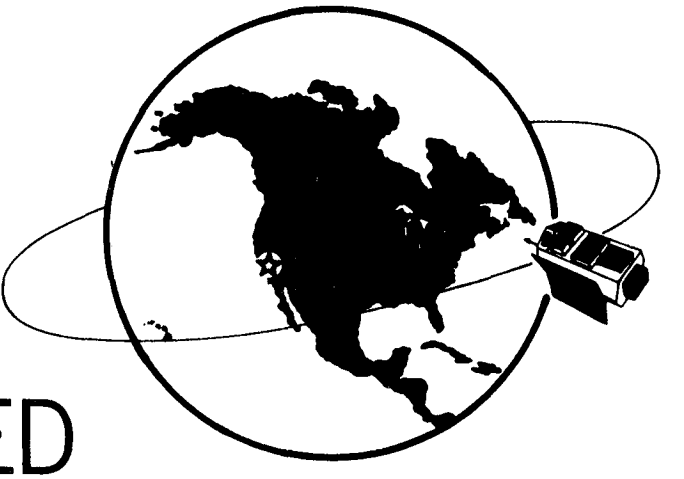

INVITED
RAPPORTEUR
HIGHLIGHT
MISCELLANEOUS

VOL. 9

PUBLICATION COMMITTEE

F.C. Jones, Chm.
J. Adams
G.M. Mason

NASA Conference Publication 2376

Published by
Scientific and Technical Information Branch
National Aeronautics and Space Administration
Washington, D.C. 20546

February 1986

For sale by the National Technical Information Service, Springfield, VA 22151

EDITORIAL FORWARD

Volumes 9 and 10 constitute the last two volumes of Conference Papers for the 19th International Cosmic Ray Conference that was held in La Jolla, USA during August, 1985. In Volume 9 are collected most of the Invited talks, all of the Rapporteur talks, and most of the Highlight talks. A few of the contributed papers have been included in this volume for reasons that will be mentioned shortly. Volume 10 contains an updated and corrected author index covering Volumes 1 through 9 and a list of names and addresses of those attending the conference.

If one studies the list of invited, rapporteur, and highlight talks on pages vii–ix it will be apparent that not all of them are printed here. In some cases press of new duties prevented the speaker from producing a manuscript; in one case the speaker was recruited as a last minute substitute and then left the country for a protracted stay immediately following the conference; one highlight speaker felt that his talk was a summary of work that was already reported in a series of contributed papers. Such reasons are understandable and we only hope that the reader is not too disappointed over the few missing papers. Fortunately, all of the rapporteur speakers were able to send a manuscript so an excellent summary of last summers conference can be found in Volume 9. Also we call the readers attention to the printed version of the presentation of the Shakti P. Duggal award to Dr. Raymond J. Protheroe.

A few contributed papers are included in Volume 9. It must be emphasized that the rule of no late papers has not been violated; these are not late papers. Every one of these manuscripts arrived in the editorial office on or before the deadline for inclusion in the regular Conference Papers volumes. Due to editorial error they were left out of or misprinted in these volumes. We have included them here in an attempt to make amends to their authors.

WE apologize for the fact that these volumes were not produced in as short a time as we had hoped; a mishap on the way to the printer made it necessary to redo much of our work. Our thanks to those authors who responded to our telegrams with such promptness. Without their help publication would have been even later.

PUBLICATIONS COMMITTEE June, 1986

Frank C. Jones, Chmn.
Jim Adams
Glenn M. Mason

Conference Synopsis

The 19th in the series of International Cosmic-Ray Conferences was held 11-23 August, 1985 in the Third College area on the campus of the University of California San Diego. About 520 scientific registrants, and an additional 200 friends, spouses and family members from over forty countries participated in the event. About 900 papers were presented in 80 parallel and over 12 plenary sessions.

The conference required the efforts of many people. The overall direction of the conference was determined by the Steering and General Organizing Committees, which were under the chairmanship of Frank B. McDonald of NASA Headquarters, and Martin Israel, of Washington University, St. Louis, respectively. The Local Oragnization was under the direction of L. Peterson, R. Lingenfelter, R. Rothschild, G. Burbidge, A. Hewitt, and their staffs devoted large amounts of time to various tasks associated with the implementation of a successful event. UnConventional, Inc., the conference management team under the direction of Karen Delaney had prime responsibility for the registration, operations during the conference, and the planning and implementation of many activities and services. Lene Hartman, UCSD Conference Coordinator, made many on-campus arrangements.

The conference was funded by NASA, NSF, DOE, California Space Institute and International Union of Pure and Applied Physics. Industrial support from the Ball Corporation, Lockheed, Rockwell International, TRW, and Kaypro, Inc. helped fund many of the social activities.

L.E. Peterson
Chairman, Local Organizing Committee

16 December 1985

INVITED
RAPPORTEUR
HIGHLIGHT
MISCELLANEOUS
VOLUME IX

19th INTERNATIONAL COSMIC RAY CONFERENCE
LA JOLLA, USA
AUGUST 11–23, 1985

INTERNATIONAL UNION OF PURE AND APPLIED PHYSICS
MEMBERS OF THE COMMISSION ON COSMIC RAYS OF IUPAP

A.E. Chudakov, Chm.
F.B. McDonald
G.C. Castagnoli
P.H. Fowler
D. Hovestadt
J. Kota
T.O. Montmerle
H. Moraal
J. R. Prescot
B.V. Sreekantan
K. Suga
J. Wdowczyk

STEERING COMMITTEE

F. McDonald, Chm.
G. Burbidge
M. Forman
T. Gaisser
M. Israel
F. Jones
R. Lingenfelter
R. Mewaldt
L. Peterson

GENERAL ORGANIZING COMMITTEE

M. Israel, Chm.
M. Bercovitch
P. Freier
R. Gall
R. Jokippi
L. Jones
V. Jones
S. Krimigis
J. Kurfess
J. Lockwood
P. Meyer
B. Price
R. Ramaty
F. Reines
M. Shapiro
M. Shea
J. Simpson
E. Stone
D. Venkatesan
J. Waddington
S. White

PROGRAM COMMITTEES

OG SESSIONS
R. Mewaldt, Chm.
G. Cassiday
C. Fichtel
A. Harding
J. Matteson
D. Muller
W. Webber

SH SESSIONS
M. Forman, Chm.
H. Hudson
G. Mason
B. McKibben
M. Pomerantz

HE SESSIONS
T. Gaisser, Chm.
K. Lande
J. Linsley
E. Loh
G. Yodh

PUBLICATIONS
F. Jones, Chm.
J. Adams
G. Mason

LOCAL ORGANIZING COMMITTEE

L. Peterson, Chm.
G. Burbidge
R. Lingenfelter
R. Rothschild
J. Arnold
W. Baity
A. Buffington
M. Burbidge
W. Fillius
R. Gall
R. Gould
H. Hudson
J. Linsley
K. Marti
G. Masek
J. Matteson
C. McIlwain
R. Mewaldt
O. Piccioni
M. Thiemens
W. Thompson
H. Ticho
R. White

Sponsored by
National Aeronautics and Space Administration
National Science Foundation
Department of Energy
Center for Astrphysics and Space Science, University of California, San Diego
California Space Institute, University of California
Department of Physics and Astronomy, University of Maryland, College Park
Ball Corporation, Kaypro Inc., TRW
Lockheed Missles and Space Division, Rockwell International

INVITED TALKS

RAPPORTEUR TALKS

V. Schonfelder (FRG)	OG1(2)3: Gamma Rays < 1 TeV
A. A. Watson (UK)	OG5(2): Cosmic Rays and Gamma Rays > 1 TeV
J. P. Meyer (France)	OG4(6,7,8): Cosmic Rays < 1 TeV
V. S. Ptuskin (USSR)	OG8(2,5,6,7): Sources, Acceleration, and Propagation
R. P. Lin (USA)	SH1,2,8: Solar Particles Gamma Rays and Neutrinos
C. K. Ng (Malaysia)	SH3(1,4): Interpalnetary Propagation and Acceleration
J. Kota (Hungary)	SH4: Modulation
E. O. Flueckiger (Switzerland)	SH5,6,7,9,10: Forbush Decreases, Geomagnetic and Atmospheric Effects and Cosmogenic Nuclides
L. W. Jones (USA)	HE1,6: High Energy Interactions and New Particle Searches
M. Shibata (Japan)	HE3: Emulsion Chamber Observations and Interpretation
R. W. Clay (Australia)	HE4: Extensive Air Showers
T. Stanev (USA)	HE5,7: Muons and Neutrinos

HIGHLIGHT TALKS

INTRODUCTION: Shakti P. Duggal Award Presentation

When, in 1959, Vikram Sarabhai wrote asking whether a post-doctoral appointment at Bartol might be available for his fine young student, he received an affirmative response by return mail. Shakti P. Duggal took up his appointment as a Bartol Fellow the following year, and for the next 22 years, he continued to make important contributions to cosmic ray physics in the field which at this International Cosmic Ray Conference is designated solar-heliospheric -- SH.

He had become a well respected member of our community when his brilliant career was cut short at its peak by his untimely death in 1982, at the age of fifty. He had been an active participant in, and contributor to, then of these Conferences, commencing with the 8th ICRC in Jaipur in 1963, and ending with the 17th ICRC in Paris in 1981. The outpouring of his colleagues from around the world upon learning of his premature passing testifies to the high regard in which he was held, and the genuine affection of all who were fortunate enough to know him.

As a fitting memorial, Shakti Duggal's colleagues and friends established an international award for outstanding work by a young scientist in the field of cosmic ray physics. The recipient of the First Biennial Award has been selected by a committee consisting of M. Casse, A. E. Chudakov, P. H. Fowler, M. A. Pomerantz, J. A. Simpson, and A. W. Wolfendale. I take this opportunity to express deep appreciation to my colleagues on this committee for carrying out the exceedingly difficult task of making a selection among the many outstanding young people who have already attained prominence in our discipline.

With great pleasure, I call upon Professor John R. Prescott to introduce Raymond J. Protheroe as the first recipient of the Shakti P. Duggal Award.

Martin A. Pomerantz
Bartol Research Foundation
of the Franklin Institute
University of Delaware

THE SHAKTI P. DUGGAL AWARD

Raymond John Protheroe

I am very happy to introduce Raymond John Protheroe as the first recipient of the Shakti P. Duggal award "for outstanding work by a young scientist in the field of cosmic ray physics". In making this award for the first time one could scarcely have wished for a candidate with a greater breadth of experience or greater versatility. Protheroe has had wide experience in the cosmic ray astrophysics field. He shows an unusual breadth of capacity for one still relatively early in his research career. At the same time there has been no sacrifice of depth and significance. His work spans three continents and two hemispheres and, although he would regard himself as a theoretician first, he is also quite at home as an experimenter. Thus, over the past eighteen months he has first developed the theoretical basis of an experimental design for a new approach to the study of primary cosmic radiation through the Cherenkov light produced by extensive air showers. He then helped put it into practice in the Australian "outback", in the desert darkness of the new moon to the howling of the dingoes, the thumping of the kangaroos and the imprecations of his colleagues.

He is an Honours graduate in Physics of the University of Durham and subsequently obtained his Ph.D. there for a thesis on the topic, "Computer Simulations of Large Cosmic Ray Showers Using Recent Models of Hadronic Collisions". He played a key role in the pioneering work of the University of Durham group in developing the atmospheric Cherenkov technique for the study of extensive air showers and hence primary composition. In this he provided some of the most significant of the theoretical input, both for design and interpretation.

Subsequently, while still at Durham, he turned his attention to studies of the nature and origin of the diffuse X- and gamma-ray background, concluding that interactions of cosmic ray electrons are responsible for a significant contribution to this diffuse radiation.

In 1979 he went to work at the NASA/Goddard Space Flight Centre in Maryland where his research centred on several related areas of cosmic ray astrophysics particularly concerned with cosmic ray propagation. There he studied the relative abundances and energy spectra of low energy (by cosmic ray standards) nuclei, positrons and antiprotons in an effort to understand their origin and details of the propagation in the galaxy.

In 1982 he was awarded a Queen Elizabeth II Fellowship to work at the University of Adelaide. These Fellowships are highly competitive across the whole field of the sciences and mathematics and, while they must be held in Australia, they attract many overseas applications. To be successful, a candidate must show "quite exceptional merit" and "have demonstrated outstanding promise and capacity for original work".

With the cosmic ray group at the University of Adelaide he has once again become involved with work on extensive air showers. He has played

a particularly important role in developing the analytical tools needed for the successful discovery of ultra-high energy gamma rays from Vela X-1 and LMC X-4, a source in the Large Magellanic Cloud. These are, respectively, the first source of such gamma rays observed in the Southern Hemisphere and the first extra-galactic source.

With the publication of the Proceedings of this, the Nineteenth Cosmic Ray Conference, Protheroe will have published some sixty papers. Citations in the literature are now approaching fifty per year and are rising exponentially with a roughly two-year doubling time. Since he is still only thirty-two years old, it seems likely that he will still be contributing at the time of the thirty-sixth Cosmic Ray Conference in the year two thousand and eighteen.

Selected Publications

Protheroe would be the first to insist that his work owes much to fruitful collaboration with others. Indeed I think it is clear to his colleagues that this is one of his great strengths. In the context of the present citation it seems appropriate not to refer to any of his co-workers specifically. Many of their names appear in the selected references that follow:

"Cherenkov Radiation in Large Cosmic Cosmic Ray Air Showers", R. T. Hammond, K. J. Orford, R. J. Protheroe, J. A. L. Shearer, K. E., K. E. Turver, W. D. Waddoup and D. W. Wellby, Nuovo Cimento, 1C, 315, (1978.

"Cosmic Ray Showers and Particle Physics at Energies 10^{15}-10^{18} eV", T. K. Gaisser, R. J. Protheroe, K. E. Turver and T. J. L. McComb, Reviews of Modern Physics, 50, 859, (1978).

"Galactic X-Ray and Gamma-Ray Emission and the Nature of the Interstellar Electron Spectrum", R. J. Protheroe and A. W. Wolfendale, Astron. Astrophys., 92, 175, (1980).

"Interpretation of Cosmic Ray Composition: The Pathlength Distribution", R. J. Protheroe, J. F. Ormes and G. M. Comstock, Ap. J., 237, 362, (1981).

"Cosmic Ray Antiprotons in the Closed Galaxy Model", R. J. Protheroe, Ap. J., 251, 387, (1981).

"First Observation of Gamma-rays from Vela X-1 at Energies greater than 3×10^{15} eV", R. J. Protheroe, R. W. Clay and P. R. Gerhandry, Ap. J. (Letters), 280, L47 (1984).

"First Observation of Ultra-high Energy Gamma-rays from LMC X-4", R. J. Protheroe and R. W. Clay, Nature, 315, 205 (1985).

J. R. Prescott,
Physics Department,
University of Adelaide
August 1985

This conference is the 19th in a series. Previous conferences in this series were held at:

Cracow, Poland	–	1947
Como, Italy	–	1949
Bagneres-de-Bigorre, France	–	1953
Guanjuato, Mexico	–	1955
Varenna, Italy	–	1957
Moscow, USSR	–	1959
Kyoto, Japan	–	1961
Jaipur, India	–	1963
London, UK	–	1965
Calgary, Canada	–	1967
Budapest, Hungary	–	1969
Hobart, Australia	–	1971
Denver, USA	–	1973
Munchen, FRG	–	1975
Plovdiv, Bulgaria	–	1977
Kyoto, Japan	–	1979
Paris, France	–	1981
Bangalore, India	–	1983

VOLUME 9

INVITED TALKS

RAPPORTEUR TALKS

VOLUME 9

HIGHLIGHT TALKS

VOLUME 9

THESE PAPERS WERE INADVERTANTLY LEFT OUT
OF THE CONFERENCE VOLUMES OR MISPRINTED

COSMIC JETS

Martin J. Rees
Institute of Astronomy, Madingley Road,
Cambridge CB3 OHA, England

ABSTRACT

The evidence that active galactic nuclei produce collimated plasma jets is summarised. The strongest radio galaxies are probably energised by relativistic plasma jets generated by spinning black holes interacting with magnetic fields attached to infalling matter. Such objects can produce e^+-e^- plasma, and may be relevant to the acceleration of the highest-energy cosmic ray primaries. Small-scale counterparts of the jet phenomenon within our own galaxy are briefly reviewed.

1. INTRODUCTION

The study of extragalactic high energy astrophysics really began just over 30 years ago, when Baade and Minkowski (1954) showed that Cygnus A, the second strongest source in the radio sky, was a remote galaxy with a redshift of 0.05. Radio studies soon confirmed that its emission, along with that from other strong sources, was synchrotron radiation, coming primarily from two blobs symmetrically disposed on either side of the optical galaxy. In the late 1950s Geoffrey Burbidge (1958, and references cited therein) calculated that the minimum energy stored in the radio lobes of such sources in relativistic electrons and magnetic fields was $\sim 10^{60}$ ergs, about the rest mass of a million suns. This was the first indication that some galaxies release non-thermal energy in a coordinated fashion, at a level millions of times surpassing a single supernova.

For many years afterwards, a regular highlight of these conferences was a debate between Professors Burbidge and Ginzburg on intergalactic cosmic rays, and whether cosmic rays pervade the entire universe with the same density as in our galaxy. The issues of cosmic ray confinement, and of how much energy could come from active galaxies, have clarified now; but radio sources are relevant to cosmic ray physics for several reasons: they are the prime candidate for producing whatever intergalactic flux there is; the extended lobes offer, in my view, a vary plausible origin for the highest energy particles we observe; moreover, studies of radio sources yield clues to the nature of acceleration mechanisms in general.

Optical astronomy made its own most crucial contribution to extragalactic high energy astrophysics in 1963, when searches for the optical counterparts of some radio sources led to the discovery of quasars — objects that resembled stars on photographic plates, but whose spectra displayed emission lines with large redshifts (Hazard *et al.* 1963, Schmidt 1963). During the last 21 years, a bewildering body of data gathered in all wavebands has borne out the general concept (adumbrated in the pioneering paper by Burbidge, Burbidge and Sandage (1963)) of 'violent activity' in galactic nuclei. Radio galaxies and quasars are the prime

examples of this phenomenon, but the objects known as Seyfert galaxies and "BL Lacs" also involve active galactic nuclei (AGNs).

Optical observations offer a wealth of information on the spectrum, polarization and variability of AGNs. From such data, physical conditions in the emission regions can be inferred. However, it is the radio astronomers who are best able to provide structural information. This is because the radio-emitting regions are often very extended, and also because the angular resolution of radio interferometers with baselines approaching the Earth's diameter surpasses anything optical imaging can yet achieve.

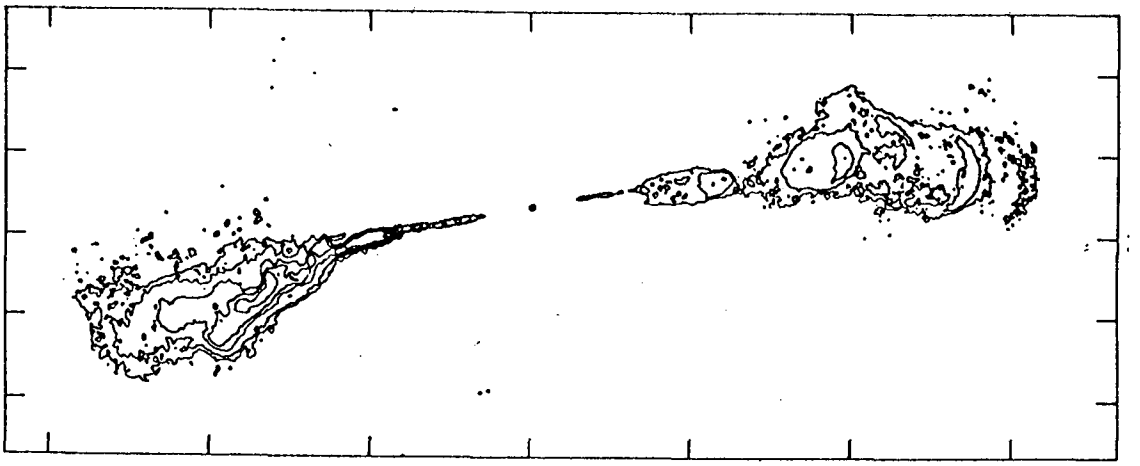

1. VLA map at 5 GHz of the giant double source Hercules A, overall size $\sim$ 1 Mpc, showing narrow straight "jets" linking the galaxy to the lobes. This high-power source is atypical in showing such conspicuous jets: normally the jets are only as strong as this (relative to the lobes) in sources of lower power. I am grateful to Dr J.H. Dreher for providing this map.

2. EVIDENCE FOR JETS

The reasons why radio sources have their characteristic double morphology, and the nature of the energetic link between the nucleus and the radio lobes, were very perplexing in the early days of radio astronomy. In particular, it was unclear whether the lobes originated in a single colossal explosion, or whether they had been gradually "inflated" by a continuing output of directed energy from the associated galaxy (Rees 1971). These issues have been clarified in the last decade, thanks mainly to the improved resolution and sensitivity of the Very Large Array (VLA) in New Mexico.

Figure 1 shows a VLA map of the double source, Hercules A (3C 348). On earlier maps, nothing could be seen connecting the central optical galaxy with the lobes $\sim 10^6$ light years away on either side, but the newer maps reveal conspicuous bridges of radio emission stretching almost all the way from the central galaxy to the lobes. Similar jet-like features are now detected in more than 100 double sources (Bridle and Perley, 1984). Some of the jets are rather inconspicuous: the recently discovered jet in Cygnus A (Perley, Dreher and Cowan, 1984) is barely detected even with the VLA's impressive dynamic range.

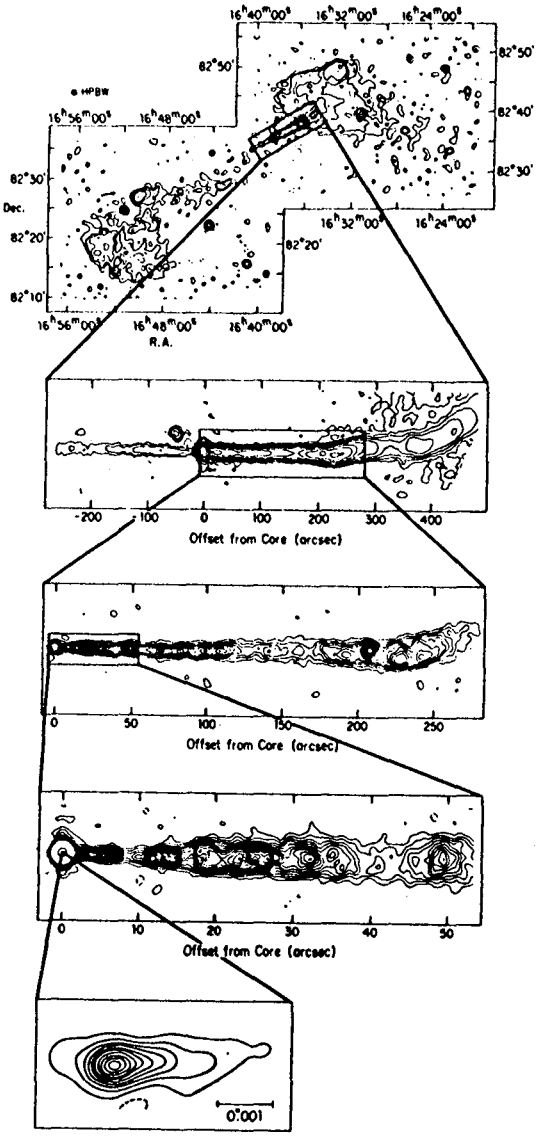

2. Montage, adapted from Bridle and Perley (1984), showing the radio source associated with the galaxy NGC 6251 over a wide range of angular scales. The top panel shows the large scale structure: a double source ∿ 2 Mpc in extent. The second panel shows the jet and the (much weaker) counterjet; lower panels show the high-surface-brightness inner parts of the jet at increasing resolution. The large brightness asymmetry between jet and counterjet, and the straightness of the jet, are characteristic of moderately high-power radio sources. The bottom panel, obtained with milli-arc-second resolution via the VLBI technique, shows that the jet emanates from a "nozzle" < 1 pc in scale at the galactic nucleus. The primary power supply probably comes from a region ∿ 5 powers of ten smaller still.

The smallest angular scales resolvable by the VLA (0.1 arc second) correspond to linear dimensions as large as several hundred parsecs in a remote extragalactic source; for finer resolution we must resort to Very Long Baseline Interferometry (VLBI). The montage of NGC 6251 (Figure 2) is specially interesting in showing direct continuity between a plasma 'blowtorch' one parsec long and the large-scale jets and giant radio structure. A common characteristic of jets in strong double sources is that they are asymmetrical: they are detected on only one side; or, if there is a counterjet, it is generally much fainter (by a factor of about 60:1 in NGC 6251 shown in Figure 2).

The jets seem to be conduits along which energy and momentum flow into the extended lobes. But the VLA maps offer no direct evidence for motion. VLBI maps, however, sometimes show dramatic evidence of this: there are several instances where blobs appear to move across the sky, in a direction away from the AGN itself, at 5-10 times the speed of light. There is nothing paradoxical about these 'superluminal' apparent velocities; they can arise from plasma moving at close to the speed of light in directions making a small angle with the line of sight. Motion with a bulk Lorentz factor γ_b ($\gg 1$) at an angle $\sim \gamma_b^{-1}$ to the line of sight yields an apparent transverse velocity $\sim \gamma_b c$. Moreover, the apparent intensity of material moving in these special directions (nearly towards us) is greatly enhanced by the Doppler effect and by aberration. Although detailed models for "superluminal" sources are still controversial, there is thus no obvious improbability in postulating that most of the compact sources in a survey down to a given apparent intensity have this special orientation. Not only, therefore, do the jets contain radiating electrons with high individual Lorentz factors, but the entire medium (electrons, protons (or positrons) and magnetic field) sometimes has a bulk Lorentz factor $\gamma_b > 5$.

The one-sidedness of the large-scale jets in powerful double sources could arise from Doppler favouritism; there would be jets on both sides, flowing in opposite directions, and unless the motion were exactly transverse to our line of sight, one side (the approaching side) would appear enhanced. The famous jet in the Virgo cluster elliptical galaxy M87 could be a relativistic phenomenon, the counterjet perhaps being suppressed by the Doppler effect. This jet, discovered by Curtis at the Lick Observatory in 1918, reminds us that it was actually the optical astronomers who first detected this phenomenon; VLA radio maps (Figure 3) show that M87 has weak double radio lobes plus a one-sided radio jet (whose brightest features coincide with the "knots" in the optical jet). The M87 jet has also been detected in X-rays; its emission in all wavebands is probably synchrotron radiation, produced by electrons accelerated at strong shocks associated with the "knots".

Miniature jets in our own Galaxy

Smaller scale jets are found within our own galaxy. The extraordinary object SS 433 (Margon 1984 and references cited therein) has twin jets with a flow speed of 0.27c (the only jet whose speed is unambiguously known). Recently, directed outflow has been found from some protostars (Bally and Lada 1982, Mundt 1984): these involve much lower energies (and shallower gravitational potential wells), though the collimation may arise from a mechanism analogous to that in the more spectacular extragalactic jets.

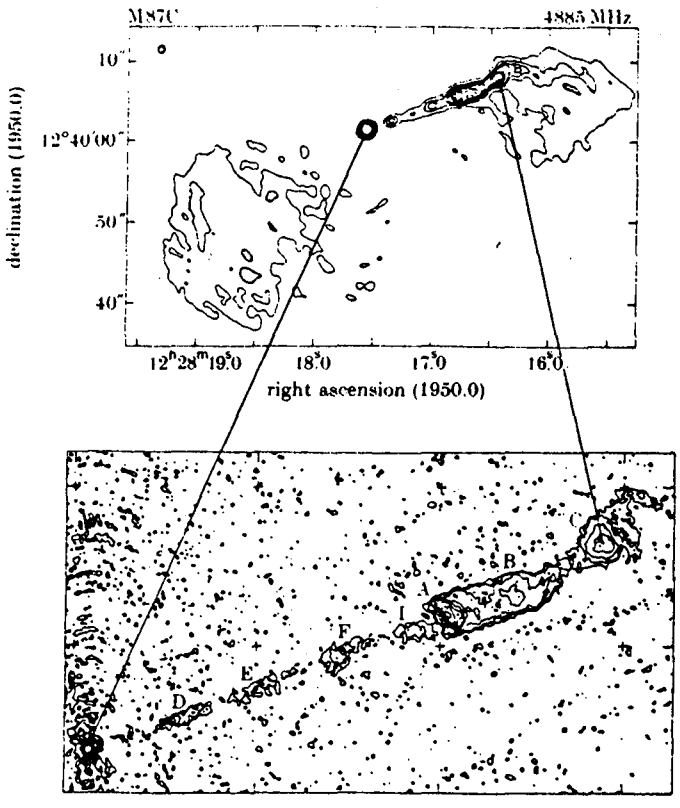

3. Two radio maps of M87. The bottom picture (from Biretta et al. 1983) shows a 15 GHz VLA map of the jet, with 0.12" resolution. The high brightness features correspond with the optical knots (the emission being synchrotron radiation in both bands). The top picture (from Owen et al. 1980) shows a more extended radio view at lower resolution, which reveals that M87 is a miniature double source, with roughly symmetrical lobes $\sim$ 2 kpc in size and a one-sided jet.

Associated with the galactic X-ray source SCO X-1 are double radio components, resembling a miniature version of an extragalactic double source (Fomalont et al. 1983).

The ICRC conferences are often enlivened by a 'topical diversion', such as the tentative (or even transient) discovery of a monopole, or a quark. This time, we shall undoubtedly hear a great deal about the claimed underground detection of high energy particles triggered from Cygnus X3. Perhaps it is worthwhile, therefore, to recall what radio astronomy tells us about this strange object. It is a variable radio source, with occasional flares lasting a few days. Such flares were well observed in 1972 and in 1982. Limited VLA data, obtained during the 1982 flare, provide just a bit of structural information. The emitting region had a 4:1 axial ratio, thereby perhaps just qualifying as a jet; and expanded at about 0.6 c during the flare (Geldzahler et al. 1984).

The jet phenomenon is ubiquitous. Many different mechanisms may be implicated - the only feature that all jets may have in common is alignment with a rotation axis. In what follows, I shall concentrate on the large-scale jets, emitting synchrotron radiation, which are primarily studied by radio astronomers.

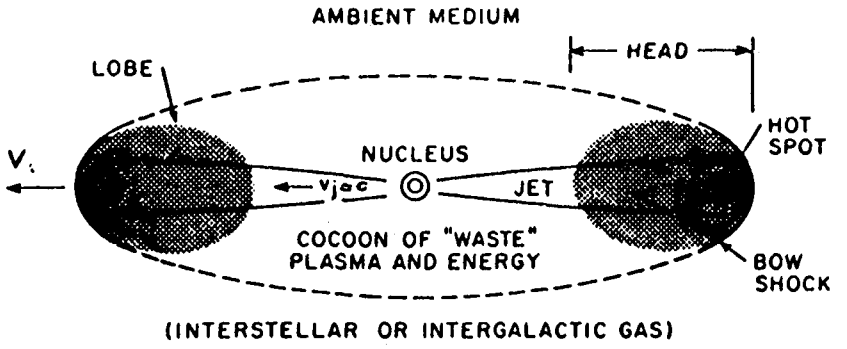

4. Theorists' view of double radio sources (Blandford and Rees 1974): schematic model and "naming of parts".

3. JET PHYSICS

The key elements of a double radio source are: i) a generator of relativistic plasma in the AGN; ii) some bifurcation and collimation mechanism whereby plasma can squirt preferentially in two opposite directions; and iii) a place far away where the relativistic plasma, having ploughed its way through the interstellar medium of the host galaxy out to intergalactic space, is stopped by interaction with the external gas in a shock front (see Figure 4).

The speed of advance V of the "working surface", where the jet is stopped by the external medium, is governed by pressure balance - the balance between the momentum density in the beam and the $\rho_{ext}V^2$ ram pressure force (ρ_{ext} being the density of the surrounding medium). The beam energy is randomized by shocks when it impinges on the external medium; particles here are accelerated and these regions are identified with the "hot spots" in the radio source components. Even if the beams are relativistic (with $V_j \cong c$), V itself is not; we therefore do not expect the same Doppler asymmetry in the lobes and hot spots as in the emission from the jets themselves. The relativistic plasma then accumulates in a cocoon of lower energy density and lower radio emissivity.

We can regard jets as basically fluid phenomena and apply fluid-dynamical analogies. This is because the gyro-radii (even for the synchrotron-emitting particles) and the Debye length are both much less than the jet dimensions, and deviations from charge neutrality are therefore small; also the relative mean velocities of the electrons and ions is small. The MHD approximation is valid: the mean-free path against 2-body collisions is enormous, but the magnetic field, with its small associated gyro-radius, makes the flow fluidlike, as in the solar wind.

The data on jets pose a whole range of questions (all discussed more fully by Begelman, Blandford and Rees, 1984).

Jet speeds

The small-scale superluminal sources certainly indicate outflow at a speed $\sim c$, but it is unclear whether the nuclei of all radio sources generate relativistic jets; nor is it clear whether high initial speeds persist over the jets' whole length, or whether frictional effects gradually slow them down. A tenable viewpoint is that jets in the strongest double sources have high Mach number, low internal dissipation, and maintain speeds $\sim c$ out to distances of several hundred kiloparsecs, thereby transporting energy to the extended components in an almost loss-free way. The fact that often only one jet is seen could then arise merely from Doppler favouritism. In lower-luminosity sources (where the jets often appear two-sided, and are more conspicuous relative to the extended lobes) the flow is presumably slower and more dissipative.

What are the jets made of?

A slow-moving jet would consist predominantly of ordinary swept-up material. However, there are reasons (discussed in section 4) for conjecturing that the 'central engine' generates an e^+-e^- plasma. The kinetic energy requirements of relativistic jets are then somewhat reduced: each electron need be neutralized by just one positron (0.51 Mev of rest mass) rather than a proton (936 Mev).

Confinement?

The flux of energy (and momentum) along the jet can be estimated by considering the dynamics of the lobes and hot spots. The internal pressure within a jet is however lower than the longitudinal momentum flux density by about the square of the Mach number $\mathcal{M}$. The value of $\mathcal{M}$ is often uncertain; a lower limit to the internal pressure (i.e. an upper limit to $\mathcal{M}$) comes from applying the equipartition argument to the radio emission from the jets themselves. This pressure may in some cases be balanced by the pressure of an external medium (e.g. the hot plasma that pervades clusters of galaxies); the latter however is constrained by the amount of X-ray bremsstrahlung, sometimes to values below the minimum inferred pressure within the jet, so we are motivated to seek other agents for confinement. One interesting possibility is that the jets may be confined by magnetic fields coiled around the jet, but the stability of these configurations is still open to question.

Stability?

The observed jets seem amazingly stable against break-up, even in cases (e.g. NGC 1265) where the jet is bent by a "side wind". Clues to why this is so can come from simulations. Aeordynamical experiments may provide valuable insights into purely hydrodynamic aspects of jet physics. They cannot, however, demonstrate the dynamical effects of magnetic fields and relativistic bulk velocity, and only restricted ranges of Mach number, density ratio, and adiabatic index are practicable in the laboratory. Propagation of intense particle beams (or, alternatively, laser beams) into an ambient gas (cf. Bekefi et al. 1980) – although the internal

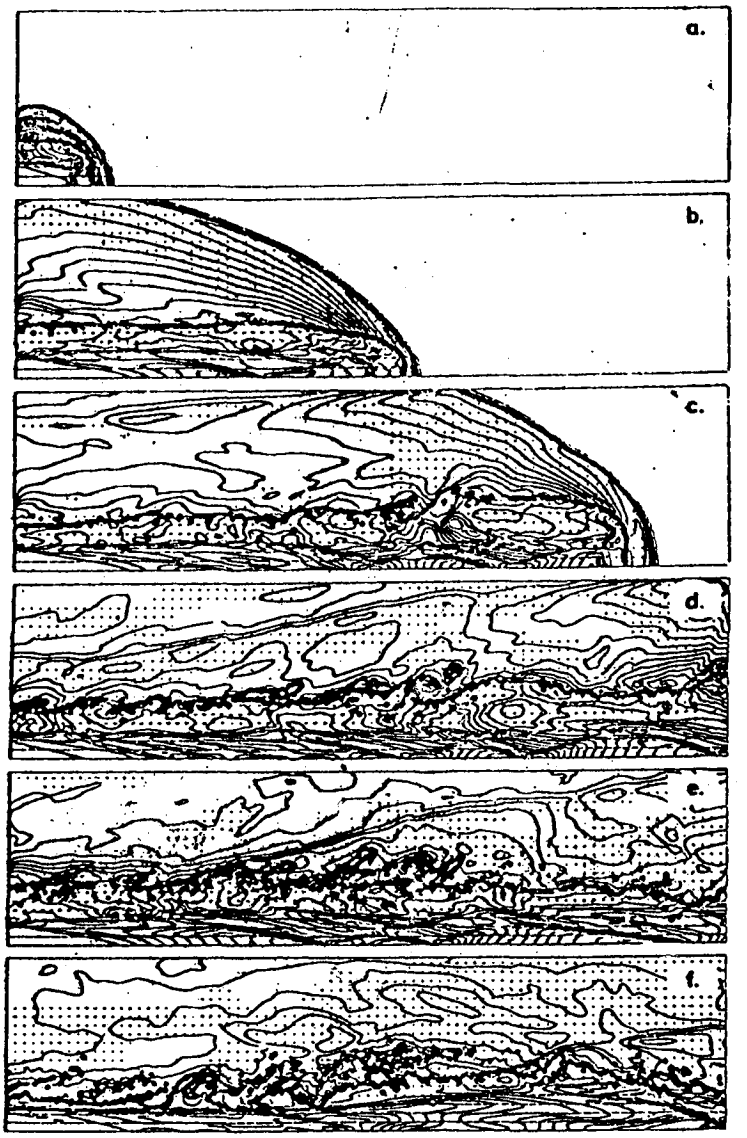

5. Computations by Norman et al. (1982) showing successive stages in the advance of a hypersonic jet into a uniform gas. (These are 2-D simulations, so axisymmetry is artificially enforced.)

dynamics of such beams differ crucially from those in the cosmic-scale beams.— could provide a much higher momentum density and higher Mach numbers than an ordinary gas jet. The interaction with the external medium as such a beam advances may simulate the structure of "hot spots" and cocoons in very strong sources.

The greatest progress will surely come, however, from use of increasingly sophisticated and powerful hydrodynamical codes. These have already (see, for instance, Figure 5) uncovered some gas dynamical properties of

supersonic flows that were unanticipated by analytical models and may have counterparts in radio maps (Norman et al. 1983; Williams and Gull 1985). Within a few years, high resolution 3-D computations incorporating electromagnetic effects (MHD) should be feasible. We can then test if it is plausible that jets are confined magnetically, and whether the polarization patterns observed in jets can be explained in terms of the kinematics of expanding shear flows.

Acceleration mechanisms: conversion of bulk kinetic energy into relativistic particles

The radiating particles in the radio lobes are presumably accelerated behind the strong shocks that occur where the beam is stopped by external matter. Moreover, *in situ* acceleration is generally required at locations along the jet which emit synchrotron radiation (e.g. the "knot" in the M87 jet shown in Figure 3), and the blobs in superluminal sources are probably associated with internal shocks within a relativistic beam. If these beams emerge from nozzles with scale much smaller than 1 parsec (see section 4) then any initial random relativistic motion would have been degraded by radiative or adiabatic losses.

We know that relativistic particles can readily be accelerated by shocks, even when the shock speed is itself only one or two percent of c (as in supernova remnants). In the present context, the shock speeds are much higher: probably $\sim$ c for internal shocks within the jet; and up to at least $\sim$ 0.1 c in the "bow shock" that advances into the intergalactic medium ahead of the jet and radio lobe. It could even be that the Poynting flux (i.e. the "kinetic energy" of the electromagnetic field) exceeds the kinetic energy of the matter itself. A high efficiency for converting bulk kinetic energy into relativistic particles in radio sources therefore occasions no surprise. The particles whose pressure we can directly infer are, of course, just the electrons (or maybe positrons) responsible for the observed synchrotron radiation. What about protons or heavier ions? It is most unlikely that these dominate electrons by factor as large as 100. Allowance for the associated extra internal energy and pressure would make it much harder to understand the confinement of the high-surface-brightness "hot spots" in radio lobes. (A well-known analogous argument applied to the Crab Nebula shows that the 100:1 ratio does not prevail there either (Trimble and Rees 1970)).

We thus have no direct handle on how many ions are accelerated. However, the large value of B x (length scale) in radio lobes like those of Cygnus A, plus the firm inference that strong shocks occur there, makes them a plausible location for the production of the very highest energy primaries (see, for instance, Cavallo (1978)). On this hypothesis, the $> 10^{18}$ev particles now reaching Earth could have originated in the Southern Hemisphere object Centaurus A. This radio source now has very diffuse extended lobes, and only low-level nuclear activity. But it must, in the (cosmologically) "recent" past have been much more active in order to have inflated and energised the giant lobes - maybe $\sim 10^8$ years ago it was a source whose power rivalled Cygnus A.

The highest energy primaries can be accounted for, without assuming an implausibly flat energy spectrum for a universal cosmic ray energy density of only $\sim 10^{-5}$ eV cm^{-3} (see, for instance, Wolfendale 1984).

This energy density is well below the electromagnetic energy output from AGNs. There is, however, a general constraint on the intergalactic cosmic ray density that could be built up by radio galaxies, pointed out by Rees and Setti (1968): the relativistic electrons in radio lobes would eventually lose most of their energy via inverse Compton scattering of the microwave background, thereby contributing to the cosmic X-ray background. The latter amounts in toto to $\sim 10^{-4}$ ev cm^{-3}, so an intergalactic cosmic ray density higher than this could be ruled out unless the fraction of energy going into electrons rather than ions were correspondingly small.

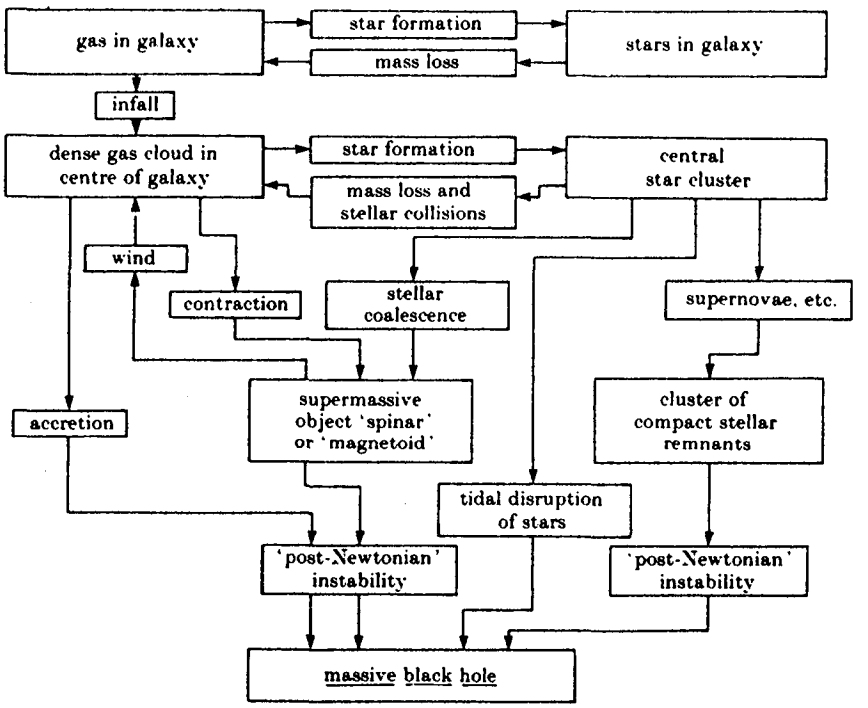

6. This flow diagram illustrates various runaway processes that could in principle occur in a galactic nucleus, causing an ever-deepening gravitational potential well. A massive black hole is the almost inevitable endpoint; accretion onto black holes, or electromagnetic extraction of their rotational energy, is the most efficient known process that could account for the luminosity of AGNs and the formation of relativistic plasma jets.

4. THE CENTRAL OBJECT IN RADIO GALAXIES

In large radio lobes energy deposited by the jets is dissipated via complex interactions with interstellar and intergalactic media: to model their intricate and environment-dependent morphology are plainly initiated on a scale of $\lesssim 1$ pc. AGNs not only generate a vast "in situ" luminosity (as in the quasars), but sometimes eject energy in these relativistic jets. The jets, however, are just one aspect of the general AGN phenomenon.

The central engines in the most powerful AGNs probably involve black holes of $\sim 10^8 M_\odot$: arguments for this point of view have been given elsewhere (e.g. Rees (1984)) and I shall not repeat them in the present written text (see, however, Figure 6 and its caption). The characteristic scale of a black hole is the Schwarzschild radius $r_s = 3 \times 10^{13}(M/10^8 M_\odot)$ cm. Most of the energy release, in all processes involving black holes, happens within a region only a few times larger than r_s. There are therefore several powers of 10 between even the smallest scales probed by VLBI and the dimensions of the primary power source.

Pair production and transrelativistic plasma in compact sources

Before focusing on processes that involve specific (relativistic) features of black holes, it might be worth mentioning some physical processes that occur in any sufficiently compact region that emits hard photons.

Suppose that a source of radius r_* emits a luminosity L_γ in the form of Mev photons. These can interact with each other to produce electron-positron pairs, the cross section being of order the Thomson cross section. Most of the photons (each carrying energy $\sim m_e c^2$) will collide with each other before escaping if $n_\gamma \sigma_T r_*$ exceeds unity, where $n_\gamma \simeq (L_\gamma/4\pi m_e c^3 r_*^2)$ is the photon density. This implies that γ-rays cannot escape freely from any source whose 'compactness parameter' L_γ/r_* exceeds a certain threshold value. The requirement is $L_\gamma > 10(m_e/m_p)(r_*/r_s) L_{Ed}$, where L_{Ed} is the Eddington luminosity $4\pi GM M_p c/\sigma_T$; this inequality is readily fulfilled by non-thermal sources associated with black holes. The primary source would then shroud itself in an optically thick photosphere of e^+-e^- pairs, which would scatter all radiation, not just the part with $h\nu > m_e c^2$. Some implications for compact and variable AGNs are discussed by Guilbert, Fabian and Rees (1983). Note that we might expect a broad (0.5 Mev) annihilation line feature in the emission from such objects.

The gravitational binding energy of a proton at distance r from a black hole is $\sim 1000(r/r_s)^{-1}$ Mev. (Except within a few times r_s, general relativistic effects are unimportant, and the potential well is basically just of "1/r" form.) For $r \lesssim 10^3 r_s$, gas pressure-supported at (or shock-heated to) the virial temperature would be so hot that electrons would be relativistic if they equilibrated with the ions. The physics of these trans-relativistic thermal plasmas has, until recently, received rather little attention. The electrons tend to be cooler than the ions because 2-body ion-electron coupling is too slow to compete with the radiative cooling losses suffered by the electrons, and because adiabatic compression during infall heats the non-relativistic ions faster than the relativistic electrons ($T_i \propto \rho^{2/3}$ whereas $T_e \propto \rho^{1/3}$). Electron-ion collisions will produce not only bremsstrahlung photons, but also e^+-e^- pairs. (This is an additional source of pairs over and above the $\gamma + \gamma \rightarrow e^+$-$e^-$ process discussed above; the extra pairs will themselves participate in radiative processes). Moreover, even the thermal ions may be energetic enough to undergo nuclear spallation when they collide (Svensson, 1985 and references cited therein).

All the above processes - important not only in AGNs, but also in smaller-scale phenomena such as γ-ray bursts on neutron stars - merit closer attention.

There is an extensive literature on AGN models powered by accretion onto massive black holes (see Rees (1984), Wiita (1985) for reviews). Such models can, in broad terms, account for the quantity of electromagnetic radiation typically observed. However, one cannot reliably predict the spectrum, nor whether the radiation is thermal or non-thermal: the hardest thing to estimate is what fraction of the power dissipated by viscous friction would go into relativistic particles (via shocks, magnetic reconnection, etc.) rather than being shared among all the particles. Nor do we know how steady or stable the inflow pattern might be. This is a topic where detailed numerical simulations would be worthwhile, particularly if these allowed us to treat unsteady accretion, non-axisymmetric instabilities, and realistic radiative emission and transfer processes.

Despite the lack of quantitative understanding of AGNs in general, the strong radio galaxies (e.g. Cygnus A) have a distinctive property which offers a clue to their central mechanism. The remarkable feature of these particular AGNs is that the "kinetic" power required to energize the extended radio lobes (transmitted by the jets in the form of relativistic particles or Poynting flux) exceeds the radiative luminosity of the nucleus itself. Is there a mechanism that could generate an intense plasma outflow, even if the accretion rate and nuclear luminosity were low?

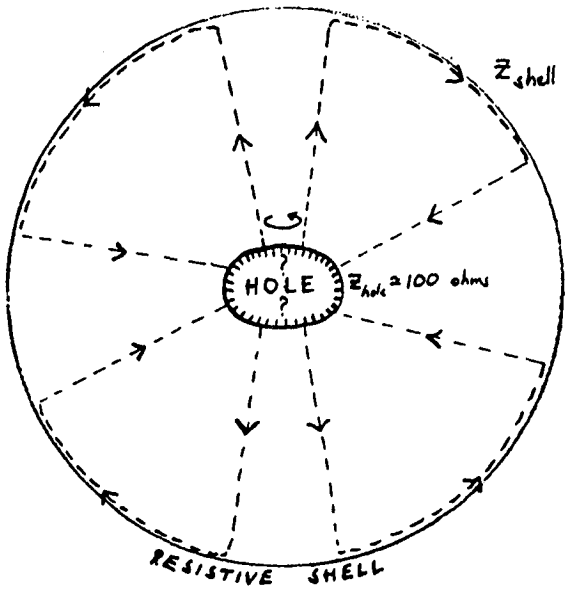

7. The unipolar inductor mechanism schematically depicted. A magnetic field (not shown) is applied to a spinning black hole surrounded by a much larger non-rotating conducting shell. A current system (dotted lines) is then induced, which dissipates energy in the hole (resistance $Z_{hole} \cong$ 100 ohms), and in the surrounding shell. The power generated in the shell (rather than going to waste down the hole) is maximised, for a given applied magnetic field, when $Z_{shell} = Z_{hole}$.

Electromagnetic energy extraction from spinning holes

There is indeed another possible source of power over and above the gravitational energy released by infalling matter: this is the rotational energy of a spinning black hole, which can in principle be extracted, as was first recognised by Penrose (1969). Astrophysically plausible mechanisms for extracting this energy depend on exploiting the remarkably close analogy between a black hole and an ordinary electric conductor. This analogy is most simply illustrated, for a Schwarzschild hole, by calculating the electric field due to a point charge held at rest near the hole (Hanni and Ruffini 1972). As the charge, with radial coordinate r_c, is moved closer to the Schwarzschild horizon, the field lines get progressively more distorted: they "wrap around" the hole so that as $r_c \to r_s$ they appear to emanate from $r = 0$, the field being essentially radial for $r - r_s \gg r_c - r_s$. It is as though the charge has spread itself over the hole's "surface". For a charge in free fall, the spreading happens in a time $\sim (r_s/c)$. Comparing this with the "classical" estimate of the time $r_s^2/4\pi\sigma$ taken for a charge to spread over a sphere of radius r_s and conductivity σ, we find that the effective resistance of a black hole is of order 100 ohms (cf. Znajek 1978).

A spinning (Kerr) black hole behaves like a spinning conductor (Blandford and Znajek 1977), in the sense that there are constraints on the orientations of any stationary electric and magnetic fields near the horizon. This analogy, spelt out in detail by Macdonald and Suen (1984), is sufficiently close that a "unipolar inductor" mechanism can indeed tap the spin energy of a hole. Specific models for radio sources based on this general concept were developed by Rees et al. (1982) and Phinney (1983) and are reviewed in detail by Begelman et al (1984).

Figure 7 depicts, very schematically, a unipolar inductor mechanism. For this to operate there must be:

(i) A magnetic field threading the hole (not shown in Figure 7).

(ii) Currents flowing in a circuit into and out of the hole.

(iii) A near-optimal impedance match, so that the currents dissipate a good fraction of their energy in the outer conducting sphere, rather than in the hole itself.

How can these requirements be fulfilled in a realistic and relevant context?

(i) There must be some conducting plasma near the hole, to carry the currents that maintain a magnetic field; even a very low level of accretion would suffice for this.

(ii) This same low-density plasma can indirectly supply the charges that carry electric current "into" the hole. Dilute plasma near a black hole would radiate inefficiently, and would be at a temperature of > 1 Mev (the virial temperature for $r < 10^3 r_s$ being higher than this). Its low-level radiative emission would then include bremsstrahlung gamma rays. Some of these will interact very close to the hole, yielding a cascade of electron-

positron pairs, with more than enough charge density to 'complete the circuit' and carry the necessary current - enough, indeed, to make the magnetosphere essentially charge-neutral, in the sense that $(n^+ + n^-) >> (n^+ - n^-)$, so that relativistic MHD can be applied.

(iii) The issue of the impedance match and the consequent efficiency, is rather more subtle. Phinney (1983) has explored the physics of the relativistic wind whose source is the pair plasma created by $\gamma + \gamma \rightarrow e^+ - e^-$ in the hole's magnetosphere, and which flows both outward along the funnel, and into the hole. He finds consistent wind solutions in which $\sim \frac{1}{2}$ of the hole's spin energy is transformed into Poynting flux and a relativistic electron-positron outflow.

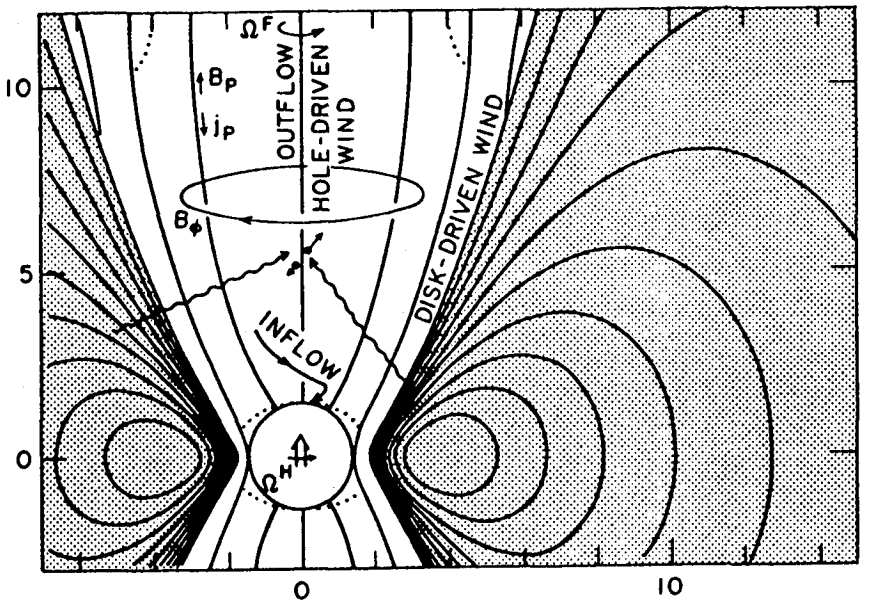

8. A model for the "central engine" in radio sources. Interaction between a spinning (Kerr) black hole and the magnetic field generates a hydromagnetic wind. External matter (shown stippled) confines a poloidal magnetic field B_p (of strength 10^3 - 10^4 G) threading the hole. (The precise geometry is unimportant; that shown is appropriate for a pressure-supported torus with constant specific angular momentum.) γ-rays (wavy lines) generated in the external matter create pairs in the otherwise empty magnetospheric region from which accreting material is excluded by centrifugal effects. On field lines which cross the event horizon, these pairs carry a current which extracts rotational energy from the hole in the form of a direct-current Poynting flux. (From Begelman et al. 1984).

The general scheme is depicted in Figure 8. Even a low-level and inefficient accretion flow can "anchor" a magnetic field that threads the hole, and thereby tap the hole's spin energy; in these conditions the extracted power naturally goes predominantly into a relativistic bifur-

cated outflow. The power extracted is of order $B^2 r_s^2 c$ (cf. an "inside out" pulsar light cylinder): for a field $\sim 10^4$G, which can be confined by plasma of density only 10^{-11} g cm^{-3}, this can be $\sim 10^{45}$ erg s^{-1}. This mechanism seems specially appropriate for strong radio galaxies such as Cygnus A (Rees et al. 1982) where the energy flowing along the jets dominates the radiative output of the AGN itself. Electron-positron pairs moving with Lorentz factors ~ 100 would transport some kinetic energy, but most of the power outflow would initially be in the form of Poynting flux associated with the magnetic field coiled round the jet axis, and "frozen in" to the pair plasma. This Poynting flux may be converted into fast particles where the jet encounters ambient material (perhaps on the scale of the VLBI radio components). The expected magnetic field in the jet has the kind of configuration that could cause magnetic confinement and collimation (see Section 3). The plasma around the hole that supplies the currents and anchors the field is just a catalyst: in principle, the power output of a radio galaxy could be sustained with *zero* accretion rate if some of the hole's spin energy were channelled into the surrounding plasma to compensate for its (small) radiative losses.

For the choice of parameters appropriate to strong sources, the maximum available e.m.f. of order $r_s \times B$, may be $\sim 10^{20}$ volts. This suggests that maybe these central regions offer a promising origin for the highest energy cosmic ray primaries. However, just as in pulsar models, the presence of charges "shorts out" the electric field and restricts the potential drop that can be attained. Pair production triggered by γ-rays from the surrounding plasma, amplified by cascade processes that occur if an outflowing wind moves through ambient radiation with a high Lorentz factor, would produce so many charges that, when the energy is shared among them, the resultant bulk flow has a Lorentz factor only $\lesssim 100$. (While shock wave acceleration could still in principle produce a power law spectrum with a tail extending to ultra high energies, the likelihood of photodissociation, etc. makes the compact central parts of AGNs a less promising site for 10^{20} ev particles than the extended lobes.)

The evolutionary context

Radio galaxies may, therefore, harbour massive black holes formed long ago via catastrophic collapse (maybe during a quasar phase of activity). The holes lurked quiescent, the galaxy being swept clean of gas, for billions of years. Then some event, perhaps interaction with a companion, triggered renewed infall - maybe at a low rate but sufficient to reactivate the nucleus by applying a magnetic field. This 'engaged the clutch', tapping the hole's latent spin energy, and converting it into non-thermal directed outflow - Poynting flux and e^+-e^- plasma - which ploughs its way out to scales $\sim 10^{10}$ times larger. If this is indeed what happens in Cygnus A and M87, then these very large-scale manifestations of AGN activity could offer the most direct evidence for inherently relativistic effects.

Massive black holes can generate a high luminosity in two quite distinct ways: straightforwardly by accretion; or via the electromagnetic process just described where the energy comes from the hole itself. The latter process tends to give purely non-thermal power. The properties of an AGN must depend, among other things, on the relative contributions of these two mechanisms, which depend primarily on the accretion rate and

the spin of the hole. The properties of AGNs must depend on other parameters - the nuclear mass M, the orientation and properties of the host galaxy etc. Ideally, one would like a unified model which explains the multifarious types of AGN in the same way that our theories for the Hertzsprung-Russell diagram do this for stars.

Conditions around black holes are extreme, but the relevant physics is known, and the key problem is at least well posed: axisymmetric plasma dynamics in a specified gravitational field, the aim being to calculate how much power is derived from accretion, and extracted from the hole's spin, and to find the form in which these respective contributions emerge. Such calculations play the same part in the modelling of AGNs that nuclear physics does in theories of stellar structure and evolution. The evidence that black holes have anything to do with AGNs is circumstantial; but the same is true for other cherished beliefs in astrophysics: the evidence that stars are powered by nuclear energy is also "merely" circumstantial. However the confrontation of models with observations - indirect even for stars - is admittedly much more ambiguous for AGNs: in stars the energy percolates to the observable surface in a relatively steady and well-understood way; in AGNs, on the other hand, it is reprocessed into all parts of the electromagnetic spectrum on scales spanning many powers of ten, in a fashion dependent on poorly-known environmental and geometrical effects within the host galaxy. The massive black hole hypothesis isn't infinitely "elastic", and could be disproved in several ways. It would, for instance, be in serious trouble if very regular periodicities were found in AGNs, or if Space Telescope studies of stellar velocity dispersions places upper limits $<< 10^8\ M_\odot$ on the central masses in any radio galaxies with large energy content.

Acknowledgements

Many of the ideas discussed in this paper have evolved in collaborative work with Mitch Begelman, Roger Blandford, Andy Fabian and Sterl Phinney. I am grateful to them, and to many other colleagues for stimulating discussion of many topics that are briefly and inadequately summarized here.

REFERENCES

Baade, W. and Minkowski, R. 1954. Astrophys. J., 119, 206.
Bally, J. and Lada, C.J. 1982. Astrophys. J., 265, 824.
Begelman, M.C., Blandford, R.D. and Rees, M.J. 1984. Rev. Mod. Phys., 56, 255.
Bekefi, G., Field, B.T., Parmentola, J. and Tsipis, K. 1980. Nature, 248, 219.
Biretta, J.A., Owen, F.N. and Hardee, P.E. 1983. Astrophys. J. (Lett), 274, L27.
Blandford, R.D. and Rees, M.J. 1974. MNRAS, 169, 395.
Blandford, R.D. and Znajek, R.L. 1977. MNRAS, 179, 433.
Bridle, A.H. and Purley, R.A. 1984. Ann. Rev. Astr. Astrophys., 22, 319.
Burbidge, G.R. 1958. Astrophys. J., 129, 841.
Burbidge, G.R., Burbidge, E.M. and Sandage, A.R. 1963. Rev. Mod. Phys., 35, 947.

Cavallo, G., 1978. Astron. Astrophys., 65, 415.
Curtis, H.D. 1918. Lick Obs. Publications, 13, 11.
Dreher, J.W. and Feigelson, E.D. 1984, preprint.
Fomalont, E.B., Geldzahler, B.J., Hjellming, R.M. and Wade, C.M. 1983. Astrophys. J. (Lett), 275, 802.
Geldzahler, R.J. et al., in Proc. IAU Symposium on VLBI, eds. R. Fanti et al. (Reidel, Dordrecht).
Guilbert, P.W., Fabian, A.C. and Rees, M.J. 1983. MNRAS, 205, 593.
Hanni, R.S. and Ruffini, R. 1972. in "Black Holes" ed. B. De Witt and C. De Witt p.1275 (Gordon and Breach, London).
Hazard, C., Mackay, M.B. and Shimmins, A.J. 1963. Nature, 197, 1037.
Hutchings, J.B. and Campbell, B., 1983. Nature, 303, 584.
Macdonald, D.A. and Suen, W-M, 1984, Phys. Rev. D (in press)
Margon, B. 1984. Ann. Rev. Astr. Astrophys., 22, 507.
Mundt, R. 1984. Proc. Toulouse Conference on "Nearby Molecular Clouds" Springer Verlag (in press).
Norman, M.L., Smarr, L.L., Winkler, K-H.A., and Smith, M.D. 1982. Astron. Astrophys., 113, 285.
Owen, F.N., Hardee, P.E. and Bignell, R.L., 1980. Astrophys. J. (Lett), 239, L11.
Penrose, R. 1969. Nuovo Cim., 1, 252.
Perley, R.A., Dreher, J.W. and Cowan, J.J. 1984. Astrophys. J. (Lett), 285, L35.
Phinney, E.S. 1983. Cambridge Ph.D. Thesis.
Rees, M.J. 1971. Nature, 229, 312 (errata p. 510).
Rees, M.J. 1984. Ann. Rev. Astr. Astrophys., 22, 471.
Rees, M.J., Begelman, M.C., Blandford, R.D. and Phinney, E.S. 1982. Nature, 295, 17.
Rees, M.J. and Setti, G. 1968. Nature, 219, 127.
Svensson, R. 1985. Proc. IAU Colloquium on Radiative Gas Dynamics, ed. D. Mihalas (in press).
Schmidt, M. 1963. Nature, 197, 1040.
Trimble, V.L. and Rees, M.J. 1970. Astrophys. Lett, 5, 93.
Wiita, P. 1985. Physics Reports (in press).
Williams, D. and Gull, S. 1985. Nature, 303, 39.
Wolfendale, A.W. 1984. in Proc. Erice Cosmic Ray School, ed. M. Shapiro (Reidel, Dordrecht)
Znajek, R.L. 1978. MNRAS, 185, 833.

GAMMA-RAY LINE ASTROPHYSICS

Richard E. Lingenfelter
Center for Astrophysics & Space Sciences, Univ. of California, San Diego
La Jolla, CA 92093 USA
and
Reuven Ramaty
Lab. for High Energy Astrophysics, NASA Goddard Space Flight Center
Greenbelt, MD 20771 USA

ABSTRACT

We review recent observations of gamma-ray line emission from solar flares, gamma-ray bursts, the galactic center, the interstellar medium and the jets of SS433, and we discuss the implications of these observations on high energy processes in these sources.

INTRODUCTION

Gamma-ray line astrophysics has developed rapidly in recent years with exciting new observations by gamma-ray spectrometers on balloons and on the HEAO, Venera, Hinotori and SMM satellites and space probes. These observations are providing unique new insights into a wide range of problems in high energy astrophysics and cosmic rays.

The relationship between gamma-ray and cosmic ray studies, of course, goes back to the very earliest observations. When Victor Hess[1] discovered the extraterrestrial origin of atmospheric ionization in 1912 he suggested that it was caused by high energy gamma rays from outside the solar system and hence named them "cosmic rays." But in 1927 on a voyage from Java to Genoa, Clay[2] discovered that the intensity of cosmic rays varied with geomagnetic latitude and thus they were charged particles not gamma rays. Extraterrestrial gamma rays were finally discovered over thirty years later when Peterson and Winckler[3] observed gamma-ray emission from a solar flare with a balloon-borne detector in 1959. Three years later Arnold et al.[4] discovered the diffuse extragalactic gamma-ray emission with a detector on the Ranger probe.

Gamma-ray astronomy has grown rapidly since then and at this conference fully one-fifth of the contributed paper sessions are devoted to gamma-ray observations and theory.

Recent developments in gamma-ray spectroscopy have revealed a diversity of gamma-ray lines in the spectra of astrophysical sources. The wide range of these observed lines, processes and sources can be seen in Table 1.

Although we reviewed[5] all of gamma-ray astronomy just three years ago, there have been a number of important new observations since then that need to be discussed here. In particular, gamma-ray spectra from solar flares have been observed[6] in much greater detail by the spectrometer on the Solar Maximum Mission (SMM), providing new information on both the flare accelerated particles and on chemical abundances in the solar atmosphere. A gamma-ray line from radioactive ^{26}Al was seen[7] from the interstellar medium by a high-resolution spectrometer on the Third High Energy Astronomical Observatory (HEAO-3), providing new information on processes of explosive nucleosynthesis in the Galaxy. Gamma-ray lines have been reported[8] also by HEAO-3 from the compact galactic object SS433, possibly providing clues to the understanding of the acceleration of the jets that are revealed by optical and radio observations. We will review all of these and other important sources of gamma-ray line emission.

Table 1
OBSERVED ASTROPHYSICAL GAMMA RAY LINES

Observed Lines	Processes	Sources
Cyclotron emission & absorption ~50 keV	Emission & absorption by electrons in $\gtrsim 10^{12}$ gauss magnetic fields	Gamma-ray bursters X-ray pulsars Crab pulsar(?) (magnetic neutron stars)
$e^{\pm}$ pair annihilation radiation 0.511 MeV	$e^+e^- \rightarrow 2\gamma$ by e^+ from: $\gamma\gamma \rightarrow e^+e^-$ $\gamma e^- \rightarrow e^-e^+e^-$ $\gamma B_\perp \rightarrow B_\perp e^+e^-$ β^+ decay $\pi^+ \rightarrow \mu^+ \rightarrow e^+$ decay	Solar flares (accel. particle interactions) Galactic center (accreting black hole) Gamma-ray bursters (magnetic neutron stars)
Nuclear deexcitation 6.129 MeV 4.438 1.779 1.634 1.369 0.847	Inelastic excitation $^{16}O(p,p')^{16}O^*$ ^{12}C . . . ^{28}Si . . . ^{20}Ne . . . ^{24}Mg . . . ^{56}Fe . . .	Solar flares (accel. particle interactions) SS433 jets (jet nuclei interactions)
1.809 MeV	Radioactive decay $^{26}Al(\beta^+)^{26}Mg^*$	Interstellar gas (explosive nucleosynthesis)
Radiative capture 2.223 MeV 7.632 7.646	Neutron capture $^1H(n,\gamma)^2H$ $^{56}Fe(n,\gamma)^{57}Fe$	Solar flares (accel. particle interactions) Jacobson transient (accreting neutron star?)

SOLAR FLARES

Recent observational and theoretical studies of gamma rays and neutrons from solar flares have provided new insights into the problem of particle acceleration and have given new information on the composition of the solar atmosphere. These results have been discussed in a number of recent papers (e.g. Refs. 6, 9-12). The gamma-ray lines and neutrons result from nuclear interactions of accelerated protons and heavier nuclei, while the continuum is due to relativistic electron bremsstrahlung and the superposition of Doppler-broadened gamma-ray lines.

Theoretical studies predicted[13] that the principal gamma-ray lines should be those at 2.223 MeV from neutron capture on ^1H, at 0.511 MeV from positron annihilation, and at 4.438 and 6.129 MeV from deexcitation of nuclear levels in ^{12}C and ^{16}O, respectively. These predictions were confirmed when gamma rays were first observed[14] with a detector on OSO-7 from the solar flare of 4 August 1972. These and other weaker lines have since been observed from more than 30 flares by detectors on HEAO-1[15] HEAO-3[16], Hinotori[17] and most extensively SMM[6,10,18]. Neutrons from solar flares have also been observed, confirming earlier predictions (e.g. Ref. 19). The neutron observations consist of direct spacecraft[20,21] and ground based[22,23]

detections, as well as of the measurement[24] of the protons resulting from the decay of the neutrons in interplanetary space.

Energetic particles from solar flares have been observed in interplanetary space on numerous occasions, but there is clear evidence that the nuclear interactions that produce the gamma rays and neutrons are caused by accelerated particles that remain trapped in the magnetic fields of the flare region and interact as they slow down in the solar atmosphere. This is most clearly seen (e.g. Ref. 25) by the fact that, if the escaping particles were responsible for the observed gamma-ray emission, they should also show great enrichments in spallation products, such as ^{2}H, ^{3}H, Li, Be and B, which are not observed[26].

Further evidence for this trapping comes from the comparison of the number of particles required to produce the observed gamma rays and neutrons with the number of escaping particles, and from the comparison of the number of positrons produced at the Sun with the observed flux in the 0.511 MeV line.

The number of gamma-ray producing particles can be derived from measurements of the neutron-capture line at 2.2 MeV and the photon flux in the 4 to 7 MeV band, which is dominated[27,28] by C and O deexcitation lines. Since the effective threshold for neutron production is significantly higher than that for C and O excitations, the 2.2 MeV line and the 4 to 7 MeV band sample different portions of the accelerated particle spectrum. The ratio of the fluxes in the 2.2 MeV line and in the 4 to 7 MeV band therefore constrains the particle spectrum, while the 4 to 7 MeV flux determines the particle number. Results for several flares from which gamma rays were observed are summarized in Table 2. The spectral indexes and total proton numbers at the Sun are given for two possible forms for the accelerated particle energy spectra, a power law in kinetic energy and a Bessel function. For the former, the number of accelerated particles per unit kinetic energy is proportional E^{-S}, where E is particle kinetic energy. For the latter, this number is proportional to $K_2(12p/m_pc\alpha T)^{1/2}$, where p is particle momentum per nucleon and αT an index characterizing the hardness of the spectrum. A power law in kinetic energy is the nonrelativistic approximation of a power law in momentum, which is the spectral form expected (e.g. Ref. 29) from first order shock acceleration at a planar and infinite shock. The Bessel-function spectrum is the nonrelativistic approximation to the spectrum expected from stochastic acceleration[30]. Nonrelativistic approximations are adequate for calculations involving protons and nuclei, since the bulk of the nuclear reactions in flares occur at energies much lower than m_pc^2.

Table 2
ENERGETIC PARTICLE PARAMETERS IN SOLAR FLARES[11]

	In Solar Atmosphere				Interplanetary	
	Bessel Function		Power Law			
FLARE	αT	N_p (>30 MeV)	S	N_p (>30 MeV)	Spectral Index	N_p (>30 MeV)
	Determined from Gamma-Ray Line Measurements					
4 Aug. 1972	0.029±0.004	1.0×10^{33}	3.3±0.2	7.2×10^{32}	—	4.3×10^{34}
11 Jul. 1978	~0.032	1.6×10^{33}	~3.1	1.3×10^{33}	—	—
9 Nov. 1979	0.018±0.003	3.6×10^{32}	3.7±0.2	2.6×10^{32}	—	—
7 Jun. 1980	0.021±0.003	9.3×10^{31}	3.5±0.2	6.6×10^{31}	$\alpha T\simeq0.015$	8×10^{29}
1 Jul. 1980	0.025±0.006	2.8×10^{31}	3.4±0.2	1.9×10^{31}	—	$<4\times10^{28}$
6 Nov. 1980	0.025±0.003	1.3×10^{32}	3.3±0.2	1.0×10^{32}	—	3×10^{29}
10 Apr. 1981	0.019±0.003	1.4×10^{32}	3.6±0.2	1.0×10^{32}	—	—
	Determined from Neutron and Gamma-Ray Line Measurements					
21 Jun. 1980	0.025±0.005	7.2×10^{32}	INCONSISTENT		$\alpha T\simeq0.025$	1.5×10^{31}
3 Jun. 1982	0.034±0.005	2.9×10^{33}	INCONSISTENT		$s\simeq1.7$	3.6×10^{32}

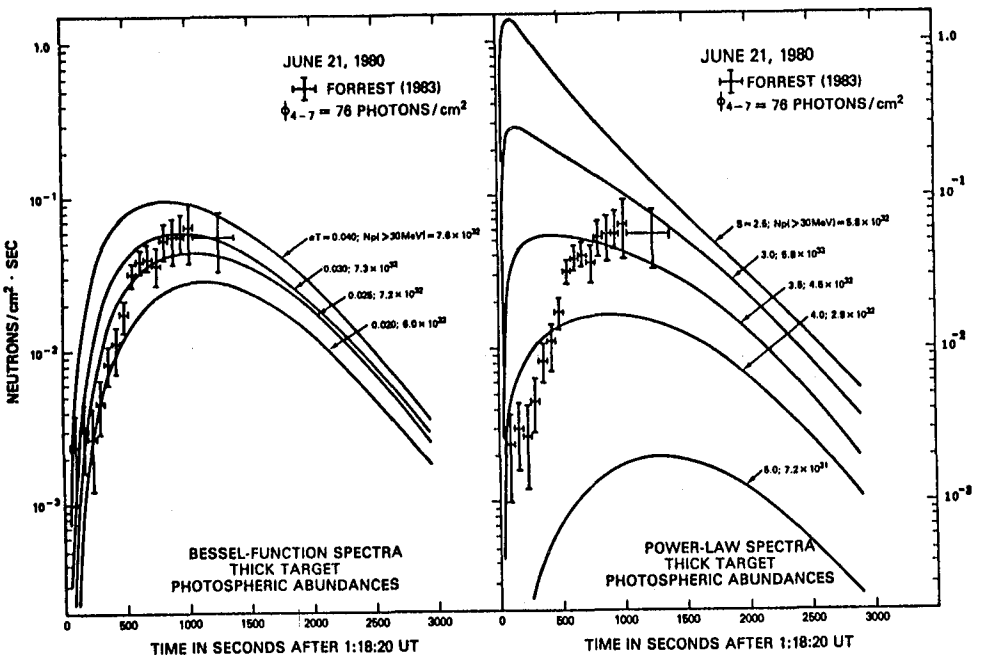

Fig. 1. Determination[11] of the number and spectrum of flare accelerated protons at the Sun from observations[6] of the time dependent neutron flux and the gamma-ray line emission in the 4-7 MeV range.

The number of neutron-producing particles and their energy spectrum can be derived from observations of the time-dependent neutron flux at Earth. For consistency, this number and spectrum must be the same as those derived from the gamma-ray observations. Observations of a time-dependent neutron flux for the flare of 21 June 1980 are shown in Figure 1 together with calculated fluxes. These fluxes are normalized such that the calculated 4 to 7 MeV flux agrees with the observed[6] flux in this energy band, $\sim$76 photons/cm^2. It is evident that the combined neutron and gamma-ray emission cannot result from particles with a power-law spectrum. For, as we see from Figure 1, none of the combinations of power-law spectra and total particle numbers that could produce the observed 4-7 MeV flux can also produce a neutron flux consistent with that which was measured. As can also be seen in Figure 1, however, both observations are quite consistent with accelerated particles having a Bessel-function spectrum with $\alpha T \sim 0.025$ and a total number of 7×10^{32} protons >30 MeV. Qualitatively, the difference between this Bessel-function spectrum and a power-law in kinetic energy is the gradual steepening of the former as the energy increases. Shock acceleration can also produce[29] such a steepening, or high-energy cutoff, if the shock is of finite size and the acceleration is of finite duration. Thus, while these results cannot definitively determine the acceleration mechanism, they demonstrate that a consistent interaction model can be set up involving either one of them.

Comparing these results with those inferred from the direct particle observations (Table 2), we see that independent of the spectral form, the number of particles that produce the observed gamma rays and neutrons are generally much higher than the number of interplanetary particles from flares which produce detectable gamma rays. This implies that the gamma rays and neutrons are produced predominantly in closed magnetic configurations from which very few charged particles escape. As mentioned above, the absence of spallation products in the escaping particles indicates that this latter population is not involved in significant gamma-ray and neutron production. We discuss separately the implications of the exceptional

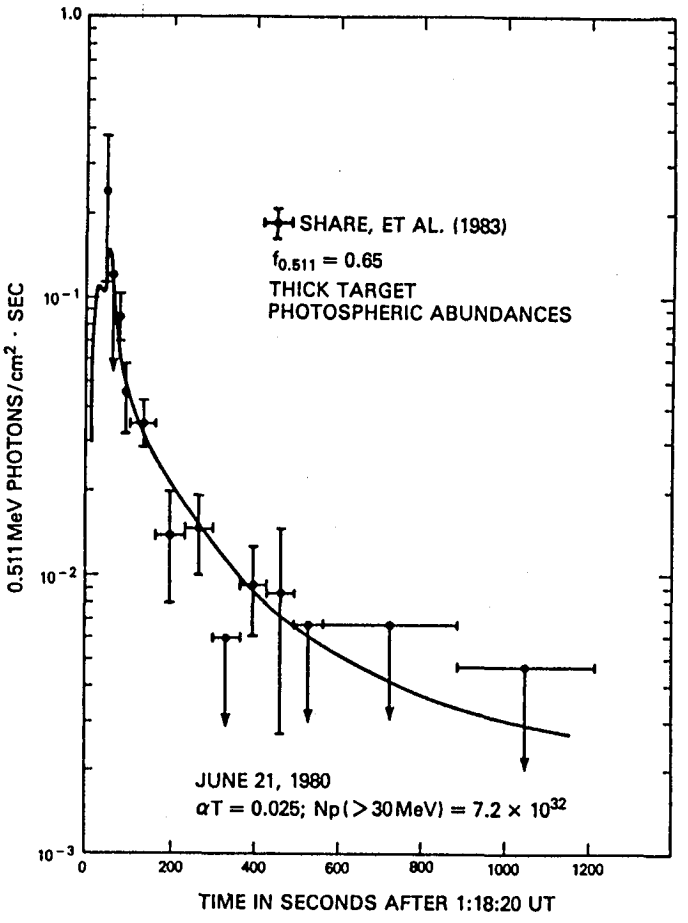

Fig. 2. Observed[31] 0.511 MeV line flux from the 21 June 1980 flare compared with that expected[11] from the number and spectrum of accelerated particles determined in Figure 1.

case of the 4 August 1972 flare for which the number of particles observed in interplanetary space was much larger than the number of trapped particles (Table 2).

Further evidence that the gamma rays are generally produced in closed magnetic configurations comes from the analysis of the time-dependent flux of the 0.511 MeV line from positron annihilation. This is shown in Figure 2 where observations[31] of the 21 June 1980 flare are compared with the calculated[11] 0.511 MeV flux. In these calculations the radioactive β^+ emitters and π^+ mesons were produced by accelerated particles with the same spectrum and total number as determined from the neutron and 4-7 MeV observations, and it was assumed that the positrons remain trapped at the Sun and annihilate essentially instantaneously. The agreement with the observations shown in Figure 2 strongly supports these assumptions. The trapping of the positrons is further evidence for the trapping of all the gamma-ray producing charged particles, while their short annihilation time implies a sufficiently high ambient density which suggests that the annihilation site, and hence also the interaction site, is in the chromosphere below the transition layer.

In addition to the 4 August 1972 flare, for which the number of interplanetary particles was much larger than that involved in gamma-ray production, there are many other flares[32]

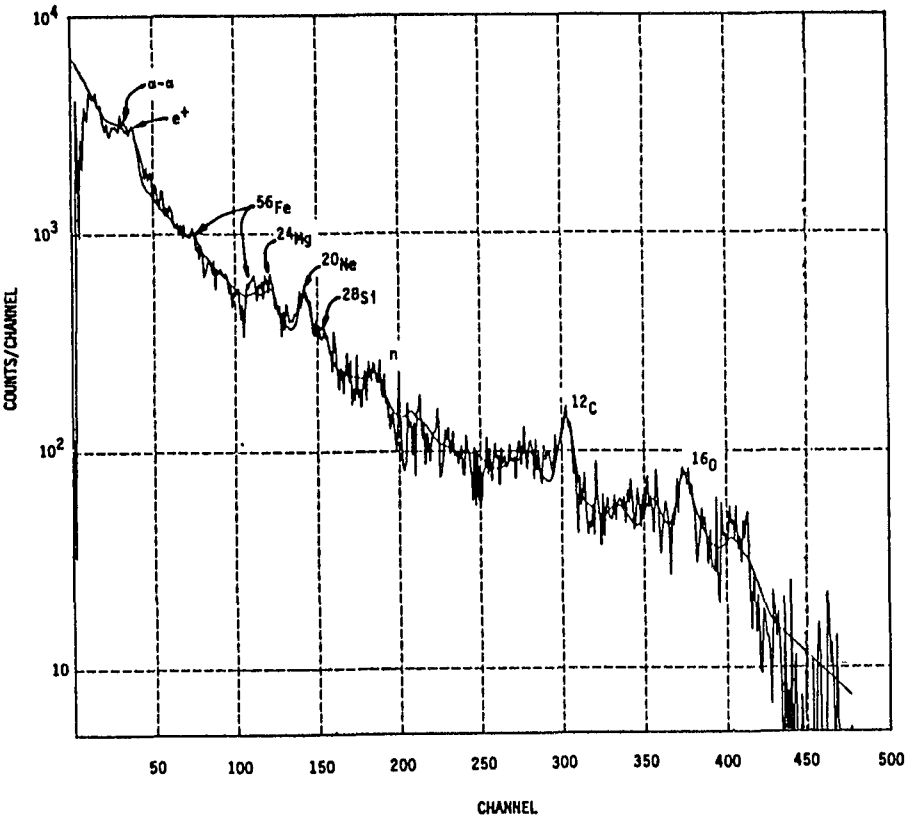

Fig. 3. Observed[6,10] and calculated[33] spectra of the 27 April 1981 flare.

which produce large fluxes of interplanetary particles without producing detectable gamma rays. These particles, always devoid of spallation products, are most likely accelerated at sites with ready access to interplanetary space.

We turn now to the determination of the relative composition of the solar atmosphere in the flare region from comparisons of the various deexcitation line intensities. A sample spectrum shown in Figure 3 was observed[6,10] from the 27 April 1981 flare by the gamma-ray spectrometer on the SMM. Nuclear reactions of accelerated protons and alpha particles with heavier nuclei in the ambient gas produce narrow lines, such as those shown at 6.129 MeV from deexcitation of $^{16}O^*$, 4.438 MeV from ^{12}C, 1.779 MeV from $^{28}Si^*$, 1.634 MeV from $^{20}Ne^*$, 1.369 MeV from $^{24}Mg^*$ and 0.847 MeV from ^{56}Fe. The inverse reactions, between accelerated heavy nuclei and ambient H and He, produce broad lines which effectively merge into a continuum. Also evident are the lines at 2.223 and 0.511 MeV. The feature just below the positron annihilation line results from reactions between accelerated alpha particles and ambient He nuclei leading to $^7Li^{*0.478MeV}$ and $^7Be^{*0.431MeV}$ line emission. The continuum, upon which the narrow lines are superimposed, is due to both relativistic electron bremsstrahlung and the Doppler broadened deexcitation lines of the accelerated heavy nuclei.

The relative intensities of the narrow nuclear deexcitation lines depend on several factors, such as the energy spectrum of the accelerated particles, but they are obviously most sensitive to the elemental abundances of the ambient gas in the interaction region. Even though the location of this region cannot be determined by direct gamma-ray imaging, a variety of indirect arguments, such as the time dependence of the 0.511 MeV line discussed above, indicate that most of the nuclear reactions take place in the chromosphere. The observed gamma-ray

spectrum, therefore, can be used to infer chromospheric abundances. The most direct evaluation[12] consists of theoretical calculations of the spectrum with variations of the abundances until the best fit to the data is achieved. The resultant best-fitting spectrum[33] is shown by the smooth curve in Figure 3.

With the normalization given by the best-fit, the principal difference between the gamma-ray and local galactic[34] abundances is the underabundance of C and O in the gamma-ray deduced abundances. The Fe, Si, Mg and Ne abundances are in good agreement, while the statistical errors for Ca, S, Al and N and the systematic errors for H and He are too large to permit any quantitative conclusion (see Ref. 12). A similar suppression of C and O in the coronal abundances relative to local galactic abundances has been pointed out in Ref. 34 where it was suggested that the suppression may be caused by charge-dependent mass transport from the photosphere to the corona. Since the photosphere is collisionally ionized at a relatively low temperature, the transport could depend on the first ionization potentials of the elements. Mass transport to the chromosphere could be influenced by similar fractionation effects. However, if the Ne abundance in the photosphere (where it has not yet been measured) is the same as in the local galactic set, then the mechanism which produces differences between the gamma-ray and photospheric abundances must include additional effects, because correlation with first ionization potential alone would predict a Ne abundance at least as low as the O abundance, contrary to that implied by the gamma-ray observation.

Independent of the mechanism responsible for the fractionation, significant abundance differences exist between various sites in the solar atmosphere. It seems inevitable that similar fractionation phenomena could affect the abundance determinations of objects other than the Sun.

GAMMA RAY BURSTS

Gamma-ray bursts were discovered[35] accidentally in 1967 by detectors on board the Vela satellites whose primary purpose was to monitor artificial nuclear detonations in space. The observational properties of the bursts and current theoretical ideas about their origin have been extensively reviewed in recent workshop proceedings[36,37].

Gamma-ray bursts are generally observed in the photon energy range from a few tens of keV to several MeV with event durations ranging from about 0.1 to 100 sec. The observed burst energy fluences (>30 keV) range from about 10^{-7} to 10^{-3} erg/cm^2, and the frequency of occurrence of detector bursts range from about ten per year with fluences $>10^{-4}$ erg/cm^2 to several thousand per year with fluences $>10^{-7}$ erg/cm^2. At fluences less than 10^{-5} erg/cm^2, the frequency of bursts falls below that which might be expected from an unbounded, isotropic and homogeneous distribution of sources[38,39]. Although it has been suggested that this results from the finite galactic distribution of sources and is thus evidence for a galactic origin, recent studies[40,41] have shown that this deviation can be explained entirely by temporal and spectral selection biases in the detectors.

The distribution of gamma-ray burst source directions on the sky is essentially isotropic, which suggests that if they are galactic the sources typically lie within a scale height of the disk ($\leqslant 1$ kpc) and release energies of $\leqslant 10^{39}$ ergs.

The determination[42] of several very precise source positions, however, has not lead to the identification of any burst sources with known objects, except for one case. That exception is the source of the 5 March 1979 burst, GBS 0526-66, whose positional error box[43] of size 0.1 arc min^2, lies within the supernova remnant N49 in the Large Magellanic Cloud which is at a distance of 55 kpc. If the burst source is at this distance, the total radiated energy is $\sim 10^{44}$ ergs, which is about five orders of magnitude larger than that inferred for a typical galactic gamma-ray burst. But the 5 March burst exhibited a number of remarkable and possibly unique observational characteristics, including[44,45] the extremely rapid rise time ($<2\times10^{-4}$ sec) of the impulsive emission spike, the relatively short duration (~ 0.15 sec) and high luminosity of this spike, the 8-sec pulsed emission following the impulsive spike, and 15 subsequent[46], apparently

nonrandom[47], outbursts of lower intensity from the same source direction over the last several years. Thus it appears[44,48] to belong to a separate class of less frequent but more energetic transients than do the typical galactic bursts.

Although searches (e.g. Ref. 49) of other positional error boxes have not produced any likely source objects, a search[50,51] of archival optical plates has revealed evidence of possible optical flashes from a couple of the burst sources in the past. Very recently optical flashes have also been detected[52] from the direction of the repeating, 5 March 1979 source direction. This appears to open a new window for monitoring such bursts, but simultaneous optical and gamma-ray observations are still needed before it can be established that gamma-ray bursts are in fact accompanied by the detectable optical flashes.

The best insight into the nature of gamma-ray burst sources has come from the discovery[53] of absorption and emission features in the energy spectra of the bursts.

The absorption features have been observed[53,54] in a number of spectra, generally in the energy range from about 30 to 60 keV, as can be seen in the spectra of the 25 March 1978 burst[54] shown in Figure 4. These features, like those in the spectra of X-ray binaries, appear to be the result of cyclotron absorption in intense magnetic fields of a few times 10^{12} gauss, which strongly suggests that magnetic neutron stars are the source of many, if not all, gamma-ray bursts. Moreover the narrowness of the observed absorption features, implying a small range of effective magnetic field strengths, further suggest that the soft burst emission (<0.1 MeV) comes from a relatively small region close to the polar cap of a neutron star and is observed at a large angle to the axis of the field. The soft continuum spectra are in fact quite consistent[55] with gyrosynchrotron emission in such fields.

As can be seen in the spectrum of the 25 March 1978, however, this soft component accounts for only a fraction ($\sim 20\%$) of the observed burst emission. Most of the emission in this burst is seen in a spectrally distinct hard component between ~ 0.25 and 6 MeV. Similar hard components, with energies extending as high as 20 MeV, have been observed[56] in many other bursts. The photon-photon $e^{\pm}$ pair production opacity of these hard photons imposes a strong constraint[57,58] on the minimum size of the emission region. This size greatly exceeds that of a neutron star polar cap, unless the star is uncomfortably close or the emission is highly beamed.

To reconcile these features it has been suggested[57,58] that the bulk of the observed burst energy was initially ejected from the polar cap of a neutron star in a highly collimated jet of $e^{\pm}$ pairs which disrupted and isotropized far above the star to form a fireball[59] that expanded until it became transparent to photon-photon pair production and the observed photons escaped. In such a model the emission time-scale is determined by the size at which the fireball becomes transparent. Thus the observed duration can give a measure of the total energy, and hence the distance, of the burst[58].

There is also evidence for possible redshifted $e^{\pm}$ annihilation line emission in the spectra of some gamma-ray bursts. The most commonly observed emission line in burst spectra falls in the energy range from 0.40 to 0.46 MeV, as seen[53] by low resolution NaI detectors in the spectra of a third of the most intense gamma-ray bursts. Such line emission may be optically thin $e^{\pm}$ annihilation radiation redshifted by the strong gravitational field of a neutron star. But in an optically thick region, stimulated annihilation radiation[60] could also produce a line at about 0.43 MeV without a gravitational redshift. A well resolved line at ~ 0.43 MeV (Figure 5) was also seen[61,62] in the spectrum of the 5 March, 1979 burst, suggesting that the source of this burst was also a neutron star.

Current theoretical ideas on gamma-ray bursts generally involve strongly magnetized neutron stars. These ideas have developed, in part, as a result of the detailed observations and modelling[63,64] of the 5 March 1979 burst even though it is quite likely that the underlying energy source of this burst in not typical of all gamma-ray bursts. The most probable energy source of gamma-ray bursts is either gravitational or nuclear. Magnetic field annihilation, responsible for rapid energy generation in solar flares, is insufficient energetically.

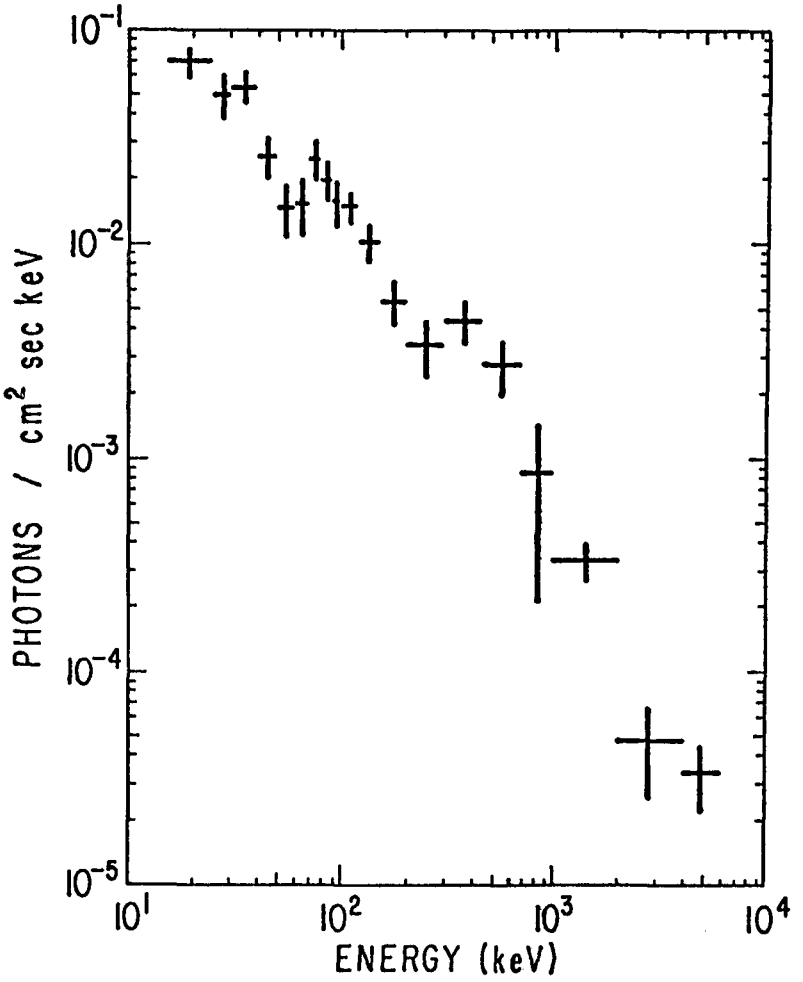

Fig. 4. Observed[54] gamma-ray spectrum of the 25 March, 1978 burst.

Gravitational energy can be released in a burst from a neutron star when a large amount of matter is impulsively accreted onto its surface, in an asteroid or comet impact[65,66] or sporadic dumping of an accretion disk by magnetospheric instabilities[67]. Such accretion releases about 100 MeV/nucleon, the potential energy at the neutron star surface. Gravitational energy could also be released in a corequake of a neutron star[63,68]. Such quakes could result[69] from a collapse following a phase transition from ordinary nuclear matter to a new state containing a Bose-Einstein condensate of pions[70]. Pion condensates are believed to exist above a critical density, about twice the nuclear density, and to have lower energies per baryon and a significantly softer equation of state than ordinary nuclear matter. As a result of accretion or reduced centrifugal forces due to a slowing rate of rotation, the core density of a neutron star may increase beyond the critical density resulting in a supercompressed metastable state which could eventually collapse to the pion condensed state. Such a collapse could release[71] about 10^{48} erg in a time no longer than the free fall time (10^{-4} sec). As much as 10% of this energy could go into neutron star vibrations if the oscillation amplitude is on the order of the radius change ($\sim$10m). Neutron star quakes can set up neutron star vibrations which dissipate mainly by gravitational radiation (e.g. Ref. 72). A fraction of the vibrational energy, however, can be

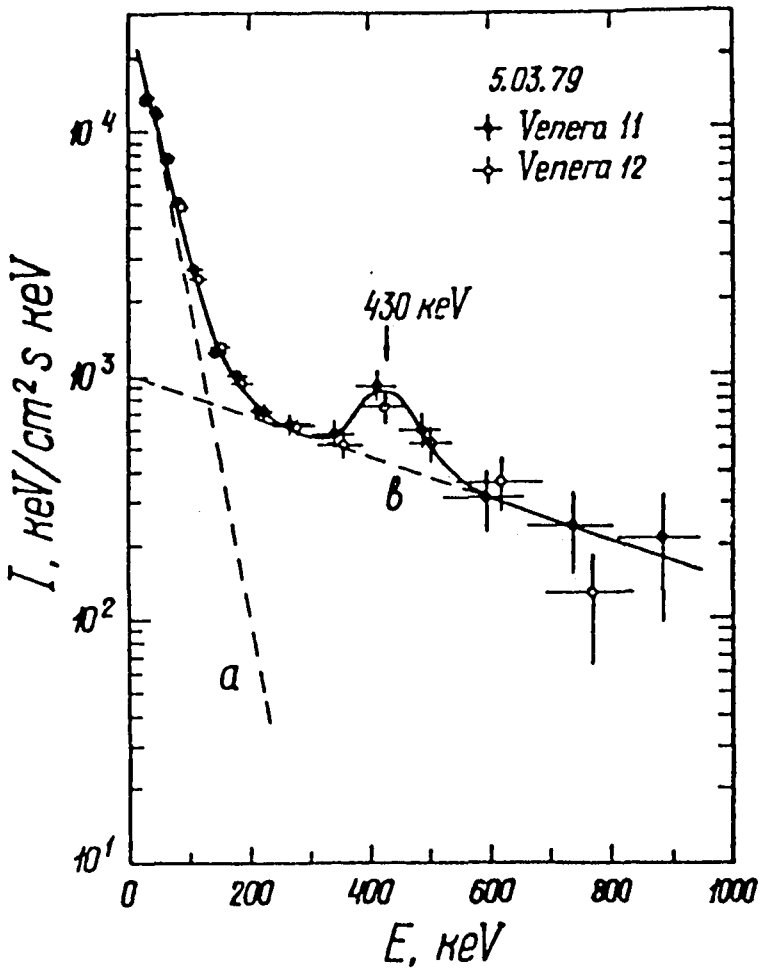

Fig. 5. The spectrum[62] of the impulsive emission spike of the 5 March, 1979 gamma-ray burst.

converted[63,69] into magnetoacoustic waves which dissipate by accelerating particles in the magnetosphere. Radiation from these particles would then be responsible for the observed gamma-ray emission.

Alternatively, impulsive energy release from neutron stars could result from a nuclear detonation of degenerate matter accumulated over a relatively long period of time by slow accretion of gas[73,74]. Such detonations release several MeV per nucleon from the burning of helium to the iron peak nuclei. All three of these processes, impulsive accretion, corequakes, or nuclear detonations, appear to be quite capable of providing the 10^{37} to 10^{40} ergs required for typical galactic gamma-ray bursts. But to account for the $\sim 10^{44}$ ergs of the 5 March 1979 burst, such large amounts of accreted matter are required that accretion and nuclear detonation appear to be ruled out, so that only corequakes appear to be capable of providing the energy needed for this burst.

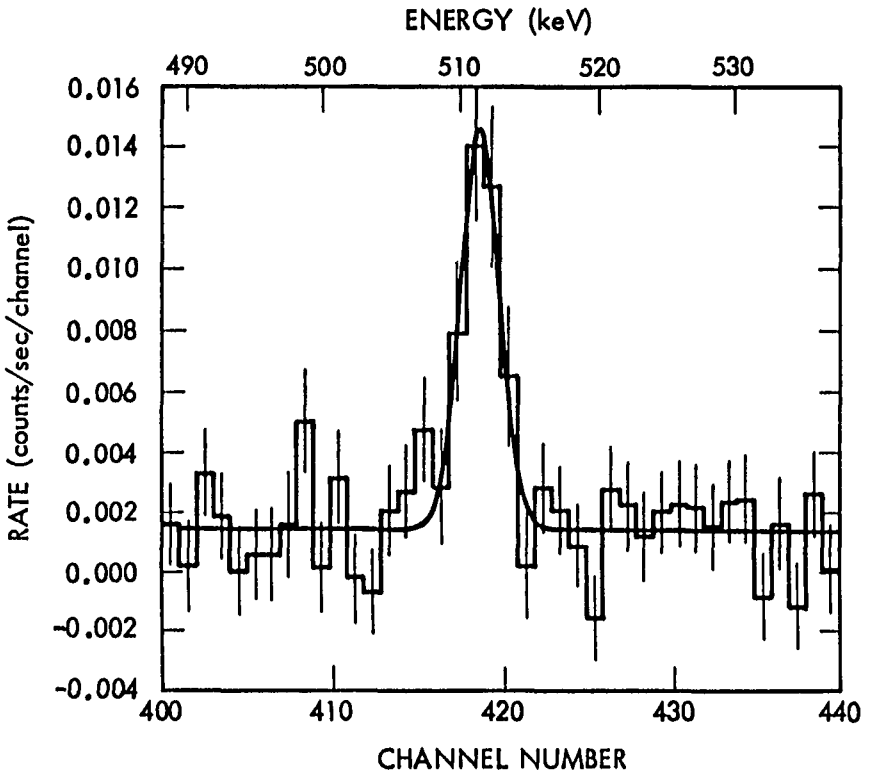

Fig. 6. Gamma-ray spectrum near 0.511 MeV observed[79] from the direction of the Galactic Center.

GALACTIC CENTER

Intense positron annihilation radiation at 0.511 MeV has been observed from the direction of the Galactic Center for over a decade. This emission was first reported in a series of balloon observations with low-resolution NaI detectors, starting in 1970[75–77]. But it was not until 1977 that the annihilation line energy of 0.511 MeV was clearly identified with high-resolution Ge detectors[78]. The latter observation also revealed that the line is very narrow (FWHM <3.2 keV) and that it shows evidence for three-photon positronium continuum emission below 0.511 MeV, implying that $\sim$90% of the positrons annihilate via positronium. Thus, the observed intensity of $\sim 10^{-3}$ photons/cm^2 sec implies an annihilation rate of $\sim 2\times10^{43}$ positrons/sec or an annihilation radiation luminosity of $\sim 3\times10^{37}$ ergs/sec at the 10 kpc distance of the Galactic Center.

Subsequent Ge detector observations[79–80] on HEAO-3 have confirmed the narrowness (FWHM <2.5 keV) of the line and have provided more precise information on the line center energy (510.90 ± 0.25 keV, see Figure 6). These measurements also showed that the direction of the source is coincident with that of the Galactic Center (within the $\pm4°$ observational uncertainty). Most important, the HEAO-3 observations revealed that the line intensity varies with time, decreasing by a factor of three in six months from $(1.85\pm0.21)\times10^{-3}$ photons/cm^2 sec in the fall of 1979 to $(0.65\pm0.27)\times10^{-3}$ photons/cm^2 sec in the spring of 1980. This decrease, confirmed by later observations[81–83] implies that the sizes of both the annihilation region and the positron source are less than the light-travel distance of 10^{18} cm. The reported annihilation line fluxes from the Galactic Center as a function of time during the last 15 years are shown in Figure 7.

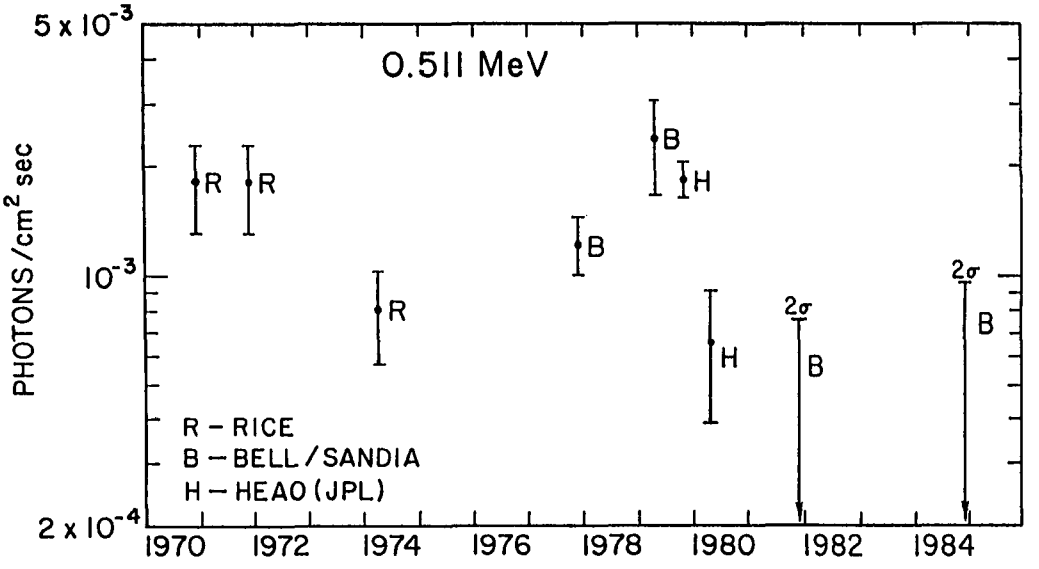

Fig. 7. Observed 0.511 MeV fluxes and upper limits from the direction of the Galactic Center.

The nature of the positron annihilation region is further constrained by the observed line width and intensity variations. The line width (FWHM < 2.5 keV) requires[84] a gas temperature in the annihilation region less than 5×10^4 K and the intensity variation requires that the density of gas at this site be high enough ($> 10^5$ cm^{-3}) that the positrons can slow down and annihilate in less than half a year. Such regions appear to exist in both the peculiar warm clouds[85] and the compact non-thermal source[86] within the central parsec of the Galaxy. While previous theoretical studies[84] suggested that the line width also constrains the ionization fraction of the ambient gas to values greater than $\sim 10\%$, it has recently been pointed out[87] that, when the results of new laboratory measurements[88] of positron annihilation in neutral H are taken into account, this constraint is no longer valid.

The nature of the positron source is strongly constrained[89] by the observed variation of the 0.511 MeV intensity and by observations at other wavelengths. The decrease of a factor of three in the line intensity in six months clearly excludes any of the multiple, extended sources, such as cosmic rays, pulsars[90], supernovae[91] or primordial black holes[92] previously proposed. Instead, it essentially requires[93] a single, compact ($< 10^{18}$ cm) source which is apparently located either at or close to the Galactic Center and which is inherently variable on time scales of six months or less. However, because the observed line-center energy shows no evidence for any gravitational redshift, the annihilation site must be removed by at least 10^3 Schwartzschild radii from this compact object.

The strongest constraints on the positron production processes are set[89] by observations[80,94] of the accompanying continuum emission at energies $> m_e c^2$. These require a high positron production efficiency, such that more than 10% of the total radiated energy $> m_e c^2$ goes into electron-positron pairs. Under the conditions of positron production on time scales comparable to that of the observed variation and in an optically thin, isotropically emitting region, only photon-photon pair production among $\sim$MeV photons can provide the required high efficiency. Moreover, the absolute luminosity of the annihilation line requires that the photon-photon collisions take place in a very compact source ($d < 5 \times 10^8$ cm). Pair production in an intense radiation field around an accreting black hole of $\lesssim 10^3 M_\odot$ appears to be a possible source[89,95]. However, if the gamma-ray continuum is beamed, the observed continuum cannot be used to determine the photon density at the source. In this case, a photon density high enough to produce pairs at the observed rate may be present in a much larger source region

than that estimated for isotropic gamma-ray emission. Such pair sources may be associated with jets in massive, million-solar mass black holes[89,93,96–99]. But the total gamma-ray luminosity in these models is much higher ($\sim 10^{40}$ erg/sec) than that of the isotropic model ($\sim 10^{38}$ erg/sec). Another important difference between the $\sim 10^3 M_\odot$ and the $\sim 10^6 M_\odot$ black hole models is that while dynamical considerations imply that the more massive hole should reside at the nucleus of the Galaxy, the currently determined positional uncertainty of the line source ($\pm 4°$) would allow a variety of locations for the less massive object. Future imaging experiments with much better angular resolution could therefore differentiate between the models.

GALACTIC NUCLEOSYNTHESIS

The search for gamma-ray lines from nucleosynthetic radionuclei in our galaxy has been carried on for over a decade to test current theories of the explosive nucleosynthetic origin of most nuclei heavier than helium. This search has at last resulted in the first observation[7,100] of such a line from ^{26}Al, made with the high resolution Ge spectrometer on HEAO-3. That this line should be detectable was pointed out earlier [101,102], but the observed intensity is nearly an order of magnitude greater than was predicted.

A rich variety of explosive nucleosynthetic lines have been proposed from both supernovae and novae. The most abundant radionucleus expected[103] from explosive nucleosynthesis in supernovae is ^{56}Ni, which decays with a 8.8 day mean-life to ^{56}Co, which, in turn, decays with a mean-life of 114 days to ^{56}Fe; 20% of the ^{56}Co decays are via positron emission. Nucleosynthesis of ^{56}Ni in supernovae is thought[104] to be the primary source of galactic ^{56}Fe.

The bulk of the gamma rays[105] and positrons[106] from the ^{56}Ni decay chain, however, are absorbed in the expanding nebula and their energy emerges only as lower energy radiation. The characteristic light curves of Type I supernovae, in fact, appear to follow the ^{56}Ni and ^{56}Co decay and optical lines from both ^{56}Co and the resulting ^{56}Fe have recently been detected[107] in the spectrum of an extragalactic supernova, SN 1972e. Any such direct gamma-ray line emission escaping from the nebula would be detectable for only a few years after the supernova explosion.

Gamma-ray lines from other longer-lived radionuclei, such as 1.1 yr ^{57}Co, 3.8 yr ^{22}Na and 68 yr ^{44}Ti from supernovae, have also been suggested[103,108,109]. But these too could only be detectable for at most about 100 years after the explosion.

There are, however, three much longer lived ($> 10^5$ yr) sources of nucleosynthetic gamma-ray lines, namely β^+ decay positrons, ^{26}Al and ^{60}Fe, which could give a direct measure of the overall galactic average rate of explosive nucleosynthesis. Since a fraction of the positrons from ^{56}Co decay are expected[105,106] to escape into the interstellar medium and since in the tenuous interstellar gas the positron lifetime against annihilation is quite long ($\sim 10^5$ yr in a density of 1H cm^3), positrons should accumulate from several thousand supernovae, assuming that galactic supernovae occur about once every 30 years. Their annihilation should thus produce[91,110] diffuse galactic gamma-ray line emission at 0.511 MeV. Furthermore, estimates (e.g. Ref. 93) of the rate of positron production by other types of sources suggest that the principal source of galactic positrons should in fact be those escaping from ^{56}Co decay produced in Type I supernovae.

Recent observations[111,112] of galactic 0.511 MeV emission with wide ($> 50°$) field-of-view detectors reveal considerably higher line intensities than would be expected from the Galactic Center source alone, which suggests that there may be a spatially diffuse source of 0.511 MeV line emission in the Galaxy. Conclusive measurements of such diffuse line emission can thus provide information on the average rate of galactic nucleosynthesis of ^{56}Fe during the last 10^5 years.

Similarly, the long-lived radionuclei ^{60}Fe (mean-life $\sim 4 \times 10^5$ yr) and ^{26}Al (mean-life $\sim 1 \times 10^6$ yr), which are also expected from explosive nucleosynthesis, should accumulate from $\sim 10^4$ or more supernovae and be well distributed through the interstellar medium before they

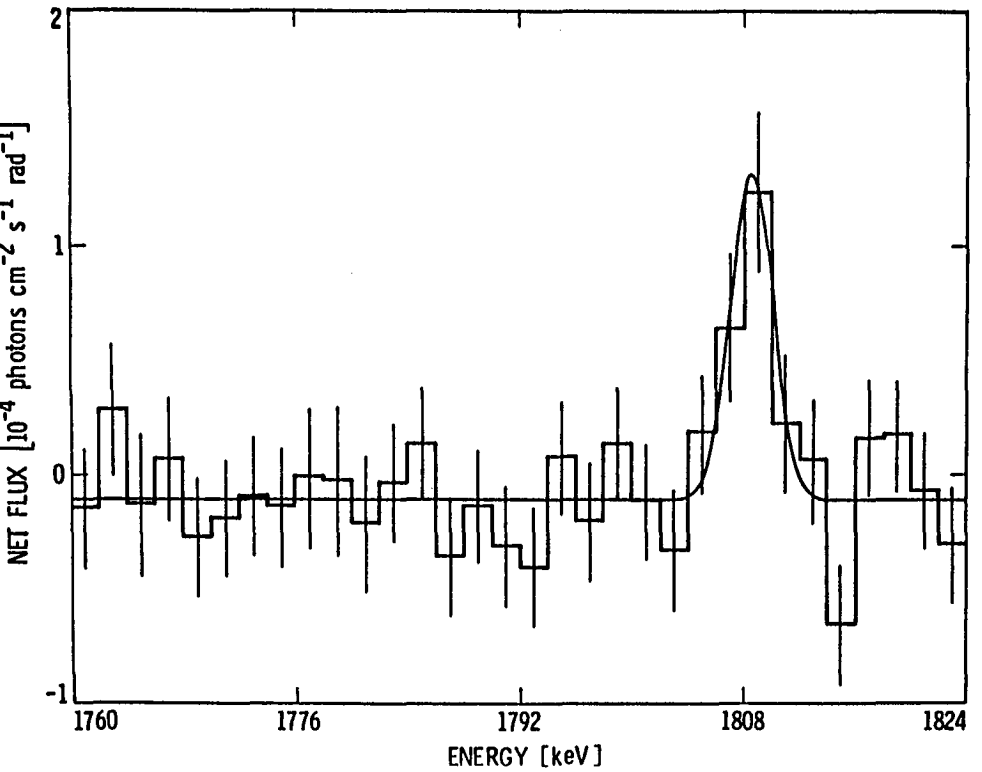

Fig. 8. Observed[100] gamma-ray spectrum near 1.809 MeV from the galactic plane in the direction of the Galactic Center.

decay. Diffuse galactic line emission is thus expected at 1.809 MeV from ^{26}Al decay to ^{26}Mg (Refs. 101,102) and at 1.332 MeV, 1.173 MeV, and 0.059 MeV from ^{60}Fe decay to ^{60}Co and its subsequent decay to ^{60}Ni (Ref. 113).

Diffuse galactic line emission at 1.809 MeV from ^{26}Al has now been measured[7,100] and confirmed[114]. The measured line, shown in Figure 8, has a width (FWHM) $\leqslant 3.0$ keV which is quite consistent with that expected solely from galactic rotation. The intensity varies with galactic longitude from $(4.8\pm 1.0)\times10^{-4}$ photons/cm^2 sec rad in the direction of the galactic center[100] to less than 40% of that in the direction of the anti-center[114]. This intensity is roughly an order of magnitude greater than that predicted[101,102] from supernova production.

The observed flux corresponds to a total mass of about $3M_\odot$ of ^{26}Al in the interstellar medium. Assuming steady state, this implies a present galactic production of $\sim 3\times10^{-6}M_\odot$/yr of ^{26}Al. By comparison the estimated present production rate of ^{27}Al is of the order of $10^{-4}M_\odot$/yr which thus requires that the production ratio of ^{26}Al/^{27}Al in the ^{26}Al source must be $>3\times10^{-2}$. Otherwise too much ^{27}Al would be produced. The calculated[115] yields of Type II supernovae, however, give a ^{26}Al/^{27}Al ratio of only (1 to 2)$\times10^{-3}$ which, like the predicted intensity, is an order of magnitude too low.

There are however other possible sources of ^{26}Al: Novae[116,117], red giants[118] and 0 and Wolf-Rayet stars[119]. For novae the calculated[116,117] production ratio of ^{26}Al/^{27}Al is of the order of unity which is more than sufficient. Moreover estimates[7,100,120] of the current galactic rate of ^{26}Al production by novae come quite close to the required rate inferred from the observations. Calculations of the ^{26}Al/^{27}Al ratio from pulsating red giants[118] is also of the order of unity and that in the winds of 0 and Wolf-Rayet stars is about 4×10^{-2} which would be just sufficient. But

the estimated total galactic production rate from these sources appears to be less than that of novae. Thus it seems at the present that the bulk of the ^{26}Al in the interstellar medium is most likely produced by novae while the bulk of the ^{27}Al may come from Type II supernovae with only about 10% of it coming from novae. The recent discovery[121] of a new low lying resonance for ^{26}Al production in the ^{25}Mg (p, γ) reaction suggest, however, that new theoretical calculations of the yields for the various sources are needed.

SS433

Intense, time-variable and very narrow gamma-ray line emission has recently been observed[8,122] from SS433 with the high resolution Ge spectrometer flown on HEAO-3. This instrument is particularly sensitive to very narrow lines (widths less than a few keV). The line with the strongest intensity and highest statistical significance was seen[8] at 1.497 MeV (see Figure 9). In addition, spectral features at $\sim$1.2 MeV[8] and $\sim$6.695 MeV[122] were also reported. All of these lines have very narrow widths (FWHM $<$ 10 keV). Searches for these very narrow lines were carried out also with a Ge spectrometer flown on a balloon[123] and the NaI spectrometer on SMM[124] whose energy resolution is much lower than that of the Ge spectrometers. Although no lines were detected in either of these searches, this negative result could be due to the time variability of the SS433 gamma-ray source.

Two different identifications of the 1.497 MeV line have been proposed, both of which assume that this line is blueshifted emission from the approaching jet. The first suggestion[8] identifies the line with the 1.369 MeV line from ^{24}Mg* excited by inelastic collisions, while the other[125] associates it with a line at 1.380 MeV from the fusion reaction ^{14}N(p,γ)^{15}O* in a very narrow resonance at a proton energy of 0.278 keV. The optically determined[126] Doppler shifts of the approaching jet of SS433 at the epoch of the gamma-ray observations are consistent with both of these identifications, as is the possible association of the 1.2 MeV feature with the redshifted counterpart of the 1.497 MeV line from the receding jet. Moreover, the inelastic excitations and fusion models, based on these identifications, each predict another line at either 6.129 MeV from ^{16}O* deexcitations[127] or 6.175 MeV from ^{15}O* deexcitations[125]. The observed feature at $\sim$6.695 MeV could be identified with either of these lines. The two models also predict other lines which have not yet been observed.

If the observed 1.497 MeV line is due to ^{24}Mg deexcitations, then the fact that the gamma-ray and optical Doppler shifts are similar implies that the Mg nuclei are moving essentially at the flow speed (0.26c) of the jets. This corresponds to a kinetic energy of $\sim$33 MeV/nucleon. At this energy, the 1.369 MeV line can be produced in nuclear reactions with either ambient protons or moving protons, provided that the proton velocity in the Mg rest frame exceeds $\sim$0.07c, corresponding to the effective threshold energy ($\sim$2 MeV) for exciting the 1.369 MeV level. But unless the relative proton velocity is less than $\sim$0.09c, corresponding to a rest frame energy less than $\sim$4 MeV, the recoil of the excited Mg nuclei in a gas would broaden the line to a width which is larger than that observed[8]. Therefore, for inelastic excitations in a gas[128], the velocity differential between the protons and the Mg nuclei must lie in a very narrow range, so that the protons have sufficient energy to excite the line, but not too much energy to broaden it excessively. Moreover, if the 6.695 MeV line is confirmed with a very narrow width, excitations in a gas can be ruled out because at proton velocities $<$0.09c required by the line width ^{16}O cannot be excited.

These constraints, however, can be eliminated[127] by a line-narrowing effect[129,130] involving deexcitations of nuclei embedded in dust grains. The grains also offer a simple explanation[127] to the fact that the strongest very narrow line is at 1.369 MeV from ^{24}Mg. For local galactic abundances and deexcitations in a gas, the strongest lines are generally at other energies, depending on the proton energy in the Mg rest frame. Since at $\sim$4 MeV the strongest line is at 1.634 MeV from ^{20}Ne deexcitations, a very strong depletion of Ne relative to Mg is required if the 1.497 MeV line is due to Mg deexcitations in a gas. In grains, on the other hand, Ne and other volatiles are naturally depleted.

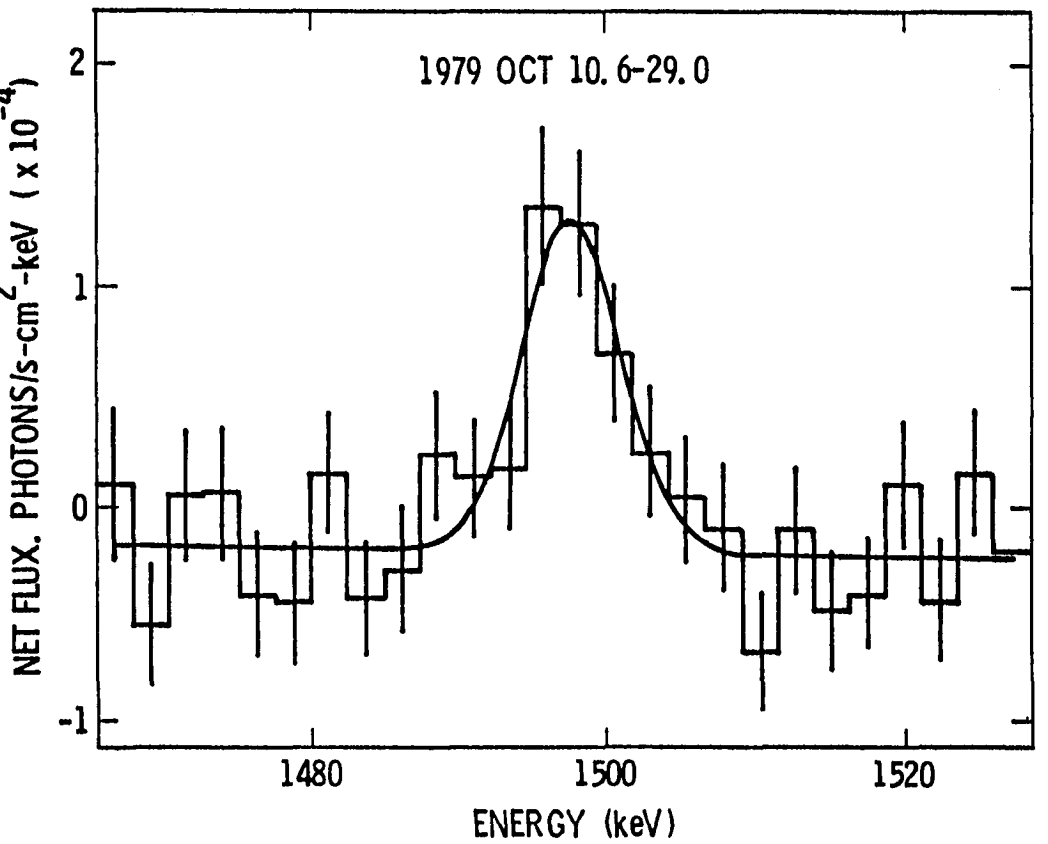

Fig. 9. Observed[8] gamma-ray spectrum within ± 30 keV of the 1.5 MeV line from the direction of SS433.

Very narrow gamma-ray lines can be produced from the deexcitation of nuclei embedded in dust grains if the sizes of the grains are large enough ($\geq 10^{-4}$ cm) and the lifetimes of the nuclear levels are long enough ($\geq 10^{-12}$ sec). If these two conditions are met, an excited nucleus produced in a grain loses its recoil energy by Coulomb collisions and stops in the grain before it deexcites. Thus, the line is not broadened by the recoil following deexcitation. A variety of very narrow grain lines are expected[129,130] with relative intensities depending on the elemental abundances in the grains, as well on the details of the interaction model.

In the jet-grain interaction model[127] refractory grains were assumed in which the abundances of Mg, Si and Fe were the same as the local galactic abundances[34], while the more volatile elements were depleted, such that the C, N and O abundances were reduced relative to the local galactic abundances by a factor f and the H, He, Ne and S abundances were set to zero. It was also assumed that the grains, moving with the jet velocity, interact with a stationary ambient medium. This corresponds to a thin-target interaction model in which the bombarding proton energy in the grain rest frame has the fixed value of 33 MeV. Alternatively, the gamma-ray lines may be produced while the grains, moving at the speed of the jet flow, sweep up the ambient protons. This would occur if the bulk of the heavy elements were in the grains and the radiation pressure which accelerates the jets couples primarily to these elements and not to the hydrogen. This corresponds to thick-target interactions where the bombarding protons in the jet rest frame have initially 33 MeV, but produce the gamma rays as they slow down and eventually stop in this frame.

The relative intensities of very narrow lines for these abundances in the thin- and thick-target cases are shown in Table 3. The line at 4.438 MeV from ^{12}C is not shown because even in grains this line is broad owing to the very short (0.06 psec) lifetime of the 4.439 MeV level. Also shown are relative intensities for MgO, a very refractory compound with a very high melting temperature, a feature that is important for the survival of the grains[127].

Table 3
RELATIVE VERY NARROW LINE INTENSITIES FROM GRAINS

Photon Energy (MeV)	Excitation Process	(O:Mg:Si:Fe) (22f:1:1.1:1) Thin Target (Ref. 127)	(O:Mg:Si:Fe) (22f:1:1.1:1) Thick Target	(O:Mg:Si:Fe) (1:1:0:0) Thick Target
0.847	$^{56}Fe(p,p')^{56}Fe^*$	0.5	0.7	0.0
0.931	$^{56}Fe(p,pn)^{55}Fe^*$	0.6	0.4	0.0
1.317	$^{56}Fe(p,pn)^{55}Fe^*$	0.5	0.3	0.0
1.369	$^{24}Mg(p,p')^{24}Mg^*$ $^{28}Si(p,x)^{24}Mg^*$	1.0	1.0	1.0
1.634	$^{24}Mg(p,x)^{20}Ne^*$	0.5	0.3	0.3
1.779	$^{28}Si(p,p')^{28}Si^*$	0.4	0.6	0.0
6.129	$^{16}O(p,p')^{16}O^*$	4.0f	4.4f	0.2

As can be seen, in all cases the strongest very narrow line is at 1.369 MeV, provided that the depletion factor f is small enough. As already pointed out, the 6.129 MeV line can be associated with the reported feature at $\sim$6.7 MeV. The confirmation of this feature and the measurement of its relative intensity would determine the depletion factor. An upper limit on the 1.634 MeV line, reported[131] at this conference, appears to be in conflict with the thin-target ratio given in Table 3, but not with the thick-target ratios. The thin-target ratio for this line in Table 3 is lower than that suggested[132] previously, where the contribution of Si spallation to the 1.369 MeV line was ignored. There is as yet no data on the other lines shown in Table 3. As can be seen, such data would provide important information on the composition of the grains.

In the absence of grains, the 1.497 MeV line could still be identified[128] with the 1.369 MeV line from inelastically excited ^{24}Mg, provided that the excitations were due to protons with velocities relative to the ^{24}Mg nuclei less than 0.09c. At higher relative velocities, the line width would be larger than observed. But the composition of the gas in which these interactions take place must be quite different from the local galactic composition[34]. For such a composition, the intensity of the 1.634 MeV line produced by protons of a few MeV is larger by about an order of magnitude than that of the 1.369 MeV line in conflict with the fact that the upper limit on the ^{20}Ne line intensity is considerably lower than the observed intensity of the 1.369 MeV line.

In the fusion model[125] for gamma-ray production in SS433, the line at 1.380 MeV results from the deexcitation of the 7.556 MeV level of ^{15}O to the ground state via a state at 6.176 MeV. The 7.556 MeV level is populated by p-^{14}N reactions through a narrow resonance at a proton energy of 0.278 MeV[133,134]. The low energy and narrow width of this resonance lead to a very narrow width for the 1.380 MeV line, provided that the temperature of the ^{14}N nuclei in the jets is sufficiently low ($< 10^8$K). This implies that the protons and the ^{14}N nuclei must have different temperatures or that the particle distributions are nonthermal. This has profound implications on the energetics of the system, as discussed below. The deexcitation of the 7.556 MeV level produces additional lines at 6.176, 0.764, 6.793, 2.374 and 5.183 MeV with intensities relative to that the 1.380 MeV line of 1, 0.40, 0.40, 0.28 and 0.28, respectively. Although as mentioned above, the 6.176 MeV line could be identified with the 6.695 MeV line, the fact that this line is observed[122] to be much weaker than the 1.497 MeV line, argues strongly against the fusion model. Searches for the other predicted lines have not yet been carried out.

Gamma-ray line production by inelastic excitations is accompanied by energy loss to Coulomb collisions. If the gamma-ray lines were due to fusion, the line production would also be accompanied by Coulomb losses, because of the nonthermal nature of the particle distributions implied by the observed line widths. But the rate of Coulomb energy loss for a given rate of gamma-ray line production is much larger for fusion than for inelastic excitation because the line production cross section for fusion in the resonance ($\sim$0.1 mb) is much smaller than that for inelastic excitation ($\sim$200 mb). The observed gamma-ray line luminosity of SS433 of $\sim 10^{37}$ erg/sec implies a Coulomb energy loss $> 10^{47}$ erg/sec for the fusion model. The Coulomb energy loss in the inelastic excitation models can be as low as $\sim 4 \times 10^{40}$ erg/sec, in the thick-target jet-grain model. Since even this value is highly super-Eddingtonian for a stellar size object, the bulk of the Coulomb energy loss should go into mass motion in the jets. This Coulomb energy loss will also heat the grains, but the estimated temperature, $<$3000K, is below the melting point of MgO. The survival of grains in the environment of the jets of SS433 has not yet been studied in detail. However, it has been suggested[135] that the presence of clumps of dense matter (e.g. grains) may be a prerequisite for the acceleration of the jets by line locking. Crucial tests of the proposed models for gamma-ray line production in SS433 will come from the confirmation of the already reported lines and from further observations of the relative intensities and widths of the predicted lines.

SUMMARY

We have highlighted some of the important recent advances in gamma-ray line astrophysics. The solar flare observations, including a remarkably detailed gamma-ray line spectrum, provide insights into problems of particle acceleration and confinement and allow the determination of elemental abundances by a powerful new technique. Recent gamma-ray bursts studies have provided much new insight into the nature of their sources, with magnetized neutron stars emerging as the best candidates. Continuing observations of the Galactic Center provided only upper limits on the 0.511 MeV line flux, but a variety of theoretical and laboratory studies have elaborated considerably the physical processes that govern the production of pairs and the annihilation of the positrons. The gamma-ray line from recently synthesized ^{26}Al has been observed and confirmed by independent observations, providing evidence for ongoing nucleosynthesis in the galaxy, and requiring some modification of current ideas. Gamma-ray lines have been observed from the compact galactic object SS433, which have very exciting theoretical implications. Further progress in these and other areas is expected from future observations with the Gamma Ray Observatory, to be launched in 1988.

ACKNOWLEDGMENTS

We wish to acknowledge very valuable discussions with Benzion Kozlovsky and financial support from the NASA Solar Terrestrial Theory program, NASA Grant NSG-7541 and NSF Grant ATM 84-18194.

REFERENCES

1. Hess, V.F., (1912), *Physik. Z. 13*, 1084.

2. Clay, J., (1927), *Proc. Acad. Sci. Amsterdam 30*, 1115.

3. Peterson, L.E., and Winckler, J.R., (1959), *J. Geophys. Res. 64*, 697.

4. Arnold, J.R., Metzger, A.E., Anderson, E.C., and Van Dilla, M.A., (1962), *J. Geophys. Res. 67*, 4876.

5. Ramaty, R., and Lingenfelter, R.E., (1982), *Ann. Rev. Nucl. Part. Sci. 32*, 235.

6. Forrest, D.J., (1983), in *Positron Electron Pairs in Astrophys.*, M.L. Burns et al., Eds., Am. Inst. Phys., N.Y. p. 3.

7. Mahoney, W.A., Ling, J.C., Jacobson, A.S., and Lingenfelter, R.E., (1982), *Astrophys. J. 262*, 742.

8. Lamb, R.C., Ling, J.C., Mahoney, W.A., Riegler, G.R., Wheaton, W.A., and Jacobson, A.S., (1983), *Nature 305*, 37.

9. Ramaty, R., Murphy, R.J., Kozlovsky, B., and Lingenfelter, R.E., (1983), *Solar Phys. 86*, 395.

10. Chupp, E.L., (1984), *Ann. Rev. Astron. Astrophys. 22*, 359.

11. Murphy, R.J., and Ramaty, R., (1985), *Advances Space Res. (COSPAR) 4*, No. 7, 127.

12. Murphy, R.J., Ramaty, R., Forrest, D.J., and Kozlovsky, B., (1985), *19th Internat. Cosmic Ray Conf. Papers 4*, 249.

13. Lingenfelter, R.E., and Ramaty, R., (1967), in *High-Energy Nuclear Reactions in Astrophysics*, Ed. B.S.P. Shen, Benjamin, N.Y. p. 99.

14. Chupp, E.L., Forrest, D.J., Higbie, P.R., Suri, A.N., Tsai, C., and Dunphy, P.P., (1973), *Nature 241*, 333.

15. Hudson, H.S. et al., (1980), *Astrophys. J. 236*, L91.

16. Prince, T., Ling, J.C., Mahoney, W.A., Riegler, G.R., and Jacobson, A.S., (1982), *Astrophys. J. 255*, L81.

17. Yoshimori, M. et al., (1985), *J. Phys. Soc. Japan 54*, 487.

18. Chupp, E.L. et al., (1981), *Astrophys. J. 244*, L171.

19. Lingenfelter, R.E., Flamm, E.J., Canfield, E.H., and Kellman, S., (1965), *J. Geophys. Res. 70*, 4077 and 4087.

20. Chupp, E.L. et al., (1982), *Astrophys. J. 263*, L95.

21. Chupp, E.L. et al., (1983), *18th Internat. Cosmic Ray Conf. Papers 10*, 334.

22. Debrunner, H., Fluckiger, E., Chupp, E.L., and Forrest, D.J., (1983), *18th Internat. Cosmic Ray Conf. Papers 4*, 75.

23. Efimov, Yu.E., and Kocharov, G.E., (1983), *18th Internat. Cosmic Ray Conf. Papers 10*, 276.

24. Evenson, P., Meyer, P., and Pyle, K.R., (1983), *Astrophys. J. 274*, 875.

25. Ramaty, R., Kozlovsky, B., and Lingenfelter, R.E., (1982), in *Gamma Ray Transients and Related Astrophysical Phenomena*, R.E. Lingenfelter et al., Eds., Am. Inst. Phys., N.Y. p. 231.

26. McGuire, R.E., and von Rosenvinge, T.T., (1985), *Advances in Space Res. (COSPAR) 4*, No. 7, 127.

27. Ramaty, R., Kozlovsky, B., and Suri, A.N., (1977), *Astrophys. J. 214*, 617.

28. Ibragimov, I.A., and Kocharov, G.E., (1977), *Son. Astron. Lett. 3*, 221.

29. Ellison, D.C., and Ramaty, R., (1985), *Astrophys. J.* (in press).

30. Ramaty, R., (1979), in *Particle Acceleration in Astrophysics*, J. Arons et al., Eds., Am. Inst. Phys., N.Y. p. 135.

31. Share, G.H., Chupp, E.L., Forrest, D.J., and Rieger, E., (1983), in *Positron-Electron Pairs in Astrophysics*, M.L. Burns et al., Eds., Am. Inst. Phys., N.Y. p. 15.

32. Cliver, E.W., Forrest, D.J., McGuire, R.E., and von Rosenvinge, T.T., (1983), *18th Internat. Cosmic Ray Conf. Papers 10*, 342.

33. Murphy, R.J., Forrest, D.J., Ramaty, R., and Kozlovsky, B., (1985), *19th Internat. Cosmic Ray Conf. Papers 4*, 253.

34. Meyer, J.P., (1985), *Astrophys. J. (Supp.) 57*, 173.

35. Klebesadel, R.W., Strong, I.B., and Olson, R.A., (1973), *Astrophys. J. 182*, L85.

36. Lingenfelter, R.E., Hudson, H.S., and Worrall, D.M., Eds., (1982), *Gamma-Ray Transients and Related Astrophysical Phenomena*, Am. Inst. Phys., N.Y. 500 pp.

37. Woosley, S.E., Ed., (1984), *High Energy Transients in Astrophysics*, Am. Inst. Phys., N.Y. 714 pp.

38. Mazets, E.P., et al., (1981) *Astrophys. Space Sci. 80*, 1.

39. Meegan, C.A., G.J. Fishman and R.B. Wilson, (1984), in *High Energy Transients in Astrophysics*, S.E. Woosley, Ed., Am. Inst. Phys., N.Y. p. 422.

40. Higdon, J.C. and R.E. Lingenfelter, (1984), in *High Energy Transients in Astrophysics*, S.E. Woosley, Ed., Am. Inst. Phys., N.Y. p. 568.

41. Higdon, J.C. and R.E. Lingenfelter, (1985), *19th Internatl. Cosmic Ray Conf. Papers, 1*, 37.

42. Cline, T.L., (1981), *Ann. N.Y. Acad. Sci. 375*, 314.

43. Evans, W.D., et al., (1980) *Astrophys. J. 237*, L7.

44. Cline, T.L., (1980), *Comments Astrophys. 9*, 13.

45. Cline, T.L., (1982), in *Gamma Ray Transients and Related Astrophysical Phenomena*, R.E. Lingenfelter et al., Eds., Am. Inst. Phys., N.Y. p. 17.

46. Golenetskii, S.V., V.N. Ilyinskii and E.P. Mazets, (1984), *Nature 307*, 41.

47. Rothschild, R.E., and R.E. Lingenfelter, (1984), *Nature 312*, 737.

48. Klebesadel, R.W., E.E. Fenimore, J.G. Laros and J. Terrell, (1982), in *Gamma-Ray Transients and Related Astrophysical Phenomena*, R.E. Lingenfelter et al., Eds., Am. Inst. Phys., N.Y. p. 1.

49. Hjellming, R.M., Ewald, S.P., (1981), *Astrophys. J. 246*, L137.

50. Schaefer, B.E., (1981), *Nature 294*, 722.

51. Schaefer, B.E., et al., (1984), *Astrophys. J. 286*, L1.

52. Pedersen, H., et al., (1984), *Nature 312*, 46.

53. Mazets, E.P., Golenetskii, S.V., Aptekar, R.L., Guryan, Yu. A., Ilyinskii, V.N., (1981), *Nature 290*, 378.

54. Hueter, G.J., (1984), in *High Energy Transients in Astrophysics*, S.E. Woosley, Ed., Am. Inst. Phys., N.Y. p. 373.

55. Liang, E.P., (1982), *Nature 299*, 321.

56. Nolan, P.L., et al., (1984), in *High Energy Transients in Astrophysics*, S.E. Woosley, Ed., Am. Inst. Phys., N.Y. p. 399.

57. Hueter, G.J. and R.E. Lingenfelter, (1983), in *Positron-Electron Pairs in Astrophysics*, M.L. Burns et al., Eds., Am. Inst. Phys., N.Y. p. 89.

58. Lingenfelter, R.E., and G.J. Hueter, (1984), in *High Energy Transients in Astrophysics*, S.E. Woosley, Ed., Am. Inst. Phys., N.Y. p. 558.

59. Cavallo, G., and M.J. Rees, (1978), *Mon. Not. R.A.S., 183*, 359.

60. Ramaty, R., McKinley, J.M., and Jones, F.C., (1982), *Astrophys. J. 256*, 238.

61. Mazets, E.P., Golenetskii, S.V., Ilyinskii, V.N., Aptekar, R.L., and Guryan, Yu.A., (1979), *Nature 282*, 587.

62. Mazets, E.P., Golenetskii, S.V., Guryan, Yu.A., and Ilyinskii, V.N., (1982), *Astrophys. Space Sci. 84*, 173.

63. Ramaty, R. et al., (1980), *Nature 287*, 122.

64. Ramaty, R., Lingenfelter, R.E., and Bussard, R.W., (1981), *Astrophys. Space Sci. 75*, 193.

65. Harwit, M., and Salpeter, E.E., (1973), *Astrophys. J. 187*, L97.

66. Colgate, S.A., and Petchek, A.G., (1981), *Astrophys. J. 248*, 771.

67. Lamb, F.K., (1984), in *High Energy Transients in Astrophysics*, S.E. Woosley, Ed., Am. Inst. Phys., N.Y. p. 179.

68. Tsygan, A.I., (1975), *Astron. Astrophys. 44*, 21 and *49*, 159.

69. Ellison, D.C., and Kazanas, D., (1983), *Astron. Astrophys. 128*, 102.

70. Haensel, P. and Schaeffer, R., (1982), *Nuclear Phys. A381*, 519.

71. Haensel, P. and Proszynski, M., (1982), *Astrophys. J. 258*, 306.

72. Wang, Q.D. and Lu, T., (1984), *Phys. Lett. 148B*, 211.

73. Woosley, S.E. and Taam, R.E., (1976), *Nature 263*, 101.

74. Woosley, S.E., (1982), in *Gamma Ray Transients and Related Astrophysical Phenomena*, R.E. Lingenfelter et al., Eds., Am. Inst. Phys., N.Y. p. 273.

75. Johnson, W.N., Harnden, F.R., and Haymes, R.C., (1972), *Astrophys. J. 172*, L1.

76. Johnson, W.N., and Haymes, R.C., (1973), *Astrophys. J. 184*, 103.

77. Haymes, R.C. et al., (1975), *Astrophys. J. 201*, 593.

78. Leventhal, M., MacCallum, C.J., and Stang, P.D., (1978), *Astrophys. J. 225*, L11.

79. Riegler, G.R. et al., (1981), *Astrophys. J. 248*, L13.

80. Riegler, G.R. et al., (1983), in *Positron Electron Pairs in Astrophysics*, M.L. Burns et al., Eds., Am. Inst. Phys., N.Y. p. 230.

81. Leventhal, M., MacCallum, C.J., Huters, A.F., and Stang, P.D., (1982), *Astrophys. J. 260*, L1.

82. Paciesas, W.S., et al., (1982), *Astrophys. J. 260*, L7.

83. Leventhal, M., and MacCallum, C.J., (1985), *19th Internat. Cosmic Ray Conf. Papers 1*, 213.

84. Bussard, R.W., Ramaty, R., and Drachmann, R.J., (1979), *Astrophys. J. 228*, 928.

85. Lacy, J.H., Townes, C.H., Geballe, T.R., and Hollenbach, D.J., (1980), *Astrophys. J. 241*, 132.

86. Kellermann, K.I., Shaffer, D.B., Clark, B.G., and Geldzahler, B.J., (1977), *Astrophys. J. 214*, L61.

87. Brown, B.L., (1985), *Astrophys. J. 292*, L67.

88. Brown, B.L., Leventhal, M., Mills, A.P., Jr., and Gidley, D.W., (1984), *Phys. Rev. Letters 53*, 2347.

89. Lingenfelter, R.E., and Ramaty, R., (1982), in *Galactic Center*, G. Riegler and R. Blandford, Eds., Am. Inst. Phys., N.Y. p. 148.

90. Sturrock, P.A., and Baker, K.B., (1979), *Astrophys. J. 234*, 612.

91. Ramaty, R., and Lingenfelter, R.E., (1979), *Nature 278*, 127.

92. Okeke, P.N., and Rees, M.J., (1980), *Astron. Astrophys. 81*, 263.

93. Ramaty, R., and Lingenfelter, R.E., (1981), *Philos. Trans. R. Soc., London, Ser. A., 301*, 671.

94. Riegler, G.R., Ling, J.C., Mahoney, W.A., Wheaton, W.A., and Jacobson, A.S., (1985), *Astrophys. J. 294*, L13.

95. McKinley, J.M., (1986), in *Proc. 3rd International Workshop on Positron-Gas Scattering*, Wayne State University, Michigan, in press.

96. Blandford, R.D., (1982), in *Galactic Center*, G. Riegler and R. Blandford, Eds., Am. Inst. Phys., N.Y. p. 177.

97. Lingenfelter, R.E., and Ramaty, R., (1983), in *Positron Electron Pairs in Astrophysics*, M.L. Burns et al., Eds., Am. Inst. Phys., N.Y. p. 267.

98. Kardashev, N.S., Novikov, I.D., Polnarev, A.G., and Stern, B.E., (1983), in *Positron Electron Pairs in Astrophysics*, M.L. Burns et al., Eds., Am. Inst. Phys., N.Y. p. 253.

99. Burns, M.L., (1983), in *Positron Electron Pairs in Astrophysics*, M.L. Burns et al., Eds., Am. Inst. Phys., N.Y. p. 281.

100. Mahoney, W.A., Ling, J.C., Wheaton, W.A. and Jacobson, A.S., (1984), *Astrophys. J. 286*, 578.

101. Ramaty, R., and Lingenfelter, R.E., (1977), *Astrophys. J. 213*, L5.

102. Arnett, W.D., (1977), *Ann. N.Y. Acad. Sci. 302*, 90.

103. Clayton, D.D., Colgate, S.A., and Fishman, G.J., (1969), *Astrophys. J. 155*, 75.

104. Woosley, S.E., Axelrod, T.S., and Weaver, T.A., (1981), *Comments Nucl. Part. Phys. 9*, 185.

105. Colgate, S.A., and McKee, C., (1969), *Astrophys. J. 157*, 623.

106. Arnett, W.D., (1979), *Astrophys. J. 230*, L32.

107. Axelrod, T.S., (1980), Ph.D. Thesis Univ. of Calif., Santa Cruz.

108. Clayton, D.D., (1974), *Astrophys. J. 188*, 155.

109. Clayton, D.D., (1975), *Astrophys. J. 198*, 151.

110. Clayton, D.D., (1973), *Nature Phys. Sci. 244*, 137.

111. Albernhe, F., et al., (1981), *Astron. Astrophys. 94*, 214.

112. Dunphy, P.P., Chupp, E.L., and Forrest, D.L., (1983), in *Positron-Electron Pairs in Astrophysics*, M.L. Burns et al., Eds., Am. Inst. Phys., N.Y. p. 237.

113. Clayton, D.D., (1971), *Nature 234*, 291.

114. Share, G.H., Kinzer, R.L., Kurfess, J.D., Forrest, D.J., Chupp, E.L., and Rieger, E., (1985), *Astrophys. J. 292*, L61.

115. Woosley, S.E., and Weaver, T.A., (1980), *Astrophys. J. 238*, 1017.

116. Wallace, R.K. and Woosley, S.E., (1981), *Astrophys. J. Suppl. 45*, 389.

117. Hillebrandt, W. and Thielemann, F.K., (1982), *Astrophys. J. 255*, 617.

118. Norgaard, H., (1980), *Astrophys. J. 236*, 895.

119. Dearborn, D.S.P. and Blake, J.B., (1985), *Astrophys. J. 288*, L21.

120. Clayton, D.D., (1984), *Astrophys. J. 280*, 144.

121. Champagne, A.E., Howard, A.J., and Parker, P.D., (1983), *Astrophys. J., 269*, 686.

122. Wheaton, W.A., Ling, J.C., Mahoney, W.A., and Jacobson, A.S., (1984), *Bull. Amer. Astron. Soc. 16*, 472.

123. MacCallum, C.J., Huters, A.F., Stang, P.D., and Leventhal, M., (1985), *Astrophys. J. 291*, 486.

124. Geldzahler, B.J., Share, G.H., Kinzer, R.L., Forrest, D.J., Chupp, E.L., and Rieger, E., (1985), *19th Intern. Cosmic Ray Conf. Papers 1*, 187.

125. Boyd, R.N., Wiescher, M., Newson, G.H., and Collins, G.W., (1984), *Astrophys. J. 276*, L9.

126. Margon, B., (1984), *Ann. Rev. Astron. Astrophys. 22*, 507.

127. Ramaty, R., Kozlovsky, B., and Lingenfelter, R.E., (1984), *Astrophys. J. 283*, L13.

128. Helfer, H.L., and Savedoff, M.P., (1984), *Astrophys. J. 283*, L49.

129. Lingenfelter, R.E., and Ramaty, R., (1977), *Astrophys. J. 211*, L19.

130. Ramaty, R., Kozlovsky, B., and Lingenfelter, R.E., (1979), *Astrophys. J. Suppl. 40*, 487.

131. Wheaton, W.A., Ling, J.C., Mahoney, W.A., and Jacobson, A.S., (1985), *19th Intern. Cosmic Ray Conf. Papers 1*, 183.

132. Norman, E.B., and Bodansky, D., (1984), *Nature 308*, 212.

133. Ajzenberg-Selove, F., (1981), *Nucl. Phys. A360*, 143.

134. Fowler, W.A., Caughlan, G.R., and Zimmerman, B.A., (1967), *Ann. Rev. Astron., Astrophys. 5*, 525.

135. Pekarevich, M., Piran, T., and Shaham, J., (1984), *Astrophys. J. 283*, 295.

CONSTRAINTS ON GALAXY FORMATION THEORIES

Alexander S. Szalay

NASA/Fermilab Astrophyics Group
and
Eötvös University, Budapest

Abstract

The present theories of galaxy formation are reviewed. The relation between peculiar velocities, temperature fluctuations of the microwave background and the correlation function of galaxies point to the possibility that galaxies do not form uniformly everywhere. The velocity data provide strong constraints on the theories even in the case when light does not follow mass of the universe.

1. Initial Conditions

The universe contains a wide dynamic range of objects : from stars (1 $M_\odot$) all the way to superclusters (10^{16} $M_\odot$). A major question that we are unable to answer yet is whether the formation of structure has started with smaller masses clustering on ever larger scales[1], or whether extremely large structures formed first, then subsequently fragmented into smaller ones[2]. If we knew the precise initial conditions then the present structure of the universe could be derived by applying the laws of physics. Let us summarize, what has to be known about the initial conditions for this ambitious project.

The fluctuations are likely to be adiabatic, since the specific entropy of the universe, n_B/n_γ is tied to microscopic parameters of particle physics. Entropy fluctuations, once popular, can be generated by huge amounts of shear, e.g. In the inflationary theories quantum fluctuations arise in a natural way. However, the necessary amplitude seems to require rather special prescriptions for the effective potential[3].

The initial perturbations are expected to be scale free, therefore their Fourier amplitude depending on the wavenumber k can be well described by a power law, $|\delta_k|^2 \propto k^n$. If the spectral index is $n = 1$, the amplitude of the different perturbations is the same when their wavelength equals the horizon size. This 'double scale-invariant' is called the Zeldovich spectrum, and is known to arise in inflationary scenarios[4].

There are severe constraints on the fluctuation amplitudes. If the fluctuations were adiabatic, the perturbations of the metrics generate fluctuations in the temperature of the microwave background. On small angular scales (4.5 arc mins) these limits are extremely small[5]:$\Delta T/T < 2.9 \times 10^{-5}$. The H-He plasma becomes gravitationally unstable only after recombination, at $Z \sim 1000$. At this point the density and temperature fluctuations are similar, 3 $\Delta T/T = \Delta\rho/\rho$. Since the standard growth of fluctuations in a flat universe is $(1+Z)^{-1}$, this does not leave enough margin for fluctuation growth, the fluctuations cannot reach the nonlinear stage our universe seems to be in today. Present calculations confirm[6] that if the universe is baryon dominated, only prohibitively high initial fluctuation amplitudes can result in the formation of galaxies. If the universe is dominated by some form of collisionless dark matter, the dark matter fluctuations are unaffected by pressure, therefore grow even before recombination. After recombination these curvature perturbations caused by the dark matter will accelerate fluctuation growth in the baryons, so the $\Delta T/T$ constraints are less stringent.

Though the initial spectrum is a power law, by the time it becomes nonlinear it will be considerably modified. When the universe is radiation-dominated, fluctuations within the horizon have a minimal increase[7], whereas the ones outside the horizon grow. This effect will bend the slope of the spectrum from n to $n-4$ for

wavenumbers higher than k_{eq}, corresponding to the size of the horizon when the matter and radiation energy densities were equal. The presence of the collisionless dark matter results in distortions of a different kind: the free motion of particles erases structures smaller than the free streaming scale[8,9,10,11]. The mass scale of this collisionless damping process can be expressed in terms of the mass and entropy of the particles the dark matter consists of. $M_x \approx 2.2\ m_p^3 m_x^{-2}$. In the case of neutrinos this mass takes the value of $M_{\nu m} = 3.2 \times 10^{15} m_{30}^{-2}\ M_\odot$, corresponding to the comoving length scale $\lambda_{\nu m} = 41\ m_{30}^{-1}$ Mpc. Depending on what the 'temperature' of the dark matter is, this damping scale can change from the above 41 Mpc to extremely small values. The neutrinos are *hot* particles, since their average momentum is close to that of the background radiation photons. Most other candidates for the dark matter like axions and photinos - yet undiscovered - would have decoupled much before the neutrinos, having a lower entropy or temperature, so they are called *cold.* They hardly move at all, their damping scale is negligible. Intermediate candidates, like a gravitino of 1 keV mass would be *warm.*

A major underlying assumption in calculating most consequences of a given fluctuation spectrum is that the phases of the individual Fourier components are random, ie. the perturbations are a random Gaussian process. One can envisage scenarios, where this will not be the case, like perturbations originating from strings[12]. For a given spectrum combined with the assumption of random phases one can calculate the distribution of mass fluctuations, density of local peaks, density profiles around local peaks, the distribution of peaks of a given size, etc.

The expansion of the universe is characterized by three quantities: $\Omega = \rho/\rho_{crit}$, the density parameter, H_0, the Hubble constant, Λ_0, the cosmological constant. If $\Lambda_0 = 0$ and $\Omega = 1$ the universe is flat, which appears to be necessary for inflation. Λ_0 is generally assumed to be negligable. Calculations of the primordial ^{4}He and

D+^{3}He abundance indicate[13], that the baryon density of the universe at the time of primordial nucleosynthesis lies in the range of $0.01 < \Omega_B < 0.1$. This suggests that if baryons dominate the mass density then the universe is open by a large margin.

Fluctuation growth also depends on the density of the universe. If $\Omega < 1$, the growth of perturbations effectively stops at the redshift $Z = \Omega^{-1}$. The detailed predictions of $\Delta T/T$ are just below the current limits if the dark matter consists of neutrinos with about 30 eV mass, and restrict Ω if the cold particles dominate the universe [6]: $\Omega \geq 0.2 \times h^{-4/3}$ where $H_0 = 100h$ km /s Mpc. In deriving this limit it was assumed that galaxies follow the mass distribution: the amplitude of the fluctuations today was normalized to J_3, the integral of the galaxy-galaxy correlation function $\xi_g(r)$.

2. Nonlinear structure

Here we would like discuss the expected structure of the universe if the dark matter is either hot, warm or cold. Once the first mass scale in a spectrum with a large damping cutoff (hot) reaches nonlinearity, particle trajectories cease expanding away from each other and converge, resulting in the temporary formation of caustics. The density becomes very high and a flat 'pancake' is formed[2]. At first they arise at isolated spots where the initial velocity perturbations had the largest gradient. Soon these regions grow, turning into huge surfaces which intersect, forming the walls of a cell-structure which is itself gravitationally unstable. The methods of catastrophe theory were applied[14] to analyze structure that develops in such potential motion. It was found that the two dimensional pancakes are only the lowest order singularities; other singular topological structures should also appear. String-like features are one example, and they can be seen in the N-body simulations.

When the intersection of trajectories takes place, gas pressure builds up, the velocity of the collapsing gas exceeds the sound speed and a shock wave is formed[2]. The gas is shock-heated up to keV temperatures and cools by emitting radiation over a broad spectrum. The UV and soft X-ray emission can photoionize the intergalactic medium, making galaxy formation in regions that have not yet formed pancakes more difficult, which would accentuate the contrast in galaxy density between the strings and pancakes vs. voids, even though the density contrast may be only 3-10.

If the dark matter is cold, then the mass autocorrelations are logarithmically divergent towards the smallest scales. These objects will collapse first, the scales determined by the baryon Jeans mass at around recombination. Collapse of larger scale systems follows subsequently. It is believed that the statistical properties on a given mass scale can be reasonably well understood by studying the Gaussian random fluctuations obtained by filtering out all the smaller scale contributions from the power spectrum. Recently as major effort has been undertaken[15], where galaxies were associated with peaks of a given height of the random fluctuation field and various properties like correlation functions, mean shapes, densities etc were calculated in a manner similar to previous work on pancakes[16]. If the dark matter is warm, it will still form pancakes, though of galactic size. There the cooling is much more efficient[17], those timescales will determine the fate of each object.

In either of the above scenarios it seems to be very hard to avoid strong initial explosions and rapidly cooling shocks, which compress the gas and provide seeds for the next generation of explosions, as suggested by Ostriker and Cowie [18]. The complicated nature of such calculations has yet prevented a very detailed discussion, but the importance of these processes is unquestionable.

3. Peculiar velocities

If we knew all the parameters listed above, it would be relatively easy to follow the evolution of the universe. Only gravitational forces act on collisonless dark matter so one can numerically solve the transport equations, even in the nonlinear regime. This has indeed been done, as we discuss here. Given the initial conditions, these numerical experiments can tell us the mass distribution in the universe. One can hope, that the structure obtained this way will resemble the real universe, ie. galaxies trace the mass distribution.

Starting from the above mentioned initial conditions extensive N-body simulations [19,20] were made. The free parameters of the calculations are Ω, H_0 and the initial amplitude of the fluctuations.For a given Ω one can use conservative limits for the age of the universe to obtain a value of H_0. If $\Omega = 1$, then $t_0 > 12$ Gy requires $H_0 < 54$ km/s Mpc. The initial amplitude can be defined in various ways. For simulations with hot dark matter the epoch of galaxy formation Z_{GF} was the redshift when 1 percent of all particles have gone through a 'caustic'. For cold dark matter, due to the growth of nonlinearity, $\xi(r)$ is rapidly increasing both in slope and amplitude, just like for hot dark matter. One can define *today* when the correlation function of the particles most resembles that of the galaxies, ie. a power law with a slope -1.8.

$$\xi(r) = (r/r_0)^{-1.8}$$

The simulations have encountered a major difficulty : the random velocity dispersion of galaxies is well known[21]:

$$< v_{12}^2 >^{1/2} \approx 300 - 400 \mathrm{km/s}.$$

Both in the neutrino and cold dark matter simulations, when the density correlations are just about right, velocity dispersions are in the 1200 km/s range, clearly too high.

$$< v_{12}^2 >^{1/2} \approx (1200 \text{ km/s})\ \Omega^{0.6} \xi_0$$

where ξ_0 is the value of the mass autocorrelations at 5 Mpc radius. Comparing this to the data, this suggest that $\Omega \ll 1$, forbidden by the $\Delta T/T$ constraints. Since a low Ω model is ruled out, the only remaining possibility is to have $\xi_0 = |\delta\rho/\rho|^2$ fairly small. Then we are in a sharp contradiction with the observed galaxy autocorrelation.

Here one should note, though, that all calculations so far have assumed, that the distribution of galaxies follows the mass distribution, ie. $\xi_g(r) = \xi_m(r)$. It is $\xi_m(r)$, which determines both the $\Delta T/T$ fluctuations and the peculiar velocities, and it is $\xi_g(r)$ that we can observe. Since $\xi_g(r)$ seems to be too large to be in agreement with either $\Delta T/T$ or $\langle v_{12}^2 \rangle$, and changing Ω does not resolve the problem, the next possible solution may be that the mass fluctuations are relatively small, whereas $\xi_g(r) \gg \xi_m(r)$. This means, that *galaxies do not form with uniform probability everywhere*, the formation rate is 'biased' towards some regions.

This can be quite natural, though, since galaxies consist mostly of baryonic gas capable of emitting and absorbing radiation. These dissipative processes, strongly density and temperature dependent, occur at a different rate at different places[17]. All these effects, combined with possible shock waves due to the finite pressure in the H-He gas, may have an important role in determining where galaxies form. As a result, the galaxies may not follow the light at all, so the mass autocorrelation should not be compared to the galaxy autocorrelation. Galaxy formation, as long as it is a random process, initiated by gravitational infall will be likely to start at the regions of highest densities. One can therefore associate the particles in these regions with galaxies. This 'biasing' of galaxy formation towards these high densities is a heuristic

procedure, but probably a fair approximation to what really happens. The physical explanation of what the threshold of the selection should be is much less clear, it can only be adjusted to the observed number density of galaxies. This 'biasing' process enhances the correlations, without invoking large peculiar velocities.

If we consider the large scale velocity fields, they provide strong upper limits to the 'biasing' factor[22]. The dispersion of the center-of-mass velocity of a sphere with radius R is given by

$$\langle V^2 \rangle = (\mathrm{H}_0 f)^2 \int_0^\infty dk |\delta_k|^2 W^2(kR)$$

where $f = \Omega^{0.6}$ and $W(kR)$ is the window function, the Fourier transform of the spherical distribution [23]. The window function effectively eliminates contributions from scales smaller than R, so $\langle V^2 \rangle$ is a genuine measure of the large scale fluctuations, which are believed to be still close to linear. During the last few years there were several attempts to determine the peculiar velocities of spheres of galaxies centered around us, although the errors are considerable[24]. The results are not yet conclusive, but potentially they are an important test of the fluctuation amplitude.

Another measure of the large scale structure of the universe is the cluster - cluster correlation function $\xi_{cc}(r)$. It has the same functional form as the galaxy autocorrelation, but the amplitude is considerably larger [25]:

$$\xi_{cc}(r) = (\frac{r}{36\mathrm{Mpc}})^{-1.8}$$

Furthermore, the amplitude is dependent upon the richness class. It has been shown recently, that this richness dependence can be nicely explained, if we assume that the universe has a scale invariant property over the volume of the Abell catalogue. For each cluster sample one can derive the mean distance between clusters ($D = n^{-1/3}$),

which would uniquely characterize the richness. If we measure the length in these units, the richness dependence disappears[26]:

$$\xi_{cc}(r) = 0.35(r/D)^{-1.8}$$

Originally Mandelbrot [27] has suggested such a 'fractal' structure for the universe. The physical meaning of this scale invariance is not absolutely clear. It is unlikely that it could be generated via nonlinear gravitational dynamics, since the corresponding velocities on 40 Mpc scales would be enormous. There are suggestions, that cosmic strings may have such an effect[28], but other explanations attribute the difference in the clustering amplitude to the fraction of galaxies associated with clusters [29].

Recent calculations indicate, that for certain kinds of fluctuation spectra the correlation function of 'biased' regions may be a power law over a wide dynamic range, and the slope of the power law would depend on the threshold set for galaxy formation [30], contrary to previous work, claiming that $\xi(r)$ would be amplified by a constant factor [31].

5. Conclusion

All the present theories of galaxy formation fail to explain the observed universe in its full complication. The recent observations of the microwave background fluctuations provide the strongest constraints on present theories. The details of galaxy correlation properties are a new challenge, indicating that galaxies are unlikely to be tracers of the mass distribution. The peculiar velocity field of galaxies and clusters may provide a way to probe the fluctuations even in this case.

I would like acknowledge useful discussions with Simon White, Dick Bond, Jim Bardeen and Lars Jensen.

7. References

1. Peebles,P.J.E. 1980, *The Large Scale Structure of the Universe*, Princeton University Press, Princeton.
2. Zeldovich,Ya.B. 1970, Astron.Astrophys., **5**, 84.
   Sunyaev,R.A. and Zeldovich,Ya.B. 1972, Astron.Astrophys., **20**, 189.
3. Guth,A. and Pi,S-Y. 1982, Phys.Rev.Lett., **49**, 1110.
   Steinhart,P. and Turner,M.S. 1984, Phys.Rev., **D29**, 2162.
4. Brandenberger,R. and Kahn,R. 1984, Phys.Rev., **D29**, 2172.
   Bardeen,J., Steinhart,P. and Turner,M.S. 1983, Phys.Rev., **D28**, 679.
5. Uson,J.M. and Wilkinson,D.T. 1984, Ap.J.Lett., **277**, 1.
6. Bond,J.R. and Efsthathiou,G.P. 1984, Ap.J.Lett;285;L45
   Vittorio,N. and Silk,J. 1984, Ap.J.Lett., **285**, L39.
7. Guyot,M. and Zeldovich,Ya.B. 1970, Astron.Astrophys., **9**, 227.
   Meszaros,P. 1974, Astron.Astrophys., **37**, 225.
8. Gershtein,S.S. and Zeldovich,Ya.B. 1966, JETP Lett., **4**, 174.
   Cowsik,R. and McClelland,J. 1972, Phys.Rev.Lett., **29**, 669.
   Marx,G. and Szalay,A.S. 1972, Proc Neutrino '72, **1**, 123.
   Szalay,A.S. and Marx,G. 1976, Astron.Astrophys., **49**, 437.
   Doroshkevich,A.G. and Khlopov,M.Yu. 1981, Sov.Astron., **25**, 521.
9. Bond,J.R. and Szalay,A.S. 1981, Proc. Neutrino 81, **1**, 59.
   Bond,J.R. and Szalay,A.S. 1983, Ap.J., **274**, 443.
   Bond,J.R., Szalay,A.S. and Turner,M.S. 1982, Phys.Rev.Lett., **48**, 1636.
10. Peebles,P.J.E. 1982, Ap.J., **258**, 415.
    Peebles,P.J.E. 1982, Ap.J.Lett., **263**, 1.
11. Pagels,H. and Primack,J. 1982, Phys.Rev.Lett., **48**, 223.
    Blumenthal,G.R., Pagels,H. and Primack,J. 1982, Nature, **299**, 37.
    Blumenthal,G.R., Faber,S.M., Primack,J.R. and Rees,M.J. 1984, Nature, **311**, 517.
12. A.Vilenkin 1984, Proc. Inner Space/Outer Space, Fermilab,in press.
13. Olive,K.A., Schramm,D.N., Steigman,G., Turner,M.S. and Yang,J. 1981, Ap.J. **246**, 557.
14. Arnold,V.I., Shandarin,S.F. and Zeldovich,Ya.B. 1982, Geophys. Astrophys. Fluid Dynamics, **20**, 111.
15. Bardeen,J.M., Bond,J.R., Kaiser,N. and Szalay,A.S. 1986, Ap.J. in press.
16. Doroshkevich,A.G. 1970, Astrofizika, **6**, 320.
    Doroshkevich,A.G., Shandarin,S.F. and Saar,E. 1978, M.N.R.A.S., **184**, 643.

17. Rees,M.J. and Ostriker,J. 1977, M.N.R.A.S., **179**, 541.
Silk,J. 1977, Ap.J., **211**, 638.
18. Ostriker,J.P. and Cowie,L.L. 1981, Ap.J.Lett., **243**, L127.
19. Davis,M., Efsthathiou,G.P., Frenk,C.S. and White,S.D.M. 1984, Ap.J. **288**, 836.
Frenk, C.S., White, S.D.M. and Davis, M. 1983, Ap.J., **271**, 417.
20. Centrella,J. and Melott,A. 1983, Nature, **305**, 196.
Klypin,A.A. and Shandarin,S.F. 1983, M.N.R.A.S., **204**, 891.
21. Davis,M. and Peebles,P.J.E. 1983, Ap.J., **267**, 465.
22. Vittorio,N. and Silk,J. 1985, Ap.J.Lett, **293**, L1.
23. Kaiser,N. 1983, Ap.J.Lett., **273**, L17.
24. Hart,L. and Davies,R.D. 1982, Nature, **297**, 191.
de Vaucouleurs,G. and Peters,W.L. 1984, Ap.J., **287**, 1.
25. Peebles,P.J.E. and Hauser,M.G. 1974, Ap.J.Suppl., **28**, 19.
Bahcall,N.A. and Soneira,R.M. 1982, Ap.J.Lett., **258**, L17.
Bahcall,N.A. and Burgett,W.S. 1985, submitted to Ap.J.
26. Szalay,A.S. and Schramm,D.N. 1985, Nature, **314**, 718.
27. Mandelbrot,B.B. 1977, *Fractals*, Freeman, San Francisco
28. Turok,N. and Albrecht,A. 1985, UCSB preprint.
29. Bahcall,N.A. 1985, submitted to Ap.J.
30. Szalay,A.S. 1985, work in progress.
31. Kaiser,N. 1984, Ap.J., **284**, L9.

ELEMENTARY PARTICLE PHYSICS

Professor D.H. Perkins

Department of Nuclear Physics
University of Oxford, Keble Road,
Oxford
ENGLAND

I shall cover the following topics, from the experimentalists' viewpoint

1. Status of the Standard Model (of electroweak and strong interactions)
2. Phenomena beyond the Standard Model (Higgs, GUTS, SUSY etc.)
3. New Accelerator projects
4. Outstanding problems, and the possible contributions from non-accelerator experiments.

1. THE STANDARD MODEL

1.1 Electroweak Interactions I - Neutral Currents

In the Weinberg-Salam model, the electroweak interactions are specified by a single parameter, $\sin^2\theta_W$ (in addition to G, α etc). All experiments to date are consistent with the W-S model and a unique value $\sin^2\theta_W \sim 0.22$. Table 1 gives a list (incomplete) of experimental results. The studies of the purely leptonic processes of $\nu_\mu e$ and $\overline{\nu}_\mu e$ elastic scattering at CERN and Fermilab are now reaching the precision to provide strong constraints on the world average value of $\sin^2\theta_W$. The other important leptonic reaction is

Table 1 Values of $\sin^2\theta_W$

Process	Experiment	$\sin^2\theta_W$
$\nu_\mu e \to \nu_\mu e$	CERN	$0.22 \pm .03$
$\bar{\nu}_\mu e \to \bar{\nu}_\mu e$	FNAL	
$\nu N \to \nu X$	CERN	$0.22 \pm .01$
$\bar{\nu} N \to \bar{\nu} X$	FNAL	
$e^-_{L,R} + d \to e^- + X$	SLAC	$0.22 \pm .02$
$\mu^\pm_{L,R} + C \to \mu^\pm + X$	CERN	$0.23 \pm .02$
Parity violation in atomic transitions	Various	$0.21 \pm .05$
$1-M_W^2/M_Z^2$	$Sp\bar{p}S$	$0.23 \pm .03$

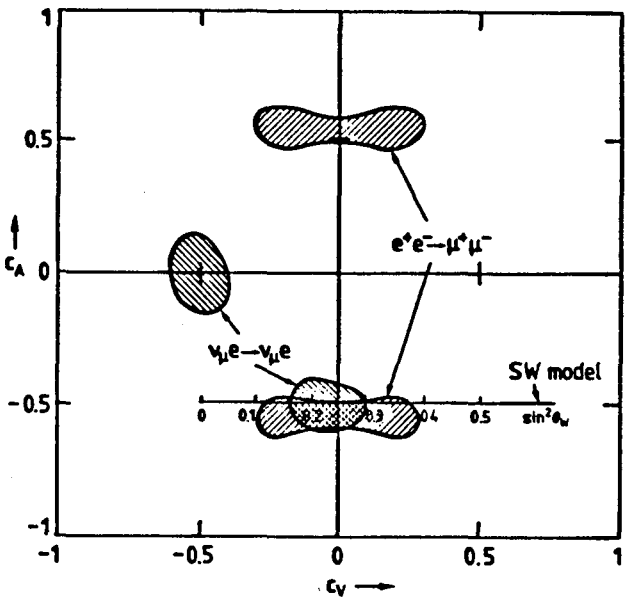

Fig.1 Values of C_A and C_V, the axial and vector coupling coefficients of the Z^o to charged leptons. The cross-sections for ν_μ and $\bar{\nu}_\mu$ scattering on electrons and the asymmetry in $e^+e^- \to \mu^+\mu^-$ each constrain solutions to two shaded areas. The common solution has $C_A \simeq -0.5$, $C_V \simeq 0$ (i.e. $\sin^2\theta_W \simeq 0.25$). (After Wu 1984)

$e^+e^- \to \mu^+\mu^-$, where Z^o as well as γ exchange gives a F/B asymmetry in the muon angular distribution. The asymmetry measures the axial vector coupling C_A of the charged leptons to the Z^o and confirms that $C_A = \frac{1}{2}$; the quantity $\sin^2\theta_w$ is not measured since the vector coupling of the charged leptons to the Z^o, $c_V = \frac{1}{2} - 2\sin^2\theta_w$ vanishes for $\sin^2\theta_w \approx 0.25$. The result of a recent survey is given in Fig.1.

The experiment on deep inelastic neutrino-nucleon scattering measure the following cross-section ratios, which are predicted to have the values

$$R_\nu = \frac{\sigma^{\nu N}(NC)}{\sigma^{\nu N}(CC)} = \tfrac{1}{2} - x + \frac{20}{27}x^2 \qquad (1a)$$

$$R_{\bar\nu} = \frac{\sigma^{\bar\nu N}(NC)}{\sigma^{\bar\nu N}(CC)} = \tfrac{1}{2} - x + \frac{20}{9}x^2 \qquad (1b)$$

where $x = \sin^2\theta_w$. Fig.2 shows a plot of R_ν versus $R_{\bar\nu}$ for recent experiments. The agreement of $R_{\bar\nu}$ with the Salam-Weinberg curve shows that the neutral/charged coupling factor $\rho = 1.00 \pm .02$ ($\rho = 1$ in the Salam-Weinberg model). The value of R_ν largely determines the value of $\sin^2\theta_w$ (≈ 0.23).

A third class of experiment deals with the deep-inelastic scattering of longitudinally polarised electrons or muons by nucleons. The SLAC experiment (Prescott et al 1979) measured the difference in cross-sections of LH and RH electrons on deuterons, resulting from the $\gamma - Z^o$ interference. The CERN experiment (Argento et al 1982) evaluated the scattering of both LH and RH μ^+ and μ^- on carbon.

Finally, atomic physics experiments measure the small parity-violation effect associated with Z^o exchange. For example, it results in a rotation of the plane of polarisation of plane-polarised light exciting energy levels in traversing bismuth vapour. The value of $\sin^2\theta_w$ in Table 1 is the average of several experiments (Fortson & Lewis 1984).

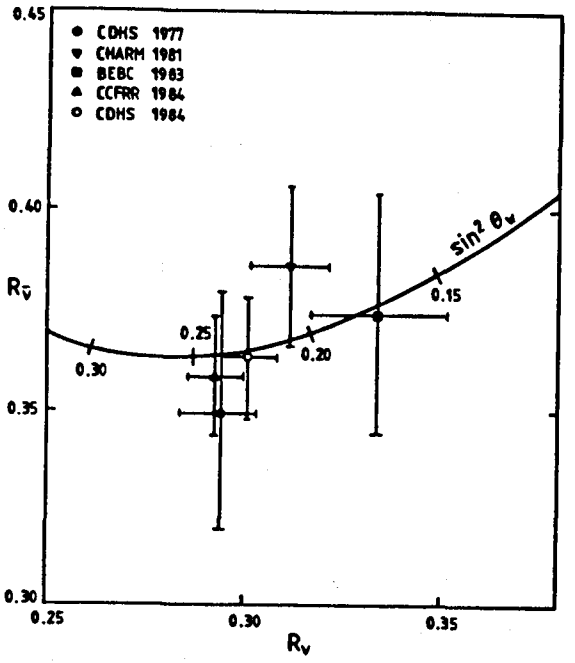

Fig.2 Values of ratio of neutral to charged current cross-sections of neutrinos and antineutrinos on nucleons. The data are consistent with the Weinberg-Salam model (full curve) with $\sin^2\theta_W \approx 0.23$.

1.2 Electroweak Interactions II - the W and Z bosons

CERN $p\bar{p}$ collider experiments have measured the W and Z masses, with recent results given in Table 2. Through the relations

$$M_W = (\pi\alpha/\sqrt{2}\ G)^{\frac{1}{2}} \frac{1}{\sin\theta_W} = \frac{37.28}{\sin\theta_W}\ \text{GeV}$$

$$M_Z = M_W/\cos\theta_W \qquad (2)$$

it is possible to calculate $\sin^2\theta_W$ from the masses: the values are included in Table 1 for completeness.

We see from Table 1 that widely different experiments are consistent with a unique value of $\sin^2\theta_W$. In fact the numbers shown need corrections if they are to be compared, since each experiment has cuts or kinematic selections, and the results should be "evolved" to the same value of q^2 (conventionally taken as $q^2 = M_W^2$). When these radiative corrections are taken into account the world average becomes

$$\sin^2\theta_W\ (M_W) = 0.215 \pm .015 \qquad (3)$$

The great triumph of the electroweak theory was of course the successful prediction of the W and Z particles, observed in UA1 and UA2 experiments (Arnison et al 1983, Bagnaia et al 1983, Banner et al 1983) at the CERN $p\bar{p}$ collider, via the reactions $p\bar{p} \to W + \ldots\ldots$, or in terms of quarks

$$u + \bar{d} \to W^+ \to e^+ + \nu_e \qquad (4)$$
$$\to \mu^+ + \nu_\mu$$

$$\begin{cases} u + \bar{u} \\ d + \bar{d} \end{cases} \to Z^o \to e^+e^-$$
$$\to \mu^+\mu^-$$

The cross-section for W or Z production in $p\bar{p}$ collisions leading to decay $W^\pm \to e^\pm + \nu_e$ can be calculated from the quark momentum distributions in the nucleon (measured in νN scattering), and the W mass, partial width $\Gamma(e\nu) = GM_W^3/6\pi\sqrt{2}$ and total width $\Gamma \simeq 12\ \Gamma(e\nu)$. For 310 GeV p on 310 GeV $\bar{p}$, one expects $\sigma(W^\pm \to e^\pm) \simeq 5$pb, that is about 10^{-8} of the total $p\bar{p}$ cross-section (60mb). The value of $\sigma(Z \to e\bar{e})$ is one order of magnitude smaller. The detection of such a rare signal is made possible because of the high p_T of the charged lepton(s) ——p_T up to $M_W/2 \sim 40$ GeV. Events are selected by requiring an isolated electron track of high p_T in the vertex detector pointing to the beam intersection region, and to a narrow electromagnetic shower without hadronic component.

Fig. 3(a) shows a plot of transverse momentum p_T^e of the single electron versus the missing transverse momentum in the whole event,

measured in the electron-beam plane. The fact that the two are roughly equal is clear evidence that an unseen particle (neutrino) was emitted to balance p_T^e, consistent with the decay $W \to e\nu$. Fig.3(b) shows the angular distributions of the decay electrons relative to the beam, evaluated in the W rest-frame. This has the $(1 + \cos\theta)^2$ distribution predicted from the V-A theory. As expected from helicity arguments (LH u quark and RH $\bar{d}$ quark in (4), leading to $J_Z = -1$ for W^+ if Z defines the proton beam direction), the e^+ from W^+ decay favours the same direction as the incident antiproton.

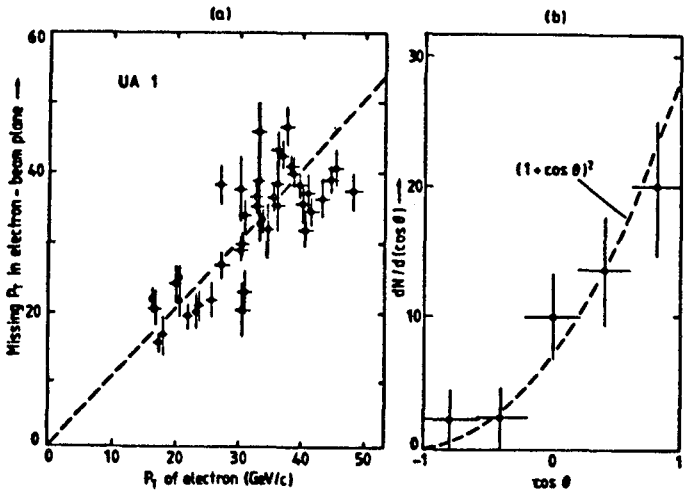

Fig.3 (a) Plot of missing p_T in electron-beam plane, against p_T of electron, in candidates for $W \to e + \nu$, from UA1 experiment.

(b) Angular distribution of electrons relative to beam axis in $W \to e + \nu$ events, (Arnison et al 1983)

The identification of $Z^o \to e^+e^-$ decays proceeds by demanding two isolated high p_T electrons of large invariant mass. The muonic decays in UA1 ($W \to \mu\nu$ or $Z \to \mu^+\mu^-$) are identified by the penetration of the muons through many interactions lengths of steel of the magnet yoke, as well as the usual requirements of isolation, matching with a muon track in the inner detector and high p_T.

A recent compilation of results is given in Table 2. The predicted masses are from the relations (2), but with upward radiative corrections to the masses of order 4% (equivalent to renormalization of α in (2)). There is good agreement between observed and predicted

Table 2 Recent data on W, Z events

	UA1	UA2	
$W \to e\nu$	172	122	Prediction (with radiative corrections)
$\to \mu\nu$	44	-	
$Z \to ee$	22	16	
$\to \mu\mu$	9	-	
M_W	$80.9 \pm 1.5 \pm 2.4$	$81.2 \pm 0.9 \pm 1.2$	83.0 ± 2.7 GeV
M_Z	$95.6 \pm 1.4 \pm 2.9$	$92.4 \pm 1.1 \pm 1.4$	93.8 ± 2.2 GeV

masses.

The width Γ of the Z^o boson, which depends on the number of neutrino generations, cannot be accurately measured at this time. However Γ_Z can be deduced by making some (fairly safe) assumptions. From the standard model one knows that

$$\Gamma_W(e\nu) = GM_W^3/6\pi\sqrt{2}$$
$$\Gamma_Z(\nu\bar{\nu}) = GM_W^3/12\pi\sqrt{2} \qquad (5)$$

Then the observed cross-section ratio

$$R = \frac{\sigma(Z^0 \to e\,\bar{e})}{\sigma(W \to e\nu)} = \frac{\sigma(Z^0 \to \text{all})}{\sigma(W \to \text{all})} \frac{\Gamma_Z(e\bar{e})}{\Gamma_Z} \frac{\Gamma_W}{\Gamma_W(e\nu)} = 0.116 \pm .027 \qquad (6)$$

The first term on the RHS, the (total cross-section ratio $\sigma(Z^0 \to \text{all})/\sigma(W \to \text{all})$ can be calculated from the quark distribution function in the nucleon (measured in lepton-nucleon scattering) and from QCD (to evolve these distributions to the appropriate value of q^2). Also, the ratio $\Gamma_W/\Gamma_W(e\nu) \simeq 12$, assuming 3 generations of quarks and leptons of mass $< M_W$. $\Gamma_Z(e\bar{e})$ is also known from the standard model. The above equation yields

$$\Gamma_Z = 2.54 \pm 0.61 \text{ GeV} \qquad (7)$$

compared with 2.75 ± .07 GeV expected for 3 lepton (and quark) generations. However, if there are further massive charged leptons of mass > $M_Z/2$ and corresponding neutrinos of small mass, the result would be an increase in Z^0 width through the decay $Z^0 \to \nu_L\,\bar{\nu}_L$ ($\Delta\Gamma$ = 180 MeV for each neutrino type). These considerations set a limit of $N_\nu < 7$ at 90% CL for the total number of lepton generations. This constraint will obviously be greatly improved at LEP or SLC.

1.3 Electroweak Interactions III - the Higgs particles

A very important component of the electroweak theory is the Higgs scalar boson and it has not yet been found. Recall that in the Weinberg-Salam model, the Higgs is postulated to account for spontaneous symmetry - breaking, through the generation of mass by self-interaction. The massless $W^\pm$ and Z^0 particles of the exact SU(2) and U(1) symmetry "eat" three of the four Higgs components (which appear as a doublet of complex fields), and so acquire mass. This leaves one massive neutral Higgs scalar as a physical particle.

The properties of the Higgs are ordained by the job it was invented to do. It cancels divergences in the process $e^+e^- \to W^+W^-$, requiring a coupling proportional to fermion mass; and in

$W^+W^- \to W^+W^-$, requiring a coupling proportional to boson mass, squared. These features determine the width of the Higgs and its decay branching ratios.

One method proposed to observe the Higgs (for $M_H < M_Z$) is via the decays

$$Z^o \to H\gamma \qquad (8)$$
$$\to H\mu^+\mu^-$$

resulting in a photon or lepton pair of unique energy. The branching ratio (on account of the small lepton masses) is small, varying from 10^{-5} for M_H = 20 GeV to 10^{-7} for M_H = 60 GeV. This might be detectable if, as expected, the annual Z^o production at LEP is 5.10^6 events. If $M_H < M_V$ where $V = t\bar{t}$ is the massive toponium state, then the decay

$$V \to H\gamma \qquad (9)$$

has a much larger (2-5%) branching ratio.

For $M_H > 0.2$ TeV, the decay $H \to W^+W^-$ will be dominant. On dimensional grounds, we expect the total width

$$\Gamma_H \propto GM_H^3 \qquad (10)$$

and an exact calculation shows $\Gamma_H \sim M_H$ for $M_H \sim 1.2$ TeV. This result implies that the Higgs (HWW) coupling is strong and the perturbation approach is wrong anyhow. One must then be entering a regime of fundamentally new physics: for example, the Higgs might be a composite rather than elementary particle, with new types of constituents and new types of coupling. If the Higgs <u>is</u> massive ($M_H > 2\,M_W$), detection is bound to be difficult, firstly because the resonance will be broad and secondly because non-resonant background processes $e^+e^- \to W^+W^- + X$ or $p\bar{p} \to W^+W^- + X$ will be important and of comparable cross-section to the signal process, $e^+e^-(p\bar{p}) \to H + X$, $H \to W^+W^-$.

1.4 Strong Interactions Between Quarks - QCD

The basis for our belief in the gauge theory (quantum chromodynamics - QCD) of the colour interactions between quarks via

gluon exchange rested, until recently, on analysis of deep inelastic lepton-nucleon scattering experiments and of the bound states of heavy quarkonium (ψ,T spectroscopy) and in the observation of multi-jet events in e^+e^- annihilation at high energy. During the last 2 years, strong and even more convincing support for QCD has been found from CERN $p\bar{p}$ collider experiment measuring directly the scattering of quarks and gluons at high momentum transfers.

The analysis is based on observation of events in which 2 jets of hadrons are produced at large angle to the colliding beams. Fig.4 shows an example of such an event in the UA1 detector (Arnison et al 1984) The 2 jets emerge at 180^o in the azimuth, as expected if they result from fragmentation of quark/gluon constituents of the incident beams after a two-body scattering. The polar angles are not equal and opposite, since in general the colliding constituents can carry different fractions of the momenta of the p and $\bar{p}$.

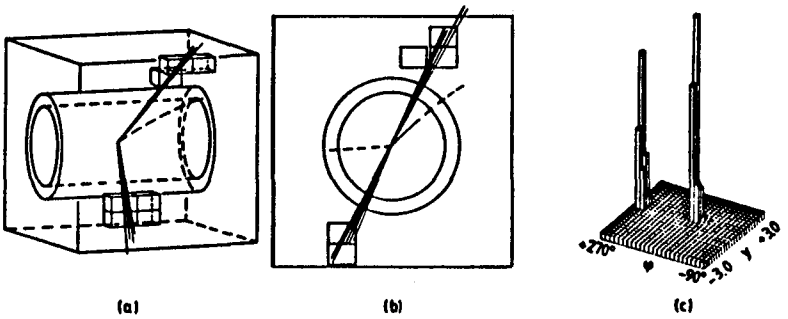

Fig.4 Example of 2-jet event in CERN SPS $p\bar{p}$ collider (a) reconstruction of event (b) projection in azimuthal plane normal to beam (c) energy deposition in calorimeter as a function of azimuth ϕ and rapidity y.

From the energies and angles, the events are first transformed into the CMS of the colliding constituents, and the scattering angle in this frame and q^2 are evaluated. When due account is taken of experimental cuts (on transverse energy, $E_T > 15$ GeV), the angular distribution is found to have the Rutherford form

$$\frac{d\sigma}{d\Omega} \sim \sin^{-4} \frac{\bar{\theta}}{2} \tag{11}$$

for small $\bar{\theta}$ - see Fig.5. Since it is impossible to know which jet originates from which beam particle, the smaller of the two possible scattering angles ($\bar{\theta}$ or $\pi - \bar{\theta}$) is taken. This fact, and the

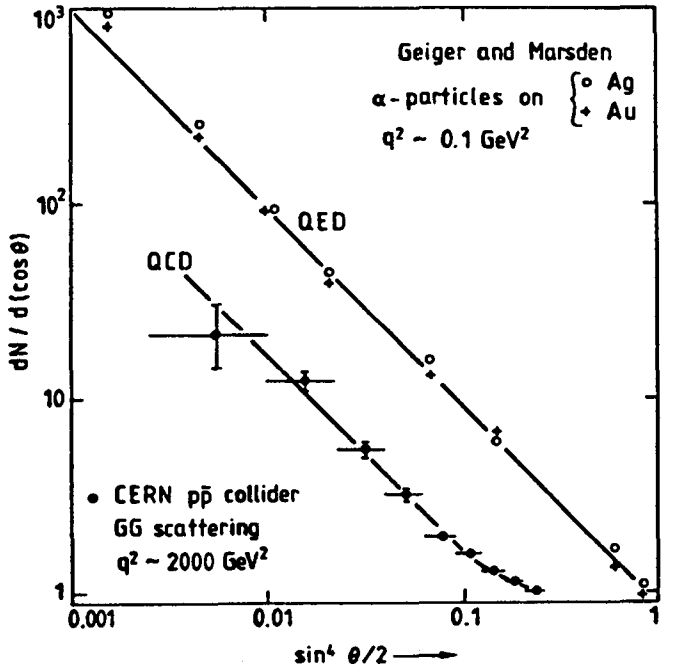

Fig.5 Differential cross-section for 2-jet events in terms of CMS scattering angle θ. Rutherford scattering predicts a $\sin^{-4}(\theta/2)$ dependence. The Geiger-Marsden results (1911) on α-particle scattering by gold and silver nuclei is shown for reference.

existence of spin terms leads to deviations from the Rutherford formula (for non-relativistic spinless scattering) near $\bar{\theta} = \pi/2$. The form of the angular distribution (11) is exactly that expected (for small $\bar{\theta}$) if the quark-quark, quark-gluon or gluon-gluon interaction is mediated by single massless vector boson (i.e. gluon) exchange.

The beam particles $(p,\bar{p})$ contain Q, $\bar{Q}$ and G constituents. There are colour coupling factors which are 9 for GG scattering, 16/9 for QQ or $Q\bar{Q}$ scattering and 4 for GQ or $G\bar{Q}$ scattering. Thus, GG scattering dominates. Although there are small differences in the angular distribution near $\bar{\theta} = \pi/2$ for the different processes, to a good approximation they can be described by the GG distribution over the angular range covered. In this case, the scattering cross-section is described by an effective structure function

$$F(x) = G(x) + \frac{4}{9}\,(Q(x) + \bar{Q}(x)) \qquad (12)$$

where G(x), Q(x), $\bar{Q}(x)$ are the momentum distributions of gluons, quarks and antiquarks in the proton (antiproton) and x is the fractional beam momentum carried by a constituent.

Fig.6 shows the UA1 and UA2 results on F(x), in comparison with the same quantity deduced at $q^2 \sim 50$ GeV^2 from deep-inelastic neutrino-nucleon scattering at CERN and Fermilab. The latter results were evolved according to QCD to the region $q^2 \sim 2000$ GeV of the collider data. There is remarkably close agreement between the two quite different types of experiment. Note that the gluon contribution is vital to account for the collider data, especially at small x. So this is a direct proof of GG scattering by G exchange, that is of the existence of the triple gluon vertex.

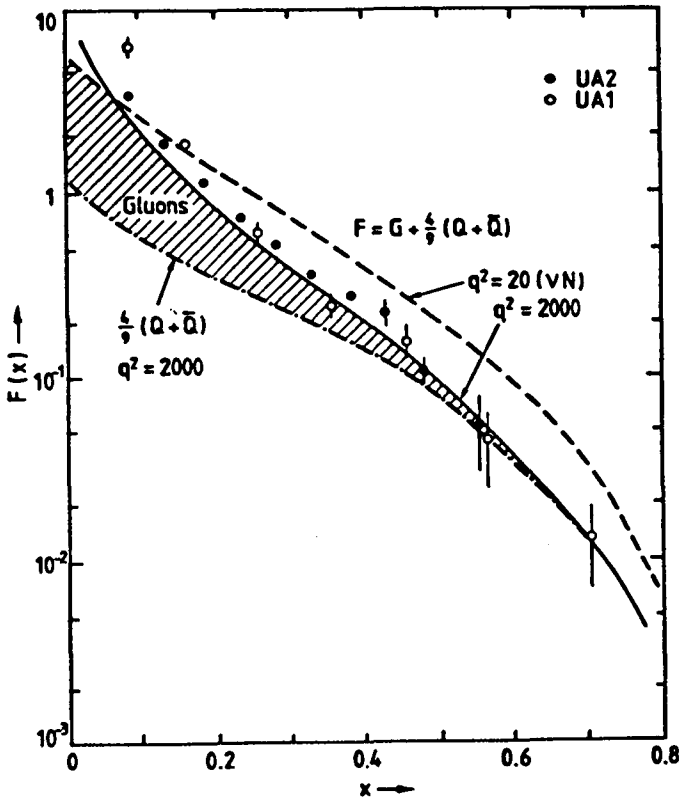

Fig. 6 Effective structure function $F(x) = G(x)$ $F(x) = G(x) + \frac{4}{9}(Q(x) + \bar{Q}(x))$ measured in $p\bar{p}$ collider experiment. The full line is the prediction from neutrino-nucleon scattering data, evolved to $q^2 = 2000$ GeV^2. Note that the gluon contribution (shaded) dominates at small x. UA1 data from Arnison et al (1984); UA2 data from Bagnaia et al (1984)

2. BEYOND THE STANDARD MODEL

We have already said that the perturbative approach of the standard model breaks down for Higgs masses $M_H \sim 1$ TeV. This is not the only potential problem associated with the Higgs. One is dealing with different mass scales for the various gauge interactions: the scale parameter $\Lambda \sim 0.2$ GeV for QCD, the scale $M_{W,Z} \sim 100$ GeV for electroweak interactions, and $M_X \sim 10^{15}$ GeV for the masses of the bosons X, Y mediating quark-lepton transitions in grand unified theories (GUTS). The GUT symmetry breaking (the difference in photon, W/Z and X/Y boson masses) is described in terms of massive GUT Higgs of mass $\sim M_X$. The theoretical values of M_W and M_Z will receive radiative contributions from the massive Higgs and lead to uncontrollable quadratic divergences unless one can arrange some clever cancellations (to the level of $M_W/M_X \sim 10^{-13}$!). So theorists have invented mechanisms to cure this so-called "hierarchy problem". One such is supersymmetry (SUSY) in which all fundamental fermions (bosons) have boson (fermion) partners. The radiative corrections to $M_{W,Z,H}$ from boson and fermion loops have opposite signs and one can get the desired cancellation. $\delta M_H \sim \alpha |M_B^2 - M_F^2|$ and thus $|M_B^2 - M_F^2| < 1$ TeV^2. Table 3 gives a list of SUSY particles. Most models involve R symmetry: particles are produced in pairs with $R = \pm 1$. Thus one gets associated production of squarks by quarks

$$q\bar{q} \rightarrow \tilde{q}\bar{\tilde{q}}$$

As a consequence of R conservation, the lightest SUSY particle (Photino?) must be stable. Decay of a squark

$$\tilde{Q} \rightarrow Q + \tilde{\gamma}$$

would be manifest in the large missing p_T of the photino, so the signature would be dramatic.

So far, no SUSY particles have been observed. Limits to the mass are more than 20 GeV for $\tilde{Q}$, $\tilde{\ell}$ and $\tilde{W}$ and more than 4 GeV for G. At new colliders with sufficient CMS energy (several TeV) to be sure of producing SUSY particles (if they exist), these new phenomena should

Table 3. Supersymmetric particles

Particle		Spin	Sparticle		Spin
Quark	Q	½	Squark	$\tilde{Q}$	0
Lepton	ℓ	½	Slepton	$\tilde{\ell}$	0
Photon	γ	1	Photino	$\tilde{\gamma}$	½
Gluon	G	1	Gluino	$\tilde{G}$	½
	$W^{\pm}$	1		$\tilde{W}^{\pm}$	½

be very easy to find.

3. NEW ACCELERATOR PROJECTS

A list of present and future colliders is given in Table 4. The e^+e^- colliders SLC at Stanford and LEP at CERN are designed to study the electroweak interactions, in particular to serve as Z^0 factories. VLEPP (Novosibirsk) is just a super linear collider (LC) proposal. The pp and $p\bar{p}$ colliders UNK (Serpukhov), LHC (CERN) and SSC (USA) are intended to attack the multi-TeV energy region mentioned above, and none of them is likely to be ready before the late 1990's.

HERA is so far the only ep collider, and provides a logical extension to $q^2 \sim 20{,}000$ GeV of lepton-nucleon scattering experiments at fixed target machines (SPS and Fermilab). The actual direction taken by colliders in the future will depend on the success or otherwise of the linear e^+e^- collider project at Stanford, physics results from the existing SPS and TeV I hadron colliders, and on developments of radically new methods of particle acceleration with high accelerating fields.

Table 4. Colliders

a)	e^+e^-	Year	#I.R.	E(GeV)	L $cm^{-2}sec^{-1}$
	SLC (LC)	1987	1	50 + 50	10^{29} - 6.10^{30}
	LEP I	1989	4	50 + 50	10^{31}
	LEP II	1992?	4	95 + 95	10^{31}
	TRISTAN	1987	4	30 + 30	-
	VLEPP (LC)	-	1	150 + 150	- (project)
b)	$pp,p\bar{p}$	Year	#I.R.	E(TeV)	
	$Sp\bar{p}S$	1982-1987	2	0.3 + 0.3	10^{29} - 10^{30}
	TeVI($p\bar{p}$)	1987	2	0.8 + 0.8	10^{29} - 10^{30}
	UNK (pp)	-	-	3 + 0.4 or 3 + 3	started
	LHC (LEP tunnel)	-	-	5 + 5	under study
	SSC (pp)	-	-	20 + 20	10^{32}; R and D
c)	ep	Year	#I.R.	E(TeV)	
	HERA	1990	2 (+2)	$0.82p + 0.03e^{\pm}_{L,R}$	10^{31} - 10^{32}

4. ROLE OF NON-ACCELERATOR EXPERIMENTS

Of the urgent problems in high energy physics that confront us now, many - such as the existence of Higgs scalars, supersymmetric particles or other new phenomena in the TeV energy range - are exclusively the province of the giant colliding beam machines.

There are many other problems which these accelerators will not address - for example, proton decay, GUT monopoles, neutrino masses and mixing. Then there is potentially new physics of which hints have come from cosmic ray studies, for example underground muons possibly related to point stellar sources (Cygnus X3, Hercules XI etc).

It is clear that non-accelerator experiments have a big role to play for very many years to come.

5. REFERENCES

Argento, A. et al Phys.Lett. 120B, 245 (1982)

Arnison, G. et al Phys.Lett. 122B, 103 (1983)

Arnison, G. et al Phys.Lett. 136B, 294 (1984)

Bagnaia, P. et al Phys.Lett. 129B, 130 (1983)

Bagnaia, P. et al Phys.Lett. 138B, 430 (1984)

Banner, M. et al Phys.Lett. 122B, 476 (1983)

Fortson, E.N. and L.L. Lewis, Phys.Rep. 113, 289 (1984)

Prescott, C. et al Phys.Lett. 77B 347 (1978); 84B 524 (1979)

Wu, S.L. Phys.Rep. 107, 59 (1984)

Invited talk presented at the 19th International Cosmic Ray Conference, San Diego, U.S.A., Aug 11-23, 1985

COSMOGENIC NUCLEI

G.M. RAISBECK

Laboratoire René Bernas, 91406 ORSAY, FRANCE

1. INTRODUCTION

Cosmogenic nuclei are, by definition, nuclides formed by nuclear interactions of galactic and solar cosmic rays with extraterrestrial (meteorites, moon, interplanetary dust, etc.) or terrestrial (atmosphere, lithosphere, etc.) matter. The nuclides produced in these reactions range from short lived radioactive species to stable isotopes. In this paper we will, for two reasons, concentrate on the long lived ($\sim 10^2$-10^7 years) radioactive cosmogenic isotopes. First, it is these isotopes which remain in various geological reservoirs today, as a link with cosmic ray activity in the past. Unlike stable cosmogenic nuclei (with some important exceptions) these long lived isotopes can readily been distinguished from "ordinary" terrestrial matter, and thus are unambigous evidence of cosmogenic production. The second reason is that the study of these long lived species has been revolutionized (and the word is not too strong) by the development in the past few years of a technique known as accelerator mass spectrometry (AMS). It is in fact the participation of our group at Orsay in the development of this technique, together with our previous interest in cosmic rays, which has led to our involvement in the study of cosmogenic nuclei.

We will not here go into any details about the technique of AMS, but rather refer the interested reader to the proceedings of the last symposium on this subject (1). Basically AMS is mass spectrometry at an energy where nuclear as well as atomic forces can be exploited in the

separation and detection steps. The result is a technique which can sensitively, and uniquely, identify a very small quantity (~ 10^6 atoms) of a given isotope in a much larger matrix of other nuclei. It is this property which makes it particularly valuable for measuring the small concentration of cosmogenic nuclei often available in geological samples.

AMS was originally developed at accelerators built for, and largely devoted to, nuclear physics. Much current work continues to be done at such accelerators. However, the potential of the technique has also led to the design and installation of five so-called "dedicated" accelerators, at Oxford University, University of Arizona, University of Toronto, Nagoya (Japan) and Gif-sur-Yvette (France). These relatively small (~ 2 million volt terminal voltage) tandem accelerators are used full time for AMS. Although originally conceived for ^{14}C measurements, we have shown that these Tandetron accelerators are also capable of measuring ^{10}Be and ^{26}Al with sensitivity and background levels comparable to the higher energy machines (2) (3). Except where noted, the results mentioned in the present paper have been obtained using the Tandetron accelerator at Gif-sur-Yvette.

The range of applications of cosmogenic isotopes is much too large to cover in any detail here. Once again, a simple perusal of ref (1) will give the interested reader some idea of the breadth of these applications. Thus, after briefly categorizing the types of these applications, I choose to describe several recent studies undertaken by our own group, which I feel might interest the attendees of this meeting. This paper is thus in no way intended to be a comprehensive or general review. The choice of subject matter is one of convenience and topicality and does not reflect any value judgement on similar or different studies being carried out by other groups.

2. GENERAL APPLICATIONS

We like to classify the applications of cosmogenic nuclei into three broad categories :

a) Dating : this is perhaps the first application that comes to mind when thinking of radioactive isotopes. With the exception of the already well developed procedure of ^{14}C dating, however, it is the application which will probably require the most extensive and detailed preliminary studies before it can be fully exploited. The reason is that, unlike ^{14}C, most of the other cosmogenic isotopes are not homogenized with their stable isotopes in the atmosphere. Their application in dating thus necessitates, at the very least, a detailed and comprehensive knowledge of the geochemistry of the isotope in question. In some cases application may require such limitating conditions as to be impractical.

b) Tracers : as mentioned above, cosmogenic nuclei are unambiguous witnesses of the interaction of cosmic rays with matter. As such they can be thought of as "tracers" of these interactions, and be used in two general ways :

- First, they can give information on the duration, place and conditions of the irradiation
- Second, once formed, they can give information on the movement of the medium (air, water, soil, ice, etc) in which they are transported.

c) Production variations, and their implications : there are basically three parameters which control cosmogenic production rates

i) Primary galactic cosmic ray intensity
ii) Solar activity (through modulation and production of solar flare particles)
iii) Geomagnetic field intensity (for terrestrial production)

The study of cosmogenic isotopes as a function of stratigraphic position in various geological reservoirs (marine and lacrustine sediments, polar ice) can thus potentially give us information on the variation of the above three parameters in the past.

3. SOME RECENT EXAMPLES

a) Primary cosmic rays : the application which probably most directly interests attendees at this meeting is the possibility of obtaining information on the variation of primary galactic cosmic ray flux in the past. Many theories of cosmic ray formation and acceleration allow, or even predict, a variable flux at the earth on a geological time scale. For example, at the Paris Cosmic Ray Conference, Axford discussed the type of variability that might be expected from the acceleration of cosmic rays by shock waves associated with supernova remnants (4). Streitmatter et al. (5) have recently described the type of variations that could result from the acceleration of cosmic rays in a "superbubble" in which the solar system is presently imbedded. At the present meeting Wolfendale et al. (OG 3.1-11) have given their predictions on the expected variability of intensity of cosmic rays associated with supernova remnants. In each of these cases, the variability is expected to be quite significant over periods of the order of $\sim 10^4$-10^7 years. This is just the period which is amenable to study using the nuclide ^{10}Be (half-life 1.5 My) which, conveniently, is also the second most abundant cosmogenic nuclide, after ^{14}C, produced in the earth's atmosphere.

Already studies on meteorites, and a few limited measurements in marine sediments, using classical counting techniques, have permitted tentative limits on cosmic ray variability (see, for example, Foreman and Schaeffer (6), and Reedy et al. (7) and references therein). However, the technique of AMS offers the promise of much more extensive and detailed limitations in the near future. At Orsay we are working on such an investigation by measuring ^{10}Be concentrations in several marine sediment cores. We have previously reported a few results from marine core RC12-65, which suggested a possible increase in production $\sim$ 10 My ago (8). We have since measured a substantially larger number of samples from this core. In addition, the chronology of the magnetic stratigraphy used to date the core has recently been subject to revision (9). This has had the effect of significantly modifying the age of the samples in

the ~ 5-9 My time range, and thus the earlier conclusions. We show in Fig. 1 some new results, expressed as $^{10}Be/^{9}Be$ ratio. In fact, one of the most difficult aspects in using ^{10}Be to deduce production variations, is the problem of how to normalize the results. Although we do not believe that ^{10}Be and ^{9}Be are completely homogenized in the ocean, we have evidence that, in some cases at least, ^{9}Be can partially compensate for varying sediment composition (in particular, the biogenic component). Thus ^{9}Be can serve as a useful, although imperfect, normalizing species.

Each sample in Fig. 1 represents ~ 1 cm depth in the core. However, bioturbation (mixing by organisms at the sediment surface) typically mixes deep sea sediments over a depth of ~ 10 cm. Using the sedimentation rates determined in the core by magnetic stratigraphy, a 10 cm depth interval corresponds to ~ 80,000 years in the upper part of the core, and ~ 20,000 years toward the bottom. This then determines the time resolution of the ^{10}Be measurements.

For the moment we have not included in Fig. 1 the earlier data of Ref (8). The reason is that the ^{9}Be measurements in that work were made under slightly different conditions, and we have not yet confirmed the reproducibility of the two techniques. The errors in Fig. 1 have been calculated using, in addition to the uncertainty in the ^{10}Be measurements, a 7 % relative uncertainty for the ^{9}Be. This is the average ^{9}Be variability observed in a series of duplicate measurements in another core (10). However it is possible that additional measurements in the present core may lead to revisions outside this range. Ironically enough, we presently have more confidence in the precision of our ^{10}Be measurements than those of the ^{9}Be.

For a perfectly constant cosmogenic production rate, and uniform sedimentation conditions, the $^{10}Be/^{9}Be$ ratio in Fig. 1 should decrease with age in the sediment with the 1.5 My half-life of ^{10}Be. Although there are some minor deviations, the most notable aspect of the data is the degree to which they follow such a trend. In addition to possible production variations, the deviations which do exist could be due to experimental error, rapid changes in sedimentation conditions, or

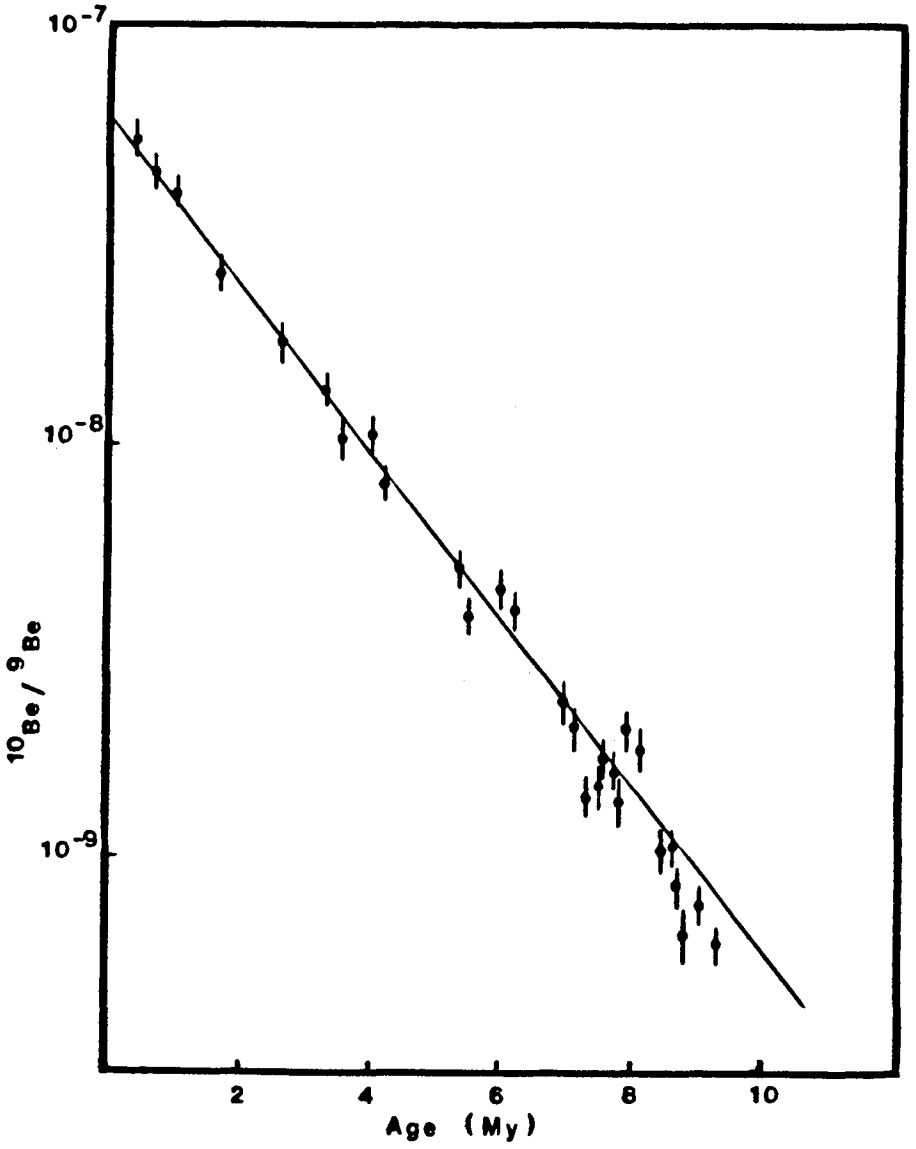

Fig 1 : $^{10}Be/^{9}Be$ ratio as function of age of samples in marine sediment core RC12-65

residual uncertainties in the chronology of the core. In order to check for such possibilities it will be necessary to make similar measurements in other cores covering the same time period.

Even if production variations are established it will be necessary, before concluding that these are due to primary cosmic ray intensity changes, to consider two other potential sources of variation mentioned above, namely solar modulation and geomagnetic field variation. The maximum expected variation due to these causes is a factor of ~ 2, and they are expected to be significantly attenuated over time periods of ~ 10^4-10^5 years (ie the time resolution of the samples in Fig. 1). Thus the type of variations which would most strongly suggest a primary cosmic ray origin would be those of large (> ~ 2) amplitude, or long (> ~ 1 My) duration.

Within the uncertainties and time resolution of the data, the measurements shown in Fig. 1 provide no compelling evidence for changes in cosmic ray flux during the past ~ 9 My (although there is a hint of a brief increase at ~ 8 My). This conclusion is similar to that arrived at by Tanaka and Inoue (11) over a shorter time period (2.5 My) or Ku et al. (12) over approximately the same time period, but with poorer time resolution. However, I wish to emphasize that the results of Fig. 1 are still preliminary, and incomplete. In addition to making more detailed measurements in RC12-65, we are extending this study back to ~ 20 My by making similar measurements in other cores. The purpose in presenting the results of Fig. 1 is thus not to give here any definitive limits to possible cosmic ray variations, but rather to illustrate the type of data that can be expected in the quite near future. Such data may then provide important constraints to theories of the origin and acceleration of cosmic rays. I would thus urge those working on such theories to try to calculate and report the time variations to be expected from their models.

b) Variation at a geomagnetic reversal : The intensity of the geomagnetic field varies on time scales of hundreds to tens of thousands of years (13) (at the present rate of change, the field would become zero in about 2000 years). The most dramatic of these changes occurs during a geomagnetic reversal. During such an event it is believed that the dipole field intensity decreases to < 20 % of its "normal" value, for a period of the order of 10^4 years. During such a time, we would thus predict that the production rate of cosmogenic nuclides in the atmosphere should increase. In order to test this idea, and obtain additional information on the details and length of the intensity changes, we have measured a ^{10}Be profile in a marine sediment core during the most recent of these reversals (Brunhes-Matuyama), which occurred 730,000 years ago. The results, shown in Fig. 2, do indeed show a significant increase in ^{10}Be at the time of the reversal (10). This increase in production occurs over a period estimated as ~ 12,000-24,000 years, and is considerably longer than the change in direction itself. Further studies along these lines should help those working on models of the reversal process itself, and on the way the magnetic signal is acquired in marine sediments.

c) ^{10}Be in polar ice cores : Some of our first measurements of ^{10}Be by AMS were made on samples from an Antarctic ice core. One of the principle motivations for that work was to look for variations caused by variable solar modulation. We did indeed find increased ^{10}Be during the period 1645-1715 AD, known as the Maunder Minimum (14). Somewhat more surprising, we also found increased ^{10}Be concentrations in ice deposited during the last ice age. More recent work by a Swiss collaboration, using ice cores from Greenland, has confirmed and extended these observations (15) (16). Nevertheless, the interpretation of the increase during the ice age has remained uncertain. We have recently had the opportunity to measure ^{10}Be in a 2083 m core taken in Antarctica by a Russian group. This core goes back in time over the entire last climatic cycle (~ 125,000 years). We once again found increased ^{10}Be concentration during the glacial stages, with concentrations similar to the

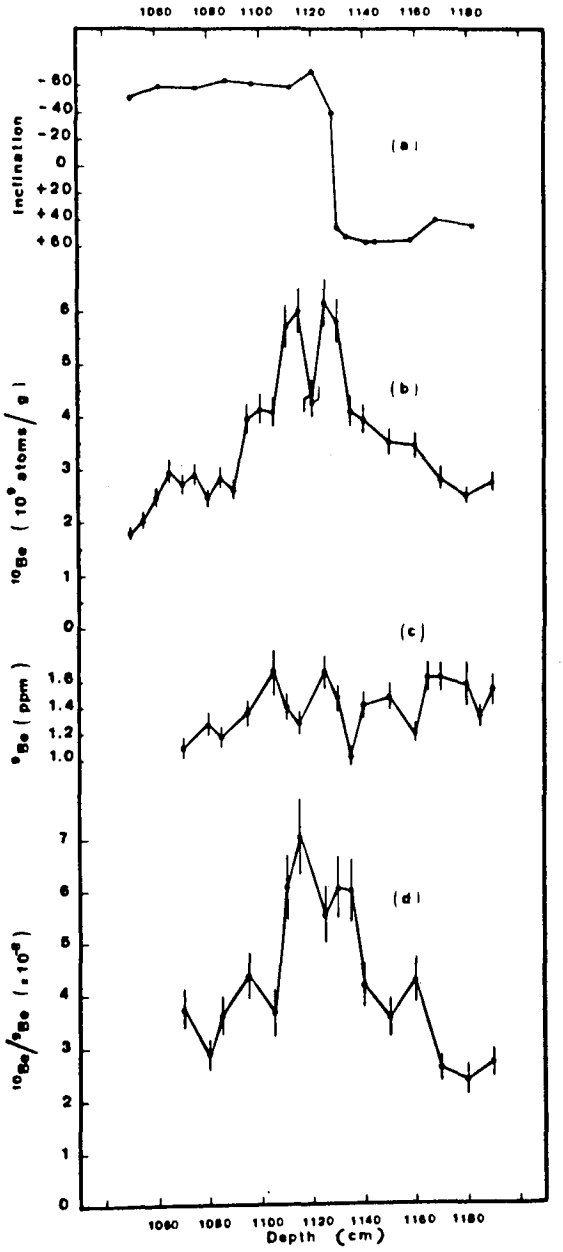

Fig 2 : (a) Magnetic inclination (b) ^{10}Be concentration (c) ^{9}Be concentration (d) ^{10}Be/^{9}Be ratio in marine core V16-58 during geomagnetic reversal (from ref 10)

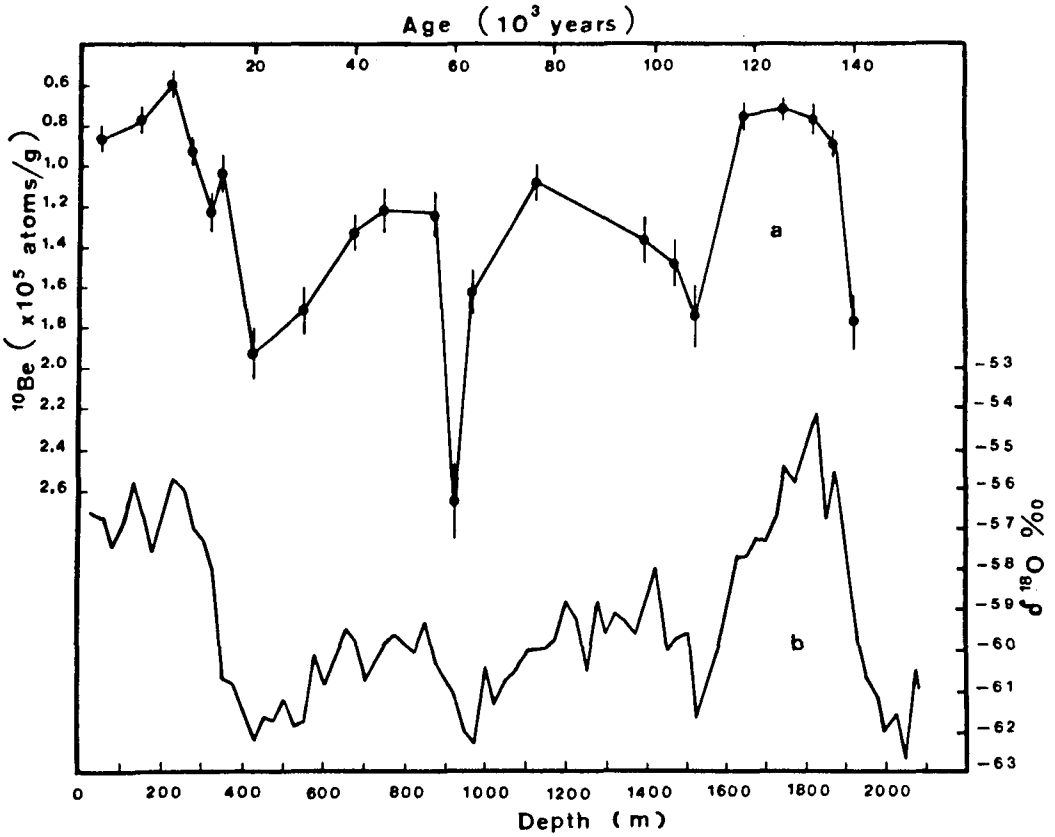

Fig 3 : ^{10}Be concentration and δ^{18}O in an ice core from Vostok station Antarctica (from ref 17) Note inverted scale of ^{10}Be to facilitate comparison between curves

present during the last interglacial (17). Our present interpretation of this phenomena is that the changes are not due to ^{10}Be production variations, but rather changes in the past precipitation rate in the Antarctic. Knowledge of such past precipitation rates is not only of interest for climatic studies, it is essential for determining the chronology of the ice cores themselves.

d) ^{10}Be and ^{26}Al in cosmic spherules : Cosmic spherules are small (~ 50-500 micron diameter), magnetic objects originally found in slowly accumulating deep sea sediments (18). An origin as ablation products from extraterrestrial material during atmospheric entry was first suggested by their discoverers, more than 100 years ago (19). The exact nature of the parent bodies has, however, remained uncertain. Several years ago, Nishiizumi, on the basis of cosmogenic ^{53}Mn data, suggested ablation from "normal" sized meteorites (20). An alternate possibility is that the parent objects could be the much more numerous small (~ 1 mg) objects that bombard the atmosphere (often observed as "shooting stars"), and that are believed to represent cometary debris.

The possibility of measuring cosmogenic ^{10}Be and ^{26}Al in the spherules suggested to us a way of distinguishing between these two possibilities. If the parent bodies were irradiated as small objects in interplanetary space, they should have a much larger $^{26}Al/^{10}Be$ ratio than that found in larger meteorites. The reason is that, in addition to formation by galactic cosmic rays, ^{26}Al can also be formed from the more numerous lower energy solar flare particles. ^{10}Be, on the other hand, being formed most efficiently by higher energy reactions, will have only a modest contribution from solar flare particles. Since the lower energy solar flare particles have a relatively short range (few millimeters) in matter, their influence will be significant for only small parent bodies. Using the University of Pennsylvania tandem accelerator, we measured the $^{26}Al/^{10}Be$ ratio in groups of (21), and individual (22) cosmic spherules. The ratios we found were in general much larger than found in meteorites, suggesting to us that these spherules are, in fact, in large part, cometary debris. Among our most recent measurements, made

with the Tandetron, we have found a ^{10}Be concentration in one spherule which is much larger than the "saturation" value for irradiation in near earth interplanetary space (23). We have suggested that this spherule may have been irradiated in part outside the solar modulation region, where the galactic cosmic ray flux is believed to be much larger than observed in the interplanetary space explored so far.

We are looking foreward to extending these studies to similar spherules recently discovered in "blue lakes" on Greenland ice (24). The collection procedure in this case does not depend on the spherules being magnetic, and they may include better preserved, and even new forms, of extraterretrial matter.

4. Conclusion

The technique of AMS opens up whole new areas of application for long lived cosmogenic nuclei. In addition to creating new links between cosmic ray physics and other domains, the possibility now exits for adding a virtually new dimension to cosmic ray studies themselves, namely that of detailed time variability over the past ~ 20 My. Such information may well provide important implications for theories of cosmic ray origin and acceleration.

5. Acknowledgements

I wish to thank first of all Francoise Yiou, who has participated in all aspects of the work discussed here. I also am deeply indebted to my other colleagues at Orsay, D. Bourles, D. Deboffle and J. Lestringuez, both for the often laborious task of preparing samples, and for help in making measurements at the Tandetron. I also have benefitted from the help of a number of others, cited in the appropriate publications, who have provided samples, or collaborated in the development of the AMS procedure.

References

(1) AMS 84, Nucl. Instr. and Meth. B5, 91 (1984)
(2) G.M. Raisbeck, F. Yiou, D. Bourlès, J. Lestringuez and D. Deboffle, Nucl. Instr. and Meth. B5, 175 (1984)
(3) F. Yiou, G.M. Raisbeck, D. Bourlès, J. Lestringuez and D. Deboffle, Radiocarbon (in press)
(4) W.I. Axford, 17th ICRC, Paris 12, 155 (1981)
(5) R.E. Streitmatter, V.K. Balasubrahmanyan, R.J. Protheroe and J.F. Ormes, Astron. and Astrophys. 143, 249 (1985)
(6) M.A. Forman and O.A. Schaeffer, Rev. Geophys. Space Phys. 17, 552 (1979)
(7) R.C. Reedy, J.R. Arnold and D. Lal, Ann. Rev. Nucl. Part. Sci. 33, 505 (1983) ; Science 219, 127 (1983)
(8) G.M. Raisbeck and F. Yiou, Nucl. Instr. and Meth. B5, 91 (1984)
(9) K.G. Miller et al., Geology, 13, 257 (1985)
(10) G.M. Raisbeck, F. Yiou, D. Bourles and D. Kent, Nature 315, 315 (1985)
(11) S. Tanaka and I. Inoue, Earth Planet. Sci. Lett. 45, 181 (1981)
(12) T.L. Ku et al., Nature 299, 240 (1982)
(13) R.T. Merrill and M.W. Mc Elhinny, The Earths Magnetic Field (Academic, London, 1983)
(14) G.M. Raisbeck et al., Nature, 292, 825 (1981)
(15) J. Beer et al. 18th ICRC, Bangalor 9, 317 (1983)
(16) J. Beer et al. Ann. Glac. 5, 16 (1984)
(17) F. Yiou, G.M. Raisbeck, D. Bourles, C. Lorius and N.I. Barkov, Nature, 316, 616 (1985)
(18) D.E. Brownlee, Ann. Rev. Earth Planet. Sci. 13, 147 (1985)
(19) S. Murrey and A.F. Renard, Rep. Sci. Results Voyage H.M.S. Challenger, (Edinburgh, Neill and Co, 1891)
(20) K. Nishiizumi, Earth Planet. Sci. Lett. 63, 223 (1983)
(21) G.M. Raisbeck, F. Yiou, J. Klein, R. Middleton, K. Yamakoshi and D.E. Brownlee, Lunar Planet Sci. 14, 622 (1983)
(22) G.M. Raisbeck, F. Yiou, J. Klein, R. Middleton and D.E. Brownlee, Proc. IAU Colloquim n°85, Properties and Interactions of Interplanetary Dust (in press)
(23) G.M. Raisbeck, F. Yiou and D.E. Brownlee, Meteoritics (in press)
(24) M. Maurette and C. Hammer, La Recherche 16, 852 (1985)

Invited Talk, XIX International Cosmic Ray Conference
La Jolla, August 21, 1985

EXTRAGALACTIC ASTRONOMY

E. Margaret Burbidge
Center for Astrophysics and Space Sciences
University of California, San Diego

I. INTRODUCTION

Most of the observational data and theoretical studies of cosmic rays concern processes at work in the Galaxy--solar activity and solar system interactions, particles produced and/or accelerated in active stellar systems and the interstellar medium, and particles ejected by nova and supernova explosions, or accelerated in the shock waves of supernova shells.

In discussing the relevance of extragalactic astronomy to cosmic ray physics, it is therefore necessary to consider what extragalactic objects exhibit physical processes of the same kind as those thought to be important within the Galaxy. In this paper, therefore, I shall describe some components of the active extragalactic universe where comparisons may be drawn with galactic cosmic ray sources.

For cosmic rays to be produced, there needs to be a source of high-energy particles (either baryons or leptons), magnetic fields which can interact with the particles, and, concomitantly, high-energy photons.

The obvious feature of galactic objects that may be sources of cosmic rays is that they must have a mechanism for ejecting high-energy particles. Since supernovae and supernova remnants, where ejection is known to occur, are seen as sources of synchrotron radiation, i.e. they produce high-energy particles in the presence of a magnetic field, we need to look at extragalactic sources of synchrotron radiation, that is, radio galaxies and quasars. Since these sometimes exhibit bulk relativistic motion, it is interesting to make a comparison between what we can only see at low resolution in extragalactic objects, because of the large distances involved, and what maybe analogous processes seen relatively nearby, where a detailed model can be constructed.

The X-ray binary star SS433 is very interesting in this respect. This system consists of a primary component orbiting about a collapsed component; infall of matter into the gravitational potential well of the latter produces sufficient heating for X-ray emission, and, most remarkable of all, the collapsed component must be rotating, have a strong magnetic field, and have an axis inclined to the axis of the orbital plane of the binary. By little-understood mechanisms, bulk matter is accelerated outward and ejected in two opposite, precessing, highly collimated beams, at the near-relativistic velocity of $\sim c/3$. The binary is surrounded by a radio source presumably originating from particles accelerated by the inner activity.

Collimated beams of relativistic electrons are the hallmark of radio galaxies and quasars, and jets are common features in these and in Seyfert galaxies, so in this paper we will discuss some recent data on radio galaxies, active galactic nuclei (AGNs), and quasars (QSOs).

II. RADIO GALAXIES, ACTIVE GALACTIC NUCLEI, AND QUASARS

There are several points to discuss from the observational standpoint. What do these categories of objects have in common, what are the differences between them, what measurements can be made and with what limitations, and what physically meaningful correlations can be found?

In searching for correlations, there is the ever-present caveat to beware of selection effects, and therefore to attempt to find samples that are complete in one respect or another. Regarding radio sources, a tractably small yet sufficiently diverse sample is the 3CR catalog (Bennett 1962), consisting of sources with radio power $\geq$ 9 Jy. Optical observations of the QSOs in this sample have been complete for some time; the radio galaxies are so much fainter that it has taken decades to achieve an almost complete set of optical identifications of those not in very low galactic latitudes (cf. Smith et al., 1976). Spectroscopic observations of these very faint objects are necessary before one can do any work on analyzing their physics--attempts to assign redshifts to optically unexamined objects result in misleading theoretical analyses. After many years of painstaking and careful work, Spinrad and collaborators (Spinrad et al., 1985) have recently produced an almost complete set of spectroscopic observations, which will be a goldmine for theoretical analyses, interpretations, and cosmological studies.

Limited areas of the sky have been searched for optical identifications of QSO's, and at radio wavelengths, to faint limiting powers. The HEAO catalog provides a catalog of X-ray emitters from which the attempt to separate high galactic latitude sources into extragalactic and galactic objects is feasible.

The search for correlations in the properties of QSOs is difficult and often frustrating. The lack of a general correlation between apparent magnitude and log (redshift) is only too well known (cf. Hewitt and Burbidge 1980; Barbieri et al. 1982, figure 4). Correlations between X-ray and radio luminosities of QSOs have been shown to exist (Zamorani et al. 1981), but correlations between line strengths and X-ray luminosities in a sample chosen to have a large spread in X-ray luminosities and to contain both radio-loud and radio-quiet QSOs have not been found (Bradley 1985).

a) Physical Properties Common to RGs, AGNs, QSOs

Common properties are that all these classes have an energy source (the most likely being ultimately gravitational in origin) in a very small volume. The central "engine" produces accelerated particles, and the relativistic leptons can be recognized by the non-thermal synchrotron emission they produce.

Surrounding the central energy source there is usually ionized gas, recognized by thermal radiation. This gas is distributed non-uniformly; usually clouds of relatively high electron density ($N_e \sim 10^{10}$ cm^{-3}) with a small filling factor are surrounded by a lower-density, higher-temperature

medium in which forbidden lines are produced. Seyfert galaxies exhibit the highest ionization in forbidden lines--up to [Fe X] in NGC 4151. Outward-directed beams of relativistic leptons produce radio emission in lobes which may be symmetrically placed either side of the central object, or which may be one-sided jets, or which may be bent or curved as though interaction with an intergalactic medium has occurred. Examples of these radio structures were described at this conference by Martin Rees.

Physical quantities which can be measured, besides morphological structure, are: optical apparent magnitudes at a selected wavelength, redshifts from optical or UV spectral emission lines, properties of the emission lines including their intensities and profiles, X-ray luminosities, radio fluxes.

The coexistence of electron beams (from collimated radio emission), X-ray beams, and "streaks" of thermal emission from hot gas or young stars can be well seen in the nearest strong radio galaxy NGC 5128 (Centarus A), as was shown by Martin Rees earlier in this conference (cf. Burns et al. 1983).

The recent work by Spinrad et al. (1985), in which 3CR radio galaxies with redshifts up to $z = 1.8$ have been measured, shows there are clearcut spectral differences between these and QSOs. First, the spectral lines are much narrower in RGs than in QSOs (smaller velocity dispension in the emitting gas). Second, [OII]λ 3727, which is quenched by electron collisional de-excitation at fairly low electron densities, is strong in radio galaxies but generally weak or absent in QSOs (e.g. 1641+399 and NRAO 140, Bradley 1985). HeII λ1640 is strong and sharp in the radio galaxy 3C256, and is not always seen in QSOs.

Spinrad et al. (1985) show in their Figure 1 a comparison between the histogram of redshift distribution between QSOs and RGs in the 3CR catalog. Both terminate at $z \sim 2$; this may be observational limitation in the case of the RGs because of their extremely faint optical emission, but is clearly an inherent property of the 3CR strong-source radio QSOs, since other radio catalogs have produced QSOs with $z \sim 3.8$ (Peterson et al. 1982).

QSOs themselves exhibit a wide range of properties. As an example, I describe a search using an objective-grating-prism (grism) at the prime focus of the Kitt Peak National Observatory Mayall telescope for QSOs with $z \sim 2$. Two areas of sky were searched, each about 1 square degree, one centered on a rich cluster of galaxies, A2151, in the Hercules supercluster, and one off the field of the cluster (Burbidge et al. 1985). Searches for radio-quiet QSOs are especially successful in finding objects with $2 < z < 3.3$, for which the Lyman-α hydrogen line, usually the strongest emission line seen in QSOs, falls in the observable region. Of 20 objects in the Hercules region, five with redshifts $z \sim 3$ had such strikingly different line profiles and relative strengths that they will provide challenging material for study of a set of QSOs in a small area of sky and a small range of redshift.

If we turn to the Seyfert nuclei, we see further striking differences between these objects and QSOs. Line profiles of permitted lines (Hα) can reach a Doppler width corresponding to $\Delta v = 18{,}000$ km/sec, and one such object shows strong narrow [Fe X]λ6374 and [Fe VII]λ6087 (Cohen 1985). Rapid continuum variability is found in both Seyferts and some QSOs, but, while short-time scale variations in permitted lines in Seyferts are well known,

results on possible line variability in QSOs are still inconclusive.

b) Bulk Ejection from QSOs

Evidence for bulk ejection of matter at high velocities from active extragalactic objects is important when we make comparisons with ejection from galactic objects, novae, supernovae, and SS433 and possibly other such evolved binaries.

There is a class of QSOs in which the normal emission lines are accompanied by broad absorption troughs on the short wavelength side. The longest-known and best-studied object of this class of broad absorption-line QSOs (BAL QSOs) is PHL 5200 (Junkkarinen et al. 1983). Widths of the absorption troughs indicate outflow velocities of 30,000 km/sec, even in some extreme cases 66,000 km/sec, or more than 0.2c (Foltz et al. 1983). Such velocities may be compared with the typical 5000-10,000 km/sec ejections seen in supernovae.

Models of optically-thick outflow (Junkkarinen 1983) have shown from the observed line profiles that the outflow cannot be spherically symmetric. It could be in jets, conical outflow, a break up of disk-like structure. The absorbing material must have a small covering factor as seen from the inner clouds that produce the fairly normal emission lines, and the inner source of continuum radiation.

Until recently, it was thought that this phenomenon occurs only in rather high-redshift QSOs, with a frequency still imperfectly determined of between 1% and 10%. However, a case of outflow at 14,500 km/sec in a QSO with the relatively low z of 1.2 has recently been found (Wilkes 1985). Since this observation was made from the ground, with the University of Arizona 90-inch telescope, only CIV λ1549 was detected. In higher-redshift objects all the resonance lines display broad troughs - CIV λ1549, SiIV λ1397, NV λ1240, Lyα, and OVI λ1035.

c) Bulk Ejection from Other Active Galactic Nuclei

Small jets, usually seen as "blue jets" close in to the nuclei of radio galaxies, have been detected in a number of cases. An interesting case of a possible jet detected spectroscopically in the UV spectrum of the active Seyfert galaxy NGC 4151 has been described by Ulrich et al. (1985). Spectra taken with the International Ultraviolet Explorer showed two unidentified emission features, variable on a time scale of several days, flanking CIV λ1549. If they represent a jet seen in CIV λ1549 with an approaching component and, on the far side, a receding component (as in SS433), the line-of-sight outflow velocities would be -6100 and +8500 km/sec.

d) Do QSOs Have a Limiting Redshift?

Studies of the distribution of redshifts of QSOs have long displayed a peak around z = 2, mainly caused by the optically-discovered radio-quiet QSOs because of the easy visibility of Lyα λ1216 between z = 2 and 2.5 (Osmer 1982), see also histograms by Hewitt and Burbidge (1980)). Beyond z = 2.5, a precipitous decline in numbers of QSOs is seen. It took 10 years for the "record" redshift of z = 3.5 for 0Q172 to be overtaken by two southern hemisphere QSOs, the largest redshift now known being 3.8 (Peterson et al.

1982). New histograms by Hewitt and Burbidge, to be presented at I.A.U. Symposium No. 119 in December 1985, in Bangalore, display these features very clearly.

There have been several speculations as to the cause of the precipitous decline. These include: this redshift corresponds to the epoch of galaxy formation; there is luminosity evolution in QSOs; regions at higher redshift are obscured by dust. The answers are not in, nor are likely to be until we have a better understanding of the relationship between galaxies and QSOs.

e) Are there Non-Cosmological Redshifts?

It is not fashionable to accept the existence of non-cosmological redshifts and the association of high-redshift active objects with low-redshift-galaxies. However, Arp and co-workers have gathered a significant amount of data on this controversial topic. The best-studied case is NGC 4319 and Markarian 205; in the presentation I showed slides taken from the work of Arp (1985), Wehinger and Wyckoff (1981), and Sulentic (1983); unfortunately these cannot be reproduced here. It seems, however, clear that there is a faint luminous bridge extending from Mrk 205 ($z = 0.07$) toward the nucleus of NGC 4319 ($z = 0.006$). What the nature of this luminous material is, and whether it really links the two objects, has not been resolved.

Other interesting cases are the aligned set of some 8 QSOs around NGC 3379 (Arp et al. 1979) and three QSOs within the arms of NGC 1073 (Arp and Sulentic 1979; Burbidge et al. 1979). A review of these apparent associations has been given by Burbidge (1981).

III. CONCLUSION

A thorny question in cosmic-ray physics is that of whether there is an extragalactic component of cosmic rays. The preceding sections have shown that components of the active extragalactic universe undoubtedly eject high-energy (relativistic) particles and bulk matter at high velocities approaching relativistic speeds, and these ejections must affect their extragalactic environment. There are distinct differences between Seyfert galaxies, quasars, and radio galaxies, but nevertheless they have in common an interior energy source which powers these phenomena. Of the radio galaxies, as Martin Rees pointed out in his introductory paper, NGC 5128 (CenA) is the nearest very active source, and it may be capable of emitting high-speed particles that reach the environment of our galaxy. I have not discussed the results of Very Long Baseline radio interferometry, since Rees showed examples, but the remarkable "superluminal" effects seen in e.g. 3C273 (cf. popular review by Field 1984) provide yet another indication of relativistic ejection at high Lorentz factors.

It seems not unlikely that the highest-energy cosmic rays may have an extragalactic origin, and further study of Centarus A could throw light on this controversial question.

REFERENCES

1. Arp, H. C. 1971, Astrophys. Lett., 9, 1.
2. Arp, H. C. 1985, private communication.
3. Arp, H., Sulentic, J.W. 1979, Ap. J., 229, 496.
4. Arp, H., Sulentic, J.W., and Tullio, G. di 1979, Ap. J., 229, 489.
5. Barbieri, C. et al. 1982, Mem. Soc. Astron. Italiana, Catalogue.
6. Bennett, A. S. 1962, Mem. Roy. Astron. Soc., 68, 163.
7. Bradley, S. E. 1985, Ph.D. Thesis, U. Calif. San Diego.
8. Burbidge, G. 1981, Ann. New York Acad. Sci., 375, 123.
9. Burbidge, E. M., Junkkarinen, V., and Koski, A. T. 1979, Ap. J., 233, L97.
10. Burbidge, E. M., Smith, H. E., Junkkarinen, V. T., and Hoag, A. A. 1985, Ap. J., 288, 82.
11. Burns, J. O., Feigelson, E. D., and Schreier, E. J. 1983, Ap. J., 273, 128.
12. Cohen, R. D. 1985, Ap. J., in preparation.
13. Field, G. 1984, Mercury, 13, 98.
14. Foltz, C., Wilkes, B., Weymann, R., and Turnshek, D. 1983, Pub. Astron. Soc. Pacific, 95, 341.
15. Hewitt, A. and Burbidge, G. 1980, Ap. J. Suppl., 43, 57.
16. Junkkarinen, V. T. 1983, Ap. J., 265, 73.
17. Junkkarinen, V. T., Burbidge, E. M., and Smith, H. E. 1983, Ap. J., 265, 51.
18. Osmer, P. 1982, Ap. J., 253, 28.
19. Peterson, B. A., Savage, A., Jauncey, D. L., and Wright, A. E. 1982, Ap. J., 260, L27, 1982.
20. Shanks, T., Fong, R. and Boyle, B. J. 1983, Nature, 303, 156.
21. Smith, H. E., Spinrad, H., and Smith, E. O. 1976, Pub. Astron. Soc. Pacific, 88, 621.
22. Spinrad, H., Djorgovski, S., Marr, J., and Aguilar, L. 1985, preprint and Pub. Astron. Soc. Pacific, in press.
23. Sulentic, J. W. 1983, Ap. J., 265, L49.
24. Ulrich, M. H. et al. 1985, preprint.
25. Wehinger, P.A. and Wyckoff, S. 1981, Sky and Telescope, 61, 200.
26. Wilkes, B. J. 1985, Ap. J, 288, L1.
27. Zamorani, G. et al. 1981, Ap. J., 245, 357.

GAMMA RAY ASTRONOMY FROM SATELLITES AND BALLOONS

V. Schönfelder
Max-Planck-Institut für Physik und Astrophysik
Institut für extraterrestrische Physik
8046 Garching, F.R.G.

1. Introduction. This rapporteur talk deals with the field of gamma ray astronomy from satellites and balloons and therefore is restricted to energies below about 10 GeV. Ground based gamma ray observations ($E_\gamma > 1$ TeV) will be covered by the rapporteur talk of Dr. Watson.

Gamma ray astronomy provides the opportunity to study high energy phenomena in space. Many of these phenomena are directly related to questions of cosmic ray research, so gamma ray astronomy plays a central role for cosmic ray research.

Gamma ray astronomy has become a rather broad field. The different topics can be grouped under the following headings:

- gamma ray bursts
- gamma ray line spectroscopy
- galactic gamma ray sources
- broad scale distribution of galactic gamma ray emission
- extragalactic gamma ray astronomy (extragalactic sources and diffuse cosmic gamma ray background)

All these topics were covered during the conference (by in total 62 papers), and in my presentation I shall follow this subdivision.

2. Gamma Ray Bursts. During the time of their bursts cosmic gamma ray bursters are the by far brightest gamma ray sources in the sky. Our entire knowledge on bursters is essentially based on the measurement of four different properties of their bursts. These are

- their light curves
- their energy spectra
- the location of the burster in the sky
- recently, for very few gamma ray burst sources, a correlated observation in the optical range

Additional information on each of these four observational aspects was provided at the conference:

The durations of gamma ray bursts typically range from a few tenths of a second to tens of seconds. Some are as short as 10^{-2} sec, others as long as 100 sec. It seems that there is no uniform structure in the light-curves of different bursts. Some bursts show single spikes only, others very complex structures. Cline (OG 1.2-6) has speculated that all complex long duration bursts might be characterised as superposition of single spikes, which are similar for all bursts.

The energy spectra of gamma ray bursts in many cases show a thermal bremsstrahlung spectrum $N(E)dE \sim E^{-1} \exp(E/kT)$ with $kt \approx 300$ keV. Recently, however SMM-measurements (Matz et al., 1985) have shown that high energy gamma ray emission above 1 MeV is a common feature of bursts. This conclusion was confirmed by HEAO-1 observations (Hueter and Matteson, OG 1.1-1). Many bursts show power law spectra at least up to 6 MeV and are in conflict with the normal thermal model burst spectra.

Our knowledge on burster positions in the sky is mainly - with the exception of a very few measurements with position sensitive burst detectors - based on triangulation from different spacecraft locations. An overview on

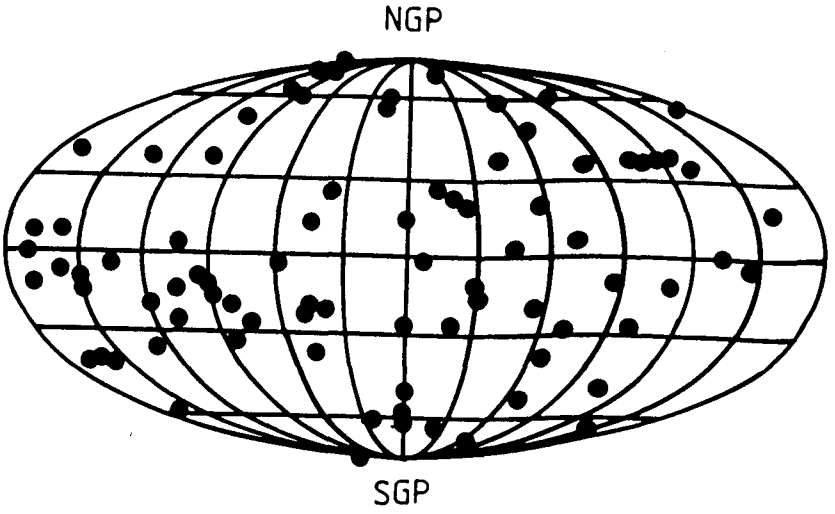

Fig. 1 Distribution of 86 bursters on the sky (from Atteia et al., OG 1.2-1).

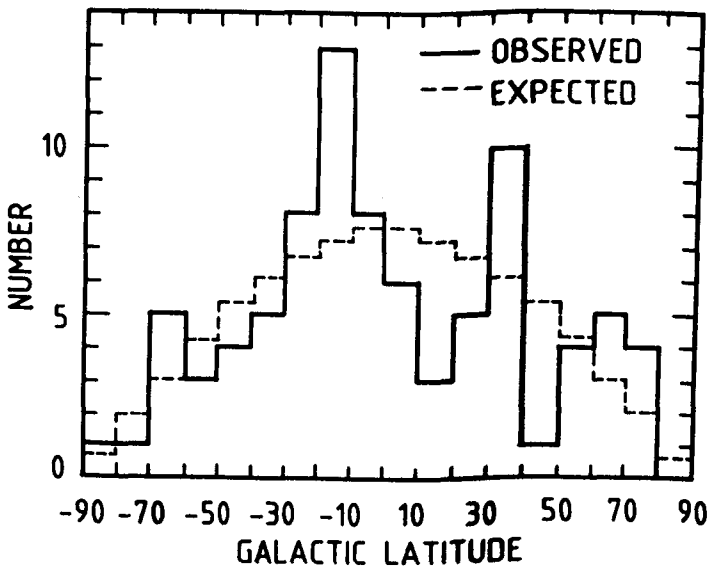

Fig. 2 Latitude distribution of the 86 bursters of Fig. 1. The dashed line is the distribution expected on the basis of isotropy (from Atteia et al., OG 1.2-1).

our present state of knowledge was given at the conference (Atteia et al. (OG 1.2-1). Fig. 1 displays the distribution of 86 bursters in the sky. Fig. 2 shows the latitude distribution of these locations as well as that expected, if the distribution is isotropic. It is clear: the observed burster distribution is consistent with isotropy.

Extensive efforts to find out whether optical phenomena are associated with gamma ray bursters were finally successful. At the positions of 3 different gamma ray bursts optical flashes could be found on archival photographs. The optical flashes occurred in 1901, 1928 and 1944 and are correlated with the gamma ray bursts of Nov. 5, 1979, Nov. 19, 1979, and January 1, 1979, respectively (Schaefer et al., 1984). The optical flashes had durations of typically 1 sec. From statistical considerations it was estimated that the recurrence time scale of the optical flashes of a burster is about 1 year. The energy emitted in gamma-rays was estimated to be about 1000-times larger than in the optical flashes. We do not yet know, whether optical and gamma-ray bursts occur simultaneously. A detailed analysis of the bursts of the Second Interplanetary Network (Atteia et al., OG 1.2-5) came to the important conclusion that the best lower limit to the repetition rate of gamma ray bursts from one and the same source is 100 months. So far only two examples of repetition are known at all (one of which is the burster with the famest outburst on March 5, 1979). Further searches for counterparts of gamma ray bursters in the optical and infrared region so far remained unsuccessful (Gehrels et al., OG 1.1.-7, Seetha et al., OG 1.1-8, and Schaefer and Cline OG 1.1-9). Such counterpart searches will definitely play an important role in gamma ray burst astronomy of the near future.

More observational "facts" on cosmic gamma ray bursters are now urgently needed in order to come to an understanding about their nature. So far, more than 40 models have been suggested to explain the origin of the bursts. During the last few years a certain consensus about the nature of the burst sources has been achieved. First, it is now generally agreed that the burst sources are contained within the Milky Way and second, there is strong evidence that a neutron star is somehow involved in the sources. Both these conclusions have to be discussed in more detail:

The galactic origin of most of the gamma ray bursts so far was mainly derived from the log N (> S) - log S diagram, which shows a -1.5-slope at high fluences (time integrated gamma ray flux) S and a flattening at lower fluences. This shape has been generally interpreted as evidence for the galactic origin of bursts: it is expected from an isotropic burster distribution up to about 300 pc distance and a disk like distribution for larger distances, if all bursts are assumed to have the same intrinsic gamma ray luminosity. Such an interpretation, however, is inconsistent with the distribution of measured burst positions on the sky (see Fig. 1 and 2), which show complete isotropy. Many people have worked on this problem. It has been shown that a halo-distribution of bursts can also reproduce the observed log N (> S) - log S curve, if a proper luminosity distribution is assumed (for a review see Jennings, 1984). In case of an extragalactic origin the log N (> S) - log S curve should have the -1.5-slope over the entire range and should show much more structure, because the bursters would be expected to be clustered in certain galaxies. In addition, it is difficult to explain the resulting very high luminosities of typically 10^{46} erg instead of typically 10^{38} erg for a galactic origin.

During the conference strong arguments were put forward that the flattening of the fluence distribution at low fluences actually is only an observational selection effect due to variations in durations and energy spec-

tra of different bursts (Higdon and Lingenfelter, OG 1.2-3 and Nishimura and Yamagami, OG 1.2-10). The selection effect on duration is due to the fact that burst detectors do not trigger on a minimum fluence, but on a minimum flux increase within a fixed time. Similarly, different energy spectra of bursts lead to a selection effect, because a given burst detector samples only a limited energy band and not the entire energy range of the burst. The result of the energy selection effect is illustrated in Fig. 3. Here the peak

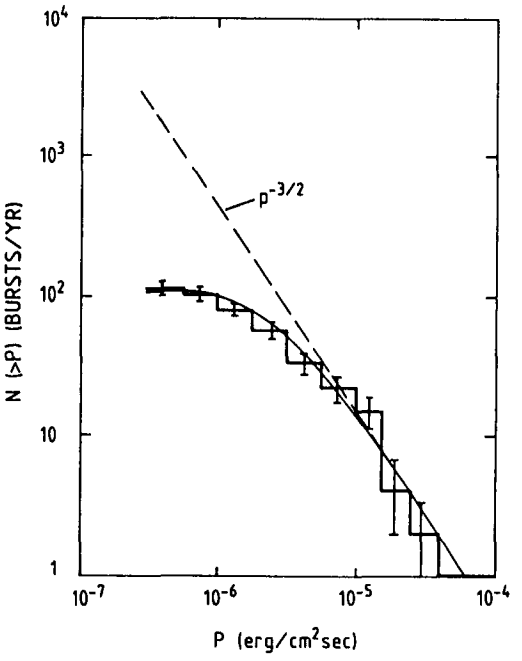

Fig. 3 Burst size-frequency distribution of peak energy flux, N (> P) as function of P. Measuring points are from Venera-data. Solid line is derived from an isotropic burst distribution with a certain assumed intrinsic energy distribution. The flattening of the solid curve at low P-values is caused by spectral selection biases of the burst-detectors (from Higdon and Lingenfelter, OG 1.2-3).

energy flux P is used instead of the fluence S, because P is more directly related to the burst detector response than the fluence and because the influence of variations in burst duration is minimised, if P is used. In Fig. 3 the size frequency distribution for bursts observed by Venera is compared with that expected from an isotropic distribution of sources, which have a certain assumed distribution of energy spectra. As can be seen, spectral selection biases can indeed account for the observed deviation from the simple -1.5 power law distribution. The flattening of the size frequency distribution therefore no longer seems to be an argument for the galactic origin. The strongest arguments for the galactic origin at present are the luminosity argument and the neutron star hypothesis.

Why do we believe that a neutron star is somehow involved in the burst sources? First, there is some observational evidence: namely the existence of absorption lines between 30 to 70 keV, which are interpreted as cyclotron lines and, therefore, require magnetic field strengthes which are

available only on the surface of a neutron star. Furthermore, about 7% of all bursts show an emission line at about 420 keV, which is interpreted as red-shifted annihilation line in the gravitational field of a neutron star. In addition to these (and a few other) observational evidences there are also some good theoretical reasons, why neutron stars should be involved: it is easy to account for the observed energy release by means of their gravitational and/or magnetic field energy, and the high magnetic field density provides a means to confine the source region against the radiation pressure of the gamma-rays.

Essentially four different classes of models exist, in which a neutron star is the main cause of the gamma ray bursts: The four causes are:

- accretion of matter onto the surface of a neutron star (either from interstellar space or from a companion star). The material is heated and may lead to an explosion after some reservoir of accreted matter has reached a critical mass (nuclear flash model).
- star quakes, which generate shocks
- magnetic instabilities near the surface of the neutron star
- impact of a comet or asteroid onto the neutron star surface.

It is quite clear that further observations are needed to confirm the neutron star hypothesis and to distinguish between these models. The future aspects of gamma ray burst astronomy are quite promising: once, due to the burst capabilities of GRO and then due to efforts which are presently undertaken to observe large numbers of correlated optical flashes.

3. Gamma Ray Line Astronomy. Gamma ray line astronomy is no longer a field for theoreticians only. Gamma ray lines by now have been detected from solar flares, from gamma-ray bursts and transient sources, and from some steady sources. In the following I shall restrict myself to line-emission from steady sources only (solar flare gamma ray line emission will be discussed in the SH-session). Three such sources are listed in Table 1:

Table 1: Sources of Gamma Ray Line Emission

galactic center	511 keV-annihilation line
interstellar space	1.8 MeV-line from radioactive Al^{26}
SS 433	lines at 1.5 MeV and 1.2 MeV

New results on each of the sources were presented at the conference: The 511 keV-line from the galactic center region has first been detected in the 1970's and since then has turned out to be variable in intensity on a time scale of about half a year. A new attempt of the joint Bell/Sandia gamma-ray astronomy group to detect the line in a balloon flight in November last year was not successful. The source was still in the "off"-state (MacCallum and Leventhal, OG 2.5-5). Considering the large flux of the line, the rapid variability, the line width (< 2.5 keV FWHM), and the absence of other nuclear gamma ray lines from the center region a black hole model provides the easiest and most natural explanation for the origin of the line.

The 1.809 MeV line from Al^{26} in interstellar space is the first line from a radioactive nucleosynthesis product. The line was first detected by HEAO-3 (Mahoney et al. 1984) and now also by SMM (Share et al., OG 3.2-1). The HEAO-3 line profile is shown in Fig. 4 (from Mahoney et al., OG 3.2-3). Al^{26} is a long lived isotope of half-life $1.4 \cdot 10^6$ years. Therefore

the presently observed line intensity is the sum emission over more than a million years. The observed abundance ratio Al^{26}/Al^{27} is a factor of 10 too high to be explained by supernovae alone. It therefore is concluded that most of the Al^{26} is produced in novae (Clayton, 1984). Other possible contributors are massive stars and red giants (Prantzos et al., OG 3.2-5). In order to better understand the origin of the line it would be necessary to measure the angular distribution of the line: whereas the novae-distribution is strongly peaked towards the galactic center, supernovae and massive stars have a much broader distribution.

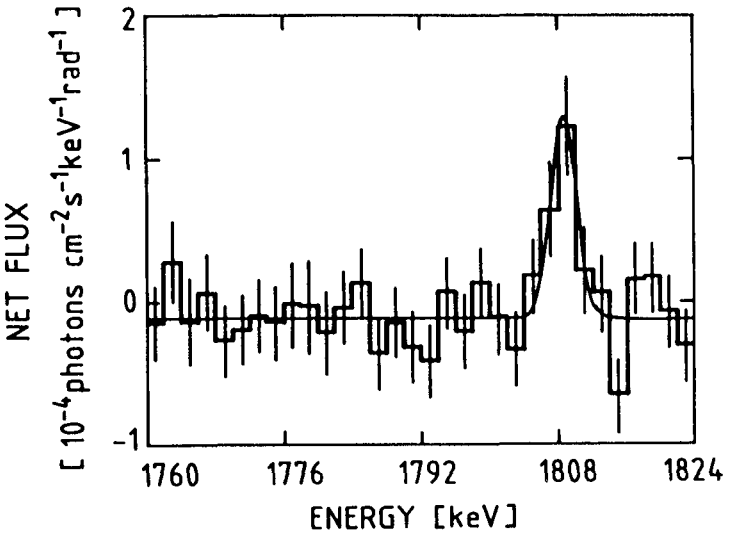

Fig. 4 The 1.809 MeV-line in the diffuse galactic gamma ray emission from the center region as observed by HEAO-3 (from Mahoney et al., OG 3.2-3).

Gamma ray line emission at 1.5 and 1.2 MeV from the binary system SS 433 was reported by HEAO-3 (Lamb et al., 1983 and Wheaton et al. OG 2.4-9). These two lines were interpreted as Doppler shifted lines from Mg^{24} (1.369 MeV) or from N^{14} (1380 MeV). The SMM-investigators (Geldzahler et al. OG 2.4-11) have analysed 468 days of their data, during which SS 433 was within the field-of-view. The line is not seen! The upper limits derived by SMM are at least an order of magnitude below the fluxes of HEAO-3. Either SS 433 shows unusual variability at gamma ray energies or statistical/systematic fluctuations were misinterpreted by the HEAO-3 group. The HEAO-3 group believes the latter possibility to be very unlikely, at least for the 1.5 MeV line.

In addition to the three lines discussed so far, other line observations are reported in the literature. However, most of them are at the limit of statistical significance. We therefore have to wait for more sensitive observations. The intensities of so far detected lines are in the range of $10^{-3}/cm^2$ sec or somewhat lower. GRO will be able to detect line intensities down to $10^{-5}/cm^2$ sec. A next generation of high resolution gamma ray spectroscopy instruments with senstivities down to $10^{-6}/cm^2$ sec will be needed, however, to open the full potential of gamma ray line spectroscopy.

4. Galactic Gamma Ray Sources. Most of the known galactic gamma ray sources are contained in the second COS-B catalog. So far only 3 sources of

this catalog are identified, namely the quasar 3C 273; the only extragalactic object in this catalog, and the two radio pulsars Crab and Vela. A fourth source 2CG 353+16 which was tentatively identified with the ρ -Ophiuchi cloud has been resolved in the meantime (Hermsen, 1983). Not contained in this catalog is the Orion nebula which covers a field of the sky of a few hundred square degrees and which was resolved by COS-B.

The remaining 21 sources of the catalog are still unidentified in spite of tremendous efforts to find counterparts in other spectral ranges. Because nearly all sources are located along the galactic plane, it is obvious that most of them are galactic. The attempt to identify some of the sources by observation of correlated time variability in different spectral ranges so far was not successful (Caraveo et al. OG 2.5-9). A third issue of the COS-B catalog is in preparation. Pollock et al. (OG 3.1-9) presented results from a new point source search along about half of the galactic plane. So far this analysis was restricted to high energies only (> 300 MeV). An extension to all energies and to the rest of the galactic plane is in preparation.

During the conference new results were presented on some of the COS-B sources and on a few others as well.
These are

- Crab pulsar
- Cyg X-3
- Geminga
- ρ -Ophiuchi
- Loop I remnant
- the unidentified COS-B sources in general

Each of these objects will now be discussed separately.

Crab-pulsar. The Riverside group (White et al. OG 2.3-8) presented final results from a balloon flight which was carried out already in 1978 with their Compton telescope. The derived pulsar spectrum in the 1 to 30 MeV range follows the single power law spectrum $\sim E^{-2.2}$ which is generally observed between about 50 keV and 2 GeV. The new fluxes agree well with previous values obtained by Graser and Schönfelder (1982) in the same energy range. The final analysis of the balloon flight did not confirm the results of a preliminary analysis on the existence of MeV-lines in the pulsar spectrum, which were presented at the Bangalore conference (Long et al., 1983).

Cyg X-3. Cyg X-3 is a binary X-ray source with a periodicity of 4.8 hours. The situation of Cyg X-3 in the gamma ray range around 100 MeV is controversial. The SAS-2 experimenters had claimed the detection of this source above 35 MeV (Lamb et al., 1977). They identified the total excess observed in the Cyg-region with Cyg X-3 and found the total excess to be pulsed with the 4.8 hour period. COS-B has looked at the Cygnus region seven-times from 1975 to 1982. No evidence for pulsed emission with the 4.8 hour period was found. The 2 σ upper limits are an order of magnitude below the flux reported by SAS-2. The COS-B analysis has shown that the emission in the Cygnus-region is structured and that it can be explained as being the sum of a diffuse emission in interstellar space plus a contribution from two point-like gamma ray sources as illustrated in Figure 5 (from Hermsen et al., OG 2.2-2). There is no excess emission at the position of Cyg X-3 which is indicated by the cross at the time of the COS-B observations. To resolve the contraversy it is recommended to the SAS-2 experimenters to repeat their analysis of the Cygnus region using all the information on molecular hydrogen which is now available - more than 10 years after the first analysis. Gamma

ray observations of Cyg X-3 at ultrahigh energies are discussed in the rapporteur talk of Dr. Watson.

Geminga (2CG-195+04). The Geminga gamma ray source was discovered by SAS-2 (Thompson et al., 1977); it is one of the strongest gamma ray sources in the sky. Based on 121 detected gamma-ray photons the SAS-2 observers had claimed the existence of a 59 sec-period emphasizing, however, that this periodicity would have to be confirmed with better statistics.

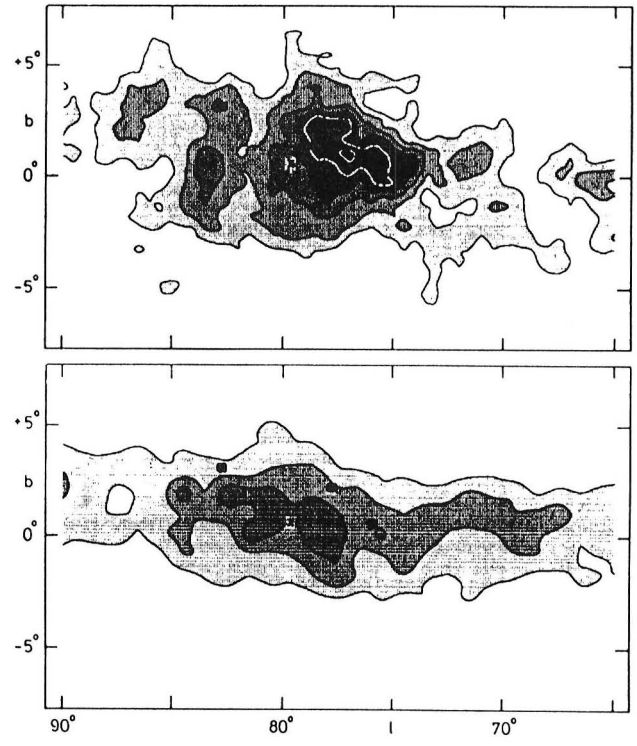

Fig. 5 Gamma ray intensity distributions in the Cygnus-region above 500 MeV as observed by COS-B (from Hermsen et al, OG 2.2-2). Upper half: contours as measured by COS-B. Lower half: estimated from total gas distribution (HI and CO-data). Position of Cyg X-3 is indicated by X. The positions of 3 γ-ray sources are also indicated (■).

Recently, Bignami, Caraveo and Paul (1985) reported that they have identified the gamma-ray source with the X-ray source 1E 0630+178. They found the X-ray source, which was observed by the EINSTEIN- and EXOSAT-satellites, to show a 50% periodic emission at a period of about 59 sec. The coincidence of the temporal signature was used for the identification of Geminga with the X-ray source. Buccheri et al. (1985) have reviewed the statistical significances of all reported detections and conclude that the identification cannot be made. The COS-B collaboration ((Buccheri et al., OG 2.4-3) has now performed a comprehensive analysis of all their Geminga data (214 days of observation). The analysis does not confirm the presence of a 59 sec pulsation with the characteristics reported by SAS-2. A sinusoidal signal at this period, however, at present cannot be excluded. The identification of Geminga is still open.

ρ-Ophiuchi. Whereas the analysis of the gamma ray data from the Orion complex has shown that the nebula is penetrated by a cosmic ray density equal to that observed near the Sun, the conclusion is different for the ρ - Oph complex: if the observed gamma-ray emission from the direction of ρ - Oph is linked to the gas in the cloud, then an increase of the cosmic ray density inside the cloud by a factor of about 2 is needed. Montmerle and Feigelson (OG 2.5-1) have looked for possible X- and radio objects, which are not correlated with ρ -Oph, but could explain the observed excess in gamma-ray intensity from this direction. They do not find such a source and therefore conclude that the most probable explanation of the excess remains the interaction of cosmic rays of enhanced density with the cloud.

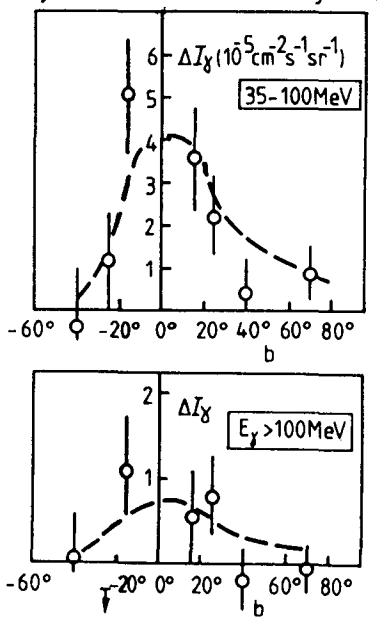

Fig. 6 Excess gamma ray intensity (using SAS-2 data) associated with Loop I as function of galactic latitude. For details see text. From Bhat et al., (OG 3.1-10).

Loop I Supernova Remnant. The Loop I SNR, which is clearly visible in radio synchrotron radiation and known as North Polar Spur, is only ~ 130 pc away; its radius is about 115 pc. Evidence for enhanced gamma-ray emission from the remnant was found by three different groups independently (Bhat et al., OG 3.1-10, Lebrun and Paul OG 3.1-1 and Strong et al. OG 3.1-3). Fig. 6 shows the excess gamma-ray intensity from the direction of Loop I as a function of b^{II}: ΔI_γ is the difference between observed and expected intensity for the Loop region minus the same quantity outside the Loop. The dashed curve corresponds to the 408 MHz radio intensity, which shows the same behaviour. There is clear indication of enhanced gamma-ray emission along the Loop. It is most interesting to note that the cosmic ray density within the remnant which is required to explain the observed ΔI_γ is consistent with the one needed, if the bulk of cosmic rays with energies below 100 GeV is produced in galactic supernova remnants.

Unidentified COS-B sources. The understanding of the unidentified COS-B sources remains an unsolved puzzle. The low luminosity of the sources in all

other spectral ranges in comparison to the gamma-ray luminosity is a constraint for the object behind these sources. Fast radio pulsars, SNR's, giant HII-regions and giant molecular clouds (very often in combination with SNR's) are possible candidates. Theoreticians nowadays concentrate on molecular clouds in combination with SN's. In most cases the mass of molecular clouds is not large enough to produce the required gamma-ray emission in the environment of a cosmic ray density equal to the one near the Sun. Indeed, recently Pollock et al. (1985) reported that only 3 out of the 8 COS-B sources in the first quadrant (2CG 036+01, 2CG 065+00, 2CG 095+04) may simply reflect the clumpiness of the interstellar gas. For the other 5 sources, either a large enhancement of the cosmic ray density within the cloud is needed or these sources are independent of the gas. Since shock waves appear to be an efficient means to accelerate cosmic rays, the combination of interstellar clouds with shocks is of special interest. The shock may come from SN's either inside or outside the cloud. Stephens (OG 2.5-2 and OG 2.5-3) has investigated a scenario, in which SN envelopes explode into dense clouds, and Montmerle (OG 2.5-4) has looked for correlations between gamma-ray sources and giant HII-regions which contain SNR's or stars with strong stellar winds. He proposes that 10 of the unidentified COS-B sources in the second and third quadrant may be of this tpye.

5. Large Scale Galactic Gamma Ray Distribution. The large scale distribution of high energy gamma ray emission - say above 50 MeV - within the Milky Way is of fundamental importance for cosmic ray research. It is expected to give an answer to the important question, how cosmic rays are distributed within the Galaxy.

It is now generally agreed that the diffuse galactic gamma-ray emission at high energies mainly results from interactions of cosmic ray nuclei and electrons with interstellar matter via π^0-decay and via bremsstrahlung, respectively. The production of gamma-rays by inverse Compton scattering of cosmic ray electrons with the ambient photon field is believed to play a minor role - however cannot be neglected totally (Bloemen, OG 3.1-2).

The gamma-ray emission from interactions of cosmic ray nuclei and electrons with interstellar matter is determined by

$$(1) \qquad \Delta I_{\gamma,ISM} = \int \frac{q(r)}{4\pi} n_{H,tot}(r)\, dr$$

where $q(r)/4\pi$ is the gamma-ray emissivity at distance r in units of gamma-rays produced per H-atom sec ster and $\int n_{H,tot}(r)\, dr$ is the column density of interstellar hydrogen. The production rate at distance r is proportional to the cosmic ray density at this distance:

$$(2) \qquad q(r) = q_o \frac{n_{CR}(r)}{n_{CR}(r=o)}$$

Therefore, by measuring the gamma-ray intensity $\Delta I_{\gamma,ISM}$, the distribution of cosmic rays within the galaxy can be inferred, if the local gamma-ray production rate q_o and the total interstellar hydrogen density is known.

The determination of $\Delta I_{\gamma,ISM}$ has some problems: First, the contribution of discrete sources has to be subtracted from the measured overall gamma-ray intensity. Second, the instrumental and cosmic background has to be known accurately in order to be subtracted, too. Indeed, small errors in the background may introduce significant errors in the broad scale distribution of $\Delta I_{\gamma,ISM}$. A better understanding of the total COS-B background was achieved only recently. Third, the inverse Compton component has to be estimated and then to be subtracted, too.

The local gamma-ray emissivity q_0 is normally determined by interpretation of the diffuse galactic gamma-ray emission at medium galactic latitudes $|10^o| < b < |20^o|$. The total hydrogen column density is determined from galaxy count data. Because gamma-rays from this medium latitude range are produced within the next - say 0.5 kpc - it is justified to take a constant value of q, which then by definition is the local one. Strong et al. (OG 3.1-3) applied this method in a more elaborated way to derive local q_o-values for atomic and molecular hydrogen separately. Lebrun and Paul (OG 3.1-1) question the usefulness of this method. They found that the detectability of galaxies - and hence the galaxy count rate - strongly depends on the field star density in the corresponding part of the sky. When correcting for this effect, they find significant variations in the emissivity from one direction to the other and therefore conclude that the definition of an average emissivity in the solar neighbourhood appears rather meaningless.

The largest uncertainty in the interpretation of the gamma-ray data is caused by our poor knowledge on the total interstellar hydrogen column density. Whereas the distribution of neutral hydrogen (HI) is known reasonably well from observations of the 21 cm line, the situation of molecular hydrogen (H_2) is controversial. The H_2 column density cannot be measured directly, but is normally obtained indirectly by observation of interstellar CO which is excited by collisions with H_2-molecules.

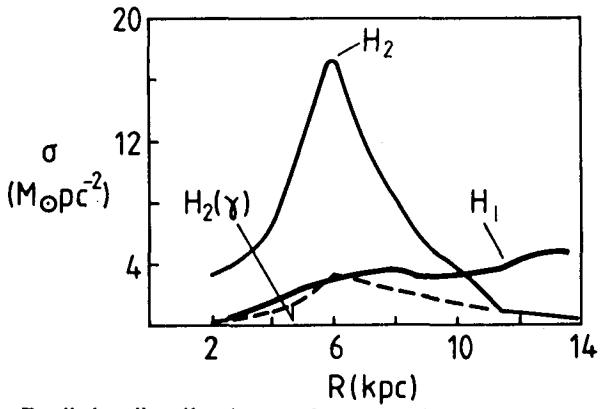

Fig. 7 Radial distribution of neutral and molecular hydrogen in the Milky Way (from Bhat et al., 1985).

Fig. 7 shows two rather extreme cases of the molecular hydrogen content within the Milky Way. The high H_2-curve is from Sanders, Solomon and Scoville (1984), and the lower dotted one from the Durham group. At 6 kpc from the galactic center both H_2-distributions differ by a factor of about 6. The neutral hydrogen density is also indicated.

It is quite clear that such differences in the gas distributions must have a significant effect on the interpretation of the gamma-ray data. The standard way to determine the gamma-ray volume emissivity within the galaxy so far was based on an unfolding of the gamma-ray longitude distribution under the simplifying assumption of cylindrical symmetry. Stecker and Harding (OG 3.1-4) again followed this approach using the complete set of SAS-2 and COS-B data and new CO-data. They found a maximum of the cosmic ray density - for both electrons and nuclei - at about 5 kpc from the center, where the density of supernovae remnants and pulsars is greatest. Goned and Wahdan (OG 3.1-5) came to a similar conclusion.

The Durham group (Bhat et al., OG 3.1-8) took a different approach: They used the distribution of supernova remnants as probable distribution of the cosmic ray density in the galaxy and then determined the gas distribution from the gamma-ray data. Due to the assumed high cosmic ray density in the inner part of the galaxy (a factor of 2.5 higher at 6 kpc than at 10 kpc) they derive the low H_2-density shown in Fig. 7. The factor of 6 difference in their H_2-density compared to that of Sanders, Solomon and Scoville (1984) is explained by them by different conversion factors between the measured CO-intensity and the derived H_2-column density. With their new and very low mass estimate of the interstellar gas in the Milky Way the Durham group found wide attention. It is one of the rare astronomical results which was reported in the Frankfurter Allgemeine Zeitung (FAZ from April 24, 1985).

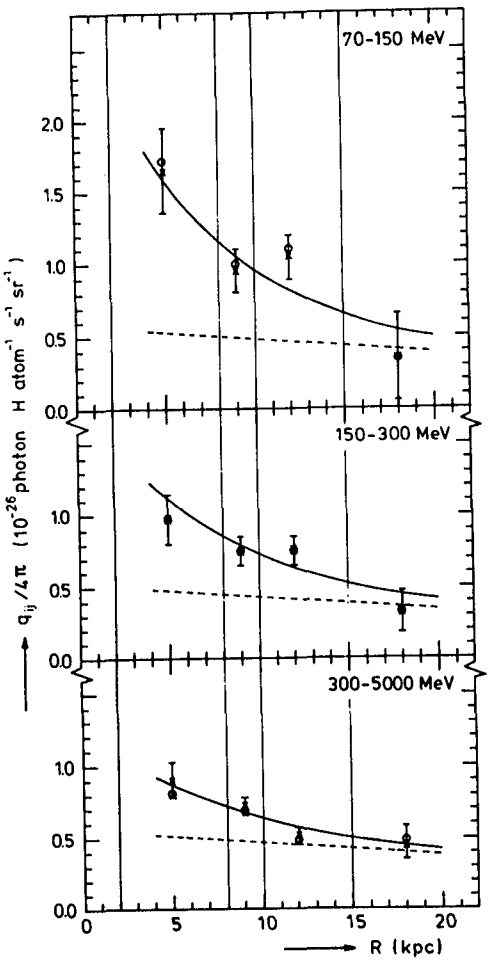

Fig. 8 Galactocentric distribution of the gamma ray emissivity for 3 energy intervals. The dashed lines indicate the π^0-decay contribution from cosmic ray nuclei only (from Bloemen et al., (OG 3.1-6).

Again a different approach was taken by the COS-B collaboration (Bloemen et al., OG 3.1-6). They made a maximum likelihood fit of the gamma-ray intensity (observed in $1^o \times 1^o$ bins) to the entire data of HI and

CO. The emissivity parameter of HI, the conversion factor between CO-intensity and H_2-column density, and the total instrumental and cosmic background were free parameters. The total line of sight was subdivided into 4 galactocentric distance intervals. The velocity information of the HI- and CO-lines was used as distance indicator. The result of this analysis is shown in Fig. 8, where the emissivity per H-atom is plotted as a function of galactocentric distance. At 10 kpc the q-values are consistent with the ones derived by Strong et al. (OG 3.1-3) from medium galactic latitudes. In each energy interval the emissivity increases towards the inner part of the galaxy. The gradient is stronger at lower than at higher energies. Because the contribution of electron bremsstrahlung to the total gamma-ray emission dominates at lower energies (as we know from the gamma-ray energy spectrum), it is concluded (and derived quantitatively) that the observed overall gradient in the low energy interval is mainly due to electrons. The lower energy gradient is consistent with the electron gradient derived from non-thermal radio measurements. The density of cosmic ray nuclei, however, is found to be practically constant throughout the entire galaxy (dashed line). The same conclusion was already earlier derived by the COS-B collaboration, when analysing gamma-ray data from the anticenter region alone in a similar way. The analysis of the anticenter is in so far easier, as the uncertainty in the contribution of H_2 does not exist, because of its relatively low contribution in this part of the galaxy.

With this conclusion the old question, whether the bulk of cosmic rays is galactic or extragalactic is open again. Though the gradient in the distribution of cosmic ray electrons confirms their galactic origin, the constancy of the cosmic ray nuclei component either requires a large galactic halo distribution or cosmic ray nuclei of predominantly extragalactic origin. In case of a galactic origin the cosmic ray nuclei density does not follow the distribution of supernovae in the Galaxy.

I think the battle on the interpretation of the broad scale galactic gamma ray distribution will continue for quite a while. New data on H_2, and also future gamma-ray data will definitely stimulate further discussions. GRO will not only provide more precise gamma-ray data from our own galaxy, it will also provide information on the interstellar gamma-ray emission in our neighbouring galaxies (see also Berezinsky et al., OG 2.7-15).

6. Extragalactic Gamma Ray Astronomy. Extragalactic gamma ray astronomy may - at some time in the near future - turn out to be the astronomy of active galactic nuclei and quasars. These two classes of objects at present belong to the most interesting objects in astronomy and astrophysics. Due to their high luminosity and their extreme compactness it is supposed that an accreting black hole is the powering engine in the center of these galaxies.

Although COS-B has devoted nearly one third of its observation time to extragalactic pointings ($|b| > 15^o$), only one source, the quasar 3C 273, could be detected. For other potential sources like normal galaxies in the local group, Seyfert galaxies, BL-lac objects, and other quasars only upper limits to the gamma ray flux could be derived.

The quasar 3C 273 has its maximum of luminosity at energies of a few MeV, as can be derived from an interpolation of its X-ray and high energy gamma ray spectrum. Many other galaxies, especially Seyferts should also have their maximum of luminosity in the range between several 100 keV and a few MeV, as can be concluded from their hard X-ray spectra in combination with the existing upper limits at gamma ray energies above 35 MeV. Hard X-ray and low energy gamma ray observations are therefore expected to provide special insight into the source mechanism of these objects.

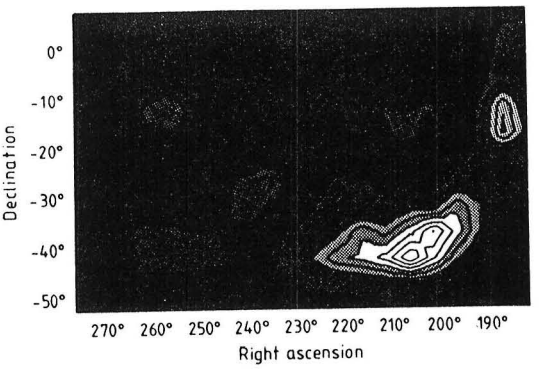

Fig. 9 Observation of Cen A with the Compton-telescope of MPI-Garching between 1 to 20 MeV (from v. Ballmoos et al., OG 2.7-7).

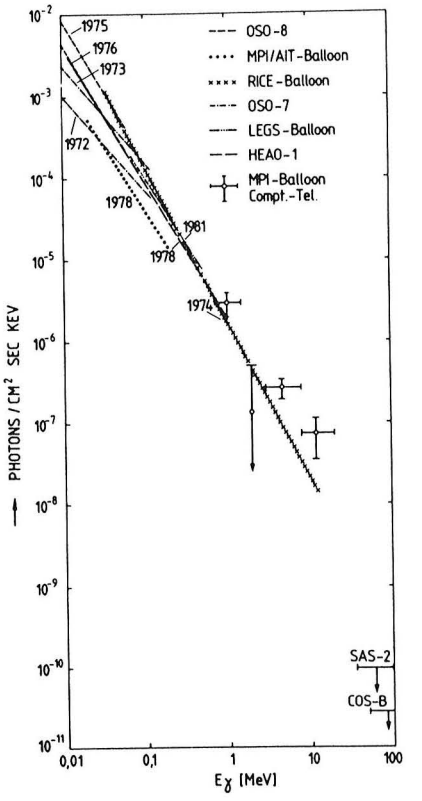

Fig. 10 The energy spectrum of Cen A from X-ray to gamma ray energies (from v. Ballmoos et al., OG 2.7-7).

During this conference my own group (v. Ballmoos et al., OG 2.7-7) reported on an observation of Centaurus A at MeV-energies. Cen A is the nearest active galaxy in the sky. Fig. 9 shows a reconstructed image of the part of the sky which we observed during a balloon flight with our Compton-telescope. The contour lines are a measure of the likelihood for the existence of a source. The likelihood is greatest near Cen A. A detailed analysis showed that the statistical significance of the source detection at the position of Cen A was 4.1σ. The derived energy spectrum is shown in Fig. 10. It is seen that the spectrum at MeV-energies well connects to the X-ray spectrum with practically constant slope. This fact, together with the position of the excess in the previous figure seems to indicate that the observed gamma ray emission is related to Cen A.

Assuming the validity of the upper limits above 35 MeV from SAS-2 and COS-B also for the time of the balloon flight, it has to be concluded that the Cen A spectrum must steepen rapidly somewhere beyond 8 or 20 MeV in order to meet the upper limits. This spectral shape, which again places the maximum of luminosity of Cen A in the MeV-range, allows interesting discussions on the source size and the radiation mechanism involved.

Damle et al. (OG 2.7-8) reported on a balloon observation of another active galaxy, namely the Seyfert galaxy 3C 120 at gamma ray energies above 5 MeV. The detection of the source had a statistical significance of 2.75σ only, and therefore definitely needs confirmation.

Let me finally turn to the topic of the diffuse cosmic gamma ray background, which has been of special interest since the very early beginning of gamma ray astronomy. It is now generally agreed that unresolved active galaxies to some extend contribute to the cosmic gamma ray background. The degree of this contribution, however, still contains considerable uncertainties.

Gruber et al. (OG 3.1-12) presented new results on the diffuse cosmic X- and gamma-ray energy spectrum between 15 keV to 4 MeV from HEAO-1 observations. Their new results agree with the compilation of experimental data between 2 keV and 200 MeV, as shown in Fig. 11. Whereas the X-ray background below 1 keV is mostly galactic, the galactic contribution above 2 keV is only a few percent of the measured flux. The high degree of isotropy, especially in the 2 to 10 keV range, is evidence for its extragalactic origin.

As can be seen from Fig. 11, there is much structure in the spectrum. Between 3 to 50 keV a thermal bremsstrahlung spectrum of kT = 40 keV fits the data quite well. Though the spectrum between 40 keV and 400 keV gives a smooth connection to the lower energy range, it does not follow the thermal bremsstrahlung shape. In the MeV-range all the existing measurements (including the new HEAO-1 results of OG 3.1-12) show the existence of a bump above the extrapolation from X-ray energies. Above about 5 MeV the spectrum becomes very steep.

Unresolved normal galaxies make only a minor contribution to the background flux (see Lichti et al., 1978). A significant contribution of unresolved active galaxies, however, especially Seyferts, is generally accepted around 100 keV (Rothschild et al., 1983).

The contribution of unresolved quasars to the high energy gamma ray background (> 35 MeV) was estimated from SAS-2 data by Lau and Young (OG 2.7-10) to be about 25% of the total observed flux. After more than 100 quasars have been observed at X-ray energies by the EINSTEIN observatory, estimates of the quasar contribution to the 1 to 3 keV X-ray background range from 25% to 100%. If all quasars would have the same spectral

shape as 3C 273 between 1 keV and 800 MeV, then their summed contribution at 100 MeV would supersede the observed gamma-ray flux by more than a factor of 10. It must therefore be concluded that the spectrum of 3C 273 cannot be typical for most of the other quasars. The typical quasar spectrum should break off already below 100 keV, otherwise it would be in conflict with the well established contribution of Seyferts at 100 keV.

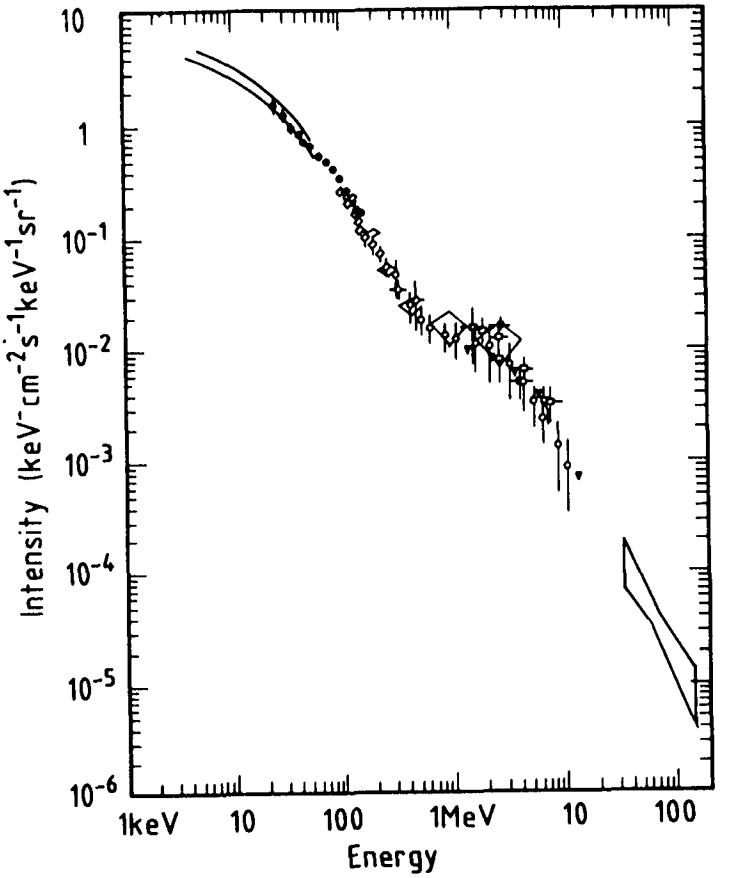

Fig. 11 The energy spectrum of the diffuse cosmic X- and gamma-ray background. The X-ray measurements are from HEAO A-2 and A-4, the low energy gamma ray measurements are from Apollo, the two Compton-telescopes at Riverside and MPI-Garching and a shutter type telescope at Nagoya. The high energy gamma-ray spectrum is from SAS-2.

In view of this discussion it is perhaps not surprising that no single power law dependence is observed over the entire X- and gamma-ray range, since different types of galaxies may contribute and dominate at different energies. The question of a remaining really diffuse component like the one from matter-antimatter annihilation in a baryon symmetric universe can only

be answered if much more information on the X- and gamma-ray emission of active galaxies and quasars is available. Only then will it be possible to derive that part of the background spectrum that cannot be explained by unresolved sources.

7. Conclusions. The major conclusions at the Cosmic Ray Conference in the field of gamma ray astronomy were:

- MeV-emission of gamma-ray bursts is a common feature. Variations in duration and energy spectra from burst to burst may explain the discrepancy between the measured log N - log S dependence and the observed isotropy of bursts.
- The gamma-ray line at 1.809 MeV from Al^{26} is the first detected line from a radioactive nucleosynthesis product. In order to understand its origin it will be necessary to measure its longitude distribution in the Milky Way.
- The indications of a gamma-ray excess found from the direction of Loop I is consistent with the picture that the bulk of cosmic rays below 100 GeV is produced in galactic supernova remnants.
- The interpretation of the large scale distribution of gamma rays in the Milky Way is controversial. At present an extragalactic origin of the cosmic ray nuclei in the GeV-range cannot be excluded from the gamma ray data.
- The detection of MeV-emission from Cen A is a promising step towards the interesting field of extragalactic gamma ray astronomy.

It is obvious: each new result raises new questions. The future of gamma-ray astronomy will be very exciting!

8. References

Bignami, G.F., Caraveo, P.A., and Paul, J.A., (1985), Nat. 310, 464
Bhat, C.L., et al., (1985), Nat. 314, 511
Buccheri, R., et al., (1985), in press
Clayton, D.D., (1984), Ap.J. 280, 144
Graser, U. and Schönfelder, V., (1982), Ap.J. 263, 677
Hermsen, W., (1983), Sp. Sci., Rev. 36, 61
Jennings, M.C., (1984), in High Energy Transients in Astrophysics, ed. S.E. Woosly (AIP Conf. Proc. 115, 412)
Lamb, R.C., et al., (1977), Ap.J. 212, L63
Lamb, R.C., et al., (1983), Nat. 305, 37
Lichti, G.G., et al., (1978), Astrophys. & Sp. Sc. 56, 403
Long, J.L., et al., (1983), Proc. of 18th ICRC, Vol. 9, 41
Mahoney, W.A., et al., (1984), Ap.J. 286, 578
Matz, S.M., et al., (1985), Ap.J. 288, L37
Pollock, A.M.T. et al., (1985), Astron. & Astrophys. 146, 352
Rothschild, R.E. et al., (1983), Ap.J. 269, 423
Sanders, D.B. et al., (1984), Ap.J. 276, 182
Schaefer, B.E., et al., (1984), Ap.J. 286, L1
Thompson, D.J., et al., (1977), Ap.J. 213, 352

Rapporteur paper presented at 19th Int. Cosmic Ray Conference, La Jolla 1985

COSMIC γ-RAYS AND COSMIC NUCLEI ABOVE 1 TeV

A.A. Watson

Department of Physics, University of Leeds, Leeds 2, U.K.

ABSTRACT

This paper is based on a rapporteur talk given at the 19th International Cosmic Ray Conference in August 1985. In it the most exciting and controversial aspects of work on cosmic γ-rays and cosmic nuclei above 1 TeV are described and evaluated. The prospect that γ-ray astronomy above 1 TeV will give new insights into high energy cosmic ray origin within our galaxy is particularly bright.

1. Introduction. The search for the origin of cosmic rays has been a long and conspicuously unsuccessful one. At high energies ($> 10^{14}$ eV) it had been anticipated that careful study of the small anisotropies which are present, allied with a sound knowledge of the mass composition and energy spectrum, would yield indirect information about the sources. At the very highest energies ($> 10^{19}$ eV), where the Larmor radii of protons in galactic magnetic fields exceed 3 kpc, strong directional anisotropies had been expected if the sources of these multi-joule particles were galactic, while a sharp cut-off in the spectrum above about 4×10^{19} eV has been predicted if the sources were at cosmological distances. Of the three measureable parameters, spectrum, anisotropy and mass composition, only the first can even now be said to be well-known (although the question of the Greisen-Zatsepin cut-off remains under debate) and our understanding of the data available on arrival directions continues to be hampered by very limited knowledge about the primary mass composition.

At the Bangalore conference it was recognized that perhaps a fourth channel of information about cosmic ray origin was opening to us. At that meeting evidence of γ-ray emission at $\sim$1 TeV from several sources, including the Crab pulsar and Cygnus X-3, was reported. In addition the possibility that point sources of γ-rays up to 10^{16} eV might exist had been signalled through the claim by the Kiel group (Samorski and Stamm 1983a) of emission from Cygnus X-3 of 10^{15} eV γ-rays modulated with the 4.8^{h} orbital period of the binary X-ray source. The significance of this latter result, confirmed by Lloyd-Evans et al (1983) by the time of the Bangalore meeting, is that it seems impossible to explain the γ-rays as arising from other than π^{0}-decay. Thus for the first time a source of cosmic ray nuclei may have been identified. Not surprisingly this meeting has seen the fruits of the burgeoning interest in γ-rays above 1 TeV while work on cosmic ray nuclei has continued with all its former vigour. I have thus had to be very selective in choosing the topics discussed below but they are, I believe, the most stimulating and controversial culled from a particularly vigorous area of the cosmic ray field.

2. Gamma-ray emission above 1 TeV. The idea that there should be detectable sources of γ-ray emission above 1 TeV is an old one. At the Moscow conference Cocconi (1959) proposed that particle arrays of adequate angular resolution should be built at high altitude, with the aim of searching for point sources of γ-rays. In particular he estimated that a

flux of $\sim 10^{-7}$ photons cm^{-2} s^{-1} above 1 TeV was expected from the Crab Nebula. To workers at that time the idea seemed beyond the limits of technical feasibility, but it prompted Chudakov and Zatsepin in the Soviet Union to develop searchlight mirror/photomultiplier combinations to search for cosmic ray point sources using the atmospheric Cerenkov light produced by γ-ray initiated air showers. This technique had been pioneered in Britain by Galbraith and Jelley (1953) for the study of more energetic cosmic rays. These searches were not immediately rewarded but in 1972 Stepanyan and colleagues at the Crimean Astrophysical Observatory (CAO), using the Cerenkov method, reported the detection of Cygnus X-3 in a flaring state following the 1972 radio outburst and, on many subsequent occasions, with the 4.8^h modulation of intensity known since the 1968 Uhuru observations at X-ray energies. At this conference γ-ray emission from many objects has been claimed and I have space to review details about only a few of them; results on others will merely be stated.

2.1. Cygnus X-3. By far the most attention has been given to observations of Cygnus X-3 - partly because it is a strong source and visible from the Northern hemisphere - but also because details of its binary nature are reasonably well understood. Above 500 GeV measurements have been reported by 14 independent groups and in addition it has received much theoretical attention. It is believed to be the site of nucleonic acceleration (up to 10^{17} eV/nucleon) and possibly the major cosmic ray source active in our galaxy at the present time. Furthermore, in one of the most exciting announcements made at a cosmic ray conference for many years, the Durham group reported evidence of a pulsar within the source of period 12.5908 ± 0.0003 ms (Chadwick et al, submitted to Nature, July 1985).

Cygnus X-3 has been extensively studied at X-ray energies since its discovery by the Uhuru satellite in 1968. The X-ray emission is modulated in an approximately sinusoidal manner with a period close to 4.8 hours. This period is believed to be associated with the co-rotation of a neutron star and a star of several solar masses. The peak of X-ray emission occurs at a phase $\phi \simeq 0.65$ with respect to the time of X-ray minimum ($\phi = 0$) at which the X-ray intensity is $\sim$ 40% that at maximum. A detailed analysis of the X-ray behaviour, as deduced from EXOSAT observations, has been given by Willingale et al (1985) and the long term behaviour, as observed by the Vela 5B satellite, has been reported by Priedhorsky and Terrell (1986).

Observations above 500 GeV are made using the air-Cerenkov technique (500 GeV - 30 TeV) and with conventional air-shower arrays (30 TeV - 10 PeV; 1 PeV $\equiv 10^{15}$ eV). Typical light curves over the 4.8^h period are shown in Figure 1 for some of the experiments described at this meeting. The light curves show much sharper peaks than the near-sinusoidal emission pattern seen at X-ray energies. In all the data there are peaks close to $\phi \simeq 0.65$, the peak of the X-ray emission. The results at 3×10^{13} eV from the group at the Whipple Observatory, Mt. Hopkins, are of particular interest as they were taken with ultra violet filters during a period close to full moon. The technique has yet to be calibrated so that the energy estimate is only approximate but if it can be further developed it will provide a very useful overlap with the EAS method which comes in at a similar energy. All these data have been

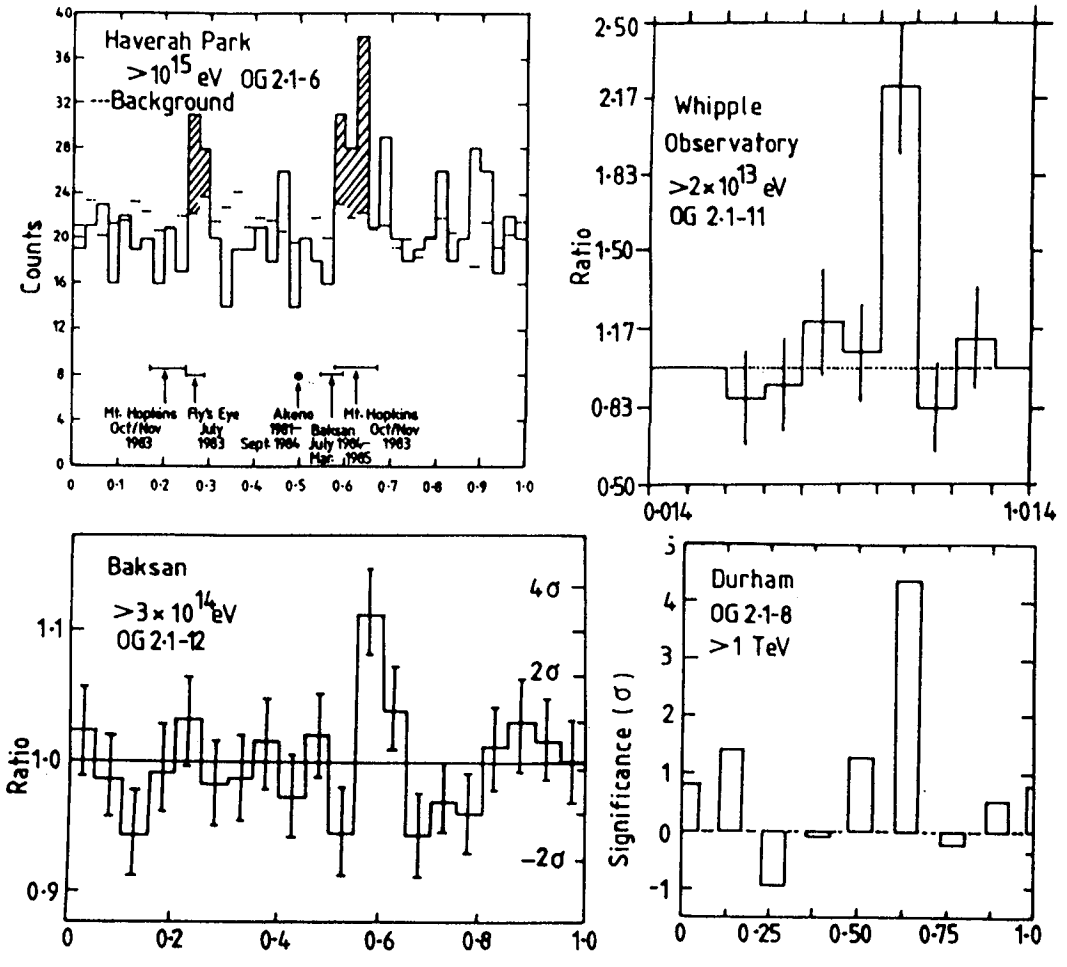

Figure 1: Cygnus X-3 light curves as determined from recent observations at different energies.

analysed using an ephemeris derived by van der Klis and Bonnet-Bidaud (1981) from a number of satellite observations and it is recommended that this ephemeris (or revised versions of it) be used in all data reduction on this source to restrict confusion when comparing results from different experiments.

The integral spectrum of Cygnus X-3 above hard X-ray energies (> 20 keV) to beyond 10 PeV is shown in Figure 2. The X-ray data (Reppin et al 1979, Meegan et al 1979) from balloon flights in October 1977 are represented by integral spectra derived from the published differential spectra. The measurements of Reppin et al are time-averaged over the phase interval 0.18 to 0.60 observed during one 2 hour period of the balloon flight while measurements of Meegan et al, covering the interval 0.45 to 0.91, have been averaged over the 4.8^h cycle to conform with the practice above 500 GeV. The difference in slope and intensity between the two hard X-ray

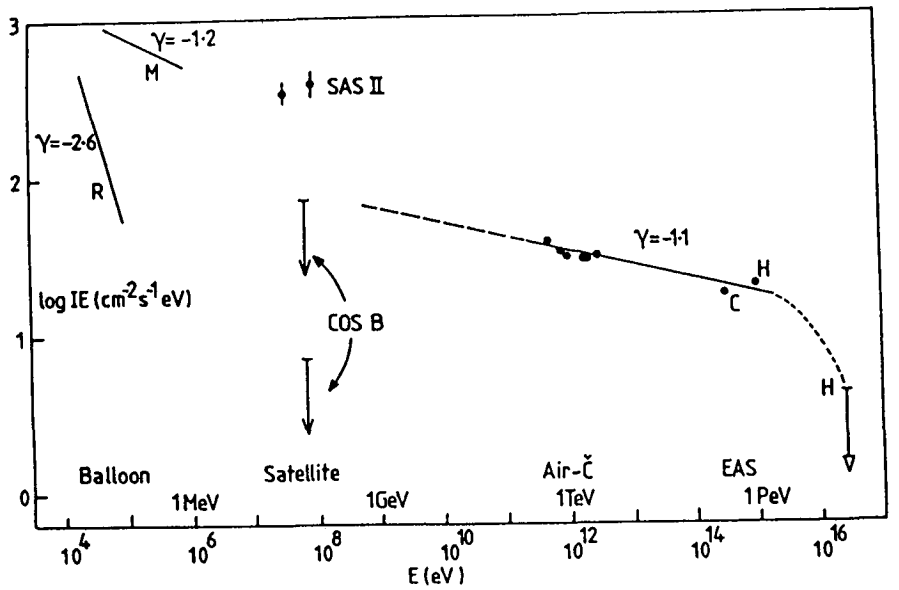

Figure 2: The integral spectrum of Cygnus X-3 above hard X-ray energies. R (Reppin et al 1979); M (Meegan et al (1979); SAS II (Lamb et al 1977), COS B (OG 2.2-2); points near 10^{12} eV (see caption of Figure 5); C: Baksan (OG 2.1-12); H: Haverah Park (OG 2.1-6).

measurements made at different phases in the orbital period is regarded as real (Meegan et al 1979) and, coupled with the known flux variability at lower X-ray energies, complicates the question of what should be the extrapolated flux in the region of the COS B and SAS II experiments. The possibility that the SAS II observations are genuine and conform to a high γ-ray state for Cygnus X-3 during 1973 (R.C. Lamb, private communication) is not excluded from examination of these data although a contrary view has been stressed forcefully by the COS B collaboration (OG 2.2-2) at this conference. All measurements shown above 500 GeV were made post-1979; the 6 points at around 1 TeV are from independent observations (see caption of Figure 5 for details). Above 10^{14} eV the measurements shown are from the Baksan (C) (OG 2.1-12) and Haverah Park (H) (OG 2.1-6) experiments which were nearly contemporaneous (C: July '84 to Feb '85; H: 1984) and for which the energy calibration is reasonably firm. Above 500 GeV the source spectrum is likely to be quite different from the spectrum at the top of the atmosphere as there is the complication of γ-ray absorption ($\gamma + \gamma \rightarrow e^+ + e^-$). At TeV energies optical photons close to the source may suppress the signal (Apparao 1984) while near 10^{15} eV the mean free path for absorption by the 2.7K background ($\lambda \sim 7$ kpc) is less than the lower limit of 11 kpc set to the source distance (Dickey 1984). At intermediate energies we may have to worry about the presence of a significant flux of far-infrared photons in the waveband not explored by the IRAS survey. The energy output of the source is difficult

to assess in view of these uncertainties. However, the slope of the spectra is very flat above 1 TeV and the flux above 1 PeV is $\simeq 10^{37}$ erg s^{-1}.

It is difficult to summarise all of the data above 500 GeV succinctly as one possibility which has emerged at this meeting is that Cygnus X-3 may be time-variable both in the nature of its light curve and its amplitude. It is, of course, disappointing (and powerful material for the sceptics) to discover that this remarkable object is time-variable but I believe this to be an experimental fact (and one which sets severe demands on the type of experiment which we should be thinking of doing in the future).

Before addressing the time-variability evidence I will attempt to summarise data on the light curve in broad terms. Near 1 TeV recent measurements (post-1980) have tended to show a strong, relatively broad, peak ($\Delta\phi \lesssim 0.1$) near $\phi \simeq 0.6$ although there have been reports of significant effects at $\phi \simeq 0.2$, particularly in the pre-1980 data of Stepanyan's group. There is some evidence that when a signal is seen near $\phi \simeq 0.2$ the initiating γ-rays are of higher energy than those seen at $\phi \simeq 0.6$. Above 10^{15} eV emission has been seen near both $\phi \simeq 0.2$ (1976 - 1983) and at $\phi \simeq 0.6$ (1984) and the peak of emission appears to be narrower ($\Delta\phi < 0.1$ and sometimes ~ 0.03) than at lower energies. The phase information is likely to be of major importance in modelling of the source and the available data are summarised in Figure 3. The evidence for emission near $\phi \simeq 0.25$ and $\phi \simeq 0.65$ is compelling. The significance of each signal (in sigma) has been taken directly, or estimated, from the published light curves. In the case of the Kiel experiment (K) (Samorski and Stamm (1983a)) account has been taken of their 4.4σ detection of the source before phase analysis. All data have been analysed using the van der Klis/Bonnet-Bidaud ephemeris except for the Akeno (A) and Kashmiri data (B) for which the probable phase adjustments are indicated by arrows.

I have also marked on the diagram the phase band in which the Soudan group (Marshak et al 1985) and the NUSEX group (Battisoni et al OG2.1-3) have reported a peak in a time-modulated signal seen in their underground muon detectors. Clearly whatever is the cause of this signal it cannot be some anomaly in γ-nucleon cross-sections or there would be phase coincidence. However if the mechanism suggested by Stecker et al (1985) works, and the signal is enhanced beyond straightforward expectation, it might be worth looking for the neutrino events expected at large zenith angles in the underground data in narrow phase windows centred on the γ-ray phases.

The most exciting result reported during the sessions on Cygnus X-3 was that of the Durham group (Chadwick et al 1985) who claim to have detected within the TeV emission the long-sought pulsar in the Cygnus X-3 system. Figure 4 is from their discovery preprint and shows the probability of agreement with a uniform distribution as a function of period for a 7 minute stretch of data near $\phi \simeq 0.65$ taken on 12 Sept 1983. The evidence for a pulsar of period 12.5908 ms looks strong and is supported by similar data taken on 2 October 1983. Both observations were made close to the time of maximum of the 18.7 day period claimed

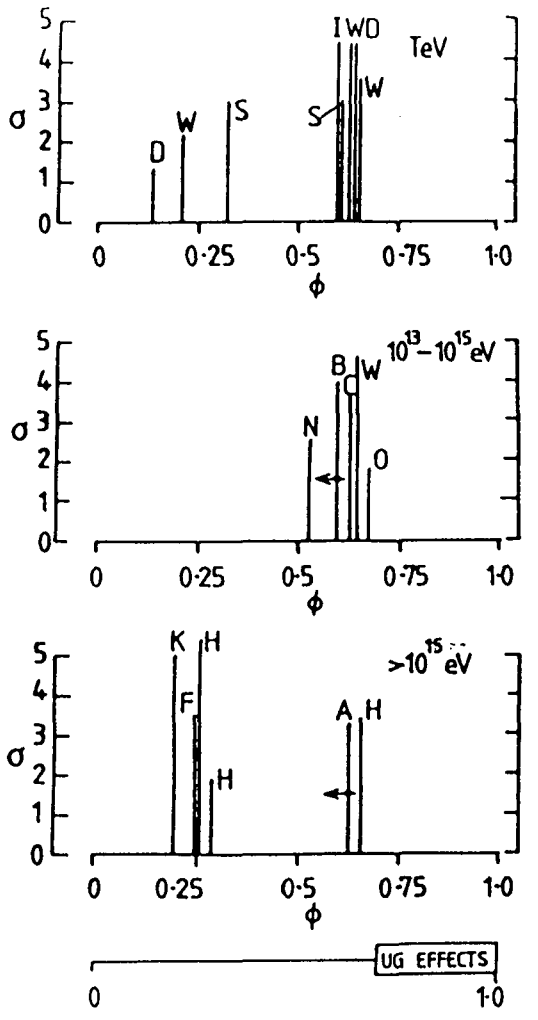

Figure 3: Summary of phase of maximum γ-ray emission from Cygnus X-3. D (Durham), W (Whipple Observatory), S (Stepanyan), I (Riverside/ JPL/Iowa State), N (Plateau Rosa), B (Khasmir), C (Baksan), O (Ooty), K (Kiel), F (Fly's Eye), A (Akeno) and H (Haverah Park). The phase of the underground muon signal claimed by Soudan and NUSEX is shown by 'UG effects'.

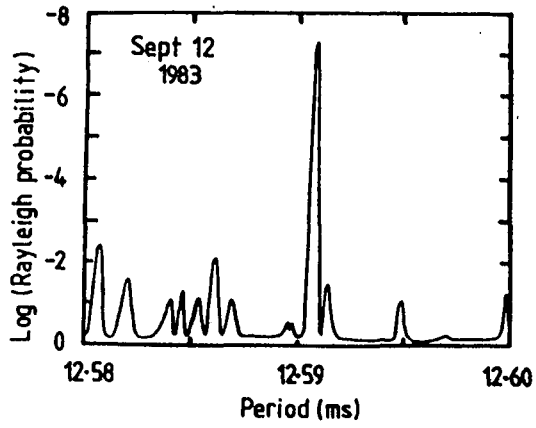

Figure 4: The chance probability for periodicity in 450 events containing the count rate excess from Cygnus X-3 as a function of trial period (from Chadwick et al 1985).

for the source (Bonnet-Bidaud and van der Klis 1981). This result, stated to have a probability of $< 3.10^{-7}$ of arising by chance, obviously supplies a major constraint to models of particle acceleration within the source.

The phase picture (Figure 3) is reasonably tidy but the same cannot be said of the situation with regard to flux. The experiments used for Figure 3 have all (with the exception of the Whipple Observatory result at 3×10^{13} eV) provided intensity estimates (so far only in integral form because of the limited statistics) and these are shown in Figure 5. Clearly there is considerable scatter between the results reported by different groups at a particular energy. Two major reasons for the scatter are poor statistics and uncertain energy calibration; these difficulties will surely disappear in time.

An extreme explanation for the scatter in Figure 5 has been advanced by Bhat et al (OG 2.10-10) who suggest - largely on the basis of their own measurements with an uncollimated light collection system - that the flux above 10^{13} eV is decaying exponentially with a time constant of 1.7 ± 4 years. Most models of Cygnus X-3 couple the presence of TeV γ-rays to the production of 10^{15} eV γ-rays, through what Hillas (1984) has described as an extensive stellar shower, and it is hard to reconcile the decay proposed by Bhat et al with the relative constancy of the TeV signal between 1972 and 1985. Factors of 2 or 3 variations have been seen but a change of the magnitude proposed (> 450) over this period is not credible. Furthermore above 10^{15} eV the Haverah Park group (OG 2.1-6) have observed essentially the same flux between 1979 and 1982 as in 1984 (but at a different phase).

There is, however, convincing evidence of a less dramatic nature for amplitude and phase variations on a time-scale of months. The Mt. Hopkins group observed a 4.4σ effect at $\phi \simeq 0.6$ in the Oct/Nov 1983 dark period but no signal was detectable with identical equipment and similar observing conditions during the Nov/Dec 1983 dark period (Cawley et al 1985). This group reported a similar effect in 1981 (Weekes et al 1981). The Fly's Eye group, working at 10^{15} eV, found a 3.5σ effect during 9-13 July 1983 at $\phi \simeq 0.25$ but observing nothing during the dark periods of August and September 1984. The Haverah Park group observed a change of the preferred phase of emission between 1979-1982 ($\phi \simeq 0.25$) and 1984 ($\phi \simeq 0.66$, with weak emission at $\phi \simeq 0.29$). It is interesting to note that the Mt. Hopkins result was obtained just after the 1983 Sept/Oct radio flare and that similar enhancements of TeV emission have been reported previously after other flares (Vladimirsky et al 1973 (following the famous 1972 flare) and Fomin et al 1981 (after the 1980 flare)).

Preliminary analysis of an observation of a flare from Cyg X-3 in which a flux level of 6×10^{-11} cm^{-2} s^{-1} was measured above 3×10^{13} eV was reported at this meeting by the Fly's Eye group. This event was seen on 16 June 1985 during one of 13 nights of observation. Even at this level of intensity existing air shower arrays would have great difficulty in detecting such a signal: an array of 30 m radius and angular resolution 10^{-2} sr, sensitive above 300 TeV would expect to record only about 3 Cygnus events above a general cosmic ray background of about 1 event! The Fly's Eye event did not show pulsed emission and may be of the

genre of the shorter flare transients observed by Nesphor et al (1979), Weekes (1982) and the Durham group (Gibson et al 1982).

Figure 5: Time averaged integral γ ray spectrum above 5×10^{11}eV from Cygnus X-3.

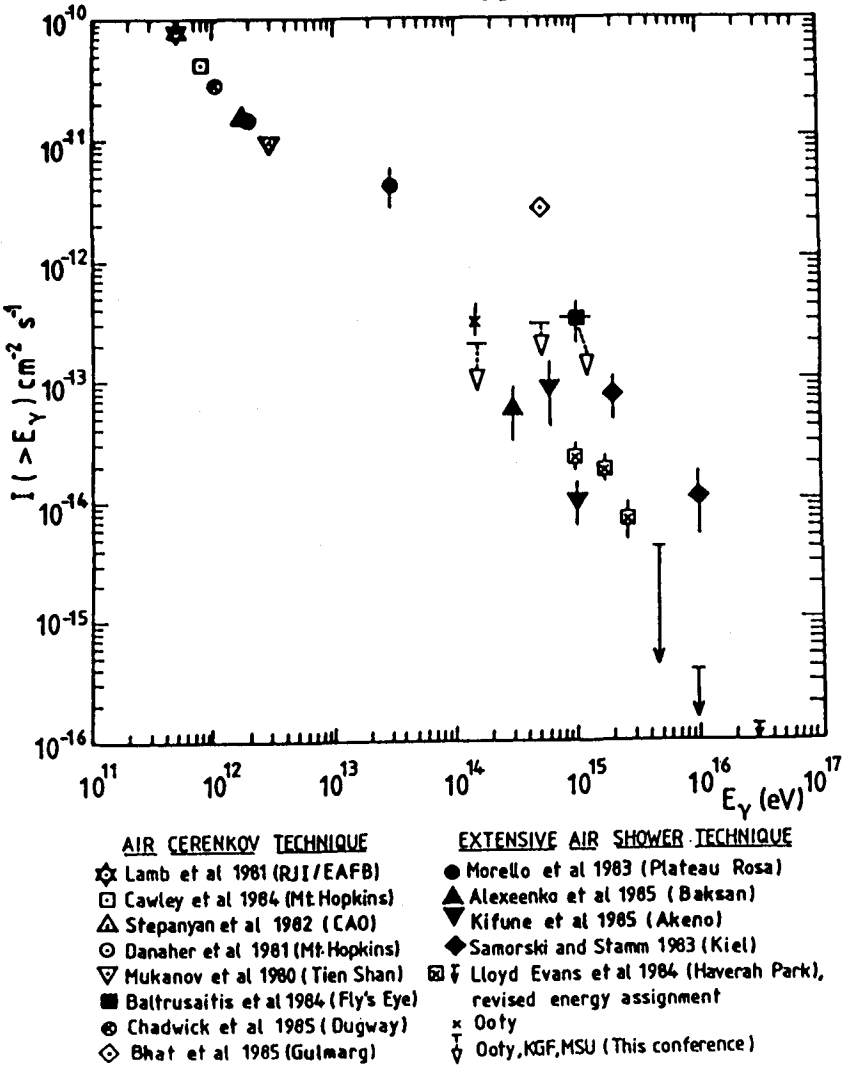

I know of no group who have observed Cygnus X-3 and reported a null result at an intensity level which contradicts those shown in Figure 2 and conclude that this source is indeed a γ-ray emitter above 500 GeV and probably up to 10 PeV. There remain, however, some questions to be answered about data from the PeV region before the matter can be regarded as being finally settled; these are:-

(a) Muon content of γ-ray showers:- The Kiel group (Samorski and Stamm 1983b) reported that their Cygnus X-3 events had a muon content $\sim$ 80% that of 'normal' showers, a result which was in sharp contradiction with theoretical expectation and is now questioned further by data from the Akeno group (OG 2.1-5) who were able to detect Cygnus X-3 only after selection of events having a muon/electron ratio less than 1/30 of that found in the bulk of showers. The Nottingham group (OG 2.1-4), hampered by poor statistics, a poor signal/noise ratio, and the small area (10 m^2) of muon detector presently available at Haverah Park, have been unable to make a statement about the muon-content in the small number of Haverah Park events for which there is coincident data. It is not clear how to resolve this question but the possibility that some of the signal seen in the Kiel detector (which is not a tracking detector) may be due to 'punch-through' of very low energy photons ($\lesssim$ 10 keV) does not yet seem to have been eliminated. Some relevant experimental data have been discussed (HE 4.5-1) by the Nottingham group but more are needed.

(b) Age selection of γ-ray showers:- The Kiel group adopted the selection requirement that the shower age, s, should be greater than 1.1 in the expectation of enhancing the γ-ray content of their sample. A similar cut was used by the Adelaide group in their detection of Vela X-1 (Protheroe et al 1984). The justification for this approach is not clear and indeed the Ooty group (OG 2.6-8) find their most significant signal ($\sim 1.5\sigma$ at $\phi = 0.675$) when showers of all ages are used. However the Ooty array is at a depth of 800 g cm^{-2} and it may be that the age restriction is effective for data taken at sea-level. Further theoretical study of this problem would be helpful.

(c) The source ephemeris:- For their discovery paper the Kiel group used the ephemeris of Parsignault et al (1976) and had not corrected their data to the heliocentre. Subsequent reanalysis after heliocentric correction and with the van der Klis/Bonnet-Bidaud ephemeris broadens the peak in phase and shifts it to the interval 0.1 to 0.3. However, the 4.4σ detection before phase analysis is unaffected and overall the Kiel result remains significant.

An overview of the Cygnus X-3 situation, with particular emphasis on what can be inferred about the production of γ-rays within the source, is available in the written version of the 'Highlight Talk' of A.M. Hillas elsewhere in this volume. Theoretical studies of the object are reviewed by V.S. Ptuskin in his rapporteur paper.

2.2. The Crab Nebula and Pulsar (PSR 0523+21). As usual in γ-ray astronomy the Crab Nebula and pulsar have attracted considerable attention. Prior to this conference the Durham group (Dowthwaite et al 1984a) had reported strong evidence of a pulsar signal from the Crab above 1 TeV with a light curve which peaked in coincidence with the main pulse of the radio emission. In a further report (OG 2.3-9) they lay particular stress on the extreme narrowness (< 0.4 ms) of the emission peak. This result is shown in Figure 6 together with the light curve at 100 MeV from COS B (Wills et al 1982) and the new result from the Riverside/JPL/Iowa State group (OG 2.3-3) at 200 GeV. The latter light curve also exhibits a

single peak although a broader one than found by the Durham group. The fluxes reported by both groups (RJI (> 200 GeV) = $(2.5 \pm 0.8) \times 10^{-11}$ cm^{-2}s^{-1} and Durham (> 1 TeV) = $(7.9 \pm 1.8) \times 10^{-11}$ cm^{-2}s^{-1}) are compatible.

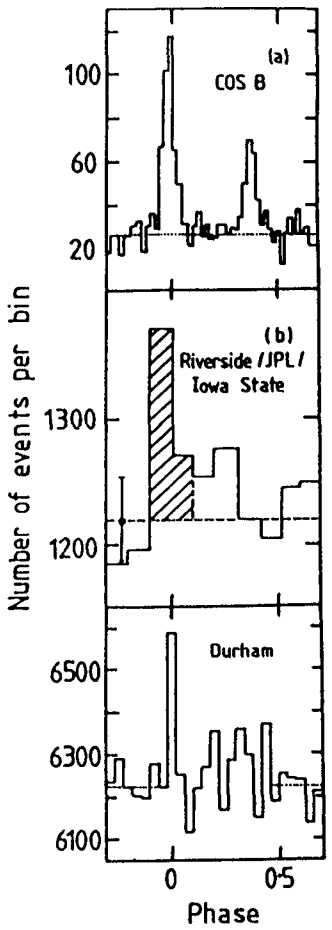

Figure 6: The light curve of PSR 0523+21 as measured at 100 MeV (COS B), 200 GeV (Riverside/JPL/Iowa State) and 1 TeV (Durham). For references, see text.

The Crab pulsar has also been studied by the Tata group (OG 2.3-4) at $\sim$1 TeV. Results were reported orally. During an extended series of observations in 1984-85 they were able to detect no pulsed signal within the sum of their data. However between 1711 and 1726 UT on 23 Jan 1985 they detected pulsed emission at the level of 5.1σ with the emission peak coincident with the radio peak. This group have also reported (OG 2.3-4/5) the continued detection of 'microbursts' from the Crab first discussed at the Bangalore conference. A microburst is defined to be the occurrence of 4 consecutive events with less than 1.5 ms between successive events. Over 100 such microbursts have been detected in 57 hours at a rate more than twice the background rate. These detections have not been replicated at Mt. Hopkins. The Tata group are continuing observations with two similar detector systems separated by 11 km.

Above 400 GeV the Mt. Hopkins group (OG 2.3-1), using a new algorithm to reject non γ-ray events, have reported a convincing (5.6σ) DC signal at a flux level of 6×10^{-11} cm^{-2}s^{-1}. Above 3×10^{13} eV Morello et al (OG 2.2-12), using conventional air shower techniques, have obtained a DC upper limit of 10^{-11} cm^{-2}s^{-1}. At higher energies the Tien Shan group (OG 2.3-2) have used the muon-poor technique to optimise a γ-ray signal from the Crab direction ($\alpha, \delta \pm 7.5^{o}$) above 3.5×10^{14} eV and 5.5×10^{14} eV. These results, based on 12 events, are plotted in Figure 7 together with the flux reported above 10^{16} eV by the Lodz group (Dzikowski et al 1981) and upper limits obtained in other experiments. Also included is a typical pair of data from the earlier Fly's Eye experiment (Boone et al 1984) in which emission was observed (3.1σ) on 9 December 1980 but not during February 1981. Even the very hard ($\gamma \simeq 0.8$) spectrum inferred from the Tien Shan/Mt. Hopkins result cannot be reconciled with the Lodz claim which is also strongly contradicted (factor of 200) by Haverah Park work (OG 2.6-9). Future studies with the improved Haverah Park γ-ray array (OG 9.4-7) in which a pulsed detection will be sought may clarify this situation before the next

conference. Note, that the angular resolution in the Tien Shan, Lodz and Fly's Eye experiments are much poorer than that at the Mt. Hopkins so that there is no convincing evidence that the signals claimed by these groups are associated with the nebula.

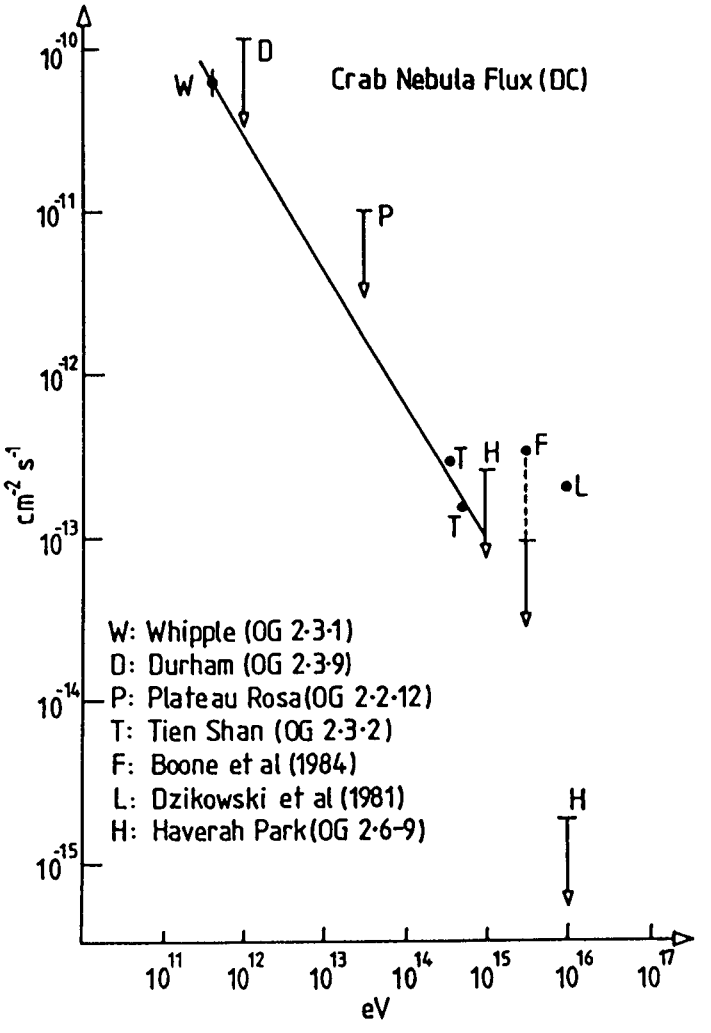

Figure 7: The integral energy spectrum of γ-rays from the Crab nebula. The solid line is an eyeball fit to W and T and has $\gamma \simeq -0.8$.

2.3. Observations on other sources. Many other sources have been observed using the techniques of very high energy ($\sim$ 1 TeV) and ultra high energy γ-ray astronomy. A number of upper limits have been set (for example the Durham group (OG 2.3-9) have reported upper limits at about 2×10^{-11} cm^{-2} s^{-1} on 7 radio pulsars) but there are 8 objects (in addition to Cygnus X-3 and the Crab) from which positive effects have been claimed; two of these (both in the Southern hemisphere) have been examined only above 1 PeV. Details of the observations are given in Table 1.

Lamb and Weekes (1985) have suggested that 4U0115+63 (a transient X-ray source) is to be identified with Cas γ-1, a TeV source reported previously by the CAO group (Stepanyan et al 1972). This proposal further emphasises Stepanyan's role in founding very high energy γ-ray astronomy. The Vela pulsar (PSR 0833-45) appears to be variable at TeV energies but its detection is probably secure. Of the sources in this list which have been detected above 1 PeV there is need for confirmations in all cases. Her X-1 was not observed by the Durham group in an observing period contemporaneous with the Fly's Eye detection. There is some evidence in the Chacaltaya data (OG 5.3-2) to support the Vela X-1 detection by the Adelaide group; 11 events are seen in a box ($\Delta\alpha = 30^{\circ}$, $\Delta\delta = 20^{\circ}$) centred on the source when 5.2 are expected. A phase analysis is not supportive but the ephemeris cannot be extrapolated to 1967 (the time of the Chacaltaya observations) with confidence. LMC X-4 is reported above 10^{16} eV; the significance is claimed at 1% and the source would be 20 times as powerful as Cygnus X-3.

Table 1

Summary of detections of sources other than Cyg X-3 and Crab Nebula

Object	Reference	Significance/chance probability at ∿ TeV	at ∿PeV	Comments and Periodicity
4U0115+63	Durham (OG 2.6-11)	2.5×10^{-6}	-	Pulsar: 3.6 s
	CAO (Stepanyan et al (1972))	3.9σ on Cas γ-1	-	DC Cas γ-1 ≡ 4U0115+63 (Lamb & Weekes 1985)
PSR 1953	Durham (OG 2.6-11)	5.4σ	-	Pulsar: 6.1 ms Binary: 117.3 days
PSR 0833-45	SAO/Sydney (Grindlay et al 1975a)	Variable	-	Pulsar: 89 ms
	Tata group (OG 2.3-10)	99.3% CL		
M31	Durham (Dowthwaite et al 1984b)	1% $2.2 \pm 0.7 \times 10^{-10} cm^{-2} s^{-1}$ at 1 TeV	-	DC not confirmed by Mt. Hopkins
	Mt. Hopkins (OG 2.7-3)	$< 1.6 \times 10^{-10} cm^{-2} s^{-1}$ at 400 GeV		
Her X-1	Durham (OG 2.6-11) (Dowthwaite et al 1984c)	7×10^{-5} (17 April 1983)		Short bursts at pulsar period: 1.24 s
	Mt. Hopkins (OG 2.2-9)	2×10^{-4} (4 April, 5 May 1984)		
	Fly's Eye (OG 2.2-7) (Baltrusaitis et al 1985)	-	2.10^{-4} (11 July 1983)	Durham observation contemporaneous with Fly's Eye saw no signal
Vela X-1	Adelaide (Protheroe et al 1984)	-	10^{-4}	Binary: 8.96 d
LMC X-4	Adelaide (OG 2.6-10) (Protheroe & Clay 1985)	-	1%	Binary: 1.4 d
Cen A	SAO Sydney (Grindlay et al 1975b)	4.5σ (> 10^{11} eV)		DC
	Adelaide (Clay et al 1984)	-	2.7σ (10^{16} eV)	DC, but ultra high luminosity unless IG magnetic field is low (<< 10^{-7} G)

I have not listed Geminga (2CG195+4), the brightest unidentified source in the COS B catalogue, in Table 1. The detections reported near 1 TeV (OG 2.4-2, OG 2.4-5) are inconsistent and unconvincing and no DC or pulsed signal has been detected by the Mt. Hopkins group at 400 GeV (OG 2.4-4). Recently Buccheri et al (1985) have pointed out some of the statistical pitfalls that await the unwary who study this source and at the moment there appears to be no firm evidence at low energy of periodicity near 59.5 sec with which to support the statistically weak TeV claims.

2.4. Summary of sources above 1 TeV. There are at least 6 sources (Cyg

X-3, Crab nebula and pulsar, Her X-1, 4U0115+63, PSR 1953 and the Vela pulsar) for which the claimed detections near 1 TeV can be said to be quite firm. At $\sim$1 PeV and above confirmatory detections have been made only for Cyg X-3 (and there remain some unanswered questions, see section 2.1). Of the 6 strongest candidates two are pulsars and four are X-ray binaries. In the case of the X-ray binaries the similarity of their light curves (Figure 8) has led to the suggestion that all such objects are TeV γ-ray emitters (see, for example, A.M. Hillas, Highlight Talk). The light curve observed at higher energy by the Fly's Eye group is quite different with a peak at ϕ = 0.75 in the 1.24 s period.

Models of proton 'beam dumps' in precessing accretion disks are being developed by many authors to explain the complex features of these sources (Brecher and Chanmugan, OG 2.2-5; Eichler and Vestrand, OG 2.2-8).

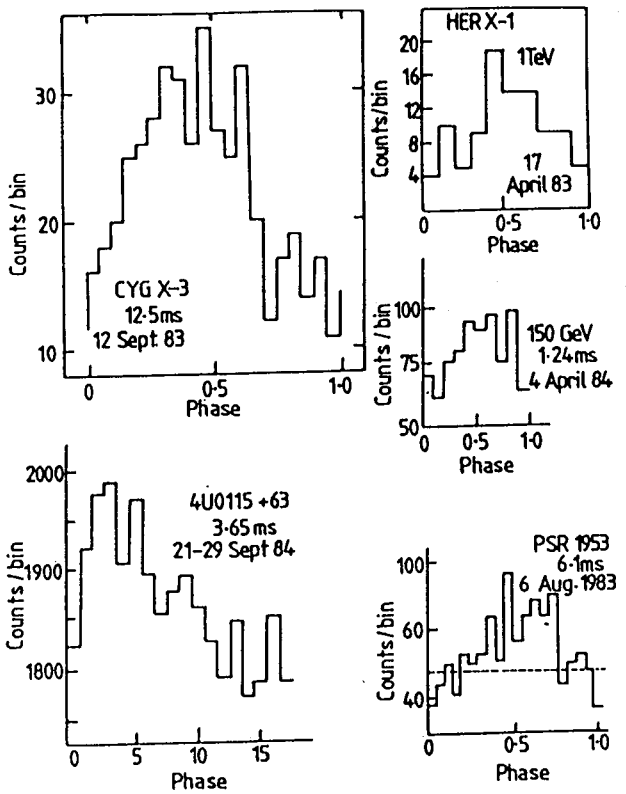

Figure 8: The light curves of TeV γ-rays from 4 binary X-ray pulsars. The period of each pulsar and the date of each observation is shown in the diagram. All observations (except Her X-1 on 4 April 1984) are by the Durham group. See Table 1 for references.

2.5. The future of γ-ray astronomy above 1 TeV. The future success of γ-ray astronomy at $\sim$1 TeV seems assured. New experiments are funded for the Durham group (in Australia) and the Potchefstroom group (South Africa) to survey the Southern Hemisphere sources and there are many plans to extend existing facilities and build new ones in the Northern Hemisphere.

While TeV astronomy is a healthy youngster, by contrast PeV astronomy is only in its infant stages. Above 100 TeV a few air shower arrays, having angular resolution approaching 1^{o} and of area $> 10^{4}\ m^{2}$, are operating, or soon will be, but it is important to recognize that $10^{4}\ m^{2}$ is only about the area monitored by existing TeV telescopes where the flux is at least 100 times higher. Thus, with the exception of the Fly's Eye instrument, these arrays are too small for serious study of short time-scale phenomena which have proved such a rich field of work in astrophysics since the discovery of pulsars in 1968. By 1987 (the Moscow Conference) I predict that Cygnus X-3 will be clearly established as a PeV source but the rest of the sky will be strewn with doubtful '3 sigma' detections where confirmation has been difficult to get because of the limited sky region ($\pm\ 40^{o}$ in declination) available to any detector, poor statistics, and time variability. Lest such a situation continue (and the whole subject became faintly disreputable) there should be a concerted effort, probably requiring international collaboration, to build a number of large γ-ray facilities at different latitudes. By large I mean about $1\ km^{2}$ (with $> 10^{3}$ detectors); such an array would detect about 10 γ-rays above 3×10^{14} eV from Cygnus X-3 per 4.8 hour cycle. (The present world total of γ-rays above this energy is probably less than 200.) Hillas pointed out to me (and I know others have realized it too) that the South Pole is an ideal place for seeing X-ray binaries: there are plenty to see, they are 'up' all day and the altitude (~ 2500 m) is about right! With such areas we may even anticipate detecting sources which have not been seen at other wavelengths (as did COS B).

Why is PeV γ-ray astronomy of more importance to cosmic ray physics than TeV astronomy? The answer is simple. I suspect that many clever theorists can explain TeV emission through electron synchrotron or curvature radiation but none (yet) has suggested that PeV γ-rays can arise from other than π^{o}-decay. We thus have the prospect of taking a major step in solving the cosmic ray origin problem while at the same time linking our subject very securely to the mainstream of astrophysics: I hope this is a chance we will not miss.

3. Can γ-rays explain cosmic ray anisotropy? Soon after the early reports of ultra high energy γ-ray emission from Cygnus X-3 and other objects Wdowczyk and Wolfendale (1983) pointed out that as the γ-ray spectra from various sources appeared to be flatter than the cosmic nuclei spectra then the γ/p ratio would increase with energy so that much of the anisotropy, hitherto attributed to the nucleonic component, might be due to γ-rays. At this meeting (OG 5.4-11) they have extended and quantified their discussion. Below $\sim 10^{13}$ eV it seems probable that the observed anisotropy ($\sim 0.1\%$) is due to the nucleonic component because the majority of measurements have been made using underground detector systems. Between 10^{13} and 10^{15} eV observations have usually been made at mountain altitude so that the nature of the primaries causing the observed anisotropy is open and γ-rays might contribute. Alexeenko and Navarra (1985) have obtained a remarkably good fit to the anisotropy observed between 10^{13} and 10^{14} eV by extrapolating the diffuse γ-ray flux measured by the COS B satellite. The best experimental data in this energy range are those from the Baksan experiment (Alexeenko et al 1984) from which the following 1st and 2nd harmonics in right

ascension have been reported:-

$a_1 = (5.8 \pm 0.3) \times 10^{-4}$ with maxima at $\theta_1 = 1.2 \pm 0.2$ h

$a_2 = (1.6 \pm 0.3) \times 10^{-4}$ with maxima at $\theta_2 = 6.1 \pm 0.5$ h in sidereal time.

The fit achieved is shown in Figure 9; there is no normalisation so that the agreement between prediction and observation is particularly striking. However, until more is known about the spectrum of the ultra high energy γ-ray sources, this interpretation of the observed anisotropy can only be considered as tentative.

Indeed it is not entirely clear what the characteristics of a γ-ray anisotropy above 10^{13} eV should be. Very recently Bhat, Kifune and Wolfendale (1985) have suggested that the latitude dependence may be a complex function of γ-ray energy. For example at 7×10^{15} eV severe synchrotron losses suffered by electrons in the magnetic field of the galactic disk lead to the prediction that the γ-ray flux at b = 0° will be nearly an order of magnitude lower than at b = 30°; these statements apply to longitudes near 0°. Better data are needed to test these predictions.

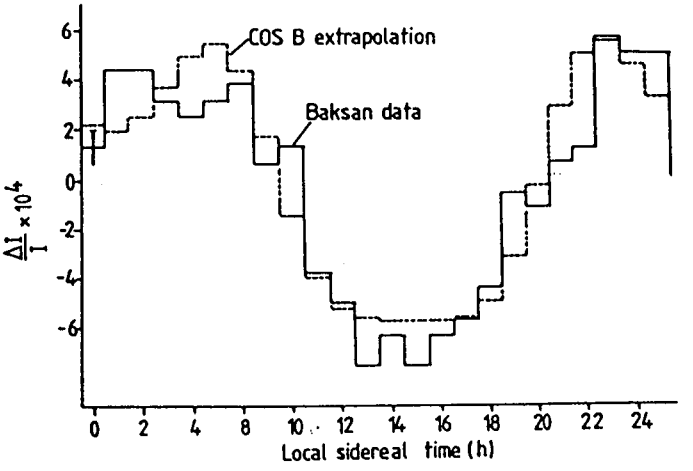

Figure 9: (after Alexeenko and Navarra 1985)
The cosmic ray sidereal daily variation, shown as departures from the mean, is compared with the extrapolated COS B measurement of the diffuse flux from the galactic plane.

To determine γ-ray anisotropies with certainty requires experiments which are sufficiently sensitive to isolate those 10^{-3} or so of events which are γ-ray initiated from the general cosmic ray background. The approach which has usually been adopted - but about which there must now be some doubt in view of the μ-poor/Soudan-effect controversy with regard to Cygnus X-3 - makes use of the expectation that γ-ray initiated showers are deficient in muons by comparison with those initiated by nuclei. Some success with this technique has been achieved in the case of Cygnus X-3 by the Akeno group (OG 2.1-5) as mentioned above. At this meeting the Lodz group (OG 2.6-7) (using 14 m^2 of muon detector with a 0.5 GeV threshold and 40 m^2 with 5 GeV threshold) have claimed an excess of events above expectation in the latitude range $|b < 17.5°|$ when showers are

selected with 0-3 muons. The effect is an excess of 234 events over about 2300 expected in this latitude strip. Formally this is a 5σ signal but the latitude strip was not picked 'a priori' and appears to have been chosen to maximise the effect. Also it is not clear that normalisation of the experimental histograms, made in the latitude interval 17.5 - 77.5°, is justified. These data are shown in Figure 10; the effect is confined to showers with electron number $> 10^6$ ($E \gtrsim 5.10^{15}$ eV).

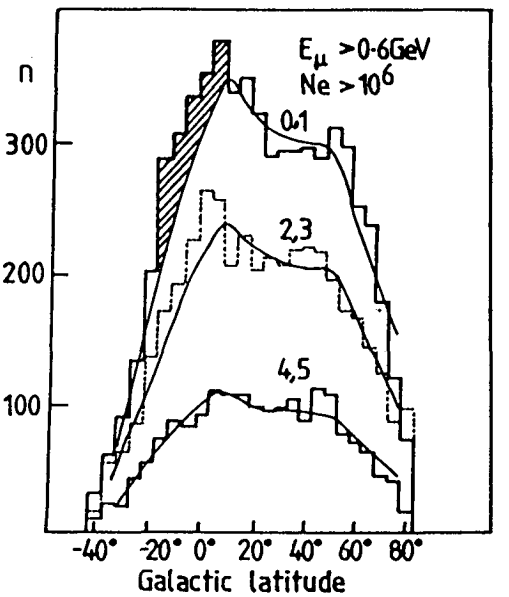

Figure 10: (from OG 2.6-7) Galactic latitude distribution of showers with $N_e > 10^6$ and various numbers of muons > 0.6 GeV. The excess claimed as due to γ-rays is shaded on the 0, 1 muon histogram.

A similar 'μ-poor' approach was developed many years ago at Chacaltaya using the 60 m^2 muon detector located there. Updated results have been reported here (OG 5.3-2) for $E \sim 10^{15}$ eV. A peak, based on 269 low-mu showers, is noted at RA = 210° when data are summed over the 70 degrees of declination scanned in the experiment. It is not totally compelling (confidence level = 91%) in the absence of any 'a priori' expectation that it should be seen in that direction. The authors note that the preferred direction is close to the direction of the maximum of the 1st harmonic for all showers recorded with $3 \times 10^{16} < E < 10^{18}$ eV. The Yakutsk group (OG 5.1-14) using 108 m^2 of muon detector (threshold 1 GeV) have begun a study of the muon content of showers produced by primaries $> 10^{17}$ eV. So far from 10^3 events they have identified one in which the muon content is 12 times less than normal. The galactic co-ordinates of the primary are (153°, -8°) and, if really a γ-ray, the intensity is about 3×10^{-14} m^{-2} s^{-1} sr^{-1}.

An alternative explanation to the γ-ray proposal for explaining anisotropies close to the 'knee' in the energy spectrum has been forwarded by Clay (OG 5.4-10). He shows that for data near 10^{15} eV the peaks in the distribution lie close to the 'spiral-in' direction on the galactic plane while the two measurements in the Southern Hemisphere exhibit troughs in the 'spiral-out' direction. He interprets this observation as implying that cosmic ray flow at these energies is diffusive with its source in the inward spiral arm direction.

4. Primary mass composition > 1 TeV. Below about 100 TeV/nucleus the primary mass composition can be measured rather directly using balloon or satellite exposures. At higher energies inferences about the

composition have to be drawn from the properties of air showers observed at ground level or from muons observed underground. The information from direct measurements is summarised in Table 2 where a measure of the mean mass, $< \ln A >$, which is appropriate for discussions of shower data about 100 TeV (Linsley 1983; Linsley and Fichtel OG 5.4-4), has been adopted.

Table 2

Mass composition above 1 TeV from direct measurement	Energy (TeV)	$< \ln A >$
	1	1.50
	10	1.68
	100	1.57 ± 0.3

The first two data are from the summary of Juliusson (1975); the 100 TeV estimate is from the direct but limited statistics exposures of the JACEE project (Burnett et al 1982). There is no evidence for any enrichment of the primaries by heavy nuclei between 10 and 100 TeV and the enrichment between 1 TeV and > 10 TeV can be understood either in terms of a diminished path length at higher energies, resulting in reduced fragmentation of the heavier nuclei, or in terms of a change in the source spectrum. The experimental situation between 1 and 100 TeV has changed little since the last conference.

As a basis for discussion of the mass composition above 100 TeV I have reproduced in Figure 11 part of a figure from OG 5.4-4 (Linsley and Fichtel). Here $< \ln A >$ is shown as decreasing above 2×10^6 GeV, where the value is about 1.7, to a value near 0 (pure protons) above 10^7 GeV. Although the bulk of the data come from an interpretation of one experiment (Acharya et al 1983 and OG 5.2-10) the conclusion is supported by reviews of the variation of depth of shower maximum (X_m) with energy (e.g. Kvashnin et al 1983) made before this meeting which showed that the elongation rate, the rate of increase of X_m with energy, changed from about 120 $g cm^{-2}$/decade below 10^{17} eV to about 60 $g cm^{-2}$/decade above 10^{17} eV. Such a change requires a decrease in $< \ln A >$ of about 1.5 between 10^{15} and 10^{17} eV.

Further support for a mass composition lighter above 10^{15} eV than below comes from an analysis made by Hillas (1984a) of the integral spectrum of shower size (N) observed at different atmospheric depths. He has shown that an explanation of the absolute rates and the shape of the shower size spectrum can be given in terms of a bimodal mass model in which the Fe-spectrum steepens from $\gamma = 2.7$ to 3.3 at 1.8×10^{15} eV/nucleus and the proton spectrum steepens from 2.7 to 3.1 at 5×10^{15} eV. Above 10^{15} eV these spectra, with 40% protons, fit the data on size spectra from depths in the range 540 - 1030 $g cm^{-2}$. Note that the Fe-spectrum steepens before the proton spectrum on this model, counter to the frequently discussed rigidity model in which the Fe and proton spectra steepen at the same rigidity. On the Hillas model the knee at 5×10^{15} eV reflects a feature of the proton spectrum, not the Fe-spectrum. If the proton knee is due to rigidity dependent-galactic leakage then the break in the Fe-spectrum must be explained some other

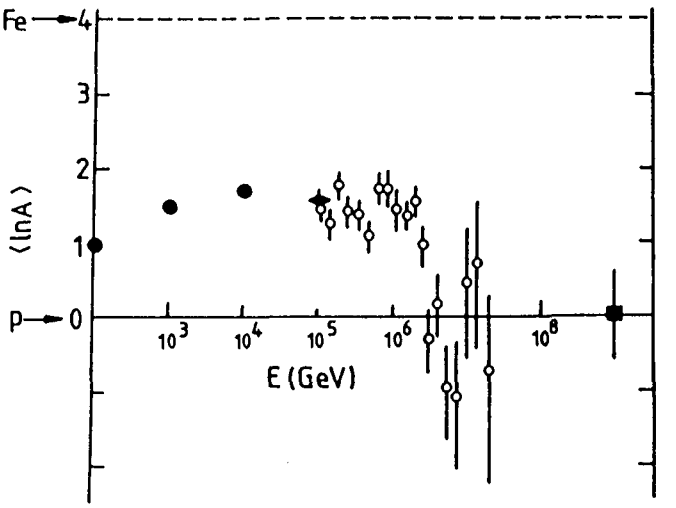

Figure 11: (from OG 5.4-4) The energy dependence of $\langle \ln A \rangle$ closed circles, balloon experiments; diamond, JACEE; open circles, Acharya et al (1983); square, Linsley and Watson (1981).

way. Hillas proposes that the Fe-knee may be intrinsic to the source. One possibility which has been explored in OG 5.2-10 is that the break in the iron-spectrum (and in the spectra of nuclei down to He) arises from photo-disintegration. In this paper Acharya et al confirm Hillas's analysis of the number spectra data and supplement their interpretation with their measurements of the number of 220 GeV muons in showers of size $10^4 < N < 10^7$. The variation of N_μ (> 220 GeV) with N is believed to be nearly twice as sensitive to changes in mass composition as the variation of N_μ (< 10 GeV) with N, which is more often measured (Grieder 1983). Acharya et al find a discontinuity in their N_μ-N plot which is explicable in terms of a break in the Fe-spectrum at about 3×10^{15} eV. Other support for a lighter composition above 10^{16} eV come from work at Yakutsk: Dyakonov et al (OG 5.1-13) claim >85% protons above 10^{18} eV while Glushkov et al (OG 5.1-14) have evidence for >40% protons beyond 10^{17} eV. Similarly from an analysis of N_μ-N data Muraki (OG 5.1-12) has concluded that Fe does not dominate between 2.10^{16} and 2.10^{17} eV.

The discussion of the last two paragraphs might be taken to imply that there is a consensus that the mass composition is lighter above 10^{15} eV than below it. While that is my own view I must point out that there are several papers in these proceedings which argue the counter view, namely that Fe-nuclei begin to dominate beyond 10^{15} eV, i.e. it is an iron-knee rather than a proton-knee. For example the Adelaide group (OG 5.2-11) have measured the lateral distribution of Cerenkov light produced by showers in the energy range 10^{15} to 5×10^{16} eV and derived the distribution of X_m. They have explored the triggering biases of their experiment using Monte Carlo calculations and claim, assuming a bimodal composition, that a mixture of 95% Fe and 5% protons produces a distribution consistent with the data. The Maryland group have been arguing for some years that Fe-nuclei become more dominant above the knee in the energy spectrum. In the latest discussion of their experiment on delayed hadrons in showers (OG 5.2-2) the Maryland

group use Monte Carlo calculations to predict the shower rate and the 'delayed event' rate. Very satisfactory agreement is found with an input composition in which there are rigidity spectral breaks for all components (p, α, CNO, Si, Fe) at 200 TeV. The proton spectrum is steeper than the Fe-spectrum both before and beyond the break (γ(p): -2.75 to -3.33; γ(Fe): -2.55 to -3.1). Additionally they claim that such input spectra propagate to produce number spectra in agreement with mountain altitude and sea-level measurements. This latter result is in direct contradiction to that of Hillas (1984a) just discussed. The Mt. Fuji group, from an analysis of γ-ray families having $10^2 < \Sigma E_\gamma < 5 \times 10^3$ TeV, argue that the proton spectra must steepen at around 10^{14} eV. There is also controversy over the experimental data on N_μ (> 200 GeV) vs N. While the Tata group (OG 5.2-10) find a flattening of the N_μ vs N plot near $N = 3 \times 10^5$ no such feature is evident in magnetic spectrograph data reported by the Moscow group (OG 5.2-10).

It should be clear from the above discussion that the answer to the mass composition question above 10^{15} eV is still uncertain. Not all of the experimental data can be correct and there must be large systematic effects in several experiments. There is no agreement about a common shower model to use when analysing data and it is certainly naive to assume that a bimodal composition is the appropriate model to explore above 10^{15} eV. However it is perhaps worth emphasising that no-one is advocating the view that above 10^{18} eV the primaries are all iron. The Fly's Eye group (OG 5.1-2) ($\sim$ 40% protons) and the Yakutsk group (OG 5.1-13) ($\sim$ 85% protons) support earlier claims by the Haverah Park group (Walker and Watson 1983) for at least 40% protons at 10^{19} eV. Above 10^{14} eV progress could perhaps best be made by a long exposure (LDEF?) of a JACEE module.

Further discussions of mass composition above 10^{14} eV are contained in the rapporteur papers of R.W. Clay and T. Stanev in these proceedings. Work relevant to the problem is to be found in the OG and HE volumes.

4. Can anisotropy measurements tell us anything about mass composition?

It has been recognized since the early sixties that studies of muon-poor and muon-rich showers might reveal anisotropies associated with γ-rays and heavy nuclei (A > 12) respectively. The latter measurements make use of the galactic magnetic field as a sort of magnetic spectrometer.† One of the design aims of the Akeno array (Kamata 1977) was to exploit this possibility through the construction of $9 \times 25\ m^2$ muon detectors with threshold energy 1 GeV. The success of this enterprise in the context of γ-ray astronomy has already been referred to and at this meeting new results on the anisotropy of μ-rich showers have been reported (OG 5.3-3). These extend, and partially confirm, results on this topic reported at the Bangalore conference (Hara et al 1983a) and recently submitted for publication (Kifune et al 1985a). The work is continuing and an interpretation of the data so far presented (Kifune et al 1985b and orally at this conference) can doubtless be further refined but I

† *The possibility of using the solar magnetic field in this context has been examined quantitatively at this meeting independently by Lloyd-Evans (OG 5.1-9) and by Linsley (OG 9.5-7).*

wish to discuss it in some detail as it appears to offer a different approach to the study of mass composition which may eventually relieve the somewhat pessimistic picture of this subject just painted.

In the first of two experiments the Akeno group (1981 - 82) used an electron trigger sensitive to showers with $N > 3 \times 10^5$. For 2.4×10^5 events having $3 \times 10^5 < N < 6.8 \times 10^6$ they found the mean N_μ/N_e to be 0.03. Of these 2.2×10^4 having $N_\mu/N_e > 0.06$ were defined to be μ-rich and assumed to have been initiated by primaries enriched in heavy nuclei. These events (9.1% of the total) exhibit a large and very significant anisotropy in right ascension: $a_1 = 4.0 \pm 1.0\%$, $\theta_1 = 226 \pm 14^o$ RA with chance probability of 2×10^{-4}. This amplitude is for showers of median energy $\simeq 5.5 \times 10^{15}$ eV and is larger by a factor of about 10 than that for all showers of this energy (see Watson 1984 for a summary). Furthermore, as Kifune et al (1985b) have emphasised, the phase is quite different from the best estimate of the phase at an energy E/Z lower in energy. Taking Z = 10 the phase at 5.5×10^{14} eV of about 300 ± 20^o (Linsley and Watson 1977) is to be compared with 226 ± 14^o found in the Akeno experiment. Anisotropies measured at 5.5×10^{14} eV probably refer to the proton component so that Kifune et al suggest that the phase difference indicates a different origin for the two components.

Kifune et al go on to estimate the fraction of heavy nuclei ($A > 12$) in the primary beam. The fraction of heavies (F_H) is related to the fraction of μ-rich showers selected (η), the relative proton and heavy nucleus shower sizes at fixed energy (ε) and the efficiency of selection of heavy primaries (g) through the equation $F_H = \eta \varepsilon g$. Adopting values appropriate to the range of experimental data available from Akeno, Tokyo and Haverah Park, estimates of the fraction of heavies as a function of energy have been derived as shown in Figure 12. A lower limit to the heavy fraction comes from the assumption that the heavy nuclei have the maximum possible (point-source) anisotropy.

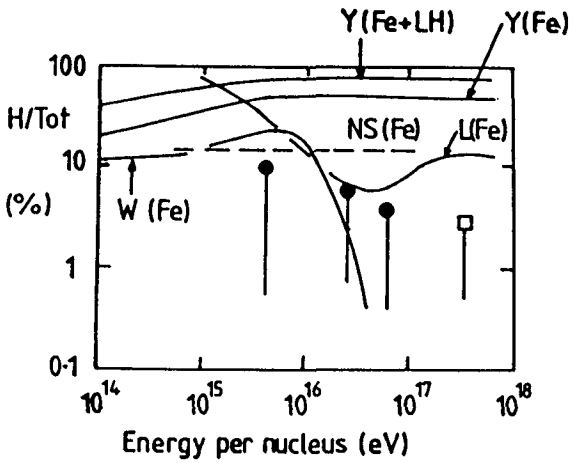

Figure 12: (from Kifune, Wdowczyk and Wolfendale 1985) Y: Yodh et al (1984) NS: Nikolskii and Stanev (1983) L: Linsley (1981) W: Wdowczyk (1985). Data points are derived as outlined in the text; the last two use measurements by Hasegawa et al (1961) and Blake et al (1975).

In a second experiment (1983-84) described in OG 5.3-3 the Akeno group used a trigger in which 4 muons were required in each of $4 \times 9\ m^2$ detectors. This selection was chosen to determine the primary energy more exactly and to reduce the effects of shower development fluctuations. A μ-rich sample, of similar median energy, was again defined by requiring $N_\mu/N_e > 2 < N_\mu/N_e >$: for this trigger 33% of the initial 6×10^4 events were thus selected. Although the phase of the sample was similar (216 ± 34^o RA) the amplitude was smaller and less significant ($1.7 \pm 1.0\%$, $p \simeq 0.25$). Because of the effects of shower fluctuations in the first experiment it is not clear that a cut which retains 33% of the events was appropriate and perhaps a deeper cut (< 10%) should have been used. The result of the second experiment does not weaken the major conclusion of the first experiment which is that muon-rich events produced by primaries of $E \sim 5 \times 10^{15}$ eV have a stronger anisotropy than the bulk of cosmic rays of this energy and also have a different phase from protons of similar rigidity. Although the composition estimates of Figure 12 may require revision, the technique offers real hope that anisotropy measurements can yield valuable information on mass composition.

5. The primary energy spectrum. Measurements of the primary spectrum continue to attract attention. The main points of interest are its detailed shape near the 'knee' and above 10^{19} eV.

5.1. The spectrum from $10^{14} - 10^{18}$ eV. The Adelaide (OG 5.1-6) and Samarkand (HE 4.4-14) groups have carried out measurements near the knee in the spectrum at about 5×10^{15} eV. Both of these determinations are based on the Cerenkov light technique and although dependent on assumptions about mass composition and particle physics they are in reasonable accord with previous work. The Samarkand measurement ($\gamma = -2.6$) supports the view that the spectrum before the knee is somewhat flatter than the spectrum at energies less than 10^{14}eV. The differential spectrum, from $10^{14} - 10^{20}$ eV, is shown in Figure 13. The absolute intensity of the all-particle spectrum is probably known to within 20% in the region of the knee. Also shown are 6 points derived by Linsley (OG 5.1-4) from a calorimetric analysis. These data are in excellent agreement with previous estimates of intensities between 5.10^{15} and 10^{18} eV. The Akeno result (Nagano et al 1985) lies about 10% below these estimates; this must be regarded as excellent agreement considering the difficulties of these measurements. Overall a reasonable description of the spectrum from 10^{16} eV (beyond the knee) to about 10^{19} eV is given by

$$J = 2.1 \times 10^7\ E^{-3.06}\ m^{-2}\ s^{-1}\ sr^{-1}\ GeV^{-1},$$ where E is measured in GeV.

5.2. The energy spectrum above 10^{18} eV. At this meeting four groups have reported spectra which contain relatively large amounts of data beyond 10^{19} eV. These results are relevant to the shape of the spectra and in particular to the question of the Greisen/Zatsepin cut-off. The exposures achieved at the various arrays are given in Table 3.

A particular feature of this conference has been the wide range of results reported by the Fly's Eye group. They are to be congratulated on bringing into successful operation a unique instrument which images

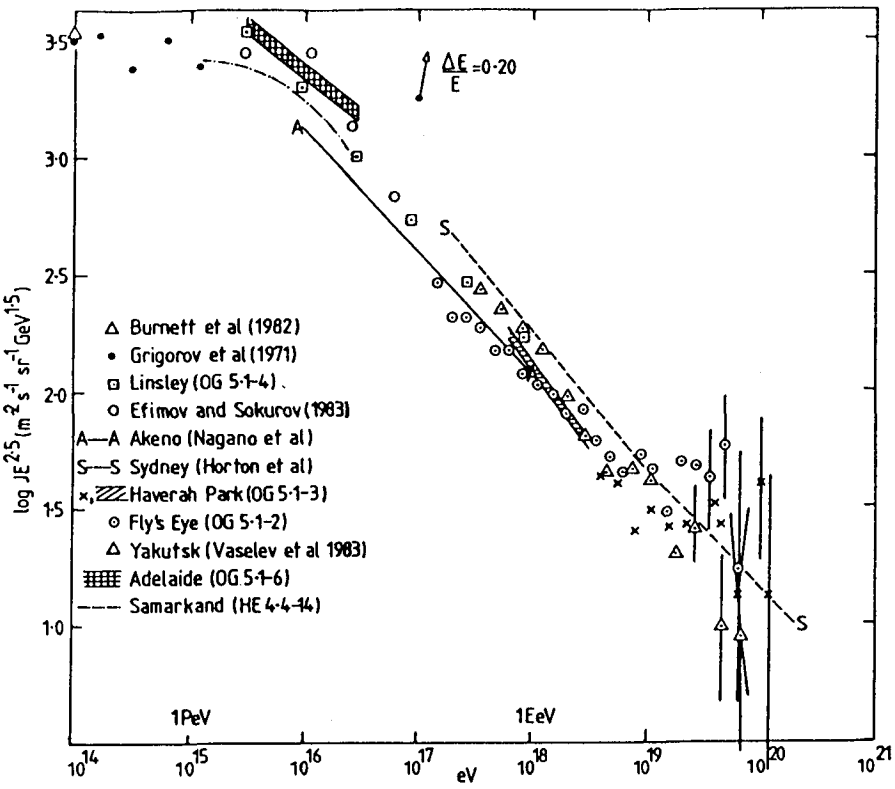

Figure 13: The differential energy spectrum from $10^{14} - 10^{20}$ eV. No attempt has been made to normalise data from different experiments. A systematic change in the energy assignment of 20% would shift each point as shown by the arrow; such a systematic effect could well be present in any data set and probably accounts for much of the scatter.

Table 3

Array	Exposure (km^2 y sr)	Events > 10^{20} eV
Volcano Ranch	∿100	1
Haverah Park (OG 5.1-3)	320 ($\theta < 45^o$)	4
	660 (used for anisotropy)	8
Yakutsk (OG 5.1-17)	200	0
Sydney (Horton et al 1985a)	1000	8
Fly's Eye (Baltrusaitis et al 1985a)	145	0
	Total	17

the development of air-showers in the atmosphere through the fluorescence light which they produce. For the first time individual cascade curves of reasonable precision are available. A typical cascade curve (HE 4.4-1), reconstructed with data from two 'Eyes' separated by 3.3 km, is shown in Figure 14. This curve is for a 2×10^{18} eV primary at 27°; the depth of maximum is estimated to be (740 ± 40) g cm^{-2}.

Figure 14:

(from HE 4.4-1)

A cascade curve produced by a 2.10^{18} eV primary as observed by Fly's Eye I and II. The depth of maximum is estimated as (740 ± 40) g cm^{-2}.

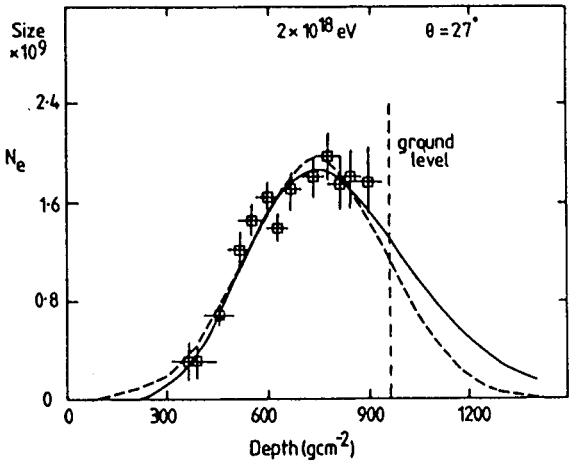

The effective aperture of the Fly's Eye device varies with energy and must be evaluated by detailed Monte Carlo calculations. The spectrum reported just prior to the meeting (Baltrusaitis et al 1985a) and in OG 5.1-2 is reproduced in Figure 15 except that the error bars, which corresponded to ± $\sqrt{n}$ (n = event number) in these papers, have been replaced by lines which indicate 68% confidence bands, following the recommendation of Regener (1951). The 95% and 84% upper limits have also been added for the differential bin above that which contains a single event. In my view there is insufficient evidence to justify a claim for observation of a 'cut-off' or bump in the spectrum (Baltrusaitis et al 1985) and in his highlight talk Cassiday described a slightly revised version of the Fly's Eye spectrum in terms of a power law between $10^{17} < E < 5 \times 10^{19}$ eV with slope = -3.02 ± 0.02, the error estimate being statistical only. This spectral slope is somewhat flatter than that found by the Sydney group (Winn, Highlight Talk and Horton et al 1985a). A comparison of the two measurements is made in Figure 16; for this figure (unlike Figure 13) the Sydney energies have been re-estimated using Yakutsk data (Diminstein et al 1983) on N_μ vs E (Linsley 1983).

In Figure 17 the Fly's Eye spectrum is compared with that from Haverah Park (OG 5.1-3) and in Figure 18 the Haverah Park and Yakutsk spectra are shown. The Yakutsk spectrum is taken from Vaselev et al (1983) in which

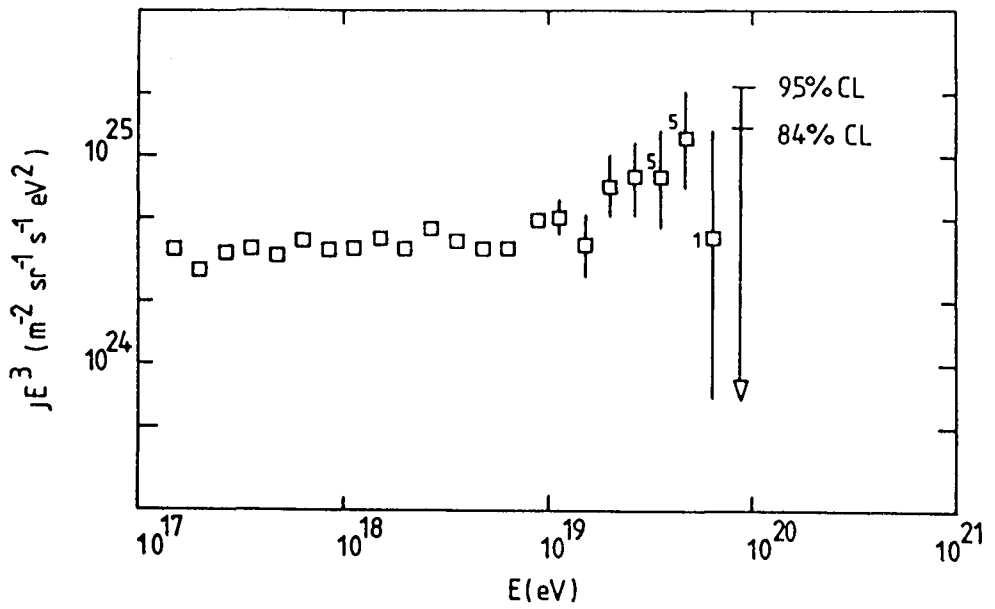

Figure 15: Differential energy spectrum measured by the Fly's Eye group (Baltrusaitis et al 1985a). The 68% confidence bands are calculated following Regener (1951).

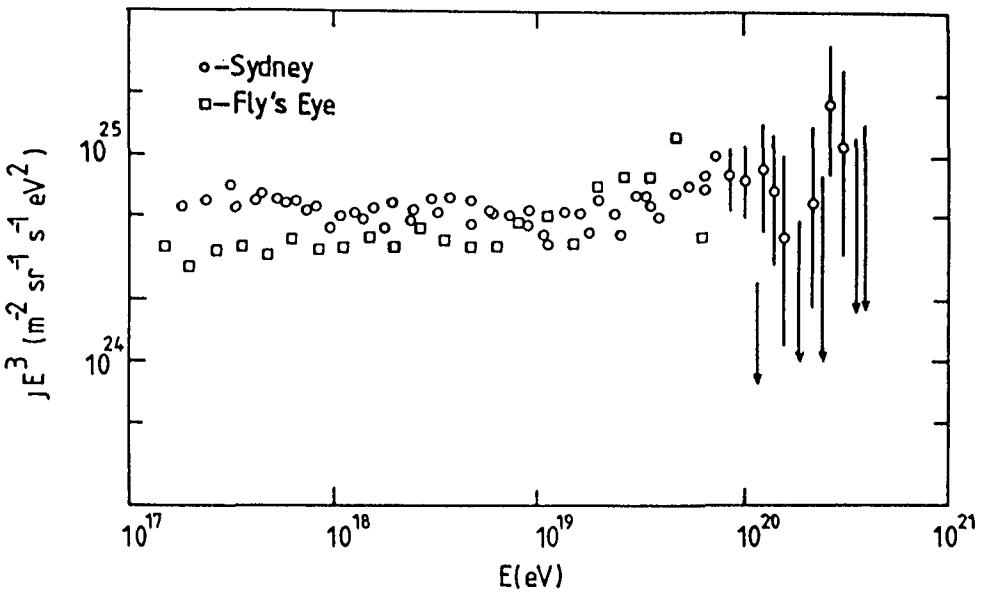

Figure 16: Comparison of the Fly's Eye (Baltrusaitis et al 1985a) with the Sydney spectrum (1985a). The latter has been calculated from N_μ using the calibration of Diminstein et al (1983).

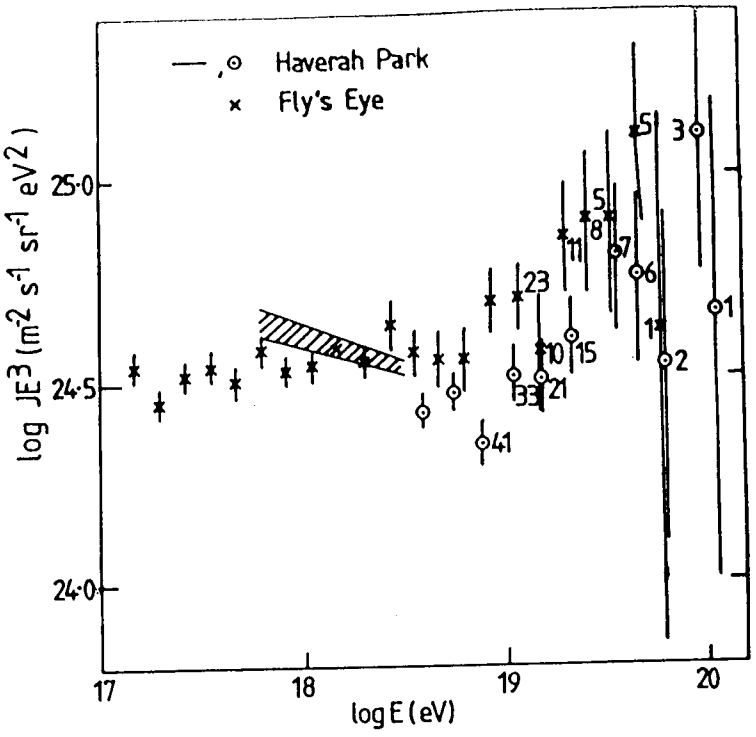

Figure 17: Comparison of Fly's Eye and Haverah Park spectra (OG 5.1-3).

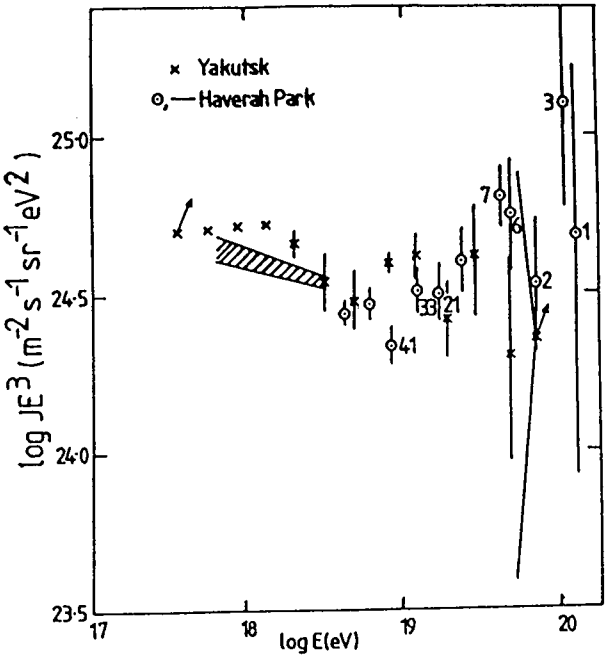

Figure 18: Comparison of Haverah Park and Yakutsk spectra. The arrows on the extreme Yakutsk points indicate the shift caused by their revised energy calibration (OG 5.1-7).

the scintillator density at 600 m, S(600), from the shower axis was related to the primary energy by calorimetric methods via the relation

$$E = (4.1 \pm 1.5) \times 10^{17}.S(600)^{0.96} \text{ eV}.$$

At this meeting (OG 5.1-7) the Yakutsk group did not present a differential energy spectrum but note that a reassessment of the atmospheric transparency requires the E/S(600) relation to be revised to $E = (5.0 \pm 1.4).10^{17} S(600)^{0.96}$ thus increasing the primary energy calculated for each event by about 22%. The magnitude of this shift is shown in Figure 18; the discrepancy between the two measurements is increased near 10^{18} eV.

It is clear from examination of Figures 15-18 that it may be a long time before the shape of the spectrum above 10^{19} eV is agreed and it is certainly premature to discuss the existence or otherwise of the 'bump' discussed by Hill and Schramm (1985). The present position can be summarised as follows:-

1. The Haverah Park, Sydney and Volcano Ranch groups claim that the spectrum is flatter above 1 or 2×10^{19} eV than below. The joint total of events believed to be 10^{20} eV is now 17.

2. The Yakutsk group, who have performed a careful calorimetric calibration of their experiment, find some evidence for a steepening of the spectrum above $\sim 4 \times 10^{19}$ eV. They point out that their calibration has only been checked to about 2×10^{19} eV. However, it appears to agree well with the Haverah Park and Volcano Ranch conversions at least to 5×10^{19} eV (Bower et al 1983).

3. The Fly's Eye measurements are consistent with a flat spectrum from 10^{17} to 5×10^{19} eV.

4. There are events in Haverah Park, Sydney and Volcano Ranch data which are claimed to have energies well beyond the Greisen/Zatsepin cut-off. Extensive details of the Volcano Ranch and Haverah Park events have been published (Wada 1980) and their energy assignments are thought to be secure. Independent assessment of these claims - perhaps by a non-EAS person? - is highly desirable.

5. The best estimate of the integral intensity at 10^{20} eV is

$$I(> 10^{20} \text{ eV}) = \left(3^{+2}_{-1}\right) \times 10^{-16} \text{ m}^{-2} \text{ s}^{-1} \text{sr}^{-1}$$

$$\text{or} \simeq 1 \text{ km}^{-2} \text{ sr}^{-1} \text{ century}^{-1}.$$

6. Anisotropy of cosmic rays $> 10^{19}$ eV. Apart from the 'μ-rich anisotropy discussed above there has been no important change in our knowledge of cosmic ray arrival directions since the last conference, with one major exception. The Sydney group (Horton et al 1985b) have finalised their arrival direction study of cosmic rays above 5.10^{17} eV as seen in the Southern Hemisphere. This important work awaits detailed examination but there is one immediate and striking fact within their paper which

relates to the question of anisotropy of cosmic rays > 4×10^{19} eV as seen from the Northern Hemisphere. Data from Haverah Park and Volcano Ranch, when combined, yield a first harmonic amplitude above 4×10^{19} eV, based on 43 events, of $(54 \pm 22)\%$ at $\theta = (190 \pm 23)^{\circ}$RA (chance probability = 0.043). Because the direction of the excess lies close to the centre of the local supercluster, which may well provide an enhancement of the cosmic ray intensity above this energy (e.g. Strong et al 1974), there has been speculation that this anisotropy is real. There are 19 Sydney events with $E > 4 \times 10^{19}$ eV and $\delta > 0^{\circ}$; for these the 1st harmonic in right ascension is represented by $a_1 = (45 \pm 32)\%$ and $\theta_1 = (134 \pm 40)^{\circ}$RA. The joint Haverah Park, Sydney, Volcano Ranch harmonic is $a_1 = (47 \pm 18)\%$, $\theta_1 = 175 \pm 22^{\circ}$ and $p = 0.033$. The three largest Sydney events which have $\delta > 0^{\circ}$ all arrive from close to the North Galactic Pole and the very largest event in Sydney listing has $\alpha = 188^{\circ}$, $\delta = 32^{\circ}$. These 3 events are plotted in Figure 19 together with the 43 events from Haverah Park and Volcano Ranch. This is a tantalising result but as the Volcano Ranch and Sydney experiments are now closed down, and little increase in the Haverah Park data set is to be expected, confirmation or otherwise must come from the Fly's Eye experiment and from the new giant array being developed at Akeno (OG 9.4-8).

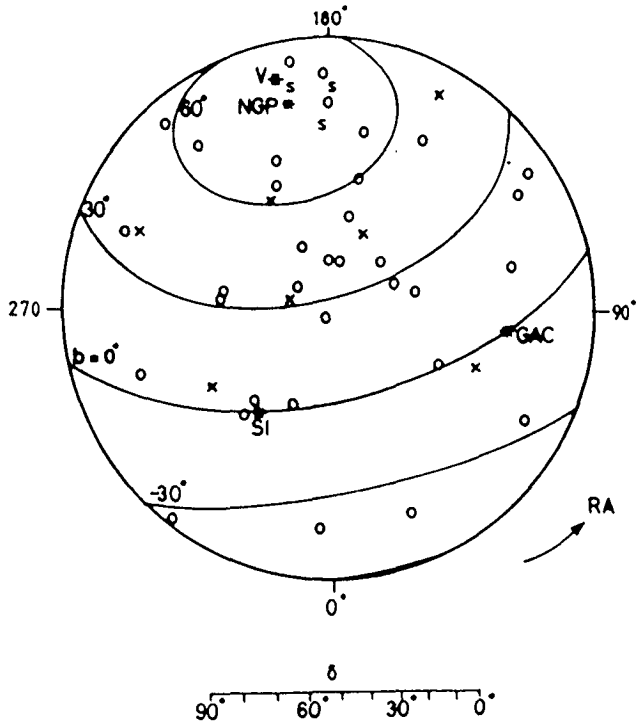

Figure 19: Events from Haverah Park (O), Volcano Ranch (X) and Sydney (S) above 4×10^{19} eV and with declination $>0^{\circ}$. Only the 3 largest Sydney events in this category have been plotted.

There is no evidence from the Northern or Southern Hemisphere for any clustering near the Galactic Plane. If the 4×10^{19} eV anisotropy is strengthened through future studies and if the particles at the highest

energy really are protons then the accelerators of these particles must surely lie in some of the more unusual objects within the local supercluster.

Acknowledgements. I would like to thank the organisers of the 19th International Cosmic Ray Conference for inviting me to be a rapporteur. My work has been made easier through discussions with many colleagues, including George Cassiday, Michael Hillas, George Khristiansen, Dick Lamb, Al Lambert, John Linsley, Jeremy Lloyd-Evans, Manfred Samorski, Ted Turver, George Wdowczyk and Trevor Weekes. I am also very grateful to Julie Ingle for her work on the diagrams and above all to Angela Vaughan for her speedy and accurate typing of a difficult manuscript.

References to pre-conference papers and pre-prints
ICRC ≡ International Cosmic Ray Conference

B.S. Acharya et al 1983 Proc. 18th ICRC (Bangalore) 11, 334.
V.V. Alexeenko et al 1984 Izv. Akad. Nauk SSSR Ser. Phys. 48, 2126.
V.V. Alexeenko & G. Navarra 1985 Lettre al Nuovo Cimento 42, 321.
K.M.V. Apparao 1984 Ap. J. 287, 338.
R.M. Baltrusaitis et al 1985 Ap. J. Lett. 293, L69.
R.M. Baltrusaitis et al 1985a Phys. Rev. Lett. 45, 1875.
C.L. Bhat, T. Kifune & A.W. Wolfendale 1985 submitted to Astron. Astrophys.
P.R. Blake et al 1975 Proc. 14th ICRC (Munich) 8, 2768.
J.M. Bonnet-Bidaud and M. van der Klis 1981 Astron. Astrophys. 101, 299.
J. Boone et al 1984 Ap. J. 285, 264.
A.J. Bower et al 1983 J. Phys. G 9, L53.
R. Buccheri et al 1985 Nature 316, 131.
T.H. Burnett et al 1982 in Workshop on Very High Energy Interactions, University of Pennsylvania 1982, p.220.
M.F. Cawley et al 1985 Ap. J. (in the press).
P.M. Chadwick et al 1985 submitted to Nature.
R.W. Clay, P.R. Gerhardy & D.F. Liebing 1984 Aust. J. Phys. 37, 91.
G. Cocconi 1959 Proc. 6th ICRC (Moscow) II, 309.
J.M. Dickey 1984 Ap. J. Lett. 273, L71.
O.S. Diminstein et al 1983 Proc. 18th ICRC (Bangalore) 6, 118.
J.C. Dowthwaite et al 1984a Ap. J. Lett. 286, L35.
J.C. Dowthwaite et al 1984b Astron. Astrophys. 136, L14.
J.C. Dowthwaite et al 1984c Nature 309, 691.
T. Dzikowski et al 1981 Proc. 17th ICRC (Paris) 1, 8.
N.N. Efimov & V.F. Sokurov 1983 Proc. 18th ICRC (Bangalore) 2, 123.
V.P. Fomin et al 1981 Proc. 17th ICRC (Paris) 1, 28.
W. Galbraith & J.V. Jelley 1953 Nature 171, 349.
A.I. Gibson et al 1982 Proc. Int. Workshop on VHE γ-ray astronomy Ootacamund, India, p.97.
P. Grieder 1983 Proc. 18th ICRC (Bangalore) 11, 323.
J. Grindlay et al 1975a Ap. J. 201, 82.
J. Grindlay et al 1975b Ap. J. Lett. 197, L9.
N.L. Grigorov et al 1971 Proc. 12th ICRC (Hobart) 5, 1746.
T. Hara et al 1983 Proc. 18th ICRC (Bangalore) 9, 198.
H. Hasegawa et al 1961 Proc. 7th ICRC (Kyoto) 3, 86.
C.T. Hill and D.N. Schramm 1985 Phys. Rev. D 31, 564.
A.M. Hillas 1984 Nature 312, 50.
A.M. Hillas 1984a Proc. of XIXth Recontre de Moriond, La Plagne, France.
L. Horton et al 1985a Sydney University pre-print, 'The Cosmic Ray Energy Spectrum above 10^{17} eV'.
L. Horton et al 1985b Sydney University pre-print, 'The Arrival Directions of Cosmic Rays above 10^{17} eV'.
E. Juliusson 1975 Proc. 14th ICRC (Munich) 8, 2689.
K. Kamata 1977 Proc. 15th ICRC (Plovdiv) 12, 102.
T. Kifune et al 1985a submitted to J. Phys. G.
T. Kifune, J. Wdowczyk & A.W. Wolfendale 1985b submitted to J. Phys. G.
M. van der Klis & J.M. Bonnet-Bidaud 1981 Astron. Astrophys. Lett. 95,L5.
A.N. Kvashnin et al 1983 Proc. 18th ICRC (Bangalore) 11, 394.
R.C. Lamb et al 1977 Ap. J. Lett. 212, L63.
R.C. Lamb & T.C. Weekes 1985 submitted to Nature.
J. Linsley 1981 Proc. 17th ICRC (Paris) 2, 141.
J. Linsley 1983 Proc. 18th ICRC (Bangalore) 12, 135.

J. Linsley & A.A. Watson 1977 Proc. 15th ICRC (Plovdiv) 12, 203.
J. Linsley & A.A. Watson 1981 Phys. Rev. Lett. 46, 459.
J. Lloyd-Evans et al 1983 Nature 305, 784.
M.L. Marshak et al 1985 Phys. Rev. Lett. 54, 2079.
C.A. Meegan, G.F. Fishman & R.C. Haynes 1979 Ap. J. Lett. 234, L123.
M. Nagano et al 1984 J. Phys. G 10, 1295.
Yu. I. Nesphor et al 1979 Astro. Sp. Sci. 61, 349.
S.I. Nikolskii & J.N. Stamenov 1983 Proc. 18th ICRC (Bangalore) 2, 115.
D.R. Parsignault et al 1976 Ap. J. Lett. 209, L73.
W. Priedhorsky & J. Terrell 1986 Ap. J. (1 Feb. issue).
R.J. Protheroe, R.W. Clay & P.R. Gerhardy 1984 Ap. J. Lett. 280, L47.
R.J. Protheroe & R.W. Clay 1985 Nature 315, 205.
V.H. Regener 1951 Phys. Rev. 84, 161.
C. Reppin et al 1979 Ap. J. 234, 329.
M. Samorski & W. Stamm 1983a Ap. J. Lett. 268, L17.
M. Samorski & W. Stamm 1983b Proc. 18th ICRC (Bangalore) 11, 244.
F.W. Stecker, A.K. Harding & J.J. Barnard 1985 Nature 316, 418.
A.A. Stepanyan et al 1972 Nature Phys. Sci. 239, 40.
A.W. Strong, J. Wdowczyk & A.W. Wolfendale 1974 J. Phys. G 7, 1767.
I.V. Vaselev et al 1983 'Cosmic Rays with Energy $> 10^{17}$ eV', Yakutsk Branch of Academy of Science USSR, EDK 537.591, p.19.
B.M. Vladimirsky et al 1973 Proc. 13th ICRC (Denver) 1, 456.
M. Wada (Editor) 1980 World Data Catalogue of Highest Energy Cosmic Ray Showers N° 1: published by World Data Center for Cosmic Rays.
R. Walker & A.A. Watson 1983 Proc. 18th ICRC (Bangalore) 6, 114.
A.A. Watson 1984 Adv. Space Res. Vol. 4, 35.
J. Wdowczyk & A.W. Wolfendale 1983 Nature 305, 609.
J. Wdowczyk 1985 Int. School of Astrophysics, Erice (in press, D. Reidel).
T.C. Weekes et al 1981 Astron. Astrophys. 104, L4.
T.C. Weekes 1982 Proc. Int. Workshop on VHE γ-ray astronomy, Ootacamund, India, p.272.
R. Willingale, A.R. King & K.A. Pounds 1985 Mon. Not, R. Astr. Soc. 215, 295.
R.D. Wills et al 1982 Nature 296, 723.
G.B. Yodh et al 1984 Phys. Rev. D 29, 892.

GALACTIC COSMIC RAY COMPOSITION

Jean-Paul Meyer
Service d'Astrophysique
Centre d'Etudes Nucléaires de Saclay
France

The plan of this report on our knowledge of galactic cosmic-ray composition as it stands after the La Jolla Conference (August 1985) may seem somewhat odd to the reader. This is why I felt it prudent to give an explicit table of contents, which might help him to find his way in this maze.

In Part I, I just highlight various key new observations brought up at the conference. In Part II, I specify what I think we know on the cosmic-ray elemental composition at the sources, and on its correlation with first ionization potential (FIP). In Part III, the most important in my view, I discuss the various areas where the correlation with FIP is, really or apparently, insufficient to explain the data as they stand. The isotopic anomalies will be discussed in this context. It might also sound a bit bizarre to the reader to find the entire problem of cosmic ray propagation (compositional aspects) treated as kind of a long parenthesis in the discussion of the source abundance of Nitrogen ! In Part IV, I summarize the situation and make recommendations on key points for future work.

CONTENTS

PART III THE PROBLEMS WITH THE GALACTIC COSMIC RAY SOURCE COMPOSITION AND PROPAGATION - BEYOND THE CORRELATION WITH FIRST IONIZATION POTENTIAL

III-1. The Hydrogen and Helium deficiency problem
- III-1.1. H and He source spectra, and behaviour in SEP's
- III-1.2. Deficiency of H and He : direct injection out of the hot interstellar medium (HIM) ?

III-2. The Nitrogen deficiency problem - Cosmic ray propagation - The B-^{15}N contradiction - Distributed reacceleration ? Truncation of the PLD ?
- III-2.1. Low energy cosmic-ray propagation - The B-^{15}N contradiction - Distributed reacceleration ?
- III-2.2. The ^{14}N source abundance from low and high energy data
- III-2.3. Truncation of the exponential Path Length Distribution (PLD) ?
  - III-2.3.1. Truncation of the PLD in the GeV/n range - Data for $Z \leq 30$ - The role of interstellar He
  - III-2.3.2. Truncation of the PLD in the GeV/n range - UH nuclei data
  - III-2.3.3. Truncation of the PLD in the few 100 MeV/n range
  - III-2.3.4. Summary on the truncation of the PLD

III-3. The Germanium-Lead deficiency problem
- III-3.1. Defining the Ge and Pb/Pt anomalies
- III-3.2. The low Pb/Pt ratio : probably not explainable in terms of a truncation of the PLD
- III-3.3. The low Pb/Pt ratio - Interpretations in terms of nucleosynthesis
- III-3.4. Ge and Pb as volatility indicators
- III-3.5. Questioning the LG reference abundances for Ge and Pb
- III-3.6. Summary on the Ge-Pb deficiency problem

III-4. The C, O, ^{22}Ne, ^{25,26}Mg, ^{29,30}Si excesses
- III-4.1. Estimating the ^{22}Ne, ^{25,26}Mg, ^{29,30}Si excesses in GCR sources
- III-4.2. The common and new wisdom on He-burning and weak s-process in Wolf-Rayet stars
- III-4.3. Relating the excesses in GCRS to those in the (WR) processed component material - FIP effects in the dilution
- III-4.4. Discussion : types of dilution, observed and predicted ^{22}Ne excesses
- III-4.5. Excess ^{22}Ne : preferential injection at the decay of ^{22}Na ?

III-5. The excess of elements with $Z \geq 40$
- III-5.1. Estimating the excesses in the processed component material - FIP effects in the dilution
  - III-5.1.1. The dilution problem
  - III-5.1.2. Consequences of differential dilution
- III-5.2. Evidences for s and/or r-process excesses
  - III-5.2.1. What happens at $Z = 40$?
  - III-5.2.2. The $_{52}$Te, $_{54}$Xe, $_{56}$Ba, $_{58}$Ce quartet
- III-5.3. UH element excesses - Summary and overview

PART IV SUMMARY AND RECOMMENDATIONS

IV-1. Summary

IV-2. Recommendations for future work.

APPENDIX : Formalism for the dilution of the ^{22}Ne-rich or other processed components.

PART I

HIGHLIGHT OF KEY NEW OBSERVATIONS

I-1. ABUNDANCE OF SUB-IRON NUCLEI UP TO 200 GeV/n

It has been known since Juliusson's (1974) first study that the abundance ratios of secondary to primary nuclei decrease with energy between $\sim$ 2 and at least $\sim$ 30 GeV/n. But there was as yet no unambiguous evidence that this trend was continued beyond $\sim$ 30 GeV/n (e.g. Webber 1983a; Garcia-Munoz et al., 1984; Juliusson et al., 1983). Taking advantage of the relativistic rise of ionization chambers to resolve high energies, the HEAO 3 Heavy Nuclei Experiment (HEAO-C3) team has shown that the purely secondary/primary ratios in the Fe region definitely continue to decrease, at roughly the same rate, up to at least 200 GeV/n (Jones et al. 2, 28; fig. 1) [1].

The approximate constancy of the primary/primary Ni/Fe ratio in fig. 1 shows that the data are not affected by any large systematic bias. As regards Ar and Ca, both the secondary and the primary component are significant. Accordingly, the Ar/Fe and Ca/Fe ratios decrease with energy, but less steeply than the purely secondary/primary ratios. Beyond $\sim$ 200 GeV/n the observed ratios are however strange, with an apparent trend to rise again. The authors are very prudent as regards these highest energy points, which just represent the present state of their data analysis. It must however be noted that a preliminary analysis of balloon gas Cerenkov data by the Goddard group also suggests an increase of sub-Fe/Fe ratios somewhere beyond $\sim$ 100 GeV/n (Balasubrahmanyan et al. 2, 44). But here also the authors are prudent (and their Cr does not fit well into the picture)!

In principle, composition observations reaching energies where the secondary component is much reduced can yield most accurate values for the source abundances. Based on the data up to $\sim$ 200 GeV/n, Jones et al. (2, 28) have indeed derived estimates of the primary Ar/Fe and Ca/Fe ratios, corresponding to source ratios Ar/Fe $\approx 0.023 \pm 0.003$ and Ca/Fe $\approx 0.085 \pm 0.004$ (fig. 1) (these source ratios are $\sim$ 12 and 10% lower than the surviving primary ratios given by the authors). I feel however that these estimates cannot be considered really solid as long as the highest energy points puzzle is not solved, one way or another.

[1] Throughout this report, the papers presented at the La Jolla Conference will be quoted directly by their volume and page number in the proceedings. They are not listed at the end of the paper.

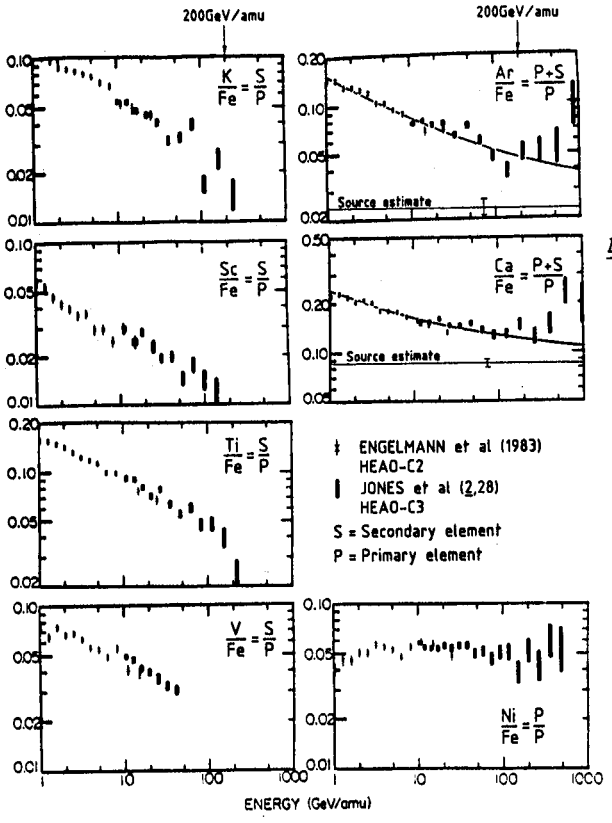

Fig. 1 Sub-Fe/Fe ratios at very high energy, as measured by the HEAO-C3 team, together with the lower energy ratios from the HEAO-C2 team (from Jones et al. 2, 28 ; fig. slightly adapted). Left column : purely secondary/primary ratios. Right column : Ni/Fe = primary/primary ratio ; Ar,Ca/Fe = mixed ratios. Also plotted are the author's fit to the data on Ar,Ca/Fe below 200 GeV/n, and the derived source ratios.

I-2. ISOTOPIC COMPOSITION OF HEAVY NUCLEI

The mass resolution now achieved by Webber et al. (2, 88) in the 400 to 700 MeV/n range for elements between N and Ca is very impressive (fig. 2). Of particular significance are the well resolved N, Mg and Ca isotopes, and especially the low ^{29,30}Si fluxes (§ II-1.2.2., III-2. and 4.).

Wiedenbeck (2, 84) and Krombel and Wiedenbeck (2, 92) also obtained quite good mass resolution on Cl, Sc and Ca around 250 MeV/n (fig. 3). They found radioactive ^{36}Cl depleted, as expected, and contributed to tightening up the source Ca abundance, based on the primary ^{40}Ca isotope, which is well resolved from the heavier, secondary isotopes (fig. 3). Webber et al. (2, 88)'s data can be used for the same purpose (§ II-1.2.2.; fig. 14).

At high energy, the HEAO 3 French-Danish experiment (HEAO-C2) team has provided new geomagnetic mean mass estimates at 3 GeV/n for elements between N and Fe (Ferrando et al. 2, 96, and priv. comm. of ^{15}N/N = 0.49 ± 0.06), whose significance, combined with the earlier HEAO-C2 data, will be discussed later (§ III-2. and 4.). Herrström and Lund (2, 100) have also shown that the ^{22}Ne enhancement at source does not vary with energy between 0.1 and 6 GeV/n.

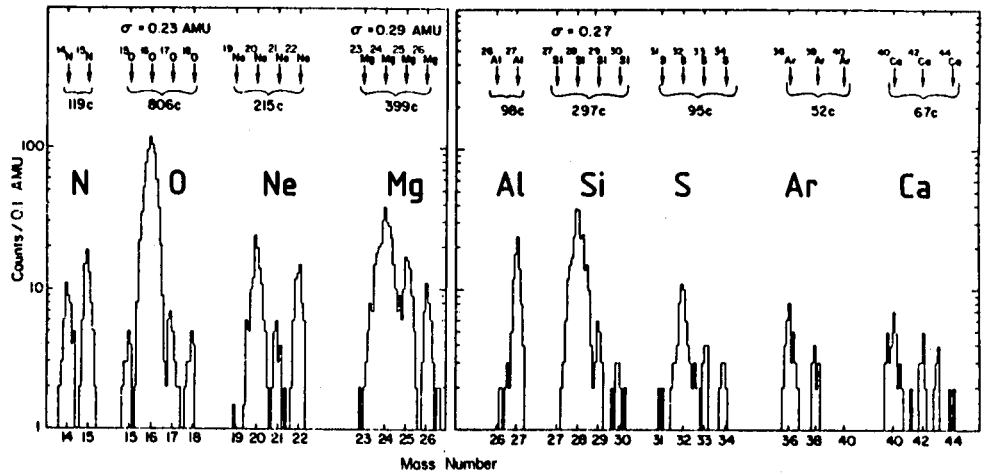

Fig. 2 *Cosmic-ray isotopes from N to Ca, as beautifully resolved by Webber et al. (2, 88).*

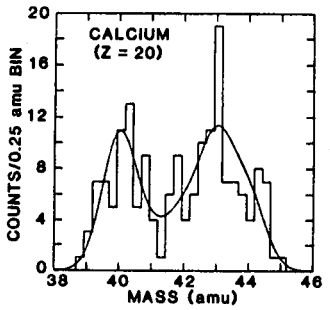

Fig. 3 *Isotopic analysis of cosmic-ray Ca, by Krombel and Wiedenbeck (2, 92).*

I-3. SPALLATION CROSS-SECTIONS

In response to a crucial need, and taking advantage of the facilities offered by the Berkeley Bevalac, a very massive effort is now being invested on spallation cross-section measurements. Let me insist on the materiality of the need : with the high accuracy now achieved in the cosmic-ray measurements, especially with the HEAO-C2 data, the check of the self-consistency and the refinement of the propagation models (truncation of the path length distribution ? distributed reacceleration ?), and a fortiori the determination of the source abundances of key largely secondary elements and isotopes (N, Na, ^{25,26}Mg, Al, ^{29,30}Si, P, Ar, Ca) are essentially limited by our knowledge of spallation cross-sections (§ II-1.2., III-2. and 4.1.). It is important to measure cross-sections for a great variety of energies and incident nuclei. In the interpretation of secondary nuclei abundances, it is indeed not worth having their production cross-sections from a few dominant parents determined with utmost accuracy, as long as the cross-sections for a large number of other contributing parents remain entirely unmeasured (Table 2). Measurement of spallation cross-sections on He are also becoming necessary now (Ferrando et al. 3, 61 ; § III-2.3.1.).

I-3.1. Measurements of spallation cross-sections on H

Following the early work of the Orsay group (e.g. Raisbeck and Yiou 1976) and the first studies on the Bevalac (Lindstrom et al. 1975 ; Olson et al 1983), in recent years the New Hampshire group has been leading the way as regards cross-section measurements (Webber and Brautigam 1982 ; Webber et al. 1983a,b ; Webber 1984 ; Webber and Kish 3, 87). Other groups are now joining the effort : Louisiana State U. - Berkeley collaboration (Guzik et al. 2, 80), Cal Tech (Lau et al. 1983 ; 3, 91), and the HEAO-C3 team in the Ultra-Heavy range (Brewster et al. 1983 ; Kertzman et al. 3, 95).

In the Be, B, C, N, O range, absolutely essential new data on the reactions $^{12}C \rightarrow$ Be, B and $^{16}O \rightarrow {}^{14,15}N$ have been provided by Webber and Kish 13, 87) and Guzik et al. 2, 80). They are summarized in fig.4. When these data are combined with those for $^{16}O \rightarrow$ B and $^{20}Ne \rightarrow {}^{14,15}N$ (Webber et al. 1983b), respectively $\sim$ 81%, 74% and 91% of the production of B, ^{14}N, ^{15}N between $\sim$ 0.3 and 2 GeV/n results from reactions whose cross-sections are measured (§ III-2.1. ; Table 2). While the very small errors quoted by the New-Hampshire group are sometimes questioned in view of the importance of their thick target correction, the agreement between the various data sets in fig. 4 shows that no large systematic error affects the data.

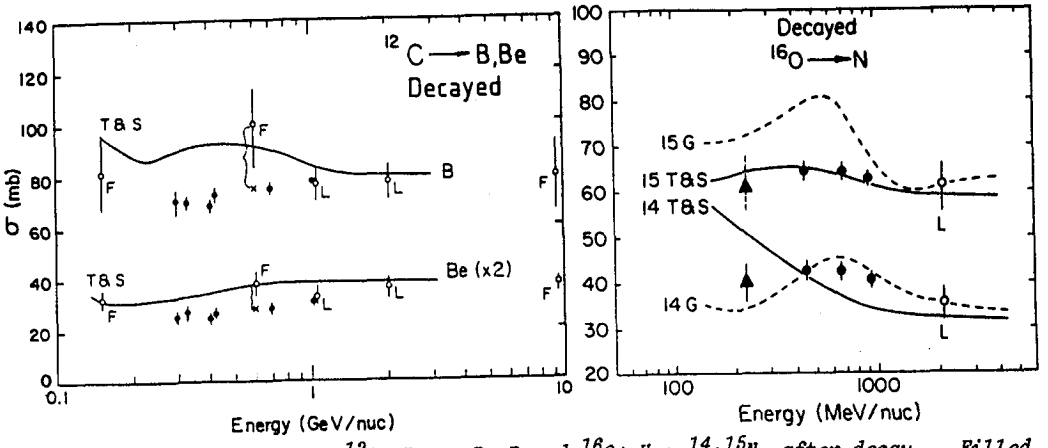

Fig. 4 Cross-sections for $^{12}C + H \rightarrow$ Be,B and $^{16}O + H \rightarrow {}^{14,15}N$, after decay. Filled circles : Webber and Kish (3, 87) (see also Webber 1984), and Webber et al. (1983b). Triangles : Guzik et al. (2, 80). Open circles : Lindstrom et al. (1975) (or Olson et al. 1983) and Fontes (1977). Curves : semi-empirical estimates by Tsao and Silberberg (1979) and Guzik (1981).

As regards the spallation of ^{56}Fe specifically, some of the discrepancies between the recent New-Hampshire data (Webber and Brautigam 1982 ; Webber et al. 1983a ; Webber 1984) and earlier studies (e.g. Perron 1976 ; Orth et al. 1976) are being removed by refined analysis of the recent data. Anyway, there is excellent agreement on the sum of the cross-section for formation of Sc+Ti+V+Cr. The new data on the energy dependence of the Fe cross-sections at low energy (down to 300 MeV/n ; Webber 1984 ; Lau et al. 3, 91) is of particular interest, and should allow a broad revision of the semi-empirical formulae for low energies.

Spallation cross-sections for ^{28}Si and ^{40}Ar between 500 and 1300 MeV/n have been measured by Webber and Kish (3, 87), who should also provide us soon with new cross-sections for spallation of ^{32}S, ^{40}Ca and ^{58}Ni. These measurements complement the above mentioned New-Hampshire data on ^{56}Fe spallation. For ^{40}Ar, and to some point ^{28}Si spallation, the new data imply that, at 650 MeV/n, the semi-empirical estimates (Tsao and Silberberg 1979) underestimate the cross-section, by factors of up to $\sim$ 1.9 for products with Z = 12 to 14 (fig. 5). If the same trend is present for other, neighbouring parent nuclei (which will be checked soon, ^{32}S, ^{40}Ca), it is of extreme importance, since it will decrease the estimate of the source abundances of Na, Al, $^{25,26}Mg$ and $^{29,30}Si$, which are at present critical issues (§ II-1.2.1. and 1.4., III-4.; figs. 14 and 29). The effect of such a correction on the determination of the source abundance of Al is illustrated in fig. 6 (from Webber et al. 3, 42).

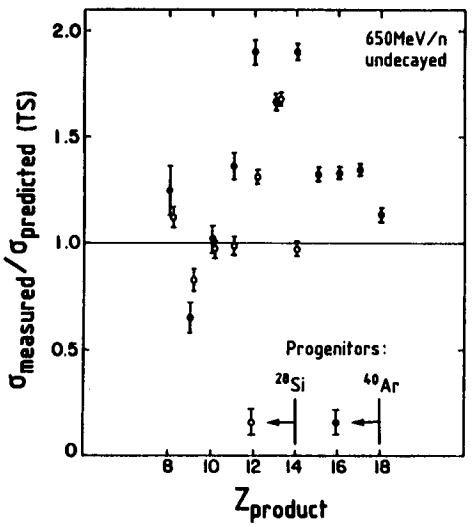

Fig. 5 Ratios of the charge changing cross-sections of ^{28}Si and ^{40}Ar on H measured by Webber and Kish (3, 87), to those estimated by Tsao and Silberberg (1979) (650 MeV/n, undecayed).

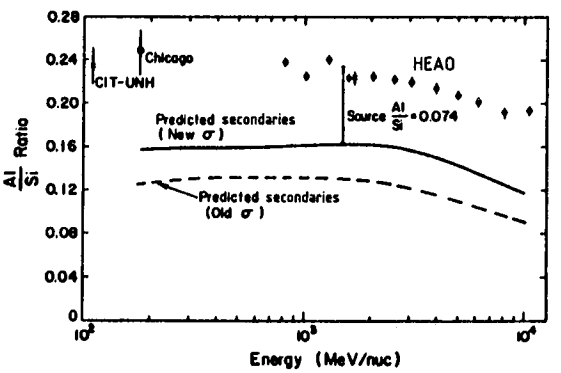

Fig. 6 Effect of the new ^{28}Si and ^{40}Ar cross-section measurements by Webber and Kish (3, 87) (fig. 5), extrapolated to neighbouring parent nuclei, on the derived Al source abundance (from Webber et al. 3, 42).

Relative cross-sections for spallation of ^{40}Ar and ^{56}Fe measured around 300 MeV/n by Lau et al. (1983; 3, 91) also give useful information to refine semi-empirical estimates. In particular, these authors note the effect of closed neutron shells: the cross-sections for formation of products with 1 neutron less than a magic number are found very small, probably because neutron emission out of a closed shell is difficult.

In the Ultra-Heavy (UH) range, beautiful new data on the spallation of $_{54}Xe$, $_{67}Ho$ and $_{79}Au$ around 1 GeV/n have been provided by Brewster et al. (1983) and Kertzman et al. (3, 95). Their measured total cross-sections σ_{tot} show that extrapolation of Westfall et al.'s (1979) formula for projectiles beyond Fe leads to slight overestimates for σ_{tot} (by 15% for $_{67}Ho$ on H). Figure 7 displays the measured charge yields on H. It shows that, when normalized to σ_{tot}, the charge yield is approximately a universal function of the charge change ΔZ, independent of the charge of the incident UH nucleus. Comparison with the semi-empirical estimates by Silberberg and Tsao (1979) (fig. 8) shows that the estimates are fairly good (generally to within a factor of 1.5) for the more important nearby products ($\Delta Z \lesssim 10$), but can underestimate by factors of up to 2 the smaller cross-sections for more distant products. Figure 8 also shows that the departures of the estimated cross-sections from the measured ones cannot be described by a unique pattern valid for all UH parent nuclei.

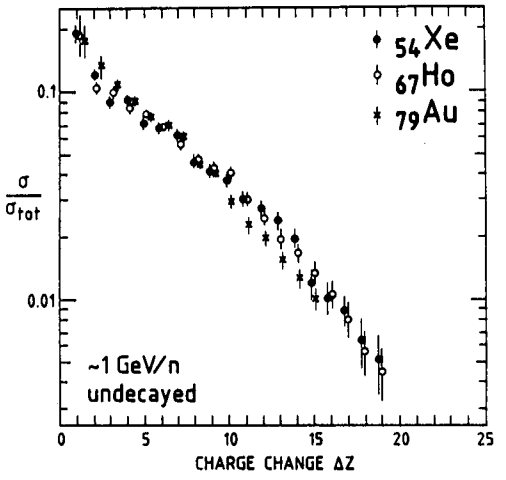

Fig. 7 Charge changing cross-sections for $_{54}Xe$, $_{67}Ho$ and $_{79}Au$ on H, as measured by Kertzman et al. (3, 95), normalized to the total cross-section ($\sim$1 GeV/n, undecayed). The values for Au have been revised since Brewster et al. (1983)'s study.

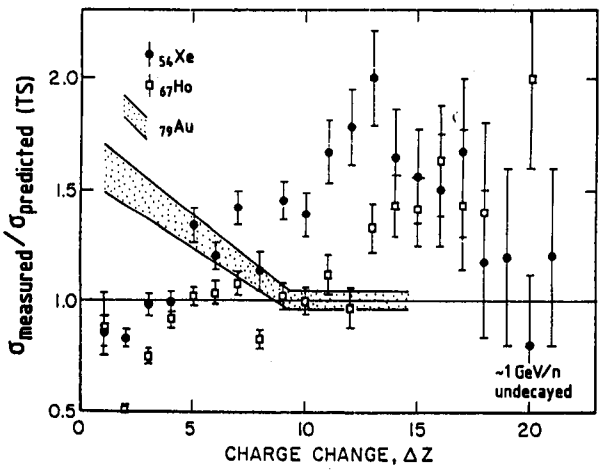

Fig. 8 Ratios of the charge changing cross-sections of $_{54}Xe$, $_{67}Ho$ and $_{79}Au$ on H measured by Kertzman et al. (3, 95), to those estimated by Tsao and Silberberg (1979) ($\sim$1 GeV/n, undecayed).

I-3.2. Semi-empirical estimates of spallation cross-sections on H

As regards semi-empirical estimates of unmeasured cross-sections (Silberberg and Tsao 1973a,b ; Silberberg et al. 1985 ; Tsao et al. 3, 103), it is clear that they will remain necessary. Estimating their accuracy is however still not easy: on the one hand, Letaw et al. (3, 46) give evidence that the errors on the semi-empirical cross-sections are uncorrelated and generally less than 35% below Fe at 4 GeV/n; on the other hand, recent cross-section observations show that the semi-empirical estimates for some major cross-sections are off by factors of up to ~ 2 around 0.6 GeV/n (fig. 5; § I-3.1.; Webber et al. 1983b ; Webber and Kish 3, 87). With the large body of recent and forthcoming measurements of cross-sections for the spallation of ^{12}C, ^{16}O, ^{20}Ne, ^{24}Mg, ^{28}Si, ^{32}S, ^{40}Ar, ^{40}Ca, ^{56}Fe, ^{58}Ni in the 0.3 to 1.7 GeV/n range by the New-Hampshire group, time will soon be ripe for a deep revision of the parametrization of the cross-section systematics, possibly including new physical effects (e.g., closure of neutron shells ; Lau et al. 3, 91 ; § I-3.1.). In particular, comparison of the data for ^{40}Ar and ^{40}Ca spallation will shed light on the effect of the neutron-richness of the parent nucleus. The detailed measurement of the behaviour of the Fe spallation cross-sections down to ~ 300 MeV/n (Webber 1984) is also an invaluable source of information (but one pending problem is to within which accuracy the cross-sections measured at Bevalac up to at most 1.7 GeV/n are constant beyond that energy ; see, e.g., Perron 1976). In the UH range, the new data by Kertzman et al. (3, 95) should also allow improved estimates. As a general rule, adjustment factors for individual cross-sections should, of course, be avoided, since they do not permit improved predictions for unmeasured cross-sections.

I-3.3. Nucleus-nucleus cross-sections

Since all the Bevalac measurements of spallation on H (§ I-3.1.) have actually been performed by comparing data for spallation on CH_2 and on C, they have also given information on nucleus-nucleus interactions. In addition Heinrich et al. (3, 99) have specifically addressed this problem, by performing measurements of ^{40}Ar and ^{56}Fe spallation on $C_{12}H_{18}O_7$ and Ag and discussing the scaling of the cross-sections as compared to cross-sections on H (see also their list of references). They are at present developing analytical expressions for nucleus-nucleus cross-sections. I shall not discuss this topic here, which is however important as regards nuclear physics, for atmospheric and instrumental corrections, and as giving hints on spallation cross-sections on He, which may become crucial for refined studies of interstellar propagation (truncation ; Ferrando et al. 3, 61; § III-2.3.1.).

I-4. OBSERVATIONS OF ULTRA-HEAVY (UH) NUCLEI

I-4.1. The HEAO-C3 and Ariel VI data

Improved data on UH nuclei (Z > 30) from the HEAO-C3 and Ariel VI spacecraft experiments have been presented at this conference by Newport et al. (2, 123), Klarman et al. (2, 127) and Waddington et al. (9,...), and by Fowler et al. (2, 115, 119).

The Ariel VI team has provided an improved analysis of their data for both $Z \lesssim 48$ (where only high geomagnetic cut-off portions of the orbit can be used, to avoid pollution by low-energy Fe nuclei) and $Z \gtrsim 48$ (where the entire orbit can be used) (Fowler et al. 2, 115, 119). Their "apparent charge" histogram for $Z \gtrsim 48$ is shown in figure 9; the median energy of these particles is fairly low, $\sim$ 2 GeV/n. From such histograms, elemental abundances are derived by deconvolution with an instrumental resolution function extrapolated from that of Fe. Corrections for interactions within the (rather thin) instrument are not large. The corrected abundances are plotted in figure 10 (for $Z \gtrsim 62$, grouped into broad ranges of elements, see also Table 1).

In the higher Z range $Z \gtrsim 50$, the HEAO-C3 team has also provided improved data for higher energy nuclei (recorded when the geomagnetic cut-off was > 5 GV; median energy $\sim$ 6 GeV/n) (Klarman et al. 2, 127; Waddington et al. 9,...). Their brutto "apparent charge" histogram is also shown in figure 9. Exploiting these data for $Z \gtrsim 62$, the authors felt it more realistic to give only abundances for broad ranges of elements, in view of the limited charge resolution and statistics. They are given in Table 1 and plotted in figure 10. These values have been approximately corrected for the interactions within the HEAO-C3 instrument, which is much thicker than Ariel VI (see caption of fig. 10).

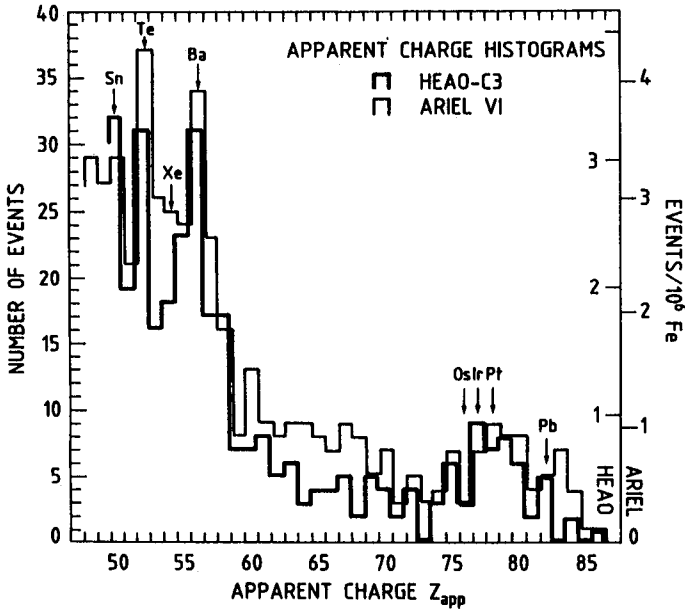

Fig. 9 The brutto "apparent charge" (Z_{app}) histograms prior to any correction for $Z \gtrsim 48$, obtained by both the HEAO-C3 and the Ariel VI experiments (Waddington et al. 9, ... ; Fowler et al. 2, 119). As can be seen, the charge resolution and the number of counts (Table 1) are comparable for both experiments in this charge range. There tends to be more Pb relative to Pt, and more secondaries with $Z \approx 62$-73 in the Ariel VI data. The latter point may be an energy dependent effect(see § I-4.2. and fig.11).

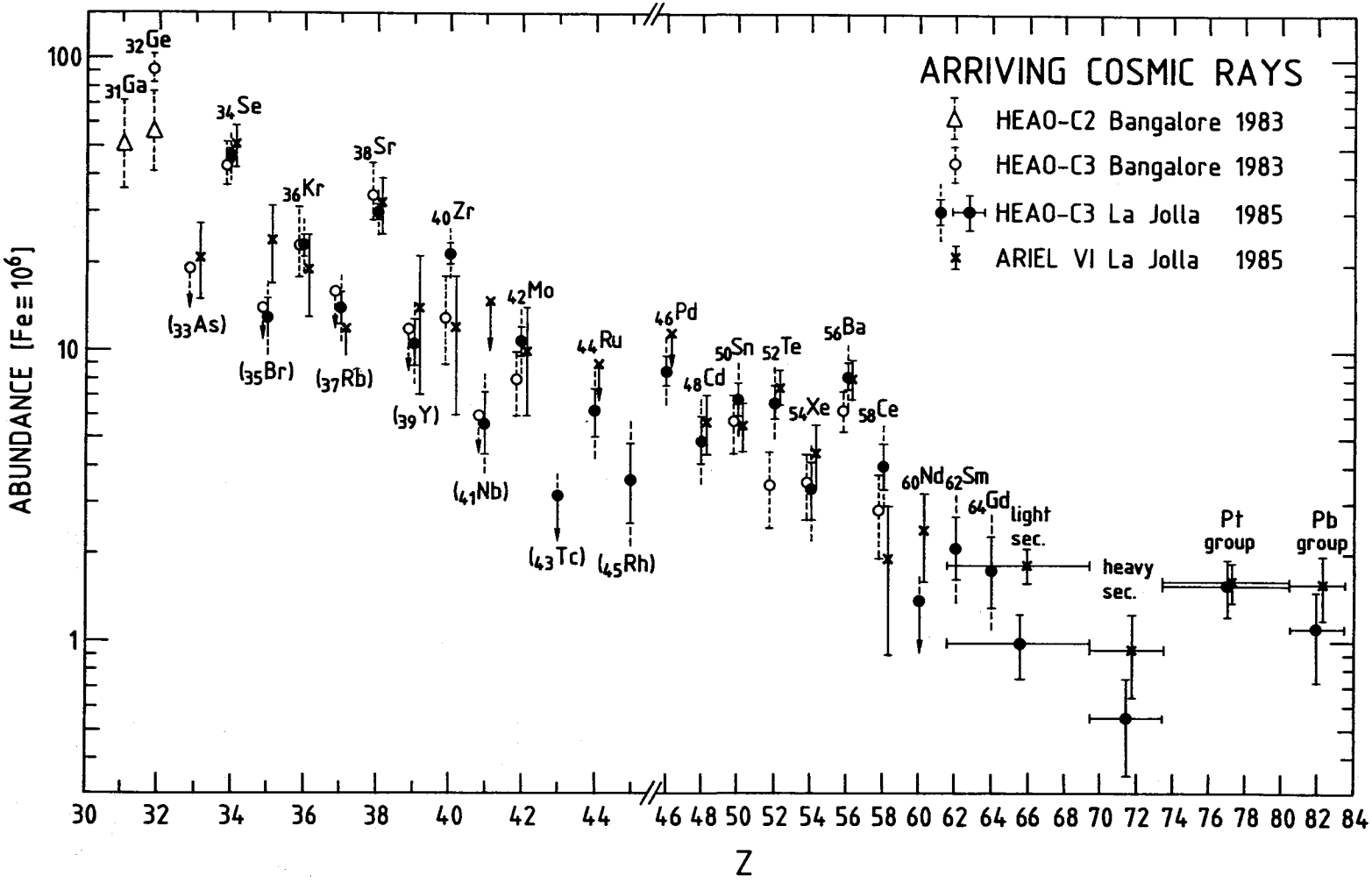
ARRIVING COSMIC RAYS
HEAO-C2 Bangalore 1983
HEAO-C3 Bangalore 1983
HEAO-C3 La Jolla 1985
ARIEL VI La Jolla 1985
ABUNDANCE [Fe≡10⁶]
Z
100
10
1
30 32 34 36 38 40 42 44 46 48 50 52 54 56 58 60 62 64 66 68 70 72 74 76 78 80 82 84
31Ga
32Ge
34Se
36Kr
38Sr
40Zr
42Mo
46Pd
48Cd
50Sn
52Te
54Xe
56Ba
58Ce
60Nd
62Sm
64Gd
(33As)
(35Br)
(37Rb)
(39Y)
(41Nb)
(43Tc)
(45Rh)
light sec.
heavy sec.
Pt group
Pb group

At lower Z = 34 to 64, the HEAO-C3 group is now developing a new technique of analysis in order to take advantage of their full statistics, by using the particles from the entire energy range covered by their detectors (Newport et al. 2, 123). Medium energy particles were previously excluded from the analysis, because their individual charge and velocity cannot be unambiguously determined from their ionization chamber and Cerenkov signals. The authors now perform a maximum likelihood adjustment of the elemental abundances, that accounts best for the entire ionization chamber-Cerenkov two-dimensional histogram. The useful statistics is thus almost doubled. But, of course, the method is delicate, and no conventional "charge histograms" can be produced.

Very preliminary elemental abundances obtained by this method are shown in figure 10, together with the "classical" earlier data presented at the Bangalore conference (Binns et al. 1983; Stone et al. 1983). These data have been presented at the Conference, but are not in the proceedings. The stated errors are only statistical ones within a given fitting model, and the final uncertainties will certainly be larger (E.C. Stone, private comm.; see caption of fig. 10).

Fig. 10 Abundances of arriving cosmic-rays with Z ≥ 31, deconvolved from the original "apparent charge" histograms or matrices (e.g. fig. 9). For Z ≤ 45 both even and odd-Z element abundances are given, but (except for $_{31}$Ga measured by the HEAO-C2 instrument with adequate resolution) none of the given odd-Z abundances should be considered really significant ; they are rather order of magnitude estimates that improve the estimate of the even-Z element abundances. For Z ≥ 46, only even-Z element abundances are given ; they include those of adjacent odd-Z elements (the systematic bias thus introduced is generally small with respect to the uncertainties). The HEAO-C2 points for $_{31}$Ga and $_{32}$Ge are from Byrnak et al. (1983b). The HEAO-C3 Bangalore Conference points are from Binns et al. (1983) and Stone et al. (1983). They are derived from charge histograms of a fraction of the data (see § I-4.1.). The new HEAO-C3 points up to Z = 64 are very preliminary results of a new two-dimensional analysis of the entire set of data (Newport et al. 2, 123). The stated errors are only statistical ones, within a particular fitting model ; the final errors will be larger (E.C. Stone, private comm.), which I have recalled by plotting an arbitrary dashed prolongation to the statistical error bars. This is in particular true for the odd-Z elements, whose abundances are highly dependent upon the fitting procedure; some of them were implausibly low in the authors' original graph. I have taken the liberty to raise them to a plausible level; the resulting corrections on the adjacent even-Z element abundances are not large (<18%). But I stress that the intrinsic charge resolution of the instrument is quite adequate to resolve even-Z elements (see Binns et al. 1983, 1984 ; Stone et al. 1983). The deconvolved Ariel VI data, with poorer intrinsic charge resolution below Z = 48, give comparable abundances for even-Z elements up to Z = 60 (Fowler et al. 2, 115, 119). For Z ≥ 62, where charge resolution and statistics are becoming poor in both experiments (fig. 9), I have followed the choice of the HEAO-C3 team and plotted only average abundances (per even-Z element) over broad, physically significant, ranges of elements (Table 1 ; Klarman et al. 2,127 ; Waddington et al. 9,...; Fowler et al. 2, 119). The normalisation to Fe of the HEAO-C3 data for Z ≥ 62 is not perfectly determined (corrections for interactions within the detector). Based on discussions, I have applied a global correction factor of 1.20 ± 0.15 to the HEAO-C3 figures relative to Fe (Table 1). For the sake of clarity, all error bars extending over a factor of ≥ 4 have been replaced by upper limits. The higher "secondary element" fluxes observed by Ariel between Z = 62 and 73 is probably an energy dependent effect (see § I-4.2. and fig. 11).

I-4.2. UH data, overview

The general picture apparent from fig. 10 can be described as follows. Up to Z ≈ 45, the intrinsic resolution of the HEAO-C3 instrument is significantly superior to that of Ariel VI (Binns et al. 1983, 1984 ; Fowler et al. 2, 115). The new two-dimensional analysis of the entire set of HEAO-C3 data (Newport et al. 2, 123) yields quite small statistical errors and is very promising, although the additional non-statistical errors have not yet been assessed. For even Z-elements, these new values are generally in good agreement with both the earlier HEAO-C3 analysis and the Ariel VI data, except for $_{40}$Zr, for which the earlier errors were very large. Tentative odd-Z-element abundances have been plotted in figure 10, but the instrument resolutions are such that none of them can be considered significant (except for $_{31}$Ga, observed with adequate resolution, though low statistics, by the HEAO-C2 experiment ; Byrnak et al. 1983b). Rough odd-Z-element abundance estimates are however useful to improve the fit of the even-Z-element abundances (which are not much affected by the associated uncertainties, except perhaps for $_{40}$Zr).

In the range Z = 46 to 60, where only even-Z-elements are given in figure 10, the resolution of the two experiments is becoming almost comparable (fig. 9). There is a very good agreement between the two experiments on the main s- and r-process peak elements from Z = 50 to 56 (in particular $_{52}$Te is no longer low in the HEAO-C3 analysis).

Beyond Z = 62, figure 9 clearly shows that in both experiments, neighbouring even-Z-elements are no longer well resolved (see, e.g., near Z = 75 and Z = 80), and that the statistics is low. There may, in addition, be small systematic shifts of the charge scale (see, e.g. $_{82}$Pb) (e.g., Newport et al. 3, 287). Accordingly, only abundances for the wide,

Table 1 - The data on UH nuclei with Z ≥ 62

Z_{app} [a]	Denomination	HEAO-C3 [b]				ARIEL VI [c]			
		brutto counts	relative corrected	normal.to Fe corrected		brutto counts	relative corrected	normal.to Fe corrected	
26	Fe	(9.6 ± 0.5).10^6	-	≡ 10^6	≡ 10^6	8.68.10^6	-	≡ 10^6	≡ 10^6
62-69	"Light Sec."	34	0.33 ± 0.06	4.0 ± 1.0	5.1 ± 1.1	63	0.44 ± 0.06	7.4 ± 1.0	9.3 ± 1.0
70-73	"Heavy Sec."	10	0.09 ± 0.03	1.1 ± 0.4		18	0.11 ± 0.04	1.9 ± 0.6	
74-80	"Pt group"	42	0.46 ± 0.07	5.5 ± 1.2	6.9 ± 1.5	46	0.34 ± 0.05	5.7 ± 0.9	7.7 ± 1.0
81-86	"Pb group"	10	0.12 ± 0.04	1.4 ± 0.5		22	0.12 ± 0.04	2.0 ± 0.5	
62-86	Sum Z ≥ 62	96	≡ 1.00	12.0 ± 2.3	12.0 ± 2.3	149	≡ 1.00	17.0 ± 1.4	17.0 ± 1.4
(62-73)/(74-86)	Sec/"PtPb"	-	0.73 ± 0.15	-	-	-	1.21 ± 0.20	-	-
(81-86)/(74-80)	"Pb"/"Pt"	-	0.25 ± 0.09	-	-	-	0.35 ± 0.10	-	-
≥ 87	Actinides	0.5 [d]	-	∿ 0.06	-	3	-	0.4 ± 0.2	-

[a] Z_{app} = "apparent charge", not including possible non-Z^2 effects in the real charge scale (e.g., Newport et al. 3, 287).
[b] Klarman et al. 2 , 127 ; Waddington et al. 9,... . The authors have applied a correction for the effect of nuclear interactions in their, comparatively thick, detector on the relative abundances of Z ≥ 62 nuclei. The effect of the interactions on the abundances with respect to Fe is not straightforward. Based on discussions, I have applied an additional global correction factor of 1.20 ± 0.15.
[c] Fowler et al. 2, 119. The corrections include deconvolution of the "apparent charge" histogram, and corrections for nuclear interactions in the, comparatively thin, detector.
[d] Fixsen et al. (1983) have observed 1 actinide nucleus for 17.4·10^6 Fe nuclei.

physically significant charge ranges defined by the HEAO-C3 team have been plotted in figure 10. They are defined in Table 1, which gives also key abundance ratios.

Figures 9 and 10 show that both experiments agree well on the "Pt-group" element abundances, and that Pb is better defined and somewhat higher in the Ariel VI data.

As regards secondaries, in the Z = 62-73 region, they are also higher in the Ariel VI data. Now, recall that the HEAO-C3 data are taken when the rigidity cut-off R_c is > 5 GV (median energy of the recorded particles ∿ 6 GeV/n), while the Ariel VI data include locations with much lower cut-off (median energy of the particles ∿ 2 GeV/n). When only location where R_c > 5 GV are selected in the Ariel VI data, the difference with respect to HEAO-C3 seems to disappear (fig. 11; P.H. Fowler, private comm.). So, the data simply seem to indicate an increase of the secondary/primary ratios towards lower energies. (See discussion in terms of a low energy increase of the grammage and especially cross-sections in § III-2.3.2.).

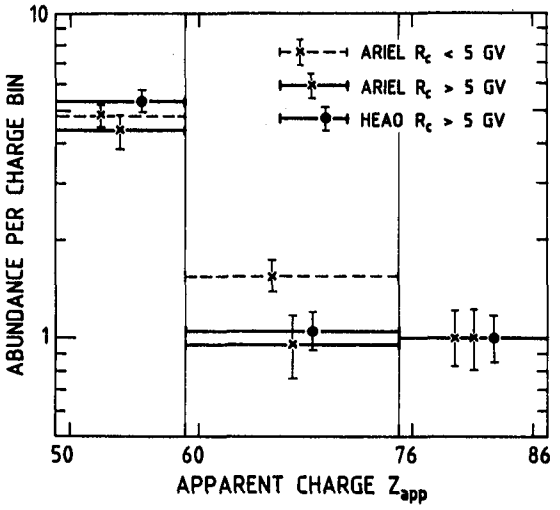

Fig. 11 Comparison between the Ariel VI data obtained at low cut-off rigidities R_c < 5 GV and the Ariel VI and HEAO-C3 data obtained at high R_c > 5 GV. Brutto data, averaged over wide charge ranges, are used. Normalized to the Pt-Pb region (Z_{app} = 76 to 86). Based on P.H. Fowler, private communication. The HEAO-C3 and Ariel VI data obtained at equal, high R_c agree.

The total abundance of nuclei with Z = 62-83, both primary and secondary, is marginally higher in Ariel VI (17.0 ± 2.6) than in HEAO-C3 (12.0 ± 2.0, relative to Fe = 10^6). These figures give a rough indication of (strictly, a lower limit to) the abundance of primary nuclei emitted at the sources). The small difference between Ariel VI and HEAO-C3 cannot be simply accounted for in terms of more spallation at low energy, which would produce the opposite effect. It might, however, have to do with the energy dependence of the shape of the mass yield (Kaufman and Steinberg 1980), on which the data of Kertzman et al. (3, 95) give information at 1 GeV/n only (§ I-3.1.; fig. 7).

As regards Actinides, the Ariel VI team has 3 candidates (Fowler et al. 2, 119). The HEAO-C3 team reported 1 candidate in Bangalore (Fixsen et al. 1983). See Table 1. The HEAO-C3 value for the ratio (Th+U)/(Pt+Pb group) is close to the LG value ∿ 10^{-2}, the Ariel value is ∿ 4 times higher.

I-5. DEUTERIUM, HELIUM-3 AND ANTI-PROTONS

Beatty (2, 56), Evenson et al. (2, 60) and Mewaldt (2, 64) have provided new data on low energy D and ^{3}He, which are purely secondary isotopes. The conclusion of the three studies is that most of the existing low energy D and ^{3}He data are readily accounted for by standard propagation and modulation models that account for the heavier nuclei abundances (escape length $\lambda_e \approx 6$ to 8 g.cm^{-2}). [2]

The high ^{3}He/^{4}He ratio $\approx 0.24 \pm 0.05$ at 6 GeV/n (Rigidity $\sim$ 13 GV) recently reported by Jordan and Meyer (1984) and Jordan (1985) is most probably an overestimate. The authors have indeed stressed that this result is highly sensitive to the value of the ^{4}He rigidity spectral index γ_R near Earth at the time of the observation (with $d\Phi/dR \propto R^{-\gamma_R}$), in the sense of a positive correlation between the derived value of ^{3}He/^{4}He and γ_R. To get the above value of the ^{3}He/^{4}He ratio, the authors have assumed that $\gamma_R = 2.65$ around 13 GV, near Earth, in April 1981. Now, Golden et al. (2, 1) have measured $\gamma_R = 2.58 \pm 0.05$ between 10 and 25 GV, in September 1976. [3] The value of γ_R near 13 GV in April 1981 can be only lower, because the spectrum is bent within the above rigidity range, and because of the much higher degree of solar modulation in 1981 (e.g. Lockwood and Webber 1984). Earlier measurements, as summarized by Smith et al. (1973) or Webber and Lezniak (1974), also clearly point towards lower values of $\gamma_R \sim 2.40$ to 2.50 at 13 GV, near Earth.

The standard leaky-box models fitting the B/C ratio with rigidity dependent escape yield ^{3}He/^{4}He $\approx 0.17 \pm 0.05$ at 6 GeV/n (scaled from Meyer 1974 ; Lagage and Cesarsky 1985). [4] Jordan (1985)'s observations lead to values of ^{3}He/^{4}He in this range for values of γ_R between 2.52 and 2.62, a perfectly plausible range for γ_R at the time of his observations. There is therefore no hint whatsoever for an anomaly.

Jordan (1985)'s data, together with the low energy data on D and ^{3}He, can be used to set lower limit to the intrinsic thickness of the thick sources invoked to explain a possible cosmic-ray anti-proton excess (Cowsik and Gaisser 1981 ; Cesarsky and Montmerle 1981 ; Tan and Ng 1983; Lagage and Cesarsky 1985 ; Tan 2, 346).

---

[2] There is, however, a problem for the high deuterium fluxes observed by Webber and Yushak (1983), which, like the earlier data of Hsieh et al. (1971), remain a mystery. Such data could be understood only if, at the time of the data taking, the interplanetary deceleration was so weak that the bulk of the deuterons due to the $p + p \rightarrow d + \pi^+$ process, with energies below $\sim$ 200 MeV/n in the interstellar medium, were still observable near Earth (Meyer 1975; Webber and Yushak 1983). This would be extremely difficult to accept, considering all evidences on solar modulation. In addition, Evenson et al. (2,60) noted the constancy of their observed D/^{4}He and ^{3}He/^{4}He ratios between 1978 and 1983 (a period which, however does not include extreme solar minimum conditions, e.g. Lockwood and Webber 1984).

[3] The larger value published by Golden et al. (2,1) in the proceedings is not that measured near Earth, but refers to the derived demodulated He spectrum. These results replace those published by Badhwar et al. (1979).

[4] With the assumption of rigidity dependent escape, the equilibrium ^{3}He/^{4}He ratio at a given energy/nucleon is 20% higher than predicted based on the formation rates only, because the residence time of ^{3}He in the galaxy is longer than that of ^{4}He at the same energy/nucleon. (Therefore, if the bulk of the grammage is spent near the sources, where the rigidity dependent escape takes place, the predicted ratio near Solar System is ^{3}He/^{4}He = 0.14 only.)

I-6. ENERGY SPECTRA OF PRIMARY NUCLEI

At this conference, a number of studies have been devoted to this subject : Golden et al. (2, 1) ; Engelmann et al. (2, 4) ; Webber et al. (2, 16) ; Derrickson et al. (2, 20) ; Burnett et al. (2, 32, 48) ; Sato et al. (2, 36); Streitmatter et al. (2, 40); Vernov et al. (2, 52).

Although I regard this subject as important, I will not discuss it here. [5]

I-7. ELECTRONS AND POSITRONS

Nishimura et al. (9, ...) have provided improved e^- spectra up to 2000 GeV (fig. 12). The presence of e^- fluxes at such high energies, where the e^- lifetime against synchrotron loss is $\lesssim 10$ years, implies that their sources are close by, within a few 100 pc. These data, confronted with the constraints from CR nuclei, also favour a nested leaky-box model for propagation, a standpoint already advocated by Nishimura et al. (1981), Tang and Müller (1983), Müller and Tang (1983), Mauger and Ormes (1983), and Tang (1984).

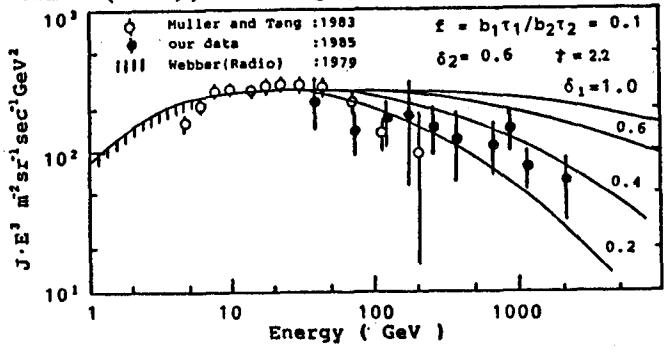

Fig. 12 New data on the high energy electron spectrum up to 2000 GeV by Nishimura et al. (9,...).

Golden et al. (2, 374) and Müller and Tang (2, 378) have provided new measurements of the $e^+/(e^+{+}e^-)$ ratio between 5 and 20 GeV (fig. 13). The high values observed for this ratio are probably due to a rapid decrease of the e^- flux above a few GeV.

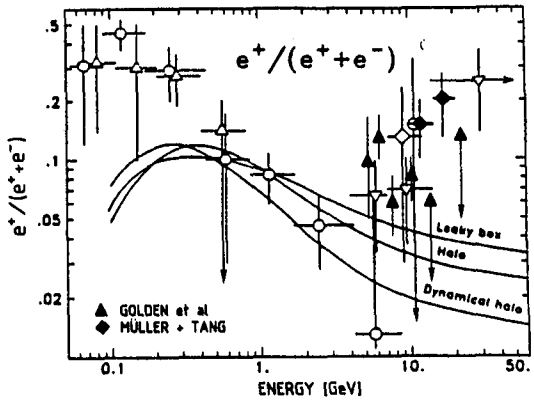

Fig. 13 The new observations of the $e^+/(e^+{+}e^-)$ ratio between 5 and 20 GeV by Golden et al. (2, 374) and Müller and Tang (2, 378), along with earlier data.

[5] This is the shortest paragraph in my report!

PART II

ASSESSING THE GALACTIC COSMIC-RAY SOURCE (GCRS) ELEMENTAL COMPOSITION CORRELATION WITH FIRST IONIZATION POTENTIAL (FIP)

II-1. GCRS ELEMENTAL COMPOSITION UP TO Z = 30

Up to Z = 30 the cosmic ray data are very reliable and a comparison is possible with Solar Energetic Particles (SEP) abundances. After having specified the Local Galactic (LG) abundances I shall use as a reference (§ II-1.1.), I am going to discuss the various available determinations of the elemental composition (fig.14) as to obtain an "adopted" GCRS composition (fig. 15 ; § II-1.2.). I shall then compare the GCRS, SEP and Solar Coronal compositions (fig. 17 ; § II-1.3.) and discuss their common properties (§ II-1.4.).

II-1.1. The Local Galactic (LG) reference abundances used

The LG abundances used for reference are mostly those of Meyer (1979a,b ; 1985a,b), generally in good agreement with recent analysis of Anders and Ebihara (1982) and Grevesse (1984a,b). For S, Cu and Zn, the improved agreement between the recent type I carbonaceous chondrite (hereafter C1) and photospheric determinations have led me to slightly modify the values and considerably reduce the error bars : S = 45 (1.15) [6], Cu = 0.047 (1.10), Zn = 0.124 (1.08) on the scale Si = 100. Note, however, that there is an apparently significant difference between C1's and photosphere for Fe, which seems higher by a factor of 1.45 ± 0.11 in the Photosphere than in C1's!!!. This is all the more a puzzle since the siderophile elements Cr, Co, Ni, Pd definitely do not show the same trend, and are found equally abundant in C1's and Photosphere (Grevesse 1984a). By contrast, there seems to be another significant discrepancy for Ti, a refractory, not siderophile element. As regards the C1 and photospheric abundances of volatile Ge and Pb, see Grevesse and Meyer (3, 5) and § III-3.5. .

In figures 14 and 15, I have kept the traditional C1 value to LG Fe, but have also indicated where Fe would lie if the photospheric value would be adopted as a reference instead.

II-1.2. GCRS composition up to Z = 30: the data and the adopted composition

Figure 14 gives up to date information on the GCRS/LG abundance ratios for elements up to Zn, versus First Ionization Potential (FIP). I have avoided, as much as possible, determinations based on low energy data ($\leqslant$ 500 MeV/n), whose interpretation may pose specific problems related to strongly energy dependent low energy cross-sections and possible distributed reacceleration (Silberberg et al. 1983). As will be shown in the discussion of the B vs. ^{15}N problem (§ III-2.1.), this hypothesis may have to be taken very seriously.

[6] Throughout this paper such figures between parentheses denote error factors: "within a factor of...".

II-1.2.1. Source abundances derived from elemental data

The basic determinations used are those from the HEAO-C2 experiment, derived from high energy observations between 1 and 25 GeV/n (Engelmann 1984 ; Lund 1984). At this conference, Webber et al. (3, 42) have reestimated the source abundances, based on the HEAO-C2 data specifically at 1.5 GeV/n, taking into account their new cross-section measurements up to $\sim$ 0.8 to 1.3 GeV/n (Webber and Kish 3, 87 ; see § I-3.1.). They have assumed that the trend for an enhanced production of secondaries with Z = 12 to 14 observed in the spallation of ^{28}Si and ^{40}Ar was also valid for other neighbouring parent nuclei. This leads, in particular, to a decrease of the estimated source Al abundance (fig. 6). Whenever different from the previous values, these new estimates of the GCRS/LG ratios have been given in fig. 14. HEAO-C3 data have also been used for Zn (Binns et al. 1984), as well as for Ar and Ca, for which the data of Jones et al. (2, 28) up to $\sim$ 200 GeV/n, i.e. at highest energies where the secondary component is much reduced, should in principle yield very accurate source abundances. However, for the reasons discussed in § I-1., I think these latter determinations should be considered preliminary at the present stage.

II-1.2.2. Source abundances derived for isotopic data

For N, Ar and Ca, we have also source abundance determinations based on low energy ($\sim$ 200 to 600 MeV/n) isotopic observations of ^{14}N, ^{36}Ar and ^{40}Ca, which are the predominant isotopes in the sources. These source abundance determinations should, in principle, be much more accurate than those based on elemental observations only, since the secondary component to be subtracted is comparatively much smaller.

As regards Ca, the cross-sections for secondary formation of ^{40}Ca are extremely small so that, while surviving primaries make up only 30 to 55% of arriving elemental Ca for energies from 1 to 25 GeV/n, they make up 95% of arriving ^{40}Ca at 0.6 GeV/n (fig. 16). ^{40}Ca is thus essentially a pure primary, and the Ca source abundances derived from ^{40}Ca isotopic data are therefore extremely clean (e.g., Krombel and Wiedenbeck 2, 92). They are essentially limited by the statistics of the isotopic observations (the mass resolution is generally adequate to separate mass 40 from $\geq$ 42, ^{41}Ca being very scarce; figs. 2 and 3). Following the summary by Krombel and Wiedenbeck (2, 92), I have plotted in fig. 14 the Ca GCRS/LG ratios resulting from the five available isotope measurements (Tarlé et al. 1979 ; Young et al. 1981 ; Webber 1981 ; Webber et al. 2, 88, source ^{40}Ca/Fe = 0.113 ± 0.027 derived by myself ; Krombel and Wiedenbeck 2, 92).

As regards Ar, the situation is less favourable: while surviving primaries make up $\sim$ 25 to 55% of arriving elemental Ar for energies from 1 to 25 GeV/n, they still make up only 50% of arriving ^{36}Ar at 0.6 GeV/n (fig. 16). So, the secondary contribution remains important, even for ^{36}Ar. The two available determinations (Webber 1981; Webber et al. 2, 88, source ^{36}Ar/Fe = 0.062 ± 0.024 derived by myself) thus give source Ar values which are sensitive to the conditions of propagation and secondary formation at low energy. I shall show in § III-2.1. that these conditions pose very serious problems.

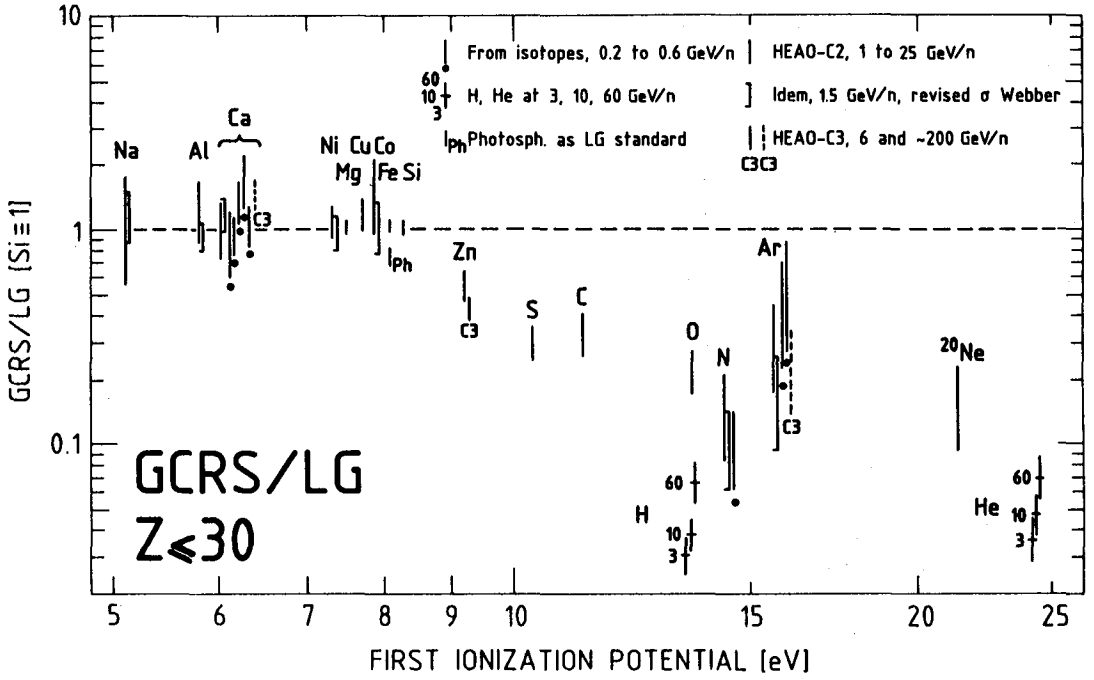

Fig. 14 GCRS/LG abundance ratios vs. FIP, for Z ≲ 30 : the various determinations. Normalized to Si. The errors are the quadratic sum of the GCRS and the LG errors (§ II-1.1.). For Fe, I have also plotted its GCRS/LG ratio if the photospheric value is taken as LG standard (marked by "Ph" ; § II-1.1.). For Ne, for which the minor isotope ^{22}Ne is greatly in excess (§ III-4.1. ; fig. 29), the plotted ratio refers to the dominant isotope ^{20}Ne only. [As regards Mg and Si, possibly also slightly isotopically anomalous (fig. 29), considering only the dominant isotopes ^{24}Mg and ^{28}Si would yield a negligible correction]. As regards H and He, they are given at a given energy/nucleon for three different energies (3, 10 and 60 GeV/n), based on the data compiled and propagated back to the sources by Engelmann et al. (1985) (see § II-1.2.3.). The various determinations of the GCRS abundances : for each element, the first bar on the left is the HEAO-C2 determination based on observations over the range from ∿ 1 to 25 GeV/n (Engelmann 1984 ; Lund 1984). Next comes, as a left-oriented bracket, the new estimate by Webber et al. (3, 42), based on the HEAO-C2 data at 1.5 GeV/n and on new cross-sections, especially from Webber and Kish (3, 87) (see § I-3.1. and II-1.2.1.). It is given only when the new estimate differs significantly from the original one. Next come, marked by a dot below the error bar, source abundances derived from low energy (∿ 200 to 600 MeV/n) isotope observations (see § II-1.2.2.). For Ca, they are, from left to right, due to Tarlé et al.(1979), Young et al. (1981), Webber (1981), Webber et al. (2, 88), and Krombel and Wiedenbeck (2, 92), and for Ar to Webber (1981) and Webber et al. (2, 88) (see discussion in § II-1.2.2. and III-2.1.). For N, the isotope bar summarizes a number of low energy isotope studies (see § III-2.1. and 2.2.). Finally, the bars marked "C3" result from the HEAO-C3 data, at GeV/n energies for Zn (Binns et al. 1984), and at ∿ 200 GeV/n for Ca and Ar (Jones et al. 2, 28) ; the latter two values, with dashed error bars, are still preliminary (see § I-1. and II-1.2.1).

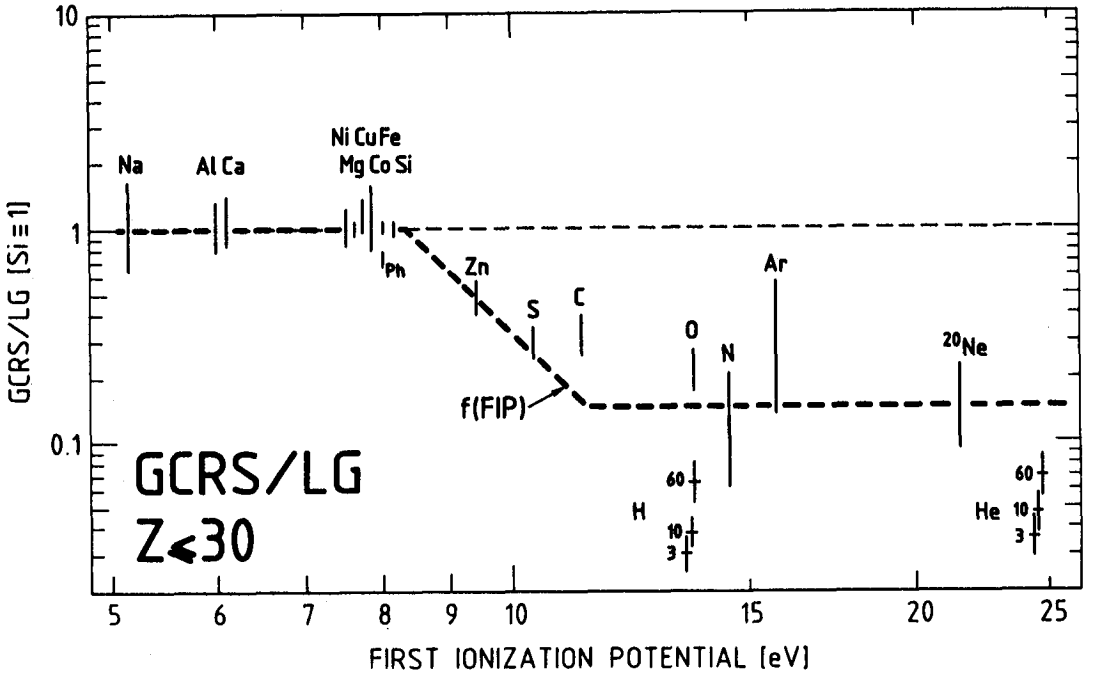

Fig. 15 GCRS/LG abundance ratios vs. FIP, for Z ≤ 30 : adopted values, derived from fig. 14. See caption of fig. 14, and text § II-1.2.4.. Also plotted is f(FIP) the adopted shape of the correlation between GCRS/LG vs. FIP for Z ≤ 30 (§ II-1.4.). As discussed in this §, f(FIP) does not fit C, O, H and He (see also fig. 17).

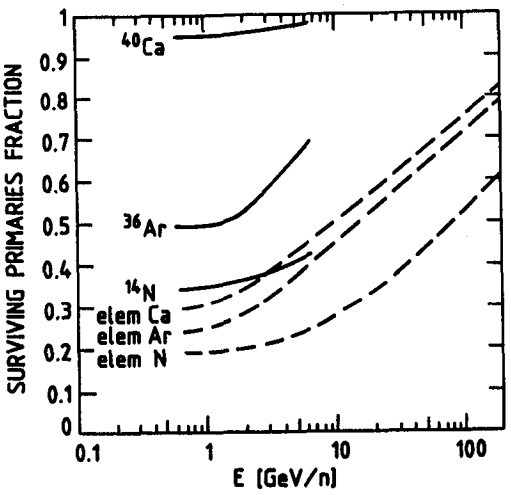

Fig. 16 Fraction of surviving primaries among arriving GCR's for elemental ^{14}N, Ar, Ca (dashed), and for isotopic ^{14}N, ^{36}Ar, ^{40}Ca (solid) as a function of energy (§ II-1.2.2. and III-2.2.). The assumed source ratios are ^{14}N/O = 6.0%, ^{36}Ar/Fe = 2.8%, ^{40}Ca/Fe = 6.3%.

The situation is even worse for N: surviving primaries make up $\sim$ 20 to 35% of arriving elemental N for energies from 1 to 25 GeV/n, but still make up only $\sim$35% of arriving ^{14}N at 0.6 GeV/n (fig. 16). Actually, the lower source N/O ratios ($\sim$ 3%) found from low energy isotopic ^{14,15}N data, and their contrast to higher values ($\sim$ 6%) derived from high energy elemental measurements have been discussed at length in recent years. I shall discuss that point in detail in § III-2., from a new standpoint.

II-1.2.3. Hydrogen and Helium at sources

Now consider H and He. According to current shock wave acceleration theories, the relevant parameter for acceleration is momentum per nucleon (or, equivalently, energy per nucleon), not rigidity (e.g. Krimsky 1977 ; Axford et al. 1977 ; Bell 1978a,b ; Blandford and Ostriker 1978 ; Axford 1981). It is therefore preferable not to discuss the source H/He ratio at a given rigidity, and I shall consider this ratio at a given energy/nucleon. But rigidity dependent escape from the galaxy (which acts differently on H and He at a given energy/nucleon) is essential in properly deriving the source H and He spectra from the observed ones. The study of Engelmann et al. (1985 ; see their fig. 12) shows that, when this is done, the H and He source spectra, in the range in which they are both precisely determined ($\sim$ 3 to 60 GeV/n), are such that : (i) The H/He ratio is remarkably constant and normal ($\approx$10); (ii) the abundance ratios of H and He to CNO are energy dependent; they increase by a factor of $\sim$ 2 (1.5) between 3 and 60 GeV/n (based on all existing data for the CNO spectrum, not merely those of HEAO-C2, which tend to be steeper than the other ones; Engelmann et al. 1985, and 2,4). Note that no significant energy dependence of any heavy element/heavy element source abundance ratio could ever be noticed between $\sim$ 0.5 and $\sim$ 25 GeV/n. This energy dependence of the H,He to heavier nuclei ratios has been shown in figs. 14 and 15.

II-1.2.4. "Adopted GCRS composition for Z $\lesssim$ 30

Based on the detailed data on GCRS composition presented in fig. 14, I derive an "adopted" set of elemental GCRS/LG ratios for Z $\lesssim$ 30, which is shown versus FIP in fig. 15. In these adopted abundances I have taken into account, though with some prudence, the trends associated with the new cross-section estimates by Webber and Kish (3, 87) and Webber et al. (3, 42), in particular as regards the lower Al abundance. For Ca, I have kept an error bar which is consistent with all elemental and especially isotopic determinations. For the more difficult cases of N and Ar, for which the interpretation of the isotopic data depends strongly on low energy propagation (§ III-2.1.), I have kept very large error bars, encompassing essentially the entire range of existing estimates. In fig. 15, I have also marked the position of Fe if the photospheric value is taken as a standard, instead of the C1 meteoritic value (§ II-1.1.; Grevesse 1984a) : Fe would then be deficient by a factor of $\sim$ 1.40 in GCRS, relative to Al, Mg, Si, Ca, Co, Ni, Cu.

II-1.3. Comparison with Solar Energetic Particles (SEP) and Solar Coronal compositions

Before discussing the properties of the obtained GCRS/LG correlation with FIP (§ II-1.4.), I want to compare the GCRS and the SEP abundances. It is now well established that the GCRS composition pattern versus FIP is remarkably similar to the basic pattern of SEP, as well as to the solar coronal composition, which differs from that of the photosphere and C1's ("Local Galactic") (Webber 1975, 1982b; Cook et al. 1979, 1980, 1984 ; Mc Guire et al. 1979, 1986; Mewaldt 1980 ; Meyer 1981a,b,c, 1985a,b ; Breneman and Stone 4, 213, 217). Using γ-ray line spectroscopy data, Murphy et al. (4, 249, 253) have, at this conference, found once again the same pattern of abundances in the upper chromosphere or lower transition region material (except for Ne, which is a problem!).

These similarities in composition, together with other arguments, led to the suggestion that SEP and GCRS compositions are, to first order, a reflection of the composition of solar-stellar coronae (F to M stars), out of which they have first been extracted (Meyer 1985b ; see also Montmerle, 1984). As regards the reason why the solar coronal composition is biased according to FIP, it is not known. Two scenarios are at present attempting to understand it, one in terms of a dynamical ionization model in spicules (Geiss and Bochsler 1984), the other in terms of gravitational settling of neutrals in the presence of the magnetic field within the chromospheric plateau (Vauclair and Meyer 4, 233).

Figure 17 compares the GCRS abundances to SEP abundances for $Z \lesssim 30$. Two sets of SEP abundances are taken: (i) the "mass-unbiased" baseline composition of Meyer (1981a, 1985a), which represents the composition of these events in which the abundances are least perturbed by rigidity (and hence, roughly Z -) dependent acceleration and propagation effects, as judged from their Fe/Mg,Si ratio [7] ; in these events the correlation of abundances with FIP, presumably an image of their coronal source material, is cleanest. (ii) the new 10-flare average presented at this conference by Breneman and Stone (4, 213, 217), who suggest that, on the average, rigidity dependent acceleration-propagation effects do not entirely cancel out in SEP's, so that the average SEP composition is slightly biased as a function of A/Q (or, roughly, Z) with respect to the original coronal composition (where Q = mean effective charge). (This conclusion however depends somewhat upon the adopting of the photospheric, rather than C1, value as a standard for Fe; the properties of this average over 10 flares will also have to be confirmed by a much broader averaging).

I now discuss the GCRS/SEP ratios plotted in fig. 17:

(i) Fig. 17 confirms that the two compositions are very similar. The strong dependence of the GCRS/LG ratio upon FIP (fig. 15) has to first order disappeared in the GCRS/SEP plot.

[7] Using the photospheric instead of the C1 value as a standard for Fe would only slightly modify the derived "mass-unbiased" baseline SEP composition (Meyer 1985a).

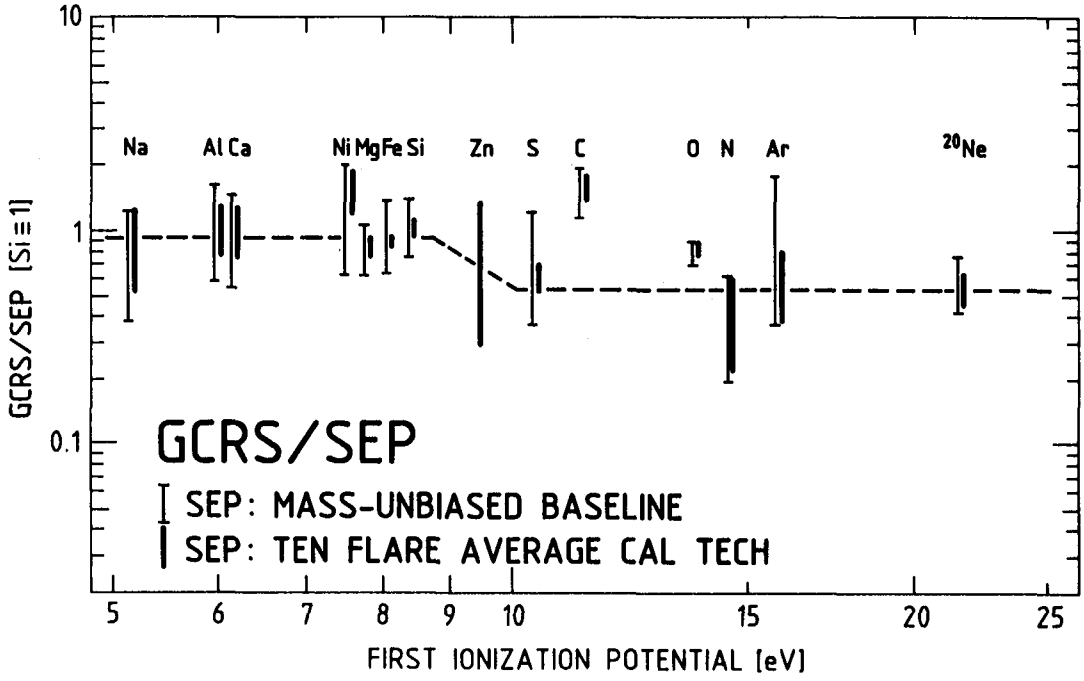

Fig. 17 GCRS/SEP abundance ratios, vs. FIP, for Z ≤ 30 (§ II-1.3). The GCRS values are those adopted in fig. 15 (with the errors on the LG denominator taken out). The SEP values are (i) the "mass-unbiased baseline" defined by Meyer (1985a), and (ii) the 10-flare average reported at this conference by Breneman and Stone (4, 213, 217). To zeroth order, the FIP-dependent bias has disappeared here. However the line, drawn to guide the eye, suggests that the depletion of high-FIP elements relative to low-FIP ones is slightly more pronounced in GCRS than in SEP's (by a factor of ∿ 1.5 ; Meyer 1985b ; Webber et al. 3, 42). C, and probably O, are above the correlation, i.e. are distinctly in excess in GCRS relative to SEP.

(ii) Fig. 17 shows that C (and, to a lesser extent, possibly O) is much above neighbouring "high-FIP" elements (FIP > 9 eV). In particular, the C/O ratio itself, extremely well determined in both GCRS and SEP's, is about twice as high in GCRS as in SEP's. See discussion in terms of the GCRS excess of ^{22}Ne and ^{25,26}Mg in § III-4.

(iii) Based on the other "high-FIP" elements ^{20}Ne, Ar, N and S, fig. 17 suggests that the depletion of "high-FIP" elements relative to "low-FIP" elements (FIP < 9 eV) is somewhat higher (a factor of ∿ 6 instead of ∿ 4) in GCRS than in SEP. This point, already noted by Meyer (1985b) is confirmed by the analysis of the new SEP data by Webber et al. (3, 42).

(iv) In this context the GCRS N abundance is very critical : if the correlation of GCRS/LG with FIP (fig. 15) and the similarity with SEP (fig. 17) are to hold, the GCRS/LG and GCRS/SEP ratios for N may not be lower than those for Ar and especially ^{20}Ne. This condition requires that N/O ≳ 6% at GCRS. It requires that the actual GCRS N abundance lies in the upper part of the adopted error bar, in agreement with the abundances derived from the high energy elemental observations (1-15 GeV/n), but in conflict with those derived from low energy (30 to 600 MeV/n) isotopic data (see discussion in § III-2.).

II-1.4. Shape of the GCRS/LG correlation with FIP for Z ≤ 30

At this conference, many papers have discussed the shape of the correlation between the GCRS/LG abundance ratio and FIP, based on data for Z ≤ 30 (Jones et al. 2, 28 ; Krombel and Wiedenbeck 2, 92 ; Webber et al. 3, 42) or for Z > 30 (Fowler et al. 2, 115 and 119 ; Klarman et al. 2, 127 ; Waddington et al. 9,... and 3, 1; Binns et al. 3, 13 ; Letaw et al. 1984).

As regards elements with Z ≤ 30, figs. 14 and 15 show that the Al and Ca abundances seriously tie down (to a factor of ≤ 1.4) any possible systematic excess of elements with lower FIP relative to elements with FIP ≈ 8 eV. In SEP's, in which no correction is required for spallation, there is not either any indication for such an excess (Meyer 1985a,b; Breneman and Stone 4, 213, 217; Mc Guire et al. 1986).

All exponential fits of the GCRS/LG pattern versus FIP are inadequate, as illustrated in fig. 18. They are totally unable to reproduce the steep drop in the Si, Zn, S, C, O, N region, together with the flat behaviour of GCRS/LG at lower and higher FIP's. Relative to Mg, Si, Fe (FIP ≈ 8 eV), exponential fits, either (i) fit more or less Zn, S, C, O, N and are much too low for Ar and Ne and too high for Na, Al, Ca, or (ii) fit Ar and Ne and are much too high over the entire region from Zn to N (fig. 18). The fit proposed by Letaw et al. (1984) is more adequate, but also somewhat high in this region.

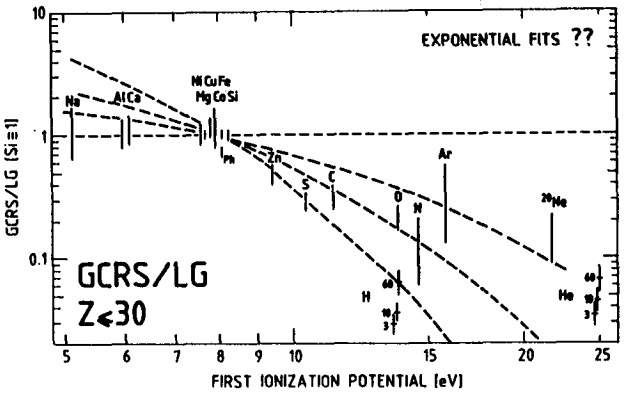

Fig. 18 Same as fig. 15, except that, instead of f(FIP), various exponential functions, normalized to the Mg Fe Si region, are tested to fit the behaviour of GCRS/LG vs. FIP for Z ≤ 30. None of them works (§ II-1.4.).

It seems to me that the obvious shape of the pattern of the GCRS/LG ratio versus FIP is that indicated as f(FIP) in fig. 15 : two plateaus at low and high FIP, with a narrow intermediate region (Zn, S). C and O, the two elements that are overabundant with respect to SEP's (fig. 17 ; § II-1.3.) have been left above the correlation curve f(FIP) ; such an excess of ^{12}C and ^{16}O is actually quantitatively predicted in connection with the ^{22}Ne and $^{25,26}Mg$ excesses, if the latter are due to the presence of a small fraction of He-burning material in GCRS, possibly originating in Wolf-Rayet stars (§ III-4. ; Meyer 1981c, 1985b ; Cassé and Paul 1982 ; Maeder 1983 ; Prantzos 1984a,b ; Prantzos et al. 1983 and 3, 167 ; Arnould 1984). The N abundance problem, mentioned in § II-1.3., will be discussed in § III-2.. H and He, whose abundances relative to

heavier elements vary with energy (§ II-1.2.3.) and which do not behave like heavier elements in SEP's (e.g., Mason et al. 1983 ; Meyer 1985a), are also left out of the correlation.[8]

This two-plateau structure of f(FIP) resembles that found in SEP's and solar corona (e.g. Cook et al. 1984 ; Meyer 1985b ; Breneman and Stone 4, 213, 217). Physically, it cannot be easily understood as representing simply the ionized fraction in a gas at a single temperature or with a monotonic distribution of temperatures (Arnaud and Cassé 1985 ; Meyer 1985b). It rather suggests a situation where ions and neutrals are selected with different efficiencies out of a plasma at ∿ 6000 K (Meyer 1985b ; Geiss and Bochsler 1984 ; Vauclair and Meyer 4, 233) (see § II-1.3.).

II-2. GCRS ELEMENTAL COMPOSITION FOR Z > 30 ("ULTRA-HEAVY" NUCLEI, UH)

II-2.1. The Local Galactic (LG) reference abundances used for UH nuclei

The LG abundances used for $Z \lesssim 30$ have been discussed in § II-1.1. For Z > 30, the C1 meteoritic values of Anders and Ebihara (1982) have been adopted; their error is usually much smaller than the GCRS error. Photospheric abundances, which are certainly a more undisputable image of the abundances in the protosolar nebula, are often lacking or still very inaccurate for UH nuclei; but, whenever they are accurately determined, they generally agree well with the C1 values (Grevesse 1984a,b). This may, however, not be always true, especially for volatile elements, and Grevesse and Meyer (3, 5), at this conference, have found possibly significant differences between C1 and photospheric abundances for Ge and Pb (§ III-3.5.).

As regards C2 meteorites, which are a mixture of 50% C1-like material, plausibly unfractionated, and of 50% highly fractionated "pebbles", there is no reason whatsoever to believe that their bulk composition might have any relevance as a standard (Anders 1971 ; Meyer 1979a,b ; Ebihara et al. 1982 ; Anders and Ebihara 1982). And C2 abundances indeed yield strange discontinuities at $_{46}$Pd-$_{47}$Ag refractory-volatile junction (Meyer 1979a). As regards the noble gases $_{36}$Kr and $_{54}$Xe, their abundances are interpolated, and the associated error difficult to assess.

II-2.2. The GCRS composition of UH nuclei

In fig. 10 (§ I-4.), I have summarized the recent observations of arriving UH nuclei. From these data, I have derived rough values of the source abundances of selected elements in the range Z = 31 to 58. The resulting GCRS/LG ratios have been plotted versus FIP in fig. 19, together with the data for $Z \lesssim 30$ and with the correlation f(FIP) adopted for these lighter elements (fig. 15). The case of Pt and Pb, for which, like most authors, I dare not derive some abundances relative to Fe or Si, will be discussed later (§ III-3.1.).

---

[8] In § III-4. and 5. and in the Appendix, f(FIP) will be expressed as f_{ik}(FIP), denoting the value of f(FIP) for species i normalized to that for a reference species k.

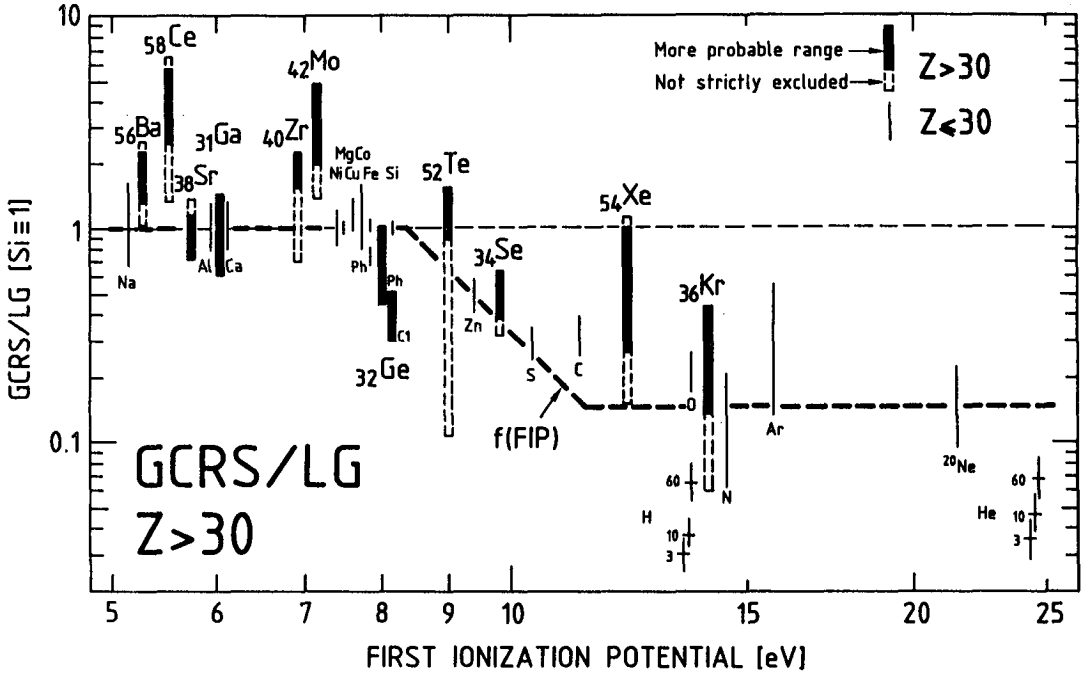

Fig. 19 GCRS/LG abundance ratios vs. FIP, for Ultra-Heavy (UH) elements with Z > 30 (thick bars), and for elements with Z ≤ 30 (thin bars, from fig. 15). The correlation f(FIP) defined in fig. 15 based on the data for Z ≤ 30 (§ II-1.4.) has also been reproduced. See caption of fig. 14. For UH elements, the thick, solid bars indicate the more probable ranges, based on the new, preliminary analysis of the HEAO-C3 data by Newport et al. (2, 123) and on conservative estimates of the spallation correction (cf. Israel et al. 1983). The dashed, white prolongations give ranges that cannot yet be strictly excluded, considering all the data in fig. 10 (Ariel VI data, Fowler et al. 2, 115,119; earlier analysis of the HEAO-C3 data ; see § I-4.) and broader assumptions for the spallation correction (§ II-2.2.). For Ge and Fe, the values of the GCRS/LG ratio is also given if the photospheric measurement ("Ph") is adopted as LG standard, instead of the more usual meteoritic value ("C1") ; see footnote # 10 (§ II-1.1., 2.1. ; III-3.5.).

The solid error bars for UH elements in fig. 19 correspond to what I believe to be the more probable range for their source abundances, based on the new, preliminary analysis the HEAO-C3 data by Newport et al. (2, 123) [9], and on conventional corrections for spallation adapted from those of Israel et al. (1983). For many elements the results of Newport et al. (2, 123) are actually in good agreement both with the earlier analysis of the HEAO-C3 data and with the Ariel VI data (fig. 10 ; § I-4.). For many elements too, the spallation corrections are not very large, so that they cannot be a major source of uncertainty.

For a few elements, however, there are large differences between sets of data (especially $_{40}Zr$, $_{52}Te$, $_{58}Ce$) and/or large spallation corrections which could be very significantly altered by slightly different

[9] To account for possible systematic errors in the fitting procedure, a standard 20% error has been quadratically added to the purely statistical errors of Newport et al. (2,123) (§ I-4.1.).

propagation models or cross-sections ($_{36}$Kr, $_{54}$Xe, possibly $_{52}$Te). Taking into account all data in fig. 10 and allowing for more extreme spallation corrections, the solid error bars in fig. 19 (giving the more probable range of source abundances) have been prolongated by dashed white bars representing ranges that, though much less likely, cannot yet be entirely excluded.

For Ge, I have plotted two values in fig. 19, one relative to the usual C1 value, one relative to the photospheric value as a LG standard (Grevesse and Meyer, 3, 5 ; § III-3.1. and 3.5.) [10].

II-2.3. Discussion – UH nuclei, correlated with FIP ?

This discussion will be based on the more probable GCRS abundances indicated by the solid bars in fig. 19, the dashed bars giving only indications as to what is really definite and what might possibly still change.

When compared to the quite orderly pattern of GCRS/LG ratios versus FIP for elements with $Z \lesssim 30$ (fig. 15), the points for UH nuclei in fig. 19 give an impression of disorder. Clearly, the same simple correlation with FIP found for $Z \lesssim 30$ does not entirely account for the UH nuclei data. But the general pattern with FIP nevertheless seems to some extent present : higher-FIP $_{34}$Se, $_{54}$Xe, $_{36}$Kr do seem depleted relative to lower-FIP elements.

The general picture is that, while a few UH elements lie on the correlation established for $Z \lesssim 30$, many of them lie above (with only $_{32}$Ge being perhaps below, depending upon whether one uses the C1 or the photospheric value as a standard; § III-3.5.). It is particularly clear that four low-FIP elements are overabundant (certainly $_{58}$Ce and $_{42}$Mo, seemingly by factors of $\sim$ 3 to 4 ; and most probably $_{56}$Ba and $_{40}$ Zr). The striking point is that these excesses are not at all correlated with FIP. [11,12]

---

[10] One should not mechanically couple the choices of a C1 or of a photospheric value as LG standard for Ge (and Pb) and for Fe (figs. 19 and 20). The problems involved in the photospheric and C1 determinations are totally different and uncoupled for Fe and Ge (and Pb). Both problems are, independently, open.

[11] The case of $_{42}$Mo is especially compelling. Its FIP (7.1 eV) is close to those of Mg, Si, Fe; when the earlier data from both HEAO-C3 and Ariel VI repeatedly indicated a high abundance for Mo, we (or at least, I) did not pay too much attention to them, surmising that with improved statistics and data treatment, its abundance would gently fall off and get normal. The improved data from both HEAO-C3 and Ariel VI (fig. 10 ; § I-4.) now confirm and even slightly increase the apparent Mo excess. Note also that Mo is a refractory element for which there exists both good C1 data [Mo = 2.52 (1.05), for Si = 10^6] and reliable photospheric data [Mo = 2.32 (1.12)], which agree perfectly (Anders and Ebihara 1982; Grevesse 1984a,b). So, the LG abundance of Mo cannot be questioned. The spallation correction, taken into account in the Mo value plotted in fig. 19, is not either very important (e.g., Israel et al. 1983). Similarly, the $_{40}$Zr LG abundance cannot be questioned [Zr = 10.7 (1.12) in C1's and 10.1 (1.12) in the Photosphere], and its spallation correction is small.

[12] Only the slightly high $_{56}$Ba could be interpreted as an indication of a slight slope of the low-FIP elements plateau. But aside from Al and Ca, UH $_{38}$Sr and $_{31}$Ga would not confirm this view.

Actually, the UH elements that are clearly above the correlation with FIP valid for $Z \lesssim 30$ tend to be the heavier ones ($Z \gtrsim 40$), while lighter $_{31}Ga$, $_{32}Ge$ (?), $_{34}Se$, $_{36}Kr$, $_{38}Sr$, both low-FIP and high-FIP elements, are roughly conistent with the correlation f(FIP).

To try to separate FIP-dependent from other, e.g. Z-dependent effects, I am going to correct the GCRS/LG ratios of all elements for the bias with FIP, i.e. plot the ratio [GCRS/LG]/f(FIP) versus Z. [13] This procedure yields fig. 20 (in which Pt and Pb are still lacking, see § III-3.1.). Fig. 20 represents enhancement factors for each element in GCRS, relative to a "normal", or "main" CR component assumed to obey the correlation f(FIP) (cf. § III-4. and 5.). For completeness the GCRS excesses of the minor isotopes ^{22}Ne, $^{24,25}Mg$ and $^{29,30}Si$ relative to standard LG isotope ratios have also been plotted (fig. 29; § III-4.1.).

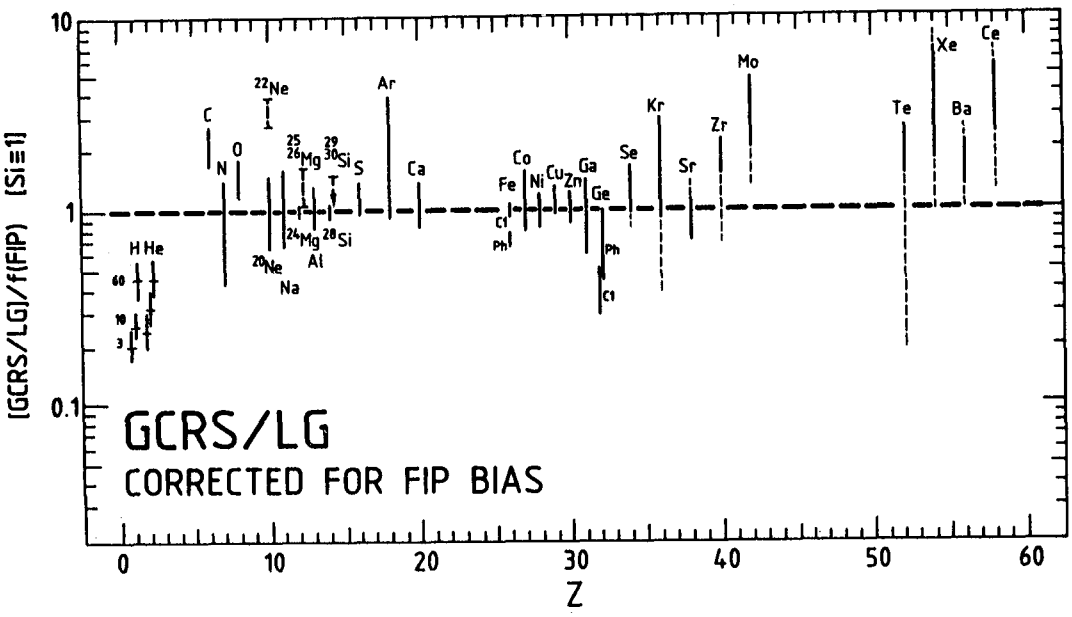

Fig. 20 [GCRS/LG]/f(FIP) ratio vs. Z for elements between Z = 1 and Z = 58 (as derived from fig. 19 ; § II-2.3.). Normalized to ^{28}Si (see fig. 14 caption). It represents the GCRS/LG ratios corrected for the bias with FIP, as described by f(FIP) which characterizes the data up to Z = 30 (figs. 15, 19 ; § II-1.4.). It also represents the excess for each species in GCRS, relative to a "normal" or "main" CR component assumed to obey the correlation f(FIP) [i.e. the quantity $E_{ik}^{*}{}_{,CR}$ in the notations of the Appendix ; § III-4. and 5.]. For Ne, Mg, Si, the elemental abundances are replaced by those of the dominant isotopes ^{20}Ne, ^{24}Mg, ^{28}Si. The excesses of the minor isotopes ratios have been plotted as dashed bars (fig. 29 ; § III-4.1. ; see footnote # 27). For H and He, the excess is energy-dependent, and given at 3, 10 and 60 GeV/n (§ II-1.2.3. ; figs. 14, 15). For Fe and Ge, two ranges are given, corresponding to the adoption of the more usual meteoritic ("C1") or to the photospheric ("Ph") value as LG reference ; see footnote # 10 (§ II-1.1., 2.1. ; III-3.5.). For $Z \gtrsim 34$, the error bars include a more probable range (solid), and a broader range which, though much less likely, cannot be entirely excluded (dashed) (fig. 19 ; § II-2.2.). The Pt-Pb region is absent from this plot, and will be treated separately (§ III-3.1., 3.5.).

[13] I recall that f(FIP) is the function describing the correlation of GCRS/LG with FIP for $Z \lesssim 30$ (figs. 15,19 ; § II-1.4.).

PART III

THE PROBLEMS WITH THE GALACTIC COSMIC RAY SOURCE COMPOSITION AND PROPAGATION - BEYOND THE CORRELATION WITH FIRST IONIZATION POTENTIAL -

To first order, the GCRS composition is characterized by its correlation with FIP. The question I am going to ask now is : what is beyond ? Where does the correlation with FIP not work ? Or, at least, where is it insufficient to account for the data ?

In fig. 20, the deviations of the ratio [GCRS/LG]/f(FIP) from the value 1, when really significant, indicate the nuclei for which the FIP-dependent filtering is insufficient to account for the data (for the Pt-Pb region, see § III-3.1.). I see five areas of problems in fig. 20, which I classify in three types:

a - The Hydrogen and Helium deficiency, which is a very specific problem (§ III-1.).

b - Excesses of heavy nuclei. They can in principle be accounted for by the presence of minor components highly enriched in specific nuclei, highly diluted in a dominant component that obeys the FIP correlation. (The abundances of the other nuclei may thus remain unaffected by the presence of the minor components). I see two areas of this kind: the C, O, ^{22}Ne, ^{25,26}Mg, ^{29,30}Si area (§ III-4.) and the $Z \geqslant 40$ area (§ III-5.).[14]

c - Depletions of heavy nuclei. They cannot be accounted for in the same way. The depletion of a single, isolated heavy species, if really proven, would imply that the bulk of GCR's originate in a medium specifically depleted in that species. Such an evidence would be sufficient to question the relevance of the entire apparent correlation with FIP and of the similarity with SEP and Solar Coronal compositions. I see three possible areas of this kind: Nitrogen (which will lead me to discuss the problems of CR propagation; § III-2.), and Germanium and Lead, which will be discussed together (§ III-3.).[15]

I am now going to discuss these various areas of problems in turn.

---

[14] Ar and Kr, with their large error bars, are also just consistent with the value 1 in fig. 20. I do not think we have to worry there. The errors are large, both on the spallation correction and on the LG value.

[15] I shall not discuss here the problems that arise if the photospheric value is adopted for LG Fe (figs. 15,20). Note that a deficiency of a group of neighbouring elements might be accounted for by (A/Q) dependent effects at high temperatures, superimposed on the correlation with FIP (as present in daily SEP composition, e.g. Meyer 1985a, and possibly in the average SEP composition, Breneman and Stone 4, 213,217). But, relative to a photospheric standard, GCRS Fe would be underabundant relative to its neighbours Co, Ni, Cu as well as to Mg, Si (figs. 15, 20), so that the above type of explanation would not work.

III-1. THE HYDROGEN AND HELIUM DEFICIENCY PROBLEM

III-1.1. H and He source spectra, and behaviour in SEP's

As shown in § II-1.2.3., the GCR observations, propagated back to the sources using a rigidity dependent escape length λ_e, imply:

- that the He/H-ratio at the sources is remarkly constant and normal ($\sim$ 10%), at least between $\sim$ 3 and $\sim$ 60 GeV/n, when taken at a given energy/nucleon (the relevant parameter according to current shock wave acceleration theory ; e.g., Krimsky 1977 ; Axford et al. 1977 ; Bell 1978a,b ; Blandford and Ostriker 1978 ; Axford 1981);

- that the roughly common spectral shape of H and He differs from that of heavier nuclei (CNO), which is steeper in this range (3 to 60 GeV/n). Meanwhile, no significant difference in source spectral shape between any two heavy nuclei has ever been found, over the range $\sim$ 0.5 to 25 GeV/n.

These facts are expressed in our plot of the abundances of H and He relative to heavies at three different energies (3, 10 and 60 GeV/n) in figs. 14,15,19,20,21,22.

In SEP's, H and He do not follow the orderly dependence on FIP and (A/Q) of all heavier species. This is in particular true for the variations of their abundances with time, a crucial parameter we have access to in SEP's, not in GCR's ! (e.g. Mason et al. 1983 ; Meyer 1985a).

So, H and He, the dominant elements, behave distinctly differently from the trace heavy elements we are studying, both in SEP's where their variations do not correlate with those of heavies, and in GCRS where they have a different spectrum. I therefore do not worry if they do not fit in the abundance pattern for the trace elements. Clearly, other phenomena are going on.

III-1.2. Deficiency of H and He : direct injection out of the Hot Interstellar Medium (HIM) ?

Attempts have been made to account for the low H and He abundances, assuming direct rigidity dependent injection of GCR's out of the HIM (Eichler 1979 ; Ellison 1981, 1985 ; Ellison et al. 1981 ; Eichler and Hainebach 1981). At this conference Binns et al. (3, 13) have tried to test this hypothesis by plotting the GCRS/LG ratios versus the ratio (A/Q_{120}) for all available elements way up to Z = 58, where Q_{120} is the approximate charge of the ions in a $\sim 10^6$ K plasma (Q_{120} is estimated by assuming that all electrons with ionization potential < 120 eV have been

removed). Their plot, shown in fig. 21 (updated), shows that the heavy element abundances are not at all organized in terms of (A/Q_{120}). This confirms earlier studies based on more accurate calculations of the charge Q in hot plasmas, but limited to $Z \leqslant 30$, by Cesarsky et al. (1981; 1985, quoted by Cassé 1983), which showed (fig. 22) that, for temperatures between 10^5 and 10^6 K, the GCRS/LG ratios plotted versus A/Q are characterized by discontinuities which cannot be accounted for by the smooth A/Q dependence of the composition predicted by the models assuming direct injection out of the ISM. These models would also have trouble in accounting for a normal He/H ratio (fig. 22).

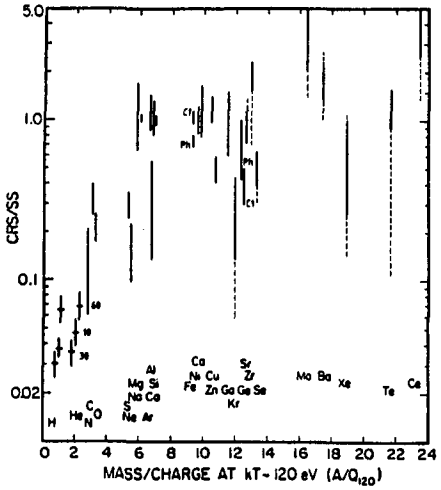

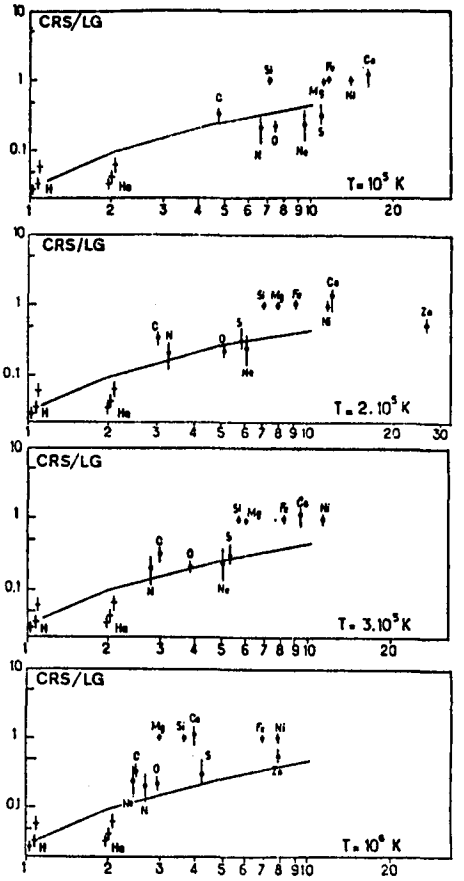

Fig. 21 GCRS/LG ratio for elements between Z = 1 and 58, versus mass to charge ratio A/Q in a 10^6 K plasma, after Binns et al. 3, 13 (updated). The charge Q = "Q_{120}" is roughly estimated by assuming that all electrons with ionization potential < 120 eV have been removed from the atoms. As regards the GCRS/LG ratios given in ordinates, I have updated them, using the values of fig. 19. See captions of figs. 14 and 19. Like in these figures H and He are given at 3, 10 and 60 GeV/n, Fe and Ge are given referred to both C1 and Photospheric LG abundances, and the error bars for UH nuclei include a more probable and a less probable range. Following the authors, I conclude that mass to charge ratio in a 10^6 K plasma does not order the data. This is a difficulty for models assuming direct injection of the particles out of the hot ISM plasma (§ III-1.2.).

Fig. 22 GCRS/LG ratio for elements between Z = 1 and 30, versus mass to charge ratio A/Q in 10^5, $2 \cdot 10^5$, $3 \cdot 10^5$ and 10^6 K plasmas, after Cesarsky et al. (1981 ; 1985, quoted by Cassé 1983). I have updated the graph for H and He, plotted at 3, 10 and 60 GeV/n. The charges Q are mean charges resulting from refined models of ionization equilibrium by Arnaud and Rothenflug (1985). The curves, normalized to H at ∿ 10 GeV/n are the enhancements predicted by Eichler and Hainebach (1981), very similar to those of Ellison (1981), assuming direct injection of the particles out of the hot ISM plasma. As can be seen, they do not account for the "observed" discontinuities of GCRS/LG vs. A/Q (§ III-1.2.).

III-2. THE NITROGEN DEFICIENCY PROBLEM - COSMIC RAY PROPAGATION - THE B - ^{15}N CONTRADICTION - DISTRIBUTED REACCELERATION ? TRUNCATION OF THE PLD ?

Is N depleted in GCRS relative to other high-FIP species, as compared to LG and/or to SEP abundances ? The best high-FIP species to which N can be compared is ^{20}Ne, since Ar is poorly determined and C and O are enhanced in SEP's relative to GCRS's, most probably because they are synthesized in large quantities together with the excess ^{22}Ne and ^{25,26}Mg (§ III-4.). The most stringent condition comes from the comparison with SEP (in which N/^{20}Ne is better determined and a bit higher than in LG matter, see figs. 15 and 17). The condition that N be not deficient relative to ^{20}Ne in GCRS, as compared to SEP, is equivalent to the condition that N/O $\gtrsim$ 6% in GCRS.

As noted in § II-1.2.2., most of the low energy studies based on isotopic observations of ^{14}N yield source N/O ratios $\sim$ 3%, which would imply that the correlation with FIP and the similarity with SEP's are not relevant, while high energy elemental studies yield N/O $\sim$ 6%, and thus make no problem (low energy isotope data : Pretzler et al. 1975; Wiedenbeck et al. 1979 ; Guzik 1981 ; Mewaldt et al. 1981 ; Webber 1982a,1983b; Webber et al. 2, 88 ; high energy elemental data : Goret et al. 1981 ; Webber 1982b ; Engelmann 1984 ; Lund 1984 ; Dwyer and Meyer 1985 ; Webber et al. 2,16; further discussions : Mewaldt 1981; Silberberg et al., 1983; Wiedenbeck 1984 ; Meyer 1985b ; Guzik et al. 2, 80 ; Webber et al. 3,42).

The surviving primary fraction is $\sim$ 34% among arriving low energy isotopic ^{14}N, and ranges from $\sim$ 19 to $\sim$ 31% (average $\approx$ 23%) for the high energy elemental N observed between $\sim$ 1 and $\sim$ 15 GeV/n by the HEAO-C2 instrument (fig. 16 ; assuming N/O = 6% at sources). So, the superiority of the low energy isotopic data as regards surviving primary fraction is not overwhelming. But the relevant cross-sections are most precisely measured at low energy, up to $\sim$ 1 GeV/n (fig. 4 ; § I-3.1.), so that the high energy estimates of the source N/O ratio require an extrapolation of the cross-sections to higher energies. Although the cross-sections are known not to vary much in the GeV range for such light nuclei (which is confirmed by the existing higher energy measurements, fig. 4), we do not know to within which accuracy this is true.

The HEAO-C2 isotopic data points for ^{14}N/O at high energy (E = 2.5 to 6 GeV/n; fig. 25), obtained from different subsets of events with various methods of geomagnetic isotope analysis, are at present too scattered to be decisive (Goret et al.1983 ; Byrnak et al. 1983a; Ferrando et al. 2, 96 and priv. comm. ^{15}N/N = 0.49 $\pm$ 0.06). Let me just note that the region of marginal agreement of all HEAO-C2 error bars on ^{14}N/O in fig. 25 (1σ errors are plotted) corresponds to N/O = 6% at the source; [while the corresponding data range for ^{15}N/O, fig. 24, agrees with the ^{15}N/O ratios predicted from the high energy B/C ratios].

I am now going to discuss cosmic ray propagation at low energy.

III-2.1. Low energy cosmic ray propagation - The B-^{15}N contradiction - Distributed reacceleration ?

Figs. 23 and 24 compare observed data to the result of propagation calculations for two (presumably) pure secondary to primary ratios: B/C and ^{15}N/O. The species considered are close in mass, so that the compared predictions for the two ratios are not sensitive to the exact shape of the Path Length Distribution (PLD; which may be truncated or not).

The PLD's used throughout figs. 23,24,25,26 are the pure exponential distributions with rigidity dependent escape length λ_e used by Soutoul et al. (2, 8). They are adjusted to best fit the observed B/C ratio, with the most up to date cross-sections. At high energy, they fit the HEAO-C2 data of Engelmann et al. (1983), with the relevant modulation parameter ϕ = 600 MV. [To fit the B/C ratios just obtained by Webber et al. (2, 16), slightly lower grammages would be required]. At lower energies, below R = 5.5 GV or E $\approx$ 2 GeV/n, two behaviours of λ_e are considered : λ_e = cst = 7.7 gcm^{-2}, and λ_e = 7.9 β gcm^{-2} (pure H). Two levels of modulation are also considered, ϕ = 350 and 490 MV. Actually λ_e = cst and ϕ = 350 MV on the one hand, and $\lambda_e \propto \beta$ and ϕ = 490 MV yield about the same results.[16] The value ϕ = 490 MV is probably more adequate for the Chicago IMP-8 data, so that their data on B/C tend to favour $\lambda_e \propto \beta$ (fig. 23). But the important point here is that the dispersion of the curves that encompass the plausible fits to the low energy B/C data points is not large, neither in fig. 23, nor in figs. 24,25 and 26.

I have also included in figs. 23,24,25,26 an estimate of the uncertainty on the calculated curves due to the cross-section uncertainties around 600 MeV, based on the figures given in Table 2. I have distinguished the errors associated with measured cross-sections, for which I have used the published uncertainties, from those associated with unmeasured cross-sections for which I have attributed a standard 35% error to the semi-empirical estimates.[17] I have simply linearily summed the two contributions.

Comparison of figs. 23 and 24 shows that the propagation models (values of λ_e) that fit the purely secondary B/C ratio do not at all fit the nearby purely secondary ^{15}N/O ratio at low energies.[18] This is another way of expressing the problem earlier addressed by Guzik (1981) and Guzik et al. (2, 80).

---

[16] For a higher degree of interplanetary deceleration ϕ, the low energy particles observed near Earth had originally higher energies in interstellar space. In the few 100 MeV/n $\sim$ 1 GeV/n range in interstellar space, higher energy particles have higher B/C ratios. Therefore a higher value of the modulation parameter ϕ yields higher B/C ratio near Earth.

[17] This 35% error may seem large since the sum of a large number of unmeasured cross-sections is involved, whose errors should largely compensate each other on the average (e.g., Letaw et al. 3, 46). On the other hand, recently measured cross-sections often deviate much more than expected from the semi-empirical estimates (e.g., Webber and Kish 3, 87) (fig. 5 ; § I-3.).

[18] The lower B/C ratios just obtained by Webber et al. (2, 16), plotted in fig. 23, would require still lower values of λ_e, thus amplifying the contradiction.

Table 2 - Contribution of various parents (fraction f) and associated cross-section errors (when unmeasured, adopted error = 35%) to the formation of secondary B, ^{14}N, ^{15}N, Sc-Cr around 600 MeV/n

Daughter / Parent	B			^{14}N			^{15}N			Sc-Cr		
	f	% error	Product	f	% error	Product	f	% error	Product	f	% error	Product
C	0.554	2.6%	1.4%	-	-	-	-	-	-	-	-	-
N	0.111	35.0%	3.9%	0.179	35.0%	6.3%	-	-	-	-	-	-
O	0.252	8.2%	2.1%	0.648	4.9%	3.2%	0.810	3.5%	2.8%	-	-	-
F,Ne	0.084	35.0%	2.9%	0.095	10.3%	1.0%	0.103	8.4%	0.9%	-	-	-
≥ Na				0.078	35.0%	2.7%	0.087	35.0%	3.0%	-	-	-
Mn, ^{54,55,57,58}Fe,Co,Ni	-	-	-	-	-	-	-	-	-	0.260	35.0%	9.1%
^{56}Fe	-	-	-	-	-	-	-	-	-	0.740	3.0%	2.2%
Fraction yielded by measured σ	0.806	-	-	0.743	-	-	0.913	-	-	0.740	-	-
∑ errors measured σ	-	-	3.5%	-	-	4.2%	-	-	3.7%	-	-	2.2%
∑ Errors Total	-	-	10.3%	-	-	13.2%	-	-	6.7%	-	-	11.3%

The contradiction is cleanest in the ∿ 300 to 500 MeV/n range, where we have in fig. 24 four independent solid points for $^{15}N/O$ by Webber and coworkers, obtained with good to excellent instrumental isotope resolution (fig. 2; § I-2.), which lie ∿ 30% above the predictions that fit B/C. The interpretation of the data in terms of solar modulation in this energy range is also less critical than for the lowest energy points (≲ 100 MeV/n), which, however, point toward the same problem (Guzik 1981; Guzik et al. 2,80). This energy range is also the one where the cross-sections have been best measured recently (§ I-3.1. ; fig. 4). It is clear from figs. 23 and 24 (Table 2) that the discrepancy is far beyond those permitted by reasonably estimated combined cross-section errors (± 13%).

Again, changes in the exact shape of the PLD (truncation) will not remove the contradiction for such nearby nuclei. So, unless there are gross, unknown errors, either in the CR data, or in the measured cross-sections for B and/or ^{15}N - which seems improbable -, I can imagine no way of understanding simultaneously the low energy B/C and $^{15}N/O$ observations within the classical propagation framework.

At this state, I can think of only two ways out [19] :

(i) A special propagation history for C (and O?) nuclei ?

The first one is very speculative, certainly difficult to check, but should still be kept in mind as a possibility. According to our current knowledge, ∿ 50% of the GCR C nuclei originate, together with the ^{22}Ne excess, in special environments, plausibly Wolf-Rayet stars (§ II-1.3. and III-4. ; figs. 17, 20 and 30). It is not impossible - although there is no particular astrophysical justification for this

[19] Here I exclude the hypothesis that a significant fraction of the ^{15}N be primary. This would imply an excess of ^{15}N by a factor of ∿ 100 in GCRS, as compared to excesses by factors of ∿ 2 to 2.5 for ^{12}C and ∿ 3.2 for ^{22}Ne. A strong dilution of the ^{15}N-rich material with normal material would then be difficult to accept. Most CR's probably ought to originate in the ^{15}N-rich material.

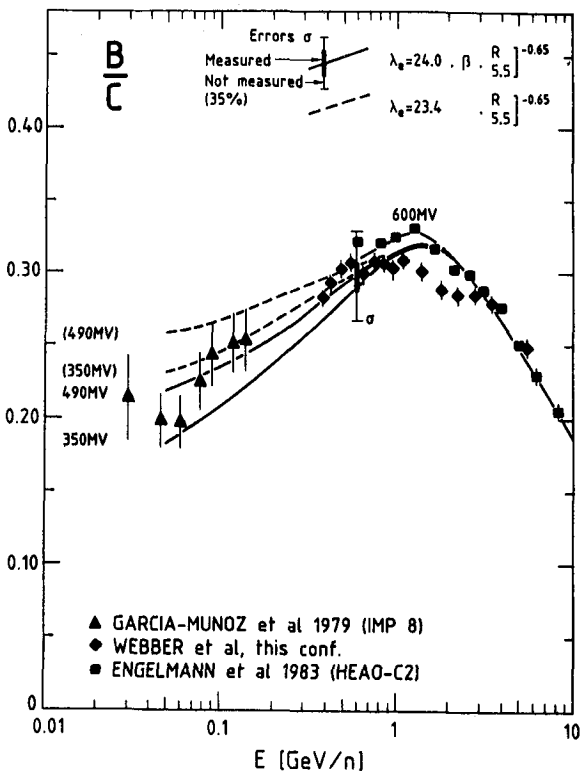

Fig. 23 *The B/C ratio, vs. energy. Observations are from : Garcia-Munoz et al. 1979 (IMP-8) ; Webber et al. 2, 16 ; and Engelmann et al. 1983 (HEAO-C2). The calculated curves are adjusted as to best fit the observed ratios. They refer to pure exponential PLD's with λ_e = f(R) or f(R,β) as indicated on the figure, based on Soutoul et al. (2, 8) [λ_e in g cm^{-2} of pure H ; R in GV ; the bracket with R and 5.5 indicates that for R < 5.5 GV, the R dependence ceases, and R is to be replaced by 5.5]. The full curves include a β-dependence, the dashed curves do not. Three values of the modulation parameter φ are considered ; 600 MV is believed to be adequate for the HEAO-C2 data, and 490 MV for the low energy IMP-8 data, thus favouring a β-dependence of λ_e. An estimate of the uncertainty on the curves due to cross-section (σ) errors is given around 600 MeV/n ; I have indicated separately the errors associated with the measured cross-sections and those due to the unmeasured ones, taken as 35% (§ III-2.1., Table 2).*

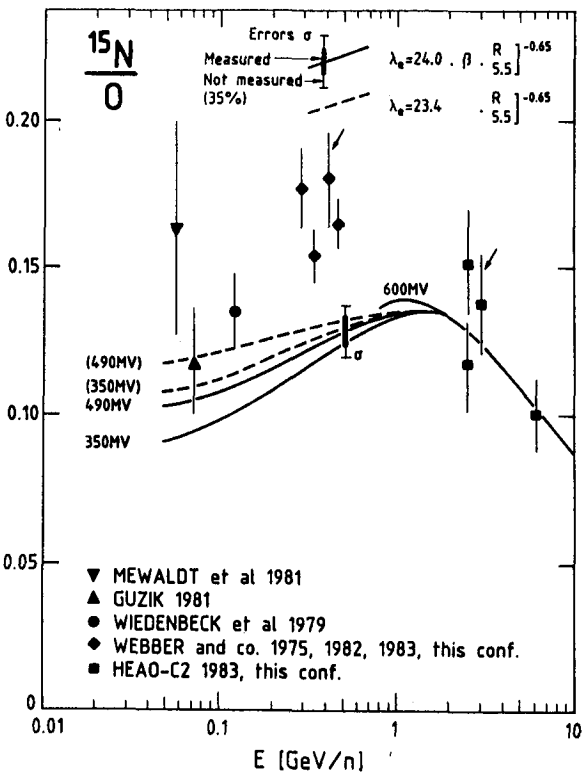

Fig. 24 *The ^{15}N/O ratio, vs. energy. Observations are from : Mewaldt et al. 1981 (ISEE 3) ; Guzik 1981 (IMP 7-8) ; Wiedenbeck et al. 1979 (ISEE 3) ; Pretzler et al. 1975 ; Webber 1982a, 1983b ; Webber et al. 2, 88; Goret et al. 1983 (HEAO-C2) ; Byrnak et al. 1983a (HEAO-C2) ; Ferrando et al. 2, 95 and priv. comm. (HEAO-C2). New data presented at this conference are marked by an arrow. Calculated curves, adjusted as to best fit the B/C ratio : see caption of fig. 23.*

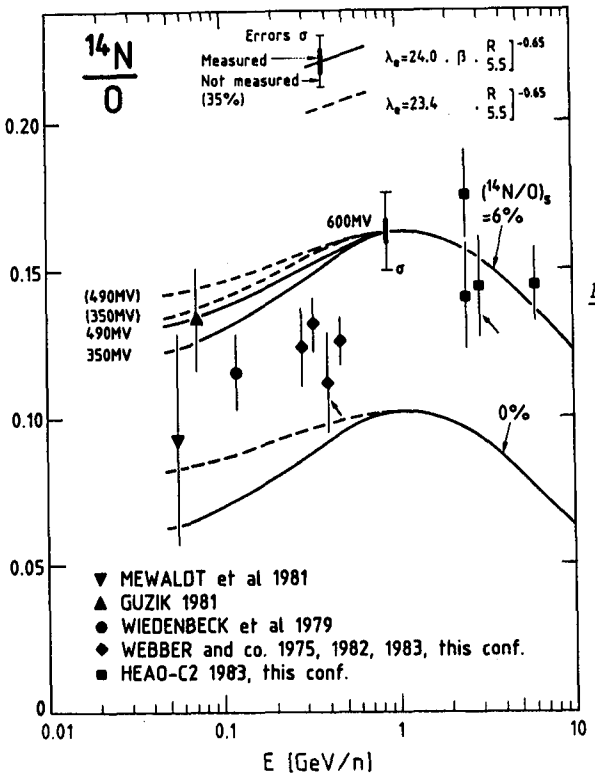

Fig. 25 The $^{14}N/O$ ratio, vs. energy. References for the observations : same as in fig. 24. Calculated curves, adjusted as to best fit the B/C ratio : see caption of fig. 23. The curves are given for source ratios $(^{14}N/O)_s$ = 0% and 6% and would scale linearly in between.

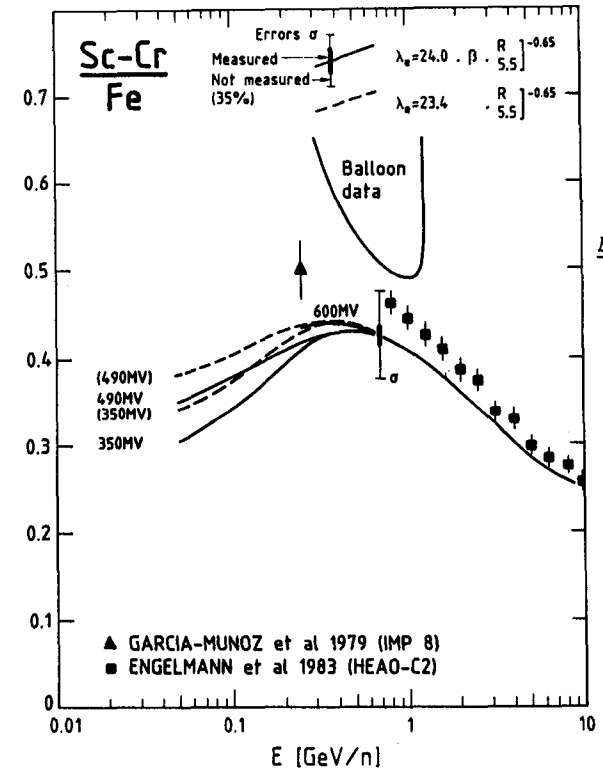

Fig. 26 The Sc-Cr/Fe ratio, vs. energy. Observations are from Garcia-Munoz and Simpson 1979 (IMP-8) and Engelmann et al. 1983 (HEAO-C2). An envelope is given for various earlier balloon data, which often yield ratios above those calculated for $\lambda_e = \infty$. Calculated curves, adjusted as to best fit the B/C ratio : see caption of fig. 23. [LG abundances have been assumed for the source abundances of Sc, Ti, V and Cr, all low-FIP elements, relative to Fe].

hypothesis - that these nuclei have a propagation history different from that of the bulk of the CR nuclei and traverse on the average significantly less matter, thus yielding comparatively low B/C ratios. The B/C ratio would then not be a good cornerstone to discuss propagation in general. An immediate argument against this hypothesis would be that, in the same framework, it is expected that $\sim$ 30% of the O also originates in Wolf-Rayet stars (fig. 30), so that the difference in propagation history is not so large for the daughters of C and of O. [This figure of $\sim$ 30% of O from Wolf-Rayet stars is, however, probably more model dependent than the 50% for C]. When good cross-sections become available, study of almost purely secondary Fluorine may be very instructive in this context.

(ii) Distributed reacceleration ?

The second way-out I can think of at the moment is less speculative, and certainly more liable to check : it is the hypothesis of distributed reacceleration. In this hypothesis, the CR's we observe in the few 100 MeV/n range have earlier been propagating a long time at lower energy (say, $\lesssim$ 100 MeV/n), before they got boosted up in energy by factors of a few units by passing weak supernova shocks (Silberberg et al. 1983, and 3,238 ; Letaw et al. 1984 ; Simon et al. 3,230). The relevant cross-sections for secondary formation are then largely thecross-sections below 100 MeV/n, which sometimes show strong peaks followed by a steep decrease down to threshold. Silberberg et al. (1983) have noted several problems with CR composition, specifically at low energy, which might be solved if distributed reacceleration is at work.

At high energy, distributed acceleration has less effect on composition, because the cross-sections are much more constant with energy. Note that, at this conference, Simon et al. (3, 230) have shown that distributed reacceleration is not in conflict with the observed decrease of the secondary/primary ratios at high energies ($\sim$ 2 to 200 GeV/n).

A serious difficulty with the hypothesis that the particles have traversed a lot of matter at E $\lesssim$ 100 MeV/n before we observe them at a few 100 MeV/n, arises from the strong energy loss and its Z^2 dependence at low energy, which may well kill selectively heavier nuclei such as Fe and especially UH elements. [This is the problem first posed by Eichler (1980) and Epstein (1980a) regarding the injection problem; at very low energies $\lesssim$ 3 MeV/n, however, the pick-up of electrons by heavier nuclei is sufficient to cancel the Z^2 dependence of the energy loss (Meyer 1985b) ; but this is no longer true in the 10-100 MeV/n range where the nuclear interactions involving the low energy cross-sections are supposed to take place]. Small reaccelerations must be frequent enough that Fe and UH nuclei do not get preferentially thermalized. This is a problem.

Anyway, I think that the lower energy B-^{15}N contradiction is perhaps a clear case for distributed reacceleration. To check this hypothesis, I recommend: (i) measurement of key unmeasured spallation cross-sections below $\sim$ 100 MeV/n, down to threshold ; (ii) detailed analysis of the consistency of our data on secondary ^{6}Li, ^{7}Li, ^{7}Be, ^{9}Be, ^{10}B, ^{11}B, ^{15}N, ^{17}O, ^{19}F at low energy, with and without distributed reacceleration; (iii) studies of the energy loss problem for heavier nuclei: can it be overcome ?

III-2.2. The ^{14}N source abundance from low and high energy data

Fig. 25 is the twin-figure to fig. 24, for $^{14}N/O$. Here, of course, a significant source component is expected, and I have plotted the $^{14}N/O$ ratios expected from the purely secondary production, $(^{14}N/O)_S = 0\%$, and for source $(^{14}N/O)_S = 6\%$. In between, calculated curves would scale roughly linearly with $(^{14}N/O)_S$.

As well known, the bulk of the low energy points indicate $(^{14}N/O)_S \approx 3\%$, if the values of λ_e that fit the B/C ratio (fig. 23) are adopted. Of course, if one were to increase the low energy λ_e's so as to fit the $^{15}N/O$ ratio instead, the predicted secondary yields for ^{14}N would increase accordingly and the ^{14}N source values derived from the low energy points correspondingly decrease down to values close to zero.

I think that, as long as the low energy B-^{15}N contradiction is not solved, we cannot say anything serious on the ^{14}N source abundance as derived from low energy data. Assuming that the CR data are correct, some cross-sections ought to be wrong : those for B formation ? for ^{15}N formation ? and then, how about those for ^{14}N formation ? As mentioned above, I do not think the recent cross-section measurements for production of these very species from their principal progenitors can be that wrong. Errors on estimates of other, not measured cross-sections are not either likely to make the difference (Table 2 ; figs. 23 and 24). That is why I think some other ingredient must interfere. The most likely one I can think of at the moment is distributed reacceleration. The relevant cross-sections could then largely be those below $\sim$ 100 MeV/n, and we would indeed be using wrong cross-sections at present ! And before the very low energy cross-sections are known (those for Li, Be, B formation have been largely investigated, e.g. Read and Viola 1984, but not those for $^{14,15}N$) and propagation with distributed acceleration has been modelled, only God knows whether this hypothesis solves the B-^{15}N contradiction (while being consistent with the data on ^{7}Be, ^{9}Be, ^{10}B, ^{11}B, ^{15}N, F), and which source ^{14}N abundance it yields.

At high energies (where, anyway, distributed reacceleration would not significantly affect the composition), the marginal consensus of the various HEAO-C2 isotope analysis around 3 GeV/n and the point at 6 GeV/n yield $^{15}N/O$ ratios which are consistent with the predictions from the B/C ratio, and converge on $(^{14}N/O)_S \approx 6\%$ (figs. 24 and 25; plotted are 1σ errors).

6% is also the value for $(^{14}N/O)_S$ derived from the N/O elemental data between $\sim$ 1 and 15 GeV/n (HEAO-C2 data, Engelmann 1984, Lund 1984; in excellent agreement with the new data of Webber et al. 2, 16 and of Dwyer and Meyer 1985).

III-2.3. Truncation of the exponential Path Length Distribution (PLD) ?

A truncation at low pathlengths of the roughly exponential PLD of CR's in the galaxy means a dearth of particles having traversed a small amount of matter, say ≤ 1 gcm^{-2}, between source and earth. The simplest interpretation of such a dearth is that many sources are surrounded by dense matter, in which newly accelerated CR's are trapped before escaping into the general galactic medium: this is the nested leaky-box model (Cowsik and Wilson 1973).

Whether the PLD is truncated or not can be decided by comparing observed secondary to primary ratios, for groups of nuclei with widely different nuclear destruction lengths λ_{nucl} (some with $\lambda_{nucl} \gtrsim \lambda_e$, others with $\lambda_{nucl} << \lambda_e$, where λ_e is the escape length from the Galaxy; e.g., Webber et al. 1972). The PLD may actually be truncated for some energies, and not for others. At this conference, a number of investigators have addressed this problem, at both high and low energy, based either on data for $Z \leq 30$ (Soutoul et al. 2,8 ; Margolis 3,38 ; Webber et al. 3,42; Letaw et al. 3, 46 ; Ferrando et al. 3, 61 ; see also Garcia-Munoz et al. 1984), or on data for UH nuclei (Fowler et al. 2, 119 ; Klarman et al. 2, 127 ; Waddington et al. 3,1 ; Giler and Wibig 3,17 ; see also Brewster et al. 1983 and Letaw et al. 1984). In view of the very small value of λ_{nucl} for UH nuclei, the latter studies should in principle be the most powerful tool to investigate a possible dearth of short pathlengths.

I shall discuss in turn the evidence for and against truncation (i) at high energy ($\gtrsim 1$ GeV/n) based on elements with $Z \leq 30$; (ii) at high energy, based on UH elements; and (iii) at low energy (< 1 GeV/n), based on elements with $Z \leq 30$.

III-2.3.1. Truncation of the PLD in the GeV/n range - Data for $Z \leq 30$ - The role of interstellar He

From the comparison of the B/C and Sc-Cr/Fe ratios, there is a general agreement that no significant truncation is required beyond 1 or a few GeV/n. This is, in particular, illustrated in the comparison of figs. 23 and 26, based on Soutoul et al. (2, 8). The purely exponential PLD that best fits B/C also fits almost perfectly Sc-Cr/Fe at high energy (and certainly within the cross-section errors). The fit is, however, slightly low, and a limited amount of truncation cannot be excluded either.

Ferrando et al. (3, 61) have suggested that the need for truncation may be reenforced when interstellar He is included in the propagation calculations in a physical way (i.e. using as much as possible real cross-sections on He; not just scaling the cross-sections on H, which is merely equivalent to a change of "units" for λ_e). Referred to the total cross-section, the spallation of Fe on He yields less nearby products (Sc-Cr) than its spallation on H, while the spallation of C yields about as much Be on He as on H. When interstellar He gets properly taken into account, one may therefore expect a decrease of the calculated yield for Sc-Cr as compared to that for Li Be B. Then more truncation of the PLD will be required. I think that this idea must be studied more precisely, based on all available data on spallation on He (or, for lack of such

data, on spallation on heavier targets such as Be and C). Also, production of B, for which we have much better CR data, should be considered, rather than of Be. [B will probably be comparatively less produced than Be in the spallation of C on heavier targets, more like Sc-Cr; the above effect should therefore be smaller for B than for Be; on the other hand, as much as $\sim$ 45% of B is produced out of parents heavier than C (Table 2), for which B is not a nearby product]. Anyway, this problem requires measurements of spallation cross-sections on He.

III-2.3.2. Truncation of the PLD in the GeV/n range - UH nuclei data

As regards UH nuclei, Klarman et al. (2, 127) have in particular compared the observations to the predictions for purely exponential PLD's for two mainly secondary/primary ratios : (Z = 62 to 69)/"Pt Pb" and (Z = 70 to 73)/"Pt Pb", where "Pt Pb" stands for (Z = 74 to 83) (fig. 27). The predictions are obtained using a cross-section systematics derived from the latest cross-section measurements by Kertzman et al. (3, 95) at 1 GeV/n (fig. 7 ; § I-3.1.). Fig. 27 shows that the agreement between the HEAO-C3 measurement and the predictions is excellent. It may, however, be coincidental. The HEAO-C3 data indeed refer to a median energy of $\sim$ 6 GeV/n, while the new cross-sections measurements have been performed at $\sim$ 1 GeV/n. Now, the study of Au spallation by Kaufman and Steinberg (1980) shows that, for $\Delta A \leqslant 40$, spallation cross-sections peak around 1 GeV/n and decrease by factors of $\sim$ 2 between 1 and 6 GeV/n [20]. So, the secondary yields at 6 GeV/n predicted for a pure exponential PLD could well be twice lower than apparent in fig. 27, which would be a case for truncation. In addition, the Ariel VI group finds higher fluxes of secondary nuclei (figs. 27 and 9, 10). They refer to lower energies than the HEAO-C3 data, and the difference is believed to be real (fig. 11). Their median energy, $\sim$ 2 GeV/n, is actually much closer

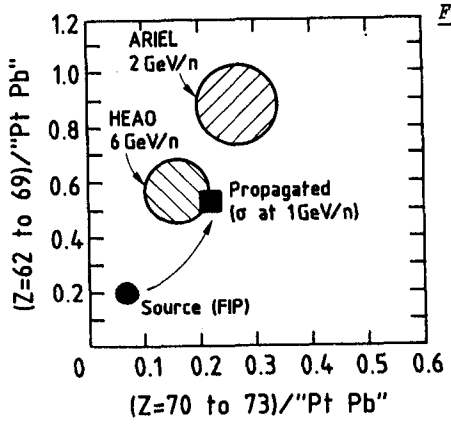

Fig. 27 Cross plot of the two mainly secondary to primary ratios (Z = 62 to 69)/"Pt Pb" vs. Z = 70-73/"Pt Pb", where "Pt Pb" stands for (Z = 74 to 83), adapted from Klarman et al. (2 127) [see also Binns et al. 1985]. The source ratios assume LG abundances biased according to f(FIP) (fig. 15). The propagated ratios have been obtained assuming a pure exponential PLD, and using cross-sections derived from the latest measurements by Kertzman et al. (3, 95) at 1 GeV/n (fig. 7 ; § I-3.1.). The observed ratios are those of the experiments HEAO-C3 around 6 GeV/n and Ariel VI mainly around 2 GeV/n (figs. 9, 10 ; § I-4.). It is important to note that a subset of the Ariel VI data around 6 GeV/n agrees well with the HEAO-C3 point at the same energy (fig. 11). See discussion in § III-2.3.2..

[20] This behaviour is not simple. Both the energy at which the cross-section peaks (it falls again at lower energy) and the relative amplitude of the peak depend on ΔA (Kaufman and Steinberg 1980).

to the energy at which the cross-sections have been measured, so that these Ariel VI data, together with the above mentioned calculation [21], could provide further support for truncation (fig. 27).

The above arguments are valid, unless distributed reacceleration, working at higher energy as well, makes the cross-sections at 1 GeV/n relevant for 6 GeV/n ! (we might then also have problems in explaining the high secondary fluxes in the Ariel data at lower energy !).

III-2.3.3. Truncation of the PLD in the few 100 MeV/n range

Below 1 GeV/n, comparison of the data for B/C and Sc-Cr/Fe [22] in figs. 23 and 26, shows that the purely exponential PLD's that fit B/C indeed do not produce as much Sc-Cr as observed at low energy. However, the discrepancy is only marginal, when considering the uncertainty on the prediction associated with the unmeasured cross-sections (taken to be good to within 35%, perhaps somewhat pessimistically; fig.26, Table 2).[23]

Much more important, the low energy discrepancy between B/C and Sc-Cr/Fe (figs. 23 and 26), which we tend to interpret in terms of a truncation of the PLD, is much smaller than that between B/C and $^{15}N/O$ (figs. 23 and 24), which is totally not understood (and certainly not due to truncation)!!! [24] So, I think that, as long as the B-^{15}N contradiction is not understood, it would be very imprudent to draw any conclusion regarding truncation of the PLD at low energy.

III-2.3.4. Summary on the truncation of the PLD

At high energy ($E \gtrsim 1$ GeV/n) there is a consensus that the data up to Fe do not suggest any significant truncation of the PLD. They should actually allow to place strict limits to acceptable truncations. However, a realistic introduction of spallation in interstellar He might increase the need for truncation. The UH data, which are extremely sensitive to truncation, are difficult to interpret because of probable energy dependence of the cross-section. They might well favour some truncation. Distributed reacceleration, if present, may further complicate the picture.

At low energy, ($E \lesssim 1$ GeV/n) no conclusion can be drawn before the B-^{15}N contradiction is solved (§ III-2.1.).

---

[21] These UH secondary/primary ratios, while very sensitive to a truncation of the PLD, are very insensitive to the exact value of λ_e (which is anyway >> λ_{nucl}), and to its $\sim$ 50% increase between 6 and 2 GeV/n.

[22] At low energy, I shall consider essentially the IMP 8 data from the U. of Chicago. There exists a large body of diverging balloon data, most of which are above the saturated Sc-Cr/Fe ratio (corresponding to no escape at all) (Soutoul et al. 2,8).

[23] The discrepancy between B/C and Sc-Cr/Fe may appear larger when expressed in terms of the λ_e's for pure exponential PLD's required to fit both ratios (Soutoul et al. 2,8). But this λ_e is not a good parameter since a small increase of Sc-Cr/Fe, obtained by a small amount of truncation of the short pathlengths, would require a large increase of λ_e in a purely exponential framework (since λ_e >> λ_{nucl}).

[24] Actually, a larger λ_e at lower energy that would fit $^{15}N/O$ would roughly fit Sc-Cr/Fe.

III-3. THE GERMANIUM-LEAD DEFICIENCY PROBLEM

I shall discuss together the Ge and Pb deficiency problems, because both may be volability indicators, and because for both the Cl meteoritic abundance standard might have to be questioned (see below § III-3.4. and 3.5.).

III-3.1. Defining the Ge and Pb/Pt anomalies

It is immediately apparent in figs. 19 and 20 that Ge is low in GCRS as compared with elements with similar FIP (Fe, Mg, Si), when referred to the standard Cl meteoritic value as LG abundance (§ II.1.1. and 2.1.).

Pt and Pb have not been plotted in the above figures, because their source abundances relative to Fe or Si cannot yet be reliably determined. Even the even-Z elements are not individually resolved in this range, neither on HEAO-C3, nor on Ariel VI (fig. 9), so that charge groups have had to be defined "Pt-group" $\equiv$ (Z = 74 to 80) and "Pb-group" $\equiv$ (Z = 81 to 86) (§ I-4 ; fig. 10 ; Table 1). Second, extrapolation to the sources of the observed abundances relative to Fe or Si is still very uncertain, model dependent (truncation of PLD, § III-2.3. ; cross-sections, § I-3.1.) (e.g. Giler and Wibig 3, 17). I shall therefore discuss only the "Pb-group"/"Pt-group" ratio, without reference to Fe or Si. And, rather than deriving this ratio at the sources from the observations, I shall follow most authors and more prudently investigate which source abundances may, or may not, be consistent with the observed ratio. I recall that the observed "Pb-group"/"Pt-group" ratios are 0.25 ± 0.09 and 0.35 ± 0.10 from the HEAO-C3 and Ariel VI experiments respectively (Table 1 ; Waddington et al. 9,... ; Fowler et al. 2, 119). These observed ratios have been plotted on fig. 28. Possible non-Z^2 effects in the HEAO-C3 instrument might further slightly reduce the ratio (fig. 28 ; Waddington et al. 9,... ; Newport et al. 3, 287).

I shall now ask the question : are the observed "Pb-group"/Pt-group" ratios consistent with what would be predicted by the simplest model : source abundances following standard meteoritic Cl values biased according to FIP, and later modified by standard pure leaky-box propagation in the galaxy ?

Fig. 28 addresses this question. Based on standard Cl values, the LG ratio "Pb-group"/"Pt-group" = 1.00 (1.11) (Grevesse and Meyer, 3, 5). Correction for FIP bias according to the pattern f(FIP) adopted in fig. 15 increases this ratio by a factor of $\sim$ 1.55 (1.15), since FIP(Pb) = 7.4 eV and FIP(Os, Ir, Pt) $\approx$ 8.9 ± 0.2 eV. We thus get "Pb-group"/"Pt-group" = 1.55 (1.19) at the sources, after bias with FIP. The modification of this ratio during propagation is not small, because a large fraction of the interacting "Pb-group" elements is transformed into one of the numerous "Pt-group" elements. With the best-available scalings of cross-sections (§ I-3.1.) ; Kertzman et al. 3, 95 and priv. comm.) and a simple leaky-box model, propagation reduces the "Pb-group"/"Pt-group" ratio by a factor of $\sim$ 0.48 (1.20) (my estimate of the error, perhaps quite optimistic ; § I-3.1. and III-2.3.2. and 3.2.). The clear conclusion of fig. 28 is that the "Pb-group"/"Pt-group" ratio is indeed anoma-

lously low, based on the most standard assumptions, and in particular starting from standard C1 values as LG abundances.

Of course, since we are unable to provide a reliable link with the abundances of much lighter elements, we cannot tell whether Pb is underabundant or Pt overabundant !

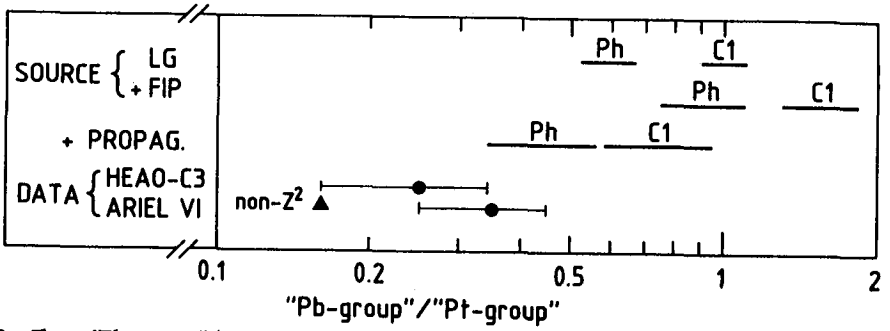

Fig. 28 The "Pb-group"/"Pt-group" abundance ratio (see Table 1 for def.), studied in the framework of the standard cosmic-ray model. Based on Waddington et al. (9,...) and Grevesse and Meyer (3, 5). From top to bottom : LG abundance ratio, equal to 1.00 (1.11) based on C1 meteoritic data (C1), and equal to 0.59 (1.14) based on solar photospheric data (Ph) (§ III-3.5.). If the usual bias with FIP applies, the presumable GCRS ratio is increased by a factor of 1.55 (1.15) relative to its LG value (§ III-3.1. ; fig. 15). Pure leaky box propagation between sources and Earth in turn decreases the ratio by a factor of 0.48 (1.20) (§ III-.3.1. ; on the figure, these various uncertainties have been summed quadratically). The two bottom lines give the data observed by the HEAO-C3 and Ariel VI experiments (Waddington et al. 9, ... ; Fowler et al. 2, 119 ; § I-4. ; Table 1 ; figs. 9, 10). Possible non-Z^2 effects on the HEAO-C3 charge scale might displace the HEAO-C3 point to the position of the triangle (e.g., Newport et al. 3, 287). The clear conclusion of this figure is that the observed "Pb-group"/"Pt-group" ratios are definitely inconsistent with the most standard CR model if C1 meteoritic abundances are adopted as a LG basis, but are not inconsistent if the solar photospheric values are adopted instead.

III-3.2. The low Pb/Pt ratio : probably not explainable in terms of a truncation of the PLD

It is clear from § III-2.3.2. that the question of a limited truncation of the PLD, to which UH elements would be extremely sensitive, is still open. The main problem is here the energy dependence of the relevant cross-sections, which are measured at 1 GeV/n (§ I-3.1.) and are used at 6 and 2 GeV/n, a range in which they are likely to significantly decrease with energy (Kaufman and Steinberg 1980). If too large cross-sections are actually used, truncation is actually needed.

But this trade-off between cross-sections and truncation is about the same when considering the (Z = 62-73)/"Pt Pb" ratio and the effect of secondaries on the "Pt-group"/"Pb-group" ratio. Fig. 27 shows that, with the cross-sections used as they are and no truncation, the (Z = 62-73)/"Pt Pb" data of HEAO-C3 and Ariel VI (high energy part of the data, identical to those of HEAO-C3 ; see fig. 11) are well fitted. Therefore not much can be changed by some trade-off between cross-sections and truncation as regards the calculated "Pt-group"/"Pb-group" ratio.

III-3.3. The low Pb/Pt ratio - Interpretations in terms of nucleosynthesis

It is well known that in ordinary matter Pb is primarily a s-process element while elements of the Pt group are mainly formed by the r-process. On this line Giler and Wibig (3, 17) have proposed a model in which the parameters governing nucleosynthesis of UH elements in GCR material differ from those for ordinary, "solar-mix", material : for GCR material, neutron fluences and densities, temperatures and time scales are adjusted in such a way that the s-process does not reach beyond Z = 58, and the shape of the GCR Pt-Pb peak is reproduced by a specific type of r-process. [25]

On the other hand, Margolis and Blake (3, 21) note that, in "solar-mix" material, the standard s-process that fits s-nuclides up to ^{204}Pb (1.5% of Pb) underproduces the dominant, heavier Pb isotopes. It is generally believed (Clayton and Rassbach 1967 ; Beer and Macklin 1985) that most of the missing Pb is produced in specific sites with particularity intense neutron exposures ("recycling s-process"), which are identified as low mass stars ($M < 1\ M_\odot$). The sites for production of most Pb being different from those for lighter s-nuclides, a deficiency of Pb in GCR's would be explained if the nucleosynthetic yield of these sites, i.e. stars with $M < 1\ M_\odot$, was underrepresented in GCR's as compared to "solar mix". [26]

The difficulty with such explanations of the deficiency of a specific element in terms of nucleosynthesis is always the same : they imply that the vast majority of GCR's must originate in specific sites of current nucleosynthesis, while their bulk composition resembles so much the "solar-mix" modified by simple atomic selection effects (the same selection effects found present in the solar Corona and SEP), and correlates so poorly with the outcome of the major cycles of nucleosynthesis and with the calculated pre-supernova and supernova compositions (Arnould 1984 ; Meyer 1985b).

Of course, there remains the possibility that Pb be not low, but that "Pt-group" elements be high, as a specific excess of r-nuclides (see § III-5.3.).

---

[25] This adjustment is also tuned as to reproduce other features of the UH source abundances for lower Z (some of which are, however, in my opinion, very unreliably derived from the abundances observed near Earth). Selection according to FIP is assumed to apply for s-process elements, not for r-process species.

[26] Käppeler et al. (1982) had erroneously attributed to r-process the entire difference between the observed Pb abundance and that estimated for conventional s-process, thus forgetting about the important contribution of the "recycling s-process" (Käppeler et al., private circular ; Beer and Macklin 1985). On this erroneous track, Fixsen (1985) has reevaluated a r-process Pb abundance, which is also much too high (as noted by Fixsen himself, by comparison with the neighbouring r-process components of Tl and Bi). This high r-process Pb abundance is however the one adopted by Binns et al. (1985) and Waddington et al. (9,...) ; I shall not consider it further in my discussion. These authors, however, note that the CR data may be consistent with a "Pb-poor r-process" (similar to the more standard one considered by Giler and Wibig 3, 17).

III-3.4. Ge and Pb as volatility indicators

It is now well known that, for most elements, the degree of volatility is (positively) correlated with the value of the FIP so that the apparent correlation of abundances with FIP might as well be interpreted as a correlation with volatility (Cesarsky and Bibring 1980 ; Epstein 1980a ; Bibring and Cesarsky 1981). Only a few low-FIP, though volatile, elements that are exceptions to the general rule permit to distinguish between the two types of correlation. Two indicators, Cu and Zn, though not entirely clear-cut, tend to favour FIP. But the best available indicators are at present Ge and Pb (Meyer 1981d ; Grevesse and Meyer 3, 5).

The fact that Ge and Pb are simultaneously found underabundant is striking ! At face value, it implies in this context that volatility, not FIP, is the relevant ordering parameter, and that GCR's are primarily interstellar grain destruction products. This is an interesting possibility, but not an easy one to live with ! The models of grain destruction and preferential injection in shock waves, while accounting fairly easily for the relative abundances of the refractory and volatile reactive heavy elements and for the low abundances of H and He, have a hard time in accounting for the roughly normal abundances of heavier noble gases (Ne, Ar, Kr, Xe) relative to O. Note also that, if GCR's are grain destruction products, their similarity in composition with SEP and Solar Corona is purely fortuitous.

III-3.5. Questioning the LG reference abundances for Ge and Pb

LG reference abundances have been discussed in § II-1.1. and 2.1.. As mentioned there, I think that C2 meteoritic abundances are irrelevant as a standard, which does not mean that C1's are necessarily perfectly representative of the protosolar nebula for all elements.

The study of Grevesse and Meyer (3, 5) shows that the C1 meteoritic abundances are well defined for both Ge and Pb.

As regards the solar Photosphere, this study shows that the Ge abundance can be reliably determined from 2 lines, and that of Pb from 1 line. This represents very few lines indeed ! However, with the quality presently reached by the solar atmospheric models, it is no longer unreasonable to determine the abundance of an element based on 1 or 2 lines only. A critical treatment of the errors in the photospheric abundance determinations, especially on the log gf values, leads to the conclusion that, to the best of our present knowledge, there is a significant discrepancy between the C1 and the photospheric abundances of Ge and Pb, both being found lower by a factor of ~ 1.6 in the Photosphere. If the photospheric values are adopted, there is no longer any significant underabundance of Ge relative to Fe, Mg, Si (figs. 19 and 20) and of Pb relative to Pt (fig. 28).

Can one meaningfully pick-up specifically two elements and adopt for them photospheric rather than C1 meteoritic values ? Once again, C1 values are better measured, but their relevance as representative of the abundances of the protosolar nebula is not straightforward, especially for volatile elements (§ II-2.1.). And we are specifically considering two volatile elements (especially Pb, which is extremely volatile) ! Consideration of fig. 2 in the review by Grevesse (1984a) shows that there is still some leeway for limited differences between photospheric and C1 abundances among volatile and highly volatile elements (not to speak of the problems with siderophile Fe and refractory Ti ; § II-1.1.).

III-3.6. Summary on the Ge-Pb deficiency problem

The low Ge and Pb abundances in GCRS seem at first to indicate that volatility, rather than FIP, is the parameter governing GCR abundances, and that GCR's are primarily grain destruction products. (However other, less clear-cut indicators, Cu and Zn, do not confirm this view). This hypothesis is not easy to live with : it has difficulties in explaining the noble gas abundances in CR's ; in addition, it would imply that the similarity between GCRS, SEP and solar coronal abundances is fortuitous.

On the other hand, models based on specific nucleosynthetic processes have been proposed to account for the low Pb. These are, in my view, not appealing. They would, indeed, require the entire cosmic radiation to originate in sites of specific nucleosynthetic processes. This seems highly improbable, in view of the similarity of the main features of GCRS composition to LG, SEP and solar coronal composition, and of its dissimilarity to predicted outcome of the main nucleosynthetic cycles and to calculated global pre-supernova and supernova compositions.

A more acceptable possibility, to be kept in mind, would be a specific excess of the r-nuclides around Pt, with respect to which a normal Pb abundance would appear low (see § III-5.3.).

One possible way-out is to question the C1 meteoritic standard used for reference. If the - apparently significantly - lower photospheric values were used as a standard, Ge and Pb would no longer appear depleted in GCR's. The question is open.

III-4. THE C, O, ^{22}Ne, $^{25,26}Mg$, $^{29,30}Si$ EXCESSES

The C, and to a lesser extent, O excesses in GCRS are most conspicuous when the GCRS composition is compared to that of SEP's, the two compositions being otherwise quite similar (fig. 17 ; § II.1.3.). In particular the C/O ratio itself, extremely well determined in both populations, is about twice as high in GCRS as in SEP's. I surmise that these excesses relative to SEP's are highly meaningful ; and the shape of f(FIP), the basic FIP-dependent pattern of GCRS relative to LG composition defined in fig. 15, has been chosen accordingly : f(FIP) does not try to fit the GCRS/LG values for C and O, which are in excess, like in fig. 17 (§ II-1.4.). In addition such C and O excesses are known to be expected, associated with the ^{22}Ne and $^{25,26}Mg$ excesses, if these are due to a small fraction of He-burning material appearing in GCR's.

But let me first review the evidences for or against the existence of ^{22}Ne, $^{25,26}Mg$ and $^{29,30}Si$ excesses is GCRS.

III-4.1. Estimating the ^{22}Ne, $^{25,26}Mg$, $^{29,30}Si$ excesses in GCR Sources

Fig. 29 summarizes our knowledge on the Ne, Mg and Si isotopic composition. I have plotted the estimated composition from Wiedenbeck's (1984) summary at Graz, which is mainly based on low energy data (< 600 MeV/n), the new data brought at this conference by Webber et al. (2, 88) around 500 MeV/n, and a summary of the high energy HEAO-C2 data between 2.5 and 6 GeV/n, including those presented at this conference (Ferrando et al. 2, 96 ; Herrström et al. 2, 100) (§ I-2.).

In this figure, I have given both the isotope ratios measured near Earth and those derived for the sources, thus evidencing the crucial importance of the correction for secondaries in estimating the $^{25,26}Mg$ and $^{29,30}Si$ excesses (or absence of excess !!!) at the sources. These corrections differ somewhat from calculation to calculation. An important new point is that the cross-sections for secondary production of Mg and Si isotopes out of ^{28}Si and ^{40}Ar just measured by Webber and Kish (3, 87) are higher than was expected (§ I-3.1. ; fig. 5). These higher cross-sections, when extrapolated to other neighbouring parent nuclei (the question is of course : how to extrapolate ?), yield significantly higher secondary production, hence lower source abundances, for $^{25,26}Mg$ and $^{29,30}Si$ (as for Al, illustrated in fig. 6). In fig. 29, these higher cross-sections are applied to the data of Webber et al. (2, 88), but I have not modified the other corrections accordingly.

Extreme prudence is in addition required since, except for the HEAO-C2 data (which are conclusive, neither for Mg, nor for Si), all estimates are based on low energy studies. But we have shown in § III-2.1. that the B-^{15}N contradiction suggests that we understand poorly propagation at these energies, and that distributed reacceleration possibly completely blurrs the picture there. If this were the case, the corrections for secondary formation of ^{22}Ne, $^{25,26}Mg$ and $^{29,30}Si$ might have to be based on the cross-sections below 100 MeV/n, which are unknown.

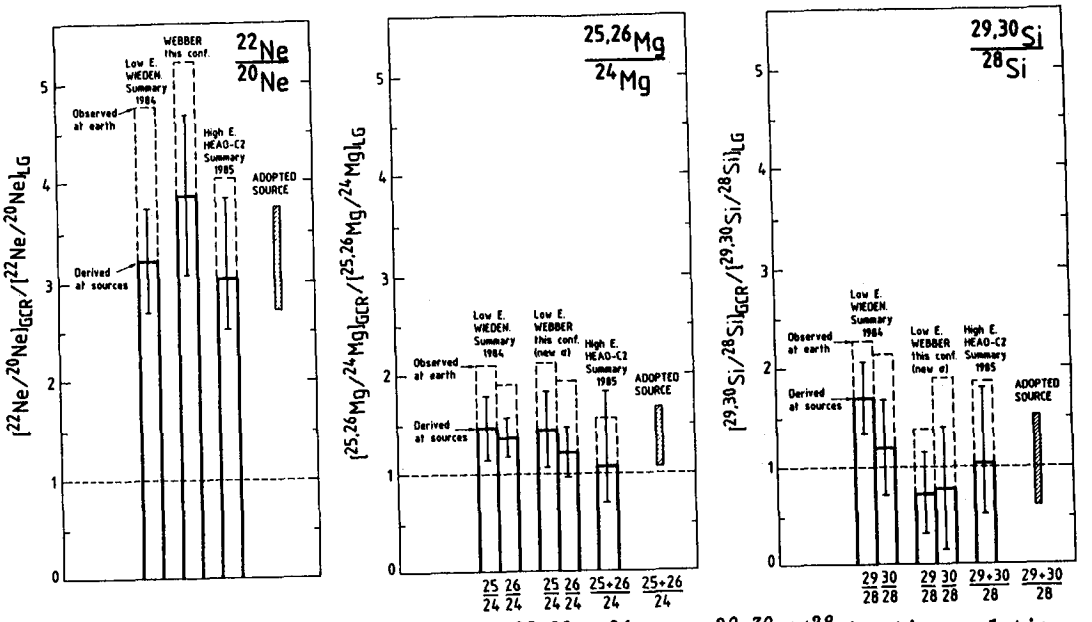

Fig. 29 Excesses in the GCR $^{22}Ne/^{20}Ne$, $^{25,26}Mg/^{24}Mg$ and $^{29,30}Si/^{28}Si$ ratios, relative to standard LG (see footnote # 27). For each set of data, I give the excess as observed at Earth (dashed ; error bar omitted for clarity) and that derived at source after correction for secondary production as derived by the authors (solid). From left to right in each plot : (i) Wiedenbeck's (1984) summary of the data existing in 1984, based mainly on low energy data (E < 600 MeV/n) ; (ii) the new data by Webber et al. (2, 88) around 500 MeV/n, the correction for secondary production being based on new, larger cross-sections, recently measured or estimated (§ I-3.1. ; figs. 5, 6) ; (iii) a summary of the HEAO-C2 data at high energy, mainly near 2.5 GeV/n but up to 6 GeV/n, based on Byrnak et al. (1983a), Goret et al. (1983) ; Ferrando et al. (2, 96) and Herrström et al. (2, 100) ; (iv) an "adopted" source excess. For Mg and Si, the various ratios plotted are indicated at the bottom of the figure.

An important point in fig. 29 is the low abundance of $^{29,30}Si$ observed near Earth by Webber et al. (2, 88), with an excellent resolution and a decent statistics (fig. 2 ; § I-2.). Together with the increased correction for spallation, it yields very low $^{29,30}Si/^{28}Si$ source ratios. Considering all the data for Si together, there may be a slight excess of $^{29,30}Si$ at the sources, but the data are also perfectly consistent with a totally normal source $^{29,30}Si/^{28}Si$ ratio.

As regards $^{25,26}Mg$, the data do suggest on excess in GCRS, but are not really compelling in view of all the uncertainties on the secondary correction. And, even if real, the excess could be very small.

Only the ^{22}Ne excess is established beyond any doubt, and is rather precisely determined.[27]

The adopted GCRS excesses of $^{22}Ne/^{20}Ne$, $^{25,26}Mg/^{24}Mg$ and $^{29,30}Si/^{28}Si$ have been plotted in fig. 20.

[27] No error has been associated with the LG $^{22}Ne/^{20}Ne$ isotope ratio, taken on the basis of SEP's (Meyer 1985b). If the Solar Wind value turned out to be more representative (e.g., Geiss 1985), the GCRS excess would be slightly larger.

III-4.2. The common and new wisdom on He-burning and weak s-process in Wolf-Rayet stars

It is now common wisdom that the simultaneous conspicuous ^{22}Ne and C excesses in GCRS (relative to LG and especially SEP abundances) are an indication that a small fraction GCR's originates in He-burning material. The smaller excesses of $^{25,26}Mg$ and O, if confirmed, indicate a more limited contribution from the subsequent stage of nucleosynthesis where ^{22}Ne is turned into $^{25,26}Mg$ and ^{12}C into ^{16}O. It is also well known that Wolf-Rayet (WR) stars, in which the nucleosynthetically active core has been bared by huge stellar winds which disperse the newly "cooked" material, are a very plausible site for providing this processed component without further alteration.

More precisely, it has been shown that the ^{22}Ne-C and possible $^{25,26}Mg$-O excesses are explained if material from WC-WO type stars (the WO stage is very rapid) is diluted in GCR's in $\sim$ 50 times as much nucleosynthetically standard, solar-mix material (to be precise, this dilution factor applies to high-FIP species that are unaffected by the local nucleosynthesis, such as ^{20}Ne ; see § III-4.3. and footnote # 29). If one considers material from the entire WR stars sequence, which includes 40% of WN stars (which are not enriched in ^{12}C, ^{22}Ne), one GCR ^{20}Ne nucleus out of $\sim$ 30 should originate in a WR star of any type (Meyer 1981c, 1985b ; Cassé and Paul 1981, 1982 ; Maeder 1983 ; Blake and Dearborn 1984 ; Arnould 1984 ; Prantzos 1984a,b ; Prantzos et al. 1983 ; 3, 167).

Note that a high abundance of Ne (presumably ^{22}Ne) has indeed been recently observed by IRAS in the atmosphere of a WC star (Van der Hucht and Olnon 1985).

One strong conclusion from the above studies is that, while $^{25,26}Mg$ can be produced in the destruction of ^{22}Ne, there is no way of producing $^{29,30}Si$ in the same context. To explain excesses of $^{29,30}Si$, additional, extrinsic hypothesis would have to be invoked, such as supermetallicity (i.e. CR's coming from far away in the inner galaxy), or galactic evolution, which are not straightforward (Woosley and Weaver 1981 ; Cassé 1981, 1983). The new observations by Webber et al. (2, 88) (§ I-2 and III-4.1. ; fig. 2 and 29) indicating that there may well be no $^{29,30}Si$ excess at all, if confirmed, would greatly simplify the situation.

In addition, liberation of neutrons at the time of the ^{22}Ne destruction by the $^{22}Ne(\alpha, n)\ ^{25}Mg$ process leads to the predicted formation of other n-rich species (weak s-process), which have been estimated quantitatively in the framework of a consistent WR evolution scheme by Prantzos et al. (1983), Prantzos (1984a,b) and at this conference by Prantzos et al. (3, 167) who have integrated over the contribution of WR stars with initial masses > 50 $M_\odot$. The predicted excess of these other n-rich species in GCRS can be related to the ^{22}Ne excess through the time scales of the WR star evolution and the dilution factor required for ^{22}Ne. These results will be discussed in the next § III-4.3. (figs. 30 and 31).

Note that a possible N excess originating in WN-stars (largely lower mass stars, < 50 $M_\odot$) has not been studied quantitatively in the same framework. Recall, however, that, even at the end of CNO cycle, N

is overabundant by a factor of at most ~ 17 (to be compared to 120 for ^{22}Ne in the He-burning phase) (Prantzos 1984a ; Meyer 1985b). Quite small dilution factors for the WN star material would be required to produce an observable N excess in GCRS, while only $\sim 40\%$ of WR stars are of type WN, 60% of them being of type WC-WO.

III-4.3. Relating the excesses in GCRS to those in the (WR) processed component material. FIP effects in the dilution

This is all nice, but there is a problem.

In order to characterize the sources of the processed material, we have to correctly relate the excesses in that processed component to those in GCRS as derived from the observations. The key point here is to properly take into account the dilution of the processed component in the main component, for each particular element.

The studies performed up to now have, in my view, not dealt with this point correctly. As pointed out in Meyer (1985b), it has been forgotten that, in the main component in which the processed material is believed to be diluted, low-FIP elements such as Mg are overabundant by factors of ~ 6 relative to high-FIP C, O, Ne. Then, while we do not know what atomic selection effects might affect the processed component, two simple cases should be considered (see formalism in the Appendix) :

(i) The processed component is affected by the same bias with FIP as the main component

Then, of course, all elements are diluted by the same factor ; and the existing studies, that simply ignore differences in dilution factor between elements, give correct results (Meyer 1981c, 1985b ; Cassé and Paul 1981, 1982 ; Maeder 1983 ; Blake and Dearborn 1984 ; Arnould 1984 ; Prantzos 1984a,b ; Prantzos et al. 1983 ; 3, 167). Then, as shown in the Appendix, the classical formula applies :

$$E^{*}_{ik,CR} = 1 + p_k \cdot E_{ik,proc,nucl} \qquad \text{(A3)}$$

where (see Appendix)

$E^{*}_{ik,CR}$ = enhancement in GCRS relative to LG after correction for bias with FIP, i.e. [GCRS/LG]/f(FIP), the quantity plotted in fig. 20, for species i relative to a reference species k which is not affected by the nuclear processing.

$E_{ik,proc,nucl}$ = enhancement in the processed component material relative to LG, due to nuclear effects only, for species i relative to the same, unaffected, reference species k.

p_k = fraction of the unaffected species k originating in the processed component ($1/p_k$ = dilution factor for species k).

I regard this situation as astrophysically implausible. It would indeed be quite odd to have the same filtering according to FIP occur independently in the main component and in the processed component, which certainly originates in a cahotic environment ; the proposed

favourable objects, Wolf-Rayet (WR) stars, are very hot, so that all elements are ionized on their surface and FIP does not have a chance to play a role.

The only way-out would then be : the filtering according to FIP should occur after mixing of the main and the processed components (i.e. at a common injection or acceleration phase).

But the presence of the refractory, condensable elements in the main GCR component and its bias with FIP seem to reflect the composition of coronae of solar-like F-M stars (as well as that of SEP's), which are likely to be the injection sites of this main component (Meyer 1985b). The cause for the bias with FIP of the main component therefore probably lies in the composition of the medium they have been extracted from, not in later, distant injection or acceleration processes. [28]

Note however that the above formula ignoring any differences in dilution between elements gives, anyway, correct results when applied only to elements on the same FIP-plateau, e.g. ^{20,22}Ne, C, O, for which it has actually been first used (see Appendix).

In the top graph of fig. 30, the data on the GCRS excesses (from figs. 20,29 and Wiedenbeck 1984) are compared to the excesses predicted for GCRS, based on Prantzos et al. (3, 167)'s He-burning and weak s-process calculations in 50-100 $M_\odot$ WO-WC star atmospheres, and on the above eq.(A3) to describe the dilution of this processed component. The dilution factor ($p_{^{20}Ne} \approx 1/50$ for the WC-WO material) [29] is adjusted as to fit the GCRS ^{22}Ne excess of ≈ 3.2 (figs. 20,29). The depicted species are those produced in WC-WO stars, whose excess in GCRS is, or may become observable (as a reminder ^{29,30}Si, which is not produced in this context, has also been plotted).

In the top graph of fig. 31, the enhancement factors in the source medium of the processed component, as derived from the GCRS data using eq.(A3), are compared with those directly predicted by the stellar evolution codes for WC-WO atmospheres. The same value $p_{^{20}Ne} = 1/50$ is used to adjust the excesses derived from the GCRS data to the ^{22}Ne enhancement calculated for time averaged WC-WO atmospheres.

---

[28] I believe that we definitely have two completely different injection sites for the main and the processed component. The final, high energy accelerations may take place, either (i) prior to mixing of the two components, in different environments; for instance, the WR component might be specifically accelerated by the WR's own stellar wind terminal shock, or (ii) after mixing of the two injected suprathermal populations, by a common agent. The lack of detectable difference between the source spectral shapes of C, O, ^{22}Ne and other heavy nuclei between ~ 1 and ~ 20 GeV/n (Engelmann et al. 1985 ; Herrström and Lund 2, 100) is consistent with the second hypothesis, but not necessarily inconsistent with the first one. Of course, search for such differences in spectral shapes should continue, especially at higher energies.

[29] Choosing ^{20}Ne as the reference species k unaffected by the local nucleosynthesis is not strictly adequate, since a small amount of ^{20}Ne is produced at the end of the WO stage (Prantzos et al. 1983 ; Prantzos 1984b ; time integrated excesses : ^{20}Ne : 1.6 ; ^{22}Ne : 108). But after dilution, the ^{20}Ne excess is completely negligible, and we can forget about it.

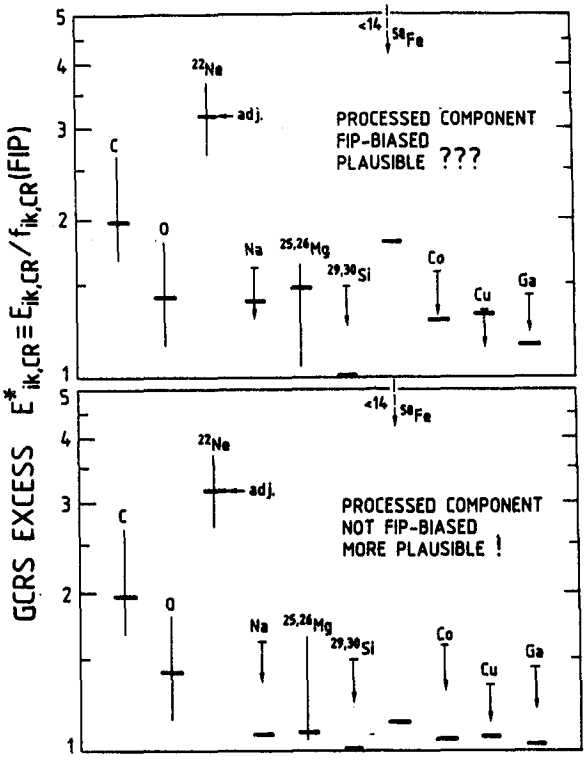

Fig. 30 *Plotted are excesses $E^*_{ik,CR}$ in GCRS, relative to the FIP-pattern $f_{ik}(FIP)$ describing the main GCRS component (cf. fig. 20) (§ III-4.3. and 4.4. ; Appendix). The species plotted are those formed by He-burning and weak s-process, for which excesses in GCRS are, or may become, observable (as a reminder $^{29,30}Si$ which is not produced in this context, has also been plotted). Vertical error bars, identical in both graphs : GCRS excesses derived from the observations (figs. 15, 20, 29). Thick horizontal marks : predictions based on Prantzos et al. (3, 167)'s model of He-burning and weak s-process in WC-WO stars, diluted in the main component by a factor of $1/p_k$ = 50 for ^{20}Ne (adjusted as to fit the "observed" GCRS $^{22}Ne/^{20}Ne$ excess). Top graph : the processed WC-WO component is assumed to be FIP-biased like the main component, so that all species are diluted by the same factor ; this assumption has been made in existing studies, but is not very plausible. Bottom graph : the processed component is not FIP-biased, so that its low FIP elements are ∿ 6 times as diluted as its high-FIP elements ; this hypothesis is much more plausible.*

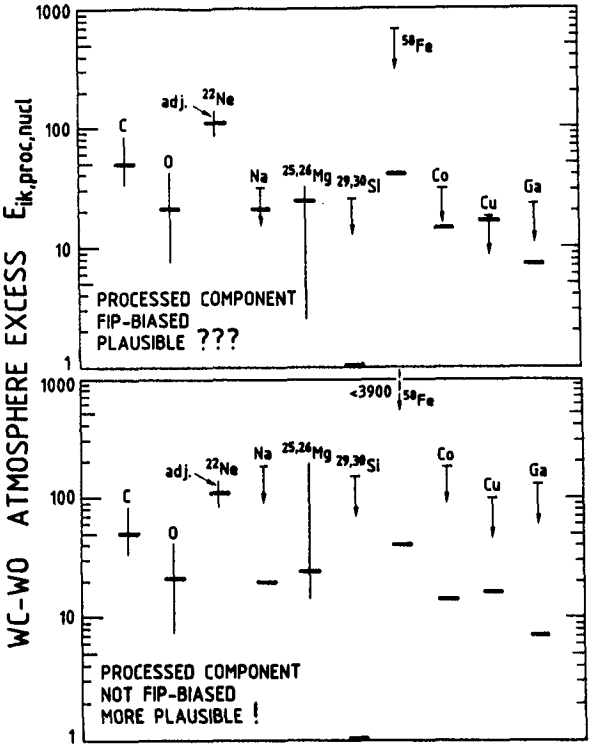

Fig. 31 *Plotted are excesses $E_{ik,proc,nucl}$ in the surface material of WC-WO stars, relative to LG composition (§ III-4.3. and 4.4. ; Appendix). Thick horizontal marks, identical in both graphs : excesses directly predicted by Prantzos et al. (3, 167)'s model of He-burning and weak s-process in WC-WO stars. Vertical error bars : excesses in the processed component source material, as derived from the "observed" GCRS excesses, assuming a dilution in the main component by a factor of $1/p_k$ = 50 for ^{20}Ne (adjusted as to fit the calculated ^{22}Ne excess in WC-WO stars). Top graph : the processed component is FIP-biased. Bottom graph : it is not FIP-biased. See caption of fig. 30.*

(ii) The processed component is not affected by atomic selection effects.

We now consider the situation in which the processed component is not affected by the same bias with FIP as the main component. As just discussed, this is the more plausible situation. Other atomic selection effect, unrelated to FIP, may of course be present in the processed component ; but in the absence of any information on them, we can only ignore them and take for the processed component the composition given directly by the local nucleosynthesis.

Then we have, as shown in the Appendix :

$$E^{*}_{ik_{CR}} = 1 + \frac{p_k}{f_{ik}(FIP)} \cdot E_{ik,proc,nucl} \qquad (A4)$$

with the notations defined above for eq.(A3) and $f_{ik}(FIP)$ being the value of f(FIP) for species i normalized to that for species : $f_{ik}(FIP) = f_i(FIP)/f_k(FIP)$.

Here $f_{ik}(FIP) = 1$ for high-FIP species (reference species k = ^{20}Ne), and $f_{ik}(FIP) \approx 6$ for low-FIP species (fig. 15). Equation (A4) thus simply expresses the 6-fold higher degree of dilution of "processed" low-FIP species as compared to high-FIP species (Meyer 1985b). The dilution factor $p_{^{20}Ne} = 1/50$ relevant for high-FIP species becomes 1/300 for low-FIP species.

When eq.(A4) is used to describe the dilution, the new connections between the excesses in GCRS and those in the WC-WO processed component are depicted in the bottom graphs of figs. 30 and 31.

III-4.4. Discussion : types of dilution, observed and predicted excesses

Figs. 30 and 31 include only three high-FIP species, C, O and ^{22}Ne, all heavier species being low-FIP elements. Comparison of the top and bottom graphs shows that :

- as regards the high-FIP species, the top and bottom graphs are, of course, identical (since the dilution is adjusted as to fit the high-FIP $^{22}Ne/^{20}Ne$ ratio). As has been known for a while now, the same degree of dilution of the WC-WO material fits simultaneously the ^{22}Ne, C and O excesses.
- For all other, low-FIP, species, the 6-fold higher degree of dilution in the bottom graphs (in which the processed component is no longer assumed to be affected by the bias with FIP) decreases the expected excesses at GCRS by that same factor of 6 (fig. 30). [Conversely, it increases the excesses in the processed material, required to fit the observed GCRS excesses (fig. 31)].
- As regards specifically $^{25,26}Mg$, produced together with O, the predicted GCRS excess drops from ~ 1.48 if the WR component is biased with FIP (as usually implicitely assumed up to now), down to ~ 1.08, i.e. a minute enhancement, in the much more probable opposite case. The present data (fig. 29) do not really exclude either of the possibilities. We really need higher statistics observations and safe, accurate secondary corrections.

- As regards the other low-FIP species, produced by the weak s-process (Prantzos et al. 3, 167), their predicted enhancements are also very small if the WR component is not biased with FIP (fig. 30, bottom). Even in the unlikely case that this component were FIP-biased, the predicted excesses would still be below all present upper limits to the GCRS excess (fig. 30, top). The most promising species that might set limits in this case are, first, Ca, and then Na, Co, Ga. Present upper limits on ^{58}Fe are still very far up.
- Note finally that, if the processed component is not FIP-biased, the existing data on Mg and Si isotopes in GCRS do not exclude equal excesses of ^{22}Ne, ^{25,26}Mg and ^{29,30}Si in the material of the processed component (fig. 31, bottom). This leaves the door slightly open for the proponents of the supermetallicity hypothesis to explain the ^{22}Ne, ^{25,26}Mg, ^{29,30}Si excesses (Woosley and Weaver 1981). It would remain to see how the C and O excesses would then fit into the picture.

III-4.5. Excess ^{22}Ne : preferential injection at the decay of ^{22}Na ?

A shrewd, totally new mechanism to explain the ^{22}Ne excess has been proposed at this conference by Yanagita (3, 175). Although I am not too convinced that it will finally work out as a very plausible scenario for ^{22}Ne, I think it deserves attention becauses it contains a lot of new ideas which may be fruitful in this, or other occasions.

The idea is that, at the moment of β-decay, the daughter nucleus gets both ionized and selectively heated, hence "injected", by the recoil energy of the electron emission. The mechanism therefore concerns nuclear species which originate from the β-decay of some other, directly synthesized progenitor. Now, it is well known from Ne-E in meteorites that some ^{22}Ne is produced via β-decay of ^{22}Na, which is itself largely synthesized by explosive H-burning in novae and possibly massive supernova envelopes (e.g., Arnould and Norgaard 1978,1981 ; Arnould et al. 1980 ; Hillebrandt and Thielemann 1982). This ^{22}Ne could be preferentially injected, hence be in excess in GCRS.

Now, among the various species thus formed via β-decay from some other directly synthesized nuclide, why should only ^{22}Ne be enhanced in GCRS ? Yanagita (3, 175) remarks that the mechanism does not work for radioactive progenitors other than ^{22}Na ($\tau_{^{22}Na}$ = 2.6 yr) because, either they are too short-lived so that the decay occurs within a stellar medium, inappropriate for acceleration, or they are rapidly locked in grains. Only ^{22}Na both has a long enough period and remains volatile in space.[30]

Many questions remain to be solved with this scenario : (i) the suprathermal ^{22}Ne must be picked up by an accelerating shock wave before it gets thermalized, which takes about 1 year ; (ii) the total production of ^{22}Ne via ^{22}Na in novae can be estimated through the observed ^{26}Al γ-ray line emission, provided most of the ^{26}Al is indeed produced by

[30] There might however be another possibility with fission products (Xe) formed in supernovae.

explosive H-burning in novae (Arnould et al. 1980 ; Hillebrandt and Thielemann 1982), which is not obvious [31] ; even then, the process requires that as much as 6% of all the ^{22}Na nuclei ejected by novae get accelerated and become cosmic-ray ^{22}Ne ; this would be a very high efficiency indeed ! (iii) the energetics remains to be precisely worked out.

Of course, this interesting mechanism, when applied to GR ^{22}Ne suffers from an additional weak point : it takes care only of the ^{22}Ne excess, so that an independent cause must be found for the C excess, as well as for the weak $^{25,26}Mg$ and $^{29,30}Si$ excesses, if they exist (figs.29 and 20 ; § III-4.1.). [32]

III-5. THE EXCESS OF ELEMENTS WITH Z ⩾ 40

The conspicuous really new event in fig. 20 is the probable excess of all of the six nuclei with Z ⩾ 40 for which GCRS abundances have been estimated (see also fig. 19). As discussed in § II.2.2., the solid error bars in fig. 20 indicate the more probable ranges for the excesses of UH nuclei, while their dashed prolongations indicate ranges which cannot yet be entirely excluded, but are by far less likely. As can be seen, the excesses seem certain for $_{42}Mo$ and $_{58}Ce$, and probable for $_{40}Zr$, $_{52}Te$, $_{54}Xe$, $_{56}Ba$. The discussion that follows is based essentially on the solid bars, and thus assumes that all six excesses are real. The dashed bars however tell us where there is still a slight degree of doubt.

The excesses appear roughly comparable in magnitude for elements in the ranges Z = 40-42 and Z = 52-58, and also for predominantly s ($_{40}Zr$, $_{42}Mo$, $_{56}Ba$, $_{58}Ce$) and for predominantly r ($_{52}Te$, $_{54}Xe$) elements But this point will have to be discussed more seriously in § III-5.2..

A very striking feature is that there is no trend for an excess up to Z = 38 : the excess starts abruptly at Z = 40. It is true that $_{34}Se$ and $_{36}Kr$, with their large error bars on fig. 20, could apparently be also in excess ; but further analysis will show that this possibility is only apparent (§ III-5.1.2.). As regards $_{38}Sr$, a refractory element for which good C1 meteoritic data agree with the photospheric value (Anders and Ebihara 1982 ; Grevesse 1984a), which is well measured in CR's (fig. 10), and for which the spallation correction is negligible (e.g., Binns et al. 1983), it is definitely not in excess (see also fig. 19). By contrast, most probably $_{40}Zr$, and definitely $_{42}Mo$ are in excess. For these two elements the LG values and the spallation corrections cannot either be questioned (see footnote # 11). [33]

---

[31] There are other, competing processes for ^{26}Al formation, in red giants (Norgaard 1980) and in Wolf-Rayet stars (Dearborn and Blake 1985 ; Prantzos and Cassé 1985).

[32] For these weak excesses, galactic evolution effects or the supermetallicity hypothesis might do the job (Cassé 1981, 1983 ; Woosley and Weaver 1981).

[33] Atomic selection effects are not good candidates to explain the jump. As regards FIP-dependent effects (actually taken out in fig. 20), $_{38}Sr$, $_{40}Zr$ and $_{42}Mo$ have very similar low values of FIP (fig. 19). In a 10^6 K plasma, fig. 21 shows that they also behave quite alike. Only in a very specific temperature range between ∿ 15000 and ∿ 80000 K would $_{38}Sr$ (in its Kr-like state) behave differently from $_{40}Zr$ and $_{42}Mo$.

III-5.1. Estimating the excesses in the processed component material - FIP effects in the dilution

III-5.1.1. The dilution problem

Before discussing the possible significance of the excesses in fig. 20, we must make sure that we understand them correctly. We are indeed faced with the same problem as in the study of the ^{22}Ne and its associated excesses in § III-4.3.. Most likely, we have again a processed component, highly enriched in specific species, which is highly diluted in the FIP-biased main CR component. We need to derive the nuclear anomalies in the source material of this processed component from the GCRS excesses in fig. 20. This requires to properly take into account the differences in degree of dilution of the various elements of the processed component, due to the FIP-bias in the composition of the main component itself (cf.§ III-4.3.).

We shall, again, start from the fundamental eq.(A2) of the Appendix, explicited for $E_{ik,proc,nucl}$:

$$E_{ik,proc,nucl} = \frac{E^{*}_{ik,CR} - 1}{p_k} \cdot \frac{f_{ik(FIP)}}{f_{ik,proc(atom)}} \qquad (A2')$$

with the notations of § III-4.3. and of the Appendix [$f_{ik,proc}(atom)$ describes any atomic selection effects in the processed component]. This equation is valid for $p_k << 1$ (high degree of dilution) and $E_{ik,proc,nucl} >> 1$.

The situation however differs from the one we had when studying the ^{22}Ne anomaly : here we have no model at hand to theoretically estimate $E_{ik,proc,nucl}$ and therefore have no way to know the dilution factor $1/p_k$ (which I just assume to be large). $E_{ik,proc,nucl}$ can therefore be derived only to within an unknown factor. This is why fig. 32, otherwise similar to fig. 31, is labelled in arbitrary units (actually normalized to the $_{42}Mo$ excess $\equiv 10^n$, where n is an unknown, non integer, number).

Like in § III-4.3., we have two choices :

(i) the processed component has gone through the same FIP-filtering as the main component ; then all differential effects on dilution cancel out ; $f_{ik,proc}(atom) = f_{ik}(FIP)$, and the second factor in eq.(A2') vanishes (fig. 32 ; top) ; for the reasons developed in § II-4.3., I consider this situation as implausible ;

(ii) the processed component did not go through the same FIP filtering ; other atomic selection effects may of course be at work, probably not related with FIP ; in the absence of any information on them, we can only ignore them and set $f_{ik,proc}(atom) = 1$; we are thus left with a factor $f_{ik}(FIP)$ in eq. (A2'), which just describes the lower degree of dilution of the processed species belonging to elements which are underabundant in the main component (fig. 32, bottom) ; this should be a better approximation to reality.

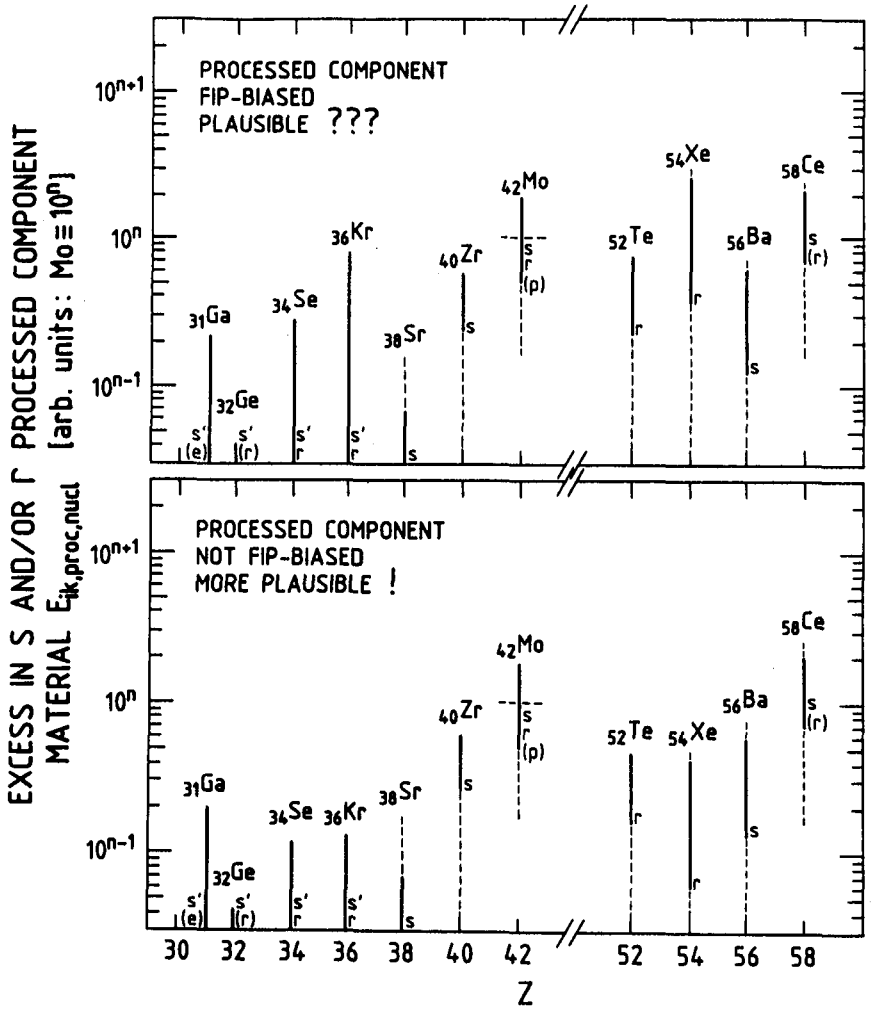

Fig. 32 *Plotted are excesses $E_{ik,proc,nucl}$ in the s and/or r-processed component material, relative to LG composition (§ III-5.1. ; Appendix). This figure is similar to fig. 31. The excesses in the processed component are those derived from the GCRS composition (figs. 19, 20 ; § II-2.2.) ; they are known only to within an unknown dilution factor for the processed component ($1/p_k$, assumed large), so that only relative values of the excesses are given (normalized to the $_{42}$Mo excess ≡ 10^n). For each element, the thick, solid error bar gives the more probable range, and its thin, dashed continuation a range that is much less likely, but cannot yet be entirely excluded (figs. 19, 20 ; § II-2.2.). Of course, bars reaching the bottom lines are only upper limits, consistent with no enhancement at all. Also given are the main processes responsible for the synthesis of the various elements in the "solar mix" : e, s, r, p processes, and s' = s due to the weak component of the neutron irradiation (see footnote # 35). One symbol plotted : ≥ 80% one process ; two symbols : two processes contribute about equally ; second symbols in parenthesis : contributes about 1/3 of total. Top graph : the processed component is assumed to be FIP-biased like the main component, so that all species are diluted by the same factor ; this assumption is quite implausible. Bottom graph : the processed component is not FIP-biased, so that in GCRS its low-FIP elements have been more diluted than its high-FIP elements ; it is the more plausible hypothesis.*

III-5.1.2. Consequences of differential dilution

Introducing the differential effects of dilution changes the picture in some respects, which are apparent when comparing figs. 20 and 32, top and bottom. In fig. 32, I have marked the predominant nucleosynthetic processes responsible for the formation of the various elements in the usual "solar mix" (Käppeler et al. 1982 ; Fixsen 1985 ; Binns et al. 1985).

Elements $_{34}Se$, $_{36}Kr$ and $_{38}Sr$ are all three consistent with no enhancement at all (fig. 20). Figs. 20 and 32 (top), however, do not exclude the possibility that $_{34}Se$ and $_{36}Kr$, with their large upward error bars be in excess, while $_{38}Sr$ is definitely not. Since about half the $_{34}Se$ and $_{36}Kr$ are formed by r-process while $_{38}Sr$ is almot pure s, one could have considered a specific enhancement of r-nuclides in this range [however the enhancement of $_{40}Zr$, also almost pure s, would have poorly fitted into the picture]. When differential dilution is included (fig.32, bottom), this possibility of an enhancement of $_{34}Se$ and $_{36}Kr$ relative to $_{38}Sr$ in the source material of the processed component disappears.

In the $_{52}Te$ $_{54}Xe$ $_{56}Ba$ $_{58}Ce$ quartet, introduction of differential dilution specifically reduces the excesses of the two r-elements $_{52}Te$ and especially $_{54}Xe$ (which happen to be high- or intermediate-FIP elements, fig. 19) in the processed component material (fig. 32).

III-5.2. Evidences for s and/or r-process excesses

I am now going to discuss the excesses in the processed component material, under the most plausible assumption that this component has not gone through the FIP-dependent filter of the main component (§ III-4.3. and 5.1.). Fig. 32 (bottom) will therefore serve as the main basis for the discussion.

III-5.2.1. What happens at Z = 40 ?

As noted earlier, and obvious from figs. 20 and 32 (top as well as bottom), the most striking feature in the data is the sharp onset of the excesses, specifically between Z = 38 (no excess) and Z = 40 (provided the $_{40}Zr$ excess is confirmed, § II-2.2.).

At Z = 38 to 40, we are right at the neutron magic number N = 50 (fig. 33) ! This fact very strongly suggests an s-process anomaly. $_{38}Sr$ and $_{40}Zr$ are almost pure s elements, while $_{42}Mo$, for which the excess is best established, is about 44% s, 32% r and 24% p (Käppeler et al. 1982 ; Fixsen 1985 ; Binns et al. 1985).

As shown in fig. 33, all isotopes of Sr have $N \leqslant 50$ neutrons ; but one isotope dominates by far, ^{88}Sr (82%), which has N = 50 neutrons. As regards Zr, all its isotopes have $N \geqslant 50$ neutrons ; the most abundant isotope, ^{90}Zr, which makes up 52% of Zr, has also N = 50 neutrons. Both ^{88}Sr and ^{90}Zr lie right near the bottom of the first precipice of the σN_S curve (e.g., Ward and Newman 1978 ; Käppeler et al. 1982). So, ^{88}Sr is definitely not enhanced in GCRS, while ^{90}Zr, with the same magic number of neutrons N = 50, may be enhanced, or not. The responsibility for the enhancement of elemental Zr might indeed rest only with its isotopes with $N \geqslant 51$, which make up 48% of elemental Zr.

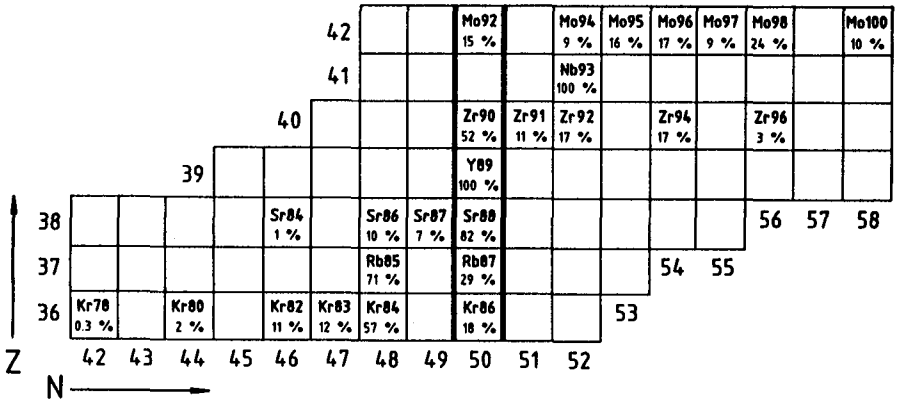

Fig. 33 The critical part of the chart of the nuclides around Z = 40, i.e. around magic N = 50 neutrons (§ III-5.2.1.). Only stable nuclides are given. The percent contribution of each isotope to the elemental abundance in the "solar mix" is indicated. For the contribution of the various processes to each nuclide, see Käppeler et al. 1982, Fixsen 1985, Binns et al. 1985 (see also fig. 32). The CR data indicate that $_{40}$Zr and $_{42}$Mo are probably enhanced in CR sources, while $_{36}$Kr and $_{38}$Sr are not (figs. 10, 19, 20, 32 ; § II-2.3. and III-5.). This may suggest that nuclides with N ≳ 51 neutrons are specifically in excess in GCRS.

So the enhancement of s-species precisely from Z = 40 upwards might mean that only species with N ≳ 51 neutrons, beyond the magic N=50, are enhanced in GCRS. [34] This would imply that products of comparatively strong s neutron irradiations, with average number of neutrons captured per Fe nucleus $n_c \gtrsim 54$, are overrepresented in GCR's (e.g., Clayton 1968, Fig. 7-22). Some material having undergone specifically such strong irradiations should be injected in the CR accelerating machine ! A very important conclusion indeed ! [which however depends on the confirmation of the [35] $_{40}$Zr excess ; $_{42}$Mo lies beyond N = 50, and is almost as much r as s].

III-5.2.2. The $_{52}$Te $_{54}$Xe $_{56}$Ba $_{58}$Ce quartet

In the r- and s-peaks region between Z = 52 and 58, we have evidence for enhancement of all four studied elements, by comparable amounts for predominantly r $_{52}$Te and $_{54}$Xe and for predominantly s $_{56}$Ba and $_{58}$Ce (figs. 20 and 32, bottom).

The best established enhancement is that of $_{58}$Ce, which is 65% s and 35% r in "solar mix" material. Almost pure s $_{56}$Ba is probably also enhanced.

---

[34] In this context, a reliable determination of the CR abundance of the single isotope pure-s element $^{89}_{39}$Y, which has also 50 neutrons, would be worth a very specific effort, if feasible at all.

[35] For A ≲ 86 (i.e. from $_{36}$Kr downwards) an additional frequent weak neutron irradiation is required to account for the s-species abundances, which are higher than predicted by the main irradiation law which make up all s-species up to ^{204}Pb (Ward and Newman 1978 ; Käppeler et al. 1982). Elements largely produced by this extra irradiation, i.e. $_{31}$Ga, $_{32}$Ge, $_{34}$Se, $_{36}$Kr, denoted by s' in fig. 32, are clearly not enhanced in CR's. One could imagine that the enhancement starts right beyond this zone, when the main irradiation law sets in. But the limit would then lie between $_{36}$Kr and $_{38}$Sr, not between $_{38}$Sr and $_{40}$Zr as it does.

The data as they stand tell us that r-nuclides in this range are enhanced by comparable factors (fig. 32, bottom). But the two predominantly r elements we have, $_{52}$Te and $_{54}$Xe are not among the nuclides whose excesses are best established (fig. 19). The HEAO-C3 data for $_{52}$Te have changed a lot between the earlier and the new analysis, which however agrees with the Ariel VI data (fig. 10). $_{54}$Xe is poorly resolved between more abundant elements in both HEAO-C3 and Ariel VI experiments (fig. 9) [not to speak of the question of the $_{54}$Xe LG abundance]. For both elements, secondary formation by spallation is not negligible, so that a limited downward revision of the observed abundance can result in a large revision of the source abundance. Finally, both excesses are sensitive to the exact choice of f(FIP), which is of course also subject to an uncertainty, especially in the relevant intermediate- and high-FIP region (fig. 19).

For these reasons, the r-process excess in the Z = 52-54 peak, while suggested by the data, should still be taken with caution.

III-5.3. UH element excesses - Summary and overview

There is no enhancement of, either s, or r nuclides for $Z \leqslant 38$ (fig. 32, bottom).

There is quite convincing evidence for s-process enhancements beyond Z = 38, from (fig. 32, bottom) : (i) the jump between the almost pure s elements $_{38}$Sr, not enhanced, and $_{40}$Zr, probably enhanced, right at the limit N = 50 (magic) ; (ii) the well established excesses of largely s $_{42}$Mo and $_{58}$Ce (which have, however, also very significant r components in the "solar mix") ; (iii) the probable excess of almost pure s $_{56}$Ba. This implies that some specific material having undergone strong s neutron irradiations (average number of neutrons captured/Fe nucleus $n_c \geqslant 54$, Clayton 1968) is probably present in CR's.

There is evidence for comparable excesses of r-nuclides in the Z = 52-54 r peak (fig. 32, bottom), but it is weaker : it rests on two elements, $_{52}$Te and $_{54}$Xe whose excesses are probable, but not very strongly established.

It must be stressed that the real strength of the evidence for a s-process excess rests on the sharp jump right at N = 50 (fig. 33), i.e. on the reality of the $_{40}$Zr excess, which becomes our cornerstone. Its LG abundance is very reliable. But as can be seen in fig. 10, its excess is observed only in the new analysis of the HEAO-C3 data. It needs confirmation.

If this $_{40}$Zr excess happened not to be confirmed, the entire picture would be much more ambiguous : all elements $_{42}$Mo, $_{52}$Te, $_{54}$Xe, $_{58}$Ce have significant r contributions, and a predominant excess of r nuclides could not be excluded [36]. Only $_{56}$Ba, whose excess is not very strongly established, would definitely not fit in. Recall, too, that the low "Pb-group"/"Pt-group" ratio (§ III-3.), usually discussed in terms of a low Pb abundance, can also be interpreted in terms of an excess of the r elements forming the "Pt-group".

[36] Although it would then seem odd to have the almost pure r elements $_{52}$Te and $_{54}$Xe apparently less enhanced than the mixed elements $_{42}$Mo and $_{58}$Ce (fig. 32, bottom).

PART IV

SUMMARY AND RECOMMENDATIONS

IV-1. SUMMARY

A few key new observations have been brought at the La Jolla Conference : observation of sub-Fe nuclei up to 200 GeV/n (§ I-1. ; fig. 1) ; improved isotopic data, which are especially important for Si (§ I-2. ; figs. 2, 3) ; a whole bunch of results from continuing efforts on systematic spallation cross-section measurements (§ I-3. ; figs. 4 to 8) ; a breakthrough in the accuracy of the Ultra-Heavy (UH) nuclei abundance measurements up to $Z \approx 60$ (§ I-4. ; figs. 9 to 11) ; improved data on low energy deuterium and ^{3}He, and evidence (related to new spectral measurements) that the recently claimed high ^{3}He fluxes at high energy is probably an overestimate (§ I-5.) ; energy spectra of primary nuclei (§ I-6. ; not discussed) ; improved observations of e^- fluxes up to 2000 GeV and of e^+ around 10 GeV (§ I-7. ; figs. 12, 13).

From these and earlier data, the Galactic Cosmic Ray compositions at Sources (GCRS) can be inferred. This implies correcting for the effects of interstellar propagation, which I discuss now.

As regards CR propagation, we have two strong facts :

(i) At very high energies, observations of sub-Fe nuclei have shown beyond doubt that the escape length λ_e continues to decrease, at roughly the same rate, up to at least 200 GeV/n (§ I-1 ; fig. 1).

(ii) While in the GeV/n range, the observations of secondary nuclei yield a reasonably consistent picture of CR propagation, at low energies ($\lesssim$ 600 MeV/n) we have a flat contradiction between two presumably pure secondary to primary ratios : B/C and ^{15}N/O. They cannot be fitted simultaneously with classical propagation models (§ III-2.1. ; figs. 23 and 24). The contradiction is well beyond reasonable errors on both the CR data and the cross-sections, which happen to be particularly well measured for the relevant nuclei and at these energies (§ I-3.1.; fig.4 ; Table 2). The nuclei concerned are also too close in mass for refinements of the propagation model (truncation of the PLD) to have any chance to solve the problem.

One way out would be to have ^{15}N enhanced by a factor of $\sim$ 100 in CR sources, but it does not sound plausible to me (footnote # 19). I therefore think that some really new ingredient must be introduced in our understanding of low energy CR propagation.

One may note that a large fraction of C_2 (and a smaller one of O) is believed to originate, together with the ^{22}Ne excess, in a specific

environment, plausibly Wolf-Rayet stars (§ III-4.2.). One cannot exclude that these nuclei might have a propagation history different from that of the bulk of other CR's, and traverse on the average less matter. This hypothesis cannot be strictly ruled out, but it is completely speculative, ad hoc, and difficult to check (§ III-2.1.).

The only other way-out I can think of at this point is the hypothesis of distributed reacceleration, in which CR's still increase their energy by a factor of a few units while propagating, as they meet extended weak SN shock waves. This idea, which is much less far-fetched and more liable to check, was first advocated by Silberberg et al. (1983) to ease various problems in cosmic ray composition, especially below a few 100 MeV/n (§ III-2.1.). The relevant cross-sections for secondary formation could then be largely those below $\sim$ 100 MeV/n, which are often unmeasured, but known to be far from constant ; for nearby secondaries, they tend to sharply peak at low energy before decreasing towards threshold. I think the low energy B-^{15}N contradiction may be a good case for distributed reacceleration, and justifies a serious effort to investigate the point (see next § IV-2. for recommendations).

Anyway, as long as the low energy B-^{15}N contradiction is not understood, I think the determination of source abundances of ^{14}N and other largely secondary nuclei (Na, ^{25,26}Mg, Al, ^{29,30}Si, P, Ar, Ca) from low energy data ($E \lesssim 600$ MeV/n) cannot give reliable results. At higher energies, the cross-sections are much more constant, at least for comparatively light nuclei, so that distributed reacceleration, if present, has much less effect on the interpretation of the data.

As regards specifically the ^{14}N source abundance (§ III-2.2.), we are left with the high energy studies based on elemental data, which lead to $(N/O)_{source} \approx 6\%$, and with the high energy isotopic values, which, though scattered, are all consistent with that same value (fig. 25). The ratio $(N/O)_{source} \approx 6\%$ implies no deficiency of N relative to other high-FIP elements (at least those not affected by the Wolf-Rayet nucleosynthesis ; § III-4.) (figs. 14, 15, 17).

The B-^{15}N contradiction also precludes any conclusion on a truncation of the exponential pathlength distribution (PLD) at low energy (§ III-2.3.3. ; figs. 23, 24 and 26). At higher energies, the situation is open : studies of elements up to Fe do not request a truncation, but could allow a limited one (fig. 26) ; properly taking into account spallation on interstellar He could possibly increase the need for truncation (§ III-2.3.1.). Interpretation of the data on UH nuclei, which are most sensitive to truncation, is complicated due to an energy dependence of the cross-sections that extends up to very high energies [where distributed reacceleration, if present, would further change the picture] (§ III-2.3.2. ; fig. 27).

After these remarks on CR propagation, we can get back to the source composition. Let me first discuss the elemental GCRS composition up to Z = 30 as derived, for safety's sake, mainly from observations in the GeV/n range (§ II-1. ; figs. 14, 15). Up to Z = 30, there is no great novelty : the GCRS/LG (LG : "Local Galactic" abundance standard) ratios follow the well known correlation with First Ionization Potential

(FIP) ; it is clear that this correlation does not follow an exponential law (fig. 18), but has rather a two-plateau structure (fig. 15) ; it is very similar to that found in Solar Energetic Particles (SEP) and, more important, in coronal composition [except for a distinct excess of C and a probable one of O in GCRS] (fig. 17). This structure is not too consistent with an ionized fraction in a gas at any simple temperature or with a monotonic distribution of temperatures. It rather suggests a picking out, with different efficiencies, of both ions and neutrals out of a gas at $\sim$ 6000 K, such as the gas in the chromospheres underlying the coronae of the Sun and of most main sequence F to M stars (§ II-1.3. and 1.4.).

It should be stressed that H and He, which have a unique, odd temporal behaviour in SEP's, have a GCR source spectrum that is distinctly flatter than the common source spectrum of heavier species (between 3 and 60 GeV/n) (§ II-1.2.3. and III-1.1. ; e.g. fig. 15). H and He are both deficient relative to heavier nuclei, but the He/H ratio itself is remarkably normal and energy-independent. The attempts to explain the H, He deficiency by a rigidity-dependent injection of GCR's directly out of the hot ISM gas face very serious difficulties : they do not account for the normal He/H ratio, nor for the discontinuities of the heavy element GCRS/LG ratios versus Z (§ III-1.2. ; figs. 21, 22).

Back to the C and O excesses in GCRS as compared to SEP, they are probably related to the ^{22}Ne and associated isotopic anomalies. Where do we stand as regards our knowledge of the ^{22}Ne, $^{25,26}Mg$, $^{29,30}Si$ excesses at GCR sources (§ III-4.1.) ?

The ^{22}Ne excess is, of course, confirmed. As regards the heavy Mg and Si isotopes, observed mainly at low energy, new data do not find any more evidence at all for a $^{29,30}Si$ excess (§ I-2. and III-4.1. ; figs. 2 and 29). In addition, new cross-section measurements (§ I-3.1. ; fig. 5) suggest a larger than expected secondary contribution to the observed $^{25,26}Mg$ and $^{29,30}Si$. This, together with the unknown effects of a possible distributed reacceleration, leads me to very prudent about the magnitude of the $^{25,26}Mg$ excess itself, which has, however, still a good chance to be real (§ III-4.1. ; fig. 29).

A lack of $^{29,30}Si$ excess, if confirmed, could fit well into the helium-burning (Wolf-Rayet) scenario for the excess ^{12}C, ^{16}O, ^{22}Ne, $^{25,26}Mg$, in which heavy Si isotopes are not produced.

But atomic selection effects interfere with this interpretation of ^{12}C, ^{16}O, ^{22}Ne, $^{25,26}Mg$ and correlated weak s-process excesses in terms of a small fraction of CR's originating in He-burning material, plausibly at the surface of WC-WO Wolf-Rayet stars (§ III-4.2.). A question should indeed be posed : did the processed component go through the same FIP-filtering as the main CR component ? As regards the main component, we now have good reasons to believe that the cause for its bias with FIP lies in the composition of the cool star coronal medium they have been extracted from, rather than in the injection or acceleration process (§ II-1.3. , III-4.3.). There is no reason whatsoever for the source material of the ^{22}Ne rich component to have been affected by the same FIP-filtering, especially if it originates in hot WC-WO stars. So,

the processed component, in all likelihood not FIP-biased, is diluted in a main CR component in which low-FIP elements are comparatively $\sim$ 6 times as abundant as high-FIP elements. Therefore the processed low-FIP $^{25,26}Mg$ and weak s-process species are $\sim$ 6 times as diluted as the high-FIP ^{12}C, ^{16}O and ^{22}Ne. Their predicted excesses at GCRS thus become minute, essentially impossible to evidence (§ III-4.3. and 4.4. ; fig.30, bottom). The large uncertainty on the presently determined $^{25,26}Mg$ source abundance does not conflict with these views (fig. 30, bottom).

Conversely, if the GCRS $^{25,26}Mg$ and/or $^{29,30}Si$ excesses eventually turned out to be significant (say, a factor of $\sim$ 1.5), it would probably imply roughly equal excesses of ^{22}Ne, $^{25,26}Mg$ and/or $^{29,30}Si$ in the source material of the processed component (fig. 31, bottom), which could no longer be explained in terms of He-burning in WC-WO stars. Other hypothesis, such as supermetallicity, should then be considered.

Now, let us turn to "Ultra-Heavy" (UH) elements, beyond Z = 30. There, we have real new stuff ! The most important point brought up at this conference is serious evidence for excesses of all elements for which we have source abundance determinations between Z = 40 and 58, relative to the FIP pattern f(FIP) describing the composition for elements with $Z \leqslant 30$ [excesses of $_{40}Zr$, $_{42}Mo$ and of the r-s-peaks elements $_{52}Te$, $_{54}Xe$, $_{56}Ba$, $_{58}Ce$; the excesses of $_{42}Mo$ and $_{58}Ce$ are certain, the others are probable] (§ II-2. ; figs. 10, 19, 20). Once again, I tend to interpret these excesses in terms of a specific processed component, highly diluted in the main, solar coronal-like, CR component. In deriving the excesses in the processed component material itself from the "observed" GCRS excesses, we again have to take into account the fact that, in all likelihood, the processed component itself is not FIP-biased (§ III-5.1. ; fig. 32, bottom).

A key point here is that elements in the range Z = 30 to 38, and in particular definitely $_{38}Sr$, are not enhanced : they just nicely follow the correlation f(FIP) (figs. 19, 20, 32 bottom). So, the enhancements seem to start abruptly at Z = 40. Actually, the enhancement of $_{42}Mo$ is established beyond any doubt, while that of $_{40}Zr$ is probable, but not yet certain (fig. 10). This $_{40}Zr$ excess (or lack of excess) is the cornerstone of the interpretation of all these UH excesses, and is worth any effort to be confirmed (or not).

If $_{40}Zr$ is indeed in excess, the sharp onset of the excesses between $_{38}Sr$ and $_{40}Zr$, right after the neutron magic number N = 50 (fig. 33) is almost a signature of a s-process contribution, implying that a specific component having undergone strong neutron irradiation (average number of neutrons captured per seed Fe nucleus $n_c \geqslant 54$, see Clayton 1968) is present in the cosmic radiation. It is then very tempting to interpret the excesses of predominantly s $_{42}Mo$, $_{56}Ba$ and $_{58}Ce$ in terms of this same intense neutron irradiation. There seems to be also an r-process excess, as judged from $_{52}Te$ and $_{54}Xe$. But the excesses for these two elements are not very strongly established from the data (fig. 19 ; § III-5.2.2.).

If, by contrast, the $_{40}Zr$ excess is not confirmed, the interpretation of the various excesses in terms of s and/or r-process excesses is

much more confused, since the elements for which we have best evidence for an excess, $_{42}$Mo and $_{58}$Ce, (figs. 19, 20, 32 bottom) have both significant s and r components in "solar mix" material. If r-process excesses are present, the may be related to a possible excess of Pt-group elements (see below).

Finally, we have still the old puzzles of the low Ge and low Pb/Pt ratio, unusually interpreted in terms of an underabundance of Pb. Contrary to excesses, deficiencies cannot be explained by admixture of a specific extra-component ! Thus explaining a low Pb in terms of a special nucleosynthesis requires the bulk of the cosmic radiation to originate in a spot of active nucleosynthesis, while we have so much evidence that most CR's are made of nucleosynthetically "solar mix" material, just fractionated like solar coronal gas. An excess of r-process Pt would be more plausible (§ III-3.3. and 5.3.). On the other hand, a coupled deficiency of Ge and Pb could indicate a fractionation of "solar mix" material according, not to FIP, but to volatility ; this would indicate that CR's are interstellar grain destruction products, another hypothesis not easy to live with [similarity with solar corona and SEP's ; noble gas abundances] (§ III-3.4.). Finally, the standard abundances to which we refer the CR abundances of Ge and Pb may be inadequate, in which case they could be not deficient at all ! For these two elements, the photospheric value indeed seems to differ significantly from the usually adopted C1 meteoritic value (§ III-3.5. ; figs. 19, 20, 28). This would be the easiest explanation. But the question is open.

IV-2. RECOMMENDATIONS FOR FUTURE WORK

(i) Distributed reacceleration

The hypothesis of distributed reacceleration should be throroughly investigated (§ III-2.1.). Only its modelling (in the presence of solar modulation) will allow to tell whether it can, not only solve the low energy B-^{15}N contradiction, but consistently account for the fluxes of D, ^{3}He, ^{6,7}Li, ^{7,9}Be, ^{10,11}B, ^{15}N, ^{17}O, F and sub-Fe nuclei observed at low energy. Also, will it yield low energy source abundances for ^{14}N,Na,Al,P,Ar, Ca consistent with the higher energy determinations ? Will it have an effect on the ^{22}Ne, ^{25,26}Mg and ^{29,30}Si source abundances, which are mainly determined from low energy data ? One must also investigate the problem posed by the differences in energy loss rates between nuclei, if they are kept a long time at low energy, say below 100 MeV/n. Last but not least, such a study requires a program of very low energy cross-section measurements (all the way down to thresholds) which I shall evoke below.

(ii) Fluorine

I insist on the possibility to get independent information on propagation from F, a purely secondary element, close to B and ^{15}N, but not made from C and O [in recent CR experiments, F is well resolved from O]. It might help to understand what is going on in the Li, Be, B, ^{15}N region (§ III-2.1.). But, first, we need cross-sections.

(iii) Energy range for source abundance determinations

In order to get safest source abundances of comparatively light nuclei, CR observations and propagation studies should concentrate in the range $\sim$ 1 to 2 GeV/n. At higher energies, we cannot get any more cross-section measurements at the Bevalac, and have to use extrapolated cross-sections (which, however, usually remain quite constant with energy for lighter nuclei). At lower energies, the combined effect of the strong cross-section variations below $\sim$ 100 MeV/n and of possible distributed reacceleration (plus modulation !) casts doubt on any results one may obtain [for heavier nuclei, such as Fe or UH nuclei, the cross-sections become energy-independent only at significantly higher energies ; e.g. Webber 1984 ; Kaufman and Steinberg 1980].

(iv) Zr abundance and s-process

In the UH range, make all efforts to confirm (or not) the high abundance of $_{40}Zr$, which is essential in the interpretation of the UH element excesses in terms of a CR component having undergone a specific s-process (fig. 10 ; § III-5.2.1. and 5.3.). If feasible at all, an estimate of the abundance of the neighbouring odd-Z single isotope element $^{89}_{39}Y$ (N=50) would also be valuable.

(v) Cross-sections

Although much effort has been invested in recent years on cross-section measurements and semi-empirical estimates (§ I-3.), insufficient knowledge of spallation cross-sections is still the weak point of many a CR problem :

- A major specific effort must be undertaken to measure all relevant cross-sections at lowest energies, down to thresholds (below the $\sim$ 300 MeV/n lower bound of the Bevalac range). Such a program is essential to investigate the reality of distributed reacceleration and to assess its consequences (§ III-2.1.).

- Measurements of cross-sections on a He target are necessary to progress on the question of the truncation of the PLD (§ III-2.3.1.).

- Measurement of cross-sections for the formation of F can give an essential new tool to untangle the low energy propagation puzzle (isotopic cross-sections ; undecayed elemental cross-sections are always much less useful) (§ III-2.1.).

- Be conscious that, once the cross-sections for the major contributors to the formation of a daughter product have been accurately measured, the much larger errors on the unmeasured cross-sections for the numerous minor contributors can become dominant (see, e.g., Table 2 and figs. 23 to 26). Therefore, measurements on a large number of parent nuclei are useful and, for lack of it, a significant improvement of the semi-empirical estimates is essential. This remark applies in particular to crucial nuclei whose formation cross-sections from dominant parents have been intensively measured recently :

  - B, $^{14,15}N$: (Table 2). Note the importance of $^{14,15}N$ parents in the formation of B and even ^{14}N !

- Se-Cr : (Table 2). Note the importance of parents other than ^{56}Fe (mainly Mn, $^{54,55}Fe$, Ni).
- $^{25,26}Mg$, $^{29,30}Si$: to the secondary production of $^{25,26}Mg$, while Si contributes $\sim$ 63 %, Al makes $\sim$19 %, S $\sim$ 9 % and heavier nuclei $\sim$ 9 % ; to that of $^{29,30}Si$, while S contributes $\sim$ 52 %, Ar makes $\sim$ 12 %, Ca $\sim$13 %, Sc-Mn $\sim$15 % and Fe $\sim$8 %.

- As regards UH nuclei, where cross-sections remain energy dependent up to very high energies, try to semi-empirically combine the recent Bevalac data on $\sigma = f(Z_{parent})$ at $\sim$ 1 GeV/n (§ I-3.1. ; fig. 7) with the comprehensive data on $\sigma = f(E)$ for a Au target over the wide range of energies from 0.2 to 6 GeV/n by Kaufman and Steinberg (1980). [If possible, of course, complement the Bevalac measurements at $\sim$ 1 GeV/n by other ones at other (including lower) energies within the $\sim$ 0.3 to 2 GeV/n Bevalac range]. To master the energy-dependence of the cross-sections is obviously essential to interpret the UH data in terms of propagation (truncation problem ; § III-2.3.2. ; fig.27).
- Try to diversify the groups performing cross-section measurements, to permit inter-laboratory check of the results. In particular check thick target against thin target data.
- With the large body of recent and forthcoming measurements of spallation cross-sections for ^{12}C, ^{16}O, ^{20}Ne, ^{24}Mg, ^{28}Si, ^{32}S, ^{40}Ar, ^{40}Ca, ^{56}Fe, ^{58}Ni and of the low energy dependence of the cross-section for ^{56}Fe, time should be ripe for real improvement of the parametrization of the (still essential) semi-empirical formulae. These should be based, as much as possible, on a better physical understanding of what is going on (see detailed discussion in § I-3.2.).

Acknowledgements

I am first of all highly indebted to Aimé Soutoul for a number of essential discussions we have had before and after the Conference, and for introducing me to the delights of the Saclay HEAO-C2 team propagation code. Many of the ideas put forward in this report, especially on CR propagation, originated in these exchanges with him. I also profited from discussions with Philippe Ferrando and Philippe Goret. From Jean-Jacques Engelmann and Michel Cassé, I got wise criticism of the manuscript. I also wish to thank a large number of colleagues for the patience with which they endured my endless inquisitorial questioning under the ever present beautiful sun (or moon) of La Jolla. I am highly indebted to the HEAO-C3 team, and particularly to Ed Stone, for their permission to print the results of the preliminary, but capital new analysis of their data, which have been given only orally at the Conference and are thus not present in the printed "Conference Papers". I apologize for not having discussed the important field of the shape of the CR spectra (see footnote # 5), nor other interesting papers dealing with the properties of the interstellar medium in which CR's propagate. Finally, last but not least, I wish to thank Franck Jones and the Publications Committee for they patience in waiting for the arrival of this never-ending manuscript.

APPENDIX

FORMALISM FOR THE DILUTION OF THE ^{22}Ne-RICH OR OTHER PROCESSED COMPONENTS

With X_i being the mass fraction of the nuclear species i, let me define various excesses E_{ik} of species i relative to species k : [37]

(i) As regards elemental composition, I define the GCRS "main component", biased according to FIP, as following strictly the correlation f(FIP) defined in fig. 15. As regards isotopic ratios, they are assumed to have standard LG values. Thus, the excesses relative to LG for the main component are :

$$E_{ik,main} \equiv \frac{X_{i,main}}{X_{i,LG}} \Big/ \frac{X_{k,main}}{X_{k,LG}} = \frac{f_i(FIP)}{f_k(FIP)} \equiv f_{ik}(FIP)$$

where $f_i(FIP)$ and $f_k(FIP)$ are the values of f(FIP) for species i and k, and $f_{ik}(FIP)$ is its value for species i normalized to its value for species k. An uncertainty should be associated with f(FIP) ; for simplicity, I shall ignore it here.

(ii) In the "processed component", we have :

$$E_{ik,proc} \equiv \frac{X_{i,proc}}{X_{i,LG}} \Big/ \frac{X_{k,proc}}{X_{k,LG}}$$

$E_{ik,proc}$ describes abundance anomalies of any origin in the processed component : local nucleosynthesis and, if any, atomic selection effects on this component. To separate the two possible effects, atomic and nuclear, let me define :

$$E_{ik,proc} \equiv f_{ik,proc}(atom) \cdot E_{ik,proc,nucl} \cdot$$

I choose as a reference species k a species whose mass fraction is not affected by the nuclear processing (e.g. ^{20}Ne, ^{28}Si). Since in addition, $f_{ik,proc}(atom)$ is normalized to species k, we have $X_{k,proc}/X_{k,LG} = 1$.

(iii) In the GCRS composition, obtained after mixing of the two components (for brevity, I use the symbol CR), we have :

$$E_{ik,CR} \equiv \frac{X_{i,CR}}{X_{i,LG}} \Big/ \frac{X_{k,CR}}{X_{k,LG}}$$

$E_{ik,CR}$ is essentially a "measured" quantity, which will later have to be confronted with the model-related excesses $E_{ik,main}$ and $E_{ik,proc}$.

---

[37] Working directly on the excess of mass fraction of a single species (without reference to a comparison species, e.g. $E_{i,CR} \equiv X_{i,CR}/X_{i,LG}$ is very inconvenient because $X_{i,CR}$ depends on the behaviour of H and He in GCR's, which is irrelevant here (cosmic rays are not a closed system with fixed mass).

It will often be more significant to consider the GCRS excess relative to the FIP pattern f(FIP) describing the main component (i.e. the quantity plotted in fig. 20) ; let :

$$E^{*}_{ik,CR} \equiv \frac{E_{ik,CR}}{E_{ik,main}} = \frac{E_{ik,CR}}{f(FIP)} = \frac{X_{i,CR}}{X_{i,main}} \Big/ \frac{X_{k,CR}}{X_{k,main}}$$

Now let p_k be the fraction of the species k (unaffected by the nuclear processing) in GCRS that originates from the processed component. So $1/p_k$ is the dilution factor for species k. I shall work in the approximation $p_k << 1$, implying that the processed component is a minor one, highly diluted in the main component (for a more general treatment - though not entirely adequate, as we shall see below - see Maeder 1983).

When $p_k << 1$, it is readily shown that :

$$E_{ik,CR} = E_{ik,main} + p_k \cdot E_{ik,proc} \qquad (A1)^{38}$$

$$E_{ik,CR} = f_{ik}(FIP) + p_k \cdot f_{ik,proc}(atom) \cdot E_{ik,proc,nucl}$$

Or, dividing by $f_{ik}(FIP)$:

$$E^{*}_{ik,CR} = 1 + p_k \cdot \frac{f_{ik,proc}(atom)}{f_{ik}(FIP)} \cdot E_{ik,proc,nucl} \qquad (A2)$$

This is the general expression (for $p << 1$) we need. It relates the observed excess at GCRS $E^{*}_{ik,CR}$ (corrected for the bias with FIP), the excess in the processed component material $E_{ik,proc,nucl}$, and the dilution factor $1/p_k$; and it includes possible atomic selection effects in the processed component. It can be used either way to derive one of three quantities from the other two.

The traditional treatment (Meyer 1981c, 1985b ; Cassé and Paul 1981, 1982 ; Maeder 1983 ; Blake and Dearborn 1984 ; Arnould 1984 ; Prantzos 1984a,b ; Prantzos et al. 1983 ; 3, 167) assumes $f_{ik,proc}(atom) = f_{ik}(FIP)$ and gets hence :

$$E^{*}_{ik,CR} = 1 + p_k \cdot E_{ik,proc,nucl} \qquad (A3)^{39}$$

As discussed in the text (§ III-4.3. ; Meyer 1985b), I think this assumption is not a plausible one.

---

38 In eq.(A1) the reference to LG composition has merely introduced a constant factor $X_{i,LG}/X_{k,LG}$ on both sides of the equation, which is superfluous. So, the relationship between $E_{ik,CR}$, $E_{ik,main}$, $E_{ik,proc}$ and p_k is unaffected by changes of, and hence uncertainties on the LG standard. Uncertainties on the LG composition of a large number of elements (not specifically species i and k) intervene when $E_{ik,main} = f_{ik}(FIP)$ is being defined ; I ignore this uncertainty here. On the other hand, $E_{ik,CR}$ is an observational quantity, and, when this excess has to be determined, uncertainties on the LG abundances of species i and k fully play their role.

39 It is also equivalent to forget about any atomic selection effect whatsoever in both the main and the processed component, as Maeder (1983) did.

In our ignorance of possible other atomic selection effects in the processed component, we can also simply not consider any, and set $f_{ik,proc}(atom) = 1$. Then we get the more plausible, though possibly oversimplified expression :

$$E^*_{ik,CR} = 1 + \frac{p_k}{f_{ik}(FIP)} E_{ik,proc,nucl} \qquad (A4)$$

which expresses simply the effect of the higher degree of dilution of the "processed" species belonging to elements more abundant in the main component (low-FIP elements).

Of course, expressions (A3) and (A4) do not differ when dealing with elements in the same FIP-plateau as the reference element k, since then $f_{ik}(FIP) = 1$. With $k = {}^{20}Ne$, the two formulae yield identical results for ^{22}Ne, C, O (see footnote 29).

As regards the ^{22}Ne excess (§ III-4.), $p_k = p_{^{20}Ne}$ is determined from (A3) or (A4), from the "observed" $E^*_{ik,CR}$ and the reliable theoretical estimates of $E_{ik,proc,nucl}$ for $^{22}Ne = i$ (Meyer 1981c, 1985b ; Cassé and Paul 1981, 1982 ; Maeder 1983 ; Blake and Dearborn 1984 ; Arnould 1984 ; Prantzos 1984a,b ; Prantzos et al. 1983 ; 3, 167).

To build up fig. 30, eqs. (A3) and (A4) have been used, while these same formulae, explicited for $E_{ik,proc,nucl}$ have been used for fig. 31. In both figures, the top plot results from eq.(A3) and the bottom one from (A4).[40]

As regards the excesses of UH nuclei (§ III-5.), we do not have any theoretical estimate of $E_{ik,proc,nucl}$, so that p_k cannot be derived from eq. (A3) or (A4). $E_{ik,proc,nucl}$ can only be related to the "observed" $E^*_{ik,CR}$ to within an unknown factor p_k, corresponding to the unknown degree of dilution (of whatever species k). Fig. 32, otherwise similar to fig. 31, has been built up in this way, and gives only relative enhancements $E_{ik,proc,nucl}$. [Since there is no calculation to compare the data with, there is no point in drawing an analog to fig. 30].

[40] On the r.h.s. of eq. (A2) through (A4), should strictly appear the term $[E_{ik,proc,nucl} - 1]$. Since it is assumed that $E_{ik,proc,nucl} >> 1$, the 1 has been neglected. In figs. 31 and 32, where the equations are explicited for $E_{ik,proc,nucl}$, it must be clear that, in case of a small excess, $E_{ik,proc,nucl} \to 1$, and not $\to 0$.

References

Anders, E. 1971, GCA 35, 516.
Anders, E., and Ebihara, M. 1982, GCA 46, 2363.
Arnaud, M., and Cassé, M. 1985, Astr. Ap. 144, 64.
Arnaud, M., and Rothenflug, R. 1985, Astr. Ap. Suppl. 60, 425.
Arnould, M. 1984, Adv. Space Res. 4, N°2-3, 45.
Arnould, M., and Norgaard, H. 1978, Astr. Ap. 64, 195.
Arnould, M., and Norgaard, H. 1981, Comments Ap. 9, 145.
Arnould, M., Norgaard, H., Thielemann, F.K., and Hillebrandt, W. 1980, Ap. J. 237, 931.
Axford, W.I. 1981, 17th ICRC, Paris, 12, 155.
Axford, W.I., Leer, E., and Skadron, G., 1977, 15th ICRC, Plovdiv, 11, 132.
Badhwar, G.D., et al. 1979, 16th ICRC, Kyoto, 1, 345.
Beer, H., and Macklin, R.L. 1985, Phys. Rev. C 32, 738.
Bell, A.R. 1978a, MNRAS 182, 147.
Bell, A.R. 1978b, MNRAS 182, 443.
Bibring, J.P., and Cesarsky, C.J. 1981, 17th ICRC, Paris, 2, 289.
Binns, W.R., et al. 1983, 18th ICRC, Bangalore, 9, 106.
Binns, W.R., et al. 1984, Adv. Space Res. 4, N°2-3, 25.
Binns, W.R., et al. 1985, Ap. J. 297, 111.
Blake, J.B., and Dearborn, D.S.P. 1984, Adv. Space Res. 4, N°2-3, 89.
Blanford, R.D., and Ostriker, J.P. 1978, Ap. J. Letters 221, L29.
Brewster, N.R., et al. 1983, 18th ICRC, Bangalore, 9,259.
Brewster, N.R., Freier, P.S., and Waddington, C.J. 1983, Ap. J. 264, 324.
Byrnak, B., et al. 1983a, 18th ICRC, Bangalore, 9, 135.
Byrnak, B., et al. 1983b, 18th ICRC, Bangalore, 2, 29.
Cassé, M. 1981, 17th ICRC, Paris, 13, 111.
Cassé, M. 1983, in "Composition and Origin of Cosmic Rays", M.M. Shapiro ed.,(Reidel), p.193.
Cassé, M., and Paul, J.A. 1981, 17th ICRC, Paris, 2, 293.
Cassé, M., and Paul, J.A. 1982, Ap. J. 258, 860.
Cesarsky, C.J., and Bibring, J.P. 1980, IAU Symp. N°94, Origin of Cosmic Rays, G. Setti, G. Spada, A.W. Wolfendale ed., p. 361.
Cesarsky, C.J., and Montmerle, T. 1981,17th ICRC, Paris, 9, 207.
Cesarsky, C.J., Rothenflug, R., and Cassé, M. 1981, 17th ICRC, Paris, 2, 269.
Cesarsky, C.J., Rothenflug, R., and Cassé, M. 1985, in preparation.
Clayton, D.D. 1968, Principles of stellar evolution and nucleosynthesis, Mc Graw Hill.
Clayton, D.D., and Rassbach, M.E. 1967, Ap. J. 148, 69.
Cook, W.R., Stone, E.C., and Vogt, R.E. 1980, Ap. J. Letters 238, L 97.
Cook, W.R., Stone, E.C., and Vogt, R.E. 1984, Ap. J. 279, 827.
Cook, W.R., et al. 1979, 16th ICRC, Kyoto, 12, 265.
Cowsik, R., and Gaisser, T.K. 1981, 17th ICRC, Paris, 2, 218.
Cowsik, R., and Wilson, L.W. 1973, 13th ICRC, Denver, 1, 500.
Dearborn, D.S.P., and Blake, J.B. 1985, Ap. J. Letters 288, L 21.
Dwyer, R., and Meyer, P. 1985, Ap. J. 294, 441.
Ebihara, M., Wolf, F.R., and Anders, E., 1982, GCA 46, 1849.
Eichler, D. 1979, Ap. J. 229, 419.
Eichler, D. 1980, Ap. J. 237, 809.
Eichler, D., and Hainbach, K. 1981, Phys. Rev. Letters 47, 1560.
Ellison, D.C. 1981, Ph. D Thesis.
Ellison, D.C. 1985, J. Geophys. Res. 90, 29.
Ellison, D.C., Jones, F.C., and Eichler, D. 1981, J. Geophys. 50, 110.
Engelmann, J.J. 1984, 9th European Cosmic Ray Symp., Kosice, K. Kudela and S. Pinter ed., (Slovak Acad. Sci.), p. 141.
Engelmann, J.J. et al. 1983, 18th ICRC, Bangalore, 2, 17.
Engelmann, J.J. et al. 1985, Astr. Ap. 148, 12.
Epstein, R.I. 1980a, IAU Symp. N°94, Origin of Cosmic Rays, G. Setti, G. Spada, A.W. Wolfendale ed., p.109.
Epstein, R.I. 1980b, MNRAS 193, 723.
Fixsen, D.J. 1985, U. of Minn. C.R. Rep. CR-195.
Fixsen, D.J. et al. 1983, 18th ICRC, Bangalore, 9, 119.
Fontes, P. 1977, Phys. Rev. C 15, 2159.
Garcia-Munoz, M., Guzik, T.G., Simpson, J.A., and Wefel, J.P. 1984, Ap. J. Letters 280, L13.
Garcia-Munoz, M., Margolis, S.A., Simpson, J.A., and Wefel, J.P. 1979, 16th ICRC, Kyoto, 1, 310.
Garcia-Munoz, M., and Simpson, J.A. 1979, 16th ICRC, Kyoto, 1, 270.
Geiss, J. 1985, ESA Workshop on Future Missions in Solar, Heliosphere and Space Plasma Physics, Garmisch-Partenkirchen, May 1985, ESA SP-235, p. 37.
Geiss, J., and Bochsler, P. 1984, in Isotopic Ratios in the Solar System, Paris (CNES), in press.
Goret, P. et al. 1981, 17th ICRC, Paris, 9, 122.
Goret, P. et al. 1983, 18th ICRC, Bangalore, 9, 139.
Grevesse, N. 1984a, Phys. Scripta, T8, 49.
Grevesse, N. 1984b, in Frontiers of Astronomy and Astrophysics, ed. R. Pallavicini (Florence : Italian Astron. Soc.), p. 71.
Guzik, T.G. 1981, Ap. J. 244, 695.
Hillebrandt, W., and Thielemann, F.K. 1982, Ap. J. 255, 617.
Hsieh, K.C., Mason, G.M., and Simpson, J.A. 1971, Ap. J. 166, 221.
Israel, M.H. et al. 1983, 18th ICRC, Bangalore, 9, 305.
Jordan, S.P. 1985, Ap. J. 291, 207.
Jordan, S.P., and Meyer, P. 1984, Phys. Rev. Letters 53, 505.
Juliusson, E. 1974, Ap. J. 191, 331.
Juliusson, E. et al. 1983, 18th ICRC, Bangalore, 2, 21.
Käppeler, F. et al. 1982, Ap. J. 257, 821.
Kaufman, S.B., and Steinberg, E.P. 1980, Phys. Rev. C 22, 167.
Krimsky, G.F. 1977, Dokl. Akad. Nauk. SSSR 234, 1306.
Lagage, P.O., and Cesarsky, C.J. 1985, Astr. Ap. 147,127.
Lau, K.H., Mewaldt, R.A., and Wiedenbeck, M.E. 1983, 18th ICRC, Bangalore, 9, 255.
Letaw, J.P., Silberberg, R., and Tsao, C.H. 1984, Ap. J. 279, 144.
Lindstrom, P.J. et al. 1975, Lawrence Berkeley Laboratory Report LBL-3650.
Lockwood, J.A., and Webber, W.R. 1984, J. Geophys. Res. 89, 17.
Lund, N. 1984, Adv. Space Res. 4, N°2-3, 5.
Maeder, A. 1983, Astr. Ap. 120, 130.
Mason, G.M., Gloeckler, G., and Hovestadt, D. 1983, Ap. J. 267, 844.
Mauger, B.G., and Ormes, J.F. 1983, 18th ICRC, Bangalore, 2, 65.
McGuire, R.E., Von Rosenvinge, T.T., and McDonald, F.B. 1979, 16th ICRC, Kyoto, 5, 61.
McGuire, R.E., Von Rosenvinge, T.T., and McDonald, F.B. 1986, Ap. J., in press.
Mewaldt, R.A. 1980, in Proc. Conf. Ancient Sun (Boulder 1979), R.O. Pepin, J.A. Eddy and R.B. Merrill eds., p. 81.
Mewaldt, R.A. 1981, 17th ICRC, Paris, 13, 49.
Mewaldt, R.A., Spalding, J.D., Stone, E.C., and Vogt, R.E., 1981, Ap. J. Letters 251, L 27.
Meyer, J.P. 1974, Ph. D. Thesis, Universitè de Paris, Orsay.
Meyer, J.P. 1975, 14th ICRC, Munich, 11, 3698.
Meyer, J.P. 1979a, in "Les Elements et leurs Isotopes dans l'Univers", 22nd Liège Internat. Astrophys. Symp. (U. of Liège Press), p. 153, 465, 477, 489.
Meyer, J.P. 1979b, 16th ICRC, Kyoto, 2, 115.
Meyer, J.P. 1981a, 17th ICRC, Paris, 3, 145.
Meyer, J.P. 1981b, 17th ICRC, Paris, 3, 149.
Meyer, J.P. 1981c, 17th ICRC, Paris, 2, 265.
Meyer, J.P. 1981d, 17th ICRC, Paris, 2, 281.
Meyer, J.P. 1985a, Ap. J. Suppl. 57, 151.
Meyer, J.P. 1985b, Ap. J. Suppl. 57, 173.
Montmerle, T. 1984, Adv. Space Res. 4, N°2-3, 357.
Müller, D., and Tang, J. 1983, 18th ICRC, Bangalore, 2,60.
Nishimura, J. et al. 1981, 17th ICRC, Paris, 2, 94.
Norgaard, H. 1980, Ap. J. 236, 895.
Olson, D.L. et al. 1983, Phys. Rev. C 28, 1602.

Orth, C.J. et al. 1976, J. Inorg. Nucl. Chem. 38, 13.
Perron, C. 1976, Phys. Rev. C 14, 1108.
Prantzos, N. 1984a, Adv. Space Res. 4, N°2-3, 109.
Prantzos, N. 1984b, in High Energy Astrophysics, 19th Moriond Ap. Meeting, J. Audouze and J. Tran Thanh Van ed. (Ed. Frontières), p. 341.
Prantzos, N., Arnould, M., and Cassé, M. 1983, 18th ICRC, Bangalore, 9, 155.
Prantzos, N., and Cassé, M. 1985, Ap. J., in press.
Preszler, A.M. et al. 1975, 14th ICCR, Munich, 12, 4096.
Raisbeck, R.G., and Yiou, F. 1976, in Spallation Nuclear Reactions and Their Applications, B.S.P. Shen and M. Merker ed. (Reidel), p. 83.
Read, S.M., and Viola, V.E. 1984, Atom. Nucl. Data Tables 31, 359.
Silberberg, R., and Tsao, C.H. 1973a, Ap.J.Suppl. 25,315.
Silberberg, R., and Tsao, C.H. 1973b, Ap.J.Suppl. 25,335.
Silberberg, R., Tsao, C.H., and Letaw, J.R. 1985, Ap. J. Suppl. 58, 873.
Silberberg, R., Tsao, C.H., Letaw, J.R., and Shapiro, M.H. 1983, Phys. Rev. Letters 51, 1217.
Smith, L.H. et al. 1973, Ap. J. 180, 987.
Stone, E.C. et al. 1983, 18th ICRC, Bangalore, 9, 115.
Tan, L.C., and Ng, L.K. 1983, Ap. J. 269, 751.
Tang, J., and Müller, D. 1983, 18th ICRC, Bangalore, 9, 251.
Tang, K.K. 1984, Ap. J. 278, 881.
Tarlé, G., Ahlen, S.P., Cartwright, B.G., and Solarz, M. 1979, Ap. J. Letters, 232, L161.
Tsao, C.H., and Silberberg, R. 1979, 16th ICRC, Kyoto, 2, 202.
Van der Hucht, K.A., and Olnon, F.M. 1985, Astr. Ap. 149, L17.
Ward, R.A., and Newman 1978, Ap. J. 219, 195.
Webber, W.R. 1975, 14th ICRC, Munich, 5, 1597.
Webber, W.R. 1981, 17th ICRC, Paris, 2, 80.
Webber, W.R. 1982a, Ap. J. 252, 386.
Webber, W.R. 1982b, Ap. J. 255, 329.
Webber, W.R. 1983a, in "Composition and Origin of Cosmic Rays", M.M. Shapiro ed., (Reidel), p. 25.
Webber, W.R. 1983b, 18th ICRC, Bangalore, 9, 151.
Webber, W.R. 1984, Workshop on Cosmic Ray and High Energy Gamma-Ray Experiments for the Space Station Era, Baton Rouge (Louisiana State U.), p. 283.
Webber, W.R., and Brautigam, D.A. 1982, Ap. J. 260, 894.
Webber, W.R., Brautigam, D.A., Kish, J.C., and Schrier, D.A. 1983a, 18th ICRC, Bangalore, 2, 198.
Webber, W.R., Brautigam, D.A., Kish, J.C., and Schrier, D.A. 1983b, 18th ICRC, Bangalore, 2, 202.
Webber, W.R., Damle, S.V., and Kish, J.M. 1972, Ap. Space Sci. 15, 245.
Webber, W.R., and Lezniak, J.A. 1974, Ap. Space Sci. 30, 361.
Webber, W.R., and Yushak, S.M. 1983, Ap. J. 275, 391.
Westfall, G.D., et al. 1979, Phys. Rev. C 19, 1309.
Wiedenbeck, M.E. 1974, Adv. Space Res. 4, N° 2-3, 15.
Wiedenbeck, M.E., et al. 1979, 16th ICRC, Kyoto, 1, 412.
Woosley, S.E., and Weaver, T.A. 1981, Ap. J. 243, 651.
Young, J.S. et al. 1981, Ap. J. 246, 1014.

COSMIC RAY SOURCES, ACCELERATION, AND PROPAGATION

V.S.Ptuskin

Institute of Terrestrial Magnetism, Ionosphere and Radio Wave Propagation, USSR Academy of Sciences, 142092 Moscow

Review of selected papers on the theory of CR propagation and acceleration, presented in divisions CG, 2, 5, 6, 7, 8, and related problems.

I. CR propagation in the Galaxy

I.I. CR transfer in a turbulent medium.

The high isotropy and a comparatively large age of galactic CR are explained by the effective interaction of relativistic particles with random and regular electromagnetic fields in interstellar medium. The kinetic theory of CR propagation in the Galaxy is formulated similarly to the elaborate theory of CR propagation in heliosphere (see the review by Quenby, 1984). The substantial difference between these theories is explained by the necessity to take into account in some cases the collective effects due to a rather high density of relativistic particles. In particular, the kinetic CR stream instability and the hydrodynamic Parker instability is studied (see Cesarky, 1980).

The interaction of relativistic particles with an ensemble of given weak random magnetic fields is calculated by perturbation theory. The theory of CR transfer is considered to be basically completed for this case. (A new field of activities is suggested by Webb (8.3 - 8) in his paper on CR diffusion in relativistically moving plasma.) The main problem consists in poor information about the structure of the regular and the random galactic magnetic fields.

To calculate the diffusion coefficient of a particle with a gyroradius r_H, it is necessary to know the spectrum of a random field $\delta B^2(k)$ in the resonant region of wave vectors $k_{res} \sim 1/r_H$. The CR diffusion coefficient along a magnetic field B_0 is equal to

$$D_{\parallel} \approx \frac{v r_H}{3} \frac{B_0^2}{\delta B^2(\geq k_{res})}, \qquad (I.I)$$

Remember that the gyroradius is

$$r_H = \frac{pc}{ZeB} \approx 1.1 \cdot 10^{12} Z^{-1} (E/1\,GeV) \cdot (B/3 \cdot 10^{-6} G)\,cm \quad (v \simeq c). \quad (I.2)$$

The diffusion of CR with energies 10^9 - 10^{17} eV is therefore determined by random fields with a size of inhomogeneties from $3\ 10^{12}$ - $3\ 10^{20}$ cm (for $E > 3\ 10^{17} Z$ eV, the gyroradius of particles exceeds the main turbulence scale in interstellar medium, $L_t \sim 100$ pc, and the scattering becomes not very effective, $D_{\parallel} \backsim E^2$).

The existence of the random magnetic field spectrum necessary for CR diffusion has not been reliably established although it is not excluded by the available observations (Armstrong et al., 1981). At the same time, the simplest version of realization of a unique spectrum as an ensemble of linear mhd waves seems rather doubtful because of the presence of a strong wave damping.

In their papers Highdon (7.2 - 13) and Bykov and Toptygin (7.2 - 14) give a thorough theoretical analysis of turbulence formation processes in interstellar medium. The first-mentioned paper deals with a small-scale turbulence due to evolution of isobaric entropy structures in interstellar plasma. Turbulence is shown to appear even on scales substantially smaller than the Coulomb mean free path. But the two-dimensional perturbations ($\vec{k}\vec{B}_0 = 0$) arising in this case are inefficient for CR scattering. The second paper considers generation of secondary shocks appearing in the interaction of a primary shock, which is due to a supernova explosion, with interstellar clouds. The interstellar turbulence spectrum is determined. The corresponding value of the CR diffusion coefficient turned out to be equal to $D_{\parallel} \approx 5\ 10^{28}$ cm^2/s.

The problem of transverse diffusion of strongly magnetized particles in a stochastic large-scale magnetic field, which has not yet been strictly solved, is discussed in the paper by Ptuskin (7.2 - 16).

Ginzburg and Ptuskin (7.2 - 15) present a microscopic calculation of the force acting on the CR gas on the side of background plasma and discuss the applicability limits of standard hydrodynamic equations, including the CR action.

The relatively high CR pressure provides an important role played by relativistic particles in the formation of equilibrium distributions of gas and magnetic field in the galactic halo. This classical problem is considered anew by Dougherty et al. (7.2 - 18). The new element is an account of a finite pressure of mhd waves generated due to the stream instability of CR escaping from the Galaxy. The formation of an extended "tail" in the spatial distribution of gas over the galactic plane is confirmed.

I.2. Semiempirical galactic models ($E < 10^{15}$ eV)

Kinetic theory gives serious ground for using the diffusion approximation in the description of propagation of CR with energies up to $10^{15} - 10^{17}$ eV in the Galaxy. Using the "microscopic" theory only, one cannot however strictly prove the diffusion character of motion and unambiguously determine the diffusion tensor and the velocity of CR convective transfer. Semiempirical models are of particular importance in this situation. They make it possible to classify and correlate numerous observational data, to explain the specificities of the composition, energy spectra, and anisotropy of different CR components, to find the CR composition in the sources.

The diffusion galactic model is the most thoroughly developed and on the whole explains well the relative observations. Its first basic version was proposed by Ginzburg and Syrovatsky (1964) (for the modern version see, for instance, the review by Ginzburg and Ptuskin (1985). To simplify calculations, this model can in some cases (but not always!) be replaced by the leaky-box model. Many important problems remain, however, insufficiently investigated.

At the Conference particular attention was given to the analysis of the role of particle acceleration in interstellar medium, to the study of stream instability of low-energy CR (Bretthorst and Margolis 7.2 - 9), to the clarification of consequences of strong interstellar gas density variations for CR transfer and fragmentation (Morfill et al. 7.2 - 4).

The interest in acceleration in interstellar medium is connected with a great popularity of the scheme of diffusive shock acceleration by extended SN remnants. The decisive argument against the substantial CR acceleration in the course of their propagation and fragmentation in interstellar gas is the observed decrease with energy of the amount of secondary nuclei in the CR composition.

The argument which was considered doubtless is objected in the papers by Lerche and Schlikeiser (8.3 - 2, 7.2 - 8, 8.3 - I). According to formal calculations of these authors, in a continuous Fermi acceleration of CR in the entire Galaxy, the ratio of number densities of secondary to primary nuclei may decrease with energy. The crucial point of the model proposed by Lerche and Schlikeiser is the introduction of two different leakage times $T_{\ell s} = T_{\ell p}$ in the equations for concentrations of secondary and primary nuclei on the basis that the spatial distributions of interstellar gas and CR sources do not coincide. This procedure does not seem to be correct. (Under some simplifying assumptions applied to this case the whole information on propagation of stable nuclei, both primary and secondary, is contained in the particle distribution function with respect to pathlength x, $G(x,\vec{r})$, here $\vec{r}$ is the point of observation, see Ginzburg and Syrovatsky (1964).

For the leaky-box model to be applicable, it is necessary and sufficient that the distribution function have the form $G(x,\vec{r}) = \exp(-x/x_\ell(\vec{r}))$. In this case at each observation point $\vec{r}$ there exists only one value of x_ℓ ($= \bar{n}cT$), common for all nuclei, which should be used in transfer equations for CR concentration.)

Using different methods, Giler et al. (8.3 - 4) and Cowsik (8.3 - 7) have shown that a simultaneous CR acceleration and propagation in interstellar medium lead to sec/prim ratio increasing with energy (in some cases $s/p \to$ const for $E \to \infty$).

Thus, acceleration in interstellar gas, which is accompanied by nuclear fragmentation, is excluded as the main process of CR acceleration. This does not mean, of course, that particles accelerated in compact sources cannot undergo any additional reacceleration. Such a scheme seems fairly probable (Silberberg et al. 1983, 8.3 - 5).

Simon et al. (8.3 - 3) have studied a leaky-box model in which CR accelerated in their sources are then moderately reaccelerated during propagation. A model with reacceleration time approximately equal to leakage time from the Galaxy has been revealed to agree well with the data on the amount of secondary boron nuclei in the interval of $I \sim 100$ GeV/n. In this case $x_\ell \approx 4 g/cm^2$ ($R < 6$ GV) and $X_\ell \sim R^{-0.3}$ ($R > 6$ GV), whereas in the standard model without reacceleration $X_\ell = 8 g/cm^2$ and $X_\ell \sim R^{-0.5}$ ($R > 6$ GV). Thus, the real energy dependence of CR leakage time may be substantially weaker than in the standard leaky-box model (see Fig. I). This makes easier the interpetation of observations of CR anisotropy which point to a weak energy dependence of the leakage time for $E < 10^{14}$ eV.

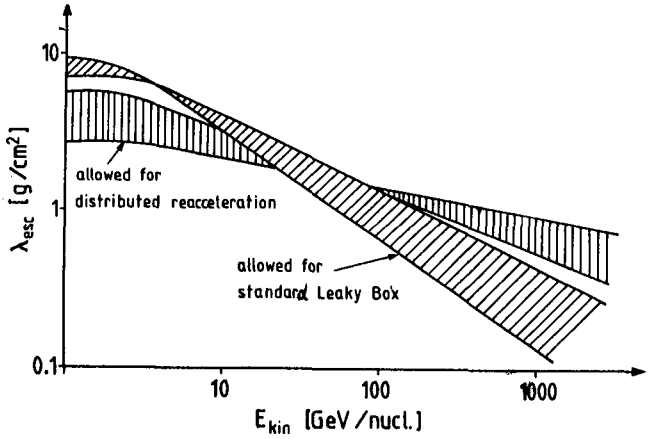

Fig. I. Schematic drawing of the energy dependence of X_ℓ (E) as predicted by the standard Leaky Box and the distributed reacceleration model. OG 8.3 - 3.

Note that reacceleration should not necesserily be associated with diffusive shock acceleration. If CR diffusion in interstellar medium is due to particle scattering by an isotropic mhd turbulence, the same scattering inevitably leads to statistical particle acceleration. It can be easily shown that the ratio of the particle leakage time from the Galaxy to the characteristic time of their acceleration is

$$T_\ell / T_a \sim \left(\frac{v_a}{c} \frac{x_\ell}{\int dz\, \rho(z)} \right)^2 \qquad (I.3)$$

Here v_a is the Alfven velocity, $\int dz\, \rho(z)$ is the gas thickness across the galactic disk. With a standard choice of parameters, we obtain $T_\ell \sim T_a$ for GeV-energy particles. As the energy increases, x_ℓ (E) decreases, and acceleration becomes inessential.

I.3. Radioastronomical evidence

Radioastronomical observations make it possible, in principle, to establish the dimension of the CR confinement region in a Galaxy (the halo dimension) and also to find the diffusion coefficient and the speed of convective CR outflow (the galactic wind speed). It is difficult to interpret the radio-maps of our Galaxy since we are inside the radiating volume. When observing other normal galaxies "from outside", it is often easier to distinguish the region of their halo. Examples are on-edge galaxies NGC 4631 and NGC 891 in which clearly pronounced radio halos were revealed.

Lerche and Schlikeiser (6.2 - I) and Cowsik and Sukumar (6.2 - 3) have constructed CR propagation models for NGC 4631 on the basis of radio continuum observations for frequencies from 327 MHz to 10.7 GHz. In the former paper it is stated that the observed dependences of the effective radio halo dimension on the frequency and of the spectral radiation index on the height over the galactic plane are an unambiguous evidence of the existence of a large-scale galactic wind and a convective CR transfer in the galaxy NGC 4631. The latter paper shows, on the contrary, that a simple diffusion model without convection explains well the available radio data.

I.4. Ultra high-energy CR

As has already been mentioned, for particles with energies $E > 3\ 10^{17} Z$ eV, scattering on inhomogeneities of the galactic magnetic field becomes inefficient and the diffusion coefficient increases rapidly with energy ($D_{\parallel} \sim r_H^2 B_0^2 / L_t (\delta B)^2$ for $r_H > L_t$). Diffusion gives turn to particle drift in an inhomogeneous regular magnetic field. At still higher energies, when the Larmor radius is comparable with the dimension of the region occupied by the regular field, the

particle motion becomes simpler, and as the energy increases, it differs smaller and smaller from the free motion. For the field strength $B = 2\ 10^{-6}$ G and for the dimension of the halo with an ordered field $h = 5$ Kpc, the condition $r_H \leq h$ holds for the energies $E \leq 10^{19}$ eV.

An informative concise presentation of the origin of ultra high-energy CR is given by Hillas (1984).

Most of the authors believe at present that particles with energies $10^{17} - 10^{19}$ eV are of galactic origin, and for $E > 10^{19}$ eV there dominates the extragalactic component. The arguments in favour of this assertion are given in the paper by Efimov and Mikhailov (5.4 - 15) (this paper is a continuation of the paper by Berezinsky and Mikhailov, 1983). The main attention is given to the weakest point of the galactic model -- to the explanation of high CR isotropy. It is assumed that CR sources are distributed in the galactic disk, the regular azimuthal magnetic field in the disk $B_\varphi = 2 - 3\ 10^{-6}$ G, in the halo $B_\varphi \lesssim 10^{-6}$ G. The corresponding trajectory calculations yield a good agreement with the observed values for the amplitude and phase of the I-st harmonic of CR anisotropy and for the southern excess of particles in the energy range from 10^{17} to 10^{19} eV. The apparent S/N asymmetry is probably connected in this case with the enhancement of particles from the general direction of the galactic plane (like in the model of galactic plane excess proposed by Wdowczyk and Wolfendale, 1984, 5.4 - II).

For the energies $E > 3\ 10^{19}$ eV the observed picture changes drastically and there appears a particle flux from high northern galactic latitudes - roughly speaking, from the direction to the supercluster Virgo. This can be explained only by the action of extragalactic sources.

The observed southern excess of particles with energies below 10^{19} eV can be explained, in principle, by a non-symmetric CR outflow across the galactic plane. In this case, the particle concentration in the region P in Fig. 2 must be lower than in the external region Q. The Hillas interpretation

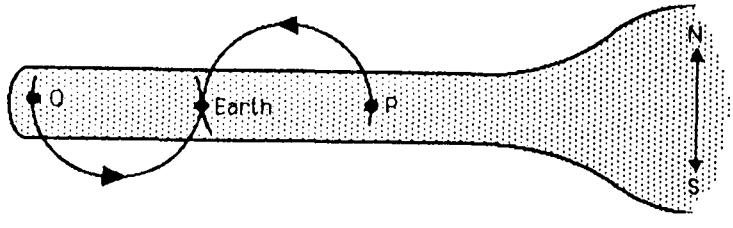

Fig. 2. Trajectories of positively charged particles in azimuthal galactic magnetic field. OG 5.4 - 9.

(1984) suggests the presence of a local CR gradient in this energy range (~ 15 % Kpc) increasing toward the Orion region. Sommers and Elbert (5.4 - 9) believe that in the region P, at a distance of several Kpc from the solar system there oc-

curs a reverse of the azimuthal field which is accompanied by a rapid evacuation of CR and a local decrease of their intensity.

Karakula and Tkaczyk (5.4 - 8) have calculated the trajectories of ultra high-energy particles and determined transparency of the Galaxy for extragalactic protons. The regular galactic magnetic field is assumed to be contained in the disk $|z| \leq 0.4$ Kpc. In constructing a concrete model of CR origin, the authors assume the isotropic flux from galactic sources to be summed up with the directed flux from the source to Virgo Cluster (these fluxes are equal to each other for 10^{18} eV).

2. Antiprotons

An understanding of the large flux of antiprotons found in CR remains an intriguing problem. The available observations (unfortunately, they have been little enriched during this Conference) can be briefly resumed as follows. The observed integrated antiproton flux was found to exceed significantly the flux of secondary antiprotons calculated from the standard model of CR propagation in interstellar medium. (See, for example, Stephens 1981). For energies 0.1 - 10 GeV, the observed total flux of antiprotons 4-10 times exceeds the flux expected in the leaky-box model for $\chi_e = 5$ g/cm^2. The observed energy spectrum of antiprotons is also unexpectedly different from the production spectrum of secondary antiprotons generated in p-p collisions. It is greatly enriched with low-energy particles and on the whole is similar to the CR proton component spectrum (in contrast with the production spectrum of secondary antiprotons which falls sharply for the energies $E < 2$ GeV).

The explanations proposed may conditionally be divided into "exotic" and "non-exotic".

Here is the list of "exotic" explanations exploiting the new physical principles: quantum evaporation of mini black holes Kiraly et al. (1984), n-$\bar{n}$ oscillations Sawada et al. (1981), Sivaram and Krishnan (1982), primary extragalactic origin Stecker et al. (1981), Stecker and Wolfendale (6.I - 8), photino annihilation in the galactic halo Silk and Srednicki (1984), Stecker et al. (6.I - 9).

The photino hypothesis is based on the assumption that in the Nature there exist stable massive photinos. These particles originate in the early Big-Bang. Photino is assumed to make up the missing mass in the galactic halo and to probide the matter density in the Universe which is close to the critical one $\Omega = I$. In the paper submitted to the Conference Stecker et al. investigate photino annihilation in the galactic halo and calculate the spectrum of antiprotons appearing in this process. An intriguing fit is obtained to all the existing data on antiprotons for a photino mass $m_{\tilde{\gamma}} \approx 15$ GeV. The cut-off of the spectrum for $E \geq m_{\tilde{\gamma}}$ is predicted. (One should remember that it is still unknown in what concrete

form, if at all, the very supersymmetry principle is realized in the real world).

Non-exotic hypotheses do not require new physical mechanisms for explanation of a high $\bar{p}$ flux. However, they require reconsideration or specification of the old habitual galactic models of CR propagation (see the Discussion in the papers by Ginzburg and Ptuskin, 1984; Lagage and Cesarsky, 1985).

It is possible, in particular, that part of CR sources (or all the sources at a certain stage of their evolution) are surrounded by a thick layer of matter in which secondary $\bar{p}$ are produced. Heavy nuclei either do not escape from such objects due to a strong fragmentation or are not accelerated in them at all. One of the possible realizations of such a model has been considered by Mauger and Stephens (1983). Primary CR are assumed to accelerate in SN explosions in dense clouds and to be confined there for several thousand years, traversing the thickness of about 50 g/cm^2. If $\sim$ 30 % of nucleons observed in CR come from such sources, one can satisfactorily explain the observations of $\bar{p}$. Now Stephens shows (6.1 - 7, 6.2 - 9, 2.5 - 3) that the fluxes of secondary positrons and gamma-quanta expected in this model do not contradict the observational data. More favourable here is the version in which the time of CR leakage from the Galaxy is almost independent of the energy. If the dependence is strong ($T_\ell \sim E^{-0.6}$), the flat CR spectrum in the sources leads to a too rigid spectrum of gamma-rays and to a too large flux of secondary positrons.

Dermer and Ramaty (6.1 - 4) have presented a model in which low-energy antiprotons appear as secondary in p - p interaction in a relativistic plasma with a temperature $kT \sim 0{,}2\ m_p c^2$. It is assumed that the appropriate conditions may exist in the vicinity of a neutron star or a black hole.

Various versions of secondary antiproton generation in dense gas clouds in models with a nonuniform CR propagation are developed by Tan (5.4 - 13, 6.1 - 6, 6.2 - 7), Dogiel et al. (8.2 - 17), Morfill et al. (7.2 - 4).

The model which would explain the high antiproton flux in the CR composition has not yet been finally chosen.

The correctness of calculations of the expected fluxes of secondary $\bar{p}$ has been verified by Bowen and Moats (6.1 - 3). The parameters $\alpha = 0.333$ - the probability of np charge exchange, and $\varepsilon/2 = 0.45$ - the average elasticity, have been determined by measuring the proton spectrum at mountain altitude. The calculated spectrum of secondary $\bar{p}$ in the atmosphere satisfactorily agrees with the measurements by Bowen et al. (1983). The contribution of atmospheric $\bar{p}$ in balloon measurements by Golden et al. (1979) and Buffington et al. (1981) has been shown not to exceed about 10 %.

3. Shock acceleration: theory and application to the CR origin problem

The diffusive shock acceleration mechanism remains the most popular with theoreticians engaged in the problem of

CR acceleration (see the reviews by Axford, 1981, Drury, 1983, Volk, 1984).

3.I. Test particle approximation

An acceleration of a fast test particle diffusing near a shock front is a version of a first-order Fermi acceleration. It is due to a repeated crossing of the shock front in a random particle walk and to an energy gain in front collisions with scattering centres embedded to the background plasma. A formal solution of the problem can be obtained using the equations for the test particle distribution function which describes spatial diffusion, convective transfer, and a regular alteration of particle energy in a nonuniform flux:

$$\frac{\partial f}{\partial t} + \vec{u}\nabla f - \nabla \hat{D} \nabla f - \nabla \vec{u} \frac{p}{3} \frac{\partial f}{\partial p} = 0, \qquad (3.1)$$

The particle density is equal to $N(p)\,dp = 4\pi p^2 f(p)\,dp$.

For a plane front the velocity profile $u(x)$ is approximated by a step function (see Fig. 3). If particle distribution in a nonperturbed medium in an upstream region has the form $f_1 \sim \delta(p - p_0)$, the stationary spectrum of accelerated particles in a downstream region has a power-law form:

$$f_2(p) \sim \theta(p - p_0) \cdot p^{-\frac{3r}{r-1}}, \qquad (3.2)$$

where $r = u_1/u_2$ is a compression ratio in a shock.

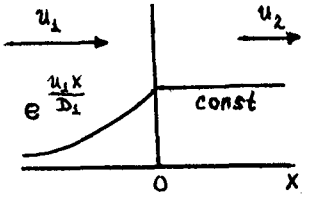

Fig. 3. Spatial distribution of accelerated test particles in the shock frame

For an extremely strong shock wave without radiation, which propagates in a gas with the adiabatic index $\gamma_g = 5/3$, the quantity $r = 4$ and, therefore, the spectrum of accelerated particles is $N(p) \sim p^{-2}$. This is close to the expected CR spectrum in the sources.

The characteristic time of particle acceleration (i.e. the time of its energy variation by a factor of e) under shock acceleration is equal to

$$t_a(p) = \frac{3}{u_1 - u_2} \cdot \left(\frac{D_1}{u_1} + \frac{D_2}{u_2} \right) \qquad (3.3)$$

Note that the estimate of the characteristic acceleration time $t_a \sim D/u^2$ is valid both for the diffusive shock acce-

leration and for the statistical Fermi acceleration. In the latter case u has the meaning of the turbulent motion velocity.

If a particle bears additional energy losses in a medium (with a characteristic time t_ℓ), then for acceleration it is necessary that the condition $t_a \ll t_\ell$ should be fulfilled. In particular, for a spherical shock wave with a radius R, the role of losses, is played by a diffusion particle escape for the time $t_d \sim R^2/D$, and therefore particles are accelerated only under the condition (the numerical factor is omitted here and it is assumed that $D_\perp \geq D_\parallel$)

$$R u_1 / D_\perp > 1. \qquad (3.4)$$

These assumptions are confirmed, in particular, by the numerical calculations made by Ko and Jokipii (8.2 - 2).

By the terminology accepted in the theory of particle propagation in a solar wind, the inequality (3.4) implies a strong CR modulation.

Since the diffusion coefficient usually increases with energy, the condition (3.4) imposes limitation on the maximum possible accelerated particle energy E_{max}. Under scattering in a magnetic field $D_\parallel > r_H v$, accordingly,

$$E_{max} \sim \frac{Ze}{c} B R u_1 \quad (D_\perp \sim r_H v, \; v \sim c). \qquad (3.5)$$

An impressive example of a possible realization of the mechanism of CR shock acceleration in the Galaxy is given by Jokipii and Morfill (8.1 - 8). They suggest that CR particles with energies $E \gtrsim 10^{15}$ eV are accelerated at a termination shock of galactic wind. If the wind in the Galaxy does actually exist (which can be strongly doubted, see, for instance, Habe, Ikeuchi, 1980) and if the large-scale magnetic galactic field has a structure similar to the Parker spiral in interplanetary space, then $B \sim B_o (R_o/R)$ for $R > R_o$, where $B_o = 3\ 10^{-6}$G is a field at a distance $R_o = 10$ Kpc. It is assumed that the distance to the shock is $R \sim 100 - 200$ Kpc, the wind velocity $u_w = 300 - 500$ km/s.

Formula (3.5) does not work in this case since in an ordered, strongly twisted spiral magnetic field, the diffusion coefficient in the radial direction is smaller

$$D_{eff} = \alpha^2 D_\parallel + (1 - \alpha^2) D_\perp \qquad (3.6)$$

where $\alpha = R_o u_w \cdot (R u_{ga1})^{-1} \ll 1$ ($u_{ga1} = 250$ km/s is the speed of Galaxy rotation), $D_\perp \approx r_H^2 c^2 / D_\parallel$ is the diffusion coefficient across a regular magnetic field.

The minimum value of D_{eff} is reached for $D \sim r_H c/\alpha \sim 20\, r_H c$. In this case, instead of (3.5) we have

$$E_{max} \sim \frac{Ze}{c} B_o R u_{ga1} = 5 \cdot 10^{17} Z \left(\frac{B_o}{3 \cdot 10^{-6} G}\right) \left(\frac{R}{100\ \text{Kpc}}\right) \text{eV} \qquad (3.7)$$

The maximum energy density of accelerated particles can be estimated by assuming that the whole power of the galactic wind ($Q \sim 5\ 10^{40}$ erg/s, according to Jokipii and Morfill) goes to accelerated particles

$$w_{cr\ max} \sim \frac{3QT_\ell}{4\pi R^3} \sim 10^{-15} \cdot \left(\frac{100\ Kpc}{R}\right)^2 \ erg/cm^3 \qquad (3.8)$$

Here the time of CR escape from the galactic wind region is $T_\ell = R/u_w \sim 3 \cdot 10^8 \cdot (R/100\ Kpc)$ years.

The CR intensity modulation effects lead, in fact, to a substantial lowering of the w_{cr} value. In this case, particles with $E \lesssim 10^{15}$ eV do not reach the observer at all. We should recall that the values observed near the Earth are w_{cr} ($>10^9$ eV) $\approx 10^{-12}$ erg/cm^3 and w_{cr} ($> 10^{15}$ eV) $5\ 10^{-16}$ erg/cm^3.

Thus, CR acceleration on the galactic wind boundaries could, in principle, be a noticeable source of particles with energies $E > 10^{15}$ eV. It remains unclear how the main energy output can be provided just in the region $E > 10^{15}$ eV (with the particle spectrum $N(E)dE \propto E^{-3.1}\,dE$) and how for $E \lesssim 10^{15}$ eV a smooth conjugation with the CR spectrum ($N(E) \propto E^{-2.7}$) generated, according to Jokipii and Morfill, in galactic SN remnants can be obtained. Note that reacceleration of CR supplied by SN is inessential in this case because due to the geometrical factor it gives not more than $(R_\odot/R)^2 \lesssim 10^{-2}$ of the CR concentration in the galactic disk. It is necessary to consider particle acceleration directly from the thermal plasma on the galactic wind boundaries.

SN remnants are regarded as "classical" astronomical objects, in which the action of diffusive shock acceleration is possible. A direct interpretation of radio data from SN remnants with an age exceeding 100 years is ambiguous. The hypothesis concerning diffusive shock acceleration is consistent with observations, but is not rigorously proved (Beck et al. 8.1 - 10, Bogdan et al. 8.1 - II, Lawson et al. 6.2 - 4).

Old remnants of the SN Loop I and III are studied in the paper by Lawson et al. Diffusive shock acceleration of electrons up to energies $E \sim 10$ GeV has been revealed. The CR diffusion coefficient in the galactic disk has been determined to be $D \sim 10^{27}$ cm^2/s.

Of importance is finding the fraction of SN explosion energy which can be transferred to CR. This problem has been solved numerically in the test particle approximation in the paper by Dorfi and Drury (8.1 - 9). With the explosion energy of 10^{51} erg and with the diffusion coefficient equal to 10^{27} cm^2/s, the effective acceleration of background relativistic particles starts at the moment $t = 6\ 10^{11}$ sec after the explosion, and by the moment $t = 2\ 10^{14}$ sec about 12 % of the initial SN energy is transferred to high-energy particles. Such an efficiency is, in principle, sufficient to replenish the observed CR energy density.

3.2. Nonlinear CR shocks

The high efficiency of shock acceleration and a comparatively large energy density of relativistic particles in cosmic plasma lead to the necessity to study the back reaction of accelerated particles to thermal plasma. (In this case the quantities $\vec{u}$ and $\hat{D}$ in equation (3.1) cannot be regarded as externally given parameters). This nonlinear problem turns out to be very complicated.

If CR are assumed to be a separate relativistic gas component with a pressure P_{cr}, an internal energy density w_{cr}, and an effective average diffusion coefficient $\bar{D}$

$$P_{cr} = \frac{4\pi}{3}\int_0^\infty dp\, p^3 v f(p), \quad w_{cr} = 4\pi \int_0^\infty dp\, p^2 E_\kappa f(p), \tag{3.9}$$

$$P_{cr} = (\gamma_{cr}-1) w_{cr}, \quad \bar{D}(x) = \Big(\int_0^\infty dp\, p^2 D E_\kappa \frac{\partial f}{\partial x}\Big)\cdot\Big(\int_0^\infty dp\, p^2 E_\kappa \frac{\partial f}{\partial x}\Big)^{-1}$$

then in the double-fluid hydrodynamic approximation the equations of one-dimensional motion of a medium, with an account of CR action, have the form

$$\frac{\partial \rho}{\partial t} + \frac{\partial}{\partial x}(\rho u) = 0, \quad \frac{\partial u}{\partial t} + u\frac{\partial u}{\partial x} = -\frac{1}{\rho}\frac{\partial}{\partial x}\left(P_g + P_{cr}\right), \tag{3.10}$$

$$\frac{\partial P_g}{\partial t} + u\frac{\partial P_g}{\partial x} + \gamma_g P_g \frac{\partial u}{\partial x} = 0, \quad \frac{\partial P_{cr}}{\partial t} + u\frac{\partial P_{cr}}{\partial x} + \gamma_{cr} P_{cr}\frac{\partial u}{\partial x} = \frac{\partial}{\partial x}\bar{D}\frac{\partial}{\partial x}P_{cr}.$$

In the study of self-consistent shock structure, one seeks for steady solutions which would describe the transition from the state given for $x = -\infty$ (upstream) to the state uniform for $x = +\infty$ (downstream), see the reviews cited at the beginning of Sec. 3.

A more complicated problem, which takes into account the finite energy of CR-scattering mhd waves, has been considered in the papers by Volk and Mc Kenzie (1982), Volk et al. (1984). These waves are assumed to be generated due to stream instability of relativistic particles before the shock front. The set of equations (3.10) must then be modified in the respective way.

An account of CR pressure changes the profile of a hydrodynamic flow near the shock front, see Fig. 4. There appears a region of smooth variation of upstream velocity (precursor), and in the general case there remains a step-like jump of velocity (subshock) determined by gas viscosity. This situation is similar to isothermal jumps for strong shocks in media with a thermal conductivity coefficient substantially exceeding the viscosity coefficient in the usual hydrodynamics (Landau and Lifshitz, 1959).

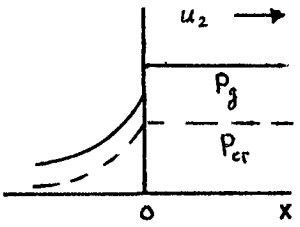

Fig. 4. A stationary modified shock

Unfortunately, one had not yet succeeded in obtaining a single-valued steady-state solution to the problem (more precisely, in obtaining generalized Rankine-Hugoniot conditions for arbitrary values of $N = P_{cr}(-\infty)/(P_{cr}(-\infty) + P_g(-\infty))$ and the Mach number of the incoming flow $M_*^2 = \rho u_1^2 \cdot (\gamma_g P_g + \gamma_{cr} P_{cr})^{-1}$. It is shown, in particular, that for $\gamma_g = 5/3$, $\gamma_{cr} = 4/3$ in the general case there may exist three solutions in the downstream region for certain upstream conditions. Such an unambiguity is caused by divergency of the quantity P_{cr} with the momentum p for flat spectra $f(p) \sim p^{-4+\varepsilon}$ ($\varepsilon \geq 0$), see (3.9). Then the definition (3.9) also loses sense for D (if $D(p)$ increases with p). Indeed, let the diffusion coefficient increase with energy and the transition region from $u(-\infty)$ to $u(+\infty)$ have the finite dimension ΔX. For particles with momenta $p \gg p_*$, where the value p_* is determined from the condition $u_1 \cdot \Delta x/D(p_*) = 1$, acceleration proceeds in the same way as on a step-like profile of the velocity $u(x) = u_1\theta(-x) + u_2\theta(x)$, and the spectrum of high-energy particles has the form (3.2). The degree of compression for a strong shock exceeds here $r = 4$ since the presence of relativistic particles in the downstream region softens the equation of state ($\gamma_{cr} < \gamma_g$). In this case the spectrum $f(p) \sim p^{-4+\varepsilon}$ and $P_{cr} = \infty$. This implies that a steady-state solution with a limited total width of the transition region is impossible. Additional difficulties are caused by the functional dependence $\gamma_{cr}(f(p))$.

It has become clear that in general either the maximum particle energy must be restricted by introducing additional loss proccesses into the problem or the acceleration must be treated as a time-dependent problem (Drury, 1984),

The time-dependent structure of a nonlinear CR shock is numerically investigated in the paper by Dorfi (8.I - 3). For not too large a value $M_* = 4.4$ and for $N = 0.5$, the transition from a gas dominated shock to a shock modified by CR takes up the time of $(30 - 40)\, D/u^2$. For a high Mach number $M_* = 10$ and for a small value $N = 0.05$, there appears no back effect of the CR pressure on the motion of background plasma up to a time $t \sim 10^3\, D/u^2$.

Beck and Drury (8.I - 4) analytically investigate the time-dependent problem. They construct a selfsimilar solution which depends on the similarity variable $\xi = x/t$. Selfsimilar shock structures are shown to contain always a subshock. The solution to the problem for shocks with a large Mach number has not been obtained.

The problem of seeking for an unambiguous solution, which has not yet been finally solved, is in a sense only of academic interest . Volk et al. (1984) have shown that in the framework of three-fluid hydrodynamics in the strong wave damping approximation the solution is unique in a wide range of reasonable astrophysical parameters.

The study of the dynamics of SN remnants with an account of the action of accelerated CR, which is of great importance for astrophysics, has been started in the paper by Volk et al. (8.I - 12), First results have been obtained on the time evolution of the kinetic remnant energy, the thermal energy of a heated gas, and the total CR energy. It has been shown that 10 - 50% of the initial energy of an explosion can be transferred into the CR energy.

Another, not hydrodynamic approach to nonlinear CR shocks is developed in the papers by Eichler and Ellison (8.I - 6) and Berezhko et al. (8.I - 13) (see also Eichler (1979, 1984), Krymsky (1981), (1983), Ellison and Eichler (1984)). This approach consists in a unified description of thermal and accelerated particles, i.e. along with acceleration one considers thermal particle injection. Particle acceleration is an inherent part of the very process of shock formation in plasma. It is assumed that there exists a maximum particle energy E_{max} above which they cannot be confined near the shock. Therefore, there exists a continuous energy flux from a system

$$q_j(x) = -\frac{j}{3}\int_{-\infty}^{x} \frac{du}{dx'} E_{K\,max}^2\, N(E_{K\,max})\, dx' \qquad (3.9)$$

(j = 2 for nonrelativistic particles and j = I for ultra relativistic particles). The diffusion coefficient D(p) is assumed to increase with momentum.

For fast particles the distribution function obeys equation (3.I). Using the mass and momentum flux conservation conditions for given upstream values, one finds a stationary solution of equation (3.I). The final solution is obtained by matching the low-energy spectrum region to the thermal background distribution.

An alternative procedure consists in the numerical solution of the kinetic equation with a simplified collision integral in the entire particle momentum region and in the definition in this way of the complete distribution function.

In the paper by Eichler and Ellison (8.I - 6) in the described scheme, the final velocity of waves generated by an accelerated particle stream is taken into account for the first time. Figures 5,6 present the obtained spectrum of accelerated particles for the case of acceleration by SN remnants in interstellar medium. The values $E_{max} = 10^{15}$ eV, $B = 3\,10^{-6}$ G, $n = 10^{-2}$ cm^{-3}, $u_1 = 10^3$ km/s were used.

It is remarkable that for a wide range of reasonable astrophysical parameters the spectrum turned out to be close to $N(E_K) \sim E_K^{-2}$. Typical is also the presence of two maxima in the function $E_K^2\, N(E_K)$ - for thermal energies and for E_{max}.

For the spectra shown in Fig 5 the kinetic energy flux going into relativistic particles makes up 72 - 26 %.

Such a calculation is in a good agreement with observations for shocks in interplanetary medium (Ellison and Eichler, 1984), but the problem as a whole cannot yet evidently be considered as finally solved. Suffice it to say that the indicated scheme must include, in particular, the theory of collisionless shocks in a usual plasma. This theory has been intensively developed for already about 30 years.

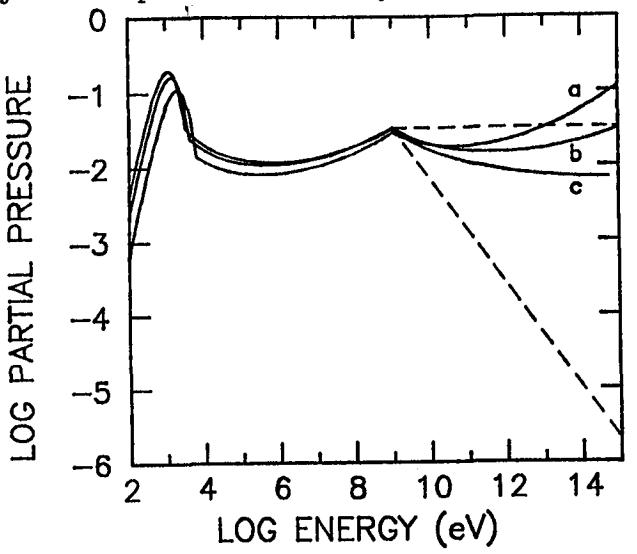

Fig. 5 Postshock partial pressure vs. energy. An energy cutoff = 10^{15}eV has been used. Each label represents a family of curves with a particular $u_1/u(GeV)$. OG 8.1-6

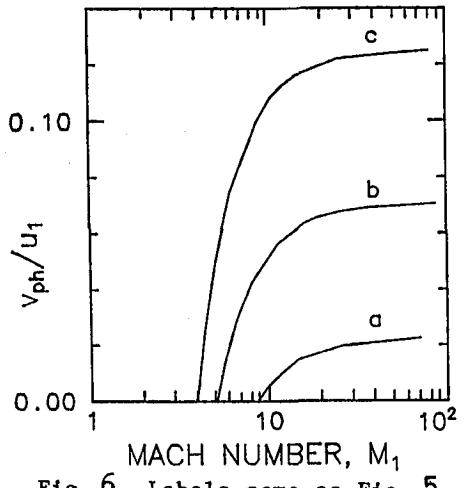

Fig. 6 Labels same as Fig. 5

It is of importance to note, however, that the difficulties in the theory of nonlinear CR shocks are due to the high efficiency of the diffusive shock acceleration and, in fact, we try to understand what it is limited to. In any case, the efficiency of the conversion of the energy of an ordered hydrodynamic stream into the energy of relativistic particles typical for the galactic model of CR origin ($\sim$ 10 %) does not seem to be excessive.

There are no essential difficulties with explanation of the observed power-law energy CR spectrum. The problem consists in obtaining a sufficiently large $E_{max} \sim 10^{17} - 10^{19}$ for galactic CR souces. So, for instance, the value $E_{max} \sim 10^{15}$ eV presented in Fig. 5 has been not calculated, but postulated. For the values $B = 3\ 10^{-6}$ G, $n = 10^{-2}$ cm^{-3} used by the authors, an SN explosion with a total energy $W = 10^{51}$ erg may, in accordance with (3.5), actually give $E_{max} = 3\ 10^{14}$ eV. In the standard model of CR propagation in interstellar medium, the value of $D_{\parallel} \sim r_H v$ entering (3.5) seems to be strongly underestimated. The value of E_{max} should rather be lowered by several orders of magnitude (for more details see Volk, 1981).

The effect somewhat increasing E_{max} is generation of a strong random magnetic field near the remnant due to the stream instability of accelerated particles. This process cannot be investigated within the theory of weak turbulence, and its analysis remains a challenge for theoreticians (see Drury 1983, Volk 1984). The possibility of hightening E_{max} (may be up to 10^{16} eV) under CR acceleration in the reverse shock inside an SNR is pointed out by Volk et al. (8.I - 12).

3.3. New problems

In their paper (8.I - 5) Dorfi and Drury have revealed a new interesting effect which accompanies CR diffusive shock acceleration. It has been shown that in the region of precursor there develops an instability of compressional disturbances of the medium, due to the CR gradient, for the wavelengths $1 << \lambda << L$ ($1 = 3D/v$ is the mean free path of a particle, $L = D/u$ is the dimension of the precursor). The instability arises for $L < |I + \delta(\ln D)/\delta(\ln \rho)| \cdot D/v_{sg}$ and develops during the time $\tau \sim L/v_{sg} M_1^2$. For $M_1 >> I$, the time τ is small as compared with the time of convectional outflow of disturbances from the prcursor region $L/v_{sg} \cdot M_1$. Slight density disturbances in the upstream medium must be substantially amplified in the precursor region.

Zank and Mc Kenzie (8.I - ?) confirm the existence of such an instability. They also investigate instability of a CR shock with respect to long-wave disturbances ($\lambda >> L$). In the presence of a relativistic CR gas, strong shocks always prove to be unstable.

The effect of these instabilities on the shock structure has not yet been investigated. One may expect a strong stochastization of the motion of the medium before a shock, the appearance of secondary shocks, an additional widening of the

front and even destruction of its plane structure.

Webb (8.I - I) was the first to study the structure of relativistic CR shocks. He points out that the effective CR acceleration proceeds for $u_1 < c\sqrt{\gamma_{cr} - I} \approx 0.58c$. In high-velocity streams ($u_1 > c\sqrt{\gamma_{cr} - 1}$) CR cool down.

4. High-energy particles in various astronomical objects

4.I. Active galactic nuclei

AGN and quasars are possibly the most powerful CR sources. It is believed now that the particles of ultra high energies $E > 10^{19}$ eV observed near the Earth have been accelerated just in AGN. To the presence of relativistic particles there testifies nonthermal AGN radiation (see Rees 1984), but concrete mechanisms of particle acceleration remain unclear.

Kazanas and Ellison (8.I - 7) consider diffusive shock acceleration of protons in accreting matter near a black hole of mass $M_9 = M/(10^9\ M_\odot)$. Accelerated relativistic protons provide the pressure to support the standing shock. They undergo inelastic nuclear collisions and generate secondary $e^\pm$, γ, ν, which are responsible for the observed radiation. For a nearly 100 % conversion of the hydrodynamic motion energy into relativistic particles, Kazanas and Ellison have calculated the expected nonthermal luminocity $L = I.5\ 10^{47} M_9 x_1^{-1}$ erg/s $= I.2\ L_E x_1^{-1}$, where $L_E = I.3\ 10^{47} M_9$ erg/s is the Eddington luminocity, $x_1 = R/R_g$ is the radius of a spherical shock in Schwarzschild radii. The model provides a natural explanation of the observed $L \backsim M$ correlation for quasars and galactic nuclei. In this case $10 \lesssim x_1 \lesssim 200$. For the case NGC 4151 ($M = 3\ 10^7\ M_\odot$, $L = 10^{43}$ erg/s) $L = 2.5\ 10^{-3} L_E$, $x_1 = 140$.

4.2. Neutron stars in close binary systems

Ultra high-energy ($> 10^{15}$ eV) γ - rays (or/and unidentified neutral particles) have been observed from Cyg X - 3 and possibly from the X-ray binary sources LMC X-4, Vela X-I. Taking the measurements at face value, we have indication of a striking efficiency of CR acceleration in the compact binary systems containing n-stars. It is sufficient to have CygX-3 alone to maintain the present flux of the galactic CR above 10^{16} eV. The extragalactic source LMC X-4 ($E_\gamma > 10^{16}$ eV) has (?) a luminosity more than 20 times the one of Cyg X-3.

Taking the Haverah Park flux for Cyg X-3 $F_\gamma (> 2\ 10^{15}\ \text{eV}) = I.I\ 10^{-10}$ erg/cm^{2}s, Hillas (5.4 - 7) obtains the following estimate for proton luminosity of the source

$$L_p(10^{16}\text{-}10^{17}\text{eV}) = \frac{\Omega}{4\pi} \times 6 \times 3 \times 50 \times 4\pi r^2 \times 1.1 \cdot 10^{-10} = \frac{\Omega}{4\pi}\ 1.7 \cdot 10^{39}\ \text{erg/s} \quad (4.I)$$

Here we have the factors taking into account the appearance of particles in a solid angle Ω, the efficiency of energy

conversion $p \rightarrow \gamma$, absorption in rout due to $e^- e^+$ pair creation on relic radiation, pulse duty ratio of the 4.8 h period of the system. The distance to Cyg X-3 is taken to be equal to r = 12 Kpc.

The proton luminosity being so high, Cyg X-3 must also be a source of secondary neutrinos (see Beresinsky 2.I - 7, Brecher and Chanmugam 2.2 - 5, Gaisser and Stanev 1985).

The hypothesis on propagation of neutral radiation from Cyg X-3 in the form of photino (V.J.Stenger) requires an improbably high proton luminosity $L_p = 2\ 10^{44}\ (\Omega/10^{-2})$ erg/s (Beresinsky 2.I - 7).

As the energy source of accelerated particles in a binary system consisting of a normal star and a magnetized neutron star, one considers two main possibilities: I) accretion from a normal star onto an n-star; 2) pulsar action of the n-star itself.

In any case, proton acceleration proceeds in the vicinity of an n-star. The primary proton spectrum has a power-law form or is a monoenergetic beam with an energy $E \sim 10^{17}$ eV. In the latter case, the power-law spectrum of radiation and of secondary particles is caused by a cascade in the target region (Hillas 1984, 5.4 - 7).

Secondary UHE γ-rays appear as a result of pp collisions in an accreting gas outside the acceleration region or in the atmosphere of the companion star. (Aharanian et al. (2.6 - 13) notice that at a rather high density of background low-frequency radiation in the source, a substantial contribution is made also by photomeson γ-ray generation).

In the source Cyg X-3 in different periods of observations in the UHE range, γ-pulses had two different values for the phase of the 4.8-hour binary orbit: $\varphi = 0.25$ and $\varphi = 0.63$. According to Hillas (5.4 - 7), in the periods of $\varphi \sim 0.6$ the target for the production of secondary γ-photons is a wake which occurs if accretion appears from a stellar wind, see Fig.7 (a similar scheme is discussed by Protheroe and Clay (1985) for LMC X-4).

The dynamics of the interaction between an accelerated particle beam and the atmosphere of a companion star is considered by Beresinsky (2.I - 7). He proposes a heating model in which radiation in the phase $\varphi \sim 0.2$ is not accompanied by the appearance of a symmetric pulse $\varphi = 0.8$.

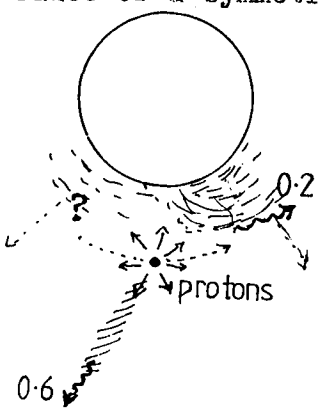

Figure 7. Supposed geometry for Cygnus X-3. OG 5.4 - 7.

To choose a concrete model of CR acceleration in binary systems, it is important to establish whether or not Cyg X-3 is a unique UHE γ-ray source.

So, for a pulsar model (Eichler and Vestrand 1984, Beresinsky 1979, 2.I - 7) a very young pulsar with a rotation speed of $10^2 - 10^3$ times per sec. is needed. Such a version is excluded for the sources LMC X-4 (P = 13.5 s), Her X-I (P = I.24 s), 4U OII5 + 63 (P = 3.61 s), but is not excluded for Cyg X-3 (the value of P in unknown).

In accretion models of CR acceleration two schemes are considered - the dynamo model in an accretion disk and shock acceleration in an accretion flow.

Brecher and Chanmugam (1985; 2.2 - 5) proposed a unipolar induction model for CR acceleration in accretion binary systems, such as Cyg X-3, Her X-I, Vela X-I, LMC X-4.

Details of the electrodynamics of such systems are not yet clear. Particle acceleration is assumed to be caused in the end by a very high potential drop across the accretion disk between the Alfven radius and the external edge of the disk. The scaling law $E_{max} \sim B^{-3/7} L^{5/7}$ ($L = GM\dot{M}/R$ is the total accretion luminosity of an n-star of mass M and radius R, B is a magnetic field on its surface) is obtained for the maximum possible energy of an accelerated particle. The maximum luminosity in relativistic particles is estimated to be $L_{p\,max} \sim 2cE^2_{max}/e^2$ (e is the particle charge). Thus, for a given magnetic field strength the higher the accretion rate, the larger the maximum CR particle energy and the higher the total particle luminosity. For $B = 10^{13}$ G the energy $E_{max} \sim 10^{17}$ eV is reached for a very high accretion rate $\dot{M} = 10^{-6} - 10^{-5}$ $M_\odot\,yr^{-1}$, i.e. $L \sim 10^{40} - 10^{41}$ erg/s. In this case to relativistic particles there goes $L_{p\,max} \sim 10^{39}$ erg/s. Most of the energy must be released in the form of a jet. In the unipolar induction model comparatively weak fields $B \sim 5\,10^9$ G are preferable. In this case $E_{max} = 10^{17}$ eV, $L_{p\,max} = 10^{39}$ erg/s $\sim L$. The value $B = 5\,10^9$ G is not excluded for Cyg X-3 (the field is unknown), but is excluded for Her X-I ($B = 4\,10^{12}$ G) and 4U0015 + 63 ($B = 10^{12}$ G).

The model of shock acceleration of particles in application to the source Her X-I is considered by Eichler and Vestrand (2.2 - 8). For an explanation of γ-radiation outbursts observed for energies $E > 10^{12}$ eV and $E > 10^{14}$ eV, they suggest a diffusive shock acceleration in an accretion column at a distance $R \sim 30$ radii of the n-star (at smaller distances acceleration is hampered by synchrotron losses). In this case $E_{max} \sim 10^7\ mc^2\ (R/10^6\ cm)^{-1/6}$. The observed γ-rays are formed in the interaction between protons and the surrounding accretion disk. The model predicts γ-ray outbursts at the onset and decline of the high-intensity X-ray state. At this time our line of sight is grazing the accretion disk. Radiation of γ-rays with an energy $E > 10^{16}$ eV is impossible in this model (see, however, Kazanas and Ellison, 1985).

The existence of such UHE γ-ray sources as Cyg X-3, possibly leads to the formation of a galactic X-ray halo (Rana et al. 2.2 - 6). Under $\gamma\gamma$ collisions with relic photons,

UHE γ -rays produce e^- e^+ pairs, and these will in turn generate hard X-rays by synchrotron radiation in the galactic magnetic field.

4.3. Stars

Normal stars may be injectors of fast particles which are further accelerated up to high energies. Bogdan and Schlickeiser (8.3 - 9) consider resonant statistical acceleration of electrons in flaring stars. The maximum particle momentum is limited in this case to the energy losses due to synchrotron radiation and in this model makes up $p \sim 1.5\ 10^8$ eV/c for the magnetic field of a star B = 100 G.

4.4. SN remnants

Most of the papers on CR acceleration in SNR have already been discussed in Sec. 3.

In some SNR (Crab), relativistic particles are supplied by a central source - a pulsar. The remnant G 29.7 - 0.3 (the distance - 19 Kpc, the dimension - I.8 pc) may also appear to be an object of this type. High resolution maps obtained with the VLA show two spectrally distinct components - a flat-spectrum core surrounded by a shell. Koch-Miramond et al. (6.2 - 10) have presented the data of Exosat observations of X-ray radiation of the remnant in the 2-10 KeV range. The search for pulsations with a period between 32 ms and 10 s in the radiation of the object has not yielded a positive result. Assuming radio and X-ray radiation to be synchrotron, they obtained the values of the field $B = 2\ 10^{-4}$G and of the total electron energy $W = I.6\ 10^{47}$erg. A continuous energy injection from the central source follows from the small synchrotron electron lifetime as compared with the SNR age.

4.5. Molecular clouds.

In the paper by Dogiel et al. (8.2 - 17) giant molecular clouds are interpreted not as passive targets for relativistic particles, but as active objects which accelerate CR up to $\sim$ 10 GeV. The energy sources are hydrodynamic motions of a neutral gas which generate a chaotic magnetic field. The galactic CR that penetrate from without undergo a statistical acceleration, as a result of which the CR energy density increases by about an order of magnitude. This explains a hightened γ -luminosity of some molecular clouds (the expected γ -ray spectrum $F_\gamma(E) \backsim E^{-1}$ for $E > 100$ MeV). An intensified production of secondary particles in clouds could explain also an anomalous amount of $\bar{p}$, d, ^{3}He, e^+ in CR.

I most sincerely thank the organisers for their risk to invite me as a rapporteur at 19 ICRC. Very useful discussions with many colleagues are gratefully acknowledged. I am thankful to Marianna Tsaplina for her assistance in preparing this paper.

References

Armstrong J.W. et al. 1981. Nature, 291, 561.
Axford W.I. 1981, 17 ICRC, 12, 155.
Beresinsky V.S. 1979. Proc 1979 DUMAND Summer Workshop, ed. J.Learned, publ. by Hawaii DUMAND Center 1980, p. 245.
Beresinsky V.S., Mikhailov A.A. 1983, 18 ICRC, 2, 174.
Berezhko E.G. et al. 1983, 18 ICRC, 2, 259.
Bowen T. et al. 1983, 18 ICRC, 2, 96.
Buffington A. et al. 1981, Ap.J., 248, 1179.
Cesarsky C.J. 1980 Ann. Rev. Astr. Astrophys. 18, 289.
Chanmugam G., Brecher K. 1985 Nature 313, 767.
Drury L.O'C. 1983. Rep. Progr. Phys. 46, 973.
Eichler D. 1984, Ap. J. 277, 429.
Ellison D.C., Eichler D. 1984, Ap.J. 286, 691.
Gaisser T.K., Stanev T. 1985. Phys. Rev. Lett. 54, 2265.
Ginzburg V.L., Ptuskin V.S. 1984. J. of Astrophys. Astronomy 5.99.
Ginzburg V.L., Ptuskin V.S. 1985. Sov Sci. Rev. E. Astrophys. Space phys. 4, 161.
Ginzburg V.L., Syrovatsky S.I. 1964. Origin of Cosmic Rays. Pergamon Press.
Golden R.L. et al. 1979. Phys. Rev. Lett. 43, 1196.
Habe A., Ikeuchi S. 1980. Progr. Theor. Phys. 64, 1995.
Hillas A.M. 1984. Ann. Rev. Astr. Astrophys. 22, 425.
Hillas A.M. 1984. Nature, 312, 50.
Kazanas D., Ellison D.C. 1985. Nature (in press).
Kiraly P. et al. 1981. Nature 293, 120.
Krymsky G.F. 1981. Izv. AN SSSR, ser. fiz. 45, 461.
Lagage P.O., Cesarsky C.J. 1985. Astron. Astrophys. 147, 127.
Landau L.D., Lifshitz E.M. 1959. Fluid Mechanics. Pergamon Press.
Mauger B.G., Stephens S.A. 1983, 18 ICRC, 9, 171.
Mc Kenzie J.F., Volk H.J. 1982. Astron. Astrophys. 191.
Protheroe R.J., Clay R.W. 1985. Nature 315, 205.
Quenby J.J. 1984, Space Sci. Rev. 37, 201.
Rees M.J. 1984. Ann. Rev. Astr. Astrophys. 22, 471.
Sawada O. et al. 1981. Ap. J. 248, 1162.
Silberberg R. et al. 1983. Phys. Rev. Lett. 51, 1217.
Silk J., Srednicki M. 1984. Phys. Rev. Lett. 53, 624.
Sivaram C., Krishan V. 1982. Nature 299, 427.
Stecker F.W. et al. 1983. Astrophys. Space Sci. 96, 171.
Stephens S.A. 1981, 17 ICRC, 13, 89.
Volk H.J. 1981 17 ICRC, 13, 131.
Volk H.J., Drury L.O'C., Mc Kenzie J.F. 1984. Astron. Astrophys. 130, 19.
Wdowczyk J., Wolfendale A. 1984. J.Phys. G. 10, 1453.

PARTICLE ACCELERATION BY THE SUN

Rapporteur paper for the 19th International Cosmic Ray Conference

R. P. Lin

Space Sciences Laboratory, University of California, Berkeley, CA 94720

I. Introduction

Large solar flares are the most energetic natural particle accelerators in the solar system, occasionally accelerating ions to many GeV and electrons to $\gtrsim 10^2$ MeV energies. Radio, X-ray and gamma-ray, and energetic particle observations obtained before the 1980 solar maximum suggest that there are at least two acceleration processes associated with solar flares. During the impulsive or flash phase electrons are often accelerated to ~10-100 keV energies, even in small flares or subflares. For some flares, the energy contained in these electrons may be a substantial fraction of the total flare energy. Thus the primary energy release mechanism for flares may initially convert stored magnetic energy into energetic electrons. These electrons can produce most of the observed impulsive phase flare phenomena through their interactions with the solar atmosphere. In large flares a second acceleration sometimes occurs which accelerates both ions and electrons to MeV energies and above. This second acceleration appears to have a close association with shock waves in the solar atmosphere as observed by type II radio bursts. Based on observations of escaping particles and hard X-ray and gamma ray bursts, the impulsive phase acceleration events occur on the order of $\sim 10^2$ time a month near solar maximum while large solar energetic particle (LSEP) events where >10 MeV ions and relativistic electrons are accelerated to observable levels occur a few times a month.

Gamma-ray observations from the SMM spacecraft in this solar maximum, however, indicate that the delays between electron and ion acceleration can sometimes be very short, ~1 s, so the separation into two types of acceleration may not be meaningful. Furthermore, the relationship between the solar energetic particles observed in interplanetary space and those which produce gamma-ray and neutrons at the Sun is unclear. Often intense gamma-ray events are observed to be associated with small energetic particle events in the interplanetary medium and vice versa.

Solar ^{3}He-rich events may represent a different type of particle injection and/or acceleration process from those discussed above. Such events have $^3He/^4He$ ratios of order unity while the typical ratios for the solar atmosphere or solar wind are a few times 10^{-4} or less. Because the particle fluxes in ^{3}He-rich events are generally quite low, these events are usually detected only by averaging over from several hours to a day. Thus the flares or other solar phenomena associated with ^{3}He-rich events have been difficult to identify. Recently, however, *Reames et al.* (1985) have found that virtually all ^{3}He-rich events are associated with impulsive ~2 to 10^2 keV electron events.

Most of the papers presented at this conference dealt with the analyses of new observations of energetic particles and energetic secondary emissions obtained over this solar maximum (~1980) by the SMM, Hinotori, ISEE, IMP, Helios and Voyager spacecraft. In this rapporteur paper I have divided the subject into the following categories: 1) solar energetic particle events observed in space; 2) ^{3}He-rich

events; 3) solar gamma-rays and neutrons; 4) theoretical work; 5) solar neutrinos; and 6) summary. In addition the reader is referred to the invited talk by Dr. E. Chupp on gamma-ray and neutron observations from the SMM spacecraft, and a highlight talk by Dr. Stone summarizing the new developments in solar energetic particle composition.

II. Large Solar Energetic Particle Events

Information on the acceleration process for LSEP events is provided by measurements of the energy spectrum, elemental and isotopic composition, and charge states of the accelerated particles, and by observations of the solar phenomena associated with the acceleration.

Kahler et al. (SH 1.3-7) showed an unambiguous case of a LSEP with >50 MeV protons and relativistic electrons which was not accompanied by a solar flare or active region or any impulsive phase phenomena (Figure 1). Only a disappearing filament and classic Hα double ribbon emission was observed on the solar disk, while a coronal mass ejection and weak interplanetary type II radio emission was observed. These phenomena suggest that the LSEP acceleration process occurred high in the corona, presumably associated with the passage of the shock wave which produced the type II radio emission. No strong complex surface magnetic fields or impulsive phase acceleration of electrons to $\sim$10-10^2 keV was necessary.

Measurements of the charge states, q, for $\sim$1 MeV nucleon ions (*Luhn et al.*, SH 2.1-11) in 12 LSEP events indicate that the ions come from regions with equilibrium temperatures of typically $\sim 2 \times 10^{6}$°K, although for a couple of elements, Ne and Mg, the inferred equilibrium temperatures are higher (Figure 2). Thus the charge state measurements indicate LSEP acceleration generally occurs in the quiet corona rather than the $\sim 10^{7}$°K flare plasma, consistent with the picture of acceleration by shock waves passing through the high corona. Also consistent with this picture is the complete absence of deuterium and tritium in LSEP events; ^{2}H and ^{3}H would be

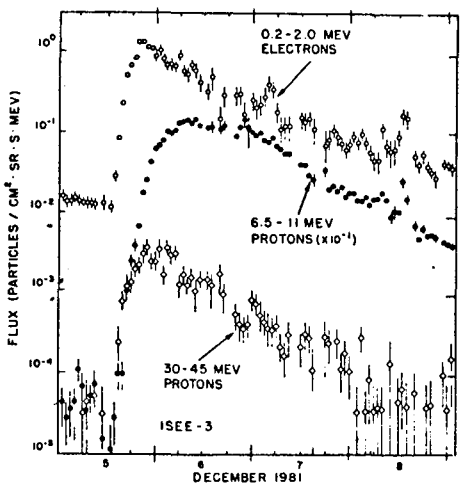

Figure 1. Flux-time plots of energetic particles for the SEP of 1981 December 5 (*Kahler et al.*, SH 1.3-7).

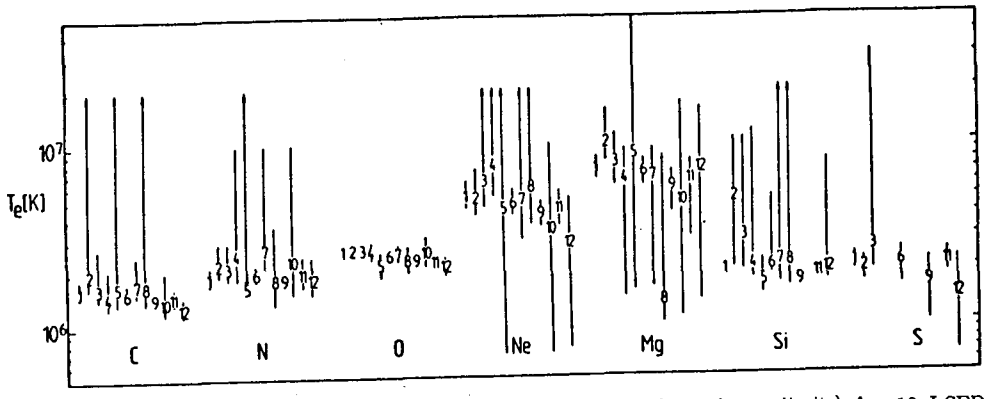

Figure 2. Equilibrium temperatures (95% confidence intervals or lower limits) for 12 LSEP periods (*Luhn et al.*, SH 2.1-11).

produced by spallation if the accelerated particles had passed through significant amounts ($\gtrsim$0.1 g/cm^2) of matter.

The papers by *Breneman and Stone,* (SH 2.1-4, 2.1-5) show that the observed elemental abundances and their variation from one LSEP event to another can be understood if the charge state of each element is taken into account. Using *Luhn et al.'s* (SH 2.1-11) average charge state measurements for each element, they show that the elemental abundances for a given LSEP event differ from the elemental abundances averaged over all LSEP events in a way which depends systematically on q/m (Figure 3). The interpretation of this result is that the combined effects of particle acceleration and propagation gives rise to a rigidity dependence which varies from one LSEP event to another, while the underlying source elemental abundances remain essentially invariant. It is well known from previous studies (see *Meyer,* 1984a,b) that when LSEP elemental abundances are plotted versus the first ionization potential (FIP) there is a depletion compared with solar photospheric abundances for elements with a FIP above ~10 eV. *Breneman and Stone* normalize the average elemental abundances for low FIP elements to photospheric abundances to remove the average q/m dependence. The resulting normalized LSEP abundances for elements with both high and low FIP are consistent with known coronal abundances, again

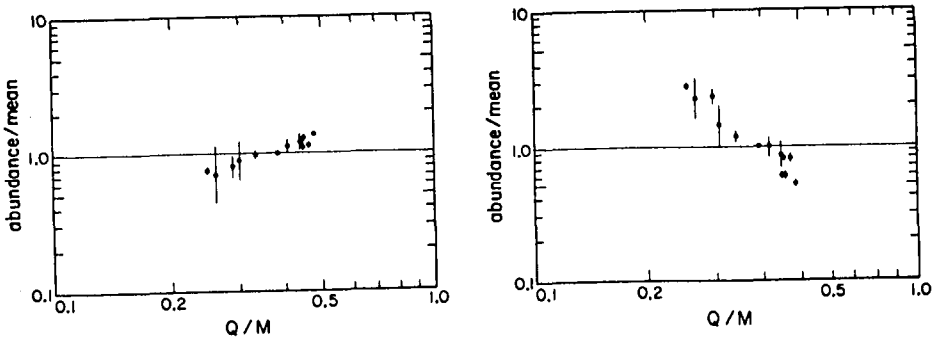

Figure 3. Abundances relative to the mean SEP abundance for two typical flares, plotted vs. q/m (*Breneman and Stone,* SH 2.1-4).

consistent with the idea of LSEP being accelerated out of normal coronal material.

The coronal structure of flares has been studied by soft X-ray (SXR) imaging telescopes aboard the Skylab (*Pallavicini et al.*, 1977). They find that two classes of flares can be distinguished in the soft X-ray images: (1) impulsive, compact, low-lying ($\lesssim 10^4$ km) flares with small volume ($\sim 10^{26} - 10^{27}$ cm^3), high energy density ($\sim 10^2 - 10^3$ ergs/cm^3), and durations of $\lesssim$tens of minutes in soft X-rays; and (2) long duration (~hours) flares with larger volumes ($10^{28} - 10^{29}$ cm^3), lower energy density ($\sim 10 - 10^2$ ergs/cm^3) located high in the corona ($\sim 5 \times 10^4$ km). These long duration SXR flares are known to accompany coronal mass ejections. *Cane et al.* (SH 1.2-12) find that all the LSEPs with 9-23 MeV proton fluxes greater than ~1 (cm^2 sec ster MeV)$^{-1}$ come from long duration SXR's. On the other hand the distributions of relativistic electron fluxes for the impulsive and long duration SXR types were almost the same. The LSEP's with impulsive SXR have previously been termed "electron rich" but a better label would be proton poor. A number of the LSEP's with impulsive SXR are associated with gamma-ray flares. It was noted that LSEP events with either impulsive and long duration SXR were generally (~80%) accompanied by type II radio emission indicating the presence of a shock wave. Many of the long duration SXR events were not accompanied by normal impulsive phenomena, i.e. type III or V radio bursts, while the impulsive SXR events usually had accompanying type III/V emission.

Evenson et al. (SH 1.2-14) found that the shape of the energy spectrum of relativistic electrons ($\sim 0.1 - 10^2$ MeV) in LSEP events also depended on whether the accompanying SXR event was impulsive or long duration. Following the method of *Lin et al.* (1982), the electron spectrum was constructed by taking the electron flux at the time of maximum (TOM) for each energy interval. For diffusive propagation with negligible energy loss the TOM spectrum reflects the injection spectrum at the Sun if the spatial dependence of the diffusion coefficient is approximately the same at all energies. Long duration SXR events produced power laws in momentum in the relativistic electron spectrum, while impulsive SXR produced power laws in energy (Figure 4). Thus there appear to be clear differences in the energetic particle emission depending on the spatial structure of the associated flare phenomena at the Sun.

The energy spectrum of LSEP protons has previously been studied by *McGuire and von Rosenvinge* (1984) who find that the characteristic Bessel function shape which is expected from stochastic acceleration generally fits the TOM spectra from ~1 MeV to $\gtrsim$80 MeV (Figure 5). They note, however, strong shocks can give a similar shape at those energies. The power law in momentum observed for electrons is also consistent with shock acceleration.

III. ^{3}He-rich Events

Solar ^{3}He-rich events represent one of the most striking composition anomalies among the observed populations of solar and interplanetary energetic particles, with ratios of the neighboring isotopes ^{3}He/^{4}He of order unity. Since the last cosmic ray conference, *Reames et al.* (1985) have found that virtually all solar $\gtrsim$1.3 MeV per nucleon ^{3}He-rich events observed by the ISEE 3 spacecraft are associated with impulsive ~2 to 10^2 keV electron events, although many electron events were not accompanied by detectable ^{3}He increases (Figure 6). Both the ^{3}He and the electrons exhibit nearly scatter-free propagation in the interplanetary medium, and the times of onset and maximum for the ^{3}He and electron increases are closely related by

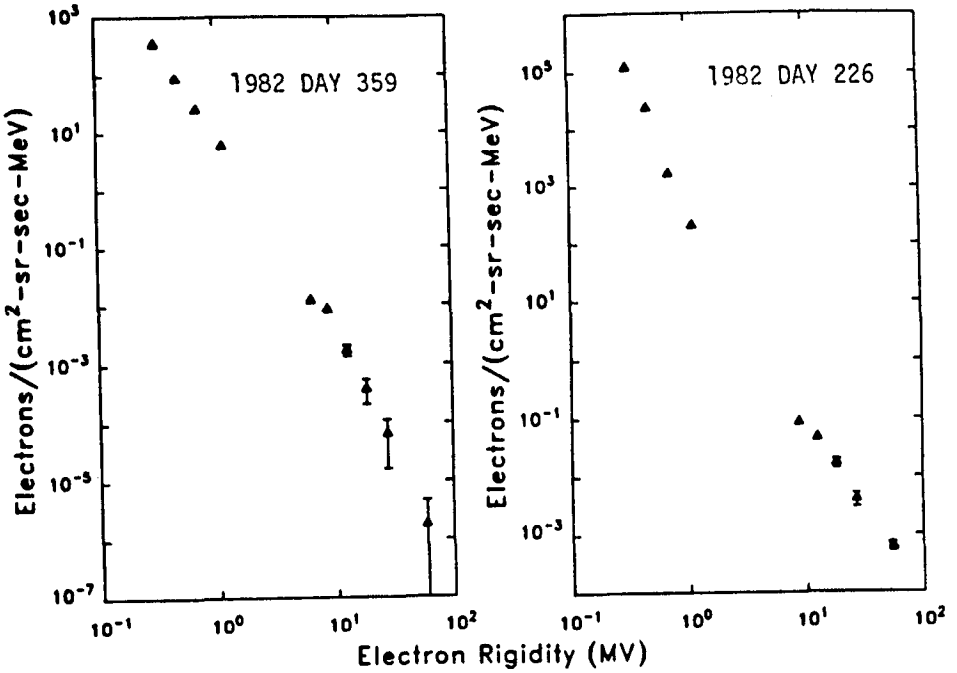

Figure 4. *(a)* Flare rigidity spectrum of a typical long duration SXR event. *(b)* Flare rigidity spectrum of a typical impulsive SXR event (*Evenson et al.*, SH 1.2-14).

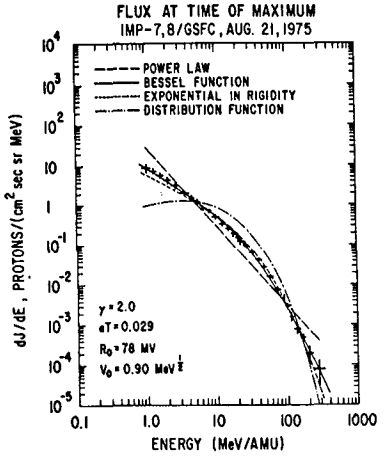

Figure 5. TOM spectrum and spectral fits for the event of 21 August 1975. The source flare was located at N26W74 (*McGuire and Von Rosenvinge*, 1984).

velocity dispersion. The electron events and their related type III solar radio bursts provide, for the first time, identification of the flares which produce ^{3}He-rich events. Thus ^{3}He appears to be accelerated at the impulsive phase of solar flares along with nonrelativistic electrons.

Reames and Lin (SH 2.2-5) systematically studied 187 solar electron events and found ^{3}He present in over half of the events. They suggest that ^{3}He would be

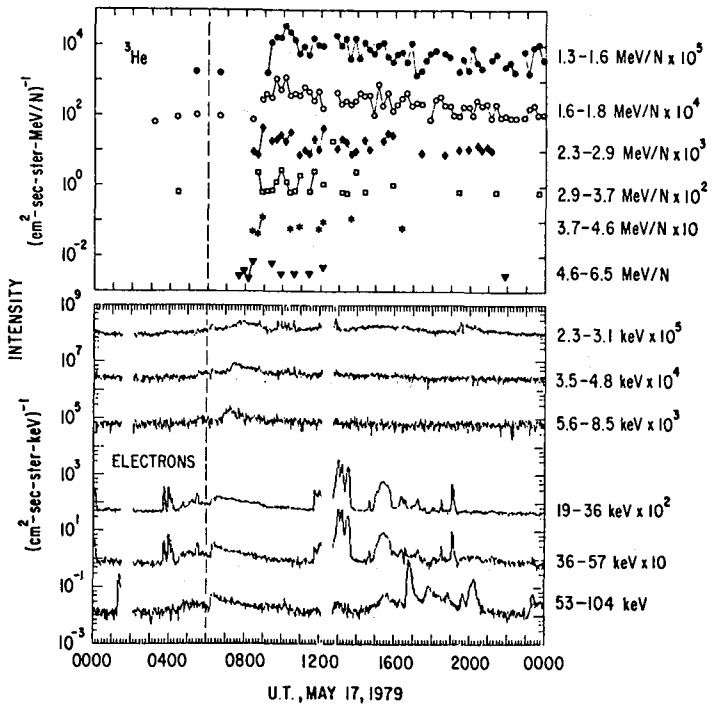

Figure 6. Time histories of the intensities of ^{3}He and electrons of the indicated energy during 1979 May 17. The appearances of the plots differ partly because of the absence of continuous background fluxes for ^{3}He. The lowest isolated points for each energy of ^{3}He represent one particle per 15 minute averaging period. The rapidly varying bursts (at ~1200 UT) observed in the higher, 19 keV, energy electron channels are due to particles from Earth's bow shock. The 53-104 keV channel also responds to solar X-rays (~0130, 1630-2030, and 2330 UT). The dashed vertical line indicates the time of the Type III solar burst. Intensity scale factors are shown to the right of the energies (*Reames et al.*, 1985).

found in all electron events if the ^{3}He detection sensitivity were better. *Reames and Stone* (SH 2.2-3) showed that in the absence of electron data, the kilometric wavelength type III bursts could be used to identify the associated flare event at the Sun. One of the events so identified is also a gamma-ray flare event. *Kahler et al.* (SH 2.2-4) studied the solar source of the ^{3}He-rich events identified by *Reames et al.* (1985) and suggest that the particle acceleration may be occurring high in the corona above the Hα flare.

Luhn et al. (SH 2.2-8) measured the mean ionic charge of silicon measured over 22 ^{3}He-rich periods in 1978-79 to be $\overline{q} \approx 14$, i.e. essentially fully ionized. The ionic charge state of iron for ^{3}He-rich flares had been previously reported to be $\overline{q} \approx 20.5$. These values are inconsistent with resonant heating by harmonics of He-cyclotron waves (*Fisk*, 1978), but are consistent with the source region for ^{3}He-rich flares having a temperature of $\sim 10^7$°K, well above the $\sim 2 \times 10^6$°K temperature inferred for normal LSEP flares.

Mason et al. (SH 2.2-7) surveyed the elemental abundances for 66 ^{3}He-rich flares observed by ISEE 3 in 1978-82 (Figure 7). It is known that He-rich flares show a tendency to be enriched in heavy ions. The enhancements over normal LSEP

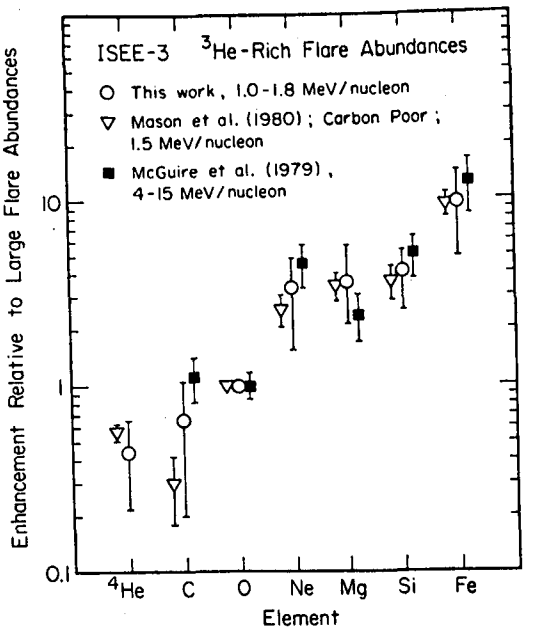

Figure 7. From *Mason et al.* (SH 2.2-7).

abundances increase with A or Z from He to Fe. *Mason et al.* show that the heavy ion abundances do not vary very much from flare to flare compared with the variation in the $^3He/^4He$ abundance. Furthermore the heavy ion abundances do not vary much with energy over the measured range of ~1 to 15 MeV/nucleon. This lack of significant variation in heavy ion abundances suggests that heavy ion enrichments are present in the ambient source plasma where ^{3}He-rich flares occur.

When ^{3}He-rich events are compared with normal LSEP events in, a consistent picture seems to emerge. ^{3}He-rich events occur in hot plasmas, $\gtrsim 10^7$°K, where most heavy elements will be fully ionized. Because q/m would then be ~1/2 for essentially all the measured heavy ions, the acceleration mechanism, which appears from LSEP events to be rigidity dependent and highly variable from flare to flare, does not alter the source composition. The high temperature, $\sim 10^7$°K, and consistent pattern of heavy ion enrichment (which must include a significant ^{4}He/H enrichment so the ^{3}He can be preferentially heated via Fisk's cyclotron resonance mechanism) are clues to the region of the solar atmosphere where the acceleration takes place. The fact that these ^{3}He-rich events appear to be closely associated with impulsive phase electron events suggests that the ^{3}He acceleration process is the same as that which accelerates the $\sim 1\text{-}10^2$ keV electrons in the impulsive phase of solar flares. It may be significant that very few ^{3}He-rich events are accompanied by shock waves.

IV. Gamma-rays and neutrons

Accelerated protons, alphas, and heavier nuclei with energies above ~10 MeV produce gamma-ray lines and neutrons via interactions with the solar atmosphere. Energetic electrons produce hard X-ray and gamma-ray continuum via

bremsstrahlung. Measurements of gamma-rays and neutrons provide unique information on the nuclear acceleration and interaction processes at the Sun. Since 1980 the SMM and Hinotori spacecraft have provided a wealth of new data on solar gamma-rays, neutrons, and other high energy neutral emissions. The results have been summarized by Dr. Chupp in his invited talk. The main points pertaining to the acceleration of particles at the Sun are:

1) Both electrons and ions are often accelerated together in the impulsive phase of the flare.

2) The acceleration can occur in seconds for both electrons and ions.

3) The maximum energies reached by the acceleration is in the GeV range for ions and $\sim 10^2$ MeV for electrons.

4) The relativistic electrons appear to exhibit evidence for directivity.

5) The spectrum of the accelerated ions at the Sun appears to show a steepening with energy which is consistent with a Bessel function shape comparable to those observed for LSEP events (Figure 5). The proton fluxes at the Sun inferred from the gamma-ray and neutron observations, however, are poorly correlated to the escaping LSEP fluxes observed in interplanetary space.

6) There is approximate proportionality between the 4-7 MeV continuum flux, which is primarily nuclear in origin, and the >0.27 MeV electron bremsstrahlung continuum flux. Chupp interprets this correlation to mean that ions may be accelerated to $\gtrsim 10$ MeV in every flare. Only relatively intense flare events, however, are detectable by the nuclear gamma-ray measurements and to a lesser extent, by the >0.27 MeV bremsstrahlung continuum measurements. *Bai and Dennis* (1985), using had X-ray (>30 keV) data, argue that the gamma-ray line flares have characteristics which distinguish them from normal flares.

Neutrons with energies ~ 1 GeV have been detected by the Jungfraujoch ground-based neutron monitors from the 3 June 1982 flare, while protons from the decay of solar neutrons have been detected for three separate flares by the ISEE 3 spacecraft (*Evenson et al.,* SH 1.2-4). This latter type of measurement gives the most accurate neutron energy spectrum since essentially all of the neutron energy is carried by the decay proton.

McDonald et al. (SH 1.3-8), *Van Hollebeke et al.* (SH 2.1-3), and *Neustock et al.* (SH 1.3-9) used data from the Helios I spacecraft to examine the energetic solar particles associated with the gamma-ray flares. The Helios I spacecraft was located close to the Sun, $\lesssim 0.5$ AU, and close in heliolongitude to the flare site for the gamma-ray flares of 7 and 21 June 1980 and 3 June 1982, so any escaping particles should be easily detectable. *McDonald et al.* and previously *McDonald and Van Hollebeke* (1985) note that small precursor energetic particle events were observed several hours prior to all three of these gamma-ray flares (these precursor events would not be detectable at 1 AU), and thus the acceleration of an existing reservoir of stored energetic (up to 60 MeV) particles could be involved in these gamma-ray flares. In support of models of re-acceleration it should be noted that the spectrum of the ions in those LSEP events is unusually hard (Figure 8). For the 3 June 1982 event, the spectrum of the escaping protons (power law exponent ~ 1.2 up to 200 MeV) appears to be inconsistent

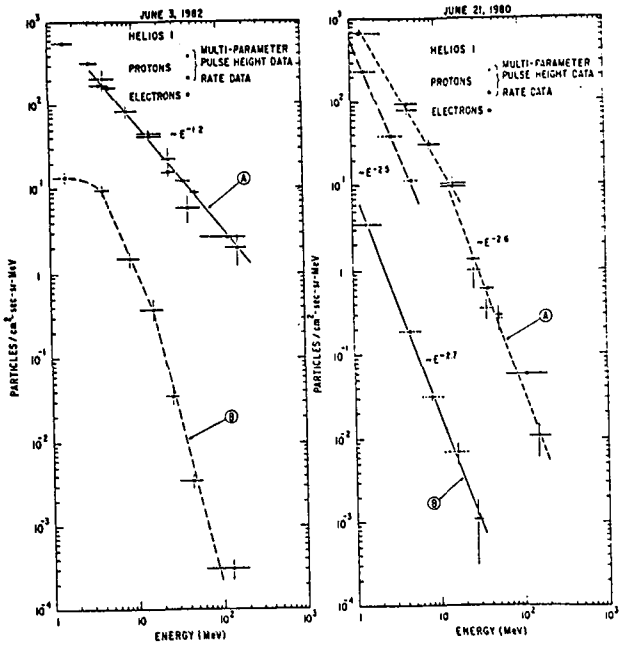

Figure 8. Energy spectra measured at the time of peak intensity for each energy interval. The measured particle anisotropy at this time is still ~60%, so convective equilibrium has not been established. For each panel the upper plot is the spectral data for the main event, and the lower data set is for the precursor event (*McDonald and Van Hollebeke*, 1985).

with the spectrum inferred from the gamma-ray and neutron observations of the impulsive phase and may require extended acceleration (*Ramaty and Murphy*, 1985). *Chupp et al.* (SH 1.4-1) and *Forrest et al.* (SH 1.4-7) show evidence from SMM for the extended production of both neutrons and pions for $\gtrsim$5 minutes beyond the impulsive phase for the flare of 3 June 1982 while electron bremsstrahlung at energies above ~10 MeV was observed only during the impulsive phase (Figure 9). The additional acceleration after the impulsive phase may have produced the hard proton spectrum observed at Helios I; *Forrest et al.* point out that ~80% of the neutral pion decay photons were observed after the impulsive phase.

McDonald et al. also point out that significant amounts of ^{3}He are observed for 3 June 1982 and 21 June 1980 as well as unusually high abundances of Fe relative to oxygen. This Fe/O enhancement is comparable to that observed for ^{3}He-rich events.

Neustock et al. (SH 1.3-9) studied the time of injection of electrons and ions on 7 June 1980. The particle fluxes were highly anisotropic, streaming along the magnetic field away from the Sun. The travel time for each particle species was subtracted to obtain a solar release time (SRT). For each of the three major flares (0117, 0302, 0725 UT) the ~0.5 MeV electron injection began promptly (within one minute) at the impulsive flare hard X-ray burst time but lasted at least several minutes longer. The 3-20 MeV protons were injected promptly at the time of the third flare, but showed three separate delayed "injections" (0345, 0440, 0635 SRT) for the second

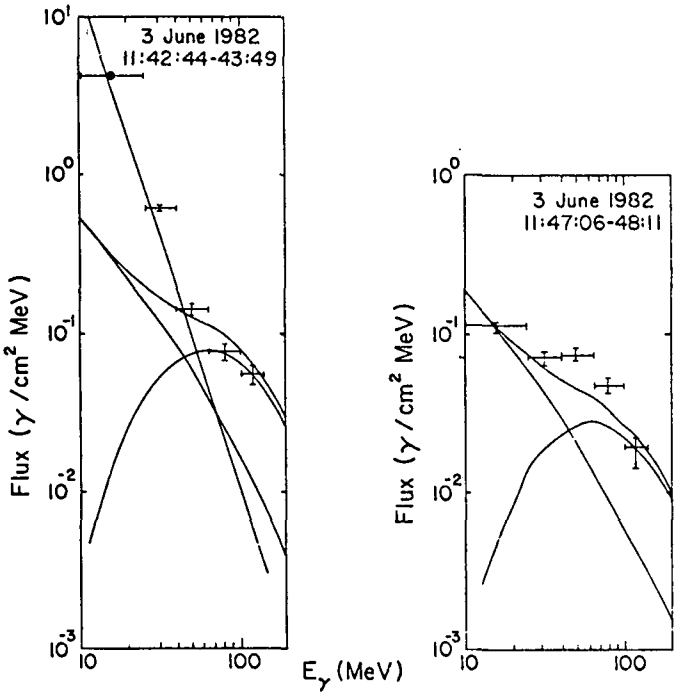

Figure 9. *(a)* The 10-140 MeV photon spectrum for the impulsive phase of the 3 June 1982 flare. The steeply falling line is a power-law fit to the electron bremsstrahlung component; the other curves are fits to the neutral pion decay component. *(b)* The 10-140 MeV photon spectrum for the extended phase, ~5 minutes after the impulsive phase. The spectrum is consistent with a pure pion decay origin without any electron bremsstrahlung component (*Forrest et al.*, SH 1.4-7).

flare (Figure 10). These delayed "injections" showed no velocity dispersion, i.e. protons of all energies were seen at Helios at the same time. One possible interpretation is that the second flare probably filled only certain channels of interplanetary field lines with energetic protons, which were then crossed by Helios. Similar channels

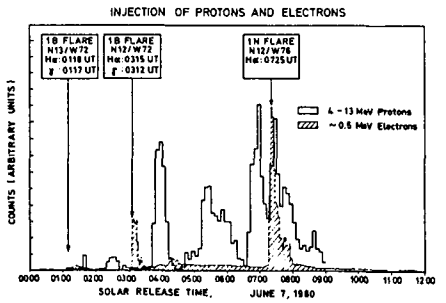

Figure 10. Solar injection of electrons and protons for the 7 June 1980 event, after correction for interplanetary travel time along the smooth interplanetary magnetic field. Solar release Time (SRT) $= -s/v$ (*Neustock et al.*, SH 1.3-9).

have been identified in ISEE 3 solar electron measurements at 1 AU (*Anderson and Dougherty,* SH 3.2-3). Finally, only the first two flares had detectable >0.3 MeV gamma-ray emission, and only the second emitted nuclear lines, but the third flare gave rise to the most intense particle event at Helios I. These fairly direct measurements of the energetic particles escaping from gamma-ray flares suggest that if the escaping and gamma-ray producing particle populations are produced by the same acceleration, then the height of the acceleration region must vary from flare to flare.

Gamma-ray line measurements provide a new method to obtain solar elemental abundances. Narrow lines are produced by the interactions of energetic protons and alphas with ambient heavy nuclei. Since the nuclear processes which produce gamma-ray lines are essentially unaffected by ambient conditions, and the theory and cross-sections for these processes are well-known, measurements with high spectral resolution ($\Delta E/E \sim 10^{-3}$) could provide accurate abundance determinations for the solar atmosphere. Even with the relatively poor spectral resolution ($\Delta E/E \sim 7\%$) of the SMM GRS instrument, *Murphy et al.* (SH 2.1-13 and -14) were able to determine the abundances of C, O, Ne, Mg, Si, Fe and O to ± 10-30%, and to show that they are significantly different from local galactic (solar) abundances, but consistent with coronal abundances.

V. Theoretical work

Since the gamma-ray measurements by SMM showed that ions are often accelerated to energies of well above ~100 MeV nearly simultaneous (within seconds) with the impulsive phase electrons, one of the key questions has been whether stochastic shock acceleration models are rapid enough. The theoretical contributions reported here suggest that shock acceleration can accelerate ions to >10 MeV energies in times $\lesssim$1 s. *Decker and Vlahos* (SH 1.1-6) show by numerical simulations of their turbulent oblique shock model that protons can be accelerated from a 100 keV injection energy to $\gtrsim$10 MeV in as short a time as ~6 msec when the shock is quasi-perpendicular. *Ellison and Ramaty* (SH 1.1-5) find that their first order Fermi shock acceleration model can reproduce the observed LSEP energy spectra for electrons, alphas, and protons for a given flare with a single shock compression ratio. They also find that the acceleration time up to ~100 MeV can be as short as ~1 s from an assumed injection energy of ~100 keV. *Droge and Schlickeiser* (SH 1.1-4) propose a combination of first and second order Fermi acceleration in shock waves. They are able to reproduce the observed correlation (*Lin et al.,* 1984) between the high and low energy spectral indices in the double power law spectrum of electrons, and the correlation between electron low energy spectral indices and proton spectral indices. As in the other models an initial injection energy is assumed; here it is 50 keV.

The question of the injection of low energy ions may be important for flare energetics as well. Low energy ~10-100 keV electrons can be observed at the Sun via the bremsstrahlung X-rays they produce. Ions below ~10 MeV, however, are essentially invisible at the Sun. *Simnett* (SH 1.2-13) argues that protons of ~10-1000 keV rather than electrons may in fact contain most of the flare energy. Computations by *Canfield and Chang* (SH 1.3-5) indicate that it may be possible to detect ~10-10^3 keV protons which are beamed downward into the solar atmosphere, via the Doppler shifted Lyman alpha radiation they produce in the process of electron pickup and loss. Clearly information on this component would be very useful.

VI. Solar Neutrinos

The solar neutrino experiment of *Davis et al.* (1983) has now been taking data for more than fifteen years with the well known result that the observed average flux of solar ^{8}B-neutrinos is only about 1/3 of that expected from standard solar models. The measurements are taken over periods of several months at a time and although the uncertainties in the data points are very large, it is remarkable that the three intervals with the largest production rates include the largest solar energetic particle events observed over that period (Figure 11). The expected production of neutrinos by the observed solar energetic particles themselves, either at the Sun or at the earth, falls many orders of magnitude below the observed increases. There remains a possibility that some process associated with very large energetic particle flares occurs beneath the photosphere to produce an increase in the neutrino flux. It would be highly desirable to determine if the association of high neutrino count rates with the largest LSEP's is in fact statistically significant.

VII. Summary

It is highly likely that the acceleration of LSEP particles is due to the passage of shock waves through the quiet corona. For a significant number of LSEP events no impulsive phase is observed. This suggests that injection of particles at suprathermal energies (50-100 keV) is not required. The acceleration process might thus be similar (but scaled up from) that observed at the earth's bow shock, where reflection of a small fraction of the solar wind thermal particles by the jump in the magnetic field at the shock apparently provides the seed population for further acceleration, which may occur via a Fermi process (see *J. Geophys. Res.*, volume 86, number A6). The spatial structure of the related solar flare or transient appears to play an important role in the acceleration process, both in determining the energetic particle fluxes which escape to the interplanetary medium and, for electrons, their energy spectrum.

The acceleration process in ^{3}He-rich events appear to be distinctly different. It occurs in regions of high, $\gtrsim 10^{7°}$K, temperatures with a characteristic pattern of enhancement of the abundances of heavy elements from He to Fe. The acceleration

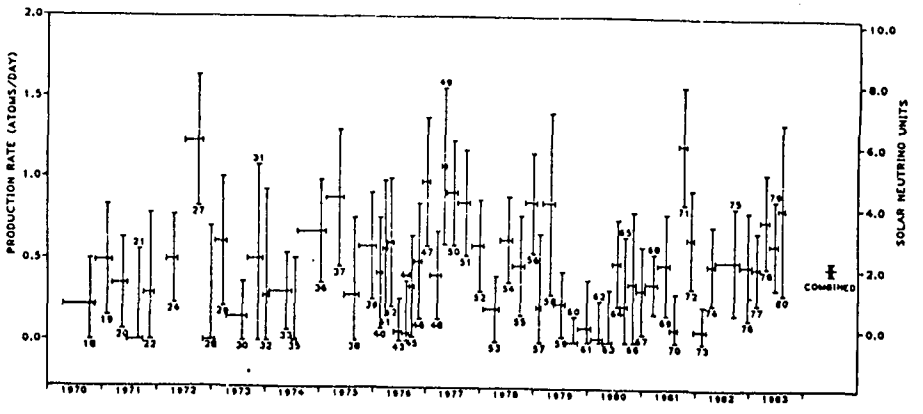

process also accelerates electrons to non-relativistic $10\text{-}10^2$ keV energies, and occurs during the impulsive phase of flares. This acceleration appears not to be shock related.

Solar gamma-ray events are generally associated with flares having intense impulsive phase phenomena, and often with impulsive, compact soft X-ray flare sources. Shock waves (i.e., type II radio emission) generally are observed as well. Often some ^{3}He and heavy element enrichments are observed from gamma-ray flares. It seems plausible that shock waves passing through low-lying compact flare structures result in an intense, rapid second-step acceleration which leads to the highly energetic ions and electrons required for the gamma-ray production. Such second step acceleration is suggested by the short delays ($\sim$1 s) that are commonly observed in the $\gtrsim$100 keV hard α-ray emission for gamma-ray flares (*Bai and Dennis,* 1985).

Gamma-ray and neutron observations from SMM and Hinotori have proved to be a powerful complement to detailed energetic particle measurements in interplanetary space for probing solar particle acceleration mechanisms. Furthermore, both types of measurements show great potential for providing highly accurate elemental and isotropic abundance measurements for the Sun. Powerful new observational techniques for measurement of both particles and photon emissions are now available to provide the next leap forward, and it is my hope that the opportunity to make that leap will come in the next solar maximum.

Acknowledgments

I wish to acknowledge useful discussion with E. Stone, R. Murphy, F. McDonald, G. Wibberenz, and R. McGuire, among others. This research was supported in part by NASA grant NAG 5-376.

References

Bai, T., and B. Dennis, 1985, *Astrophys. J., 292,* 699.

Davis, R., Jr., B. T. Cleveland, and J. K. Rowley, 1983, *Science Underground,* AIP Conf. Proc. No. 96, p. 2 (ed. M. M. Nieto *et al.*), Amer. Inst. Phys., New York.

Fisk, L. A., 1978, *Astrophys. J., 224,* 1048.

Lin, R. P., R. A. Mewaldt, and M. A. I. Van Hollebeke, 1982, *Astrophys. J., 253,* 949.

McDonald, F. B., and M. A. I. Van Hollebeke, 1985, *Astrophys. J., 290,* L67.

McGuire, R. E., and T. T. Von Rosenvinge, 1984, *Adv. Space Res., 4,* 117.

Meyer, J.-P., 1985*a*, *Astrophys. J. Suppl., 57,* 151.

Meyer, J.-P., 1985*b*, *Astrophys. J. Suppl., 57,* 173.

Pallavicini, R., S. Serio, and G. S. Vaiana, 1977, *Astrophys. J., 217,* 108.

Ramaty, R., and R. J. Murphy, 1985, *Adv. Space Res., 4,* 127.

Reames, D. V., T. T. Von Rosenvinge, and R. P. Lin, 1985, *Astrophys. J., 292,* 716.

CORONAL AND INTERPLANETARY PROPAGATION, INTERPLANETARY ACCELERATION, COSMIC-RAY OBSERVATIONS BY DEEP SPACE NETWORK, AND ANOMALOUS COMPONENT

C. K. Ng

Dept. of Mathematics, University of Malaya
Kuala Lumpur 22-11, Malaysia

1. Introduction

The purpose of this rapporteur paper is to provide an overview of the contributions presented in sessions SH3, SH1.5, SH4.6 and SH4.7 of the 19th International Cosmic Ray Conference. These contributed papers indicate that steady progress continues to be made in both the observational and the theoretical aspects of the transport and acceleration of energetic charged particles in the heliosphere.

Studies of solar and interplanetary particles have placed emphasis on particle directional distributions in relation to pitch-angle scattering and magnetic focusing, on the rigidity and spatial dependence of the mean free path, and on new propagation regimes in the inner and outer heliosphere. Coronal propagation appears in need of correlative multi-spacecraft studies in association with detailed observation of the flare process and coronal magnetic structures. Interplanetary acceleration has now gone into a consolidation phase, with theories being worked out in detail and checked against observation.

With the approach of the solar minimum, and with the Pioneers and the Voyagers spacecraft advancing steadily towards the heliospheric boundary, observation of the galactic cosmic rays and the anomalous component will soon, we hope, help to unravel the mystery of solar modulation (see Kota, 1985).

2. Coronal And Interplanetary Propagation

Flare-associated solar energetic particles (SEP) are usually assumed to have been accelerated at the sun, and to have subsequently propagated through the corona and interplanetary space before being detected. Theories tend to treat these three processes separately, using the result of the preceding stage as input to the subsequent stage.

It is however a complicated task to isolate the effects of the three processes from the observations because of the uncertainty and great variability from event to event in the flare process, and in the conditions of the corona and interplanetary space. In some cases, a large-scale shock is observed to propagate through the corona and interplanetary space. If particles are continuously accelerated by the shock on open field lines, coronal acceleration and propagation may be intrinsically inseparable, and one must also take account of the shock as a moving particle source and reflector in interplanetary space.

2.1 Coronal Propagation

Since the mid-sixties, coronal propagation has been studied by finding the dependence of the observed onset times, rise times, energy spectra and abundance ratios of SEP events on heliographic angular separation from the flare site. The angle dependence is deduced by (a) statistical analysis of single-spacecraft data from many events, or (b) concurrent multi-spacecraft data of individual events. In addition, the

coronal diffusion coefficient $K_\odot$ and coronal escape rate η have been determined for many events, using single-spacecraft data on concurrent intensity and anisotropy time histories.

The statistical studies have established the east-west asymmetry of the onset time and rise time, the existence of the fast propagation region (FPR) at 0°W - 100°W, the variation of event size with angular separation, and the correlation of p/α ratio with event size (see Van Hollebeke, 1979, and references therein). However, conflicting observations of the longitudinal variation of the proton spectra have been reported in both statistical and multi-spacecraft studies, and different conclusions regarding the rigidity and energy dependence/independence of the coronal propagation parameters have been made (see e.g. Mason *et al.*, 1984, and references therein). Nevertheless, it seems clear that the dependence of $K_\odot$ and η on energy and rigidity, if any, is weak. Some evidence seems to indicate that outside the FPR these parameters increase only with particle velocity.

The intensities and p/α ratios of solar particle events observed by the geostationary satellites GMS-1 and 2 from Feb 1978 to Sept 1984 are analysed in papers SH3.1-1 and 2 (unfortunately not presented). Using statistics from 50 events, Takenaka *et al.* (SH3.1-1) confirm the east-west effect in the rise-time and the existence of the FPR. Finding a possible correlation between short-rise time events and the occurrence of an SSC < 8 days before the events, they suggest the folowing interesting scenario. Particles from a western flare propagate rapidly in relatively smooth magnetic fields established behind an interplanetary shock, caused by a preceding eastern flare in the same active region. If confirmed, this would be relevant in interpreting the FPR and the east-west effect.

Kohno *et al.* (SH3.1-2) find that, in 14 out of 16 fast-rise events in the FPR, after adjustment for the Sun-Earth travel times, the protons in 5 energy channels between 8 to 500 MeV have almost identical intensity time profiles (Fig 1). Assuming that these reflect essentially the injection time profiles, the authors infer rigidity and energy independent coronal propagation in the FPR. We note that this appears contrary to the conclusion of Bazilevskaya & Vashenyuk (1979) for > 100 MeV protons. These onset delay times in the FPR bear no relation to angular separations from the flare site and appear consistent with the magnetic bottle model and the large-scale shock acceleration (LSSA) model (see below).

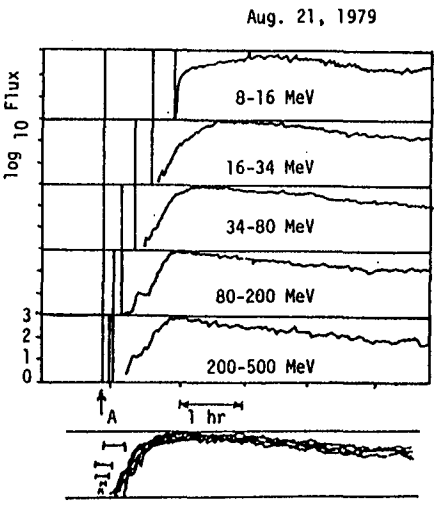

Fig 1

In paper SH3.1-3, Schellert *et al.* report on a statistical study of 36 events observed by Helios 1 and 2. From their plot of the time-to-maximum vs angular separation (Fig 2), they deduce that outside the FPR, for ~0.5 MeV electrons, $t_E t_D$ = 55 h², where t_E

and t_D are the coronal escape time and diffusion time respectively. The difference between this value and $t_E t_D$ = 800 h² for ~10 MeV protons (e.g. McGuire *et al.*, 1983; Ng and Gleeson, 1976), as well as the difference between concurrent proton and electron intensities observed on Helios 1 and 2 (their Fig. 3), show that the electrons propagate faster than the protons in the corona, leading Schellert *et al.* to reject species-independent models like the bird-cage model and the large-scale shock model (see below). From the wide range of the observed angular gradients of the maximum intensity of ~0.5 MeV electrons, apparently unrelated to the FPR (their Fig 2), Schellert *et al.* conclude that there is no universal process for coronal diffusion.

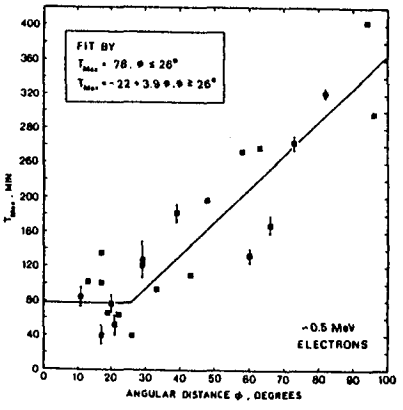

Fig 2

For the 4 Nov 1978 and 20 Nov 1978 events, when Prognoz-7 and Venera-11 were connected to neighbouring points in different unipolar magnetic field regions (UMRs) of the sun, these spacecraft observed an order of magnitude decrease in the fluxes and a large increase (~10 hr) in the rise time of ~5 MeV protons across the UMR boundary (Fig 3 from Morozova *et al.*, paper SH3.1-6, not presented). These authors deduce that the coronal propagation speed is ~ 140°/h in a UMR but drops to only 2 -5°/h across the boundary. We note that the observation may also be qualitatively consistent with the decreased efficiency of particle acceleration by a coronal shock after it has crossed a neutral sheet (Steinolfson and Mullan, 1980). It would be worthwhile to know if the UMR boundary has a similar effect on the electrons.

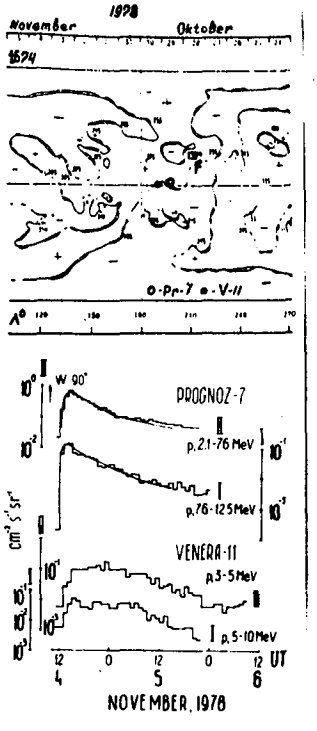

Fig 3

In summary then, the above conference papers have reported general observational confirmation of previous findings on the east-west effect and FPR, a possible correlation between fast-rise particle events and preceding SSC's, strong evidence for rigidity and energy independent injection of 8 - 500 MeV protons from the FPR, the species dependence of large scale coronal transport outside the FPR, and large attenuation in proton intensity time history across UMR boundaries.

To understand the observations, we shall discuss a few theoretical models. The angular dependence of the rise time and the event size outside the FPR can be explained by Reid's (1964) phenomeological model (called CODE model below). It assumes 2-D

particle diffusion in a thin spherical shell of radius a over the sun, with random escape into interplanetary space. The particle differential number density N(X,T,t), at kinetic energy T and heliographic angular separation X from the axis of a symmetric particle source, is governed by

$$\frac{\partial N}{\partial t} = \frac{1}{a^2 \sin X} \frac{\partial}{\partial X}\left(K_S \sin X \frac{\partial N}{\partial X}\right) - \eta N \qquad (1)$$

(Ng and Gleeson, 1976). Here $K_s(T)$ is the coronal diffusion coefficient and $\eta(T)$ the escape rate. It is customary to define the diffusion time $t_D = a^2/K_s$, and the escape time $t_E = 1/\eta$. The solution may be written in the form $N(X,T,t) = N_o(T)\, Q(X,\tau;g)$, where $N_o(T)$ is the source spectrum, and Q is a function which depends on the angle X, the dimensionless time $\tau = t/t_D$, and the dimensionless parameter $g = t_D/t_E$. For given X and T, Q and hence N attain maximum at $\tau = \tau_{max}(X;g)$, and $N_{max}(X,T) = N_o(T) Q[X,\tau_{max}(X;g);g]$.

The maximum injection rate into interplanetary space is $I_{max} = \eta N_{max}$, and its spectrum is given by

$$\frac{\partial \ln I_{max}}{\partial \ln T} = \frac{d \ln N_o}{d \ln T} + \frac{d \ln \eta}{d \ln T} - \tau_{max}(X;g)\, T \frac{dg}{dT} \quad . \qquad (2)$$

This equation is relevant for the interpretation of observations in terms of the CODE model. First, the injection spectrum at maximum may be modified from the source spectrum by an energy-dependent escape rate $\eta(T)$. Secondly, since $\tau_{max}(X;g)$ clearly increases with X, the spectrum softens with increasing X if and only if $dg/dT > 0$, i.e. t_D/t_E increases with increasing energy. This also means that the independence of the spectral index and p/∝ ratio on X do not in themselves imply rigidity-independent t_D and t_E. The conclusion only follows if one further establishes by *independent means* the rigidity independence of either t_D or t_E. For planar approximation and a point source,

$$Q(X,\tau;g) = (1/4\pi\tau)\, \exp\,(-X^2/4\tau \; - g\tau) \qquad (3)$$

(Reid, 1964). A spherical solution for a spatially extended source is given in Ng and Gleeson (1976).

The CODE model leaves the mechanism of coronal diffusion and escape unspecified. In Newkirk and Wentzel's (1978) 'bird-cage' model, particles are transported from magnetic loops to magnetic loops via field-line reconnection produced by the rearrangement of the field in the supergranulation network, resulting in rigidity and energy-independent K_s and η for < 40 MeV protons and < 80 MeV electrons.

In Mullan and Schatten's (1979) two-component model, (a) rigidity and energy independent transport in the FPR is due to the breaking of an expanding magnetic bottle ~ 15 min after a flare and (b) outside the FPR (X > 60°), the particles are scattered by magnetic inhomogeneities with scale sizes > 500 km, resulting in a coronal diffusion coefficient dependent on particle velocity but independent of particle mass. The particles also experience mainly east-west gradient and curvature drifts in the mainly north-south oriented large scale coronal loops.

In yet another model (LSSA model), suggested by Lin and Hudson (1976) and favored in a number of recent works (e.g. Mason *et al.*, 1984 , and references therein), a rapidly expanding (~ 1000 km/s) large-scale coronal shock accelerates particle on open field lines which lead directly into interplanetary space, thus obliterating the distinction

between coronal acceleration, propagation and escape.

As concluded in paper SH3.1-2, the magnetic bottle and LSSA models both appear consistent with the observed rigidity and energy independent particle injection from the FPR. It is possible that after breaking the bottle, the shock continues to accelerate particles on open field lines. However, according to Mason *et al.* (1984), the magnetic bottle model is inconsistent with the observed independence of abundance ratios (at ~ 1 MeV/nuc) on ionization loss in the corona.

Outside the FPR, the difference between the coronal transport of protons and electrons appears to support the two-component model (i.e. the CODE model). However, an *angle dependent* LSSA model may yet be consistent with this observation.

We must also point out here the important implication of the existence of two classes of flares demonstrated by Cane *et al.* in a different session (SH1.2-12). Class I flares are compact and occur low in the corona. Class II flares are diffuse, occur higher in the corona, and tend to be associated with coronal mass ejections. Whilst both classes of flares produce comparable electron events, Class I flares tend to produce far smaller proton events than Class II flares.

This suggests that coronal acceleration and transport depend on the altitude and the nature of the flare, and that more than one model of coronal acceleration/transport may be necessary. If so, the SEP data of Class I and Class II flares should be analysed separately for the effects of coronal acceleration/storage/transport.

From the above discussion, we see that progress has been made and it is hoped that a consistent picture of coronal transport will emerge in the near future. To this end, we need good angular and temporal resolution, that is, as complete as possible a set of *concurrent multi-spacecraft* data, including SEP directional intensities, spectra and composition, plasma flow (for mapping back to the corona), interplanetary and coronal magnetic fields, solar optical, radio, X and γ-ray emissions.

More theoretical work is also required. A clear quantitative difference between the predictions of the CODE model and the LSSA model is important for deciding between diffusive transport or shock acceleration outside the FPR. As the shock parameters (e.g. field-normal angle) should depend on heliographic angular separation, this fact should be taken into account in a quantitative LSSA model.

2.2 Interplanetary Propagation

After escaping from the corona to the solar-wind medium, solar energetic charged particles are guided and focused by the large-scale interplanetary magnetic field (IMF) and scattered by small-scale magnetic irregularities. Because of the large and small-scale electric fields induced by the motion of the IMF and magnetic irregularities, the particles also experience the $\underline{E}x\underline{B}$ drift, adiabatic deceleration and second order Fermi acceleration. The particles may also be reflected or transmitted at interplanetary shocks and experience energy changes during shock encounter.

In this section, we shall group the conference papers around the following headings and discuss them in that order: (a) interplanetary mean free path, (b) directional particle distributions, and (c) new propagation regimes.

2.2.1 Interplanetary Mean Free Path

In papers SH3.2-5, 3.1-8A and 3.2-9, the model of diffusion, convection and adiabatic deceleration (DCA model) is used to find the spatial and rigidity dependence of the radial mean free path λ_r from SEP events.

During the much studied 22 Nov 1977 event, Voyagers 1 and 2 at $\sim$ 1.5 AU and the earth are all well-connected to the flare site. Assuming an injection $\propto \exp(-t/\sigma)$ and a radial diffusion coefficient $K=K_o r^b$, Mason *et al.* (SH3.2-5) fit simultaneously the 0.6 -1 MeV/nuc helium intensities measured on ISEE 1 and Voyager 2, with the parameters σ = 12 ± 3 hrs, b = 1.3 ± 0.1 and λ_r = 0.10 ± 0.02 AU at 1 AU. Assuming rigidity-dependent $K_o \propto (A/Z)^{0.88}$, the intensity histories of 0.6 - 1 MeV/nuc H, C, O, and Fe are calculated (Fig 4). Except for proton (lowest rigidity) at both spacecraft and Fe (highest rigidity) at Voyager 2, all intensity fits are satisfactory. Mason *et al.* suggest rigidity-dependent interplanetary acceleration as the cause of the discrepancy.

For the same event, Hamilton *et al.* (SH3.1-8) consider not only the intensities of 1 and 25 MeV/nuc protons and helium at 1 AU and 1.6 AU, but also their anisotropies at 1.6 AU. They find $\lambda_r \sim$ 0.1 AU at 1 AU also, but have to abandon the simple power-law radial dependence of K_r in an attempt to fit all the observations.

In paper SH3.2-9 (not presented), Chebakova *et al.* fit the intensities of protons, helium and electrons of various energies in the 28 May 1967 and 2 Nov 1969 events. Assuming impulsive solar injection and $K_r \propto r^{b(R)} R^{\alpha}$, they find α = 0.27 and 0.6 for the two events and b increasing with rigidity R, thus concluding that $K_r(r,R)$ is not separable in r and R.

This conclusion, based on the assumption of impulsive injection, should be contrasted with the approach in paper SH3.2-5, in which b is assumed constant, but the injection is non-impulsive. The three papers above illustrate the difficulty of separating the effects of solar injection, interplanetary acceleration and interplanetary propagation. They underscore the importance of multi-spacecraft data and anistropy measurements, which together require fewer assumptions in the model.

In paper SH3.2-6, Lockwood and Debrunner extend previous analysis of the May 7, 1978 event at 1 AU to the observation of 70 - 500 MeV protons of the same event

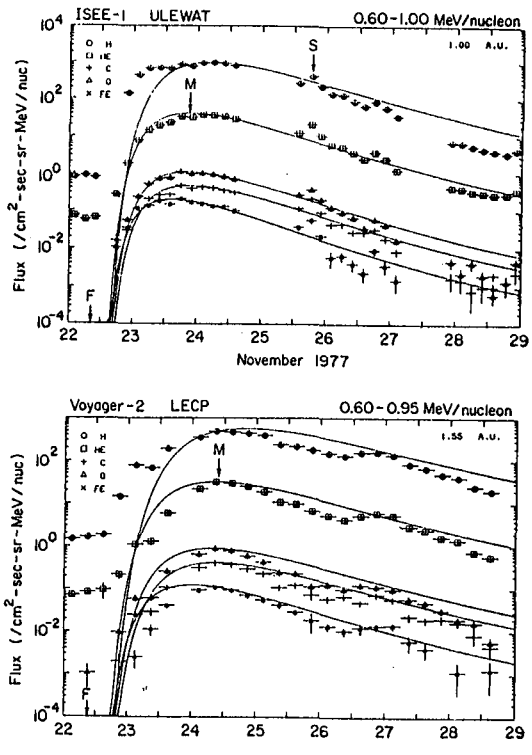

Fig 4

observed at Voyagers 1 and 2 at ~ 3 AU. They adopt (a) the Reid-Axford injection with $K_{\theta}\,[cm^2/s] = 4.4 \times 10^{18}\,(E\,[MeV])^{1/2}$ and $\eta = (2.9 + 0.5)\ hr^{-1}$, and (b) scatter-free propagation at $r < 1.6$ AU and diffusive propagation beyond. They deduce that $\lambda = 0.04$ AU beyond 1.6 AU. However, the model of coronal injection appears inconsistent with the observation at Helios A, and further studies with a more refined interplanetary transport model would be worthwhile.

In paper SH3.2-11, Lumme *et al.* fit the intensity and anisotropy of the May 7, 1978 ground level event (GLE) by a Monte Carlo simulation which takes into account adiabatic focusing, isotropic pitch-angle scattering and an injection $\propto \exp(-t/\sigma)$. They obtain $\lambda = 1$ AU and $\sigma = 11$ min, in contrast to $\lambda = 3 - 5$ AU reported in Lockwood *et al.* (1982).

The cause of the big difference is not completely clear. We note however the following. (a) The anisotropy observed by Lumme *et al.* decays somewhat faster than that observed by Lockwood *et al.* (b) The injection functions are not very different. (c) For $\lambda = 1$ AU, the theoretical anisotropy profile of Lockwood *et al.* (their Fig 5) decays significantly faster than that of Lumme *et al.* (their Fig 4). (d) Both groups simulate the distance between collisions with an exponential probability distribution: $(1/\lambda)\exp(-\Delta s/\lambda)$. However, whereas Δs is the distance projected along the field line in Lumme *et al.*, it is the actual distance in Lockwood *et al.*

Factors (a) and (d) both tend to yield a smaller value of λ for Lumme *et al.* Note that the adopted exponential distribution is very broad with 39% and 13.5% probability that $\Delta s < \lambda/2$ and $\Delta s > 2\lambda$ respectively. A probability distribution of a much smaller range would be more realistic. Since a particle travelling sunward will mirror even in the absence of scattering, the effective mean free path would be smaller than the value of λ used in the simulation.

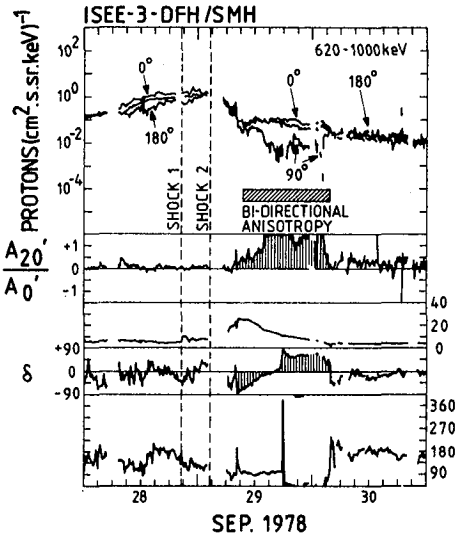

Fig 5

2.2.2 Directional Particle Distributions

With improving instrumental resolution and theoretical advance, there has been increasing interest in the directional distribution of solar energetic particles. In paper SH3.1-9, Marsden *et al.* report on a most comprehensive survey of 66 periods (> 3 hr each) of bidirectional anisotropies observed on ISEE-3 during Aug 1978 - May 1982. Fig 5 shows the bidirectional flow (BDF) event of 29 Sept 1978. They have classified and analysed the events according to magnetic field signatures and association with interplanetary shocks. They conclude that the simple model of a large-scale magnetic loop anchored on the sun cannot explain all the BDF events, and that localised effects cannot be ruled out. They also emphasise the qualitative correlation between the quietness in the

magnetic field magnitude and BDF event occurrence.

The description of a directional distribution depends on the choice of a reference frame. Transformation from the spacecraft frame to a chosen comoving frame is almost always necessary for the interpretation of the directional distribution of low-energy ions. For > 10 KeV protons, the hitherto complicated transformation procedures are rendered unnecessary by a set of second-order correct explicit transformation formulae presented by Ng in paper SH3.1-10. These are of the form

$$A_{nm}(p) = \text{function}\left\{ A^{sc}_{jk}(p),\ \partial A^{sc}_{jk}/\partial p,\ \partial^2 A^{sc}_{jk}/\partial p^2 \right\} + O(W/v)^3,$$

where A_{nm} and A^{sc}_{jk} are the spherical harmonic coefficients in the comoving frame and the spacecraft frame respectively, W the transformation velocity, v the particle velocity, and p the momentum.

In SH3.1-11, Ng describes a method to determine the particle directional distribution (in terms of pitch-angle and gyrophase), the harmonic anisotropies and associated Poisson errors from sectored particle data and concurrent field and plasma flow direction.

A concise and effective format is used to present directional solar particle data in Fig. 2 of SH3.1-11, for the 1.4 - 2.5 MeV protons of the Day 118, 1978 event observed on IMP-8. In this event, as the IMF direction varies, the variation in the transverse anisotropy in the ExB drift direction is in phase with but far larger than the variations in the Compton-Getting anisotropy. Magnetic connection to the bow shock does not appear to explain all the variations. Further work is necessary to find out the cause of this behavior.

Attempts to determine and interpret the pitch-angle distribution of the 16 Feb 1984 GLE event are reported in papers SH3.1-7, SH3.2-1 and SH3.2-2. Analysing the first two five-minute data from various stations, Fenton *et al.* (SH3.2-2) find no satisfactory mean arrival direction consistent with the asymptotic directions of the stations. On the other hand, Debrunner *et al.* (SH3.1-2) deduce the mean direction at 5°S, 5°E geographic coordinates. IMF data from ICE (ISEE-3) would be helpful in this regard.

Using the CODE model, Debrunner *et al.* calculate the intensity time profiles assuming two possible flare sites at 95°W and 130°W, and decide for 95°W upon comparison with the observation. The pitch-angle distribution observed at the time of maximum intensity (their Fig 3) is much narrower than the hourly average distribution (Fig. 6) deduced in paper SH3.2-1. This suggests that the distribution did broaden significantly in the first hour.

In paper SH3.2-13, Niskovskikh and Filipov analyse 5 GLEs associated with preceding propagating interplanetary shocks and 4 GLEs associated with preceding CIRs. They conclude that the onset delay between different stations and the ocassional second hump in the intensity are caused by

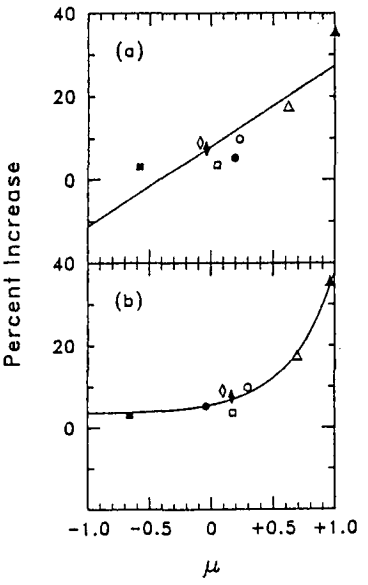

Fig 6

scatter-free propagation, partial reflection at the shock and particle mirroring near the sun.

The new idea of determining local interplanetary scattering parameters *directly* from the observation of particle pitch-angle distribution underlies the studies reported in three papers, SH3.1-13A, SH3.2-8A and SH3.2-1. This approach simplifies the hitherto involved procedure used in the fitting of the pitch-angle distributions of SEP events (e.g. Ng *et al.*, 1983). Beeck and Wibberenz (SH3.1-13A) exploit the properties of an approximate solution of the focused transport equation to deduce the pitch diffusion coefficient $k(\mu)$ directly for a number of events with λ ranging from 0.1 to 1 AU. Using a code from Ng to solve numerically the focused transport equation, Green and Schlüter (SH3.2-8A) show that the normalised anisotropic part of the pitch-angle distribution approaches quickly a characteristic function determined only by the local $k(\mu)$ and L. They also show from observations some examples that exhibit the above behaviour. In paper SH3.2-1, Bieber *et al.* assume a pitch-angle distribution of the steady-state form

$$f = C_0 + C_1 B \exp\left\{ (4-q)\,\lambda\mu\,|\mu|^{1-q}/3L \right\},$$

where μ = pitch cosine, B = magnetic field, L = magnetic scale length, λ = mean free path, and C_0, C_1, and q are constant parameters. Fitting this to the observed distributions in the 16 Feb 1984 event yields λ/L = 2 - 10 AU for > 400 MeV protons detected by neutron monitors (Fig 6), and λ/L = 2.8 and q = 1.2 for 35 -145 MeV protons observed on ISEE-3.

A number of papers are concerned with accurate solution of the transport equation in either the DCA model or the focused transport model. In paper SH3.2-10, Yang and Zhang present a method to obtain numerically accurate solution to the DCA model with λ_r = constant. In paper SH4.1-2, Earl derives a general expression of the dispersion coefficient in the theory of focused transport, for λ and L constant. This expression is relevant to an accurate numerical solution of the focused transport equation, as discussed in detail by Earl and Jokipii (SH4.1-3) and Earl (SH4.1-4).

2.2.3 New Propagation Regimes

The highly structured nature of the interplanetary medium and its influence on solar particle propagation are investigated in papers SH3.2-3 for the inner heliosphere and SH3.2-4 for the outer heliosphere. Anderson and Dougherty (SH3.2-3) identify about 50 interplanetary filaments in 1978 and 1979 mainly on the basis of 2 - 10 KeV electron intensities measured on ISEE 3, and further characterise them using concurrent plasma and field data. They find that the filaments have width of .025 ± .015 AU at 1 AU, come in clusters separated by a few hours, trace back to distinctly different regions in the solar corona than surrounding field lines, and

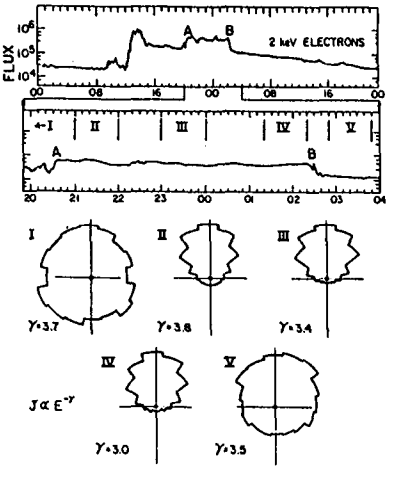

Fig 7

may exhibit decreases or increases in particle intensity relative to the surroundings. The 2 KeV electron angular distribution inside a filament often differs greatly from those outside it (Fig 7). Clearly, the existence of these filamentary channels has important implications for interplanetary propagation.

In paper SH3.2-4A, McDonald and Burlaga report on six SEP events observed between 5 and 12 AU by Pioneer 11, Voyager 1 and Voyager 2. These events are characterised by long time scales ($\sim$1 month), flat energy spectra extending to > 100 MeV and steepening with distance, and association with enhancements of MeV electrons. The authors stress that the outer heliosphere is dominated by systems of interplanetary flows, and the compressive merged interaction regions would have lower diffusion coefficient and lower adiabatic deceleration (Burlaga *et al.*, 1983).

3. Interplanetary Acceleration

Particles may be accelerated in interplanetary space by turbulent magnetic fields (second-order Fermi or statistical acceleration) and also by shocks. In an oblique fast mode shock, particles gain energy in two ways, as seen in the shock frame. (a) Shock drift acceleration (SDA) - particles gain energy by drifting in the direction of the electric field whilst gyrating back and forth across the shock. (b) Diffusive shock acceleration - particles gain energy between scatterings by the converging upstream and downstream magnetic irregularities, and also between scattering upstream and reflection at the shock front (first-order Fermi acceleration).

3.1 Numerical Simulation

There are five papers in which numerical particle trajectory-tracing technique is used to simulate second-order Fermi acceleration and shock acceleration in the presence or absence of waves.

In paper SH1.5-2 (not in the proceedings) Moussas, Valdes-Galicia and Quenby first construct a 'layer model' of the interplanetary magnetic and electric fields, using high resolution plasma and field data from Pioneer 11 at 2.5 AU, during the passage of a CIR on Day 284, 1973. Then, by following test particles in the layer model in the solar wind frame, they find, for 10 - 50 MeV protons, energy loss ahead of the forward shock where grad B is negative, and energy gain in the trailing edge of the CIR where grad B is positive. They also find a statistical energy diffusion coefficient D_{TT} ten times smaller than required to accelerate locally the anomalous component.

Using the same technique, Valdes-Galicia *et al.* (SH1.5-1) find, for a perpendicular shock observed by Helios at 0.45 AU, that there is a three-fold increase in the average energy gain of 100 MeV protons for shock plus statistical acceleration as opposed to shock acceleration only.

By using observed directional particle and field data, and following the particles backward in time, both Kessel *et al.* (SH1.5-5) and Balogh and Erdös (SH1.5-6) carry out consistency checks on the adiabatic theory of single-shock encounter. They find general qualitative agreement between theory and observation. Balogh and Erdös suggest that the model should include fluctuations in Θ_{BN}.

Decker and Vlahos (SH1.5-3) superpose wave fluctuations in an otherwise 60° oblique shock and find that in $\sim$1 hour, 10 KeV protons can be accelerated to yield a spectrum extending to 1 MeV (Fig 8). They also

conclude that the particles gain most of their energy through drift, with scattering merely returning the particles to the shock for more acceleration.

In this context, we note that in the diffusive shock acceleration theory, drift effects are included by Jokipii (1982) and reflection effects are further included by Webb (1983). Nevertheless, for nearly perpendicular shock and/or highly anisotropic particle distributions, diffusion theory may not apply and numerical simulation remains the only available tool.

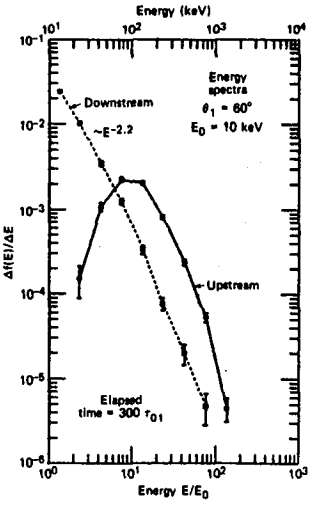

Fig 8

3.2 Observations

The pitch-angle distributions upstream and downstream of five quasi-perpendicular interplanetary shock events (Fig 9) are presented by Balogh and Erdös (SH1.5-6). As stated earlier, they find qualitative agreement with SDA theory but suggest inclusion of fluctuations of θ_{BN} in the model. They also suggest that the double loss cones observed at the higher energies in some events are due to short-lived magnetic bottles intersecting the shocks.

In paper SH1.5-4, Krimigis and Sarris present the ion spectra and the highest time resolution ($\sim$1.2s) counting rates of proton and electrons observed by Voyager 2 in the Jan 6, 1978 shock event, with θ_{BN} = 87.5° and M_A = 3.4 (Fig 10). The enhancements and fine structures down to the scale of a proton gyroradius in the near absence of field fluctuation fit the SDA theory for a quasi-perpendicular shock. A comparison between this shock event and the classic Nov 12, 1978 quasi-parallel shock event shows that in both events, the particle energy density exceeds the field energy density by a factor of 3 to 5 and is a substantial fraction of the shock energy.

Krimigis and Sarris argue that the above and other quasi-perpendicular shock events indicate that SDA at quasi-perpendicular shocks is responsible for accelerating particles to high energies in the interplanetary medium and in the astrophysical context. We refer the reader to Scholer's

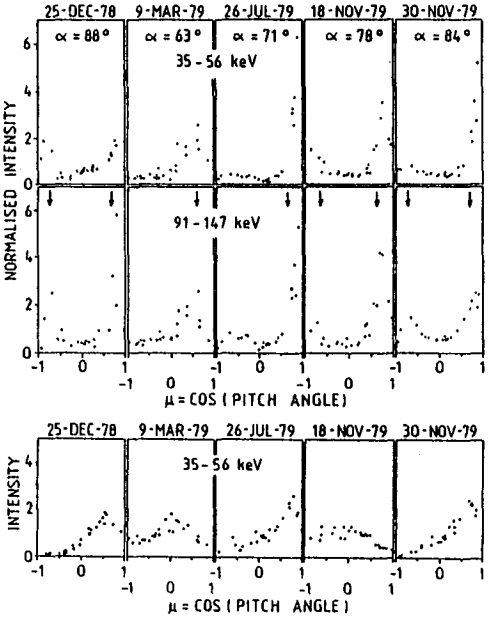

Fig 9

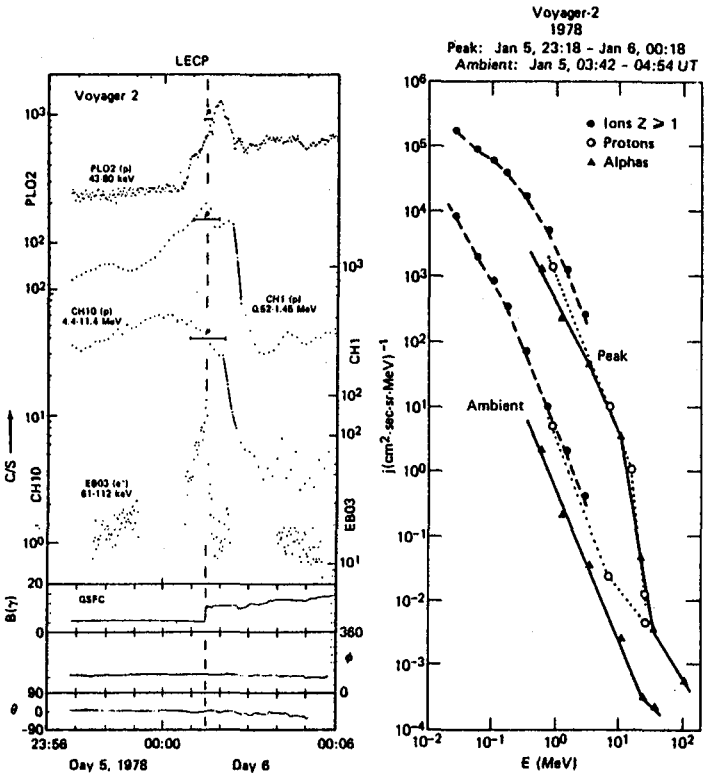

Fig 10

highlight talk at this conference for another view.

With respect to the observation, we note the following. In a single shock encounter, SDA can at most raise the particle energy by a factor of ~ 14 (Decker, 1983). Hence it appears that either the seed particles are of relatively high energies, which raises the question of their origin, or the particles must have encountered the shock many times, which implies scattering. We also note that in this case, the spacecraft is unable to measure field fluctuation in a direction parallel to the field.

In paper SH1.5-12, Gloeckler *et al.* use a novel technique to determine the parallel diffusion coefficient $K_{||}$ upstream of an interplanetary shock. By finding the frame in which the particle distribution is isotropic and thereby the diffusive flux in the spacecraft frame, they find $K_{||}$ as in Fig 11 for the 12 Nov 1978 event. The exponential rise with increasing distance is in accord with Lee's (1983) theory. However, the cause of the slower exponential decrease beyond 5×10^{10} cm is at present unknown.

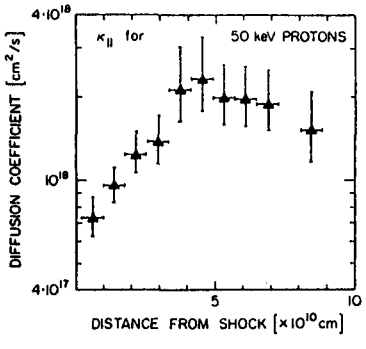

Fig 11

We now turn to shock acceleration

associated with CIRs. Gold *et al.* (SH1.5-14), taking advantage of the latitudinal separation between Voyagers 1 and 2, and picking a period free from solar particle events, show that both the number and the intensity of low energy ion enhancements associated with CIRs in the outer heliosphere (> 12 AU) are smaller at 20°N than at 0° latitude, in agreement with Christon and Stone (1985). However from the similar spectra observed, they conclude that the same acceleration process is at work at both latitudes.

One way to determine the source or the origin of the accelerated particles is to examine their composition. By carefully identifying on ISEE-3 eight CIR-associated events (including the requirement of an easterly anisotropy) in 1984/85, von Rosenvinge and McGuire (SH1.5-15) find H/He = 20 ± 8 at 4.5 - 6.5 MeV/nuc and C/O = .8 ± .2 at 1.8 - 2.8 MeV/nuc, similar to the ratios obtained in 1973/74. These ratios suggest that these particles are accelerated out of the solar wind. However they also find H/He = 67 ± 4 in the 1 Aug 1979 corotating event, and this is consistent with flare particle composition instead. They suggest that for this event, the associated high speed stream was enriched with flare particles injected by known large flares in the previous two solar rotations.

A similar idea is reached independently by Armstrong *et al.* (SH1.5-16). They select a solar active period and a solar minimum period during 1974 - 1981, and classify each day as a flare day, a quiet day, or a non-flare non-quiet day. For the solar minimum period, they find the H/He and He/CNO ratios at 2 - 4 MeV/nuc are distinctly different for the three categories of days. In contrast, in the solar active period, the composition ratios for non-flare non-quiet days are almost identical to the ratios for flare days. They suggest the latter to be due to particles of flare origin.

In paper SH1.5-17 (not presented), Petukhov *et al.* fit the quiet-time spectrum and radial gradients of < 10 MeV proton observed at 1 AU with a model of particle acceleration at the solar wind termination shock. Assuming the shock at 50 AU and reasonable parameter values, they obtain radial gradients of ~10 %/AU at 10 KeV and 5 %/AU at 1 - 10 MeV and a spectrum cut off at ~10 MeV in fair agreement with the observation.

4. Jovian Electrons

Observations of Jovian electron spectrum near Jupiter and at 1 AU are reported by Christon *et al.* (SH1.5-18) and Evenson *et al.* (SH1.5-19) respectively. Fig 12, from SH1.5-19 shows the daily rate of 10 MeV electrons observed by ISEE-3 during 1978 -1984. Apart from the ups and downs associated with the Jovian electron seasons, there is no obvious sign of solar modulation. This and the constancy of the spectrum over 6 years, indicate that solar modulation of electrons at these energies must occur well beyond the orbit of Jupiter. This is consistent with the conclusion that the bulk of the cosmic-ray modulation occur in the distant heliosphere (see below).

A comparison between the 1 AU spectrum and the spectrum measured near Jupiter by Voyagers shows that the 1 AU spectrum bends over below 10 MeV. If real, this may be an effect of rigidity-dependent propagation and adiabatic deceleration.

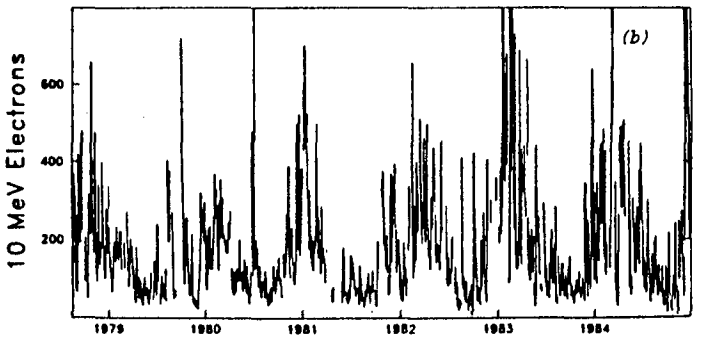

Fig 12

5. Outer Heliosphere, Radial Gradients And Anomalous Component

The network of deep space probes formed by Pioneers 10, 11 and Voyagers 1, 2 together with other spacecraft in the inner heliosphere represents a continuing *in-situ* experiment of the largest (and still expanding) distance scale ever attempted by mankind. Observation by this vast network on the spatial and time dependence of cosmic rays is important for an understanding of the solar modulation process (see Kota, 1985). For this reason, reports of the latest measurements made by this network have been looked forward to at this international cosmic ray conference, just as previous reports had been at past ICRCs. However, the reported gradients are not all in agreement.

Figure 13 (from paper SH4.7-3) shows the heliocentric distances and latitudes of the deep space probes. The wide radial and latitudinal separation between these spacecraft should be kept in mind when one compares their observations and interpretes gradient measurements.

5.1 Cosmic-Ray Intensity in the Outer Heliosphere

Time histories of the cosmic-ray intensities measured by various detectors on the deep space probes over many years are presented in papers SH4.7-1, 2, 3, 5, 6, 7, and 9. An example is given in Fig 14 (from SH4.7-3), which shows the normalised 26-day average proton and helium intensities/rates measured at five spacecraft.

By comparing the intensities at various energies < 500 MeV/nuc measured by Pioneer 10 at 24 - 28 AU in 1981 - 1982 with those measured at 1 AU during the solar minimum in 1977, McDonald *et al.* (SH4.7-3) conclude that the bulk of the modulation of these particles must occur in the distant heliosphere at that time. McKibben *et al.* (SH4.7-5), by comparing the

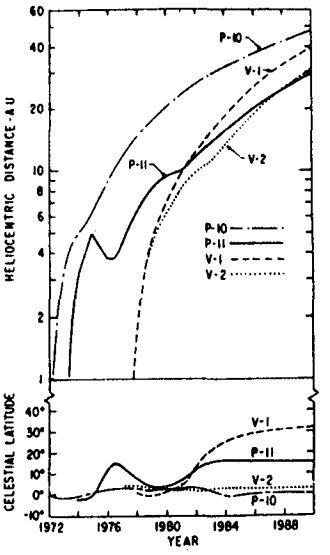

Fig 13

30 - 70 MeV/nuc proton and helium intensities at Pioneer 10 with the estimated interstellar intensities of Evensen *et al.* (1983), conclude that 95% of the modulation of these particles occurred beyond 34 AU in 1984. Similarly, Webber and Lockwood (SH4.7-1) conclude that during 1981 - 1982 about 85% of the modulation of > 60 MeV/nuc cosmic rays must occur beyond 30 AU.

By the end of 1984, the UCSD C1 counting rate of > 500 MeV/nuc ions on Pioneer 10 (SH4.7-2) had recovered to ~80% of its high level in 1978. In contrast, the 121 - 227 MeV proton flux in Fig 14 and the 30 - 57 MeV proton flux (Fig 3 of SH4.7-3) had recovered only to ~40% and ~15% of their 1978 levels. This decreasing level of recovery with lower energy or rigidity (i.e. the hysteresis effect) is true of helium as well. However, in paper SH4.7-4A, Christon *et al.* report that by early 1985, the > 50 MeV electron intensities measured on Voyagers 1 and 2 at 16 AU and 22 AU respectively had recovered to the solar minimum value in 1977, even though the b> 75 MeV proton intensity had only recovered by ~ 80%.

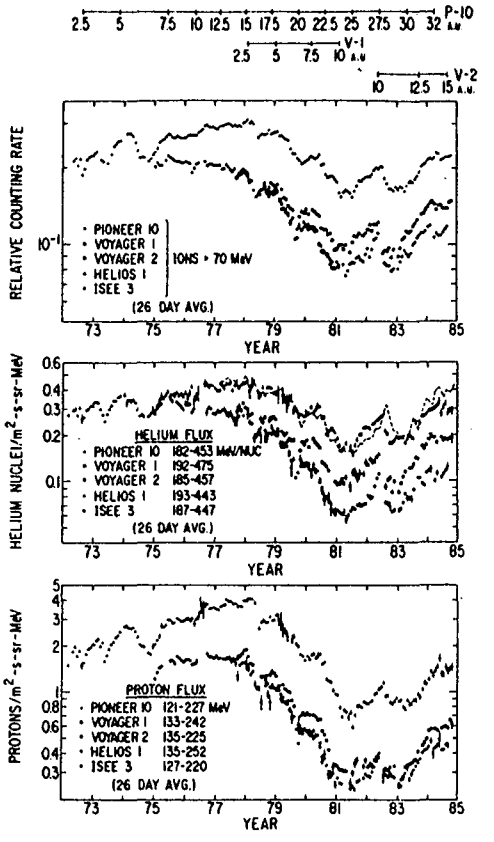

Fig 14

The outward propagation at 400-500 km/s of the step-like decreases of the particle fluxes since 1978 to the minimum level has been previously reported in the literature. In paper SH4.7-7, McKibben *et al.* use the observations of relativistic protons and 30-70 MeV/nuc ions from IMP-8 and Pioneer 10 during 1980-1984 to show that individual *increases* propagated outward at ~ 400 km/s too. However, near the time of the cosmic-ray minimum in 1982 - 1983, the intensity changes, which were not dominated by single events, propagated at ~ 800 km/s.

Forman *et al.* in paper SH4.1-12 (of a different session), show heuristically with a quasi-steady force-field model and numerically with a 3-D time-dependent model, that the phase of solar modulation propagates outward at twice and 1.85 times the solar wind speed respectively. This is caused by the solar cycle variation in the number of scattering barriers between the observer and the modulation boundary, as a result of a change in the frequency of solar emission of such barriers.

The large scale modulation and recovery associated with the huge Forbush decreases observed by Pioneers 10 and 11 in mid-1982 are analysed in paper SH4.7-9 by Pyle and Simpson, using 200-1000 MeV/nuc CNO-Fe counting rates to minimise hysteresis effect. They conclude that these intensity increases and decreases propagated radially outward at

~ 500 km/s and that azimuthal effect is small compared with radial effects.

5.2 Spatial Gradients

Measurements of radial gradients G_r are reported in papers SH4.7-1 to 6 and SH4.6-4 from various experiments aboard the spacecraft. All these (average) gradients have been calculated after time-shifting the data between the two spacecraft at a speed of 400 - 500 km/s, in order to minimise the effect of the outward propagation of modulation.

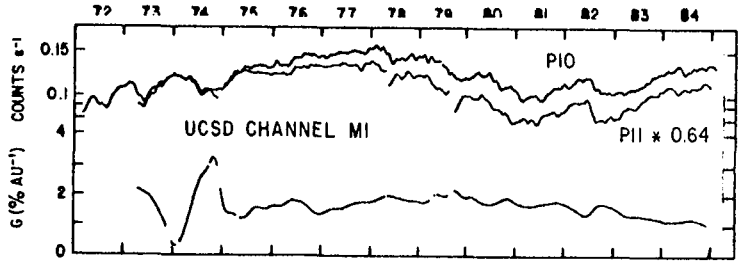

Fig 15

5.2.1 Relativistic Cosmic Rays

Figure 15, from paper SH4.7-2 by Fillius *et al.*, shows the time history of the radial gradient G_r between Pioneers 10 and 11 as measured in the M1 channels (> 80 MeV/nuc) of the UCSD detectors. It shows that since 1982, whilst the intensity has been rising, G_r between the two outermost spacecraft has been decreasing with time. This decreasing trend since 1982 is also reported for G_r measured at smaller distances by Venkatesan *et al.* (SH4.7-6) and Webber and Lockwood (SH4.7-1), but not by McKibben *et al.* (SH4.7-5). Webber and Lockwood report that G_r between IMP 8 and Pioneer 10 decreased from ~ 2.8%/AU in early 1982 to ~ 1.8%/AU in late 1984 (see also Fig 16). In contrast, McKibben *et al.* find that G_r between the same spacecraft remained nearly constant at ~ 2.5%/AU during 1978 -1984.

Figure 16 shows the radial dependence of > 60 MeV/nuc ions measured on IMP-8, Voyagers 1 and 2 and Pioneer 10 at six selected epochs, as reported in SH4.7-1. Note that in Fig 16, G_r remained independent of distance through intensity changes and even after G_r decreased in time. In contrast, Venkatesan *et al.* find that G_r was generally larger between IMP-8 and Voyager 2 than between Voyager 1 and Voyager 2.

Figure 17 summarises the various measurements reported in early 1981 and late 1984. In early 1981, the data would be consistent if the lines join to form a polygon, since Voyager 1 and Pioneer 11 were then close in radius. In late 1984, Pioneer 11 was between Voyager 1 and

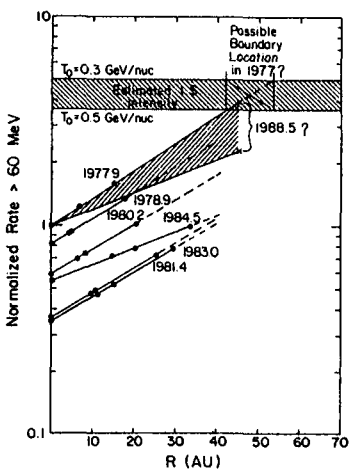

Fig 16

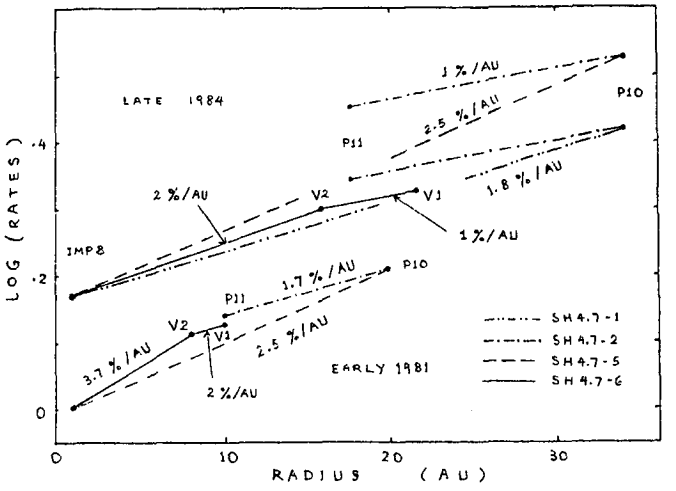

Fig 17

Voyager 2 in both latitude and radius, so the data would be consistent if the line IMP8 - P10 - P11 puts P11 close to the segment V2 - V1 on the line IMP8 -V2 - V1. The data appear consistent for early 1981 but they are inconsistent for late 1984. A (non-unique) way to remove the inconsistency is to adopt G_r somewhat less than 1.8 %/AU between IMP8 and Pioneer 10. One *might* infer that G_r between 1 AU and 20 AU decreased from $\sim$ 2.5 %/AU to $\sim$ 2 %/AU between early 1981 and late 1984, and that for both epochs, G_r decreased with heliocentric distance. However, these inferences must be regarded as controversial at the present time.

The resolution of the discrepancies in the reported spatial and time dependence of G_r probably must await the difficult task of the intercalibration of the various instruments aboard these spacecraft by the various experimental groups. Considering the immense value of the data from the deep space network, such a task may well be worthwhile.

5.2.2 Non-Relativistic Cosmic Rays

Radial gradients of proton and helium of energies < 500 MeV/nuc are reportd by McDonald *et al.* and Mckibben *et al.* Figure 18 from McKibben

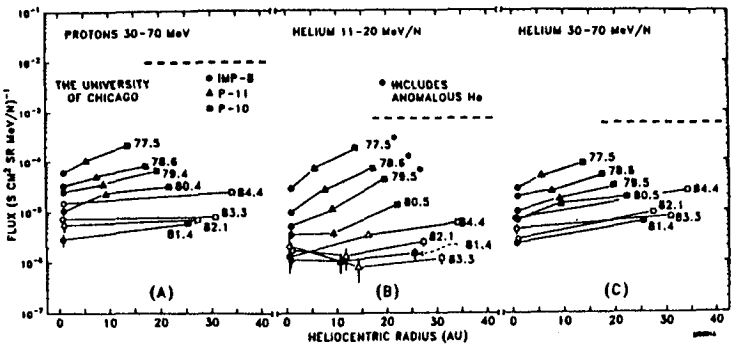

Fig 18

et al. gives yearly snapshots of the intensity versus radius for 30 -70 MeV/nuc protons and helium and 11 - 20 MeV/nuc helium. The radial gradients of these particles were much smaller at and after maximum modulation (1981) than at solar minimum (1977).

Figure 19 from McDonald *et al.* shows, at selected epochs, the radial gradients of proton and helium at various energies in the 'inner' and 'outer' heliosphere. The < 500 MeV protons generally had larger radial gradients than relativistic protons (cf. Fig 15). At solar minimum (1977), all these gradients were significantly larger inside than outside 5 AU. With the onset of solar activity, however, the spatial dependence of G_r changed in a complex manner depending on particle species and energy.

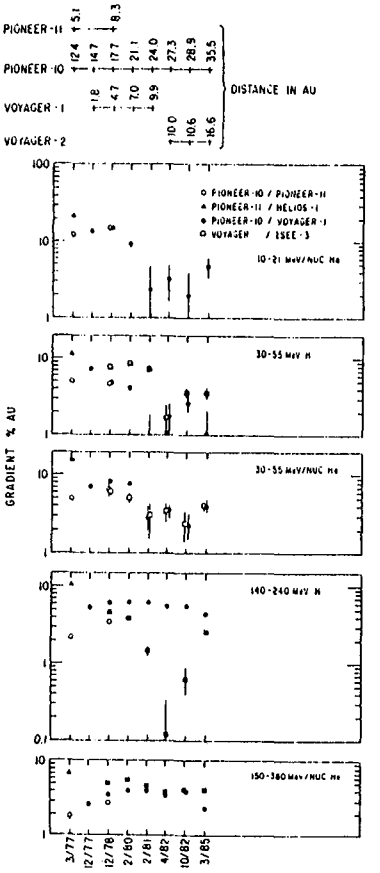

Fig 19

5.2.3 Latitudinal Gradient

The latitudinal gradient of galactic cosmic rays is considered in only one paper, SH4.7-6. Venkatesan *et al.* show that the upper limit on the latitudinal gradient of > 70 MeV protons between the Voyagers decreased from ~ 0.42 %/deg, to ~ 0.13 %/deg from early 1981 till late 1984. They also hold the view that no significant latitudinal gradient existed (Decker *et al.*, 1984).

5.2.4 Implications

A simple-minded interpretation of the gradient measurements does not seem possible. For example, Venkatesan interpret the decreasing trend of G_r to mean the approach of the modulation boundary (which would be reached when $G_r = 0$ %/AU).

In contrast, Fillius *et al.* estimate the location of the boundary by extrapolating the measured radially dependent intensity to intersect the estimated interstellar intensity. In this approach, a decreasing G_r implies that the modulation boundary is receding instead.

For more sophisticated considerations, the reader is referred to Kota (1985).

5.3 The Anomalous Component

Anomalously high quiet-time fluxes of He, N, O and Ne were first discovered in 1972 at < 30 MeV/nuc. They were observed in the solar minimum period 1972 - 1978 but have not been observed at 1 AU since 1979. Fisk *et al.* (1974) suggest that they are interstellar neutrals that, after entering the heliosphere, become singly ionised by solar UV or charge exchange and are subsequently accelerated in the interplanetary medium. Pesses *et al.* (1981) put forward a model in which these singly ionised particles are accelerated instead in the polar regions of the

solar wind termination shock, and then drift into the equatorial region of the heliosphere. This latter model predicts a 22-year modulation cycle dependent on the sign of the solar magnetic field, and that the anomalous component will not return in the coming solar minimum.

Recent observations of the intensities, radial and latitudinal gradients of the anomalous components have been closely monitored to see what light they may shed on their origin, acceleration and modulation.

5.3.1 Changes in the Intensity Spectrum of Anomalous O and He

Observations at 1 AU.

Various experimental data on anomalous O and/or He from IMP-8, ISEE-3/ICE and ISEE-1 have bee carefully analysed by Mewaldt and Stone (SH4.6-2), Mason *et al.* (SH4.6-3) and McKibben *et al.* (SH4.7-5). Their unanimous conclusion is that by end 1984/early 1985 anomalous O and He had shown no sign of recovery. However, Mewaldt and Stone as well as Mason *et al.* point out that since neutron-monitor rates had not returned to levels that imply observable anomalous O flux based on an 11-yr cycle, we probably have to wait for the next ICRC to know e.g. if Pesses *et al.*'s model applies.

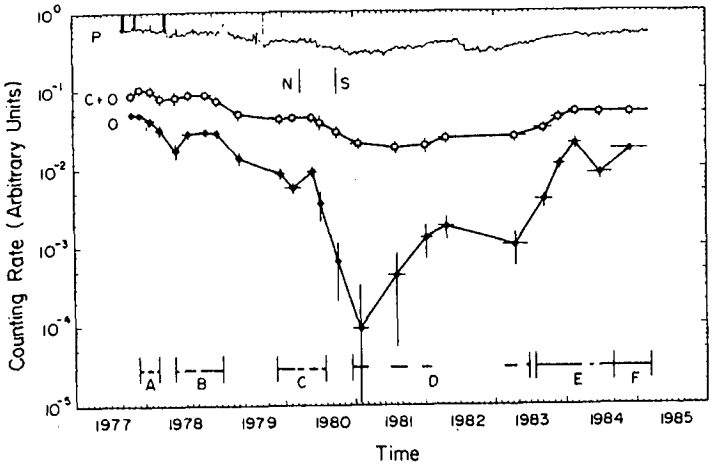

Fig 20

Observations in the Outer Heliosphere

By late 1984/early 1985, the intensity of anomalous He had not recovered at Voyagers 1, 2 and Pioneer 10 at ~16 AU, ~22 AU and ~32 AU respectively, as reported by Cummings *et al.* (SH4.6-1), McDonald *et al.* (SH4.7-3) and McKibben *et al.*(SH4.7-5). In contrast, anomalous O at Voyager 1 rose by a factor ~100 from its low level in 1981 (Fig 20, from paper SH4.6-4 by Webber *et al.*) This is consistent with anomalous O being singly ionised with rigidity ~2 GV.

Cummings *et al.* show that the anomalous O spectrum changed dramatically soon after solar field reversal in 1980 (Fig 21). They report that this is similar to the predicted spectral changes in a recent model of Jokipii (1985), which includes acceleration at solar wind termination shock and drifts.

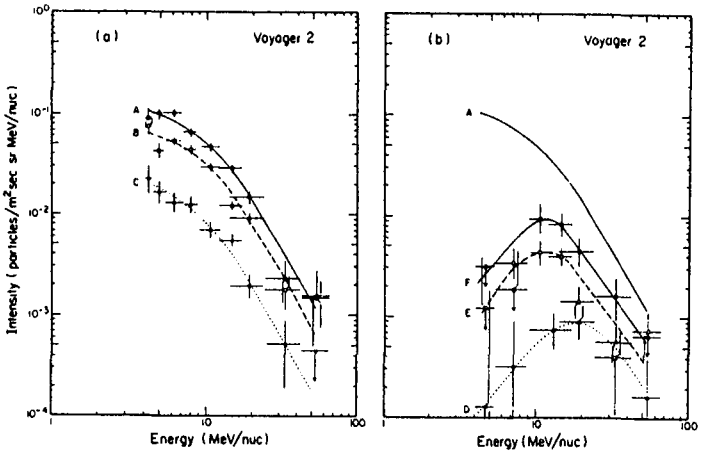

Fig 21

They also note that the observed absence of anomalous He below 30 MeV/nuc and the reduced intensity of anomalous O below 8 MeV/nuc in late 1984 are consistent if both species were singly ionised (see their Fig 4).

5.3.2 Radial and Latitudinal Gradients of the Anomalous O and He

Figure 22 from Webber *et al.* (SH4.6-4) show that the radial gradient of anomalous O as measured on Voyagers 1, 2 and Pioneer 10 in 1977 -1985 remains essentially constant at 10 - 15 %/AU although the intensity has varied by a factor of 100. They also report a latitudinal gradient of 3 ± 1 %/deg for anomalous O in the 7.1 - 10.6 MeV/nuc interval only, between Voyagers 1 and 2 at 15 - 20 AU from late 1983 to early 1985. In contrast, the radial gradient of 11 - 20 MeV/nuc He experienced a dramatic decrease in both the inner and outer heliosphere from ~10 %/AU before to 0 - 2 %/AU after the solar field reversl in 1980 (SH4.7-3 and 5, see also Figs 18 and 19).

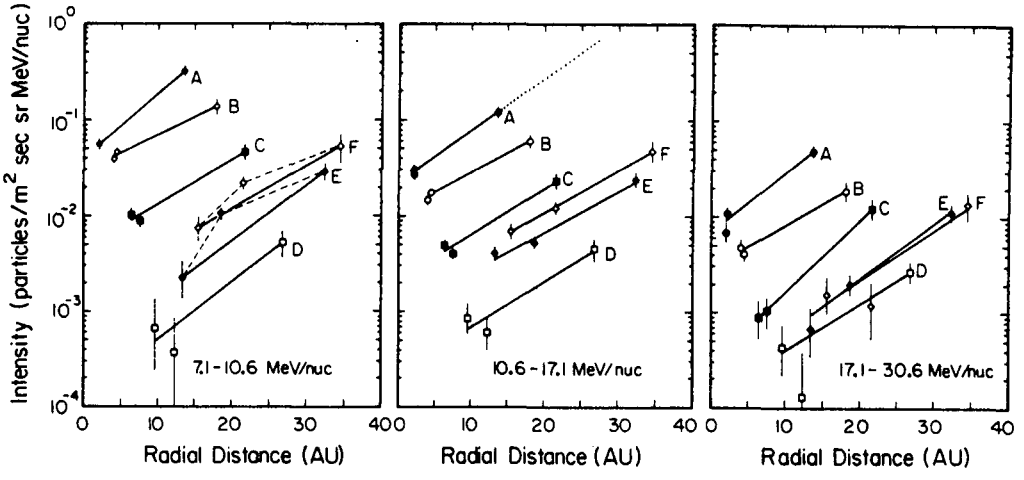

Fig 22

In terms of the conventional model of modulation, Webber *et al.* show that the intensity modulation between periods A and D in Fig 20 can be produced by a shift of 46 ± 4 AU in the modulation boundary. They further show that, if O is singly ionised, this boundary change also implies intensity modulation of a factor ~ 2 and G_r ~ 1.5 %/AU for relativistic particle of ~ 1.8 GV in rough agreement with other observations.

However, it is not clear that the conventional model can produce the spectral change of anomalous O discussed earlier. On the other hand, Pesses *et al.*'s model may have difficulty fitting the observed G_r (see section 5.3.4).

5.3.3 Origin

Observation of singly ionised He suggested to be ex-interstellar neutrals is reported for the first time by Hovestadt *et al.* (SH4.6-6). Figure 23 shows the energy spectrum of particles of M/Q = 4 measured by a time-of-flight spectrometer aboard the IRM spacecraft at 1 AU. The spectrum has a sharp cut-off at 23 KeV/Q, which for He^+ corresponds to a top speed of 2W, where W = solar wind speed. Freshly ionised helium should have a top speed of 2W sinα, where α is the angle between the solar wind flow and the magnetic field. Thus the observed cut-off energy, shown to correlate strongly with $(1/2)M(2W)^2$ rather than with $(1/2)M(2W \sin\alpha)^2$ in their Fig 3 and 4, indicate the particles have suffered substantial pitch-angle scattering since ionisation. Hovestadt *et al.* also use their observation to estimate an interstellar neutral helium density of ~ 0.01/cm³, compatible with other reported values. They suggest the observed particles to be neutral interstellar helium ionised by solar UV and that these represent the source of anomalous He as suggested by Fisk *et al.* (1974).

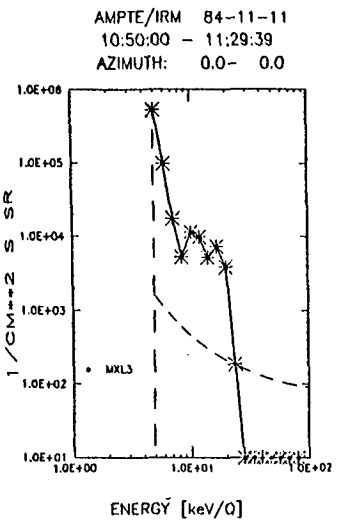

Fig 23

5.3.4 Theories

In paper SH4.6-7A, Biswas *et al.* propose that the anomolous component originates in the stellar winds of O-type stars located in a region a few Kpc around the solar system. They suggest that 10 - 100 KeV/nuc heavy ions of He^{+2}, O^{+4}, etc. in these hot stellar winds are further accelerated to 5 - 100 MeV/nuc at the shock fronts of supernova remnants, and then enter the solar system via interstellar magnetic field lines connected to the solar field. If this is correct, the anomalous component should suffer the same solar modulation as other galactic cosmic rays of comparable rigidities.

In paper SH4.6-6 Potgieter *et al.* study a model that includes gradient and curvature drifts, a diffusion coefficient appropriate for solar minimum, and a source located at various latitudes on a boundary at 50 AU. They show that for a source over the solar pole, irrespective of the IMF polarity, the radial gradient decreases very rapidly with radius

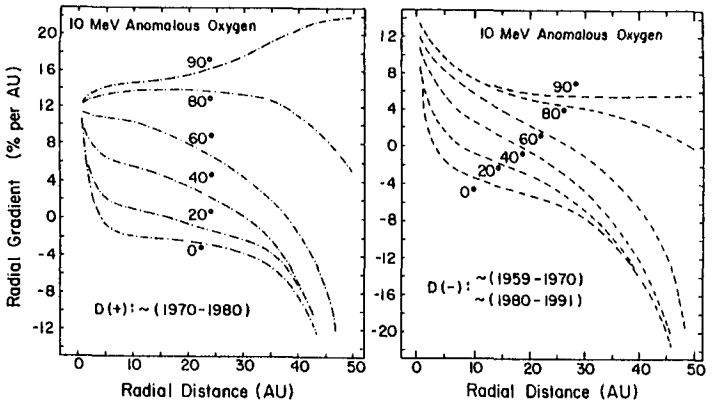

Fig 24

in the equatorial plane, from ~10 %/AU to negative values beyond ~ 5 AU (Fig 24), inconsistent with observed gradients of the anomalous O (see above). With a source located on the equator, acceptable positive gradients are produced but the predicted intensity dependence on the IMF polarity is inconsistent with observation at Earth. They conclude that models assuming termination-shock acceleration and drifts as in Pesses *et al.* (1981) cannot fit the observation. However, Jokipii claims that the predictions of his recent model with these features agree with both the spectral and gradient observations.

6. Concluding Remarks

The reports at the conference underscore the importance of

(a) analysing particle directional anisotropies in both GLEs and spacecraft observed events, in understanding pitch-angle scattering by magnetic turbulence and the focusing effect of the IMF

(b) having many observation posts ,i.e. spacecraft, to study coronal and interplanetary propagation

(c) correlative studies of multi-spacecraft particle data with solar electromagnetic emissions and synoptic maps of the coronal magnetic field, in deciding e.g. whether coronal diffusion or shock acceleration is operative far from the flare site

(d) drifts in particle acceleration by quasi-perpendicular shocks, and the inclusion of scattering in the SDA model

(e) the deep space network for studying long-term solar modulation and short-term modulation by shocks

(f) the future Ulysses mission in providing the much needed 3-D view of solar modulation.

The experimental determination of the rigidity dependence of the interplanetary mean free path below ~200 MeV is still controversial and more work needs to be done. In particular, the effect of the flare shock as a continuous moving particle source and a reflector should be

modelled.

The exact mechanism of solar modulation and the origin of the anomalous component remain controversial, although both drifts and cumulative shock modulation are recognised to be important. However, this is the subject of another rapporteur paper of this conference (Kota, 1985).

It is hoped that by the next ICRC, much progress would have been made and many of these controversies would be resolved.

Acknowledgements

I wish to thank many of the authors for stimulating and helpful discussions and to B.L. Ng for her patient typing of the manuscript.

References

Bazilevskaya, G.A. and E. V. Vashenyuk (1979) 16th ICRC, Kyoto, *5*, 156.
Burlaga, L. *et al.* (1983) Geophys. Res. Lett., *10*, 413.
Christon, S.P. and E.C. Stone (1985) Geophys. Res. Lett., *12*, 109.
Decker, R.B. (1983) J. Geophys. Res., *88*, 9959.
Decker, R.B. *et al.* (1984) Astrophys. J., *278*, L122.
Evenson, P. *et al.* (1983) Astrophys. J., *275*, L15.
Fisk, L.A. *et al.* (1974) Astrophys. J., *190*, L35.
Jokipii, J.R. (1982) Astrophys. J., *255*, 716.
Jokipii, J.R. (1985) Submitted to J. Geophys. Res.
Kota, J, (1985) 19th ICRC, San Diego, Rapporteur paper.
Lee, M.A. (1983) J. Geophys. Res.,*88*, 6109.
Lin, R. P. and H. S. Hudson (1976) Solar Phys., *50*, 153.
Lockwood, J.A. *et al.* (1982) J. Geophys. Res., *87*, 4338.
Mason, G.M. *et al.* (1984) Astrophys. J., *280*, 902.
McGuire, R. E. *et al.* (1983) 18th ICRC, Bangalore, *10*, 353.
Mullan, D.J. (1983) Astrophys. J., *269*, 765.
Mullan, D.J. and K.H. Schatten (1979) Solar Phys., *62*, 153.
Newkirk, G., Jr. and D.G. Wentzel (1978) J. Geophys. Res., *83*, 2009.
Ng, C.K. and L.J. Gleeson (1976) Solar Phys., *46*, 347.
Ng, C.K. *et al.* (1983) 18th ICRC, Bangalore, *10*, 381.
Pesses, M.E. *et al.* (1981) Astrophys. J., *246*, L85.
Reid, G.C. (1964) J. Geophys. Res., *69*, 2659.
Scholer, M. (1985) 19th ICRC, San Diego, Highlight talk.
Steinolfson, R.S. and D.J. Mullan (1980) Astrophys. J., *241*, 1186.
Van Hollebeke, M.A.I. (1979) Rev. Geophys. Space Phys., *17*, 545.
Webb, G.M. (1983) Astron. Astrophys., *124*, 163.

MODULATION AND ANISOTROPY OF GALACTIC COSMIC RAYS IN THE HELIOSPHERE

J. Kóta

Central Research Institute for Physics, Budapest, Hungary
and
University of Arizona, Tucson, U.S.A.

This rapporteur paper is intended to review sessions SH-4, which were devoted to the study of solar modulation of galactic cosmic rays. Two of the seven sessions, SH-4.6 (anomalous component) and SH-4.7 (radial gradients based on multi-spacecraft measurements) were covered by Dr. Ng in the preceding rapporteur talk. Though these sessions constitute a most important part of the recent developments in modulation studies, they will not be repeatedly reviewed here. The five sessions to be reported on contained 82 contributed papers, among which about 50 were presented at the Conference. Due to the limited scope of this paper, many excellent contributions cannot be quoted here. This report is inevitably biased, reflecting my personal views and approach. The main line of the review shall follow the classification used by the Program Committee. First, modulation models will be discussed with more time spent on two current ideas: episodic modulation and drift models, then the various types of anisotropies will be addressed. Finally, other time variations and correlation studies will briefly be reviewed.

1. INTRODUCTION

Having entered the heliosphere cosmic rays are subject to solar modulation. Charged particles are convected outward by the magnetic fields frozen in the radially expanding solar wind and also undergo adiabatic deceleration due to the expansion of the solar wind plasma. The intensity reduction and energy loss of cosmic rays are very closely connected. At a given energy, an observer inside the heliosphere sees the unmodulated galactic spectrum at higher energies, a falling spectrum should thus result in a decrease of flux. In fact, most of the modulation can be related to energy loss. In a lesser extent, an absorbing boundary near the sun may also give rise to an intensity reduction of cosmic rays without any change of energy.

By now, it is well established that, as long as the diffusion approximation applies, the transport of charged particles in the heliosphere is governed by the equation:

$$\partial f/\partial t = \mathrm{div}(\underline{\underline{\kappa}}\,\mathrm{grad}\, f) - \underline{V}.\mathrm{grad} f + (\mathrm{div}\underline{V}/3).\partial f/\partial \ln p \qquad (1)$$

where $f(r,p)$ stands for the isotropic part of the cosmic ray distribution in the 6-dimensional $(\underline{r},\underline{p})$ phase-space; the momentum-spectrum, $U_p(\underline{r},p)$ can be expressed as $U_p=4\pi p^2 f$. $\underline{V}$ is the solar wind speed. The diffusion-tensor, $\underline{\underline{\kappa}}$, has different values along and across the magnetic field, respectively, while its antisymmetric component accounts for the effects of the regular magnetic field. The anisotropy-vector, ξ, is the sum of the diffusive and convective components.

2. MODULATION MODELS

The multi-spacecraft measurements of cosmic ray intensity pose a serious challenge to modulation theories. The 2-4 %/AU value of the radial gradient of >60 MeV particles remained surprisingly stable from solar minimum to solar maximum, while the level of modulation changed considerably (Webber and Lockwood SH 4.7-1). At lower energies, there was virtually no observable gradient between 1 AU and 30 AU during solar activity maximum (McKibben, Pyle, and Simpson 1985; SH 4.7-5). For a detailed review of the radial gradients the reader is referred to the report of Ng in this volume. All these results imply that a very large part of modulation should take place at heliographic distances beyond 30 AU. It seems that either the region of modulation should be larger than believed, or modulation should be fairly effective at large heliographic distances.

There may be several possibilities to resolve this problem. In a pair of papers Gold and Venkatesan (SH 4.1-14) and Roelof (SH 4.1-24) suggested that the shocked plasma may form a buffer at large distances (>10 AU) from the sun. By reaching the distance of 10 AU, practically all the plasma must have gone through a shock: the shocked plasma is expected to be turbulent with a small diffusion coefficient. The unshocked plasma, on the other hand, is assumed to be virtually scatterfree. The authors presented an indication in favour of this hypothesis: at 1 AU a higher cosmic ray intensity was found when the connecting field line reached the shocked region at larger distances, and intensity minima were observed when this assumed shocked region happened to be near the earth.

Another possibility is the presence of a boundary effect as it was proposed by Krainev, Stozhkov, and Charakchyan (SH 4.2-19). So far, very little is known about the transition between the interstellar space and the heliospheric magnetic field. One cannot even rule out that the location of the outer boundary changes during a solar cycle. The study of the outer boundary, which has been a largely neglected subject so far, is one of the topics which should be addressed to in the next years. It would not be too surprising if the region of solar wind termination turned out to have profound effects in the transport of cosmic rays.

In the paper SH 4.1-6, Garcia-Munoz, Pyle, and Simpson demonstrated that the observed modulation of proton, helium, and carbon spectra can be explained in terms of a simple 1-dimensional force-field model. They used the helium spectrum as an input to estimate the radial diffusion coefficient, K_{rr}, which was allowed to vary from year to year. Then the thus adjusted diffusion coefficients (Figure 1) gave a good fit for the other species, too. The force-field solution (Gleeson and Axford 1968) represents the most widely usable analytical approximation to the time-independent form of the transport-equation (1). It does,

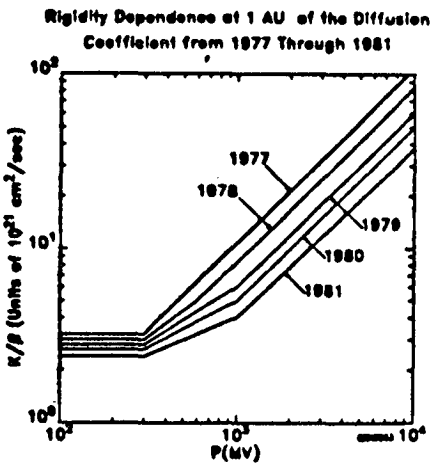

FIG. 1. - Inferred diffusion coefficients at 1 AU (SH 4.1-16)

however, rely upon the assumption of $\kappa_{rr} >> r.V$ which is violated at larger distances if, as assumed, κ_{rr} changes slowly between 1 AU and 30 AU. It remains to be determined whether the force-field solution still gives a reasonable approximation for the case of $\kappa_{rr} \approx rV$. One may expect a certain breakdown of the force-field theory, and a dramatic increase of modulation if $rV/\kappa_{rr} >> 1$. Most probably, employing a numerical method instead of the force-field approximation would result in somewhat modified diffusion coefficients at low energies but would not alter the overall picture. The results of SH 4.1-6, however, do not necessarily prove that cosmic ray transport is indeed 1-dimensional, they may show only that, at the present stage, we have still too much freedom in adjusting the values of diffusion coefficient.

2.1. Episodic modulation

It has been noted by McDonald et.al. (1981) that cosmic ray intensity shows sudden step-like decreases followed by slow, but not full, recoveries. These events, in most cases, can be associated with disturbances travelling outward in the solar system. The step-like decreases can be identified in the records of various spacecraft, the time lags correspond to a propagation speed of roughly the solar wind velocity. This led to the hypothesis that the long-term modulation is a cumulative effect of many episodic decreases. The immediate cause of the sudden decreases has not yet been clearly established, it may be, for instance, either the shock itself or the enhanced scattering in the disturbed region. Perko and Fisk (1983) assume narrow shells of enhanced scattering propagating together with the solar wind. The emission of these shells is supposed to be more frequent at high solar activity. This treatment calls for the solution of the time dependent transport equation (1). In return for the more numerical computation required, this method is also able to account for time lag between the variation of the cosmic ray intensity and the solar activity.

Venkatesan et. al. (1984) found that the phase of solar modulation propagated considerably faster than the speed of the solar wind. This seemingly surprising finding was explained by Forman, Jones, and Perko (SH 4.1-12) in an elegant way. As these authors pointed out, modulation is sensitive to the integrated effects between the observer and the outer boundary. Crudely, the integral is maximum, and intensity is at minimum, when the maximum of disturbances is halfway between the observer and the boundary. As a result, the phase of modulation may travel about twice as fast as the solar wind. The more accurate numerical work gave a value of 1.85 times the speed of the individual decraeses. It should be borne in mind, as the authors emphasized, that this derivation applies only if modulation is indeed a cumulative effect of many events. In the case of one single event or decaying disturbanceswhich do not travel to large distances, the phase of modulation should obviously propagate with the velocity of individual decreases.

There have been arguments brought forward indicating that "merged interaction regions" are responsible for the sudden intensity decreases. Burlaga, Goldstein, and McDonald (SH 4.1-11) found a most impressive agreement between the occurence of decreases in the intensity of >75 MeV/n nuclei and the passage of regions of enhanced magnetic field at the Voyager spacecraft (Figure 2). The regions of strong magnetic field are interpreted as "merged interaction regions" with turbulent fields which are formed as a result of interaction of shocks and streams. Now it is

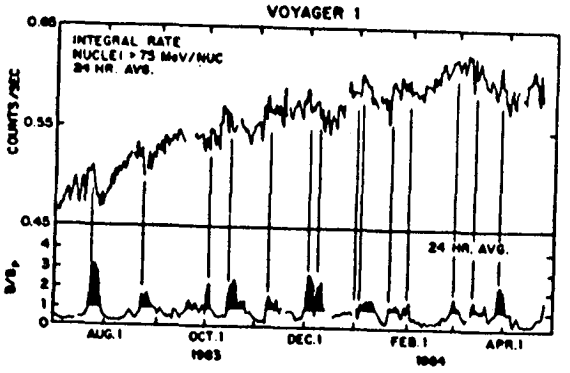

FIG. 2. - Itensity of cosmic rays)75 MeV/n vs. time (top) and magnetic field strength w.r.t. the spiral field (SH 4.1-11)

the turn of theory to provide a solid basis to the originally phenomenological description: a yet unpublished paper of Chic and Lee (1985) claims to give this theoretical support. Thus, research in this field seems to be vigorous and progress is rapid. The theoretical model permits an estimation of the diffusion tensor, the thus inferred value turns out close to the value of Perko and Fisk (1983).

At higher rigidities (1-2 GV), the effect of a sequence of shocks was investigated by Gall, Thomas, and Durand (SH 4.1-7) who applied a method based on calculating the intensity reduction from the spectrum of energy loss. The remarkable feature of this work is that it permits acceleration and decelaration at the same time. One single shock will give rise to a sharp Forbush-like decrease. If, however, there is a sequence of shocks then particles trapped between two shocks may also gain energy, and this may give rise to a slower variation of intensity. In this context it is important that shocks are assumed to widen while traveling outward otherwise div$\underline{V}$, which is responsible for energy gain or loss, could not be negative. In the overall balance deceleration is the dominant process leading to a net decrease of particle flux. The most important parameter of modulation appears to be the frequency of the shocks emitted. This work also included drift-effects which can be important at the energies considered. Indeed, a marked difference was found between the results obtained for the two opposite magnetic configurations.

In recent years, there has been a great deal of misunderstanding concerning calculations relating the modulation of cosmic ray intensity to the spectrum of energy loss. The subject of controversy is the applicability of the Liouville's theorem for diffusive processes like cosmic ray transport in the heliosphere. It can be shown, however, that the "method of energy loss" is mathematically equivalent to the use of the adjoint Green-function developed by Webb and Gleeson (1977) (see Kóta 1984). Intensity modulation and energy loss stem from the same basic physical process and there is a close and deep relation between them. Energy loss is not an extra process, but, in a sense, is rather tantamount to intensity change.

Obviously, the study of Forbush-decreases may allow a better insight into the process of modulation. An extensive statistical study of the recovery time was presented by Lockwood, Webber, and Jokipii (SH 4.1-9). They conclude that the average recovery time is fairly stable throughout the solar cycle, including the polarity reversal of the sun. It also turns out independent of particle energy, but it does depend on the heliographic distance. The longer recovery time at large radii may lead

to a more effective modulation in the outer heliosphere. By analyzing the rigidity spectra of long-term modulation and Forbush-decreases at neutron monitor energies, Fenton, Fenton, and Humble (SH 4.4-10), on the other hand, arrived at different spectral exponents, which might be considered as an indication against interpreting long term modulation as superimposed Forbush-decreases, at least at these energies.

Earl (SH 4.1-3) and Earl and Jokipii (SH 4.1-3) presented a couple of works on numerical techniques for solving time-dependent transport equations. These papers are more relevant to the propagation of solar particles where time variations are faster and numerical subtleties are more delicate. Nevertheless, they have a message to the modulation workers, too. First, the grids should be chosen carefully. One should add that in a realistic case the coefficients of the transport equation are not constant, thus the construction of an appropriate grid is not at all trivial. The main lesson, in my judgement, is that one should first understand the qualitative behaviour of the solution and then employ the numerical code.

2.2. Drift models

Drift still remained a most controversial subject, there were numerous arguments both pro and contra drift. Drift models seem to have been attracting critics ever since the pioneering work of Jokipii, Levy and Hubbard (1977). This stems from the fact that drift theories come up with very specific predictions. Curvature and gradient drifts are the only known process in cosmic ray transport which is sensitive to the electric charge. Thus, a charge dependence in the modulation should be a unique signature of drift. A charge asymmetry may appear in two obvious indirect forms. First, two consecutive 11-year cycles may be different or, in other words, the two halves of the 22-year magnetic cycle are different. Second, the location of the interplanetray neutral sheet can be important. My classification in this section (i.e. 22-year cycle, charge-asymmetry, neutral sheet effects) is largely artificial, all these result from a common origin, namely charge-dependence.

Conceptual developments

For a near isotropic distribution the particle drift velocity in a magnetic field, $\underline{B}$, is $\underline{v}_d = (pc/3q)\nabla\times(\underline{B}/B^2)$, which is also the divergence of the antisymmetric part of the diffusion tensor, provided the scattering mean free path, λ, is sufficiently larger than the Larmour radius, ρ. Positively charged particles drift (Figure 3) from the poles toward the neutral sheet in the magnetic configuration prevailing in the years 1970-1980, when field lines point away from the sun above the neutral sheet and sunward below the sheet (A>0). For the opposite configuration (A<0) the sense of drift reverses. The δ-like singularity of the drift appearing at the neutral sheet may cause some concern. The velocity of the guiding center is indeed infinite at the crossing of the neutral sheet, the average drift of a particle during a gyro-period, however, obviously remains less than the particle speed. Burger, Moraal, and Webb (SH 4.2-3) refined the concept of drift by evaluating the average (and finite, of course) drifts near the neutral sheet. Since drift velocity is divergence-free, it immediately follows that the two approaches must give the same net drift in the $(-2\rho,+2\rho)$ vicinity of the neutral sheet. The δ-singularity can also be avoided in the original

derivation, its emerge is connected with the well-known inaccuracy of the diffusion picture near a boundary.

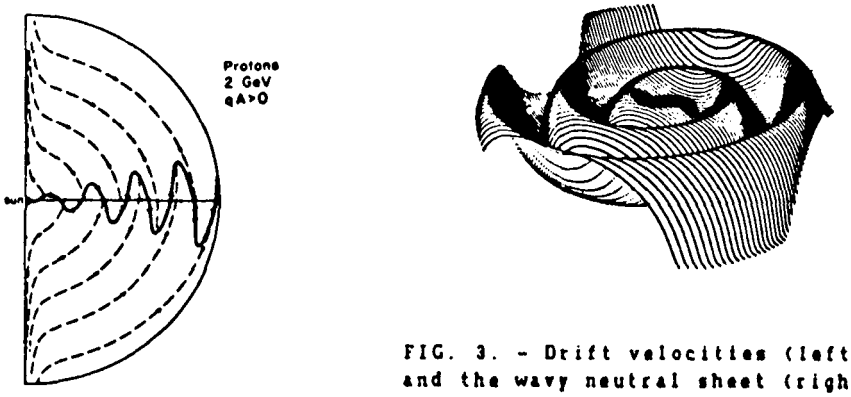

FIG. 3. - Drift velocities (left) and the wavy neutral sheet (right)

22-year cycle

The presence of a 22-year cycle first appeared in the earth-based anisotropy measurements: in the periods of A>0, the phase of the solar daily variation was observed to shift toward earlier hours with respect to the 18 hr phase of corotation. This effect can be accounted for in a natural way in terms of drift. In fact, the renaissance of drift theory started when Levy (1976) invoked drift to explain this phase shift in the solar daily wave of cosmic ray intensity variation. Anisotropies will be discussed in more detail in a later paragraph.

In an extensive numerical work Potgieter (SH 4.2-4, SH 4.2-5, see also Potgieter and Moraal 1985) was able to describe the proton and electron spectra for two consecutive solar minima (1965 and 1977) with one single set of parameters. Figure 4 shows the good agreement between the observed and calculated proton and electron ratios (1977 relative to 1965) in the 50 MeV - 1 GeV range. The predicted radial gradient of protons turns out considerably smaller for the magnetic configuration of 1977 (A>0), in accord with other drift calculations (see Kóta and Jokipii 1983, and references therein). Observations, on the other hand, seem to indicate a stable gradient or a decrease of gradient for A<0, (see the

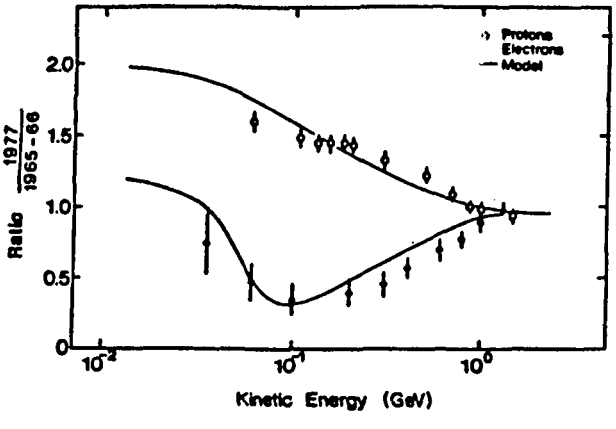

FIG. 4. - Calculated proton and electron ratios for 1977 relative to 1965 + 1966 (SH 4.2-4)

review of Ng, this volume). The radial gradient is certainly an exciting and controversial subject. The smaller radial gradient for A>0 seems to be essential in explaining the observed phase-shift of the anisotropy at GeV energies. Conversely, the smaller azimuthal streaming obtained by anisotropy measurements in the seventies implies a smaller radial gradient, at least for the GeV energies, where direct data on the gradient are scarce. The small radial gradient in the case of A>0 is a common feature of drift models. Kóta (1981) has derived a 3-D force-field solution including drift which gives a charge independent radial gradient, this model, however, relies upon specific assumptions. At low energies, the nature and extent of drift effects are not fully understood yet, the exploration of these is an important and urgent task.

Neutron monitor intensities exhibit different time evolution in the two 11-year cycles. Shea and Smart (SH 4.2-24) presented an updated statistical analysis of the correlation between cosmic ray intensity and the geomagnetic aa index. It is apparent from Figure 5 that, in the sixties, cosmic ray intensity was peaked at solar minimum, while the period of the seventies was characterized by a long plateau. This is just what one would expect from a drift model incorporating a wavy neutral sheet, with the tilt angle varying from small to larger angles as solar

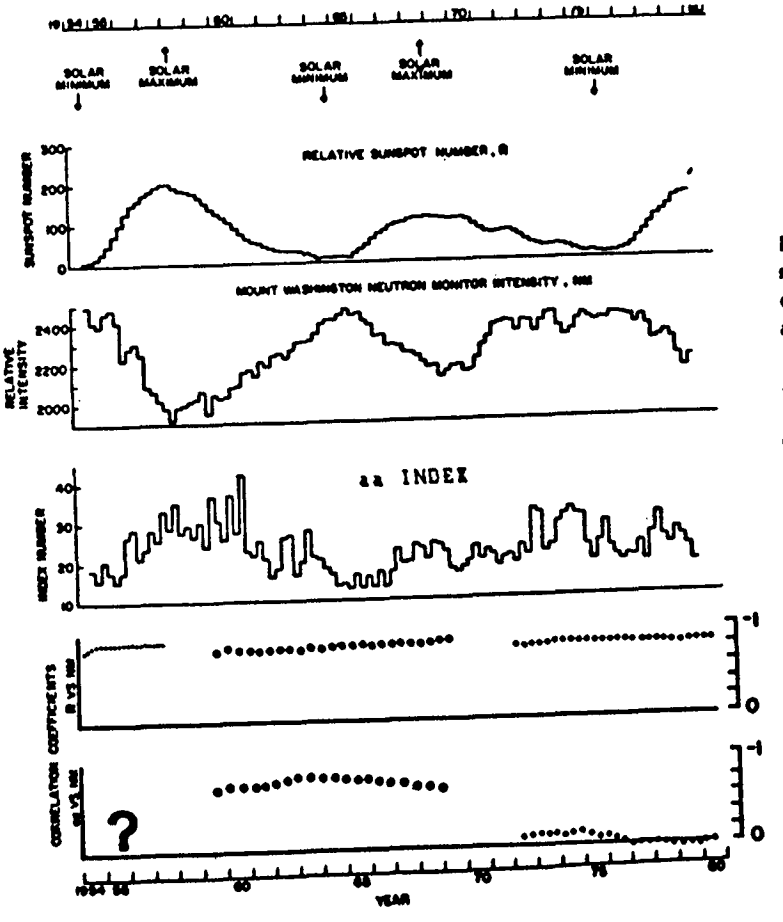

FIG. 5. - The sunspot numbers, cosmic ray flux, and aa index vs. time from 1954 to 1979. Lower panels show correlation coefficients. For details see SH 4.2-24.

activity increases (Kóta and Jokipii 1983). The correlation between the cosmic ray intensity and the geomagnetic aa index was found to be good for A<0 and poor for A>0. This, again, is in accord with the predictions of drift models. In this context, it is not crucially important that the modulation is ascribed to the wavy neutral sheet, it could be substituted by any other phenomenon which affects cosmic rays primarily in the helioequatorial region. In contrast to these results, Otaola, Perez-Enriquez, and Valdes-Galicia (SH 4.2-22) and Chirkov (SH 4.2-21) find a good correlation between the aa index and cosmic ray intensity for A>0, too. According to these authors, the aa index itself has a 22-year cycle and this is solely responsible for the asymmetry in cosmic ray counts. Similar conclusion is reached by Krivoshapkin et.al. (SH 4.4-22) at high rigidities. More studies are required to resolve the discrepancy between these works.

I also would like to mention two works here, which were presented in other sessions but bear importance in the topic of my report, too. Moraal and Mulder (SH 5.1-2) presented a statistical analysis of Forbush-decreases in the two different magnetic cycles. They find an evidence indicating that, at neutron monitor energies, the recovery is faster in the A>0 configuration. This may be interpreted as a result of drift: particles drifting down from higher latitudes (A>0) can refill the earth's vicinity more rapidly than particles coming through the equatorial region (A<0). It would be interesting to see if there is a difference between the anisotropies during the time of recovery.

One of the most interesting developments at the Conference was the reappearence of the anomalous component. The spectrum of the anomalous component has been found to shift toward higher energies with respect to the last cycle (Cummings, Stone, and Webber SH 4.6-1). This can be interpreted in terms of drift (Jokipii 1985). The anomalous component has very important implications, these will not be discussed here (for details on the anomalous component, see the report of Ng, this volume).

Charge-asymmetry

Recently Evenson and Meyer (1984) found that after the last solar maximum electron intensity recovered faster than protons while the opposite happened following the previous (1970) maximum. This is in agreement with the prediction of Kóta and Jokipii (1983), and can be interpreted as strong indication of drift effect. At this conference, Garcia-Munoz et. al. (SH 4.2-23) presented a thorough study of the helium to electron ratio from 1965 to 1985. The investigated energy ranges correspond to roughly the same rigidities, the difference in velocities is not expected to introduce a significant effect. The relative content of 70-95 MeV/n helium increased by about a factor of 2 around the polarity reversal of the sun in 1970, and decreased to its earlier (1968) level around 1980 (Figure 6). Since observations refer to the same time period, there can be little doubt that this finding should be interpreted as a clear sign of a charge dependence in the modulation of cosmic rays. It would be , however, too early to celebrate for those who believe in drift. Electrons fail to show the peaked 11-year cycle in the years of seventies, which would be a major prediction of the model of Kóta and Jokipii (1983). Instead, the time evolution of electron and helium intensities turn out rather similar (Figure 7). Certainly, further theoretical and experimental efforts are needed to clarify this subtle problem. Unfortunately, simultaneous electron and helium data are avail-

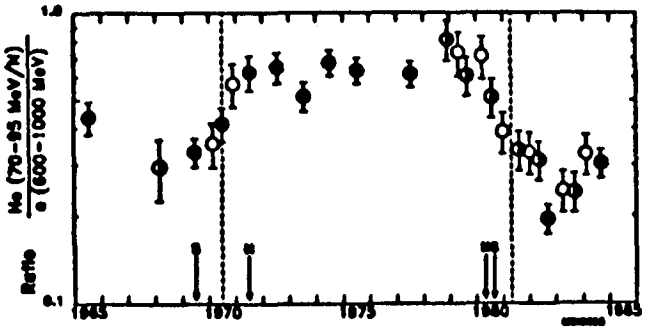

FIG. 6. - Helium to electron ratio versus time. The dashed vertical lines refer to solar polarity reversals. For details see SH 4.2-23.

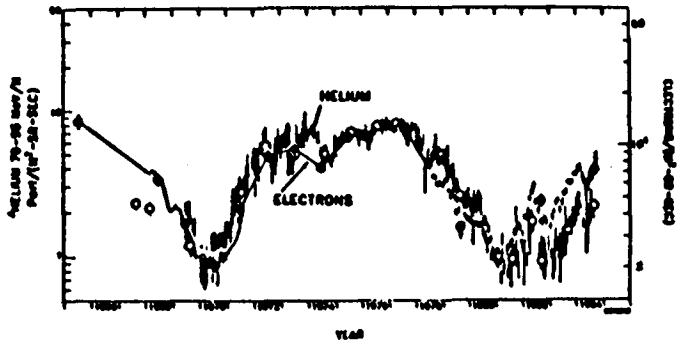

FIG. 7. - Modulation of helium and electrons in the 1970-80 cycle. Note that shapes are near the same. (SH 4.2-23)

able for one cycle only, the status of experiments will improve as the present cycle proceeds. From the theoretical side, the implications of drift should be studied more thoroughly at lower energies. Furthermore, it should be kept in mind that the model of Kóta and Jokipii (1983) does not claim to describe the period of solar maximum. The present model is certainly too simplified for that case. Unfortunately, a more sophisticated model will encounter new numerical, and also conceptual, difficulties.

Neutral sheet effects

The structure and location of the neutral sheet may affect cosmic ray transport in either a direct way via drift or an indirect way via the increase of the solar wind speed away from the neutral sheet.

A drift-model incorporating a wavy neutral sheet obviously needs a 3-dimensional calculation. The numerical studies of Kóta and Jokipii (1983, see also SH 4.2-10) represent the only full 3-D treatment available so far. Figure 8 shows the intensity contours obtained on a 1 AU sphere for both A>0 and A<0. The 3-dimensional character of the solutions is apparent. The intensity contours are best organized by the neutral sheet. It should also be kept in mind, however, that there is no obvious single parameter to fully organize the contours.

As a rule, cosmic ray intensity is predicted to rise toward the poles for A>0, and fall away from the neutral sheet for A<0. The difference in the latitudinal gradients, if observed, would be an evidence in favour of drift. Earth-based measurements give azimuthal sections in a narrow band around the heliographic equator. The 7.5° excursion of the earth about

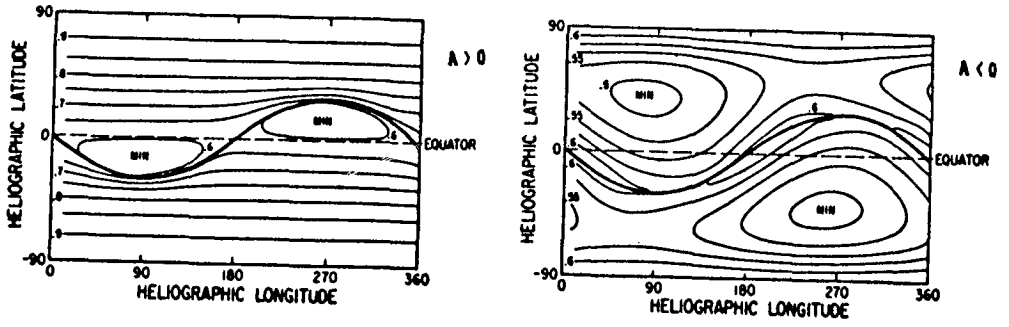

FIG. 8. - Computed contours of equal cosmic ray intensity at 1 AU, for 2.36 GeV protons, for A>0 (left) and A<0 (right). The inclination of the neutral sheet is 30 degree (Kota and Jokipii 1983).

the helioequatorial plane permits the study of the latitudinal gradient. By exploiting this, Kóta, Merényi, and Erdős (1985) arrived at a polarity dependent gradient of high rigidity (~70 GV) cosmic rays rising away from the neutral sheet in the period of 1974-79, in accord with the predictions.

When the earth-based intensities are organized according to the "heliomagnetic latitude" of the earth (i.e. distance from the neutral sheet), a negative correlation is obtained between cosmic ray intensity and heliomagnetic latitude (Figure 9) for both configurations (Newkirk and Fisk 1985; Newkirk et.al. SH 4.2-16). This result is seemingly surprising for A>0. With a numerical simulation of the experimental situation, Jokipii and Kóta (SH 4.2-10) demonstrated that a 3-D model does predict such a negative correlation (Figure 10) thus experimental results do not disprove drift. Newkirk et.al. (SH 4.2-16) have also pointed out that the model calculations of Kóta and Jokipii (1983) would give a much larger gradient for A<0, while the measurements do not show any significant difference (Figure 11). This challenge has not been answered yet. The A<0 solutions are sensitive to perpendicular diffusion, thus it is conceivable that adjusting the parameters could cure the discrepancy. Another, perhaps more probable, possibility is that calculations employed a too simplified, and too regular model.

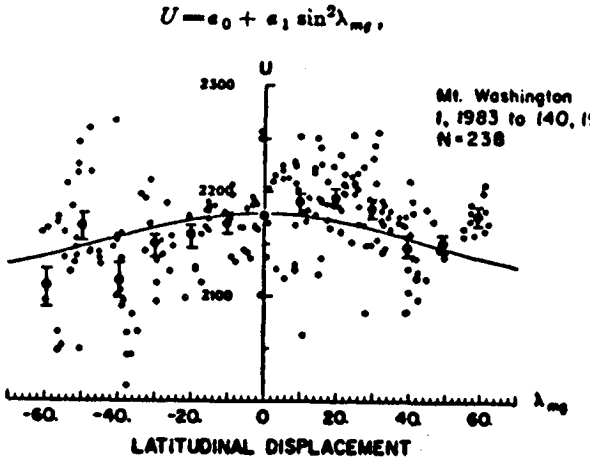

FIG. 9. - An example of the variation of cosmic ray flux vs. heliomagnetic latitude during 1983-84 (A<0) (SH 4.2-16). A very similar picture is obtained for A>0 (Newkirk and Fisk 1985).

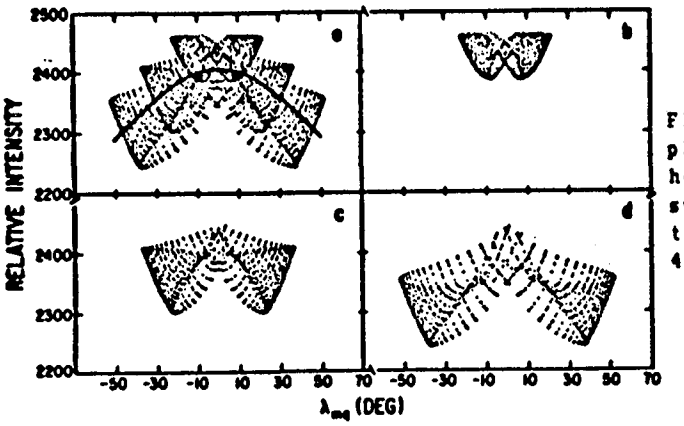

FIG. 10. - a total scatter plot of intensity versus heliomagnetic latitude, λ_{mg}, summed over three inclinations: 15 (b), 30 (c), and 45 (d) degrees (SH 4.1-10)

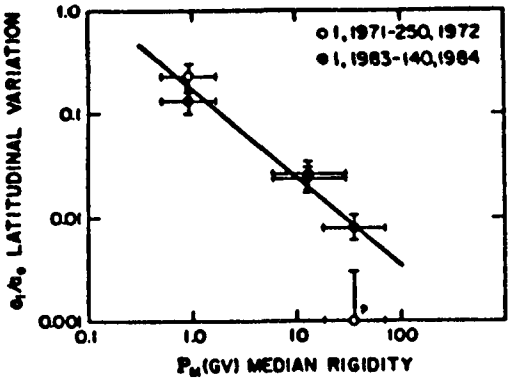

FIG. 11. - The rigidity dependence of the relative latitudinal gradients. Note the lack of a significant difference between the 1971-72 and 1983-84 intervals (SH 4.22-16).

Christon et.al. (SH 4.2-9) used the data of Voyagers to derive the latitudinal gradient of >75 MeV protons from two-point measurements in the period of 1981-83 (A<0). They found that a negative gradient became significant when a selecting restriction was employed. Crudely, this restriction selected the configurations when both spacecraft were on the same side of the sheet (say above) and, furthermore, the one at higher latitude (Voyager 1) was also more distant from the sheet. This selection enabled the authors to filter out real latitudinal effects and suppress the noise from azimuthal effects. The result is in good agreement with the predictions of drift.

Saito and Swinson (SH 4.2-8) pointed out that, in the period of 1971-74, two remarkable decreases in the counts of the Mt. Washington Neutron Monitor coincided with high inclinations of the tilt angle of the neutral sheet, just as expected from drift models. Badruddin and Yadav (SH 4.2-12) also find a negative correlation between the tilt angle and the intensity of cosmic rays, which, however, they attribute to the increase of the solar wind speed.

In a numerical study including a wavy neutral sheet, Alaniya et.al. (SH 4.2-18) confirm that cosmic ray intensity decreases as the tilt angle of the sheet is increased. This work, however, employs a 2-D code assuming azimuthal symmetry. Conceptually, the neutral sheet cannot be azimuthally symmetric, it would violate the $\mathrm{div}\underline{B}=0$ condition. The azimuthal asymmetry, in my judgement, is essential in the case of a wavy

sheet. These authors also make an ambitious attempt to derive some interesting quantities from the anisotropies obtained in different magnetic sectors. In doing so, however, they seem to assume a constant latitudinal gradient, which appears to be unjustified: the latitudinal gradient is bound to change at sector crossings.

2.3. Concluding Remarks

It seems that progress has been made since the last Conference. The field of episodic modulation is flourishing. Drift still remained a controversial subject and attracted much attention: there were new experimental and theoretical works presented both in favour of drift and challenging it. Being personally biased I would be inclined to giving more credit to the pro arguments. Drift models were successful in explaining some basic phenomena, the difficulties encountered may be connected with the simple, overly regular field models employed in the calculations. Often, the question is set in the form: is modulation caused by drift or something else? It should be remembered, that drift does not exclude other effects superimposed on it. In particular, drift models in their present form do not claim to describe the period of solar maximum when the heliospheric field should be more complex.

Spacecraft measurements in the outer heliosphere brought puzzling results which will certainly inspire theoretical research. By the time of the next Conference we reach solar minimum which then can be compared with the last minimum. We will be ahead of the exploration of high latitudes by the Ulysses mission, which makes 3-D predictions to become increasingly important. To promote the credit of model-calculations we need a better understanding of the scattering-process. Unfortunately, theory has advanced little in this field in the last years. At the Conference, there was only one theoretical paper addressing this problem: Dorman et.al. (SH 4.1-20) attempted to separate the scattering effects of "small-scale" and "large-scale" magnetic inhomogenities.

3. ANISOTROPIES

Anisotropies will be divided into three convenient groups. First, I discuss the so-called $\underline{B} \times \underline{\nabla} n$ anisotropy which is closely related to the local gradients. Then sidereal anisotropies will be reviewed, which aim to the search of a galactic signal. Finally, the term of solar anisotropies will include all solar induced anisotropies which do not fall into either of the first two categories.

3.1. $\underline{B} \times \underline{\nabla} n$ anisotropy, local gradients

The $\underline{B} \times \underline{\nabla} n$ anisotropy arises as a result of the antisymmetric term of the diffusion tensor. This streaming is connected with the regular spiralling motion in the magnetic field. It is not directly connected to particle drift: without density gradient, drift will not produce any anisotropy, while a density gradient does lead to a streaming in a homogeneous magnetic field, too. The magnitude of the resulting anisotropy is $\rho . \nabla_{\perp} n/n$, where $\nabla_{\perp} n$ is the density gradient in the direction normal to the field. Being polarity-dependent this anisotropy can be disentangled from other terms of the anisotropy, and then, knowing the Larmour radius, ρ , the gradient can be determined (Bercovitch 1970).

Fillius et.al. (SH 4.3-7) employed this method to estimate the radial gradient from the >500 MeV/n channel of Pioneer 10 (median rigidity ~5 GV) in the period of 1973-75, during which the spacecraft traveled from 3 AU to ~7 AU. The analysis gave a fairly stable gradient between 1 - 2 %/AU which is also comparable with the values of the global gradient between the earth and the spacecraft derived from the total counts. Unfortunately, the global gradient is not available for the same channel (see SH 4.7-2) during this period.

At higher rigidities (~10 GV), Bieber and Pomerantz (SH 4.2-6) convincingly demonstrate the presence of a $\underline{B} \times \underline{\nabla} n$ anisotropy, which produces a North-Shouth asymmetry in the counting rates of the neutron monitors at Thule and McMurdo, respectively (Figure 12). The inferred

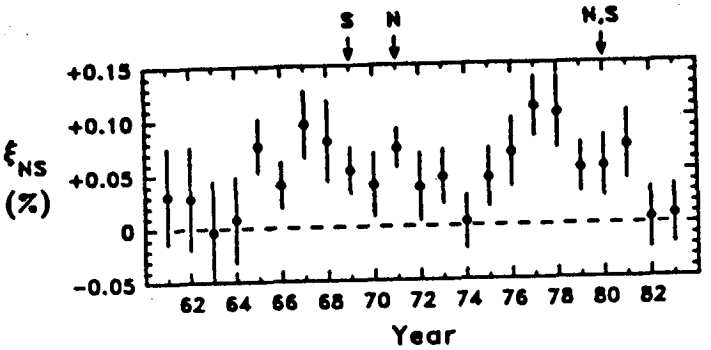

FIG. 12. - The cosmic ray North-South anisotropy, as obtained from the Thule and McMurdo NM records (SH 4.2-6)

radial gradient seems to show an 11-year cycle around a mean of 1.7 per cent/AU, and fails to show any noticeable dependence on the polarity of the solar field. The mean value of gradient agrees with that of Fillius et.al. It is intriguing that the radial gradient appears fairly stable over a wide range of energy: the values are barely larger for the >60 MeV particles (see Webber and Lockwood SH 4.7-1), despite the anticipated change of κ_{rr} in this range (c.f. Figure 1). At the lowest energies, the decrease of the Compton-Getting factor may explain the low value of the gradient, but it is hard to see a similar effect above 200 MeV.

The presence of the $\underline{B} \times \underline{\nabla} n$ streaming was also demonstrated in the work of Takahashi, Yahagi, and Chiba (SH 4.3-13) who deduced the first zonal harmonic from the data of the worldwide neutron monitor network, and showed that it undergoes sudden jumps at sector-crossings. A good correlation was found between the anisotropy and the components of the magnetic field by Xue, Zhang, and Xao (SH 4.3-15).

In a theoretical work Kóta and Jokipii (SH 4.2-11) argue that the $\underline{B} \times \underline{\nabla} n$ anisotropy may not appear in its full form. The latitudinal gradient may depend on magnetic polarity and, in this case, diffusion across the field lines will also give a polarity-dependent streaming, which may reduce the net N-S anisotropy. This effect can be important in the drift-models where latitudinal gradients are not negligible. In this case, the commonly used quantitative relation between the polarity dependent N-S anisotropy and the radial gradient may be inaccurate (the value of perpendicular diffusion coefficient should be crucial). It is also pointed out in this work that, in contrast to 2-D models, a 3-D model is able to reproduce the correct sense of this anisotropy.

The $\underline{B} \times \underline{\nabla} n$ anisotropy can also be applied to detect a steady North-South gradient as it has been shown by Swinson, Shea, and Humble (SH 4.2-7). The $\underline{B} \times \underline{\nabla} n$ streaming, in this case, adds a polarity-dependent

component to the daily variation in solar time. This study yielded a significant gradient rising toward the south for A<0, while a symmetrically rising gradient was obtained for the opposite polarity state (A>0, i.e. 1970-80). The authors attribute the asymmetric gradient to the N-S asymmetry of the sun: the northern hemisphere was observed to be more active during 1960-70, then this asymmetry disappeared after 1970. The symmetric gradient may be interpreted in terms of drift.

Significant N-S gradient has been found by other workers, too. By making use of the 7.5° inclination of the earth's orbit, Pathak et.al. (SH 4.3-14) infer an about 0.2 %/degree gradient pointing toward the south and no observable symmetric gradient during 1978-83. Since this study gives a mean variation averaged over polarities, the lack of a symmetric gradient does not deny the predictions of drift models. From the analysis of isotropic intensity waves, Duldig, Jacklyn and Pomerantz (SH 4.3-8) arrived at the conclusion that these may have resulted from a higher intensity of cosmic rays below the sheet. This is only one possible interpretation, the origin of the observed intensity waves is not yet well understood.

The presence of a small asymmetry of the heliosphere would bear some implications. For sake of simplicity, most of the theoretical works adopt simple symmetric models. One would anticipate small changes in the intensity distribution due to small asymmetries. The impact, however, would be more severe on the anisotropies which depend on a delicate balance.

3.2. Sidereal variations, galactic anisotropy

A major objective of studying sidereal daily variations is the search for a genuine galactic anisotropy. Beside a true galactic signal, there are other known effects which may also give rise to an intensity variation in sidereal time. An asymmetric heliosphere could easily produce a net stream of particles which could not be distinguished from a galactic signal. Even a symmetric heliosphere may, and does, produce 'spurious signal': the second spherical harmonics of the heliospheric anisotropy can also contribute to the sidereal daily variation. This was discussed in detail in the Highlight Talk of Mori (this volume). To eliminate this effect, most of the presented works employed the 'Nagashima-correction' (Nagashima et.al. 1983) inferring the spurious sidereal daily wave from the observed antisidereal wave. I shall return to this correction in the next paragraph.

Another difficulty in detecting a galactic anisotropy is posed by the 'magnetic optics' of the interplanetary field: the deflection of particle trajectories will distort and attenuate the original signal, random scattering will further impair the conditions of observation. An extensive study of these effects (Nagashima, Morishita, and Yasue, 1982) predicted a large dependence on the polarity of the heliospheric field. Bercovitch (1984, and also SH 4.4-1) compared these predictions with the experimental results of the Ottawa Horizontal Muon Array, and found that the expected displacements of the sidereal vectors failed to show up at the last polarity reversal. The discrepancy could not be resolved by changing the rate of scattering. This finding might imply that our model of the heliospheric magnetic field is inaccurate. It is an attractive feature of the several hundred GV particles that they may prove to be quite powerful in exploring the large-scale interplanetary field. Of course, the way of exploration is not straightforward, and these hopes

may be excessively optimistic.

Galactic anisotropy was searched for in a wide range of energies. Some of the reported first harmonics are summarized in Table 1. The lowest energies were represented in the work of Ishida et.al. (SH 4.4-2) who analyzed an impressive amount of data from the worldwide network of neutron monitors, and obtained somewhat different phases for the two polarity states. The 30 year record of the Yakutsk ionization chamber gave very small amplitude (Kuzmin et.al. SH 4.4-8). Ueno et.al. (SH 4.4-3) presented a comprehensive study of Nagoya, Misato, and Sakashita muon telescopes. Table 1 shows the results of the vertical telescopes, and also a high-energy point from the Sakashita South 60° inclined telescope is added. A similar analysis has been carried out by Swinson and Nagashima (SH 4.4-7) including the Bolivia, Embudo, and Soccoro stations. The deep-underground results of Matsushiro (Yasue, Mori, and Sagisaka SH 4.4-9) are already barely influenced by solar effects. All the quoted results are corrected for solar effects with Nagashima's method.

Paper	Station	P_m(GV)	amp $\times 10^4$	phase	
SH 4.4-2	NM network		2.0 ± 0.2	6.1 hr	A<0
			2.1 ± 0.2	8.6 hr	A>0
SH 4.4-8	ion ch. Yakutsk		< 0.5		
SH 4.4-3	muon Nagoya (V)	60	2.1 ± 1.1	4.4 hr	
	Misato (V)	145	1.2 ± 0.8	0.9 hr	
	Sakash.(V)	331	2.8 ± 0.4	4.2 hr	
	--- (SS)	540	7.2 ± 0.6	2.4 hr	
SH 4.4-7	muon Bolivia(V)	125	1.7 ± 0.5	9 hr	
	Embudo (V)	132	0.9 ± 0.3	1 hr	
	Soccoro(V)	305	2.7 ± 0.4	4 hr	
SH 4.4-9	muon Matsushiro	700	3.1 ± 0.5	2.3 hr	
SH 4.4-4	muon Poatina	1200	8.1 ± 2.5	2.4 hr	

Table 1.

Finally, the highest energy point is given by the Poatina measurement reported by Humble, Fenton, and Fenton (SH 4.4-4). The lack of significant variation in solar and anti-sidereal time confirms that the observed sidereal variation is due to a true galactic signal, and solar contamination is indeed negligible. Their first harmonic is in a good agreement with the well established galactic anisotropy obtained at somewhat still higher energies by the Musala, Norikura, and Baksan experiments, which, in a consensus, agree in a first harmonic of 0.057 percent and phase around 1.4 hr (c.f. Gombosi et.al. 1975, Sakakibara et. al. 1984, Alexeenko et.al. 1981). There is no compelling reason to expect the same anisotropy at the Northern and Southern hemispheres, respectively. The close agreement of the first harmonics is reassuring, as it implies that the structure of the anisotropy is reasonably smooth and relatively simple.

Inspection of Table 1 shows that the high-energy points tend to have a phase close to the 'expected' 1-2 hr. Measurements of median rigidities above 500 GV (Matsushiro, Sakashita SS) yield phases of 2-3 hr, the 300-500 GV range tends to shift toward later hours (around 4 hr). I would feel tempted to draw the conclusion that going down below 300 GV

it is increasingly difficult to eliminate solar effects. In particular, I would like to call attention to the possible asymmetries of the heliosphere (see previous paragraph) which are largely unkown. Experimental accuracy has vastly improved in the last decade. Our knowledge of the heliospheric field, however, may not live up to this accuracy. Now, we are able to see tiny effects which cannot be accounted for on the basis of our present knowledge. The traditional way of approach may need to be reversed: instead of taking the field model granted, we may use the anisotropy measurements to extract more information on the large scale structure of the heliosphere.

The second harmonic of the sidereal variation remains an intriguing problem. All of the Norikura, Baksan and Musala measurements show a significant second harmonic with phases around 5-6 hr, Norikura even claims a third harmonic around 7 hr (Sakakibara et.al. 1984), implying that the galactic anisotropy cannot be ascribed to a simple streaming. The Poatina results, on the other hand, do not show any noticeable second harmonic. This might be due to the limited statistics, but may as well indicate a true North-South difference. The discussion of the nature of a galactic anisotropy falls beyond the scope of this review. Yet, I feel tempted to make a remark, which stems from heliospheric background. It was proposed by Kóta (1979) that anisotropic pitch-angle scattering might be responsible for the rise of higher harmonics in the galactic anisotropy. Recently, Bieber and Pomerantz (1983) has worked out a similar, more advanced, theory including adiabatic focusing, to explain the higher harmonics of solar anisotropies. It would be interesting to see if the observed sidereal harmonics could be interpreted within the frame of the unified theory of Bieber and Pomerantz (1983).

A puzzling observation was presented by Jacklyn and Duldig (SH 4.4-6). During the years of sixties, a significant sidereal semi-diurnal wave was seen by both the Hobart and Mawson experiments. This wave disappeared after 1970 and failed to reappear after 1980. It seems hard to think of a plausible interpretation of this finding.

3.3. Solar anisotropies, higher harmonics

This paragraph is divided into two major parts. First, results on the solar daily wave will be reviewed then the higher harmonics and their effects will be considered. Among the various components of the anisotropy, the solar daily vector is the most robust, and also has the longest and most extensive history. Recently, higher harmonics seem to attract more and more attention, this can be attributed to developments in both theoretical and experimental research.

Solar daily variation

As for the very first approximation, the solar diurnal wave of intensity variation of cosmic rays was believed to be a result of a pure corotation with the sun. Corotation could be simply interpreted in the classic diffusion-convection theory if diffusion was permitted in the field's direction only. Forbush (1969) was the first to notice that the solar diurnal vector shows a 22-year wave, a phase shift occurs in association with the polarity reversal of the sun. The effect has been proved beyond doubt by numerous subsequent works: during the periods of seventies, fifties, etc., the daily vector moves toward earlier hours from the 18hr phase of corotation. This phase shift was first explained

by Levy (1976) invoking drift.

The conventional wisdom of phase shift is also apparent in the works presented at this Conference (Ahluwalia and Riker SH 4.5-7, Takahashi et.al. SH 4.5-13; Chuang, Kusunose, and Wada SH 4.5-14). Now, the main objective of the research is to find the rigidity spectrum, and find the solar parameters responsible for the year-to-year changes of the solar daily vector. Figure 13 shows the long-term variations of the amplitudes and phases as obtained by neutron monitors and muon telescopes during 1962-1979. Neutron monitor amplitudes tend to remain relatively stable while muon results undergo drastic variations. This is usually interpreted as a result of a changing cut-off rigidity.

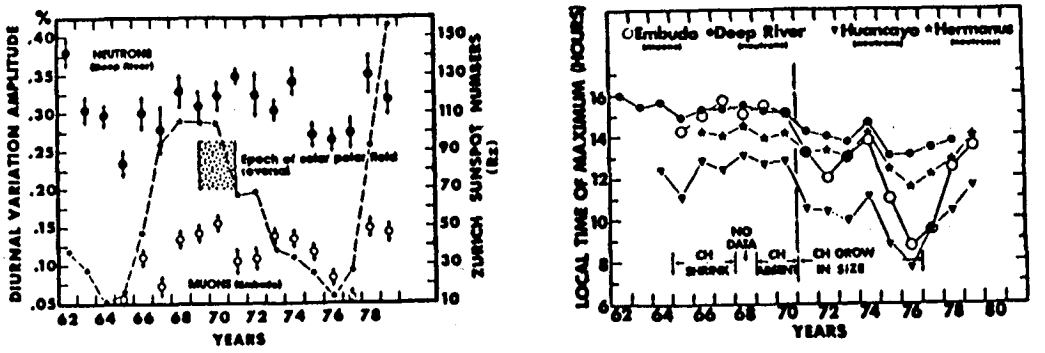

FIG. 13. - The annual mean amplitudes (left) and phases (right) of the solar daily waves, as obtained from neutron monitor and muon measurements. The dashed line shows the Zurich sunspot number (SH 4.5-7).

From the side of theory, the diffusive transport-equation (1) is applicable for neutron monitor energies. The major effect i.e. phase-shift has been reproduced by many independent numerical works incorporating drift (Potgieter and Moraal 1985; Potgieter SH 4.2-4; Kóta and Jokipii SH 4.2-11; Munakata and Nagashima SH 4.5-1; Kadokura and Nishida 1984). This consensus of the numerical results, and also our understanding of the physics involved should convince one that drift indeed gives rise to a phase shift. The quantitative features, on the other hand, are not yet all understood. Figure 14 shows the predictions of Potgieter (SH 4.2-4) together with experimental results. The agreement

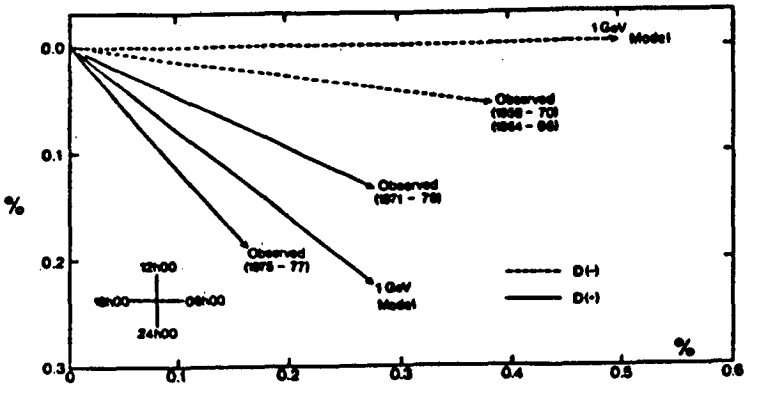

FIG. 14. - Observed (Hermanus, 4.5 GV) and computed solar diurnal vectors (SH 4.2-4)

is fairly close if we consider that model calculations are bound to be overly simplified. One might try to achieve a better fit by adjusting the input parameters. This, however, may not be very meaningful. The real solution would be the inclusion of a more realistic model of the heliosphere, which, if available, would require enormous amount of computing. At present, however, the full complexity of the heliosphere is not yet well modelled. Further studies may help to explore which features of the interplanetary field are primarily responsible for the long-term changes of the solar daily vector.

An important but conceptually obscure quantity is the upper the cut-off rigidity where solar effects cease. The upper cut-off undergoes a large variation during a 22-year cycle. It had a very low value in 1976 when virtually no anisotropy was detected by the muon telescopes (see Figure 13). On the other hand, Ueno et.al. (SH 4.5-18) reported on obtaining an anomalous large value during 1982, when the amplitude doubled at high rigidities (Sakashita, P_m=330 GV) while it remained the same at lower rigidities (Misato, Nagoya). The authors estimate a cut-off around 270 GV.

Ahluwalia (SH 4.5-4, SH 4.5-7) questioned the principle of cut-off. It is indeed a crude approximation expressing the common wisdom that solar effects should diminish at high rigidities. The Japanese groups use a 'power-exponential' formula which permits a power law at low rigidities and an exponential decrease above the cut-off. This should be a better approximation than the use of a flat spectrum with a sharp cut-off. However, both approaches are phenomenological and have little theoretical support. Admittedly, theory has been offering little help so far. At high rigidities (just around the cut-off), the whole concept of diffusive propagation breaks down, and the transport equation (1) is no more applicable. This is not only a matter of knowing the relevant parameters and solving the equation numerically. The cause of breakdown can be formulated in different ways. Physically, diffusion picture assumes the scattering mean free path to be small with respect to other distances involved. Taking a mathematical approach, one neglects higher harmonics in deriving the transport equation (1). At high rigidities, however, the spatial variation of the second harmonic becomes comparable to that of the density.

The method of Erdős and Kóta (SH 4.5-5, and references therein) may provide one part of the solution. These authors calculate energy losses along regular trajectories, disregarding scattering and retaining only the large-scale structure of the heliospheric field, including a wavy neutral sheet. This model can successfully reproduce many major aspects of the anisotropies observed at high rigidities. The predictions are similar to those of the drift models at lower energies. This is not at all surprising, since both models emphasize the effect of the regular field. The trajectory model could easily accommodate other large-scale structures, too. The inclusion of scattering would be a major step toward understanding the nature of cut-off.

In the paper SH 4.5-5, Erdős, Kóta, and Merényi predict rather gradual declines in the rigidity-spectra of solar and sidereal daily variations. For the 22-year cycle of the solar diurnal vector, they obtain a horseshoe shape, fairly similar to the loop inferred from experimental observations by Chuang, Kusunose, and Wada (SH 4.5-14) (Figure 15).

An alternative explanation of the phase shift of anisotropy was put forward by Kravtsov et.al. (SH 4.5-20) suggesting that this phase shift

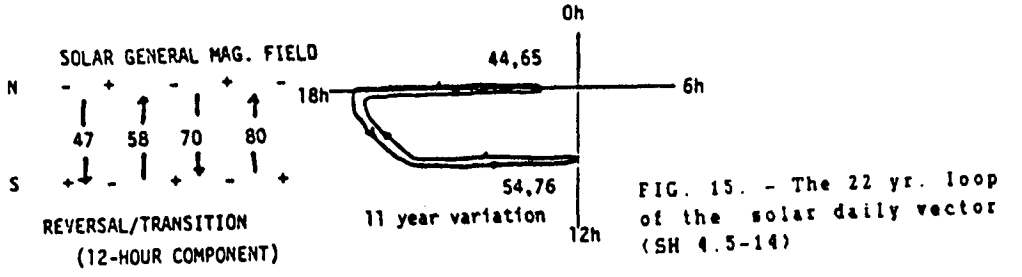

FIG. 15. - The 22 yr. loop of the solar daily vector (SH 4.5-14)

originates in the different connections of the heliospheric and interstellar magnetic fields. These 'open' and 'closed' configurations proposed by Ahluwalia (1979) deserve further study. At the present stage, however, this model is rather speculative. Drift models, on the other hand, firmly predict the observed phase shift and offer a more plausible explanation.

Higher harmonics

In general, the directional distribution of cosmic rays cannot be described with a single vector but it also contains higher spherical harmonics. As a rule, the n-th spherical harmonic may produce various daily harmonics (from n-th down to 1st, together with sidebands) in earth-based measurements. These indirect, sometimes so-called spurious, effects are still fairly tractable for the second harmonic and become increasingly complicated for the higher order terms.

The second order anisotropy has five independent components corresponding to the five spherical harmonics or, in an equivalent description, to the components of a symmetric and traceless tensor (Kota 1975). Assuming an azimuthal symmetry around the rotational axis of the sun, the resulting daily variations can be evaluated in a straightforward way. The following major terms will emerge:

semidiurnal :	solar 2nd	solar+sidereal	sidereal 2nd
diurnal :	antisidereal	solar	sidereal
zonal harmonic:	semiannual	annual	constant

Table 2

The classification is intended to express the geometrical relations. The variations in the same row have the same dependence on geographical latitude. Variations in one column arise from the same component(s) of the anisotropy, therefore there is a purely geometrical relation between them (Kóta 1975). At this Conference, Tatsuoka and Nagashima (SH 4.5-2) presented an extensive geometrical study giving all the coupling coefficients of the transformation of the second order anisotropy into earth-based intensity variations.

The direct geometrical relation between the solar semidiurnal and the antisidereal diurnal waves has been convincingly demonstrated by Swinson and Nagashima (SH 4.4-7). If the 2nd order anisotropy results from a pure pitch-angle distribution around the direction of the magnetic field, then it can be described with one single parameter, and a strict relation will hold between the sidereal and antisidereal daily waves. This constitutes the basis of the Nagashima-correction (see in paragraph 3.2.). It should

be borne in mind that the Nagashima correction involves the physical assumption of a pitch-angle distribution, while the relation between the solar semidiurnal and the antisidereal waves is purely geometrical. Of course, there are physical grounds to expect a pitch-angle distribution. The Nagashima correction has been successful in organizing the worldwide observations of the sidereal daily variations into a coherent and transparent pattern (Nagashima, Tatsuoka, and Matsuzaki 1983). The results of the Hobart underground telescope could best be interpreted by employing this correction (Humble and Fenton SH 4.4-5), giving further credit to this method.

There may also be deviations from the pitch-angle picture, at high rigidities in particular. Several works at the conference were devoted to the study of the structure of the 2nd order anisotropy. Takahashi and Yahagi (SH 4.3-12) investigated the 2nd order zonal harmonic (bottom row in Table 2) on the basis of data from the worldwide network of neutron monitors. From a pitch-angle distribution, one would expect a constant value with a semiannual wave superimposed. It would deserve a more detailed study to see if observations are in agreement with the predictions of the pitch-angle concept. The magnitude of the observed semiannual wave seems surprisingly large (about 5%) at the cut-off energy, unless the upper cut-off is overestimated. Similarly large, puzzling diurnal effect was reported by Asatryan, Babayan, and Stozhkov (SH 4.5-8) on the basis of stratospheric measurements. At present, it seems hard to think of any process leading to such huge anisotropies.

On the grounds of symmetry, Nagashima, Munakata, and Tatsuoka (SH 4.3-9) pointed out that the two components responsible for the second column of Table 2 should be polarity dependent. Analyzing the data of the multi-directional muon telescope at Nagoya, they could extricate the expected effects: a semidiurnal wave with the frequency between the solar and sidereal semidiurnal frequencies, and also a polarity-dependent contribution to the solar daily wave. This result implies that the anisotropy is not entirely axially symmetric.

Munakata and Nagashima (SH 4.5-1) endeavoured to compute the first three harmonics of the cosmic ray anisotropy. It is reassuring to see the self-consistency of the calculation, they start with computing the density distribution and then continue to proceed step by step upward in the hierarchy of the harmonics. The resulting free-space 2nd and 3rd harmonics are shown in Figure 16, together with their dependence on rigidity. A remarkable feature of the calculated 2nd harmonic is the marked deviation from the 'conventional' phase of 3 hr for the case of $A<0$. This seems somewhat surprising, and the underlying physics is not yet clear. The deviation from the 3hr phase, again, would indicate that the pitch-angle distribution is violated, and the Nagashima-correction may not perfectly eliminate the sidereal wave of heliospheric origin.

The 3rd harmonics also show different phases for $A>0$ and $A<0$, respectively. The consistently 7 hr phase for $A>0$ is not compatible with a pitch angle distribution which would predict either 1 hr or 5 hr.

Recently, Bieber and Pomerantz (1983) proposed a unified theory of the higher harmonics. The model includes adiabatic focusing and also anisotropic pith-angle scattering. The former is primarily responsible for the second harmonic, the basic process being the same as that in the loss-cone model of Fujii et.al (1971). The anisotropic scattering has more effect on the third harmonic, earlier this process was suggested to account for the higher harmonics of the galactic anisotropy (Kóta 1979).

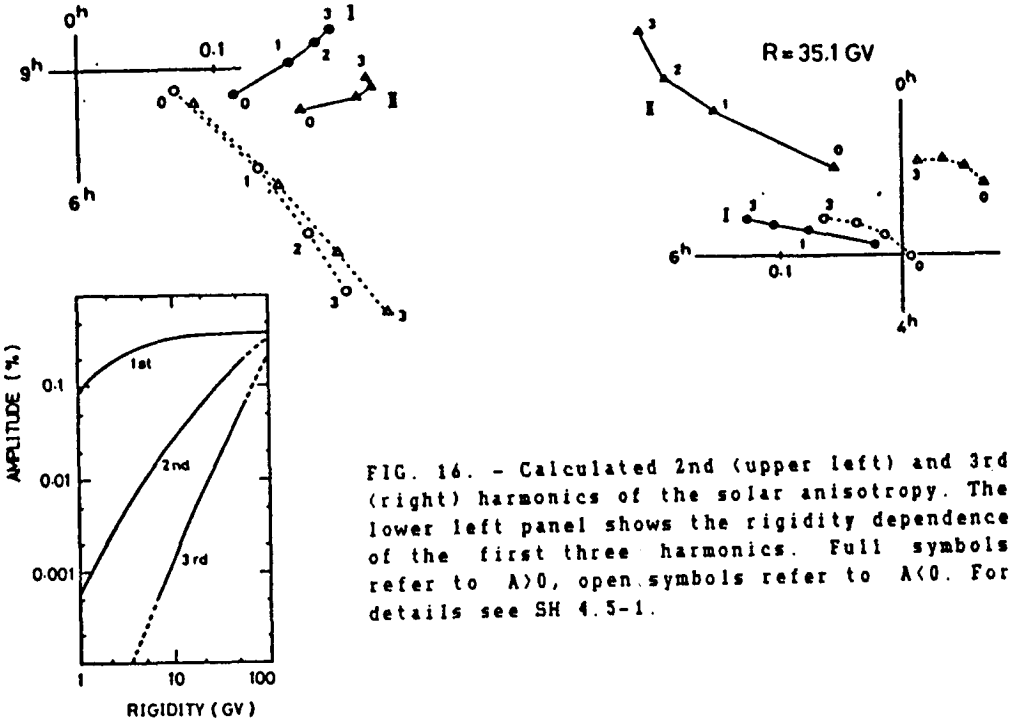

FIG. 16. - Calculated 2nd (upper left) and 3rd (right) harmonics of the solar anisotropy. The lower left panel shows the rigidity dependence of the first three harmonics. Full symbols refer to A>0, open symbols refer to A<0. For details see SH 4.5-1.

The unified theory of Bieber and Pomerantz should yield a pitch-angle distribution from the diffusive streaming, which ultimately predicts that all the higher harmonics must have either maximum or minimum at 9 hr (and 21 hr); for the first harmonic the contribution of convection should first be removed.

The unified theory predicts the relative magnitude of the second harmonic to be roughly proportional to the scattering mean free path. Bieber and Pomerantz (SH 4.5-21) used this principle to check their model. In Figure 17, the amplitudes and phases of the first three harmonics observed at Swarthmore are plotted as a function of the relative variance of the interplanetary magnetic field. The second harmonic tends to decrease with increasing field fluctuation, which also should mean increasing scattering i.e. smaller mean free path. However, this decrease seems slower than that expected from the theory.

The predictions of the unified model of Bieber and Pomerantz seem to be irreconcilable with the results of Munakata and Nagashima (SH 4.5-1). Yet, we may not need to ask which of them is correct. The model of Bieber and Pomerantz is particularly attractive to a theoretician. It is based on a firm prediction of the theory of scattering, and one would most welcome to see that the expected effect is indeed there. On the other hand, the unified model of anisotropy strongly relies on the assumption of 1-dimensional propagation. Any perpendicular diffusion or drift should modify the picture. This seems to be a plausible reason why the the model of Bieber and Pomerantz works well at lower rigidities, and may become incorrect at high rigidities where cross-field transport is much easier. This would also be in accord with the rigidity spectra shown in Figure

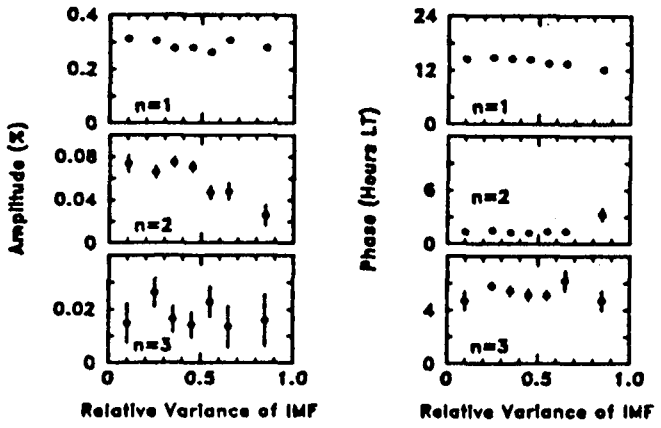

FIG. 17. - Amplitudes and phases of the first three solar harmonics observed at Swarthmore plotted vs. the relative variance of the interplanetray magnetic field. Note the decrease of the amplitude of the 2nd harmonic (SH 4.5-21)

16, which predict the relative magnitude of the 'non pitch-angle' higher harmonics to increase rapidly toward higher rigidities.

The solar tri-diurnal variation was experimentally investigated by Mori et.al. (SH 4.5-3) on the basis of the Nagoya, Misato, and Sakashita muon telescopes. The results are shown in Figure 18. The authors conclude that the best value of the phase is near 7 hr, in fair agreement with the results of Munakata and Nagashima (SH 4.5-1). Inspection of Figure 18 may also suggest the occurence of a phase shift from 1981 to 1982. It is also my impression that, in the period of 1970-80 (A>0), all the high-rigidity harmonics tend to have a phase close to 15 hr. Speaking in terms of regular motion, the ecliptic 15 hr direction represents the trajectory which has a maximum access to the neutral sheet. It is not inconceivable that this may prove to be a preferential direction.

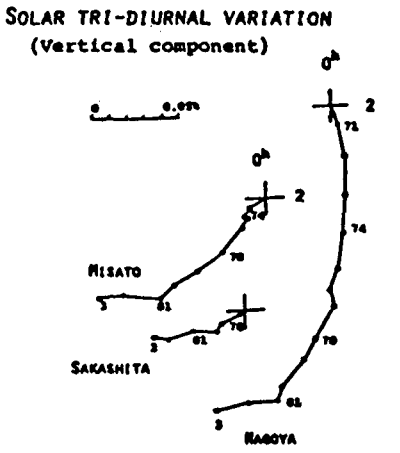

FIG. 18. - Solar tri-diurnal waves observed at Sakashita, Misato, and Nagoya (SH 4.5-3)

4. OTHER TIME VARIATIONS, CORRELATIONS

In this last, loosely organized, section, I would like to report on some interesting new developments which did not fit into the line of the previous two sections. The topics to be covered here can be summarized as time variations other than 11-year cycle or periodic variations due to the motion of the earth. For most of these variations, there is no firm theoretical prediction available. In cases such as this, when the underlying physical processes are largely unknown, the study of correlations might give an insight with helping to explore possible connections between various quantities. When doing correlation analyses, one should exercise caution, a correlation does not necessarily imply a close physical connection.

Attolini, Cecchini, and Galli (SH 4.4-14) endeavoured to discover correlations between the sunspot number, cosmic ray flux, aa index, and solar flares in narrow frequency bands. They worked out a method specifically designed for the study of narrow frequency bands. Several periodicities were found, among these the most significant is the 154 day period found in the cross-correlation of cosmic rays vs. solar flares. The method is promising even if the results are not always easy to interpret. One may hope that this new technique will be added to the already existing arsenal of the matemathical tools of correlation studies.

Analyzing variations close the 27-day rotational period of the sun, Shatashvili et.al. (SH 4.4-20) found that the period of cosmic ray recurrency increased to about 30 days between 1973 and 1975. The authors interpret this as an effect of drift. During this period, particles reached the earth through the polar regions, thus they experienced a longer period because of the differential rotation of the sun. No similar finding is apparent in the power spectrum analysis of Agrawal (SH 4.4-16).

On the basis of a large amount of observational data from 1958 to 1975, Bazilevskaya, Tyaso, and Vernova (SH 4.4-19) attempted to establish a relation between the cosmic ray flux at the earth and the longitudinal distribution of solar activity on the sun. This latter was found to undergo profoundly larger variations during the periods of solar polarity reversals. The study of correlation led to a puzzling result, which the authors find difficult to accept. The maximum correlation was obtained with a time shift of about 80 days, in the 'unexpected', implausible direction: the variation in cosmic ray flux seemed to preceed that in the distribution of solar activity. It seems incomprehensible that cosmic ray should affect solar activity in any way. An indirect effect through the solar wind is highly improbable, too. This example shows that the interpretation of a correlation is not always straightforward. The other possibilities are either an unlikely coincidence or a subtle artifact.

An interesting finding was reported by Kavlakov and Georgiev (SH 4.5-16): days of magnetic storms were observed to be preceded by enhanced daily waves in the cosmic ray counts at the Musala multi-directional telescope. This kind of 'forecast' is not inconceiveble since cosmic ray particles may experience interplanetary disturbances between the earth and the sun.

A warning came from Pandley et.al (SH 4.4-1) to those who use the solar flare index (SFI), provided by different publications. A simple correlation study gave significantly different results for the SFI-s from different sources. To avoid unwanted artifacts, correlation studies are strongly recommended to use the same source, at least within one work. This acute problem calls for an clarification of the discrepancies since the SFI is a widely used parameter of modulation research (see Agrawal, Mishra, and Jain SH 4.1-10).

Finally, the subject of bianmual variation deserves attention. At this Conference, Charakchyan et.al. (SH 4.4-21) demonstrated that the 2-year variation seen earlier in stratospheric measurements is not a geophysical effect but it can clearly be observed in satellite data, too. Cosmic ray

fluxes were shown to be in a quite sharp anti-phase with the geomagnetic Ap index, suggesting that a relatively local effect is responsible for the biannual variation of cosmic rays. Though the magnitude of this variation undergoes considerable changes, a closer look seems to rule out a close connection with solar activity. The interpretation of this phenomenon is still an open question.

ACKNOWLEDGEMENTS

I am grateful to the General Organizing Committee for inviting me to be a rapporteur. I greatly benefited from the helpful and stimulating discussions with many authors and other participants at the Conference. Special thanks are due to Dr. Ng for taking the burden of the sessions SH 4.6 and SH 4.7. This work was supported by the National Science Foundation under the Grants ATM-220-18 and INT-8400591.

REFERENCES

Ahluwalia, H.S., 1979: Proc. 16th ICRC, Kyoto, 12, 216
Alexeenko, V.V. et.al., 1981: Proc. 17th ICRC, Paris. 2, 146
Bercovitch, M., 1970: Acta Phys. Hung., 29, Suppl. 2, 169
---------- 1984: Proc. Int. Symp. 'Cosmic Rays in the Heliosphere', Morioka, Japan, 329
Bieber, J.W. and M.A. Pomerantz, 1983: Geophys. Res. Lett., 10. 920
Chic, P.P. and M.A. Lee, 1985: submitted to J. Geophys. Res.
Evenson, P. and P. Meyer, 1984: J. Geophys. Res., 89, 2647
Forbush, S.E., 1969: J. Geophys. Res., 74, 3451
Fujii, Z. et.al., 1971: Proc. 12th ICRC, Hobart, 2, 666
Gleeson, L.J. and W.I. Axford, 1968: Ap. J., 154, 1011
Gombosi,T. et.al, 1975: Nature, London, 255, 687
Jokipii, J.R., 1985: to be published
Jokipii, J.R., E.H. Levy, and W.B. Hubbard, 1977: Ap. J., 213, 861
Kadokura, A. and A. Nishida, 1984: Proc. Int. Symp. 'Cosmic Rays in the Heliosphere', Morioka, Japan, 177
Kóta, J., 1975: J. Phys. A, 8, 1349
------- 1979: Proc. 16th ICRC, Kyoto. 4, 199
------- 1981: Adv. Space Phys., 1, No.3, 135
------- 1984: Proc. Int. Symp., 'Cosmic Rays in the Heliosphere' Morioka, Japan, 153
Kóta, J. and J.R. Jokipii, 1983: Ap. J., 265, 573
Kóta,J., E. Merényi, and G. Erdős, 1985: Ap. J., in press
Levy, E.H., 1976: J. Geophys. Res., 81, 2082
McDonald, F.B., N. Lal, J.H. Trainor, M.A.I. van Hollebeke, and W.R. Webber, 1981: Ap. J., 249, L71
McKibben, R.B., K.R. Pyle, and J.A. Simpson, 1985: Ap. J., 289. L35
Fujii, Z. et.al, 1971: Proc. 12th ICRC, Hobart, 2, 666
Nagashima, K., R. Tatsuoka, and S. Matsuzaki, 1983: Nuovo Cim., 6C. 550
Nagashima, K., I. Morishita, and S. Yasue, 1982: Planet. Space Sci., 30. 879
Newkirk, G.,Jr. and L.A. Fisk, 1985: J. Geophys. Res., 90, 3391
Perko, J.S. and L.A. Fisk, 1983: J. Geophys. Res., 88. 9033
Potgieter, M.S. and H. Moraal, 1985: Ap. J., 294, 425

Sakakibara, S. et.al., 1984: Proc. Int. Symp. 'Cosmic Rays in the Heliosphere', Morioka, Japan, 314
Venkatesan, D., R.B. Decker, and S.M. Krimigis, 1984: J. Geophys. Res., 89, 3735
Webb, G.M. and L.J. Gleeson, 1977: Proc. 15th ICRC, Plovdiv, 3, 6

XIX ICRC
RAPPORTEUR PAPER FOR SESSIONS SH5, SH6, AND SH7

FORBUSH DECREASES
GEOMAGNETIC AND ATMOSPHERIC EFFECTS
COSMOGENIC NUCLIDES

Erwin O. Flückiger
Physikalisches Institut
University of Bern
CH-3012 Bern
Switzerland

This report is an attempt to give an overview and synthesis of recent developments that have occurred in the areas of Forbush decreases, Geomagnetic and Atmospheric Effects, and Cosmogenic Nuclides. Emphasis is laid on those new results and ideas which were presented in sessions SH5, SH6, and SH7 (and, if related to the abovementioned areas, also in sessions SH9 and SH10) at this conference, but some other relevant developments are discussed as well.

The complexity of the three areas and the large number of contributed papers (see Table 1) quite necessarily lead to a very personal selection of the highlights. And although this report is more comprehensive in some points compared to my oral presentation at the conference it is not a summary of the contributed papers in the abovementioned fields. My enthusiasm about new results and ideas may in addition cover some of the associated important problems. I would like to apologize for this bias. I also make my apologies to all the colleagues whose work is not mentioned explicitly in this report.

Table 1 Number of Contributed Papers in Sessions SH5, 6, 7, 9, and 10

	in Conference Papers	presented at Conference
SH 5	20	9
SH 6	18	8
SH 7	14	13
SH 9	16	11
SH10	8	3

1. Forbush decreases (Fds) have been a topic on each Cosmic Ray Conference since their discovery - and there is no evidence that this situation will change in the near future. They play a major - if not the dominant - role in the 11-year modulation of the galactic cosmic rays (see e.g. McKibben, 1981), they are associated with significant perturbations in the interplanetary medium and of the earth's magnetosphere, but the explanation of the physical processes involved has been an open question for debate for many years.

The first comprehensive review about Forbush decreases was published by Lockwood (1971). A summary of the pre-conference knowledge about Fds can be found e.g. in Iucci et al. (1984), and many of the most recent results have been published in the Proceedings of the International Symposium on Cosmic Ray Modulation in the Heliosphere, held in Morioka, Japan, August 21-25, 1984. An updated review paper on Fds including the latest developments is at present in preparation by Agrawal (1985).

Forbush decreases apparently occur at random, with a tendency to be more frequent and to have a larger amplitude during the increasing and maximum phase of the sunspot cycle. In the morphology of Fds different classifications have been proposed in the past. At present two types of Forbush decrease events with different characteristics are distinguished according to their origin (Shah et al., 1979): sporadic (non-recurrent) and recurrent (27-day period) decreases. Sporadic Forbush decreases have their origin in solar flares accompanied by type IV radioemission, occurring either on the visible or invisible hemisphere of the Sun (SH5.1-4), whereas recurrent decreases are generally related to long-lived corotating high speed solar wind streams associated with coronal holes (Venkatesan et al., 1982).

The classical Fd as recorded e.g. by a mid-latitude neutron monitor (NM) has a cosmic ray intensity-time profile as shown schematically in Figure 1. Starting immediately after a storm sudden commencement (the geomagnetic signature of the arrival of an interplanetary shock) the cosmic ray intensity decreases rapidly, typically about ∿5% (but up to several 10%) within a few hours. This decrease is then followed by a slow recovery lasting in the order of one week. Several hours prior to the fast decrease, some Fds show a distinct pre-increase with an amplitude of about 0.4 % (SH5.1-22). In many cases the descending phase of a Fd exhibits a clear two-step structure (Barnden, 1973; SH5.1-5) with two consecutive decreases in the cosmic ray intensity of approximately the same amplitude. The time period of depressed cosmic ray intensity is usually characterized by a fine structure in the intensity-time profile, including an occasional short-time (post-)increase during the minimum

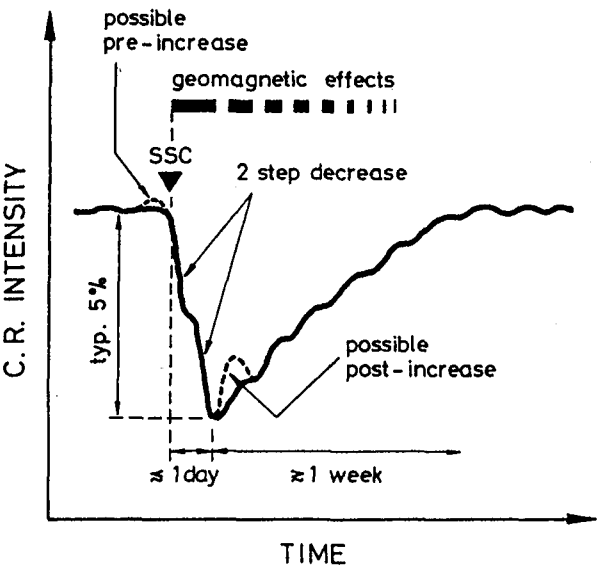

Fig. 1 The classical Forbush decrease

intensity phase (SH5.1-3). The entire event is associated with anisotropies, and for the analysis of Fds using cosmic ray data sampled on or near the earth it is also important to note that in particular the initial phase is subject to more or less pronounced geomagnetic effects. The modulation function of Fds, F(R), is often approximated by $F(R) \propto R^{-\gamma}$ (with an upper limiting rigidity of 100 GV or more) where the spectral index γ has an average value of ~ 0.8 for sporadic and of ~ 0.4 for recurrent Fds (Nachkebia and Shatashvili, 1983). Another representation of the modulation function is given by $F(R) \propto \exp(-K/R^{\gamma})$ with $0.2 \leq K \leq 1.0$ and $0.5 \leq \gamma \leq 0.9$ (e.g. Fenton et al., 1984). It was suggested at this conference by Sakakibara et al. (SH5.1-6), however, that a spectral form of fractional power type $(R^{-\gamma_1}(R+R_c)^{-\gamma_2})$ yields actually a more suitable representation of the rigidity dependence of Fds than power type or power-exponential type descriptions. For "hard" Fds during 1978-1982, i.e. for Fds with a relative change in the vertical muon intensity of more than 0.05% at the Sakashita underground telescopes (median primary rigidity R_m = 330-567 GV), they found $\gamma_1 = 0.37$, $\gamma_2 = 0.89$, and $R_c = 10$ GV. For "soft" Fds the corresponding values are $\gamma_1 = 0.77$, $\gamma_2 = 1.02$, and $R_c = 14$ GV.

One of the most significant features of the flare-associated Fds is the so-called East-West asymmetry: Fds related to solar flares in the eastern or central region of the solar disk exhibit larger amplitudes and longer recovery times than Fds related to solar flares on the western part of the solar disk. The present knowledge about the interplanetary perturbations associated with sporadic Fds within heliocentric distances of a few AU has been summarized by Iucci et al. (1984) and is shown in Figure 2. The front perturbation is a driven shock with a heliolongitudinal extent of about 100°. This shock is followed by a magnetic blob and a high-speed plasma cloud of about 0.5 AU average radial dimension at the orbit of the earth, emitted in a short time interval of usually less than 15 hours immediately after the beginning of the type IV burst. The Fd-modulated region is included between two

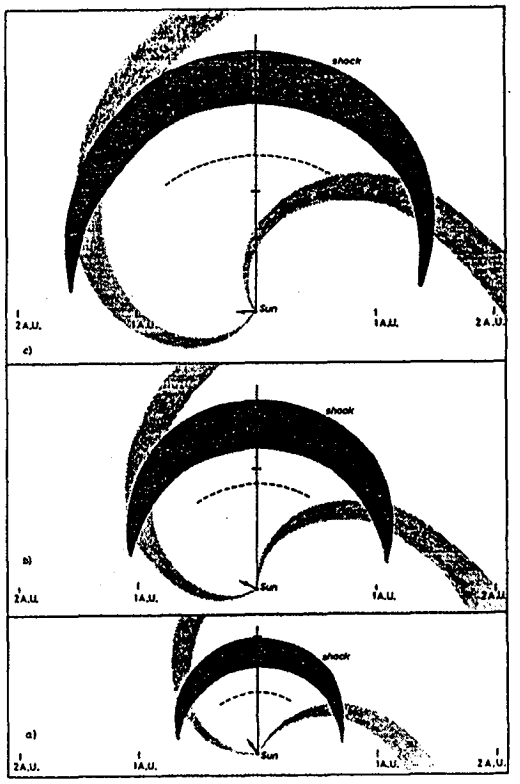

Fig. 2 Sketch on the ecliptic plane in a stationary frame of reference of the space-time evolution of a FD-producing interplanetary perturbation at three different times after the time t_0 of the type IV solar flare (SF). The flare region, indicated by the arrows, was located on the straight line at time t_0. Regions of enhanced IMF are indicated by the shaded areas (■ front perturbation, ▩ corotating lateral perturbations). The flare ejecta plasma is located between the shock and the dashed line. a) 2.5 days b) 4.5 days c) 6.5 days after the SF (from Iucci et al., 1984)

corotating boundary streams. Significant progress has been made during the last years in the understanding of the propagation of shocks in the interplanetary medium. Using either MHD theory (e.g. Wu et al., 1983) or by modelling the shock simply as a blast wave in the reference frame of the moving solar wind (Smart and Shea, 1985) it became possible to predict the arrival of a shock at the earth after a solar flare with an accuracy of 1-2 hours. Many of the associated problems were discussed recently at the STIP Symposium on Retrospective Analyses and Future Coordinated Intervals held in Les Diablerets, Switzerland, June 10-12, 1985, and will be published in the proceedings of that meeting (Shea and Smart, 1985).

In order to understand the physical processes responsible for the transient modulation of the cosmic ray intensity correlation studies with parameters describing the interplanetary medium are of crucial importance, and corresponding results can be found in several contributions to this conference (SH5.1-5, SH5.1-9, SH5.1-11, SH5.1-12, and SH5.1-13). Figure 3 taken from paper SH5.1-5 is an example for the Fd on September 29, 1978. As can be seen this Fd shows a distinct two-step decrease. The interplanetary magnetic field (IMF) data and the solar wind plasma parameters indicate that the first step begins with the shock passage at the earth. The second step is connected to the entry of the earth into a region with an enhanced magnitude of the interplanetary magnetic field and with a loop-like field configuration. This conclusion is in agreement with results obtained by Badruddin et al. for other shock-associated Fds (SH5.1-12). In a statistical analysis of the flare-associated Fds in the period 1964-1982 Iucci et al. (SH5.1-5) determined the separate contributions of the shock front and of the following magnetic perturbation to the amplitude of the first and second step of Fds as a function of the associated solar flare longitude. The corresponding result is shown in Figure 4. The polar diagram in this Figure represents (for 1 AU) the helio-longitudinal dependence, relative to the flare longitude, of the total amplitude of Fds (normalized to a maximum value of 1) together with the corresponding amplitudes of the first and second step. It can be seen that only the second step exhibits a pronounced east-west asymmetry, probably due to the longitudinal asymmetry of the magnetic perturbation following the shock.

Thomas and Gall (1984) recently showed in a theoretical study that a radially propagating perturbation similar to the one existing at the front edge of the Fd-modulated region is able to prolong the containment of cosmic ray particles behind it, leading to an additional adiabatic cooling of these particles and, therefore, to Fds in the sunward region of interplanetary space connected magnetically with the perturbation front. On the other hand, continuing previous work (and beyond a similar attempt by Badruddin et al. (SH5.1-12)) Iucci et al. (SH5.1-5) succeeded in relating empirically the total amplitude and the amplitudes of the two individual steps of Fds quantitatively to a perturbation parameter describing the strength of the front edge perturbation in the interplanetary medium made up by the shock and the magnetic blob effect, whereas the strength of the perturbation at the western boundary was found to be not correlated with the amplitude of Fds (not associated with type IV flares). These results are considered

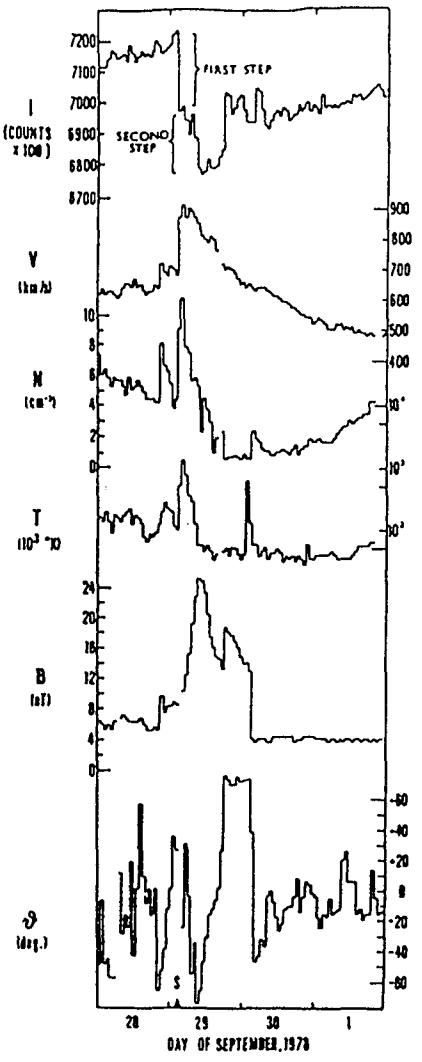

Fig. 3 Example for the time behaviour of a two-step Fd and of associated parameters of the interplanetary medium (SH5.1-5)

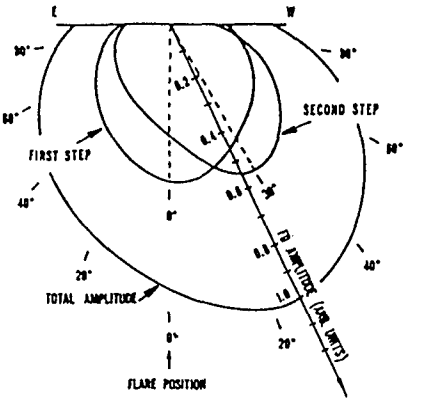

Fig. 4 Polar diagram representing the heliolongitudinal dependence, relative to the flare longitude, of the total amplitude of Fds together with the amplitudes of the first and second step (SH5.1-5)

to be important clues for the understanding of the mechanisms responsible for the cosmic ray density depression inside the Fd-modulated region.

In several papers the effect of "magnetic clouds", "magnetic cloud-like structures", and different types of high-speed solar plasma streams on cosmic ray intensity and anisotropies was discussed. Badruddin et al. (SH5.1-12) investigated the influence of three classes of magnetic clouds - shock associated clouds, stream interfaces and cold magnetic enhancements - on cosmic ray intensity. In paper SH5.1-4 Iucci et al. identified 31 short-term increases (with time duration less than 24 hours and amplitudes up to 5%) in the galactic cosmic ray intensity during Fd events of the period 1966-1977. All these increases

occurred after the passage of the compression region following the shock. They were associated with a magnetically perturbed, high velocity, low density and low temperature region in space for which in 7 cases the "magnetic cloud structure" according to the classification proposed by Burlaga (1984) could be determined. No satisfactory explanation for these observational results is, however, available yet.

The significance of periodic short-time cosmic ray intensity fluctuations for the analysis and the understanding of modulation processes has long been recognized (Dhanju and Sarabhai, 1967). A review of different techniques and applications in this field was recently published by Dorman and Libin (1984). Corresponding results were presented at this conference in papers SH5.1-7, 14, 17, and 18. By using the maximum entropy method Vainikka et al. (SH5.1-7) performed a spectral analysis of the cosmic ray intensity recorded at 9 neutron monitor stations during the large Fd of July 13-14, 1982, which was already discussed to some extent at the 18th ICRC in Bangalore (Agrawal, 1983). During the decrease phase of this Forbush event the analysis confirms the existence of a persistent oscillation with a time period of about 2 hours and an amplitude of 1-3%. This oscillation can be associated with a similar periodicity observed at the same time in the magnetospheric magnetic field. During the recovery phase the cosmic ray intensity showed a 3% variation with a time period of about 10 hours. Unfortunately, no correlation of these two periodic cosmic ray intensity variations with characteristic parameters of the interplanetary medium has yet been done and, therefore, their real origin is still unclear. Another very interesting result is discussed by Gulinsky et al. in paper SH5.1-18. Using 5-minute, 1- and 2-hour values of a large number of ground-based detectors, these authors investigated the cosmic ray power density spectrum for quiet time periods, periods with solar flares, and Fds during the years 1977-1982. Beside the known application of relating the cosmic ray power spectral density to the power density spectrum of IMF fluctuations, Gulinsky et al. demonstrate that the short-time cosmic ray variations in the GeV range also reflect the presence of large-scale perturbations in the interplanetary medium. As illustrated in Figure 5 which is based on the NM-registrations at Utrecht and Kerguelen for the time period September 7-23, 1977, the authors show that the spectral index γ in the range $10^{-5} \lesssim f \lesssim 10^{-4}$ Hz of the cosmic ray power density spectrum $P(f) = B \cdot f^{-\gamma}$ starts to increase significantly at least 18 hours prior to the onset of the Fd which occurred on September 21, 1977, whereas the quantity B decreases. In another study Sakai and Kato (SH5.1-14) found a pronounced periodicity in the cosmic ray intensity observed at Akeno with a time period of about 37 minutes during 1300-1900 UT on April 25, 1984, just one day prior to the Fd of April 26. It seems, therefore, that short-time cosmic ray fluctuations as observed by ground-based detectors are a suitable tool to probe the large-scale perturbations in the interplanetary medium and their approach to the earth.

There were some arguments in the past whether or not the characteristic properties of Fds such as the rigidity dependence (i.e. the modulation function) or the average recovery time are affected by the reversal of the solar magnetic field (as it occurred e.g. in 1980 for the last time). In this respect it was pointed out at this

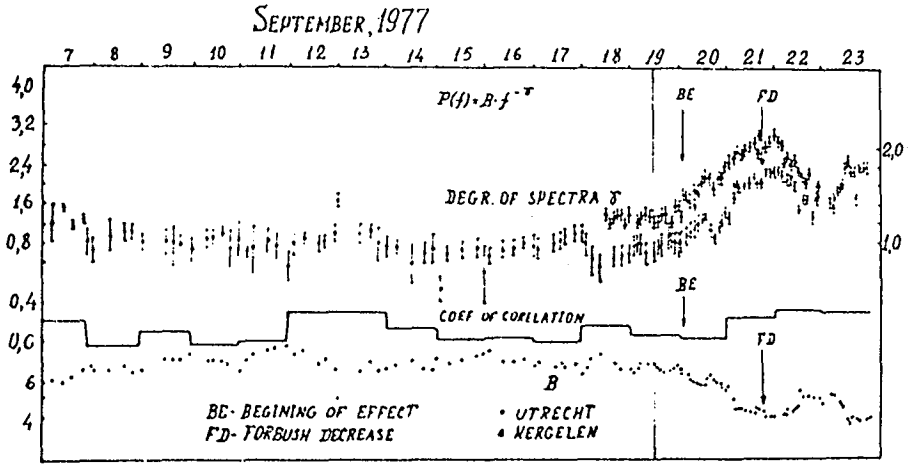

Fig. 5 Time dependence of the power spectrum of cosmic ray scintillations, $P(f) = B \cdot f^{-\gamma}$ ($f \lesssim 10^{-4}$ Hz) as determined by Gulinsky et al. (SH5.1-18) for the time period 7-23 September, 1977. The spectral index γ (top curve) starts to increase at least 18 hours before the arrival of a perturbation in the interplanetary medium at the earth and the beginning of the Fd on September 21, 1977, whereas B (bottom curve) decreases.

conference by Jain et al. (SH5.1-15) that during 1980 both the number and the magnitude of Fds was anomalously small compared to the high level of sunspot and solar flare activity. Fenton et al. (1984) performed an analysis of several shock-associated Fds during 1976-1983. Although their analysis was based on a rather limited number of comparable events, it appeared to these authors that the functional form of the Forbush-type decrease process is essentially the same now as it was during solar cycle 20. It was possible for them to conclude, however, that the rigidity dependence of the Fd is different from that of the long-term solar cycle changes during cycle 21 as it was earlier. Lockwood et al. (SH4.1-9) in a study of the intensity recovery of Forbush-type decreases as a function of heliocentric distance and its relationship to the 11-year variation arrived at the conclusions that the average recovery time t_o from transient decreases at 1 AU is energy independent and t_o is ~ 5 days, that t_o is essentially the same before and after the solar magnetic field reversal in 1980, and that t_o is constant through the solar modulation cycle. Apparently in contrast to these conclusions a remarkable result was presented by Moraal and Mulder (SH5.1-2). These authors compared the "average Fd", as observed by a specific NM during the years 1971-1980 with the corresponding "average Fd" of the years 1959-1969. The results which are consistent for different NM stations are illustrated in Figure 6 for Hermanus. They show a clear difference in the recovery phase. During 1971-1980 the cosmic ray intensity recovers to the pre-Fd level within 7 days after the onset of the decrease whereas during 1959-1969 even after 10

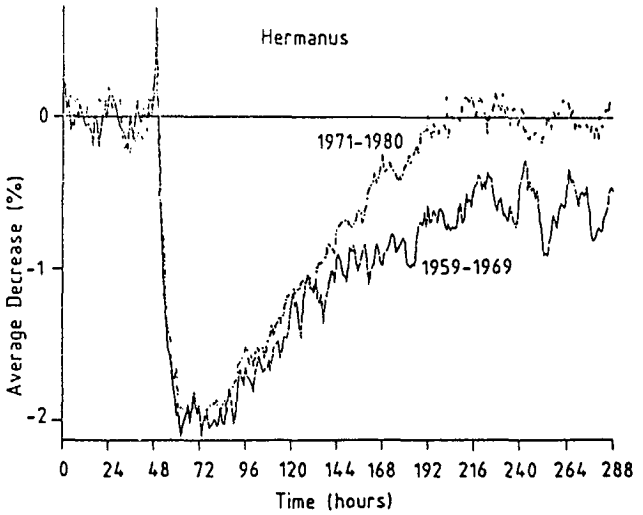

Fig. 6
The "average" Forbush decrease as observed with the neutron monitor at Hermanus during the time periods 1959-1969 (solid curve) and 1971-1980 (dashed curve). According to Moraal and Mulder (SH5.1-2) the difference in the recovery phase may be due to the drift effect.

days it is still significantly below this level. Although additional tests have to be performed to support their explanation the authors consider this effect as due to "drift", i.e. to the differences in the drift velocity field in the 1970 to 1980 IMF configuration with respect to the 1959-1969 configuration. It will certainly be most interesting to see the further development of this study.

2. Geomagnetic effects The geomagnetic field acts as a natural spectrometer for cosmic ray particles and it is, therefore, a "key instrument" in cosmic ray research. In order to relate the cosmic ray observations near or on earth to the cosmic ray flux in space, however, the transport of cosmic rays through the geomagnetic field must be understood in detail. Cutoff rigidities, asymptotic directions and/or entry points of cosmic ray particles to the magnetosphere have to be known accurately. The early work on cosmic ray motion in axially symmetric representations of the earth's magnetic field was limited to analytic considerations (Störmer, 1930; Lemaitre and Vallarta, 1936). Today, cutoff rigidities and asymptotic directions are determined almost exclusively by computer simulation of cosmic ray particle trajectories using elaborate mathematical representations of the magnetic field within the magnetospheric cavity. As a consequence of this evolution, and in order to avoid possible misinterpretations, the cosmic ray cutoff terminology needed a re-evaluation. At this conference, a final set of new definitions for use in theoretical and experimental cosmic ray studies was suggested by the experts in the field (Cooke et al., SH6.1-11).

Due to the secular changes in the geomagnetic field the trajectory calculations yielding cosmic ray cutoff rigidities and asymptotic directions have to be repeated periodically. For the Epoch 1955, 1960, and 1965 geomagnetic field models tables including the results of these calculations for the worldwide network of cosmic ray stations and/or a five degree by fifteen degree world grid have been published in the

past (e.g. Shea and Smart, 1975a, b). At present, calculations for Epoch 1980 by Shea, Smart, and co-workers are about to be completed. First results were already presented at the 18th ICRC (Shea et al., 1983a,b; Shea and Smart, 1983), and a comprehensive set of tables will again be published as an AFGL-report in the near future (Shea and Smart, 1985).

If uncertainties of the order of 5% can be accepted simple estimating procedures can be used to evaluate cosmic ray cutoff rigidities and asymptotic directions. In paper SH6.1-12 Shea et al. present useful relationships employing the McIlwain L-parameter to estimate the vertical cutoff rigidities for the twenty-five year period 1955-1980. For the effective vertical cutoff rigidity, R_c, the corresponding relation is $R_c = 16.237\ L^{-2.0353}$ GV. Flückiger et al. (1983, and SH6.1-13) discuss a method of estimating the change in the asymptotic directions of approach for vertically incident cosmic ray particles due to storm-time as well as secular variations in the geomagnetic field from a reference set of directions at a specific epoch by considering the corresponding change in the geomagnetic cutoff rigidity.

It is of considerable interest to evaluate the primary cosmic ray flux which is able to reach a satellite in earth orbit. The evaluation requires the knowledge of the geomagnetic cutoffs for all four pi steradians of possible arrival directions at every point along the spacecraft orbit. It involves in general a large number of trajectory calculations, and special computer techniques have been devised to scan the rigidity/zenith-angle space efficiently for allowed arrival directions (Cooke, 1981; Humble et al., 1983). It is possible to summarize the results of such calculations on a unit sphere of access which graphically describes the access of primary cosmic ray particles to the satellite. In the upper hemisphere of the allowed portion of this sphere the cosmic ray cutoffs can be ordered by application of Störmer theory in offset dipole coordinates (Smart and Shea, 1977). In paper SH6.1-14 of this conference Humble et al. present an empirical method to model the occluded portion of the downward hemisphere representing arrival directions which are forbidden due to the earth's cosmic ray shadow effect. Figure 7 illustrates some of their results for a satellite at an altitude of 400 km and at three locations.

Although theoretically the earth's cosmic ray shadow prohibits the arrival of all primary cosmic ray particles from directions represented by the occluded part of the downward hemisphere, reality can be different. An example for this was also given at this conference by Beaujean et al. (SH10.1-6,7) who reported on heavy cosmic ray measurements made aboard Spacelab-1. A stack of CR-39 plastic track detectors was exposed to the cosmic radiation at 250 km altitude during 10 days. As a part of the stack was rotated one revolution within 7 days the impact time of most of the particles could be correlated with the orbit position and thus with geomagnetic field parameters. In their analysis of heavy particles with charge $Z \geq 6$ in the energy range 50-150 MeV per nucleon the authors find 36 geomagnetically forbidden particles among a total of 365. Six of these particles arrived from below the horizon. It is interesting to note that these forbidden particles

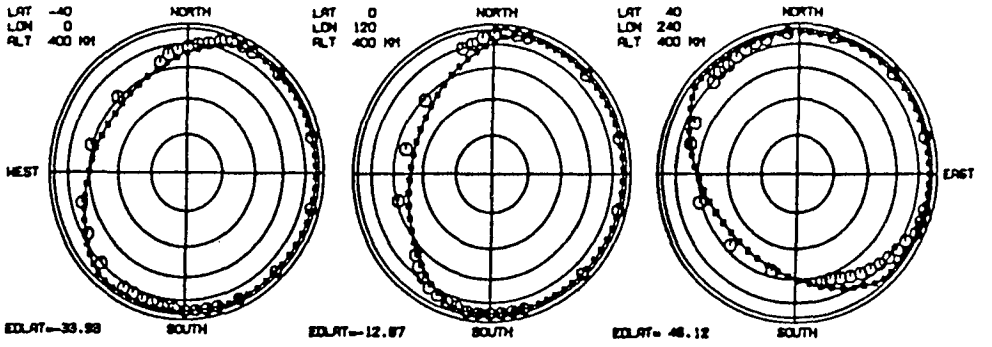

Fig. 7 Projections of the downward hemisphere of access for a satellite orbiting at 400 km altitude, at the locations 40°S/0°E, 0°S/120°E, and 40°N/240°E (Humble et al., SH6.1-14). The concentric rings represent 15° projections from the spacecraft equator to the nadir direction. Arrival directions which are completely forbidden to galactic cosmic radiation of any energy are represented by the area enclosed by the large dots in each projection. Open dots indicate where the maximum accessible zenith directions were determined by the cosmic ray trajectory-tracing method. The lines connecting the small solid squares indicate the results obtained according to the empirical model.

appeared between $\sim 49°$ and $\sim 57°$ geomagnetic latitude, with a concentration in the southern hemisphere between the geographic longitudes $\sim 30°$E and $\sim 200°$E.

The appearance of forbidden particles could be due to a temporary change in the geomagnetic field. The variation of cosmic ray cutoff rigidities during magnetic storms is well established . The maximum absolute effect occurs at mid-latitudes. Local time asymmetries were found to be correlated with longitudinally asymmetric changes in the low latitude magnetic field which are generally attributed to the presence of a partial ring current (e.g. Dorman, 1974; Debrunner and Flückiger, 1977; Arens, 1978; and references therein). In a recent study based on data of the worldwide network of neutron monitors Kudo et al. conclusively demonstrate that the amplitude of the transient cosmic ray increase associated with the depression of the cutoff rigidity during severe geomagnetic storms strongly depends on local time, and that its maximum phase is found in the evening sector (Kudo et al., 1984; SH5.1-8). According to Flückiger et al. (1985) it appears that at any time, t, during geomagnetically active periods the changes in the cosmic ray cutoff rigidity, ΔR_c, at low and mid-latitudes can be related to the weighted sum of the changes in the horizontal component of the equatorial surface magnetic field, ΔH_{eq}, sampled at intervals of one hour in local time, t_L, from 0 to 7 hours to the east of the specified location:

$$\Delta R_c(R_c, t_L, t) \simeq \sum_{n=0}^{7} g_n(R_c) \cdot \Delta H_{eq}(t_L + n, t)$$

with $g_n(R_c)$ denoting weighting factors in dependence of the cutoff rigidity, R_c, derived from trajectory calculations. But cosmic ray cutoff rigidites not only change during magnetic storms. In paper SH5.1-14 Sakai and Kato show that in general the power spectral density of cosmic rays in the frequency range of 10^{-4}-10^{-3} Hz correlates positively with the fluctuations of the geomagnetic field (represented by the Dst parameter) around 1.2 10^{-4} Hz, indicating a rather dynamic character of the geomagnetic effects on cosmic rays. The diurnal variation of cutoff rigidities was established a long time ago, and in several publications the cutoff rigidities at high latitudes were evaluated theoretically as a function of local time using a magnetic field model including the tail of the magnetosphere (e.g. Smart et al., 1969). In paper SH6.1-10 Tyasto and Danilova describe a new theoretical study on the daily variation of cutoff rigidities at mid-latitudes. Based on trajectory calculations using a model of the magnetospheric

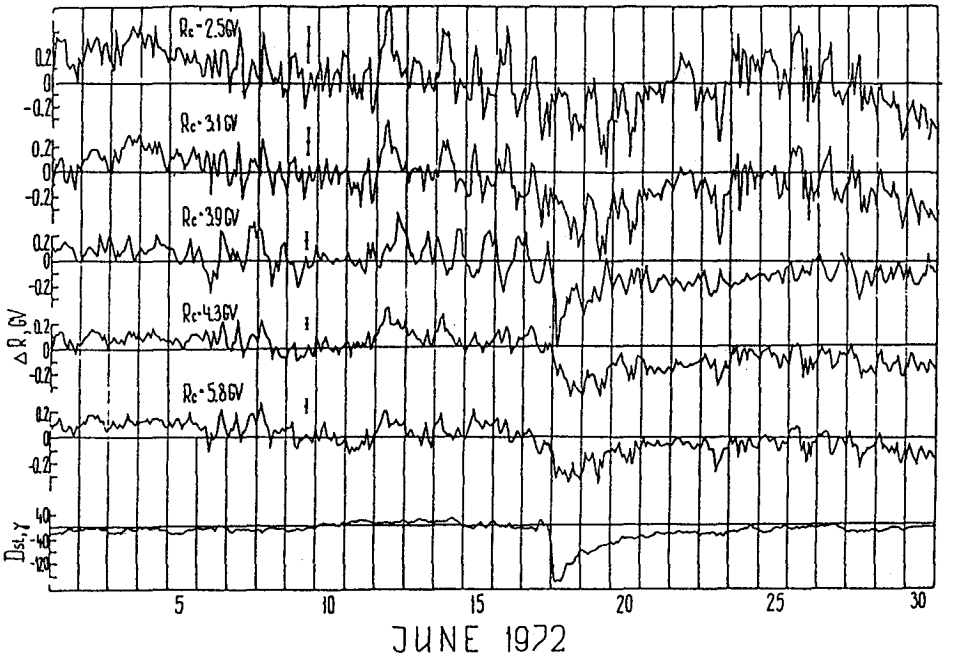

Fig. 8 Variations of the cutoff rigidity, ΔR_c, during June 1972, as determined by Dvornikov et al. (SH6.1-21) for five groups of cosmic ray stations (Kiel and Utrecht, R_c = 2.5 GV; Dourbes and Lindau, R_c = 3.1 GV; the Sayan spectrograph complex, R_c = 3.9 GV; Hafelekar, Zugspitze, Jungfraujoch, R_c = 4.3 GV; Rome and Pic-du-Midi, R_c = 5.8 GV), and Dst parameter (bottom curve).

magnetic field worked out recently by Tsyganenko and Usmanov (1982) they arrive at the conclusion that even during magnetically quiet time periods the magnetospheric effects lead to daily variations in the vertical cutoff rigidities of 0.15 GV at Moscow (cutoff rigidity R_c = 2.48 GV) and 0.02 GV at Mt. Norikura (R_c = 12.0 GV). It is interesting to compare these values with results given in paper SH.6.1-21. In this paper Dvornikov et al. discuss an experimental study in which they determined for the first time the cutoff rigidity variations at five middle and lower latitudes for the time period 1 May - 30 June, 1972, i.e. for two entire months! The analysis was based on data of 34 world network stations and a newly developed method of "spectrographic global survey". Figure 8 shows the results obtained for June 1972. Although some caution may be appropriate in accepting the absolute values of these results it is quite certain that this study provides new insight in the diurnal behaviour of cosmic ray cutoff rigidities.

In recent years, considerable progress has been made in the development of quantitative magnetospheric magnetic field models. A review discussing the state of the art with a critical comparison of different field models is found e.g. in Walker (1979) and Walker (1983). Most of the models include the major magnetospheric current systems illustrated in Figure 9 (taken from Potemra, 1984), with the restriction that the effect of field-aligned currents is not yet taken into account adequately. All the models include the dipole tilt angle as an input parameter. The magnetospheric effects constitute an important extension of the theory of geomagnetic effects on cosmic rays, and they are of significance especially for polar latitudes. A review on cosmic ray cutoff calculations utilizing magnetospheric magnetic field models is found in Pfitzer (1979), where it is shown that the cutoff values using the most sophisticated field models agree with the measurements within the experimental uncertainties. Within the extended geomagnetic theory the points of entry, i.e. the locations where cosmic ray particles enter the magnetosphere with respect to their point of detection, as well as the pitch angle of approach, i.e. the angle between the direction of approach and the neighbouring IMF, became new useful theoretical tools. Recently, Gall et al. (1984) published an extensive catalogue (free copies were available during the conference) including approach directions and points of entry of cosmic rays for 67 higher latitude cosmic ray stations. Pfitzer (1979) summarized earlier calculations on entry points with the map given in Figure 10a indicating the regions through which protons enter the magnetosphere before they are observed at the polar cap. Experimental data concerning the access of solar flare particles to the high latitude regions of the earth are discussed e.g. by Engelmann et al. (1971), Mineev et al. (1983), Ilyin et al. (1983) and Biryukov et al. (1984). Figure 10b taken from Biryukov et al. (1984) shows the structure of the solar cosmic ray proton flux in the north polar cap for energies $E_p \geq 1$ MeV according to the "Intercosmos-17" and "Cosmos-900" data for November 22-25, 1977. It is obvious from Figure 10b that a distinct structure is present, but despite the somehow restricted geographical resolution it can also be seen that this structure does not well represent the patterns given in Figure 10a. It is quite probable that the real situation is strongly marked by the field aligned currents flowing into and away from the ionosphere at these

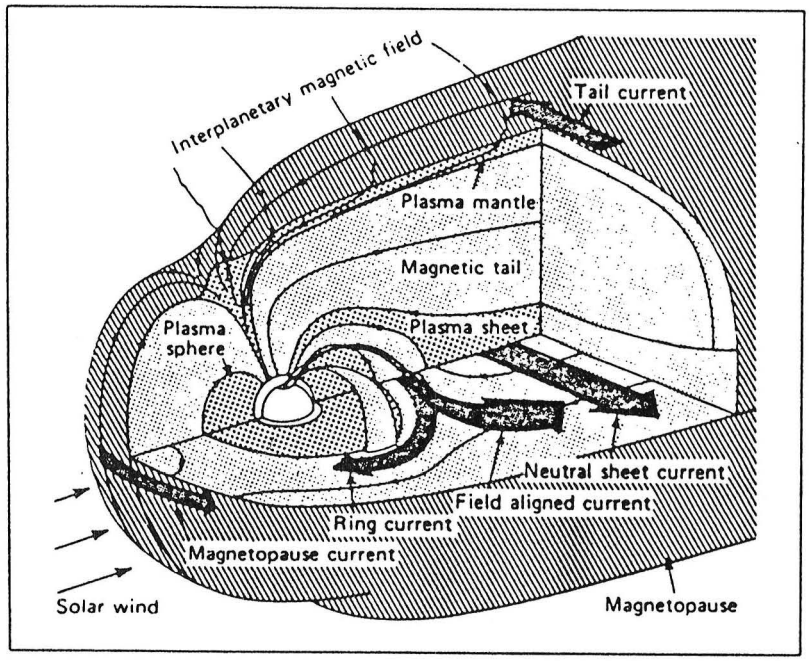

Fig. 9 The major magnetospheric current systems (Figure taken from Potemra, 1984)

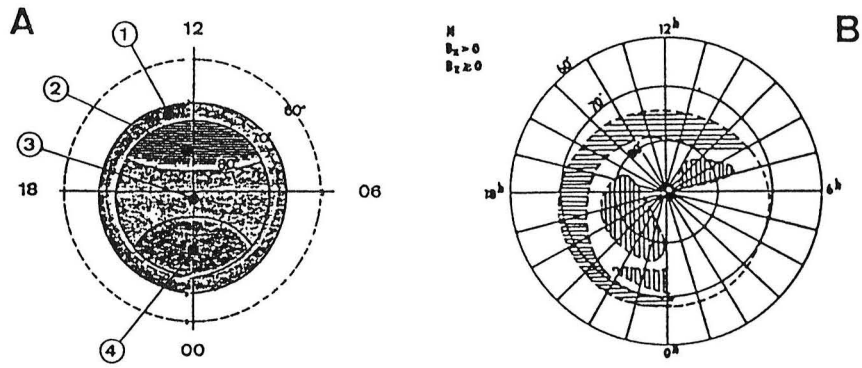

Fig. 10 Map of the polar cap showing the various regions corresponding to different entry points (to the magnetosphere) of protons observed at the polar cap

a) theoretical result according to Pfitzer (1979). The entry locations are 1) daylit dawn, 2) direct access via cusps, 3) neutral sheet, and 4) lobes of tail

b) experimental result given by Biryukov et al. (1984)

polar latitudes (see e.g. the reviews by Potemra, 1979, and Stern, 1983). New results on the access of solar cosmic ray particles to high latitude regions during quiescent and perturbed geomagnetic conditions are given in papers SH6.1-15 and SH6.1-16 (none of these two papers was actually presented at the conference). An illustration of these results is given in Figure 11, taken from Gorchakov et al. (SH6.1-15). The Figure shows the data from 3 channels of the Cerenkov detector on the low polar-orbiting satellite Cosmos-900 for the time interval 0845-1150 UT on November 22, 1977, which includes the abovementioned solar particle event starting at 1010 UT. Panel a refers to the quiet time period while panel b shows the measurements made during the solar particle event. It is important to realize that the comparisons of e.g. the equatorial penetration boundaries obtained from this kind of measurements (and as discussed in SH6.1-16) with theoretical results are a powerful tool to test the magnetospheric magnetic field models used in the calculations of cosmic ray particle transport at high latitudes.

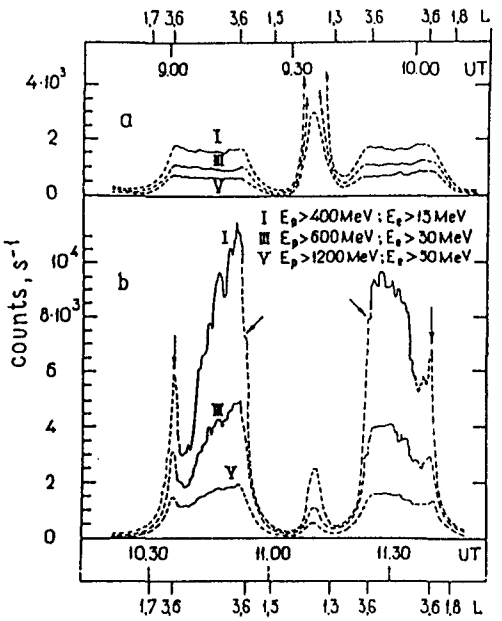

Fig. 11 The cosmic ray count rate as measured on November 22, 1972, with a Cerenkov counter aboard Cosmos-900 (Gorchakov et al., SH6.1-15):
a) in the quiet time period prior to the solar particle event
b) during the solar particle event

3. Atmospheric effects It is quite obvious that the field of meteorological effects, cosmic ray secondaries in the atmosphere, and response functions of cosmic ray detectors is no longer the focal point of interest in cosmic ray research: only four papers out of nine were actually presented at the conference in this field (SH6.1-5, 7, 8, 18). And no reference to atmospheric effects was made, after all, in the oral version of this report. Here, however, I would like to mention at least three new developments.

The flux and energy spectrum of electron and proton albedo in the energy range between 20 MeV and 1000 MeV were measured systematically a long time ago by Verma (1967) over Palestine, Texas. The measurements of proton albedos were then extended to higher energies over the same

location by Pennypacker et al. (1973). Now for the first time the flux and the energy spectrum of low energy (30 - 100 MeV) albedo protons have been measured in a low latitude region, at 4 mb altitude, over Hyderabad, India (Verma and Kothari, SH6.1-8). Preliminary results of the balloon experiment which took place in December 1984 show that the spectrum of re-entrant albedo protons agrees well with the theoretical values evaluated previously (Kothari and Verma, 1983). However, the measured flux and spectrum of splash albedo protons seem to be somewhat higher than expected. Further data analysis including also the low (5 - 24 MeV) energy splash and re-entrant electron albedo spectrum will be done.

A comparative study of cosmic ray coupling coefficients for neutron monitor stations has been made recently by Mori and Nagashima (1984) in order to obtain the most appropriate response function and also "finally the most reliable information of cosmic ray solar modulation phenomena in space from the ground-based observations". The comparison covered the three response functions derived by Lockwood and Webber (1967), Nagashima (1971) and Aleksanyan et al. (1981). The conclusions obtained are not quite unambiguous, but Sakakibara et al. (Sakakibara et al., 1984; SH5.1-6) find that the response function derived by Nagashima is the most appropriate for the analysis of the rigidity dependence of Forbush decreases.

New results were presented, finally, in paper SH6.1-18 by Alexeyenko et al. concerning short-time (10 - 20 minutes time scale) perturbations of typically 1% in the ground-level cosmic ray intensity associated with meteorological phenomena, and which cannot be explained by pressure and temperature effects (at the level of observation). These perturbations have a long history, and they were already discussed at the 14th ICRC by Alexeyev et al. (1975). In the meantime, data from an experiment carried out with the Baksan E.A.S. array and an electric field meter added to the system allow a much more detailed analysis. The authors arrive at the conclusion that the correlation between these short perturbations observed in the ground-level cosmic ray intensity and the appearance of strong (>20 kV/m) electric fields in the atmosphere is established beyond doubt. They also suggest that the effect could be due to a mechanism based on the positive excess of muons if during the time periods of perturbed cosmic ray intensity the strength of the electric field at high altitudes is much larger than the one measured at the surface of the earth.

4. Cosmogenic Nuclides New experimental techniques such as the accelerator mass spectrometry, new methods of analysis as e.g. the cyclogram method of time series analysis, and "new isotopes" such as the ^{10}Be are in the process of revolutionizing this field. New possibilities for research are open now which up to some years ago one could only dream of, and the interdisciplinary character of the field, which was not small anyway, has been increasing enormously.

A comprehensive review paper on "Cosmic-Ray Record in Solar System Matter" including some of the new developments was published by Reedy et al. (1983). Raisbeck in his invited talk presented at this

conference gave an excellent overview of the history of the field, the main techniques and isotopes used today, and he discussed a few of the most interesting applications and ongoing activities. Reference is made, therefore, to the written version of his presentation included in this volume of the Conference Papers.

New techniques and new isotopes have also been proposed at this conference: Ninagawa et al. (SH9.1-16) described the application of a spatial distribution read-out system for thermoluminescence sheets (Yamamoto et al., HE7.1-7) in dating the terrestrial age of meteorites. Nishiizumi et al. (SH7.1-4) presented a new ^{129}I - ^{129}Xe method to obtain cosmic ray exposure ages and to study the average cosmic ray flux on a 10^7 - 10^8 year time scale.

New theoretical studies on cosmogenic nuclide production by solar and galactic cosmic rays were discussed by Reedy (SH7.1-6, 7), Englert (SH7.1-9), and Zanda and Audouze (SH7.1-10), whereas the results of accelerator experiments on the contribution of secondary particles to the production of cosmogenic nuclides in meteorites were presented by Dragovitch and Englert (SH7.1-8). Because of the more fundamental character of these contributions, however, reference is made to the original papers for details.

The following discussion will be restricted to the problem of variations in the production rate of ^{14}C and ^{10}Be in the earth's atmosphere and their relation to solar modulation. In a recent paper Sonett (1984) showed that the 200-year periodicity in the time variations of atmospheric radiocarbon extends over the entire 8500-year La Jolla record and appears to be associated with a longer period between about 1500 and 2000 years. Beer et al. (1985a) find modulations with time periods of $\sim$200, $\sim$500 and $\sim$2000 years in both ^{14}C and ^{10}Be records between 3000 B.C. and 1100 A.D. As far as these long period variations are concerned they seem to be confirmed although their exact origin is still a matter of debate. Recent interest has focussed on the 11-year solar cycle in terrestrial records. Several studies (e.g. Damon et al., 1973; Baxter and Farmer, 1973; Burchuladze et al., 1980; Fan et al., 1983) on 11-year modulation effects in ^{14}C indicated a correlation between $\Delta^{14}C$ values and sunspot numbers, but in all the results cannot be considered conclusive. In recent papers it has been shown that the solar eleven year cycle is present in the series of ^{10}Be and $\delta^{18}O$ in ice cores as well as of thermoluminescence in sea sediments during the last millenia (Cini Castagnoli et al., 1984; Attolini et al., 1984; Beer et al., 1985b). As far as ^{14}C is concerned, Fan et al. (SH7.1-2) reported at this conference that from measurements in dated tree rings from 1824 - 1865 A.D. they find that, with the exception of the 1922 cycle, and with a delay of about five years, the $\Delta^{14}C$ values are anticorrelated with the sunspot numbers. The most interesting (and maybe also the most controversial) ^{14}C data, however, were presented at this conference by Kocharov et al. (SH7.1-14,15). Using scintillation equipment the radiocarbon content in dated tree ring samples from all over the Soviet Union was measured with an accuracy of 0.2 - 0.3% and with a time resolution of 1 year for the time period 1593 - 1981. They find a distinct 11-year periodicity in ^{14}C abundance before and after the Maunder Minimum. A correlation analysis between the $\Delta^{14}C$ values

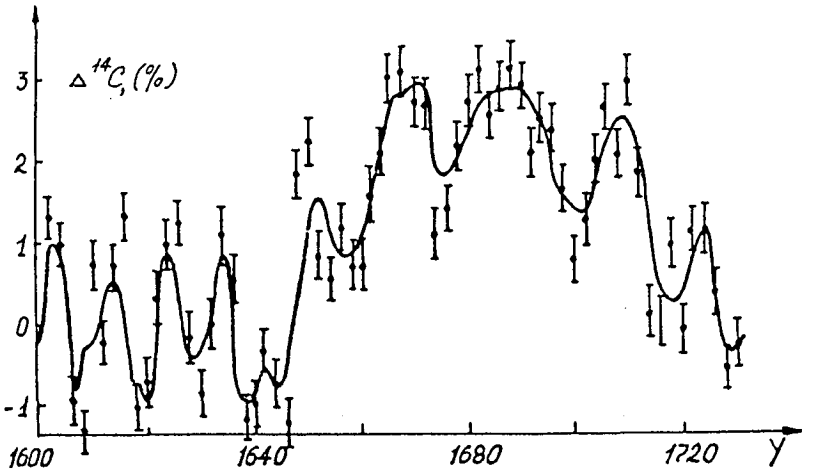

Fig. 12 $\Delta^{14}C$ data as obtained by Kocharov et al. (SH7.1-15) for the time period 1600-1730 A.D. (including the Maunder Minimum between 1645-1715 A.D.) from measurements of the radiocarbon abundance in dated tree rings.

and the Wolf sunspot number W yields a negative correlation with a time shift of about 4 - 5 years. This phase lag is in agreement with results obtained from calculations based on CO_2-models if a 11-year periodicity in the ^{14}C production rate is assumed (e.g. Siegenthaler et al., 1980). The absolute amplitude of the effect, however, appears to be somewhat large compared to the results of the model calculations.

Of special interest are the results shown in Figure 12 concerning the time period of the Maunder Minimum. It is quite obvious that between 1645-1715 A.D. the $\Delta^{14}C$ level is enhanced and that its time profile does exhibit distinct variations. In comparison with data published by Stuiver and Quay (1980) it seems that between 1670-1710 A.D. the maximum $\Delta^{14}C$ values obtained by Kocharov et al. are about 40% larger, although the 3-year running means presented at the conference appeared to be quite consistent with an average $\Delta^{14}C$-value of about 1.6% as given by Stuiver and Quay for this time period. Kocharov et al. translated the results shown in Figure 12 into ^{14}C production variations, sunspot numbers and intensity variations of the galactic cosmic rays within the rigidity range 0.5 GV $\leq$ R $\leq$ 50 GV. It is emphasized that in general extreme care must be taken in interpreting this kind of data. The authors conclude that during the Maunder Minimum the 11-year solar cycle was very weak (if present at all) but that nevertheless the cosmic ray intensity was modulated, with good indications of a 20-22-year period. It is very interesting to compare this conclusion with the

results obtained by Beer et al. (1985b) who during the Maunder Minimum find periodicities in the ^{10}Be concentrations in polar ice cores varying from 9 to 11 years.

Mechanisms for further modulation of cosmic rays also in the absence of solar flares, as e.g. the effects of polar high speed recurrent solar wind streams have been discussed by several authors (e.g. Forman, 1978; Hundhausen, 1980; Fisk, 1979). Based on a statistical analysis of ^{10}Be, sunspot, geomagnetic, and aurora data Attolini et al. (SH7.1-1, 3) suggest that the modulation of ^{10}Be in polar ice is probably due to at least two main contributions: to one which is negative and in phase with the solar flare activity modulating the cosmic ray flux in Forbush-type decreases, and to one which is positive and in phase with the appearance of large wind streams originating at both polar coronal holes. From the analysis of Aurorae the authors furthermore conclude that the high latitude solar activity is related to a stable periodicity of 11.1 years whereas the low heliolatitude activity contributes to an oscillation of the solar cycle period between 10.8 and 11.4 years on a time scale of about 200 years.

5. Concluding Comments In conclusion the progress achieved in the areas of Forbush decreases, Geomagnetic Effects and Cosmogenic Nuclides, and possible directions of related research in the near future are summarized in the following (again very personal) comments:

In the field of transient variations correlation studies between cosmic ray measurements at 1 AU and other heliocentric distances and characteristic parameters of the interplanetary medium (e.g. solar wind speed, intensity and direction of the IMF, etc.) and especially with specific types of interplanetary perturbations (e.g. shock-associated clouds, stream interfaces, cold magnetic enhancements, etc.) have been very successful in yielding new knowledge about the structure of these modulating perturbations as well as their evolution in space and time. Experimental evidence has been found for substantial differences in the effects of the various types of interplanetary perturbations on cosmic rays, and for a dependence of these effects on the three-dimensional configuration of the interplanetary medium. More of these studies are needed especially in order to explain the physical processes involved. To a larger extent, these studies should also include anisotropy effects, they should definitely include the rigidity range above 10 GV, and they should be extended to all three dimensions of interplanetary space. It is expected that the ULYSSES out-of-ecliptic mission, a joint ESA-NASA project, will contribute substantially to these analyses, but unfortunately not before $\sim$1988. The new experimental data also require an adaption of existing or the creation of new theoretical models - a comprehensive model for Forbush decreases explaining quantitatively all observational facts is still missing.

The area of geomagnetic effects has become the area of magnetospheric effects. Due to recent research great progress has been made especially in the experimental determination, the understanding and the theoretical modelling of changes in cosmic ray cutoff rigidities at low and mid-latitudes. Much work remains to be done as

far as high latitudes are concerned. In order to fully understand and to be able to simulate the (solar) cosmic ray particle access to the polar regions of the earth we need accurate models of the magnetospheric magnetic field. These models must include all major magnetospheric current systems (in particular the field aligned currents), and they should represent magnetically quiet time periods as well as different levels of geomagnetic activity. In the evolution of magnetospheric magnetic field models cosmic ray and magnetospheric physicists should work closely together since cosmic ray measurements are a powerful additional tool in the study of the perturbed magnetosphere.

In the field of cosmogenic nuclides, finally, exciting new results and developments follow in rapid succession. Thanks to new techniques and new isotopes the analysis of cosmic ray history has entered into a new dimension. Although many problems connected with experimental procedures, with data analysis, and in particular with the identification of climatic, meteorologic, transport and accumulation effects are still unsolved, the ^{14}C and especially the ^{10}Be isotopes in terrestrial records as well as the thermoluminescence in sediments are about ready to reveal the cosmic ray intensity-time profile at the earth for a time period of several thousand years back from now. And all those interested in larger time scales can expect a similar evolutionary progress in the near future from the analysis of meteorites, lunar samples, cosmic spherules and cosmic dust.

Acknowledgements I would like to thank the organizers of the 19th ICRC for the invitation to act as a rapporteur and for their hospitality in La Jolla. I am very grateful to many participants of the conference as well as to colleagues at home for helpful and pleasant discussions. Thanks are due in particular to S.P. Agrawal, J. Beer, G. Cini Castagnoli, O. Eugster, M. Galli, J.E. Humble, G.E. Kocharov, H. Oeschger, M.A. Shea, D.F. Smart, and M. Storini.

References

Agrawal, S.P., (1983), Conference Papers 18th ICRC, 12, 403

Agrawal, S.P., (1985), private communication

Aleksanyan, T.M., et al., (1981), Conference Papers 17th ICRC, 3, 225

Alexeyev, E.N., et al., (1975), Conference Papers 14th ICRC, 8, 2996

Arens, M., (1978), Partial Ring Currents and Cosmic Ray Magnetic Cutoff Rigidity Variations, thesis, Univ. van Amsterdam, Amsterdam

Attolini, M.R., et al., (1984), Proceedings of International Symposium on Cosmic Ray Modulation in the Heliosphere, Iwate University, Morioka, Japan, 21-25 August 1984, 299

Barnden, L.R., (1973), Conference Papers 13th ICRC, 2, 1277

Baxter, M.S., and Farmer, J.G., (1973), Earth Planet. Sci. Lett., 20, 295

Beer, J., et al., (1985a), Contributed Paper, 12th International Radiocarbon Conference, Trondheim, Norway, 24-28 June, 1985; publication in preparation

Beer, J., et al., (1985b), Nuclear Instruments and Methods in Physics Research, B10/11, 415

Biryukov, A.S., et al., (1984), acta physica slovaka, 34, 157
Burchuladze, A.A., et al., (1980), Nature, 287, 320
Burlaga, L.F., (1984), Space Sci. Rev., 39, 255
Cini Castagnoli, G., et al., (1984), Nuovo Cimento, 7C, 235
Cooke, D.J., (1981), Conference Papers 17th ICRC, 4, 263
Damon, P.E., et al., (1973), Earth Planet. Sci. Lett., 20, 300
Dhanju, M.S., and Sarabhai, V.A., (1967), Phys. Rev. Lett., 19, 252
Dorman, L.I., (1974), Cosmic Rays, North-Holland, Amsterdam
Dorman, L.I., and Libin, I.Ya., (1984), Space Sci. Rev., 39, 91
Debrunner, H., and Flückiger, E., (1977), Conference Papers 15th ICRC, 11, 251
Engelmann, J.R., et al., (1971), J. Geophys. Res., 76, 4245
Fan, C.Y., et al., (1983), Radiocarbon, 25, 205
Fenton, A.G., et al., (1984), Proceedings of International Symposium on Cosmic Ray Modulation in the Heliosphere, Iwate University, Morioka, Japan, 21-25 August 1984, 191
Fisk, L.A., (1979), Proc. Conf. Ancient Sun (Pepin, Eddy, Merryl), Geochimica et Cosmochimica Acta suppl., 13, 103
Flückiger, E.O., et al., (1983), Conference Papers 18th ICRC, 3, 431
Flückiger, E.O., et al., (1985), submitted for publication
Forman, M.A., (1978), EOS, 59, 1154 (abstract)
Gall, R., et al., (1984), Tables of Approach Directions and Points of Entry of Cosmic Rays for Higher Latitude Cosmic Ray Stations, Instituto de Geofisica, Universidad Nacional Autonoma de Mexico
Hundhausen, A.J., et al., (1980), Science, 207, 761
Humble, J.E., et al., (1983), Conference Papers 18th ICRC, 3, 442
Ilyin, V.D., et al., (1983), Conference Papers 18th ICRC, 3, 447
Iucci, N., et al., (1984), Nuovo Cimento, 7C, 467
Kothari, S.K., and Verma, S.D., (1983), Conference Papers 18th ICRC, 3, 483
Kudo, S., et al., (1984), Proceedings of International Symposium on Cosmic Ray Modulation in the Heliosphere, Iwate University, Morioka, Japan, 21-25 August 1984, 204
Lemaitre, G., and Vallarta, M.S., (1936), Phys. Rev., 50, 493
Lockwood, J.A., (1971), Space Sci. Rev., 12, 658
Lockwood, J.A., and Webber, W.R., (1967), J. Geophys. Res., 72, 3395
McKibben, R.B., (1981), Conference Papers 17th ICRC, 13, 163
Mineev, Yu.V., et al., (1983), Conference Papers 18th ICRC, 3, 262
Mori, S., and Nagashima, K., (1984), Proceedings of International Symposium on Cosmic Ray Modulation in the Heliosphere, Iwate University, Morioka, Japan, 21-25 August 1984, 219
Nachkebia, N.A., and Shatashvili, L.Kh., (1983), Conference Papers 18th ICRC, 10, 152
Nagashima, K., (1971), Rep. Ionos. Space Res., Japan, 25, 189
Pennypacker, C.R., et al., (1973), J. Geophys. Res., 78, 1515
Pfitzer, K.A., (1979), in Quantitative Modeling of Magnetospheric Processes, W.P. Olson (ed.), Geophysical Monograph 21, American Geophysical Union, Washington, D.C., 242
Potemra, T.A., (1979), Rev. Geophys. Space Sci., 17, 640
Potemra, T.A., (ed.), (1984), Magnetospheric Currents, Geophysical Monograph 28, American Geophysical Union, Washington, D.C.
Reedy, R.C., et al., (1983), Science, 219, 127

Sakakibara, S., et al., (1984), Proceedings of International Symposium on Cosmic Ray Modulation in the Heliosphere, Iwate University, Morioka, Japan, 21-25 August 1984, 212
Shah, G.N., et al., (1979), Conference Papers 16th ICRC, 3, 423
Shea, M.A., and Smart, D.F., (1975a), Environmental Research Papers, No. 503, AFCRL-TR-75-0185
Shea, M.A., and Smart, D.F., (1975b), Environmental Research Papers, No. 524, AFCRL-TR-75-0381
Shea, M.A., and Smart, D.F., (1983), Conference Papers 18th ICRC, 3, 415
Shea, M.A., and Smart, D.F., (1985), private communication
Shea, M.A., et al., (1983a), Conference Papers 18th ICRC, 3, 411
Shea, M.A., et al., (1983b), Conference Papers 18th ICRC, 3, 423
Siegenthaler, U., et al., (1980), Radiocarbon, 22, 177
Smart, D.F., et al., (1969), J. Geophys. Res., 74, 4731
Smart, D.F., and Shea, M.A., (1977), Conference Papers 15th ICRC, 11, 256
Smart, D.F., and Shea, M.A., (1985), J. Geophys. Res., 90, 183
Sonett, C.P., (1984), Rev. Geophys. Space Phys., 22, 239
Stern, D.P., (1983), Rev. Geophys. Space Sci., 21, 125
Störmer, C., (1930), Z. Astrophys., 1, 237
Stuiver, M., and Quay, P.D., (1980), Science, 207, 11
Thomas, B.T., and Gall, R., (1984), J. Geophys. Res., 89, 2991
Tsyganenko, N.A., and Usmanov, A.V., (1982), Planet. Space Sci., 30, 985
Venkatesan, D., et al., (1982), Solar Physics, 81, 375
Verma, S.D., (1967), J. Geophys. Res., 72, 915
Walker, R.J., (1979), in Quantitative Modeling of Magnetospheric Processes, W.P. Olson (ed.), Geophysical Monograph 21, American Geophysical Union, Washington, D.C., 9
Walker, R.J., (1983), Rev. Geophys. Space Phys., 21, 495
Wu, S.T., et al., (1983), Solar Physics, 84, 395

HIGH ENERGY INTERACTIONS OF COSMIC RAY PARTICLES[†]

Lawrence W. Jones

Department of Physics
University of Michigan
Ann Arbor, Michigan 48109

INTRODUCTION

This report focuses on the highlights of seven sessions of the Conference dealing with high energy interactions of cosmic rays. The session titles were HE 1.1: High Energy Cross Section Measurements, HE 1.2: Particle Production-Models and Experiments HE 1.3: Nuclei and Nuclear Matter, HE 1.4: Nucleus-Nucleus Collision, HE 6.1: Searches for Magnetic Monopoles, HE 6.2a: Studies of Nucleon Decay, and HE 6.2b: New Particle Searches. My task is made easier by three other related talks at this meeting; the summary of the current state of elementary particle physics in an invited lecture by Professor Perkins, the rapporteur lecture on emulsion chamber observations by Professor Shibata, and the highlight lecture on nucleus-nucleus interactions by Dr. Wosiek.

Let me begin by recalling the familiar integral flux of cosmic rays versus energy in Figure 1, where noted on the graph are the energies available and to become available with various of the proton-proton or proton-antiproton colliders. It is against this backdrop of available accelerator energies at high energy laboratories that we must temper our studies of particle interactions from cosmic rays. Let me recall Perkins' lecture and repeat his summary perspectives on the outstanding classes of problems in particle physics and the extent to which cosmic ray experiments might be useful in shedding light on these problems.

Outstanding Problems in Particle Physics and the Relevance of Cosmic Ray Data to their Solutions.*

PROBLEMS	COSMIC RAY RELEVANCE
• Massive Scalar Particles (Higgs Sector)	No
• Technicolor, Supersymmetry (New Particles, TeV Masses)	No
• Tests of GUTs (Magnetic Monopoles, Proton decay, etc)	Yes
• Neutrino Mass, Mixing; Majorana Neutrinos	Yes
• CP Violation	No
• New Interactions (Centauros, etc.)	?
• Unexpected Phenomena	Yes, if done well

*taken from D. Perkins lecture at this meeting.

[†]Supported by the U.S. National Science Foundation.

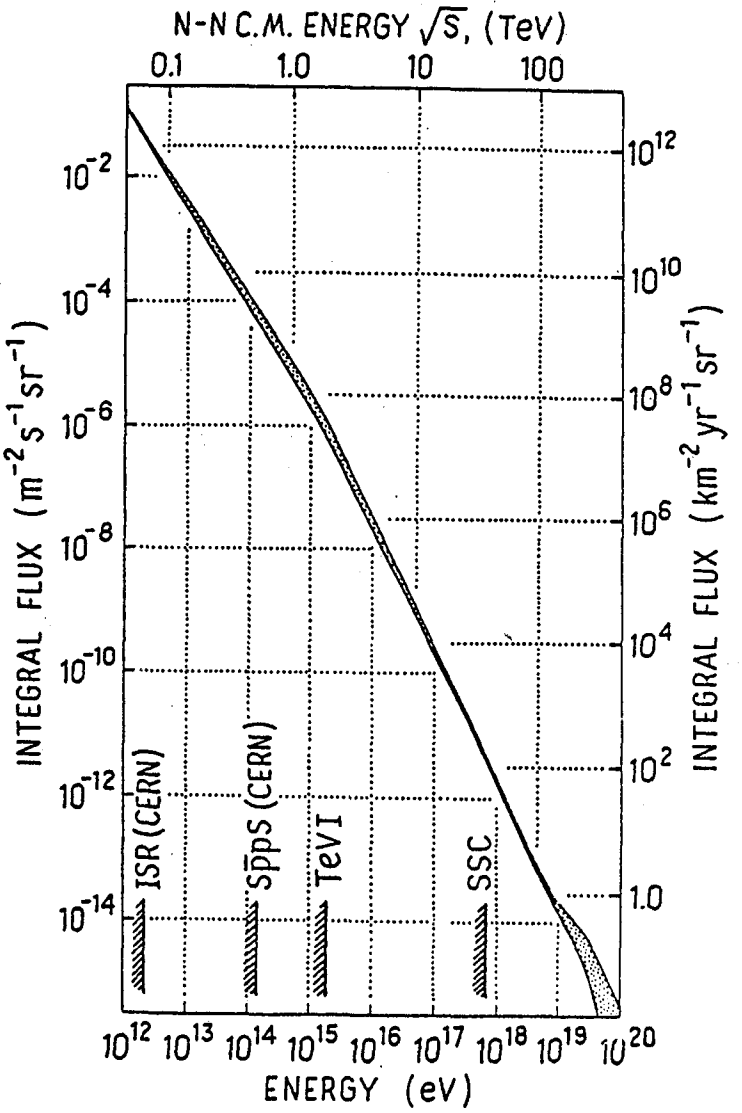

Figure 1. Cosmic ray primary integral flux spectrum vs. energy, with energies of nucleon-nucleon colliders indicated on the abscissa.

Note that the dominant problems in particle physics, the search for the Higgs particles and the search for evidence of Supersymmetry, Technicolor, or other departures from our current standard model are apparently not accessible to study by cosmic ray interactions. Looking down this list, it appears that our cosmic ray efforts have been primarily directed toward the last two items; the search for evidence of new interactions, such as Centauro events, Chirons, etc., and the search for unexpected phenomena.

I believe that Perkins' summary is a bit narrow in the context of the overall mission of our study of elementary particle physics using cosmic rays. Let me illustrate what I mean with Figure 2. In this simple sketch I attempt to indicate that the four areas: cosmic ray physics, physics of elementary particles, astrophysics, and cosmology are all interrelated. I will not in this discussion elaborate on the relationships between astrophysics and cosmology, astrophysics and particle physics or cosmology and elementary particle physics. I should note however that the relationship between cosmic rays and elementary particle physics is a two-way street. Perkins remarked specifically on the information that cosmic ray physics can provide to help us in understanding elementary particle physics. Equally, or perhaps more important, is the information that we gain from studies of elementary particle physics with accelerators which helps us to interpret cosmic ray data, often at higher energies than available in the laboratory, in order to provide insights and important information which in turn bear on questions in cosmology and astrophysics.

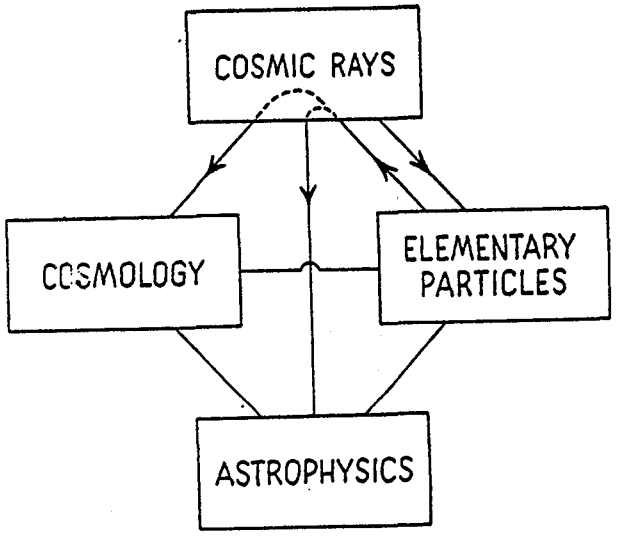

Figure 2.

I would like to propose the following list of areas where cosmic ray studies of high energy interactions are valuable.

(1) Cosmic rays can be use to exlore the fundamental nature of particle interactions at energies greater than those available with colliders, currently about 10^{15} eV. Here cosmic rays may indeed only be able to study gross features of the interactions such as total cross sections, average transverse momenta, average particle multiciplities, and so forth. Nevertheless, even this guidance to the nature of strong interactions well beyond energies accessible with accelerators is valuable.

(2) The study of proton-nucleus interaction properties at energies greater than one TeV, the highest proton beam energy currently available.

(3) The study of nucleus-nucleus reactions at energies greater than those provided by the Berkeley Bevalac or the Dubna heavy ion accelerator, which correspond to about 10^{10}eV per nucleon.

(4)The exploration of the cosmic ray energy spectrum and composition for energies greater than about 10^{14}eV. The indirect data from extensive air showers is interpretable in terms of spectrum and composition only through the use of data from accelerators.

(5) The search for new particles in cosmic rays such as magnetic monopoles, tachyons, quarks, and so forth will continue to be a domain of cosmic rays study. These particles might either be produced in very high energy interactions or, more probably, they may be relics of the early universe and primordial in nature.

CROSS SECTIONS

Let me first address the subject of proton-air cross sections and their interpretation in terms of proton-proton total cross sections. There were several papers presented here which bear on this question. Linsley (HE 1.1-1) reviewed and analyzed a large body of existing data. The Utah Fly's Eye group reported (HE 1.1-2) a relatively clean measurement of interaction mean free path of proton primaries in air and Yodh and his collaborators analyzed the proton-air data in terms of proton-proton cross sections. There were also contributions by Carlson (post-deadline paper) reporting on the UA5 collaboration results from the CERN $\bar{p}$-p collider operated at up to 900 GeV total center-of-mass energy.

The Fly's Eye result on the distribution of the height of shower maximum is reproduced in Figure 3. The data show a rise to a maximum number of events at a depth in atmosphere of about 700 g/cm^2 and then an exponential decay over the range from 800 to 1100 g/cm^2. The Fly's Eye group interprets these data as evidence for the contribution of heavier nuclei interacting at shallower depths in the atmosphere, where maximum occurs closer to the top of the atmosphere, and for proton-air interactions in the exponential tail of the interaction distribution

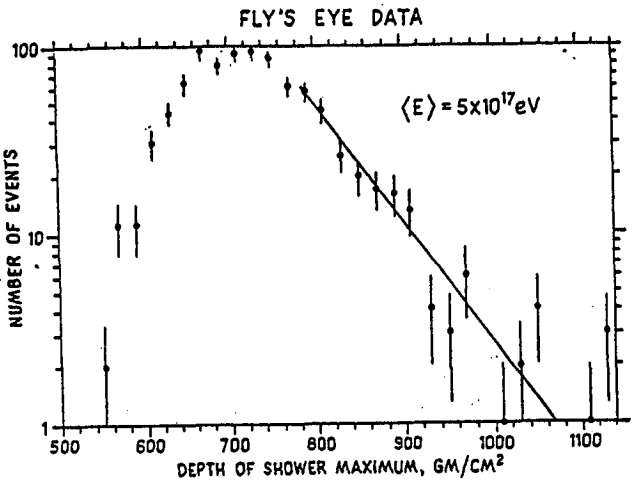

Figure 3. The Fly's Eye data on height of shower maximum showing the exponential component identified as due to proton-air events.

beyond 800 g/cm^2. From these data the Fly's Eye group interprets the interaction mean free path of protons in air as 70 ± 6 g/cm^2 at an average energy of 5×10^{17}eV. Ellsworth, Gaisser, Stanev, and Yodh (Phys. Rev. D 26, 336 (1982) have parameterized the interaction mean free path as determined from this experiment in terms of a proton-air inelastic cross sections and conclude that the proton-air cross section is 540 mb.

The interpretation of this cross section in terms of a fundamental proton-proton total cross section is indirect. The proton-air cross section may be expressed as a sum of the dominant inelastic cross section (which is that observed in the Fly's Eye and most other experiments), plus an elastic scattering contribution, plus a quasi-elastic contribution (wherein the proton scatters off a nucleon in the air nucleus leading to disruption of a nucleus without meson production), and plus a single diffraction contribution (wherein the incident proton excites a nucleon in a nucleus to a nucleon isobar, again leading to soft particle production but not contributing to an air shower). The proton-air inelastic cross section can be related to the proton-proton total cross section through Glauber theory with two added inputs; one an estimate of the quasi-elastic and single diffractive cross sections and two, the proton-proton elastic scattering slope parameter. In fact, Yodh and his collaborators (HE 1.1-3) have embphasized that there may be significant uncertainty in choosing the slope parameter and that different values lead to different values of proton-proton total cross section for the same proton-air inelastic cross section. They have been guided in their choice of the slope parameter from work of Block and Cahn. The collider data best fit a model which leads to a slope parameter

of 12 $(GeV/c)^{-2}$ at the energy of the Fly's Eye data. Yodh's analysis of the Fly's Eye proton-air inelastic measurement leads to a proton-proton total cross section at $5x10^{17}$eV of 122 mb.

NEW COLLIDER DATA

Gaisser and Halzen (HE 1.2-2) spoke on the interpretation of the rising proton-proton cross section in terms of quark-quark, quark-gluon and gluon-gluon hard scattering, or jet production. Cline reported on the recent CERN 900 GeV data observed in the UA1 detector which suggested that jet production might account for as much as 20% of the total proton-proton inelastic cross section at that energy (post-deadline paper). The recent data reported by UA1 also indicate that the average tranverse momentum continues to increase in proportion to the particle multiplicity per unit rapidity. There had been an earlier suggestion that the average transverse momemtum plateaued at greater than about 10 particles per unit rapidity suggesting that there was evidence for the onset of quark-gluon plasma phemonena, however the recent data do not support that suggestion.

Data from the CERN Collider reported by Carlson and by Geich-Gimbel of the UA-5 group also included recent measurements of average particle multiciplity, multiciplity distributions and rapidity density. One interesting result was the nature of the multiciplity distributions at these higher energies. They do not follow KNO scaling, which had become a favorite model from ISR data. In fact the suggestion here is that the better fit is to a negative binomial distribution. They also reported their best understanding at this time of the proton anti-proton total and elastic cross sections. Table I is a summary of ISR results and the CERN Collider results on cross sections.

Table I. CERN Collider Results on Nucleon-Nucleon Cross Sections

	ISR (pp)	SPS ($\bar{p}p$)		
$\sqrt{\sigma}$(GeV)	53, 64	200	540	900
σ(total)mb	44	52.3[1]	61.9	66.5
σ(elastic)/σ(total)	0.175	0.187[1]	0.215	0.235[2]
σ(elastic)mb	7.7	9.8	13.3	15.6
σ(inelastic)mb	36	42.5	48.6	50.9
σ(single diff.)[3]mb	7	4.7	5.2[4] / 8.1[5]	7.1
σ(non single diff.)mb	29	37.8	42	43.8
σ(sd)/σ(el)	0.9	0.48	0.5	0.46

1. Interpolated
2. Extrapolated
3. $M^2/s < 0.05$
4. UA5
5. UA4

One interesting feature apparent here is the rise in the ratio of the elastic to the total proton anti-proton cross section with energy.

Rapidity density fluctuatious are seen in the UA5 data which are not associated with jet production and raise interesting questions. Other results from these studies include the observation that no evidence for Centauro events is found. The rapidity distributions almost scale in the rest frame of one of the particles as one goes from the ISR energies through 900 GeV. There are some departures from scaling as suggested by Gaisser and Halzen which can be understood by the depletion of the forward particles through the increased contribution to the cross sections of large-angle jet production. The central rapidity density rises as lns through 900 GeV. At 900 GeV the average charged multiplicity is $\langle n_{ch} \rangle = 34.6 \pm 0.7$, not including single diffraction. Its energy dependence may be fit by either $\langle n_{ch} \rangle = a + b\, s^{\alpha}$ or $\langle n_{ch} \rangle = a + b \ln s + c (\ln s)^2$.

PROTON-NUCLEUS COLLISIONS

One session at this meeting was taken up with reports on nucleon-nucleus interactions. Proton-nucleus interaction systematics are necessary to understand and to calculate the cascading of cosmic ray nucleous in the atmosphere or in thick detectors, such as emulsion stacks. Thus the character of the interactions of primary protons in complex nuclei, such as the distributions in number and momentum of the secondary particles produced in the interactions, and the dependence of the distributions on the mass number of the nuclear target are all essential inputs to the modeling of extensive of air showers or the interactions of cosmic rays in thick detectors such as the nuclear emulsion chambers of high altitude experiments. However, it is less clear that there is a fundamental interest in the understanding of proton-nucleus interactions in terms of elementary particle physics. Given the availability of proton anti-proton collider data over the same range of center-of-mass energies, most of what is observed can be understood as a super-position of proton-proton interactions sumed over the nuclear targets. The uncertainty of the superposition models is greater than the differences between models of primary interactions or the statistical uncertainties in the data. In contrast, nucleus-nucleus interactions hold the promise of observing quark gluon plasma effects and with them the possible phase transition to a new state of matter. Nevertheless, some proton nucleus data are noteworthy. At this conference there were new data presented from the Armenian group (HE 1.1-5) on pion and nucleon cross sections at an average energy at 1300 GeV, as indicated in Table II. The transverse momentum distribution of proton-iron interactions has been observed (HE 1.2-11) to follow an exponential distribution with an average transverse momemtum of gammas of 0.19 GeV/c for gamma rays greater than or equal to 30 GeV/c from events of 2 1/2 to 8 1/2 TeV. Among the most interesting results reported was an observed anomalous fluctuation in rapidity density reported by Capdeville in emulsion events with incident protons and $\sum E_{\gamma} > 200$ TeV (HE 5.1-5).

Table II. Data on Inelastic Cross Sections at <E> = 1300 GeV

Projectile particle	Target element	Inelastic Cross Section (mb)
n	C	238 ± 13
p	C	236 ± 13
π	C	181 ± 12
n	Pb	1885 ± 70
p	Pb	1793 ± 90
π	Pb	1646 ± 76

NUCLEUS-NUCLEUS INTERACTIONS

Nucleus-nucleus physics was summarized at this meeting in an excellent highlight lecture by Dr. Wosiek. Several contributed papers were presented from the JACEE collaboration as well as accelerator data from the Dubna and Berkeley heavy ion accelerators. From Dr. Wosiek's highlight talk, I may repeat the essential conclusions. First, at energies below 100 GeV per nucleon the nucleus-nucleus data can be understood as a superposition of nucleon-nucleon physics together with Glauber screening, etc. Model uncertainties are at least as great as the uncertainties in the data, as remarked in the case of proton nucleus interactions. In contrast, at energies greater than 1 TeV per nucleon, the inclusive data as well as multiciplities are consistant with conventional superposition models, but there are characteristics which are not explained by superposition models. The average transverse momentum is anomalously high, there are fluctiations in rapidity density greater than one would expect from statistical arguments and super position models, and there is evidence of an increase of average transverse momentum with an increase in the energy density of the nucleus-nucleus collision system.

MAGNETIC MONOPOLES

At this conference there was a discussion of searches for magnetic monopoles. Three classes of new results were presented. Searches using gas filled proportional counters incorporating helium, where a prediction by Drell and collaborators suggests that the sensitivity to magnetic monopoles extends to lower velocities than is the case of other ionization detectors; scintillation counter detectors and ordinary gas proportional counters; and a report on searches for monopoles in geological samples of mica using track etch techniques. Let me review briefly the magnetic monopole situation. We expect monopoles to have a mass in a range predicted by grand unification theories of about 10^{16} GeV or 0.02 micrograms. The monopole velocity may be expected to fall within the range of 10^{-2} to 10^{-4} of the velocity of light. This corresponds to the range of β of our galaxy with the respect to the local super cluster, the β of the solar system through our local galaxy, or the observed β of the earth through the 3K black body radiation field. Magnetic monopoles may become attached to nuclear particles

possessing a large magnetic dipole moment, so that a magnetic monopole may arrive at the earth bound to a proton, or, in passing through the earth if not already bound to a nucleon, it might capture a heavier nucleus such as aluminum 27. Magnetic monopoles have been predicted to catalyze proton decay (the so-called Rubakov effect).

Limits to the flux of magnetic monopoles may be set by at least two effects. The Parker bound is a limit based on the observed magnitude of the galactic magnetic field and the rate at which it would be neutralized by monopoles and built up by galactic dynamo effects. The other limit comes from ascribing the missing mass of the Universe to monopoles. Second, one may argue that there is a limit on the magnetic monopole density for a given mass if monopoles accounted for the missing mass required for closure of the Universe. New limits on the flux of magnetic monopoles as a function of monopole velocity are indicated in Figure 4 where the Parker bound and missing mass limits for $M=10^{16}$ GeV are both indicated.

Experiments using helium filled proportional counters at the University of California, San Diego (HE 6.1-12) and by the Tokyo group (HE 6.1-1, 6.1-2) are indicated as well as underground measurements of the KGF group and the Baksan groups (HE 6.1-6, HE 6.1-11). The most stringent limit presented comes from the track etch technique in mica where the assumption made and the limit presented (HE 6.1-8), is that a significant fraction of the monopoles that penetrate the minerals containing the mica are bound to aluminum 27 nuclei. Without this assumption, the treshold for the mica track etch technique is not sufficient to detect single magnetic monopoles. Other monopole limits based on the lack of observation of nucleon decay cascades (the Rubakov effect) have been discussed but were not presented at this meeting. New detectors coming into operation or planned at the Homestake mine by the University of Pennsylvania group (HE 6.1-9), by the MACRO collaboration planning an experiment in the Italian Gran Sasso of tunnel (HE 6.1-4, 6.15), by upgrades of Kolar Goldfield dectectors HE 6.2-4), and by the University of California San Diego group were discussed.

I may conclude this discussion of magnetic monopoles by stating that, as of this conference, there is no evidence for magnetic monopoles.

NUCLEON DECAY

At this conference there was one session devoted to nucleon decay. One may legitimately question whether nucleon decay is an appropriate topic for a cosmic ray conference. In fact if nucleon decay were observed it would have profound cosmological as well as particle physics ramifications. However in principle there is no more reason to dicuss nucleon decay before a cosmic ray audience than the searches for

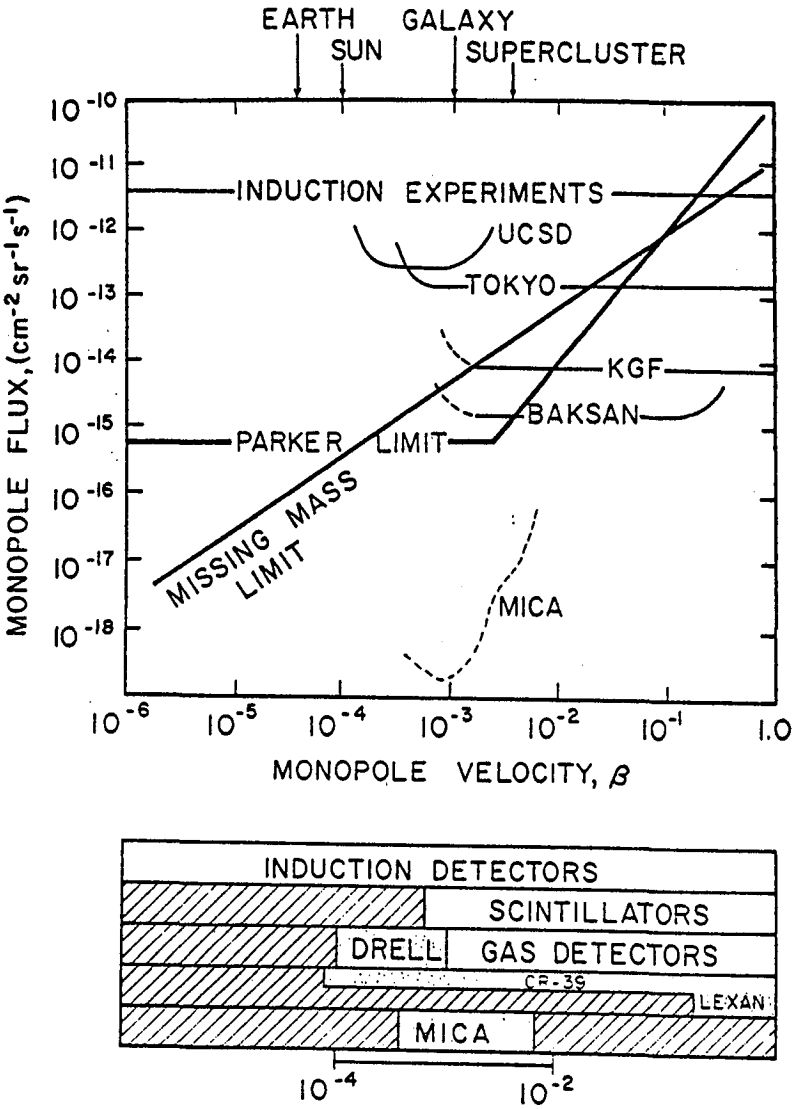

Figure 4. Monopole flux limits set by various experiments reported at this conference vs. monopole velocity, β. Also, noted are various astronomical velocities and, below the graph, the range of velocity sensitivity of various detectors.

neutrino mass, double beta decay, or parity violation in atomic hygrogen. Perhaps the reason that nucleon decay is discussed at a cosmic ray conference is simply the fact that many of the large nucleon decay experiments have been undertaken by cosmic ray groups.

Results were presented at this meeting by the Frejus group, (HE 6.2-2), the Nusex experiment (HE 6.2-6), the KGF group,(HE 6.2-3), and in a post deadline contribution by the IMB group. No report was presented here from the Kamioka experiment. Upgrades and new experiments were reported by the KGF collaboration (HE 6.2-4), and by the Minnesota Soudan group describing Soudan II (HE 6.2-5). A post deadline contribution describing the proposed MACRO experiment was presented, although information on the upgrades of the IMB detector and the Kamioka detector was not in the program. Table III reports the current limits on proton decay partial lifetimes corresponding to different decay channels as reported by the most sensitive detector operating, the IMB detector. Listed here are only proton decay limits. Comparable limits exist for the decay of bound neutrons.

The conclusions of the session can be stated at follows: Each experiment sees proton decay candidates among contained neutrino events. However there are no unambiguous candidates for proton decay, nor are there observed any statistically significant departures from the expected spectrum of neutrino interactions. The limits to proton decay can be summarized as follows: back-to-back decay modes such as $\pi^{\circ}e^{+}$ final states have a partial lifetime lower limit, $\tau/B \geq 10^{32}$ years (90% confidence level). Other modes involving K or μ final state particles have a partial lifetime limit, $\tau/B \geq 10^{31}$ years (90% confidence level). Recall that the prediction of minimal SU5 is that the proton lifetime should be about 10^{30} years with the decay going to $\pi^{\circ}e^{+}$ about 60% of the time.

MISCELLANEOUS

Several reports were presented which I would group into a miscellaneous category. There was a report on massive hadrons in airshowers by the Maryland group (HE 6.2-7); the conclusion was that there is at this time no evidence for such particles in airshowers, in contrast with earlier reports. In another paper from Akeno negative evidence for tachyons was presented (HE 6.2-8) and tachyons seem now to be definitely gone. Wada claimed some evident for charge (4/3)e quarks in cosmic rays (HE 6.2-14), however I did not find the evidence compelling. Heinreich reported on a search for anomalons using CR-39 plastic etch detector (HE 6.2-12) with strong negative results. Finally, Yakovlev presented an argument for the explanation of the "long flying component" which he has previously reported from the Tien Shan experiment (HE 6.2-17). He argues that a cross section for charm production of serveral mb could explain that observation. It seems to me, however, that such a cross section is unrealistically large in the light of current accelerator data on charm production.

Table III. Proton Decay Partial Lifetime Limits
IBM 417 Day Results*

Decay Mode	Visible Cherenkov Energy	Detection Efficiency Including Corrections	Candidates† observed	Estimated background	Partial Lifetime Limit τ/B (10^{31}yr.) 90% C.L.
$e^+\gamma$	750-1100	0.66	0	0.2	36
$e^+\pi^\circ$	750-1100	0.46	0	0.2	25
e^+K°	300-650	0.12	7	8	7.7
	750-1100	0.14	0	0.5	
$e^+\eta^\circ$	400-650	0.07	5	6	20
	750-1100	0.37	0	0.5	
$e^+\rho^\circ$	200-500	0.16	6	6	1.7
$e^+\omega^\circ$	300-600	0.19	6	7	3.7
	750-1100	0.05	0	0.5	
$\mu^+\gamma$	550-900	0.52	0	0.2	28
$\mu^+\pi^\circ$	550-900	0.32	0	0.2	10
μ^+K°	150-500	0.19	7	7	4.0
	500-900	0.14	4	6	
$\mu^+\eta^\circ$	200-400	0.12	4	5	4.6
	550-900	0.23	2	1	
$\mu^+\rho^\circ$	150-400	0.10	4	5	1.6
$\mu^+\omega^\circ$	200-550	0.18	8	8	2.3
	650-900	0.03	1	0.7	
νK^+	150-375	0.08	6	11	0.96
$\nu\rho^+$	300-600	0.07	6	7	0.84
νK^{*+}	250-500	0.08	7	11	0.96
$e^+e^+e^-$	750-1100	0.93	0	0.5	51
$\mu^+\mu^+\mu^-$	200-425	0.58	1	0.7	19

*G. Bleuitt, et al., Phys. Rev. Letters 55, 2114 (1985).

†Many observed events are candidates for more than one decay mode.

DISCUSSION

By way of conclusion, I would like to make a few remarks on this area of cosmic ray physics. I would observed that the results of cosmic ray experiments as they pertain to high energy or elementary particle physics are not always taken seriously by high energy physicists working with particle accelerators, and it is appropriate to ask why.

In the first place, since about 1960 cosmic rays physicists have made several significant discoveries. The cross section of protons on air nuclei as interpreted from airshower data was first observed to rise as a function of energy by cosmic ray physicists and this was later confirmed at particle accelerators. The systematics of the nucleon-nucleon reaction were first studied extensively with cosmic rays, well before particle accelerators provided the same class of data with much greater precision. Thus the behavior of average multiciplicity versus energy, average momentum as a function of energy, the distribution of secondary particles vs. rapidity, the observation of scaling in the forward region, the behavior of average multiciplicity vs. atomic number, multiciplicity distributions of NN reactions and so forth were all first studied with cosmic rays. Charm mesons were first observed in cosmic ray emulsion chambers and I believe that Dr. Niu properly deserves credit for their first observation, although with uncertainty of the final state particle identities he was unable to unambiguously determine the D-meson mass. The Brazil-Japan group at Chacaltaya first observed jets which are now seen so impressively in the CERN data from the proton-antiproton collider.

Nevertheless, there are ambiguous and unresolved phenomena, many of long standing, reported by our cosmic ray colleagues. These include the Centauro phenomenon, the Chiron events, the long-flying component, and many other single event and single experiment anomalies. Particularly disturbing is the fact that these puzzles remain year after year, conference after conference without definitive resolution.

However, even worse, cosmic ray physicists have made significant mistakes. Let me simply list a number of the cosmic ray mistakes reported over the last twenty years, the period over which I have been in attendance at the international cosmic ray conferences.

Table IV. Cosmic Ray Mistakes reported over the period 1965-1985

Anomalous muon production
Aleph particles
Free quarks
Proton-carbon cross sections rising rapidly with energy
Average multiplicity proportional to lns
Mandela particles
Tachyons
Magnetic monopoles
Super heavy quanta
Massive hadrons in air showers
Minicentauros
Anomalons

To be sure, many of these errors were corrected later within the cosmic ray community, and I agree that accelerator physicists and others have their own undistinguished catalogues of mistakes. Nevertheless, the listing above should be sufficient to remind us why our discovery claims are not always accepted at face value.

CONCLUSIONS

The conclusions I draw from the sessions reviewed here may be briefly stated:

- The proton-air inelastic cross section is becoming better determined, especially with Fly's Eye data, and is reported to be 540 mb at a mean energy of 5×10^{17} eV. This corresponds to a pp total cross section, σ_{pp}=122 mb, compatible with $\sigma_{p\bar{p}} \alpha \ln^2 s$.
- New CERN data at 900 GeV c.m. has expanded our knowledge of cross sections, multiplicity distributions, and other inclusive properties of nucleon-nucleon collisons. Of particular interest is the continuing increase in 2-jet events with energy, corresponding to hard scattering of nucleon constituents.
- New p-nucleus data over energies from 30 GeV to 40 TeV largely agree with superposition models.
- Nucleus-nucleus data, especially from the JACEE collaboration at energies above 1 TeV/nucleon, show unual effects and may provide the first evidence of quark-gluon plasma effects.
- There is no current evidence for physical magnetic monopoles.
- Proton decay has not been observed. There are some ambiguous events, but in any event the proton lifetime must be considerably longer than minimal SU5 predictions.
- Some effects and putative particles, previously reported, are now dead. Other enigmatic effects remain unexplained and ambiguous.

Emulsion Chamber Observations and Interpretation (HE 3)

M. Shibata
Yokohama National University, Yokohama, 240, Japan

1. Introduction

The contributions to High Energy 3 session consist of 66 papers, which mainly deal with Emulsion Chamber experiments, related methods and theories. Hereafter emulsion chamber will be abbreviated as EC. The physical interest in this field is concentrated on the strong interaction at the very high energy region ($>10^{14}$eV) exceeding the accelerator energy, also on the primary cosmic ray intensity and its chemical composition.

The majority of the papers concern the experimental results from EC experiments at mountain altitudes or at higher levels using flying carriers. There are also some papers from hybrid experiment consisting of EAS arrays or calorimeters in addition to EC.

Those experiments observe cosmic ray secondaries and give us the informations on high energy interaction characteristics through the analyses of secondary spectra, gamma-hadron families and C-jets (direct observation of the particle production occuring at carbon target). The discussions are devoted to problems of scaling violation in fragmentation region, interaction cross section, transverse momentum of produced secondaries and some peculiar features of exotic events. Already a lot of discussions for these problems have been made in Kyoto, Paris and Bangalore ICRC, however, the statistics of experimental data are steadily increasing and the quality of simulation works are also progressing, reflecting the details of new accelerator results.

The following is the classification of papers for this talk.

Secondary spectra
Primary spectra
Gamma-hadron families
Halo events (Super high energy families)
Exotic phenomena
New technics
Cascade calculations, propagations
Hybrid experiments

Some important results are described below from each section.

2. Secondary spectra

The most basic data in EC experiments are gamma and hadron spectra, which reflect the interaction characteristics of hadrons in the atmosphere as well as the primary cosmic ray intensities. It is well known that the intensity of gamma rays at mountain altitudes is quite lower than the expected value from calculations[1] based on the scaling (or quasi-scaling) interaction model and energy-independent primary chemical composition with about 40 % of protons, as it is known at energies around 10^{12} eV.

Mt.Fuji collaboration (HE 3.1-3) presented those spectra from their

(a) (b)

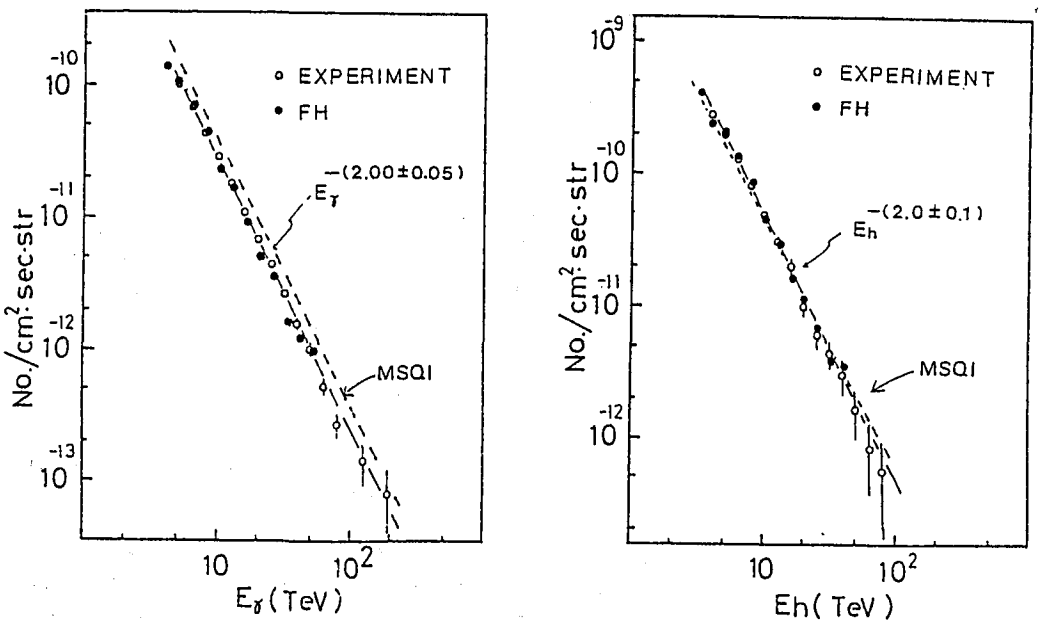

Fig.1 The energy spectrum of gamma-rays (a) and hadrons (b) at Mt.Fuji.

last exposure (Fig.1). The power indices of both components are the same within statistical errors, being 2.0. Both gamma and hadron fluxes are consistent with a calculation based on quasi-scaling model with heavy-enriched primary composition (Fig.2), where the total intensity is taken from Grigorov's[2] spectrum and the chemical composition is extrapolated from low energy data of 10^{12} eV range with an assumption that proton component has a knee around 10^{14} eV as suggested by the magnetic rigidity cut-off model of the cosmic ray propagation in the galaxy. Other components are assumed to have the knee at energies Z times greater, where Z is the atomic number. Such primary model gives proton-poor and heavy-enriched composition at energies greater than 10^{14} eV.

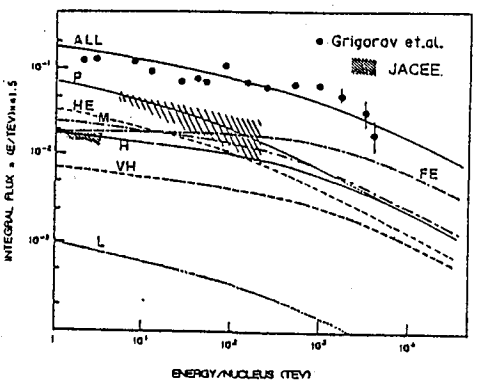

Fig.2 The heavy-enriched primary chemical composition assumed in calculations.

China-Japan collaboration also presented those spectra as shown in Fig.3 (HE 3.1-2). In a part of this experiment, iron is used instead of

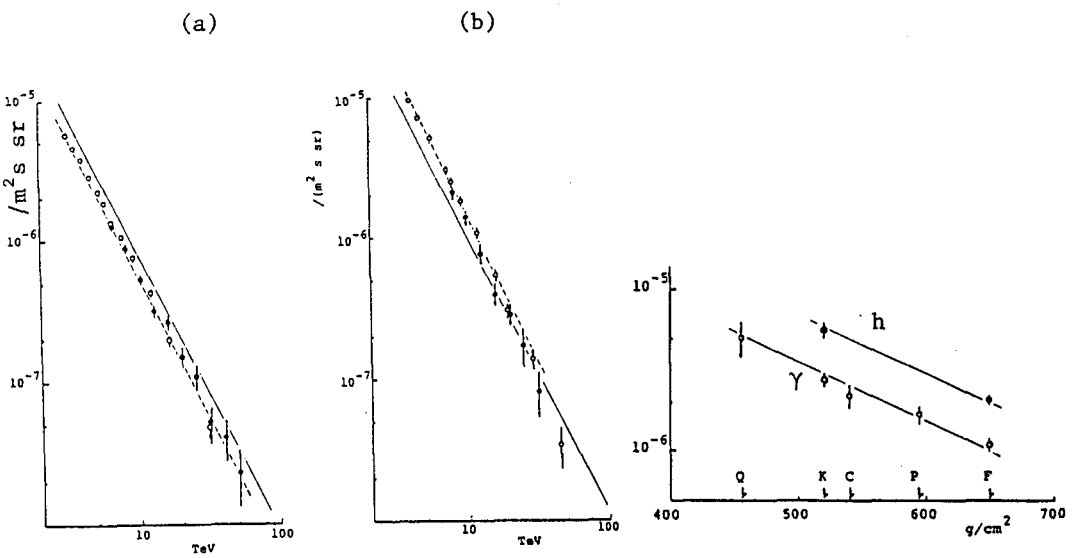

Fig.3 The energy spectrum of gamma-rays (a) and hadrons (b) at Mt.Kanbala.

Fig.4 Altitude variation of gamma-rays and hadrons.

lead and the result is consistent with that from lead chamber. Open circles and closed circles present the result from lead chamber and iron chamber, respectively. The slope and the intensity of gamma and hadron spectra are quite consistent with Mt.Fuji collaboration. The same Monte Carlo calculation as mentioned before can explain the attenuation of the secondaries in the atmosphere for world data, Qomolangma, Mt.Kanbala, Mt.Chacaltaya, Pamir plateau and Mt.Fuji. (Fig.4)

Cananov S.D. et al. presented hadron spectrum from Pamir experiment (HE 3.1-7). This new result (Table 1) is in a good agreement with other experiments.

Table 1. Hadron intensity by Cananov.S.D. et al.
(Normalized to Pamir level)

Experiment	$I_0(E > 5\ TeV)/cm^2 s\ sr$	The Slope
Mt.Fuji[3]	$(3.2 \pm 0.2)\ 10^{-10}$	2.0 ± 0.1
Mt.Kanbala[4]	$(2.9 \pm 0.1)\ 10^{-10}$	1.85 ± 0.1
Pamir Pb chamber[5]	$(1.9 \pm 0.4)\ 10^{-10}$	1.96 ± 0.1
This work	$(2.7 \pm 0.1)\ 10^{-10}$	1.9 ± 0.1

Summarizing the results of secondary spectra, all experiments are in a good agreement. The spectral indices of gamma and hadron component are about 2.0 in observed energy range of 10^{12} -10^{14} eV. The absolute intensity and the attenuation in the atmosphere for mountain altitudes are well explained by a calculations with quasi-scaling model and heavy-enriched primary composition.

Quasi-scaling model assumed in these works means that the scaling law in the fragmentation region is not violated strongly, while the increase of the rapidity density in pionization region is taken into

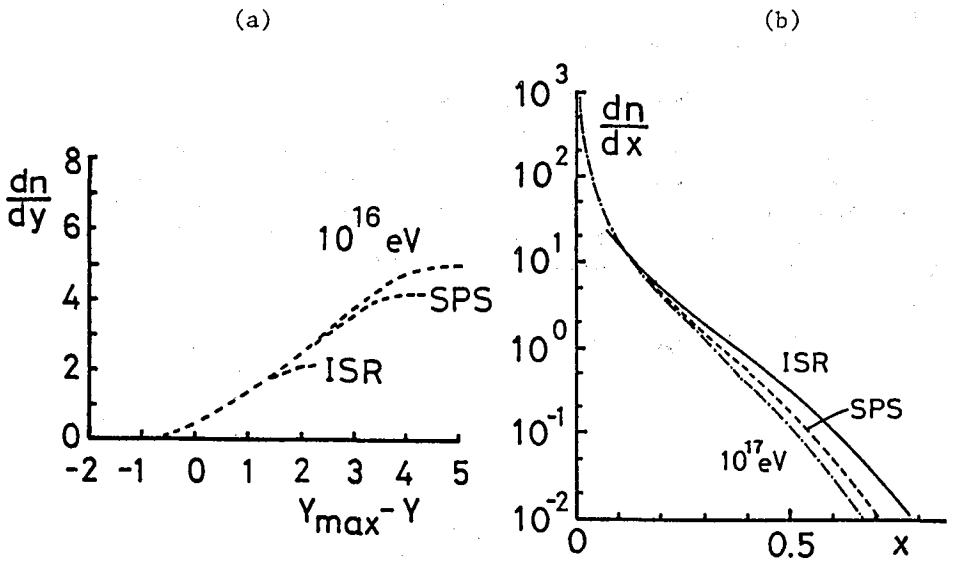

Fig.5 (a) Rapidity distribution and (b) x-distribution for quasi-scaling model.

account extrapolating ISR-SPS[6] results as illustrated in Fig.5 (HE 3.4-9) for rapidity and x distributions. The increase of proton-air cross section is assumed as $\sigma \propto E_0^{0.06}$.

However, this is not a unique interpretation of the secondary spectra because it is also possible to explain experimental data assuming stronger violation of scaling in the fragmentation region and energy-independent primary composition. This ambiguity cannot be solved when one treats only the uncorrelated secondaries. This problem will be discussed again in family phenomena.

3. Primary spectra

The observation of primary particles in the stratosphere is made by Mandritskaya K.V. et al. (HE 3.1-10). Results for 1-100 TeV range are shown in Fig.6 and compared with a mixed composition with following parameters, which are derived from the lower energy data by Ryan M.G. et al.[7], Simon M.[8], Ormes J.P. et al.[9] and Smith L.H. et al.[10] Helium and heavier components show good agreement with expected intensity. However, the proton spectrum shows steepening in 1-100 TeV range.

Another paper on the existence of the bump at 10^{15} eV in primary total spectrum was presented by Capdevielle J.N., Iwai J. and Ogata T. (HE 3.7-9)

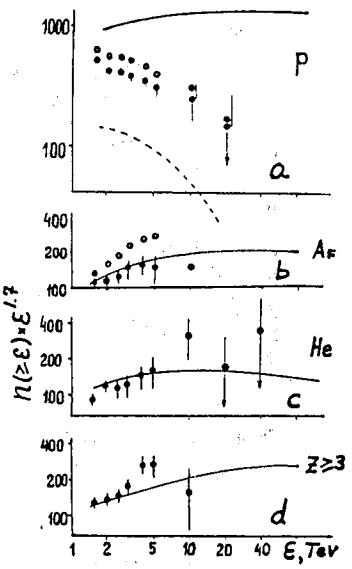

Fig.6 The primary spectra

from a compilation of Concorde[11], JACEE[12] and Japan Air Line experiments[13] as shown in Fig.7.

Summarizing the primary spectrum obtained by means of EC at energies greater than 10^{13} eV, still the situation is not clear, especially for proton intensity. A discrepancy is seen between the works by Mandritskaya et al. and the JACEE collaboration (Fig.8). One may question the statistical and/or methodical accuracy in these experiments. Therefore, at present, one cannot say definitely about the energy dependence of the chemical composition at energies greater than 10^{13} eV.

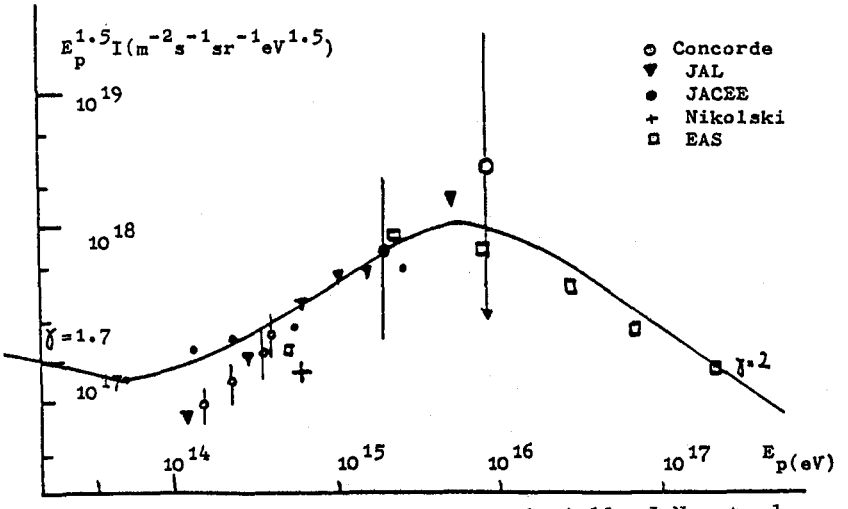

Fig.7 Primary total spectrum by Capdevielle J.N. et al.

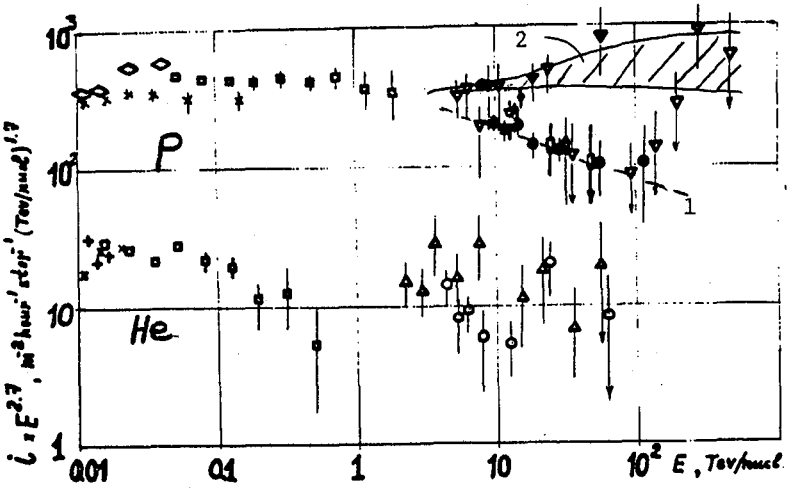

Fig.8 Comparison of proton spectrum between
1:Mandristkaya K.V. et al. and 2:JACEE collaboration.

4. Gamma-hadron families

Gamma-hadron families are generated by successive interactions of primary particles and their secondaries in the atmosphere. There has been a lot of works to account for nuclear-electromagnetic cascading effects in order to extract the characteristics of hadronic interactions from observed feature of gamma-hadron families. One of those approach is to compare experimental data with results of Monte Carlo calculations under various interaction models. Another is to try to eliminate those effects for individual events and trace back to the original interaction features. Such procedure was developed by many authors among EC experimentalists[14] and called 'clustering' or 'decascading'.

The paper presented by Mt.Fuji collaboration is using the first approach (HE 3.5-1). The intensity of gamma families is compared with results of calculations under various assumptions as shown in Fig.9, where M denotes Mixed composition, P - Proton primary, S - Scaling model, F - Fireball model of CKP type, which corresponds to the strong scaling violation in the fragmentation region, Q - that QCD jet effect is accounted, I - Increasing cross section and inside of the parenthesis is the knee energy of proton spectrum. The data are compatible with MSQI(100) model.

The energy weighted lateral spread of gamma families which reflect the transverse momentum of produced particles is compared in Fig.10, where T denotes the increase of mean Pt as $\langle Pt \rangle \propto E_0^{0.04}$, which does not seem to explain the data. Since family phenomena are very sensitive to the fragmentation region, it is suggested from this figure that the increase of mean Pt in fragmentation region is not remarkable.

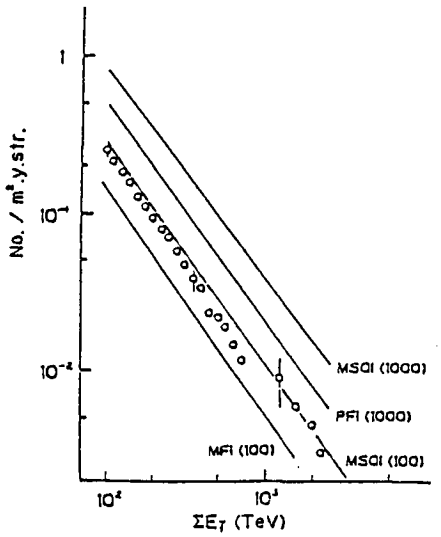

Fig.9

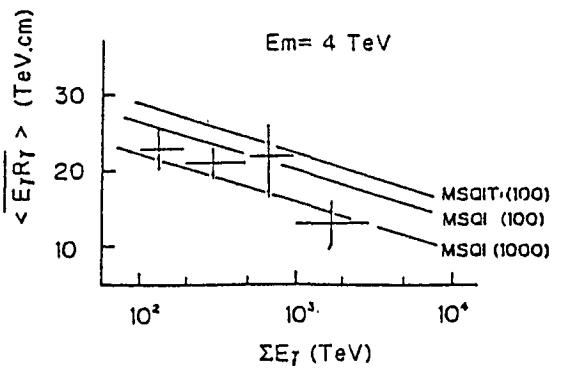

Fig.10

MSQI(100) model can also explain the binocular type events (with large lateral spread) as shown in Fig.11. The fraction of events with $\chi_{12}>100$ TeV cm is about 7 %. High multiplicity model does not explain these experimental data.

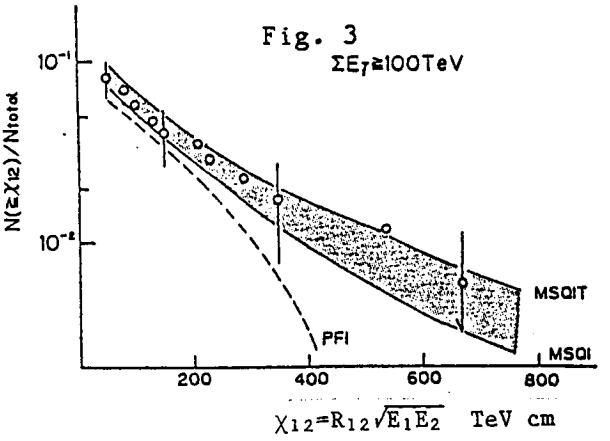

Fig.11

China-Japan collaboration (HE 3.4-2) presented a detailed analysis of an event KOE19 of the total visible energy 1537 TeV. The production height of this event is estimated from triangulation method to be less than 70 m. The clustering procedure lead to an interpretation of this event, in terms of QCD-jet, as 5-jets event with quite small sphericity (0.0074).

Navia O. and Sawayanagi K. made a cluster analysis on gamma families for Chacaltaya EC data (HE 3.2-1). From B-ER correlation, where B is the asymmetry parameter defined by A.Kryś et al.[15], they pointed out the existence of multi-jet with symmetrical structure. When the lateral structure of family is symmetrical, B is close to 1 while it is close to 0 if the showers are grouped along a straight line. Gamma families are classified by energy weighted lateral spread, then B distribution is shown in Fig.12. In the widest class of families, one can see a peak close to B=0, which can be understood as binocular type events. However, there are non-zero distribution in symmetric region too. The authors conclude that for those events the <ER> values are as large as for binocular events but the number of jets is much greater, which makes the structure more symmetrical.

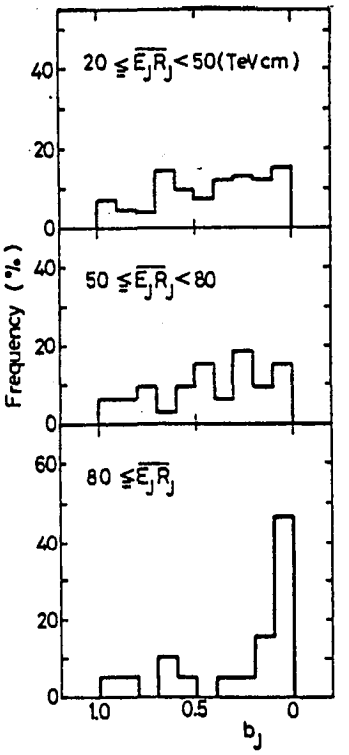

Fig.12

Azimov et al. presented a similar analysis for Pamir EC data using a symmetry parameter, α, instead of B. The definition is just opposite than of B, α is 0 for symmetric case and is unity for asymmetry (HE 3.7-1). They also showed the existence of wide and symmetrical families. Their explanation of these families as generated by heavy primary nuclei is based on the comparison of experimental data with calculations using a quasi-scaling model and mixed primary chemical composition.

Therefore, the events with large lateral spread cannot be directly connected with QCD-jet or large Pt phenomena but most of them are probably generated by heavy primary nuclei. The event KOE19 reported by China-Japan collaboration does not belong to such cases because of small lateral spread corresponding to the low interaction height. However, we need more statistics to draw a picture of multi-jet production process at very high energies.

In a paper presented by Pamir collaboration, an investigation was made for the ratio of energetic hadrons with no visible hadron accompaniment to the total hadron intensity (HE 3.1-11). It is shown that this ratio is much higher than the predictions of scaling models as shown in Fig.13. The considerations on the increasing interaction cross section or the primary chemical composition are not successful in explaining the experimental data. The violation of scaling in fragmentation region is required to explain this discrepancy, according to the authors.

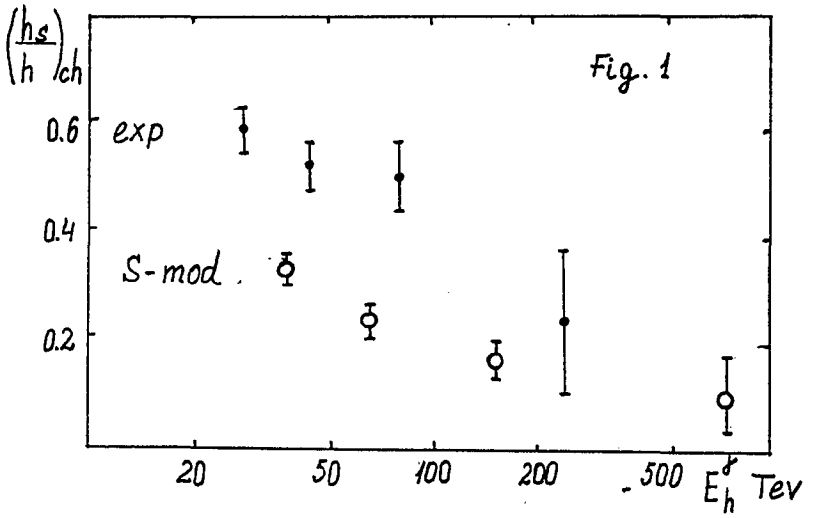

Fig.13 Single hadron ratio to total hadron intensity.

T.K.Gaisser ,T.Stanev and J.A.Wrotniak made a Monte Carlo simulation on this problem and showed the sensitivity of single hadron intensity and gamma-hadron ratio to the different interaction models (HE 3.4-7). Their results show that single hadron ratio to the total hadron intesity by Pamir experiment seems to be explained within a statistical error. However, Gamma-hadron ratio of Pamir experiment cannot be reproduced by quasi-scaling model. Possible explanations by authors are,

1. breakdown of scaling in fragmentation region,
2. there are more hadrons produced than they assume,
3. the underestimation of gamma ray energy or more probably the overestimation of hadron energy.

Summarizing the papers on gamma-hadron families, there is still an ambiguity in interpretation of the experimental data in 10^{14} -10^{15} eV range. The global features, like family intensity and lateral spread, may be explained by the interaction mechanisms extrapolated from the

accelerator results with only very slight scaling violation in fragmentation region with an assumption of heavy-enriched primary composition. The events with large lateral spread and their symmetry structures are also explained within those framework, as it is shown in clustering analysis. If the above explanations are valid, then the transverse momentum in fragmentation region seems to remain almost constant.

On the other hand, another result reported by Pamir collaboration on 'the high ratio of the energetic hadrons with no hadron accompaniment to the total hadron intesity' is not explained by above mentioned point of view. This can be explained by nuclear interactions, where no secondary particles have sufficiently high energy to be detected. Then, only survival hadron is detected with no visible accompanying particles. Such situation would be explained by strong breakdown of scaling in fragmentation region and/or the change in inelasticity with energy. Mt.Fuji experiment also found the excess of single hadrons, but less one compared to the results of Pamir experiment, being about 10 %[16]. They claim this excess would be attributed to a scanning inefficiency for low multiplicity events. On the other hand, the result, which Pamir experiment concludes to be in contradiction with scaling model, is successfully explained by the work of T.K.Gaisser et al. According to their calculations based on quasi-scaling model, also taking into account of the design of the Pamir chamber, the result does not contradict with experimental data within the statistical accuracy. This problem needs more investigations both in experiment and calculations to clarify the sensitivity to the interaction mechanism and also to the experimental bias like energy determination, scanning efficiency for accompanied particles and so on.

5. Halo events

Some of the most energetic families show a remarkable character of extremely high optical density on the X-ray films, and it is called halo. Joint paper from Mt.Fuji and China-Japan collaboration presented the intensities of the halo events (HE 3.4-9). The comparison with a Monte Carlo simulation including the halo development inside the chamber suggests more than 3 times lower proton abundance in 10^{16} -10^{17} eV range than that of 10^{12}-10^{13} eV within the framework of quasi-scaling model as shown in Fig.14. Here the geometrical size of the halo defined as an area with optical density greater than

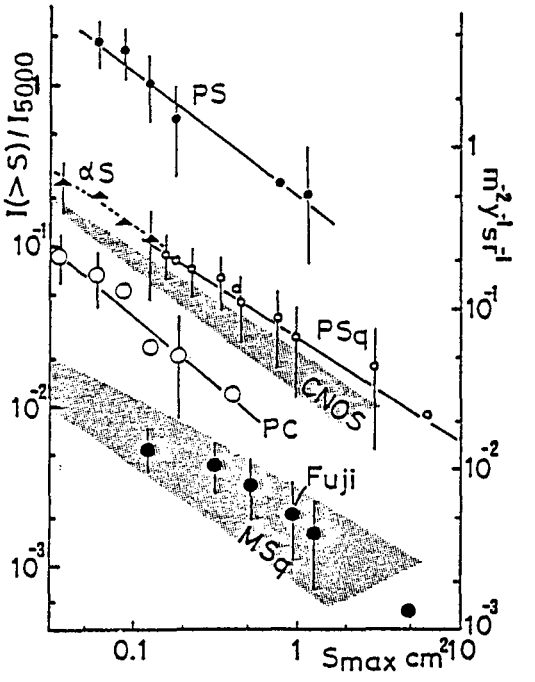

Fig.14

0.7 on N-type X-ray film is shown on horizontal axis. High multiplicity model ($n \propto E_0^{1/4}$) cannot reproduce the observed intensity of the halo events when the increase of the cross section and the primary chemical composition are adequately accounted for. Therefore, halo itself is not an exotic phenomenon but its low intensity is the largest problem. Since most of the halo events are induced by protons, such low intensity requires proton-poor primary chemical composition in 10^{16} -10^{17} eV range, say less than 10 %. Both results from Mt.Fuji and Mt.Kanbala experiment are consistent within statistical errors with the calculation based on those assumptions.

Some examples of optical density map are shown in Fig.15 for experimental data by Mt.Fuji collaboration and artificial ones by the simulation (HE 3.4-9), though the structure of those events is not fully discussed yet.

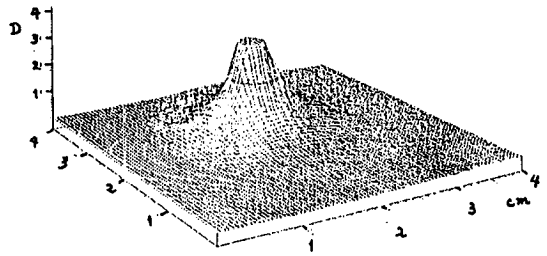

(a) Experimental:FH-89
E_{halo}=2300 TeV

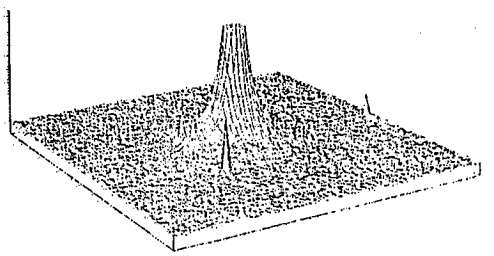

(b) Simulation:Proton primary
E_{halo} =2300 TeV

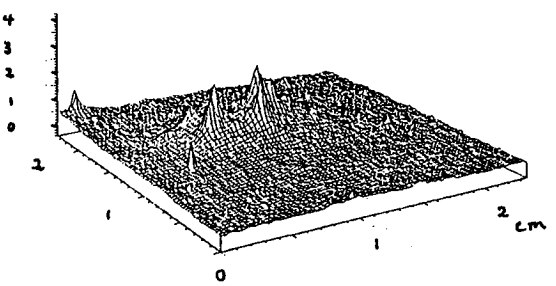

(c) Experimental:FC-104
E_{halo}=3000 TeV

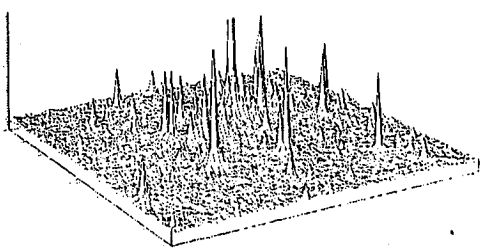

(d) Simulation:CNO primary
E_{halo}=2480 TeV

Fig.15 Optical density map of halo.

N.M.Amato, N.Arata and R.H.C.Maldonado (HE 3.4-5) presented an analysis of a halo event named P06 of the total visible energy 1300 TeV. According to their interpretation, central part of this event is formed by 'Giant-Mini-Cluster' with extremely small Pt of 30 MeV, whose characteristics are discussed by papers of Brazil-Japan collaboration (HE 3.5-4).

Another extremely exotic nature of the high energy interactions is reported by Pamir collaboration (HE 1.4-12). Some energetic events over 10^{15} eV show a coplanar emission of high energy photons as shown in Fig.16. The strong correlation among high energy photons were shown from the asymmetry analysis including the accompanied photons outside of the halo, though its interpretation is still open.

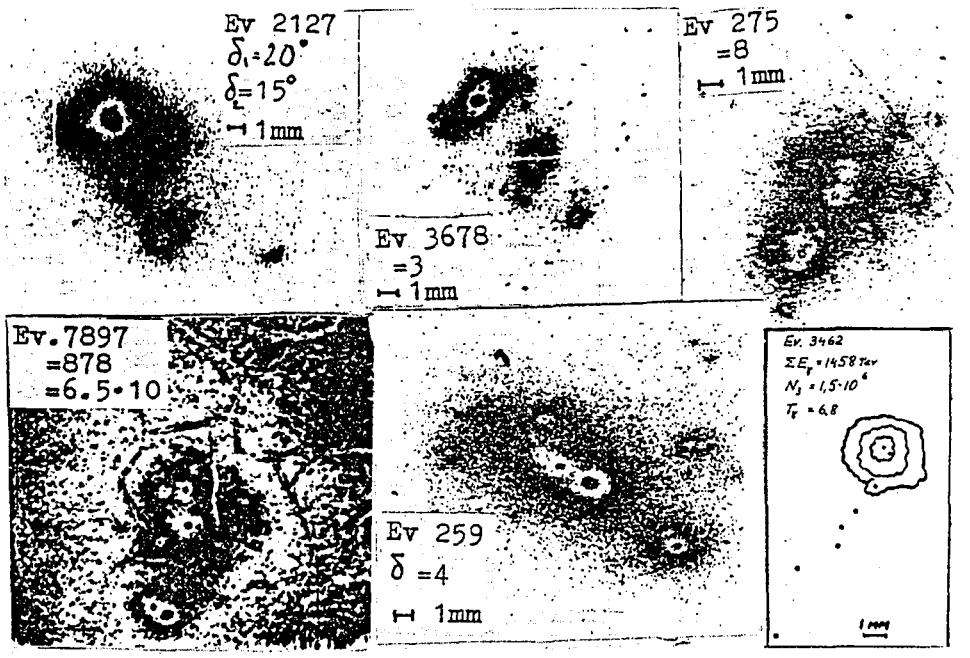

Fig.16 Coplanar events observed by Pamir experiments.

Summarizing the papers on halo phenomena, which correspond to the primary cosmic ray energy of 10^{16} -10^{17} eV, the intensity and energy flow properties are also explained by the same Monte Carlo calculations based on quasi-scaling model and heavy-enriched primary composition. In this energy range, the proton abundance was assumed as less than 10 % of the total primary intensity. If we assume more primary protons, then we need to introduce violation of scaling in fragmentation region stronger than one assumed in this calculation, though not as strong as CKP-type, because halo is created by very high energy electromagnetic particles, which are most probably produced in fragmentation region. It is reported by Pamir collaboration (HE 3.4-10, HE 3.4-11) that some of the halo events may be attributed to only few energetic photons. Sometimes only one photon produced high in the atmosphere is enough to construct observed characteristics of the halo spot. From those considerations, the fragmentation secondaries seem not to be disappearing in very high

energy interactions.

The coplanar events detected by Pamir experiment seem to indicate an existence of strikingly unknown features of very high energy interactions.

6. Exotic phenomena

Since the observation of the event 'Centauro I'[17] by Brasil-Japan collaboration, extensive searches of peculiar events were made on gamma-hadron families and C-jets by the same authors. Though no Centauro-like events were reported, a scheme of the interpretations on those interaction mechanisms was discussed in this conference. The new mechanisms are named by those authors as 'Centauro' - pinaught-less particle production, 'Mini-Centauro' - hadron-rich events, 'Chiron' - Pt ≃ 2-3 GeV/c, 'Geminion' - binocular events, 'Mini-Cluster' - Pt ≃ 10-20 MeV/c and 'Giant-Mini-Cluster' - ensemble of mini-clusters.

A search was carried out by H.Kumano for the anomalous events among C-jets at total visible energy greater than 5 TeV (HE 3.2-5). Among 150 C-jets, the author assigns 9 events as anomalous ones because of non pinaught character and/or the large transverse momenta.

Another paper by Brasil-Japan collaboration also reported exotic interactions among C-jets and Pb-jets from the systematic analysis of Charaltaya CH-19 (HE 3.2-6). The decisive characteristics common to all these exotic interactions stated by authors are : (1) - unusually large Pt and (2) - no neutral pions produced in an interaction. The origin of cascades registered in the chamber were understood to be hadrons if the shower spot was visible only in depths greater than 6 c.u., or if their cascade curves were obviously not like electromagnetic ones, or if they were showing a clearly multi-core structure. Eight events with 2 showers and another eight with 3 showers are reported because of the invariant mass greater than 200 MeV/c^2 or the association of hadrons. The resemblance of these events to Mini-Centauro interactions is shown in the Pt and fractional energy distributions (Fig.17), which may be characterized by $\langle Pt(\text{gamma})\rangle = 0.35 \pm 0.05$ GeV/c and initial

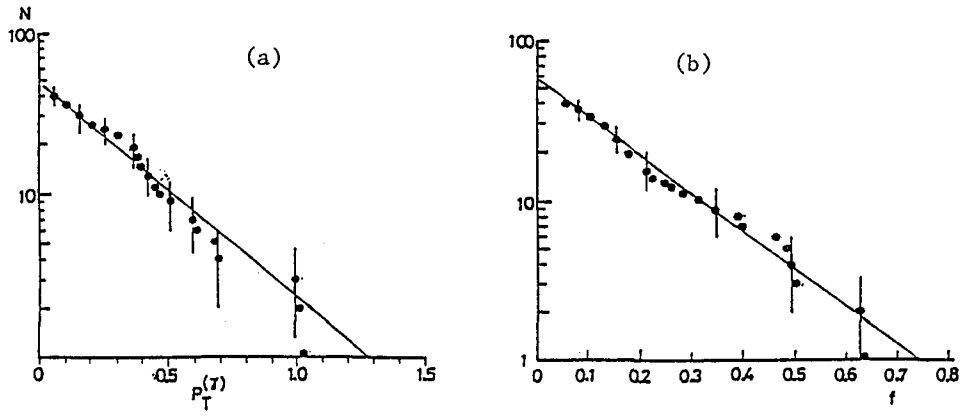

Fig.17 (a) Pt distribution and (b) fractional energy distribution for exotic C-jet events.

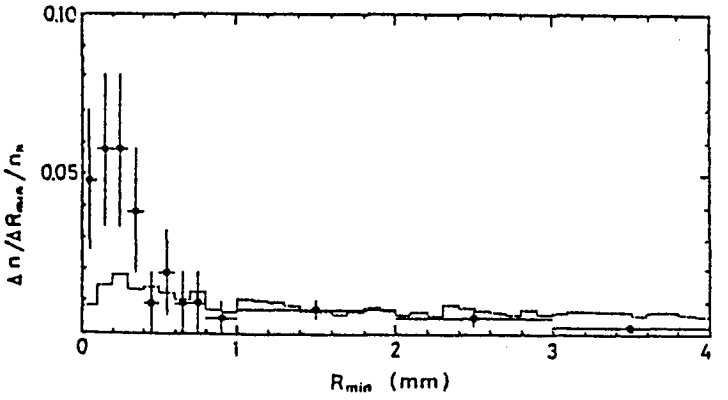

Fig.18

multiplicity $\langle m_0 \rangle = 18 \pm 3$. The parent interaction energies which give rise to these exotic events is estimated as 100 to 400 TeV.

M.Tamada showed the mini-cluster structure from the study of the correlations between hadrons and electromagnetic particles of the gamma-hadron families of Chacaltaya experiment (HE 3.3-6). There exist a number of hadrons which accompany electromagnetic showers very closely as shown in the distribution of relative distances between a hadron and its nearest neighbouring shower (Fig.18). Another feature is that the hadron carries a large portion of the cluster energy. They form a mini-cluster whose members carry transverse momentum about 10 times smaller than in normal production process.

Another paper by Brasil-Japan collaboration presented detailed characteristics of the mini-clusters (HE 3.5-3). The authors select the gamma-hadron families penetrating through both upper and lower chambers and having $\langle ER \rangle > 180$ GeV m after the decascading with Kc=6 GeV m. Single-cored and mini-clustered high energy showers (>10 TeV), spreading from 0.1 to a few mm of radius, are investigated in detail. The multiplicity distribution of mini-cluster constituents is shown in Fig.19. The lateral structure of those families is interpreted as the result of Chiron interactions with Pt $\simeq$ 2-3 GeV/c and mini-cluster formation with Pt $\simeq$10-20 MeV/c by the secondary interactions.

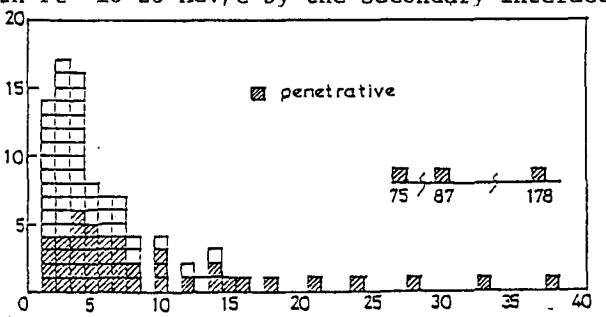

Fig. 19 Histogram of shower core number in a mini-cluster.

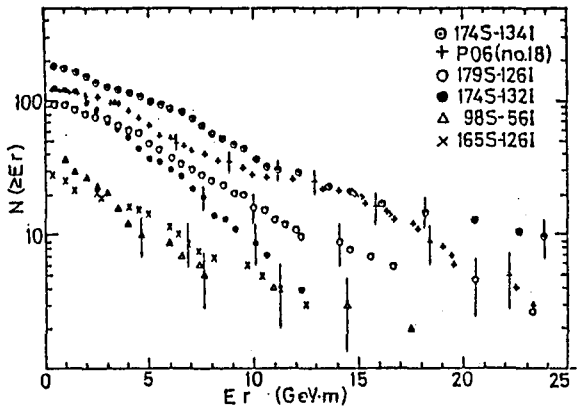

Fig.20

The mini-clusters with high multiplicity (m >30) are called 'Giant-Mini-Cluster' (HE 3. 5-4). They show small spread corresponding to extremely high rapidity density and strong penetrative power. The inner lateral distribution of giant mini-clusters shows high similarity of exponential type among different events as shown in Fig.20. Giant-mini-cluster is interpreted as an ensemble of mini-clusters and it is suggested as a possible cause of halo in large families.

The characteristics of hadron families are investigated on Charaltaya carbon chambers by H.Aoki (HE 3.3-4). The hadron multiplicity distribution is compared with current model calculations with primary protons in Fig.21. The excess of the hadron-rich events (Nh > 9) to proton-initiated artificial families is shown, though there is a possibility of explaining it with heavy primaries. In the correlation between Nh and <ERh>, the majority of experimental data are explained as fluctuations of ordinary interactions, but Centauro I and its candidates (Centauro II,III,IV) are not explained by this argument.

Summarizing the papers on exotic phenomena, Brazil-Japan collaboration concludes that 5-10 % of observed events cannot be attributed to ordinary interactions. Japan-USSR collaboration (HE 3.4-8, HE 3.5-2) also reported observing mini-clusters in Pamir carbon chambers.

The energy threshold for those exotic phenomena is

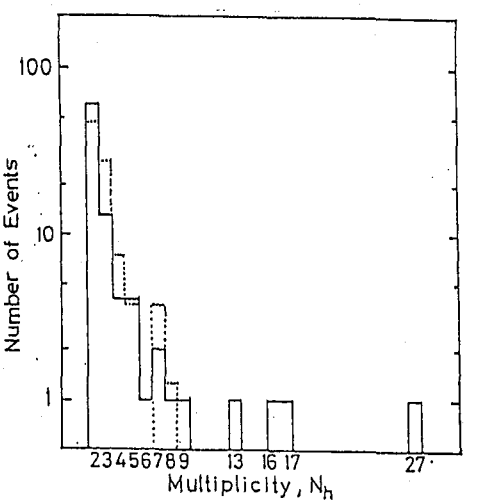

Fig.21

estimated to be around 100 TeV, though searches by present accelerator data showed negative results. This situation is explained by the authors: either the threshold energy is a little higher than SPS-energy or there is a genetic relation between the exotic phenomena, namely, the secondaries from a Chiron interaction at very high energies maintain the exotic characters and produce mini-Centauro, Geminion and mini-clusters in successive interactions in the atmosphere. These exotic phenomena reported by Brazil-Japan collaboration are derived by focusing their attention on events of unusually large lateral spread or of hadron-rich nature. This is, however, fully related to the problem of the fluctuations in 5-10 % tail. Therefore a comparison with detailed Monte Carlo simulation is needed to exclude the possibility of explaining these events as just fluctuations in ordinary interaction process. As mensioned before, the large lateral spread of 7 % of gamma-hadron families can be attributed to the heavy primary nuclei. In the discussion of hadron-rich events or the mini-clusters containing hadrons, the reliability of hadron identification is the most essential point, because mini-clusters showing transverse momentum of 10-20 MeV/c can be interpreted as trivial electromagnetic cascades if they lack hadrons inside. Those procedures of hadron identification are also related to the problem of the fluctuations in the development of electromagnetic cascades.

7. New technics

Taira T. et al. (HE 3.1-13) presented a paper on a high sensitive screen type X-ray film (Fuji G8-RXO) and luminescence sheets (Fuji 'Imaging Plate'). Those films are irradiated to the electron beam to obtain the characteristic curves. They show quite high sensitivity compared to the currently used films like N type and other similar ones. The detection threshold energy for the cascade shower observation is also tested by baloon experiment and found to be around 200 GeV.

A new clustering procedure is proposed by Nanjo H. (HE 3.7-4) based on the idea of a variable cut off value for decascading instead of the constant ER in other methods. The new method is applied to simulated data and the validity of the procedure is examined on initial number of gamma rays, initial photon energy of a cascade and the sensitivity to the transverse momentum. The results seem to be encouraging.

8. Cascade calculations, propagations

There were 11 papers on cascade studies or cosmic ray propagations in the atmosphere. A.Wasilewski and E.Kryś (HE3.6-10,HE 3.6-11) made a detailed Monte Carlo simulation both in lead and air including every possible electromagnetic processes. They gave a new approximation formula for electron lateral distribution, which shows some deviations from NKG formula. This formula explains the discrepancies between experimental data and NKG formula, for instance the change of age parameter with the distance from the shower axis.

Ivanenko I.P. et al. (HE 3.5-12, HE 3.5-13) made calculations of electromagnetic cascades for higher moment characteristics, i.e., variations, asymmetry and excess.

Other papers in this field also show some useful results, however,

due to the limited space, I would like to suggest to look at papers by A.Liland (HE 3.1-9), A.V.Plyasheshinikov (HE 3.5-9), Yu.P.Kratenko and S.A.Charishnikov (HE 3.5-10), R.M.Golynskaya et al. (HE 3.5-11), T.Yanagita (HE 3.6-7) and A.Tomaszewski and Z.Włodarczyk (HE 3.7-3).

9. Hybrid experiments

There are several stations where hybrid experiments are under operation. They are Tien-Shan station (K.V.Cherdyntseva et al. HE 3.2-7), Chikovani station (Yu.G.Verbetski et al. HE 3.2-8, HE 3.2-9), Mt.Chacaltaya station (Matano T. et al. HE 3.3-8, HE 3.3-9) and Mt.Norikura station (Shima M. et al. HE 3.3-10, HE 3.3-11).

Matano T. et al. (HE 3.3-8, HE 3.3-9) reported a detection of very high energy gamma-hadron family in an air shower core, whose age parameter is estimated to be 0.17. The association of such a young air shower to the high energy gamma-hadron family suggests that the primary particle of this event is a proton.

The installation reported by Shima M. et al. consists of EAS array, EC and burst detector below EC. EAS size spectrum is obtained in two trigger conditions. One is a usual air shower trigger and another is a burst trigger below EC. EAS size spectrum accompanied by gamma-family of total energy greater than 10 TeV is presented in Fig.22. The result agrees with the simulated data for proton poor primary composition of less than 15 % better than the proton-rich one of more than 30 %.

This kind of the experiment is a promising one because of the high sensitivity to the chemical composition of primary particles. Though the available data are limited at present, the possibility to extend the experiment is not limited compared with storatospheric experiment.

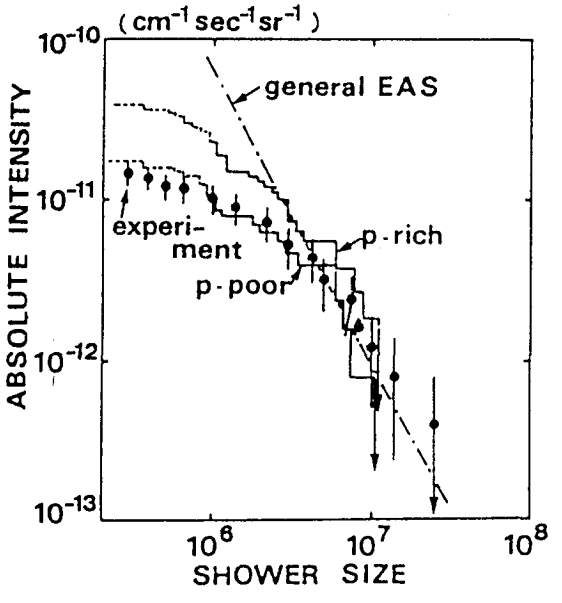

Fig.22

10. Conclusions and prospects for future

One can explain emulsion chamber data by so called quasi-scaling interaction models if primary proton spectum becomes steeper around 10^{14} eV. Already a lot of works have shown the mutual consistency among various features of the EC data. One can say, that at least no serious difficulty is known up to now in this framework.

One may argue, however, that the proton percentage at these energies is larger, and thus a more serious scaling violation in fragmentation region has to be assumed. There has been also a number of papers discussing about such possibilities[18]. In high multiplicity model, however, difficulties arise in reproducing the frequency of the binocular events and halo events, which are effectively produced in case of low multiplicity with high secondary energies. Therefore, the high multiplicity model can survive when the multiplicity distribution has a great fluctuation as discussed by J. Wdowczyk[19].

As to the exotic events, we need stronger evidence in order to confirm that they are really new phenomena. More simulations are needed to exclude the background events from fluctuations of ordinary interactions or heavy primary effects.

To get an increased sensitivity to the primary composition, an importance of hybrid experiments was discussed in this conference. Simulteneous informations from Emulsion Chamber and air shower array will bring us less ambiguous conclusions. Such experiments are being developed, for example, ANI experiment at Aragatz station, Mt.Chacaltaya, Mt.Norikura and others.

The continuation of the exposures of EC is also important to increase the statistics significantly for very high energy events like halo. The large scale EC experiments are also developing, for example, at Mt.Kanbala by China-Japan collaboration and Pamir plateau by Japan-USSR collaboration (HE 3.1-1). Fragmentation region at very high energies can be studied through those observations.

These situations are illustlated in following chart.

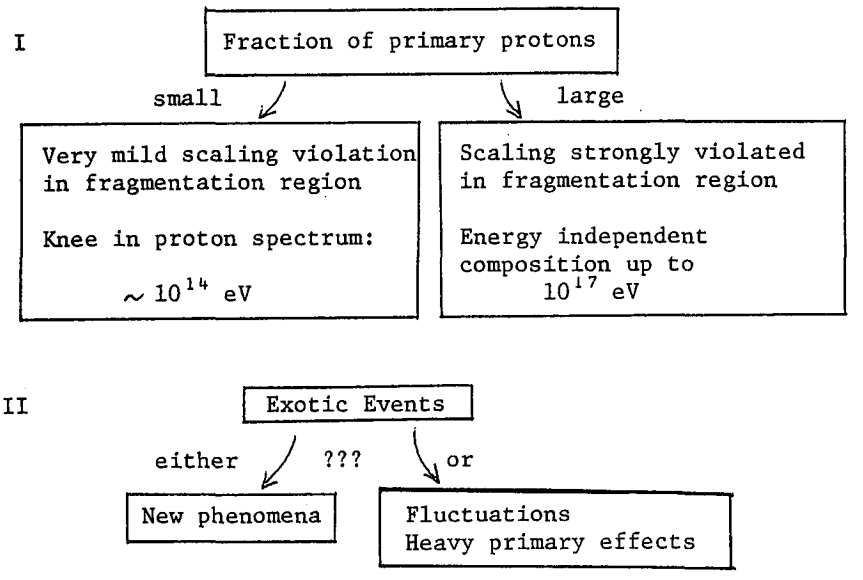

(Stronger evidence necessary)

III Importance of hybrid experiments : Increased sensitivity to composition

IV Large exposures : - halo phenomena
- fragmentation region at very high energies
- structure reflects (maybe ?) the kind of primary particle

→ Significant increase in statistics is necessary to draw conclusions.

Acknowledgement

The author is grateful for helpful discussions with many participants to this conference, in particular Profs. T.K.Gaisser, J.Wdowczyk, S.Hasegawa, J.Nishimura, I.Ohta, J.Capdevielle and L.W.Jones, also to Drs. J.A.Wrotniak, S.Torii, K.Mizutani, M.Tamada, Y.Takahashi and T.Stanev. He would like to express his gratitude to Prof.Arafune for fruitful discussions in preparing this talk.

References

1) K.Kasahara, Nuovo Cim. Vol.46A (1978) 333
2) N.L.Grigorov, Proc. of 12th ICRC, Hovart (1971) 1746
3) Mt.Fuji collaboration, 18th ICRC, Vol.11 (1983) 57
4) China-Japan collaboration, 18th ICRC, Vol.5 (1983) 411
5) Pamir collaboration, 18th ICRC, Vol.11 (1983) 122
6) W.Thomé et al. Nucl. Phys. B129 (1977) 365
G.Arnison et al. (UA1 collaboration), Phys. Lett., 107B (1981) 320, 118B (1982) 167, 123B (1983) 108, 115, 128B (1983) 336
M.Banner et al. (UA2 collaboration), Phys. Lett. 118B (1982) 203
R.Battiston et al. (UA4 collaboration),Phys. Lett. 117B (1982) 126
K.Alpgård et al. (UA5 collaboration), Phys. Lett. 107B (1981) 310, 315
7) M.G.Ryan et al., Phys. Rev. Lett, Vol.28, No.5 (1972) 985
8) M.Simon, Ap. J., Vol.239 (1980) 712
9) J.P.Ormes et al., Proc. of ICRC, London, Vol.1 (1965) 349
10) L.H.Smith et al., Ap. J. Vol.180 (1973) 987
11) Capdevielle J.N. et al., Proc. of 16th ICRC, Kyoto, Vol.6 (1979) 324
J.Iwai et al., Nuovo Cim. A69 (1982) 295
12) T.H.Burnett et al., Proc. of cosmic ray symposium, Philadelphia (1982) 236
13) J.Iwai et al., 16th ICRC, Kyoto, Vol.7 (1979) 234
14) A.V.Apanasenko et al., Proc. of Int. Cosmic Ray Symp., Tokyo (1974)
Z.Jabłoński, A.Tomaszewski and J.A.Wrotniak, Proc. of 14th ICRC, Munich, Vol.7 (1975) 2658
H.Semba, Proc. of 17th ICRC, Kyoto, Vol.11 (1981) 163, Suppl. Prog. Theor. Phys. 76 (1983) 111, Proc. of Int. Symp. on Cosmic Rays and Particle Physics, Tokyo (1984) 211
15) A.Kryś et al., Proc. of 17th ICRC, Paris,Vol.11 (1981) 187
16) Mt.Fuji collaboration, private communication
17) C.M.G.Lattes, Y.Fujimoto and S.Hasegawa, Phys. Rep. C65 (1980) 151
18) J.Wdowczyk and A.W.Wolfendale, Nuovo Cim., 54A (1979) 433
Pamir collaboration, Proc. of 18th ICRC, Bangalore, Vol.5 (1983) 425
Proc. of Int. Symp. on Cosmic Rays and Particle Physics, Tokyo (1984) 154, 178, 292
19) J.Wdowczyk, discussion during the session

Extensive Air Showers (HE-4)

R.W. Clay
Physics Department
University of Adelaide
North Terrace
ADELAIDE South Australia 5001

1. Introduction

At the conference I felt that air shower work had made genuine progress particularly due to the professionalism of work at the large arrays. More than ever, those using medium sized arrays have to be selective in their work and careful in their analysis when shower information is incomplete. Ultra high energy gamma-ray astronomy is an exciting new area for us and has added a new sense of purpose to ground based array work. There is much to be done before we properly understand U.H.E. gamma ray showers and it is important that we remain conservative with our claims whilst the properties of such showers are still not clear. Their muon content is only one of the properties to be clarified by the next conference.

There seems to have been genuine progress on primary composition. When allowance is made for detection effects there is impressive agreement on mean depths of maximum at fixed energy. It remains to be seen how well we can now progress to the second order problem of detailed interaction parameters once the gross features of our beam are clarified (see eg. Wrotniak and Yodh HE 4.1-2).

The shower disk thickness has become an area of intense study with interest in Linsley's technique for measurements of giant showers (which should have its uses but is not a complete self-contained solution to spectra and anisotropies at 10^{20} eV) and in the study of structure near the core for improving fast timing and studying delayed sub-showers.

Perhaps the most significant area of promise for the future is the study of individual shower developments with Cerenkov and, particularly, air fluorescence techniques. The importance and potential of having relatively complete information on a complete set of individual showers can hardly be overestimated. However, we must also have a complete understanding of the observation process; why we observe the showers we do and whether or not the recorded data set is complete at a given energy, apparent core distance, and zenith angle.

2. Shower Observations

Extensive air showers are usually studied with ground based detectors in arrays which first detect the presence of a shower and are then used to study a set of shower parameters. The showers are classified and ordered to give information about some parameter or about how that parameter depends on another shower property, perhaps shower size or primary energy. Unfortunately, air showers are complex and, as a general rule, the set of showers which is observed is less complete than we would like. Thus, data sets invariably contain bias in their selection and great care must be exercised when interpreting the data, particularly when mean values of parameters are derived. In some cases, intuition and experience are barely sufficient to picture the unbiased original data set

from the data which are presented and the results may then only properly be understood when compared to simulations of the whole air shower/array detection procedure.

These problems were an underlying theme in a number of areas addressed at the conference. In particular, the difficulty of comparing data obtained in terms of a shower size with data presented in terms of a primary energy was particularly apparent. The problem is usually not so much in measuring the parameters of interest but in understanding how the detection system sampled the incoming set of air showers and how the final data set was selected.

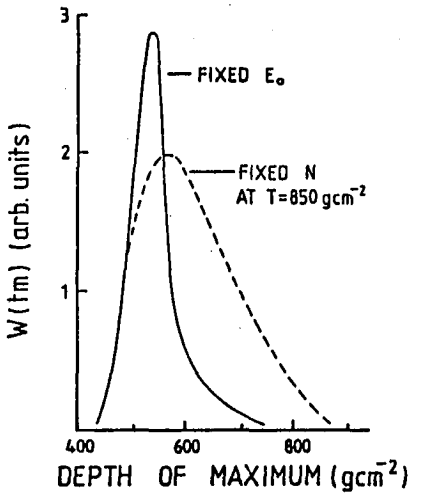

Fig 1. The difference in distributions of observed depths of maximum when shower selection is by fixed primary energy and fixed shower size. (HE 4.1-20)

Shower Size and Primary Energy

Shower size has serious limitations for use as a parameter for ordering showers in energy due to the combination of shower fluctuations and a steeply falling primary energy spectrum. Air shower arrays often trigger on particles which reach the detection level and the resulting observed distribution of showers can then be close to complete in Ne but not in primary energy. One usually wants data measured at fixed primary energy and, without further development information, the interpretation of observations can be seriously in error.

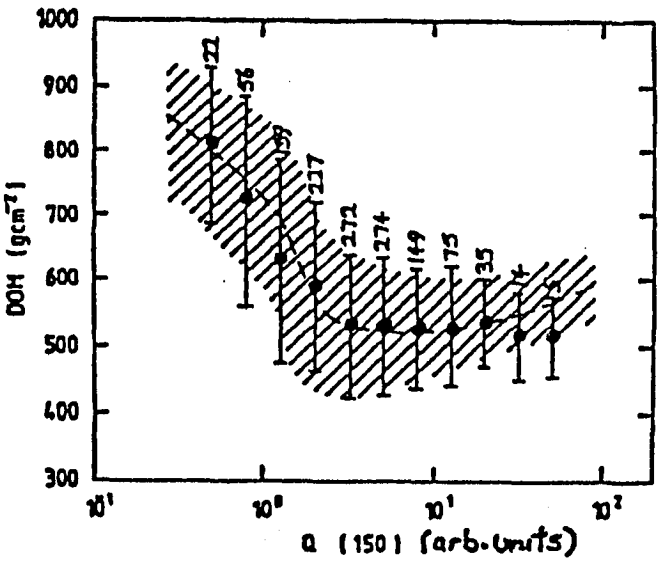

Fig 2. Experimental distribution of depth of maximum vs primary energy estimator Q(150). The hatched region is for simulated data. (OG 5.2-11)

An example of the difference between measurements in terms of primary energy and shower size is shown in figure 1 (from HE 4.1-20) where it is clear that a mean depth of shower maximum in terms of fixed primary energy

will be quite different to a mean derived for a fixed shower size; differences of up to 200 g cm^{-2} are possible. Calculations in OG 5.2-11 show other aspects of the selection of showers by real particle arrays. In terms of fixed primary energy, figure 2 shows a clear tendency to select only downward fluctuating (late developing) showers close to the array size threshold (which can be set not only by the hardware triggering but also by a software trigger if this is based on a size parameter). Also, since the energy spectrum is steep, any data set will consist preferentially of downward fluctuating low energy showers so that the system will emphasise any shower effects associated with downward fluctuations. This applies particularly if the composition of the primary beam at constant energy contains a mixture of nuclei.

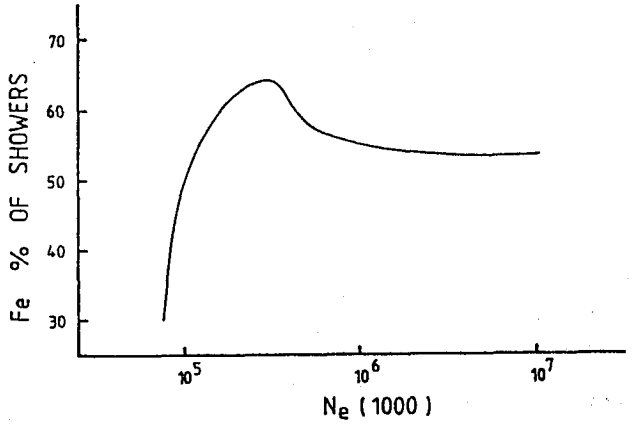

Fig 3. The fraction of all analysable sea level showers produced by iron primaries, as a function of $N_e(1000)$, for a composition of 90% Fe and 10% p. (B.R. Dawson, private communication)

In this case, proton initiated showers with their long interaction mean free path and large fluctuations will be preferentially selected. This effect is shown in figure 3 where the apparent fraction of protons in the beam is seen to be considerably enhanced when recorded by a typical array.

3. Depth of Shower Maximum

The depth of shower maximum and its fluctuations are important parameters in the studies of primary particle composition and the early shower interaction processes. Early cascade maxima are associated with short primary particle mean free paths and high secondary particle multiplicities. Similarly, small fluctuations in the depth of maximum are also associated with short mean free paths since these fluctuations largely mirror fluctuations in the depth of the first interaction. Convention has it that proton primaries are associated with long mean free paths ($\gtrsim$ 80g cm^{-2}) and large fluctuations and "iron" primaries have short mean free paths ($\lesssim$ 20g cm^{-2}) and small fluctuations. The real primary beam will probably be a mixture of species and one would wish to at least determine whether the beam is "iron dominated" or "proton dominated" at a given energy.

A substantial amount of new information on depths of maximum became available at the conference, both theoretical and experimental. These data are summarised in figures 4 and 5. The theoretical work (fig. 5) clearly confirms that the composition of the initiating particle is the major factor affecting the depth of maximum and it should be possible to interpret the experimental data in terms of composition with some confidence since the separation of the composition lines is large compared to the expected experimental errors for individual events

($\lesssim 30 g cm^{-2}$, HE 4.4-16) .

Figure 4 summarises the position on shower depths of maximum with particular reference to recent results. The data from ~ 10^{15}eV to 10^{19}eV appear to follow a consistent relationship and general agreement is remarkably good considering the variety of techniques used to obtain these data. Some comments on the experiments are necessary since some of the spread in the data is due to instrumental and technique effects.

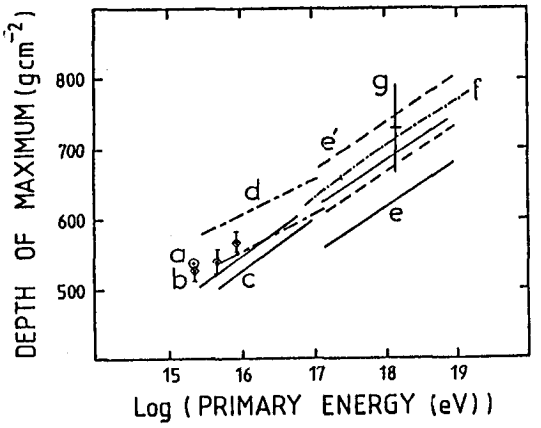

Fig 4. Measured depths of shower maximum.

(a) HE 4.4-13 (b) HE 4.4-15.
(c) OG 5.2-11 (d) Inoue et al. (1985)
(e) HE 4.1-19 (e') Before sub of 50g cm^{-2}
(f) OG 5.1-13 (g) OG 5.1-7

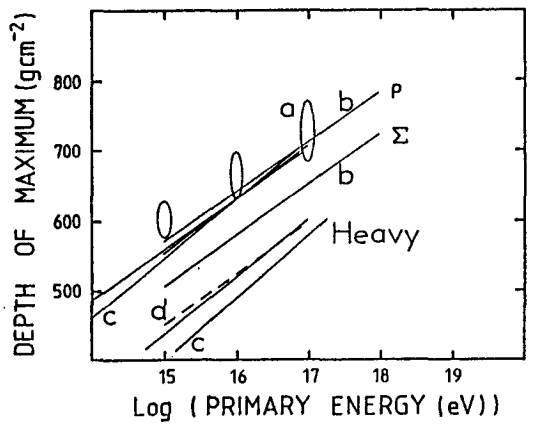

Fig 5. Theoretical Depths of Shower Maximum

(a) HE 4.1-2 (b) HE 4.4-15
(c) HE 4.1-10 (d) OG 5.2-11

The Samarkand array provides us with data at the lowest energies (HE 4.4-13). The array was used to select showers on the basis of their Cerenkov light. This provides a trigger which should approximate directly to a primary energy trigger since we expect the Cerenkov light flux at $\gtrsim$ 100m from the core to be a good primary energy estimator (fig. 6) and these should be typical core distances for the triggering detectors. In constrast, the Cerenkov flux on axis is a good measure of the ground level shower size and so the Cerenkov lateral distribution function clearly reflects shower development. The lateral distribution function can be well approximated by a simple exponential of the form $q(r) \sim \exp(-br/10^4)$ and the parameter b is thus a sensitive measure of shower development (fig. 7).

The Samarkand workers interpreted their data by simulating their experimental data with a particular composition and interaction model and showed that their experimental and simulated data fitted well at 2×10^{15}eV although their

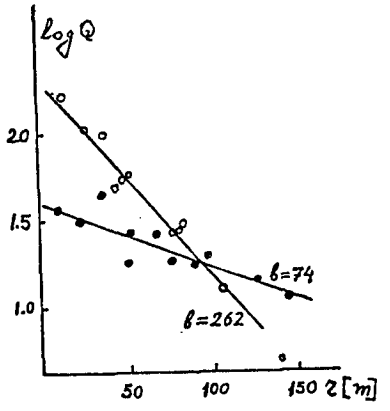

Fig 6. Cerenkov light lateral distributions for $E_0=3x10^{15}$eV but different depths of maximum. (HE 4.4-13)

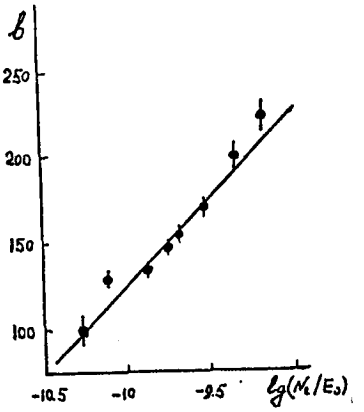

Fig 7. The relationship between the Cerenkov lateral distribution parameter b and a known depth of maximum parameter N_e/E_0. (HE 4.4-13)

observed fluctuations in depth of maximum were probably not sufficient with this model. It is not easy to judge the sensitivity of the fit between experiment and simulation to variations in the model. It is thus important that when experiments are compared to models, some measure of model sensitivity is explicitly stated. If the calculations of Patterson and Hillas (1983) are applicable at the Samarkand altitude, it is likely that the use of the Cerenkov flux at 100m from the core will cause a slight overestimate ($\sim 10 g cm^{-2}$) of the depth of maximum since the flux only becomes a really satisfactory primary energy parameter for r ~ 150m.

A similar comment might also apply to the other Samarkand result (HE 4.4-15) shown in fig. 4 since this uses the same primary energy estimator. In this case, the Cerenkov pulse shape was studied and depths of maximum at fixed primary energy were obtained which were rather higher in the atmosphere than before when a less satisfactory primary energy estimator had been used. Cerenkov pulse shape measurements are potentially very powerful but, since a great deal of information must be extracted from single pulses, they are very susceptible to selection problems and are technically demanding (see eg, Liebing et al 1984, Inoue et al 1985a). In order to be recorded, a pulse must be of a suitable amplitude and, for a given total pulse area (Cerenkov flux), this amplitude depends on shower development. A selection was made of a total of 83 events for analysis out of a recorded data set of 4000 showers. In principle, this technique of a posteriori selection of an unbiased data set is acceptable but one needs to be sure that no physics is being lost in the process. The great potential of the pulse shape technique is in its sensitivity to early shower development unlike lateral distribution experiments which are more sensitive to the cascade development past maximum. However, very good

instrumental dynamic range and wide bandwidths are necessary.

The Adelaide group (OG 5.2-11) also presented Cerenkov lateral distribution results. They interpreted their results with simulations and fitted a mixed composition model over a decade in energy. In this case, both the depth of maximum and its fluctuations seemed to be fitted by the model and the spread of acceptable models was 85-95% iron plus protons. This mixture becomes only ~50% iron in the observed beam at fixed shower size at ground level. The Adelaide data did not give such a good fit to the Samarkand composition of 40% protons plus 15% each of A = 4, 15, 31, and 56 (B.R. Dawson, Private communication) but, at this stage of sophistication, particular interaction models and detailed theory relating the lateral distribution function to development must also become important.

Inoue et al (1985a,b) have recently presented Cerenkov results from the Akeno and Chacaltaya arrays. These data are included in the figure after a conversion from their Ne to primary energy using Akeno size and energy spectrum results. Such a procedure is dangerous and has been used only since the results then represent upper limits as indicated in the original paper. Based on experience, one might expect depths of maximum to be overestimated by $\lesssim$ 50g cm^{-2} through the use of a shower size trigger and later conversion to primary energy.

Above 10^{17} eV, two data sets were presented at the Conference, by Dyakonov et al (OG 5.1-13) and by Glushkov et al (HE 4.1-19). The former data were derived from mean Cerenkov lateral distributions in a number of energy intervals obtained at Yakutsk and the latter were from a new analysis of a broad range of development-dependent parameters (electron lateral distribution function, Cerenkov light to electron ratio, and electron to muon density ratio at 300m from the core) measured at Yakutsk. Some of these parameters allowed a determination of depths of maximum in rather model independent ways (fig 8). The results were obtained in terms of fixed size parameter $\rho_s(300)$ and the authors comment that at fixed E the values of X_{max} would be ~ 50g cm^{-2} less. This correction is included in the diagram. It is not clear whether or not the work of Dyakonov et al should include a similar correction since this depends on the precise way in which shower selection and averaging were carried out.

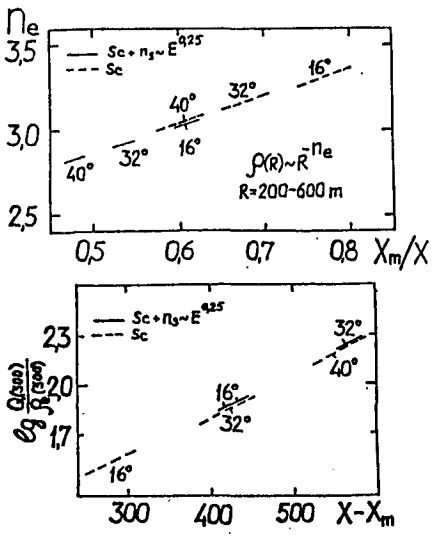

Fig 8. Relating the electron lateral distribution and the ratio of Cerenkov light to electrons (at 300m) to shower development. (HE 4.1-19)

Theory predicts such a large separation of depths of maximum of iron and proton showers that it should be possible to significantly improve our estimates of composition at fixed primary energy by looking at the actual distribution of depths in very limited energy ranges in a way

similar to that used by Nikolsky et al (1981) (see also OG 5.2-5) for fluctuations of Nμ and Ne. The resolution should be quite good with the Cerenkov techniques and sufficient events are probably already available at Samarkand and Adelaide.

Fluctuations in the Depth of Shower Maximum

Fluctuations in the depth of shower maximum should reflect primary composition through the large difference in the interaction mean free path of protons and heavier primaries. Heavy primaries should have much smaller fluctuations in depth of maximum ($\lesssim$ 30g cm^{-2}) than protons ($\sim$ 60g cm^{-2}). It is interesting that $\sigma_{x_{max}}$ can be measured through analyses of variance without a direct measurement of x_{max}. Figure 9 summarises data presented at the conference. The data favour proton like fluctuations. However, similar results would be obtained for a mixed composition, and it is unlikely that this technique is powerful except for eliminating the possibility of a pure iron primary beam (or at least lacking in light nuclei). It is interesting to see that the fluctuations at the highest energies are reduced, as one would expect for cross sections which increase appreciably with energy.

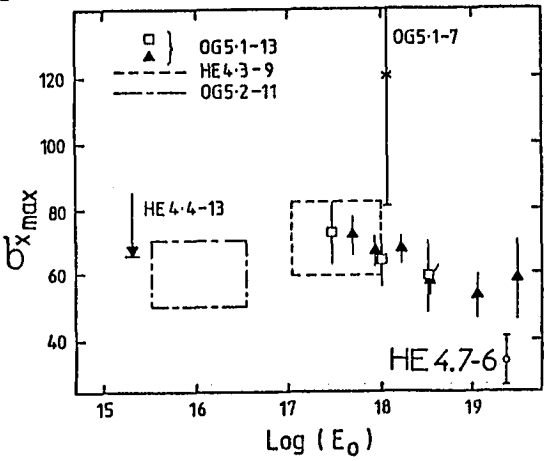

Fig 9. Fluctuations in shower depth of maximum.

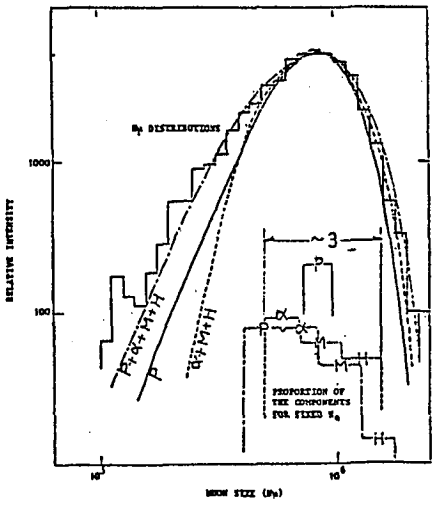

Fig 10. Observed and calculated distribution of muon size for fixed N_e. (HE 4.1-3).

There are some other results which require at least some protons in the primary beam. These are measurements of muon size at fixed Ne from Akeno (HE 4.1-3) analysed by Tanahashi which show a long tail at small Nμ due to the fluctuations of a proton component (fig 10). Also, equi-intensity cuts show a long shower attenuation length which is probably due to the large proton shower fluctuations. As a general comment on cascades discussed at the conference it is noteworthy that the cascade attenuation lengths of $\sim$ 200g cm^{-2} found with equi-intensity cuts should represent conservative upper limits to the single cascade proton development curves. A number of workers have been using much longer attenuation lengths in their models which would seem to be inappropriate.

4. Novel Techniques for the Economical Study of Giant Showers

Arrays which are used to study the very highest energy showers have now accumulated data with ~ 10^3 km^2 yrs collection in both northern and southern hemispheres. There are many questions of composition, interaction properties, anisotropy, and spectra which remain controversial or virtually undiscussed at these energies and a good case can be made for experiments which might expect to increase the data accumulation by a factor of ten in a reasonable time and at a reasonable cost. Modestly priced arrays with collecting areas of ~ 10^3 km^2 at 10^{19} eV are required. Such arrays were described at the conference using air fluorescence techniques, radio techniques, or by measuring the longitudinal thickness of the shower front at large core distances. There is potential in each technique but, though each may find its place in overall systems, none seems to be a single satisfactory answer to the replacement of conventional systems in a new generation of arrays.

The Longitudinal Thickness of the Shower Front

The thickness of the shower disk has been the subject of continuing but not major study for a number of years. It has been relevant to radio studies, fast Cerenkov studies, and particularly the risetime studies of the Haverah Park group. Recently there has been an increase in interest in this area due to a suggestion by Linsley (1983) that this parameter might be a useful direct measure of core distance thus enabling cheap EAS arrays to be built with large collecting areas for the study of giant air showers. It may not then be necessary to enclose the shower collecting area with detectors in order to obtain a useful shower analysis. In terms of shower studies, this section of the conference was unique in the sense that it was completely experimental in its outlook.

Linsley has shown (and extended his discussion here) that the thickness of the shower front can usefully be expressed as a dispersion $\sigma_t = [\int (t-\langle t\rangle)^2\, p(t)\, dr]^{0.5}$ and that as, a function of core distance, this is given by $\sigma_t \simeq \sigma_{to}\ (1+r/r_t)^b$ where σ_{to} = 2.6ns, r_t = 30m and b ~ 1.5 (or for for practical purposes a weak function of zenith angle described at the conference (HE 4.7-14)). Investigations of σ_t were presented and the extent of its usefulness was discussed in comparison with data from conventional array analyses together with specific proposals for "mini-arrays" to detect giant air showers using the "Linsley" method.

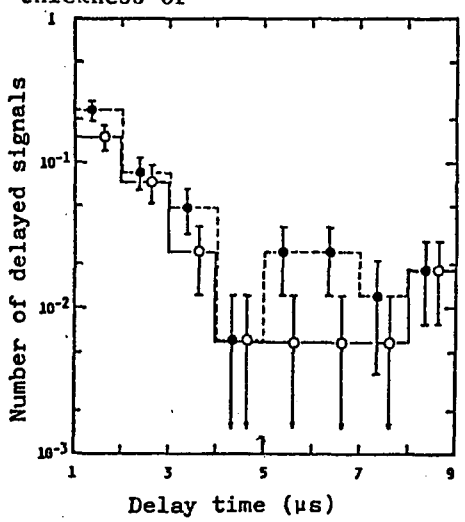

Fig 11. Delay time distribution of signals delayed by longer than 1 μs. Filled circles >0.5 particles. Open circles > 1 particle. (HE 4.7-5)

The Linsley method utilising Disk Thickness at Large Core Distances

The technique depends on σ_t or some equivalent being a

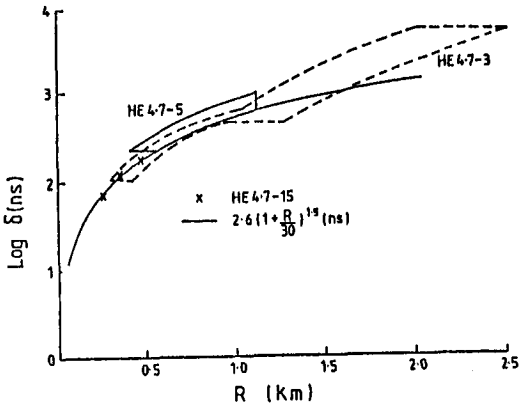

Fig 12. Arrival time dispersion of particles in the shower front.

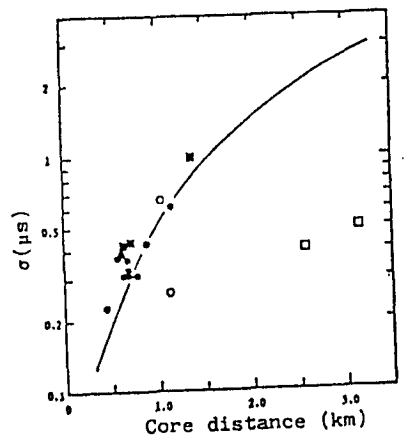

Fig 13. Time dispersions (σ) of the arrival time distributions of particles. The number of particles observed in the unshielded detectors:
filled symbols >10
open symbols <10.

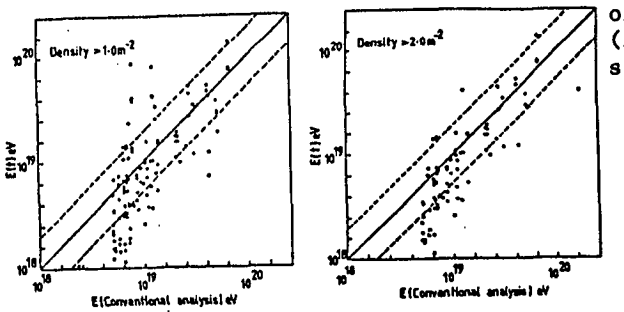

Fig 14. Plots of energy derived from risetime against energy derived from conventional analysis. (HE 4.7-6)

reliable thickness parameter at large core distances. There appear to be some late "sub-luminal" pulses associated with showers (fig 11) which are not just an extended tail of the conventional shower disk (Linsley, HE 4.7-13, Kakimoto et al, HE 4.7-5). It is possible that these are due to low energy nucleons but the tail needs more investigation with a good system impulse response before one can be sure that selection effects are not causing these very late pulses to be interpreted as a separate phenomenon. The form of σ_t is such that large values of $(t-\langle t\rangle)$ are given considerable weight and there is a need for theoretical studies to search for a suitable alternative parameter which is more linear in $(t-\langle t\rangle)$ so that a few delayed particles can not dominate the parameter.

Measurements have been made of the disk thickness at large core distances (fig 12) by Akeno and Moscow workers (HE 4.7-3/5/15) and the Haverah Park group (HE 4.7-6) investigated the Linsley technique by applying it to conventionally analysed showers. It appears that, as one might expect, agreement is best when a large number of particles is detected (figs 13, 14). Both data sets show dramatic improvements in energy estimation with increasing particle density in the detector. The Haverah Park data suggest that, for a factor of two agreement in shower energy, they would need $\gtrsim$ 64 detected

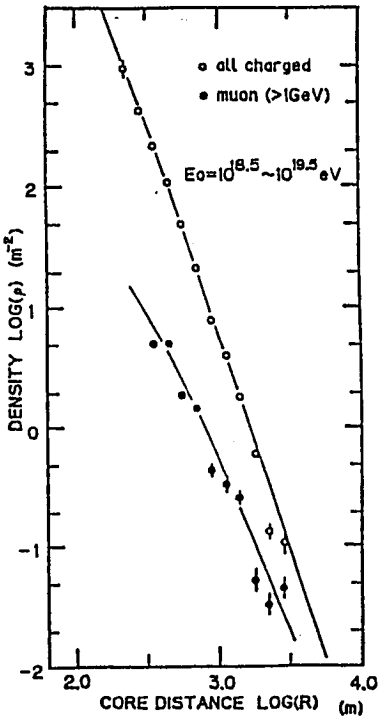

Fig 15. The lateral distribution of electrons and muons. (HE 4.7-3)

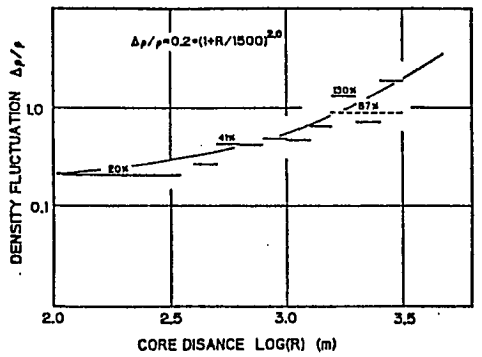

Fig 16. The fluctuation of electron densities. The broken line is derived from pulse height distribution of single particles. (HE 4.7-3)

particles ($\gtrsim 2m^{-2}$) and the Akeno group would appear to need $\gtrsim$ 10 particles for an acceptable system. It is noteworthy that at very large core distances (~2km) the technique remains to be proven and Teshima et al (HE 4.7-3) warn that an apparently steepening lateral distribution above 1km (fig 15) and large electron density fluctuations (fig 16) might finally limit the usefulness of the technique (however, Watson implied in a question that measurements of long pulses at these core distances may have caused underestimates of the density at these distances). The Akeno workers successfully used a time parameter T_{20-70} (the time between 20% and 70% of the full shower front) and such a linear parameter may well be preferable to σ_t for the reasons suggested above (fig 17). It is noteworthy that at large core distances the disk is so wide that one can reasonably expect to use simple pulse counting techniques or slow ($\lesssim$ 50MHz) sampling transient digitisers so that recording systems can be simple and economical (Ng et al, 4.7-10).

Radio Emission from Air Showers

The study of radio signals from showers might offer an inexpensive technique for constructing very large area detection arrays for giant air showers and may also provide information on shower development through the frequency spectrum of the radiation. The main period of study of radio emission was the decade from 1965-1975 but the work has continued and new results were presented at the conference. It should be remembered that interest waned in this field a decade ago through the lack of suitably large signal to noise ratios. We need to be convinced that this fundamental problem is being overcome.

Close to the shower axis, a radio system observes the shower

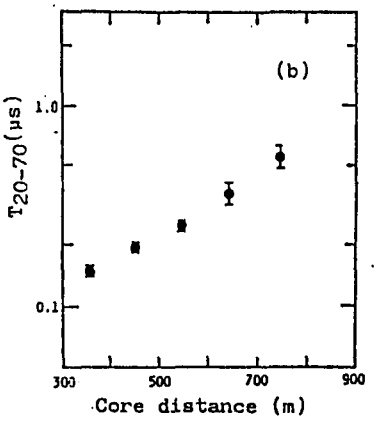

Fig 17. The average T_{20-70} of the arrival time distributions of particles. (HE 4.7-5)

with the sort of pulse widths/time periods found in fast Cerenkov work (~10ns) and the frequency spectrum thus extends typically to ~100 MHz and contains development information similar to other fast timing data. As one moves away from the axis, time compression is lost and the shower signal is observed over the full tens of microseconds of observed shower development. A frequency spectrum is then produced with important components at tens of kilohertz.

In order to make effective use of the radio technique one needs both a solid theoretical foundation and a good signal-to-noise ratio. In the VHF band, say 20 MHz to 150 MHz, Datta and Pathak (HE 4.6-4) have confirmed that we understand reasonably well the emission mechanism in terms of known charges and their motion within the shower. At low frequencies ($\lesssim$ 1 MHz) the situation has never been clearly resolved. The observed amplitude spectrum increases with decreasing frequency and there have been reports of large variations in field strengths, perhaps associated with local conditions.

Suga and his co-workers (HE 4.6-3) have begun a new attack on the low frequency region (50 kHz to 1 MHz) in conjunction with the Akeno array and have confirmed that there are large pulses to be detected from giant showers out to ~ 2 km and that these pulses are stable under varying local conditions (fig 18). This experiment is in development and use is being made of modern techniques to obtain the best possible signal to noise ratios. The current situation is that large pulses are observed but not with really large signal to noise ratios. At ~ 1 km one appears to require a 10^{10} particle shower to obtain a signal to noise $\geq$ 10:1. This is not adequate for a stand-alone system in a time-varying noise environment and more development is needed. Also, the radio emission mechanism is not yet clear at these low frequencies. Datta and Pathak were unable (along with many predecessors) to satisfactorily account for

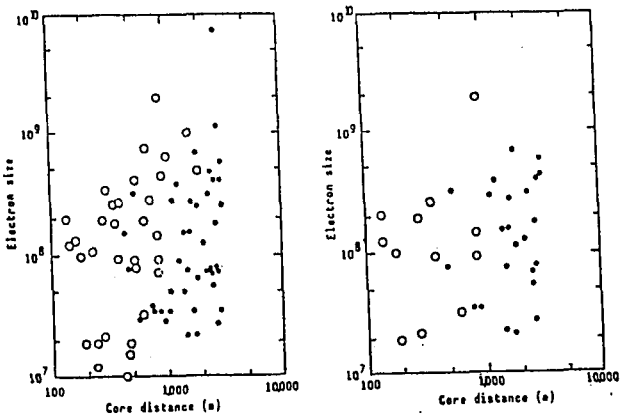

Fig 18. Air showers accompanying radio signals observed well beyond the background noise (open circles). Unaccompanied by radio signals (filled circles).

the observed field strengths (several mV. m^{-1} in a 10^9 particle shower at 1km) in terms of conventional emission mechanisms. These difficulties are of long-standing and are particularly perplexing since the problem is conceptually straightforward:- a current of $\sim 10^8$ electrons, viewed from~ 2km as it builds up and decays from ~10km to the ground.

Nishimura (HE 4.6-15 corrected in oral presentation) has specifically considered emission mechanisms in the low frequency/large core distance range and showed the dominance here of the shower negative charge excess due to positron annihilation in flight. As this number changes with altitude (or observed time), there is strong observed low frequency emission. Also, when the charges effectively disappear from the observer as the shower hits the ground, there is a process like transition radiation which gives coherent radiation preferentially at low frequencies (due to the typical time scale of the shower disk absorption of ~ 0.1 to 1 μs). At core distances of ~1km, the charge excess and transition radiation contributions should be comparable and produce a total field strength similar to (or perhaps a little below) that observed by Suga et al. In principle, the radio lateral distribution should be quite broad at low frequencies since coherence will not be lost. If a serious stand-alone system is to be developed, the impulsive time-variable background will present major problems and also some shower direction finding method will be needed if anisotropies are to be studied. Bandwidths of ~10^4 Hz preclude conventonal fast timing although it may be possible to use phase measurements for this purpose.

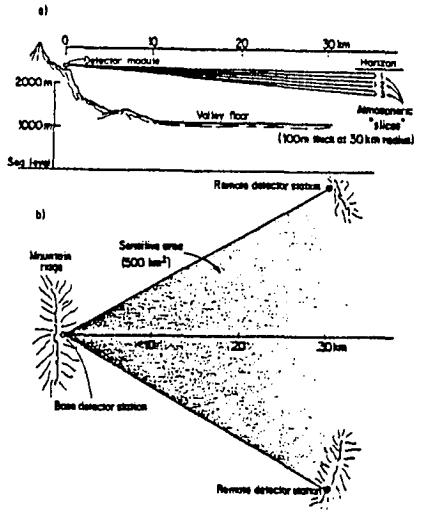

Fig 19. Proposed side-looking air fluorescence detector to observe $E_o > 10^{19}$eV air showers. (HE 4.6-6)

Air Fluorescence Techniques

Halverson and Bowen (H.E. 4.6-6) are studying the use of air fluorescence light produced near ground level by giant air showers as a basis for cheap large-area arrays. The idea involves looking down into large valleys or canyons to see fluorescent light from distances up to 35 km against a dark mountain background rather than against the relatively bright night sky (fig 19). The general properties of fluorescent light for air shower work have been proven by the Fly's Eye group and one should have confidence in the potential of the technique. To be useful however, a cheap detection system is needed and it is proposed to use cylindrical mirrors which view broad "slices" almost horizontally across the valley. Timing and amplitude measurements from perhaps three systems will contain information on the shower direction and size. However, the proposed slices are rather close together to ensure that all viewing is kept within the valleys and it would seem unlikely that good fast timing directions will be obtained vertical "baseline" of only a few hundred metres.

It is proposed that light detection will be through bars of

acrylic strips (fig 20) doped with wavelength-shifter to make good use of the ultraviolet component remaining in the light reaching the detector. The bars then act as light guides to photomultipliers. Since internal reflection at the surface is important, it may be necessary to take particular care in using such a system in a dusty desert environment which might cause progressive surface damage. Protection from unwanted local lights may be necessary.

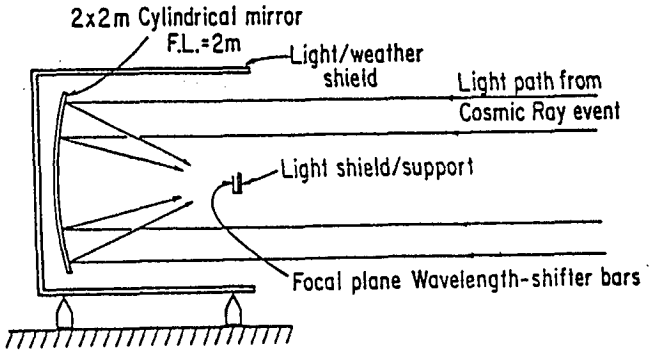

Fig 20. Side view of proposed side looking detector station. (HE 4.6-6)

5. Gamma Ray Initiated Showers

The discovery by Samorski and Stamm (1983a) of point sources of cosmic ray showers has predictably brought renewed interest in the properties of gamma ray initiated showers. One would like to have some way of picking out likely gamma ray showers from a conventional cosmic ray background and one would also wish to be able to realistically assign primary energies for the observed events. The muon component of these showers is particularly perplexing since we have long expected small values of $N\mu/Ne$ to characterise gamma ray showers whereas Samorski and Stamm (1983b) apparently observed muon signals which were not much less than those expected for conventional massive particle initiated showers.

Papers presented at this conference are in agreement that muon numbers ($\gtrsim$ 1 GeV) and hadrons in gamma ray showers produced by photoproduction should be $\lesssim$ one tenth of those expected for conventional (proton initiated) showers (eg fig 21) and the ratio is even greater if iron primaries are used for comparison (Edwards and Protheroe,HE 4.5-7). Clearly $N\mu/Ne$ should be a useful selection criterion for gamma ray showers. Indeed Stanev, Vankov and Halzen (HE 4.5-3) point out that, due to large fluctuations in muon production, most gamma ray showers will have only half the average number of expected muons.

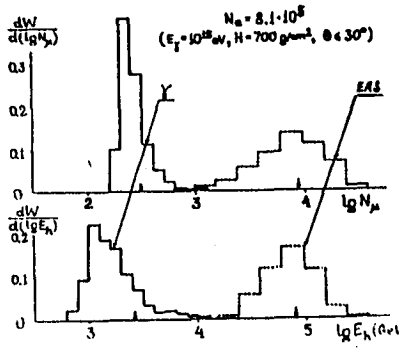

Fig 21. Expected muon number and hadron energy distributions for gamma initiated and conventional EAS. (HE 4.5-16)

The Tien Shan workers have been selecting muon-poor and hadron-poor showers as gamma-ray initiated showers and and Nikolsky et al (HE 4.5-11) have studied showers detected in this way. Through calculation and a comparison with observed muon-poor showers, Stamenov et al (HE 4.5-10) showed that theory and experiment were in agreement that, at that their altitude, $(N\mu_\gamma/N\mu_A) < 0.15$ and

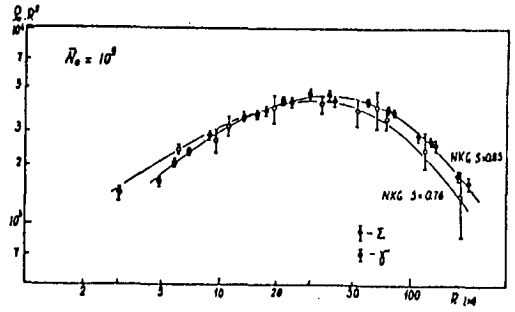

Fig 22. Electron lateral distributions measured for conventional and potential gamma initiated EAS. (HE 4.5-11)

(hadron energy/electron energy) $\lesssim 1.5 \times 10^{-2}$ were good selection parameters for such showers. A study of Tien Shan electron lateral distributions was made by Nikolsky et al. They found that muon-poor (electromagnetic?) showers were steep near the core as expected since secondary hadron transverse momenta were not involved. They also found that, at this altitude, the overall electron lateral distributions at large core distances (fig 22) were also slightly steeper for pure electromagnetic showers ($S = 0.76 \pm .02$) compared to "normal" showers ($S = 0.85 \pm 0.1$). This may be a true development effect. It is noteworthy that, since we expect gamma-ray showers to have smaller development fluctuations than background proton showers, old shower age may still be a useful gamma selection parameter since selection would tend to be against a background of young downward fluctuating proton showers. Hillas (HE 4.5-6) has calculated shower parameters for proton and gamma ray intiated showers at sea level. Again, a factor of ten is typical of the reduction in muon numbers for gamma ray showers (fig 23). He showed that a measurement of the ratio of signal in a deep water Cerenkov detector to a (5cm) scintillator detector can also provide a practical way of selecting an equivalent to muon-poor showers at large ($\gtrsim$100m) core distances (fig 23). As one might expect with a low muon content, gamma-ray showers produce a steeper lateral distribution for the deep detector, particularly at large core distances ($\gtrsim$ 100m).

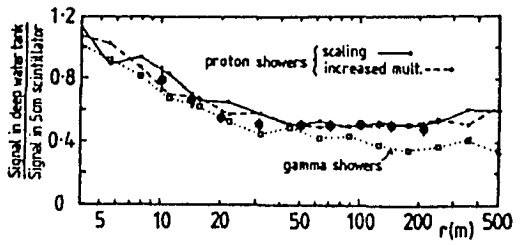

Fig 23. Ratio of particle densities recorded by two detectors in proton and gamma showers at various axial distances. (Sea level). (HE 4.5-6)

There is agreement that without the addition of some new physics to the calculations, the problem of the Kiel muon result remains. Hillas attempted to see how far one can move from conventional photoproduction to generate pions and muons more readily and still obtain results which fit conventional showers. In his model, he arbitrarily increased the hadronic cross section for photons above 1 TeV. This gives many more muons, and the required number of muons for the Kiel "gamma ray" showers can be produced. It is remarkable and salutory to note that Hillas was able to show that such an unconventional novel interaction model could still give a conventional N_μ vs N_e relationship for conventional showers (this is presumably necessary since the Kiel group have not found strange muon properties for conventional showers) and also gives a good fit to their lateral distribution functions.

It is possible that gamma-ray showers might have produced

effects in Samorski and Stamm's muon detector which fitted selection criteria for muons but were due to some other process. Stanev, Gaisser and Halzen (reported in HE 4.5-1 but withdrawn) suggested that at ~10m from the core photons might "punch through" the 880 gcm^{-2} of concrete shield and produce a signal in flash tube detectors. Blake and Nash (HE 4.5-1) investigated this possibility with data from their muon detector at Haverah Park. Their data were for core distances >20m and showed that here, "punch through" for 10cm and 20cm of lead was insignificant (fig 24). However they also used a data set of "local showers" and 20cm of lead shielding to show that below ~10m, the typical distance of the Kiel measurements, significant punch through accompanied their muons (~2:1).

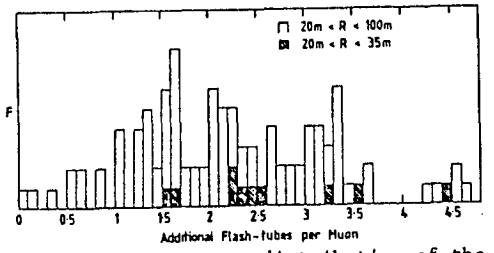

Fig 24. The frequency distribution of the electron accompaniment per muon capable of penetrating at least 5cm of lead. (HE 4.5-1)

In their presentation, Stephens and Streitmatter (HE 4.5-5) commented that, if they included incomplete screening in their calculations, pair production by low energy ($\lesssim$10MeV) gamma rays would be suppressed leading to a build up of relatively penetrating particles. It remains to be seen whether, if this is correct, the Kiel workers would have observed any effect with conventional showers but the result emphasises the need for calculations to follow the electromagnetic component correctly to the lowest possible energies.

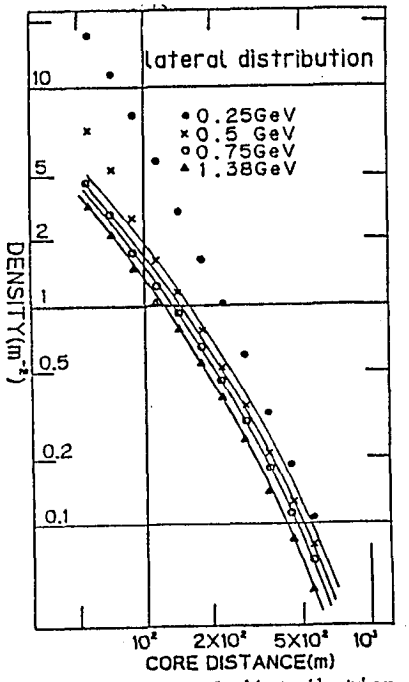

Fig 25. The lateral distribution of the density of muon signals at each layer of absorber for vertical showers. Curves are those given by the Greisen formula with R_0=280m. (HE 4.3-8)

The Akeno group has been studying the penetration of muons through concrete absorber (Matsubara et al, HE 4.3-8) and has found that at small core distances, there is a deviation from a conventional muon lateral distribution function which has a lateral distribution rather like the electromagnetic component suggesting a "punch through" effect (fig 25). This leakage occurs below 500m for 0.25 GeV threshold muon detectors, and below 150m for 0.5 GeV detectors (shower

size 10^7 particles) and may be consistent with the Kiel observation at 880 gcm^{-2} of concrete and core distances <10m.

Evidence for Low-Muon Gamma Showers

Despite the Kiel finding that there were muon-like signals associated with their gamma ray events, a muon-poor criterion has been applied apparently successfully by other groups. Akeno workers (OG 2.1-5) have observed events from Cygnus X-3 only when they applied a muon-poor content cut (set at N_μ/N_e <0.001 compared to a mean for all events of 0.03). It is noteworthy that the muon measurements in this case were made at rather large (> 50m) core distances. Kaneko et al (OG 5.3-2) appear to have confirmed the Adelaide Vela X-1 observation with muon-poor showers recorded many years ago at Chacaltaya. Kirov et al (OG 2.3-3) found an excess of events from the direction of the Crab Nebula only when a muon-poor ($N\mu/\overline{N\mu} \leq 0.11$) cut was applied. On the other hand, Blake et al (OG 2.1-4) were unable to find any evidence for a lack of muons in events from the direction of Cygnus X-3 and at the phase peak. The position is then not yet clearly for or against muon-poor astronomy.

6. The Shower Front at Small core Distances

The shower front has a thickness which increases with core distance. This allows us to study aspects of shower development through disk thickness measurements at large distances where there may also be a separation of the muon and electromagnetic fronts. At small core distances, the disk is very thin and until recently there has been a general contentment to leave it at that. However, technology for studying fronts a few nanoseconds (x c) thick is now readily available and there are also now pressing needs for such measurements. We would like to understand the Linsley broadening better, there is interesting evidence for shower front structure, and ultra high energy gamma ray astronomy requires improved angular resolution through better shower front timing.

Woidneck and Bohm (1975) provided basic data by sampling the shower front and found typical thicknesses of 2 nanoseconds (x c). At this conference, Sasaki et al (HE 4.7-1) and Inoue et al (HE 4.7-2) gave more detailed information directly from the risetime and full width at half maximum of observed scintillator pulses. The longitudinal widths were derived by correcting the observed average signal shapes for the system impulse response (fig 26). If the impulse response removal proves correct, these widths are very narrow ($\lesssim$ 2ns at 20m from the core) and seem rather narrower than measured by Woidneck and Bohm. If the fronts of gamma ray initiated showers are this narrow, one

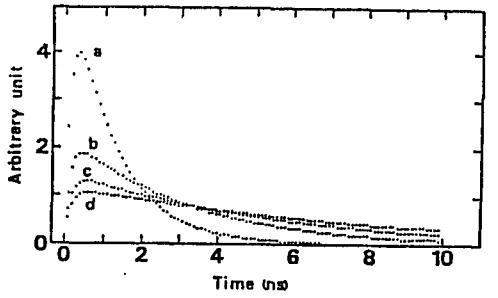

Figure 26 Corrected arrival time distributions of air shower particles for showers with sec θ of 1.0-1.2 and
(a) Ne of $3.2 \times 10^{5.5}$ - $1.0 \times 10^{6.0}$ for core distances 10m-20m
(b) Ne of $1.0 \times 10^{6.0}$ - $3.2 \times 10^{6.5}$ for core distances 20m-30m
(c) Ne of $3.2 \times 10^{6.5}$ - $1.0 \times 10^{7.0}$ for core distances 30m-40m
(d) Ne of $1.0 \times 10^{7.0}$ - $3.2 \times 10^{7.5}$ for core distances 40m-50m

might hope that shower front sampling for small U.H.E. gamma ray telescopes might not be a serious factor in limiting the array fast timing angular resolution.

Calculations on shower front thickness were presented by Nakatsuka (HE 4.4-11/12, HE 4.7-11). These were the first such calculations for some years and generally confirmed the recent observations. It is interesting to see how narrow the disk may be at the smaller core distances and also that this thickness depends a little (inversely) on distance to shower maximum (fig 27). These are results of considerable current interest and we need to see whether or not they are confirmed by more complete shower models and calculations.

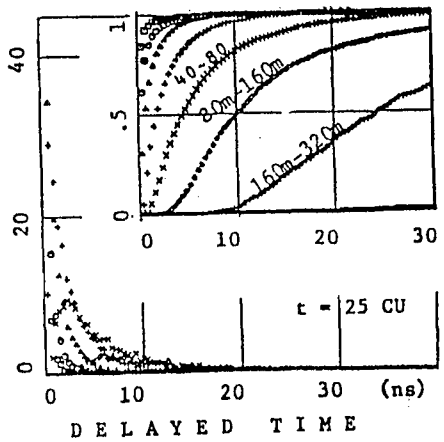

Fig 27. The arrival time structure at various distance from the axis. The distances are 0-5m, 5-10m, 10-20m,etc., (HE 4.7-11)

Structure in the Shower Front

Shower front observations sometimes show delayed structure which is correlated among a number of nearby detectors. These delayed sub-showers were discussed by Sasaki et al (HE 4.7-1) and Kamamoto et al (HE 6.2-10) and delays of a few tens of nanoseconds have been observed (fig 28). The delayed pulses do not seem to be instrumental or sampling effects on the basis of simulation of the detection procedure. Also, Sasaki et al have been able to identify delayed pulses with multiple core structure observed with the Norikura system. This interesting but difficult work is still severely limited by instrumental time resolution.

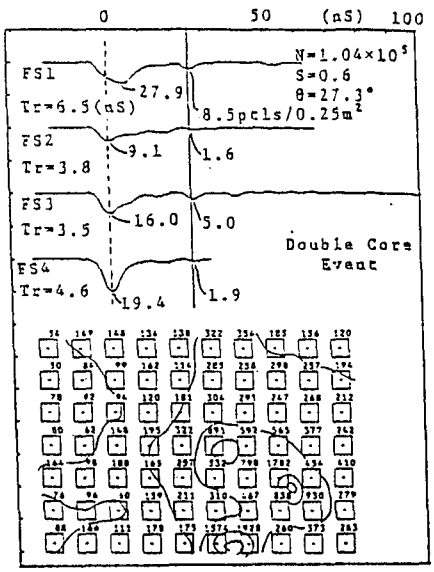

Fig 28. A multicore event showing subpeaks delayed similarly in a number of detectors (HE 4.7-1)

7. Mini-Arrays

The Hong Kong and Michigan groups have been working on the practical implementation of the Linsley array concept. In order to be successful the designs must be simple and inexpensive or the original intention will be lost. There is the need to ensure that whatever results are obtained on anisotropies and spectra will be acceptable in comparison with data obtained by more conventional means. If the technique in

principle is possible, that is the shower front width proves to be an acceptable parameter, then suitable practical means of triggering, density measurements, and direction measurement must be found.

Triggering for a Linsley array requires pulse width discrimination. Hazen and Hazen (HE 4.7-7) assume that, for a broad shower front, individual particle arrivals will be resolved and a pulse counting system in a 2μs window can give a suitable trigger (with a pulse dead time of 30-40ns). The concept of digital discriminators in this sense is new and discrimination can be done either in software or by reconstructing an analog amplitude. With such a system, it is not possible to use the discriminator output for fast timing purposes but the pulse train itself can be used. The leading particle can be timed by a fast preamplifier/discriminator (Ng, HE 4.7-9) and the arrival time of all pulses can be stored in a fast register to be read into a microcomputer.

There is some loss of useful information in such arrangments. If there is a bunching of shower particles, amplitude information will be lost and it may be preferable with some extra expense to use a simple flash digitiser (multiple level discriminator) particularly as a large shower falling relatively close-by might saturate a leading edge discriminator for an appreciable fraction of the acceptance time and, in a worst case, may be not recognised.

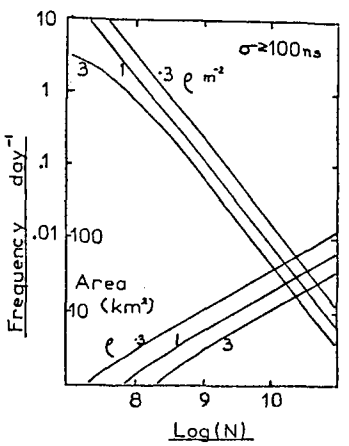

Fig 29. Expected rates for a mini array. (HE 4.7-8)

Timing for the determination of shower directions is a serious problem. With a small array, 10ns timing may not be adequate, particularly if a limited number of shower particles is spread through a ≥ 100ns front. The suggestion that track visualising detectors should be employed is being seriously studied (Ng and Chan, HE 4.5-14). An alternative being considered at Adelaide may be to use an aray of Linsley arrays in a 1km grid. Fast timing could be done in a conventional way and supplementary core location information would be available from the front width. The Linsley arrangement would reduce the data recording to $1hr^{-1}$ per detector by a reduction of the trigger rate of individual detectors. This is a cheap alternative to the two-fold local coincidence used by SUGAR.

Hazen (HE 4.7-8) has looked carefully at some practical problems of background and expected rates (fig 29). Typical rates for small (100ns) pulse widths and small (a few m^2) detector areas are ~ a few per day giving an array with a threshold of $10^{17} - 10^{18}$ eV. These rates agree well with observations made so far.

8. High Energy Muons

High energy muons are results of the early interactions in the shower and should be sensitive to early interaction parameters through both their total number (Wrontiak and Yodh HE 4.1-2, 4.1-7) and their lateral distribution function. Muons with energies greater than 200 GeV

have been discussed by Bazhutov et al (HE 4.3-16) and Cho et al (HE 4.3-7). Cho et al find that the lateral distribution function is much too steep for them to be anything but a proton dominated flux in their observations at 10^{14} to $10^{14.5}$ eV. Moscow results (HE 4.3-16) for showers in the size range above this show a rather broader distribution which fits better with their preferred mixed composition although particular interaction models have to be introduced to increase the total muon number and widen the lateral distribution a little. These characteristics are also associated with models of high atomic number primaries.

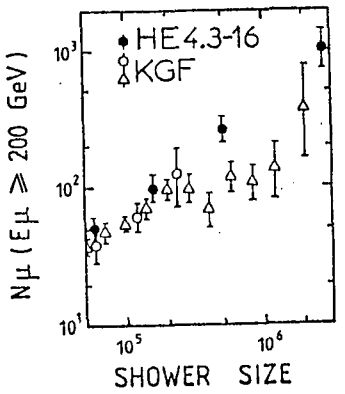

Fig 30.

Mountain altitude data (Acharya et al 1983) had indicated that, as one passed through the region of the knee, there was a reduction in muon numbers for a given Ne. A comparison of the Moscow sea level results with those data scaled to sea level failed to confirm such an effect and the source of this important discrepancy is not clear (fig 30).

9. Low Energy Muons

Lower energy muons are commonly detected in conjunction with larger air shower arrays and are studied particularly at large core distances where the muon component progressively dominates the total detector signal. The lateral distribution function, total muon number, and the muon pulse risetime are of interest in reflecting cascade development.

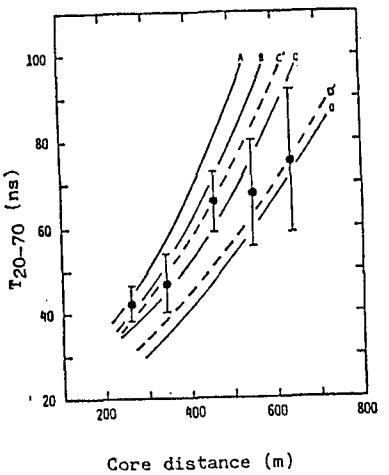

Figure 31. The average T_{20-70} of the arrival time distributions of muons with energies above 1.0GeV for showers with N_e of $10^{8.0}$–$10^{8.5}$ and secθ of 1.0-1.2 compared with those calculated from A: scaling model, B: a model with an $E^{1/4}$ multiplicity law, C: a model with an $E^{1/2}$ multiplicity law and D: a model with an enhanced $E^{1/2}$ multiplicity law and with first-interaction depths of 40gcm^{-2} for A-D and 120gcm^{-2} for C'-D'.

Muon arrival time data were reported by the Akeno (HE 4.7-4) and Haverah Park groups (HE 4.3-10). Taking into account details of the experimental arrangments (system response, muon energy threshold etc), the agreement between these experiments is good. However, agreement with the model used by McComb and Turver (private communication (1981) quoted in HE 4.3-10) is very poor, with extreme models being required to fit the data. Kakimoto et al suggest that their muon (>1GeV) risetime data indicate an early fast development of showers (Ne ~ 10^8) since the muon risetime results as a function of core distance show rather short risetimes at large core distances (fig 31). However, this may be a measurement artefact at small muon densities and also, at the present time, the statistical uncertainties in the result do not preclude many other models. It appears also that there is no evidence in these data for any muon photoproduction of 0.5 GeV muons. If the data

are correctly interpreted, the ratio of photoproduced to all muons above 0.5 GeV must be much smaller than calculated by McComb, Protheroe and Turver (1979). There is no evidence from the Akeno data (HE 4.3-8) for any substantial changes with size of Nμ/Ne. In particular, the relationship shows no evidence for any steepening associated with an increasing contribution due to photoproduction at large shower sizes (fig 32).

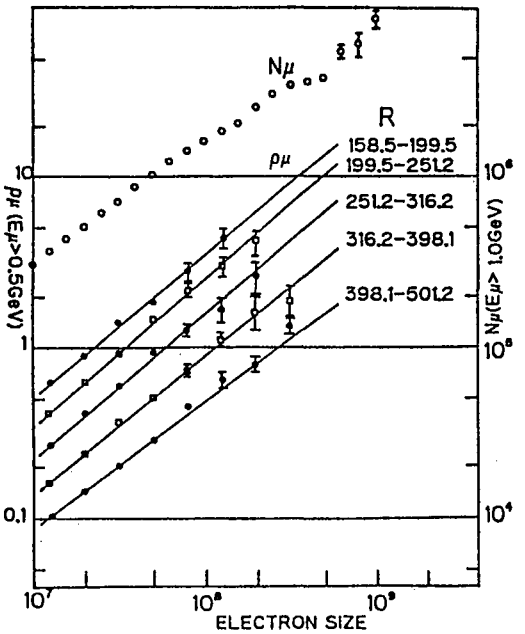

Fig 32. Size dependence of muon number and muon density. (HE 4.3-8)

Van der Walt and de Villiers (HE 4.7-12) presented some sampling statistics for shower front studies which are of interest also to those interested in shower front fast timing since the distribution of arrival times within a front probability density function determines the directional accuracy of fast timing systems. The muon lateral distributions measured at Akeno (HE 4.3-8) and Haverah Park (HE 4.3-10) are also in reasonable general agreement. At low threshold energies and smaller core distances ((0.5 GeV, <150m) and (0.25 GeV, <500m)) the Akeno group appear to find evidence for larger densities than expected. It may be that concrete shielding with depths equivalent to 0.25 or 0.5 GeV may be allowing a leakage of the electromagnetic component of the shower at the smaller core distances. This effect is shown clearly in the dependence of the observed to expected density with energy threshold and core distance. The higher the energy threshold becomes (with the sec θ absorption term), the less the leakage is observed.

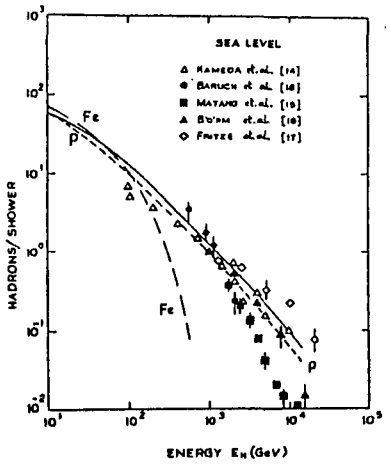

Fig 33. Hadron energy spectra. (HE 4.1-14) Dashed lines are from Grieder (1984)

10. Hadrons

In principle, studies of hadrons should give rather direct information on primary composition and early shower interactions. Indeed, there is good agreement between the various calculations presented at the conference, mainly concerning hadron energy spectra (fig 33). However, there is considerable disagreement between interpretations of experimental data. Tien Shan data can be fitted well with the calculations at nominal constant shower size but it

is not clear that in all cases proper consideration has been given in the calculations to primary energy spectra and fluctuations. Indeed, Tonwar (HE 4.1-11) has forcibly pointed out the differences between the measured parameters at various experiments (fig 34). The results depend critically

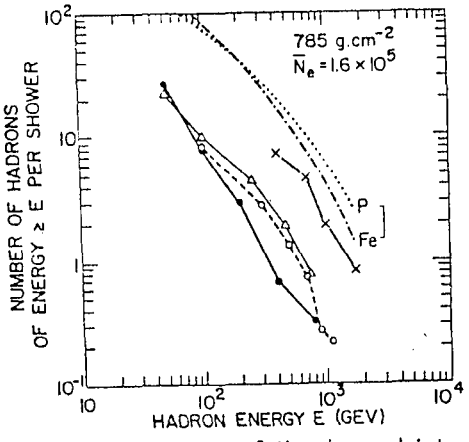

Figure 34: Comparison of the observed integral energy spectrum for high energy hadrons in air showers of average size ~1.6 x 10^5 at mountain altitudes

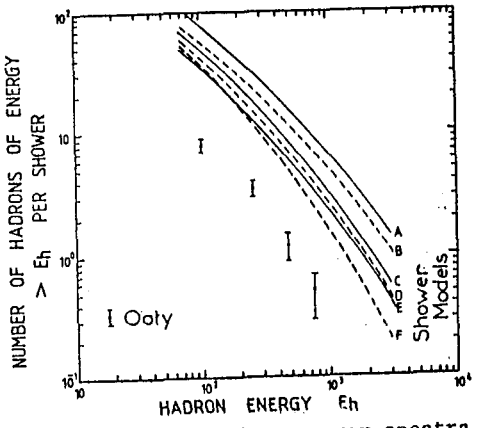

Fig 35. Measured hadron energy spectra and calculations presented in HE 4.1-11.

on how well individual hadron signals are resolved in the hadron detector. The clearest resolution, in the Tata Institute cloud chamber, gives the greatest discrepancy with calculation. Tonwar has been unable to find models which give adequate fits to the Tata data (fig 35). There is no clear route to a resolution of the discrepancies. The total experimental data as interpreted by the Tata group seems to be relatively consistent but observed high energy hadron numbers are then an order of magnitude below those expected from calculation. Conventionally measured muon and electron numbers are rather insensitive to changes in models for these highest energy interactions and discrepancies in the hadron models should not greatly affect many other air shower results.

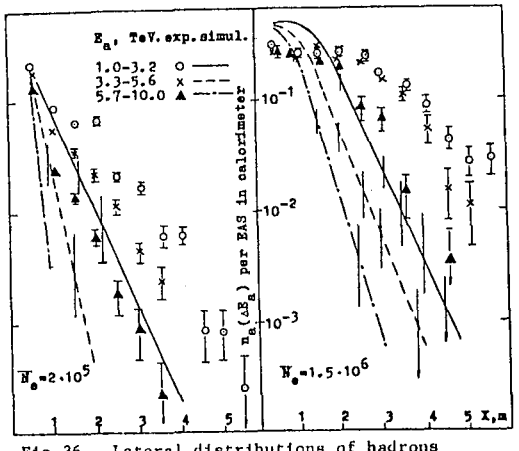

Fig 36. Lateral distributions of hadrons measured at Tien Shan compared to simulations using a scaling model. (HE 4.1-15)

Danilova et al (HE 4.1-15) examining hadron lateral distributions showed an apparent increase in large transverse momentum processes between 5×10^{14} eV and 10^{16} eV compared to those expected from lower energy accelerator p-p data (fig 36). Interestingly, the Leeds group (HE 4.2-15/16/18) have confirmed their observations of core flattening with increasing energy also in this range and thus require modification to conventional interaction models since any possible

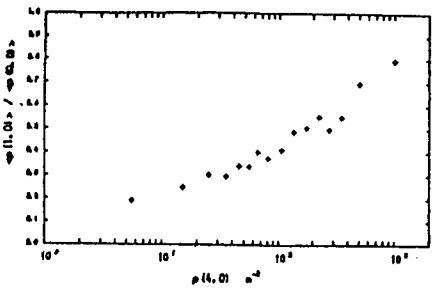

Fig 37. 'Core flattening' between 0 and 1.0m from the shower centre. The ordinate is a measure of the flatness of the lateral distribution near the core. The abscissa is a shower size parameter. (HE 4.2-10)

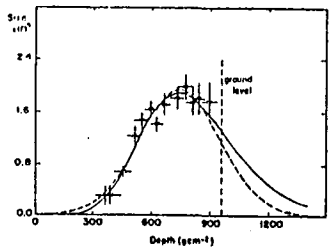

Fig 38(a). Longitudinal profile of an EAS observed by both Fly's Eye I and II simultaneously. (HE 4.4-1)

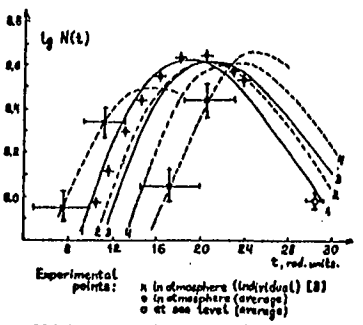

Fig 38(b). Cascade curves derived from Cerenkov pulse shape measurements. (HE 4.4-14)

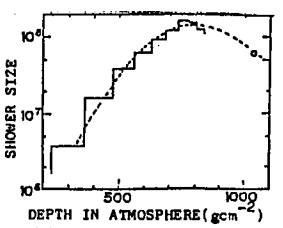

Fig 38(c). A shower curve determined from Cerenkov pulse shape. (HE 4.4-7)

composition changes appear inadequate for a straightforward interpretation of their data (fig 37). It would seem that it is necessary to ensure that a correct, broad, lateral distribution function must be included in discussions of hadron energy spectra, otherwise hadron numbers will be underestimated.

11. Cascade Functions

Many measurements we make on showers are samples of the complete shower electromagnetic cascade function. It is becoming possible to measure the complete cascade function of certain showers using atmospheric Cerenkov (Hara et al, HE 4.4-7, Fomin et al, HE 4.4-18), or air fluorescence techniques (Baltrusaitis et al, HE 4.4-1/2) (figure 38a, b, c). This study holds great promise for the next conference with the Fly's Eye group, in particular, accumulating large numbers of cascades (eg. fig 39). Already, direct measurements of E/N_{max} are becoming available for comparison with theory. The Fly's Eye group (HE 4.4-2) find

$$E_{TOT} = 1.31(\pm.14)(N_{max}/10^9)^{0.990\pm.05}$$

GeV which can be compared to the lowest value of $1.38\ N_{max}$ found in calculation by Wrotniak and Yodh (HE 4.1-2). Linsley (HE 4.4-5) has proposed the use of the function of the form

$$N = A\ \xi^q\ e^{-q\xi} \qquad (\xi = x/x_{max})$$

for fitting cascade functions and has described useful properties and applications of this function to air showers.

12. Shower Age

There is a good deal of circustantial evidence that the lateral distribution function of electrons is related to shower

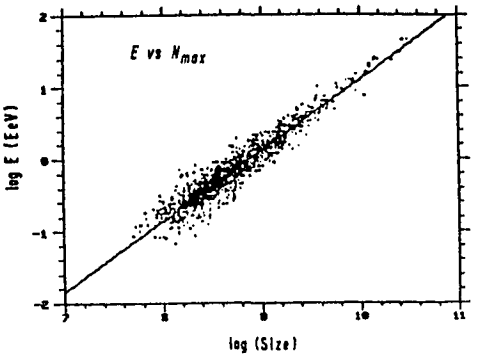

Fig 39. Scatter plot of total shower energy vs shower size at maximum as measured by the Fly's Eye. (HE 4.4-2)

development. This function, usually fitted by a N.K.G. function of age S, depends on zenith angle, shower size, (see eg., HE 4.3-4, Nagano et al 1984) and other development parameters such as the Cerenkov lateral distribution parameter b (B.R. Dawson private communication). It is unfortunate that S is not a simple parameter to use. It depends on core distance (Capdevielle and Gawin, HE 4.3-13), particularly close to the core ($\lesssim$ 10m) where it may also be affected by the transition effect, although the importance of the latter may not be great (Asakimori et al, HE 4.3-3). Close to array thresholds, the effect of selecting downward fluctuating (young) low energy showers may be seen (Chaudhuri et al HE 4.3-1).

Age probably depends on depth of maximum as $\sim 7.5 \times 10^{-4}$ per gcm (Nagano et al (1984), Fenyves et al, HE 4.3-14) and typical uncertainties are then ~0.05 - 0.07 (~70-100gcm^{-2}) so that in terms of differences in depths of maximum for iron and proton primaries discussed above, S has more potential than has yet been exploited. The problems of data sampling are now probably better understood for S than other more popular development parameters although the learning process may have damaged the reputation of age as an interesting parameter. It is particularly important to note that almost every shower can be assigned an age parameter and a data set complete in this sense is obtained.

It is not unusual to see detailed average lateral distributions fitted by NKG (S) functions for fixed shower size. I believe this process to be inappropriate because of large development (and presumably S) fluctuations for fixed Ne ; considerably distorted averages can be produced. It has been Adelaide experience in fitting lateral distributions by minimising chi-squared that the precise definition of the minimised function (in terms of observed or expected densities) can affect the fit (or absolute value of S) whilst the correct ranking in S is retained. Perhaps this should be remembered when data are compared between experiments.

13. Miscellany

Some topics in the conference are worthy of particular note as areas where progress in being made and further results should prove significant.

Constant Intensity Cuts and Attenuation Lengths

Serious efforts are being made to simulate constant intensity cuts in terms of interaction parameters and composition (Tanahashi, HE

4.1-3, Cheung and MacKeon HE 4.3-12, OG 5.2-12). This is particularly difficult for the muon component which depends on atmospheric angle as well as depth. Mixed compositions need to be simulated carefully. The use of muon data provides useful limits to the number of acceptable models.

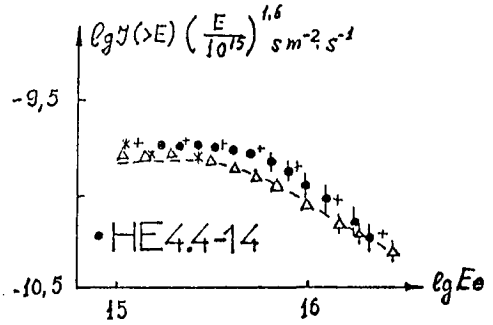

Fig 40. Integral energy spectra. The filled circles are from direct energy measurements. (HE 4.4-14)

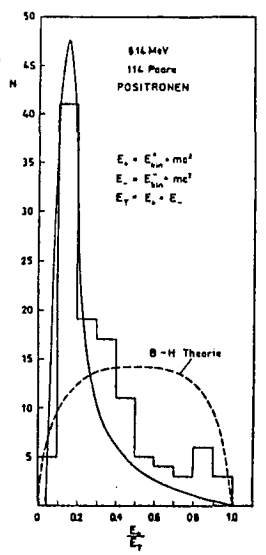

Fig 41. The positron spectrum of pairs created by 6.14 MeV gamma quanta. Note the high frequency of low kinetic energy positrons in contradiction to BETHE and HEITLER. The solid curves are as predicted by Bagge. (HE 4.4-8)

Energy Spectra

A comparison of energy and size spectra is very helpful, particularly close to the knee where detailed shape comparisons should give useful independent checks of composition models. There is a remarkable (perhaps even strange) agreement shown in HE 4.4-14 between very different techniques for deriving energy spectra (fig 40). The sharpness of spectra in Ne is often strange to me when noting that fluctuations must be taken into account.

Pair Creation Fundamentals

Bagge and his co-workers (HE 4.4-8) have been investigating deviations predicted by Bagge from the well known Bethe and Heitler theory of pair creation. The observed spectra of positrons and electrons in pair creation are shown in figure 41 and clearly deviate from the commonly assumed spectra.

Radii of Curvature

A knowledge of shower radii of curvature is important when designing fast-timing direction measurement systems. New information (fig 42) was presented in HE 4.7-15 and the radius

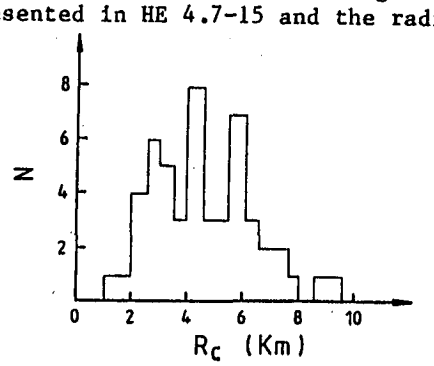

Fig 42. Shower radius of curvature distribution. (HE 4.7-15)

of curvature of the leading particles can be taken as constant at ~ 5km for core distances 200m-500m. It should be remembered that the shower front is complex with both muon and electron components and different techniques of sampling may give widely different results. As Atrashkevitch et al point out, the radius of curvature of the bulk of the particles in the shower front is likely to be much smaller, of the order of 1.5km.

Muon Charges

Moscow State University data showed no evidence for any deviation from unity of the ratio of positive and negative muon numbers.

TABLE 1

Numbers of positive I_+ and negative I_- muons.

	E_μ Gev	10-50	50-100	100-200	200-500	500-1000
r < 16 m	I_+	161	97	77	57	9
	I_-	164	91	82	56	9
r=16-32m	I_+	174	75	51	18	4
	I_-	159	68	43	15	0
r > 32 m	I_+	224	69	16	6	0
	I_-	206	61	15	6	1

14. Some Techniques

Many interesting techniques were described at the conference. Those selected below seemed to me to be particularly interesting or novel.

Fikushima et al (HE 4.2-6) described a PIN photodiode (10mm x 10mm) detection system for scintillator light from bursts (fig 43). At the present time photomultipliers are still required for small particle densities but PIN photodiode technology is clearly encroaching on their light detection area.

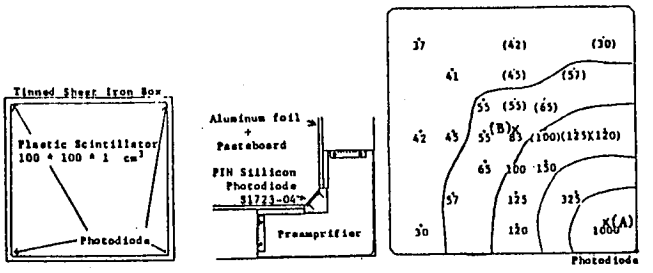

Fig. 43. Construction and uniformity of response of a scintillator burst detector using PIN photodiodes. (HE 4.2-6)

Hazen and Hazen (HE 4.7-7) described a digital "discriminator" technique for triggering when shower front particles are resolved in time and Ng (HE 4.7-9) described an antijitter constant fraction discriminator for fast timing even when these single pulses are rather slow.

Valtonen et al (HE 4.6-8) described their work on their position sensitive hadron spectrometer which should soon be operational.

Suga and his co-workers (HE 4.6-3) are studying the shape of the radio pulse (or the spectrum of radio pulses) in a rather direct way through real-time triggering of a fast fourier transform signal analyser when the shower arrives, eliminating man made frequencies from the signal, and inverting the transform to derive the original air shower pulse.

15. Some Brief Conclusions

(a) The composition shows no evidence for significant changes between 10^{15}eV (the knee) and 10^{19}eV. There is strong evidence for an early developing component and a mixed primary composition dominated by heavy nuclei when measured at constant energy.

(b) The use of shower size as an energy parameter has caused far too many problems of interpretation.

(c) The general properties of the longitudinal thickness of the shower front are well known. Linsley's suggestion of mini-arrays exploiting this parameter is worth pursuing but they will not replace conventional arrays.

(d) We cannot explain the detection by Samorski and Stamm of muon signals associated with gamma-ray showers.

(e) There is serious conflict between experiment and theory for high energy hadrons.

(f) Shower age (S) deserves more study as a shower development parameter.

(g) The measurement of complete cascade curves presents us with our best opportunity for understanding shower development.

16. References

Acharya, B.S., et al (1983) Proc 18th Int. C.R.C. (Bangalore), 9 191.
Grieder, P.K.F. (1984) Il Nuovo Cimento, 84A, 285.
Inoue, N. et al (1985a) J. Phys G: Nucl. Phys, 11, 657.
Inoue, N. et al (1985b) J. Phys G: Nucl. Phys., 11, 669.
Liebing, D.F. et al (1984) J. Phys G: Nucl. Phys, 10, 1283.
Linsley, J. (1983) Proc. 18th Int. C.R.C. (Bangalore), 12, 135.
McComb T.J.L. et al (1979) J. Phys. G: Nucl. Phys., 5, 1613.
Nagano, M. et al (1984) J. Phys. Soc. Japan, 53, 1667.
Nikolsky S.I. et al (1981) Proc 17th Int. C.R.C. (Paris), 2, 129.
Patterson, J.R., and Hillas, A.M. (1983) J. Phys. G: Nucl. Phys., 9, 1433.
Samorski, M. and Stamm, W. (1983a) Ap. J., 268, L17.
Samorski, M. and Stamm, W. (1983b) Proc 18th ICRC. (Bangalore), 11, 244.
Woidneck, C.P. and Bohm, E. (1975) J. Phys. A: Math. Gen., 8, 997.

MUONS AND NEUTRINOS

T. STANEV*
Physics Department, University of Wisconsin
Madison, Wisconsin 53706
and
Bartol Research Foundation, University of Delaware
Newark, Delaware 19716

INTRODUCTION

This conference comes at a time of major experimental developments in the underground physics. The first generation of large and precise detectors, some initially dedicated to search for nucleon decay, has accumulated significant statistics on neutrinos and high-energy muons. A second generation of even better and bigger detectors are already in operation or in advanced construction stage. The present set of experimental data on muon groups and neutrinos is qualitatively better than the one we had several years ago and the expectations for the following years are high.

The interpretation of these results, however, is far from complete. Most, if not all, of the particles observed underground are produced in cascades generated in the atmosphere by primary cosmic rays. Thus the data interpretation involves complex and time-consuming calculations of the cascade development, propagation to the detector through the surrounding rock and the detector response, which are not always consistently performed for each detector. The importance of such calculations increases with the increasing complexity of the investigated phenomenon and is, for example, crucial for the interpretation of muon groups.

The chemical composition of the cosmic-ray flux and the characteristics of the inelastic interactions in the atmosphere, two main assumptions in cascade calculations, vary widely from author or author. And while the composition is often the subject of the investigation, I do not see at the present time reasons for a drastic change of the interaction models from what is observed at accelerators. The $\bar{p}p$ collider at CERN, which works at equivalent laboratory energies up to 4.3×10^5 GeV, has established certain deviations from Feynman scaling such as energy-dependent cross section, $\ell n^2 s$ term in the average charged multiplicity and broadening of the multiplicity distribution with the energy, but has not found evidence for serious scaling violation in the fragmentation region.[1] The measurements extend to only $x \cong 0.05$, but

* On leave of absence from the Institute for Nuclear Research and Nuclear Energy, Sofia 1784, Bulgaria.

the total amount of energy released in such particles can be used[2] to estimate the behavior at higher x. Some uncertainty in the interaction model is introduced by the fact that the atmosphere provides a nuclear target and the transformation from pp to pN interactions is model-dependent. There is, however, enough lower-energy (up to 400 GeV) data, which can guide the required modification of the interaction models for hadron interactions on light nuclei.

In this talk I shall concentrate on three topics, which not only have significant scientific importance, but were also discussed at this conference by independent groups. They are:

- composition studies with underground muon groups,
- neutrino detection,
- expected extraterrestrial neutrino fluxes.

INVESTIGATION OF THE PRIMARY COSMIC-RAY COMPOSITION WITH UNDERGROUND MUON GROUPS

The studies of the chemical composition of the cosmic-ray flux at energy $> 10^{14}$ eV have produced one of the most contradictory sets of results in the whole field. The fluxes at such energies are low enough not to permit statistically adequate direct measurement and the indirect evaluations from cascade properties such as depth of maximum and muon-to-electron ratio did not allow unique interpretation and produced vastly different results.[3]

It does not seem possible from air shower data to judge even such distinctly different models as the proton-dominated light composition, suggested by J. Linsley[4] and the more conservative composition derived by G. B. Yodh and collaborators[5] from studies of delayed hadrons in air showers, which contains an increasing with the energy fraction of heavy nuclei.

The sensitivity of the muon groups to the composition arises from the different muon yields from nuclei of different mass and the same total energy. Figure 1 shows the average number of muons produced at depth 4 km.w.e. (effective $E_\mu \geq 2.1$ TeV) by protons and iron nuclei. The yield of an iron nucleus is zero before the energy per nucleon exceeds E_μ and rises faster than the proton one until an asymptotic behavior is established. The following features of the production of high-energy muons have been established in numerous Monte Carlo studies:[6]

1. $N_\mu(> E_\mu) = \frac{kA\sec 0}{E_\mu}\left(\frac{E_\mu}{E_0/A}\right)^\alpha\left(1-\frac{E_\mu}{E_0/A}\right)^\beta$ is the Elbert's formula relating the muon yield to the primary energy and mass. The sec0 dependence of the yield holds up to 60°.

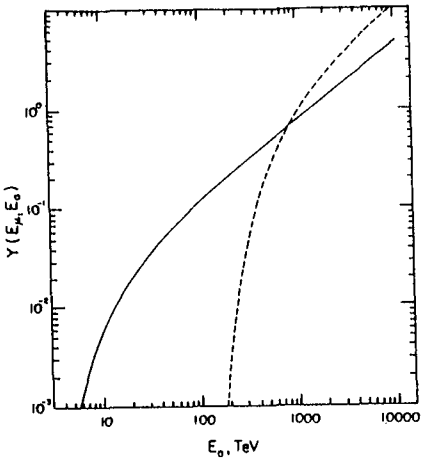

Fig. 1. Muon yields from primary protons (solid line) and iron nuclei (dash line) at depth of 4 km.w.e.

2. The muon multiplicity distribution in a single shower is very close to and can be approximated with a Poissonian.

3. The lateral distribution of muons depends on the primary energy per nucleon E_0/A and the cross section, which leads to an explicit A dependence.

The knowledge of the lateral distribution is very important in view of the fact that most detectors are not much bigger than the average muon radius and thus suffer from confinement problems. The detected number of muons is only a fraction of the total multiplicity of the muon shower, which depends on the exact shape and resolution of the detector. The detection efficiency cannot be accounted for without extensive Monte Carlo study.

Three experimental groups presented results on the primary composition from observation of muon groups. The NUSEX group [OG 5.1-5] compares the observed muon multiplicity distribution (Fig. 2) with predictions for compositions, characterized by different spectral indexes of the iron component. The plotted prediction lines account for the detection efficiency and the slant depth variation with the zenith and azimuthal angle of the event.

The conclusion from the experiment is that the spectral index of the iron component, which fits the data best, is 2.7 and data do not agree with iron spectrum flatter than $E^{-2.6}$.

The Frejus group [HE 5.1-1] shows its first results on muon groups. This detector is impressive in both size and resolution and has collected significant statistics in a short time. Cascade calculations have indicated to the Frejus group that the ratio of events with $N_\mu \geq 7$ to $N_\mu = 4$, 5 and 6 is a good measure of the composition. The experimentally measured ratio is $\frac{N(\geq 7)}{N(4+5+6)} = 0.14 \pm 0.04$, which is in good agreement with a proton-dominated composition.

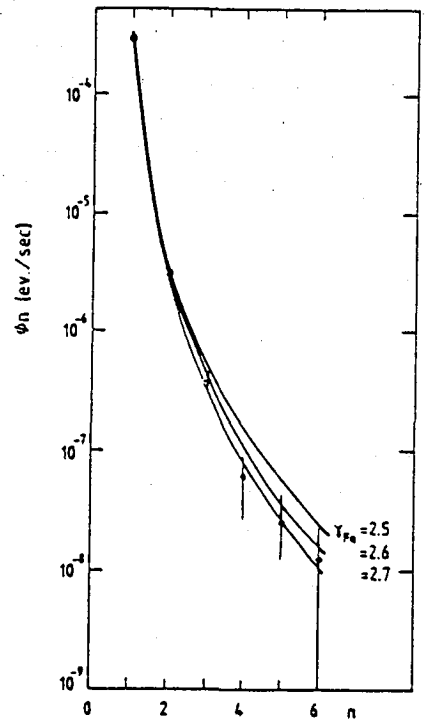

Fig. 2. Comparison of NUSEX rate of muon groups of multiplicity n to predictions from compositions with different spectral index for iron.

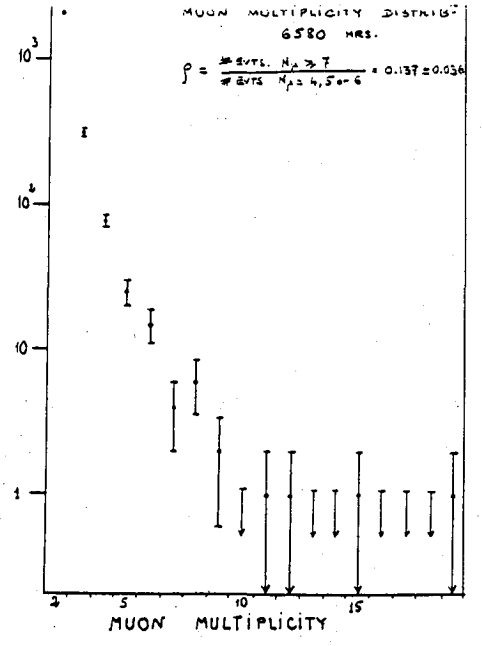

Fig. 3. Muon multiplicity distribution measured at Frejus.

The Baksan group has used two methods to derive the composition. The first one is similar to the approaches of the two other groups [HE 5.5-12]. Figure 4 shows the multiplicity distribution in the detector compared with predictions for pure compositions of different A (solid lines) and two composition models. A light energy-independent composition with $\langle A \rangle = 3.5$ best fits the data. $\langle A \rangle = \sum \beta_i A_i^2 / \sum \beta_i A_i$, where β_i is the fraction of nuclei with mass A_i on *E/nucleon* basis.

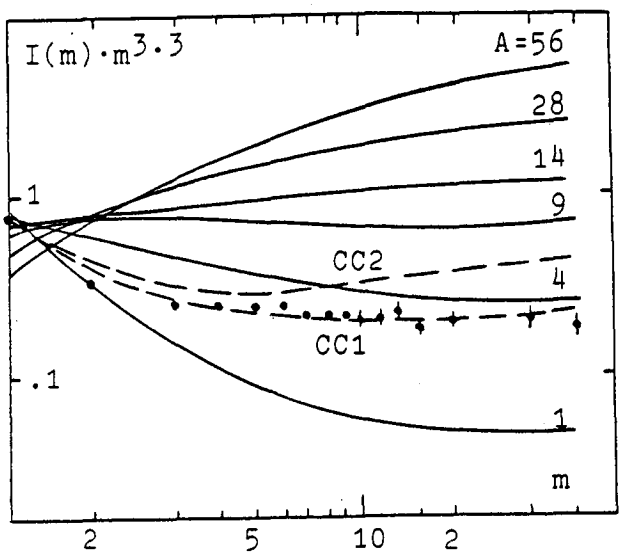

Fig. 4. Comparison of Baksan multiplicity distribution with predictions from pure (solid lines) and mixed compositions.

Note that because of the relatively shallow and large detector ($E_\mu > 0.22$ TeV) the observed multiplicities reach very high values.

The second approach is more interesting, because it involves an estimate of the primary energy [HE 5.1-13]. It is based on a calculated relation of the energy of the muon-induced showers in the detector to the primary energy per nucleon, which fits some other properties of the detected muon groups.

Figure 5 shows the observed dependence of the muon multiplicity N_μ on the primary energy E_0/A estimated through the energy of muon-induced showers in the detector. Curve 2 corresponds to a composition with $\langle A \rangle = 3.5$ and curve 3, which seems to fit data quite well, has $\langle A \rangle = 4.5$.

The conclusion from both approaches is that the primary composition does not change with energy and is dominated by protons up to 10^{15} eV.

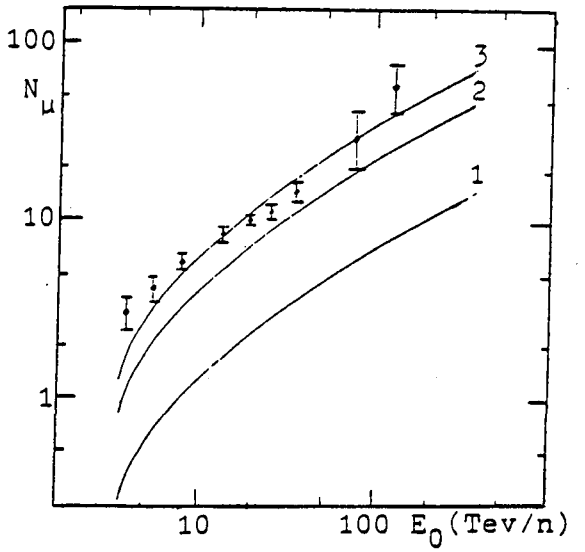

Fig. 5. Muon multiplicity at Baksan *vs.* the primary energy per nucleon. Curves correspond to compositions with $\langle A \rangle = 1$, 3.5 and 4.5.

The conclusions of all groups seem to agree with each other, although the results are expressed in different terms, and do not cover the same energy range. It would be helpful to compare the conclusions quantitatively with each other.

All conclusions are drawn from the fact that the heavy nuclei are more efficient in muon production than protons. The asymptotic behavior of the muon yield is

$$N_\mu(> E_\mu) = \left(\frac{k}{E_\mu}\right) A \left(\frac{A E_\mu}{E_0}\right)^{-0.78} \propto A^{\frac{1}{4}}$$

for equal zenith angle θ and muon energy E_μ. Since $A^{\frac{1}{4}}$ is a slowly increasing function of A, the sensitivity is not very big even for the asymptotic region, which is only partially examined in the experiments.

It seems reasonable to use as a common representation of all composition models one very simple parameter $R = \frac{L}{H}$, which is the ratio of the protons and α particles in a composition to all heavier nuclei. For energy-independent compositions $R = \text{const}$ and specifically $R \cong 2$ for the region where direct measurements are available. The energy-dependent compositions of Refs. 4 and 5 have the following R values at total energy 10^5 and 10^6 GeV:

Model	10^5 GeV	10^6 GeV
JL (Ref. 4)	1.89	2.85
MDII (Ref. 5)	0.74	0.34

Let us now calculate R for the compositions which best fit the experimental data. The two compositions favored by the Baksan results give $R = 1.7$ ($\langle A \rangle = 3.5$) and $R = 1.1$ ($\langle A \rangle = 4.5$). The only serious criticism I have of this experiment is that the interpretation does not account for the mass dependence of the muon lateral spread. The average muon spread used in the analysis is $\approx$ 13 m for vertical muons of $E = 0.22$ TeV, comparable to the dimensions of the detector, which is obviously not free from containment problems. The bigger lateral spread of iron showers might make the detector less efficient for their detection and decrease its sensitivity to composition.

The NUSEX result translates only into a limit $R \geq 0.7$. The reason is that the reference composition is already very heavy and the addition of more iron nuclei does not change significantly its basic property. The heavy reference composition also explains the low sensitivity to the iron fraction, which is obvious from Fig. 2. Despite the containment problems, the data set of NUSEX is one of the best available and certainly deserves a new analysis and comparison with lighter composition models.

The Frejus data give $R \lesssim 2$. The data set is relatively free from containment problems, but the presented interpretation has to be considered preliminary. I am not convinced that muon multiplicities $N_\mu \geq 7$ and $N_\mu = 4$, 5 and 6 reflect different components of the primary cosmic ray flux. Particularly the lower multiplicity group invevitably contains an admixture of events, generated by heavy primaries. It would probably be better to compare the multiplicity distribution with predictions of different models. Due to its big dimensions and excellent resolution, the Frejus detector is perfect for investigation of muon-induced showers. An attempt to estimate the primary energy from the energy released in the detector, in Baksan fashion, might give an additional handle on the composition problem.

Formally the papers presented at the Conference limit the value of our simple parameter $0.7 < R \leq 2$, an uncertainty not as bad as the spread of the values derived from different air shower properties. The existence of new large and precise detectors, such as Frejus and Homestake, which can collect statistics at a fast rate supports an optimistic view that with proper efforts in data analysis and interpretation the value of R will soon be determined with a reasonable precision of approximately 0.2 from measurements of underground muon groups.

NEUTRINO DETECTION

The worldwide statistics of neutrinos has been steadily growing in recent years. Table I shows the number of contained neutrino events in different detectors. Contained events are produced by neutrino interactions in the detector and the requirement for full containment is that all resulting tracks, as well as the vertex, are confined to the detector volume. Stars denote results, discussed at this conference.

Table I. Worldwide statistics on contained ν events, including nucleon decay candidates.

Experiment	Full containment	Vertex containment
IMB*[HE 5.3-7]	401	
KAMIOKANDE	107	
NUSEX*[HE 6.2-6]	32	
Frejus* Not in printed paper	13	21
KGF* Not in printed paper	19	40

Because of containment and flux restrictions, such events are produced by neutrinos of energy less than several GeV. The rate of such events can be calculated as

$$\text{Rate} = \sum_{i} \int_{E_i} \int_{E_\nu} dE_i \, dE_\nu \, \frac{dN_\nu}{dE_\nu} \, \frac{d\sigma}{dE_i} \, \epsilon_i(E_i) \, ,$$

where dN_ν/dE_ν is the neutrino flux, which we assume consists of atmospheric neutrinos only, $\frac{d\sigma_i}{dE_i}$ is the cross section for production of the i particle in a neutrino interaction and $\epsilon_i(E_i)$ is the energy-dependent detection efficiency for the i particle.

The atmospheric neutrino flux in the energy range responsible for contained events has been calculated by several authors.[7] The most recent calculation takes into account both the temporal and location variation of the neutrino flux.

The temporal variation is due to the solar modulation of the primary cosmic-ray flux and thus follows (with some delay) the 11-year variation of solar activity. Maximum flux is achieved about $1\frac{1}{2}$ years after solar minimum.

The cosmic-ray flux is further modulated in interaction with the geomagnetic field. Penetration through the field around the magnetic poles requires

less momentum than around the magnetic equator, so that the geomagnetic cut-off varies from a fraction to several tens of GV. Integrated over all zenith and azimuthal angles the influence of the geomagnetic field not only produces different fluxes at different experimental locations, but also affects the angular distribution of neutrinos at every given location.

Figure 6 shows the angular distribution of neutrinos with three different energies, calculated as in Ref. 7(e) for the location of the IMB experiment. While the angular distribution of the lower energy (0.2–0.4 GeV) neutrinos is very strongly affected by the geomagnetic field, its influence is negligible for $E_\nu > 2$ GeV. At higher energy the angular spread is only due to the different atmospheric thickness and structure at different angles.

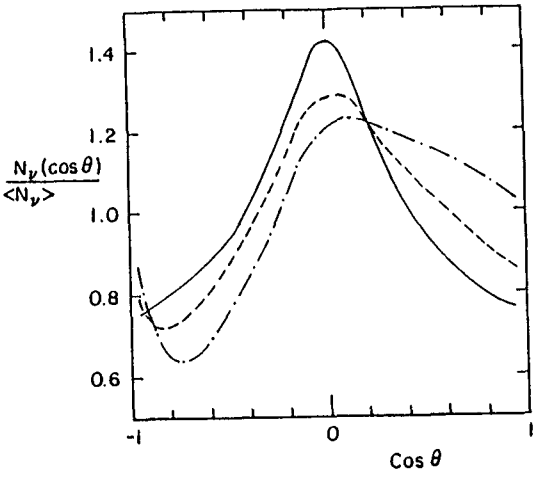

Fig. 6. Neutrino angular distribution at the site of the IMB experiment. Curves are for neutrinos of energy 0.2–0.4 GeV (dot-dash), 0.8–1 GeV (dash) and 2–3 GeV.

The cross sections in the energy range of interest here are well known for neutrino-nucleon scattering. All experiments, however, have nuclear targets, ranging from water to iron. Neutrino-nucleus cross sections are not well known and they induce an additional uncertainty in the calculated rates. As far as the majority of data on neutrinos of $E > 300$ MeV, however, this uncertainty is not very large, because in this range the nuclear cross sections are not expected to deviate very much from the cross section on free nucleons.

The detector response to the products of the neutrino interactions is studied at best by direct calibration in an accelerator beam (which was done for a fraction of the NUSEX detector) or by an extensive Monte Carlo study of the detector, as performed by the other groups.

The IMB collaboration operates an extremely large water Cherenkov detector with fiducial volume of 3.3 kt. Data from 420 days of running time has been analyzed, which gives a total exposure of 3.8 kt.yr. During that time 401 contained neutrino events have been observed, which with an overall efficiency of 0.80 gives a rate of 132 ν/kt.yr. Figure 7 shows a comparison of the experimentally observed neutrino energy spectrum in single-prong events[8] with a theoretical prediction, which combines the flux calculation of Ref. 7(e), averaged over all angles, with a detector Monte Carlo. The same approach, however, does not fit the neutrino angular distribution well, which requires a better account for the geomagnetic effect. This is shown on Fig. 8, which compares data with calculated spread in terms of $\log(E/L)$ where L is the distance to the neutrino production point, taken to be at an altitude of 20 km and corresponding to a unique zenith angle. An isotropic distribution reverses the heights of the two peaks, which reflect the solid angle subtended.

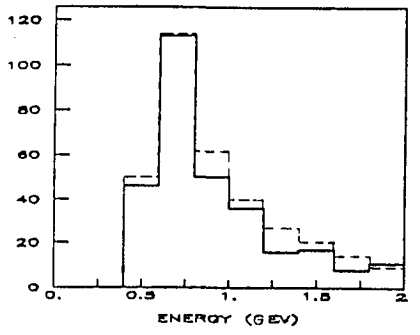

Fig. 7. Comparison of the measured neutrino energy spectrum for single-prong events (IMB) to a detector Monte Carlo (J. LoSecco) using the flux of Ref. 7(e).

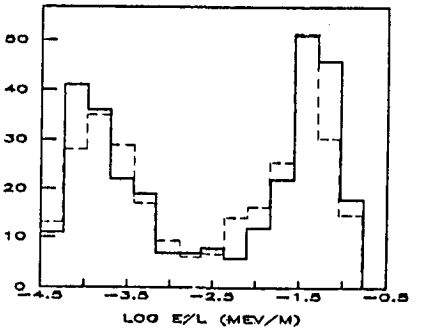

Fig. 8. Comparison of neutrino angular distribution (IMB) to the calculated in Ref. 7(e). No detector Monte Carlo. See text for definition of L.

The NUSEX detector is a cube of 3.5 m side and total mass of 150 tons. The active part of the detector consists of 43,000 plastic streamer tubes interspersed with 136 horizontal iron plates each 1 cm thick. Typical space resolution of the detector is 1 cm, but both resolution and trigger efficiency are anisotropic because of the horizontal arrangement. The operation time of the detector is 23,440 h, which gives a total exposure of 401 t/yr in which 31 contained events with visible energy $E_{vis} > 250$ MeV are detected. The neutrino rate, calculated with correction for the trigger and containment efficiency on an event-by-event basis, is 152 ± 20 ν/(kt.yr) and the ν_e/ν_μ ratio comes to a rather small value of 0.28 ± 0.11.

The apparatus of the Frejus group (fully completed in July 1985) is a big tracking detector with dimensions $6 \times 6 \times 12.3\,m^3$ and average density of 2.1 g/cm^3. A very high space resolution is achieved with 10^6 $0.5 \times 0.5\,cm^2$ flash tubes, triggered by 4×10^4 Geiger tubes. The arrangement of the sensitive and passive (1.5 mm thick iron plates) is vertical, so that the triggering efficiency is once again not isotropic. The neutrino statistics are collected with a fiducial mass of 585 tons and total exposure of 289 t.yr. A total of 22 neutrinos is observed, 14 of which are fully contained in the fiducial volume. Taking into account the average trigger and scanning efficiency this gives a rate of charge current events of 97 ± 25 ν/kt.yr. The observed ν_e/ν_μ ratio is 0.64 ± 0.30.

The prediction of Ref. 7(e) for both NUSEX and Frejus detectors, which are located nearby, is 120 ν/kt.yr for solar maximum, and the uncertainty of the calculation is at least 10%. The predicted ν_e/ν_μ ratio is 0.64.

To compare the results of NUSEX and Frejus one has first to substract the contamination of the neutral current, which from Frejus data is $\sim$ 15%, from the NUSEX rate. Then both rates agree within 1σ—a quite good agreement keeping in mind the difficulties in accounting for the efficiency and the difference in the way it is performed for the two experiments.

The difference in the measured ν_e/ν_μ ratio is more surprising. Apart from the low statistics, the efficiency for observing μ decays is low and the experiments have to rely on the shape of the track to distinguish between electrons and muons. There are some indications from the detector with higher resolution (Frejus) that some electron tracks at $E \sim 200$ MeV would look very much like muon tracks.[9] If some electron tracks were misinterpreted and counted as muons, this would cure not only the ν_e/ν_μ ratio, but also the apparent lack of low-energy electron neutrinos in the NUSEX energy spectrum.

The rate of contained events at KGF, as can be concluded from Fig. 1 of HE-6.2-3, is also in good agreement with their prediction for atmospheric neutrinos.

The conclusion, which can be drawn from the results on contained neutrino events, presented at this conference, is that all observations are compatible with the hypothesis that all observed neutrinos are of atmospheric origin. In addition to the rates, the analysis of the angular distribution, performed by J. LoSecco, shows that the account for the geomagnetic effect improves the agreement with data.

The statistics are, however, still low and the statistical errors alone give us room for some hopes for more exciting physics, some of which is contained in the next topic.

NEUTRINO FLUXES EXPECTED FROM EXTRATERRESTRIAL POINT SOURCES

The recent observations of γ rays with $E \geq 10^{15}$ eV from point sources[10] have increased the hopes for a working experimental neutrino astronomy. The idea has been suggested by different authors.[11] Cosmic-ray nuclei of very high energy interact within the clusters of matter, which we know exist in the universe, and produce neutrinos through the decay of the secondary particles. Only recently, however, we have observed γ rays with energy so high that the only reasonable production mechanism is $\pi^\circ \rightarrow 2\gamma$ decay and subsequent electromagnetic cascading. In a stellar environment a large fraction of the charged pions and kaons generated in the same interactions will necessarily decay and give rise to neutrinos.

Such neutrino fluxes are expected to be low and the only reasonable way of detection is the use of the Earth as a target for neutrino interactions. Only muons have long enough range to survive to the detectors and only the interaction $(\bar{\nu}_\mu) + N \rightarrow \mu + X$ is of practical interest. In order to calculate the observable quantity, which is the flux of neutrino-induced muons, one has to fold the neutrino flux dN_ν/dE_ν with the neutrino cross section $d\sigma/dE_\mu$ and integrate over the muon range. The double differential flux is[12]

$$\frac{dN_\mu}{dE_\mu dE_\nu} = \rho N_A \int_0^\infty dX \int_{E_\mu}^{E_\nu} dE'_\mu \, g(X, E_\mu, E'_\mu) \frac{d\sigma}{dE'_\mu} \frac{dN_\nu}{dE_\nu} ,$$

where $g(X, E_\mu, E'_\mu)$ is the probability that a muon generated with E'_μ will have energy E_μ after path X in rock. Three calculations of muon fluxes, induced by neutrinos from extraterrestrial point sources were presented at the conference.

Berezinsky, Castagnoli and Galeotti [HE 5.3-15/16] first calculated the neutrino production at a standard source. A standard source in their definition is a source of accelerated particles, embedded in a gas cloud of column density $x >> 70$ g/cm^2 and in the same time transparent to neutrinos. The flux of neutrino-induced muons is calculated from the neutrino flux at Earth using the average muon energy loss in rock and a neutrino cross section derived from the structure functions of Ref. 13.

The output from this calculation is the rate of muons with energy $> E_\mu$ in a 100 m^2 detector from a source of proton luminosity $L_p = 10^{43}$ erg/s at a distance 10 kpc as a function of the proton integral energy spectrum index γ. Table II shows some of the calculated rates for $E_\mu > 10$ GeV which depend very strongly on the value of γ.

Table II

$\gamma =$	1.1	1.2	1.4	1.6	1.8	3.0
$N_\mu(E > 10$ GeV)	1200	690	130	23	4.7	1.1

For sources at different distances and luminosities the calculated rates have to be appropriate scaled.

Gaisser and Stanev [HE 5.3-17] employ an entirely different approach. A model of the X-ray binary source[14] consisting of a pulsar and companion star is combined with a particular density model of the companion star, in which accelerated protons produce "star showers". The star properties vary with the phase and the neutrino attenuation in the star is accounted for. Fig. 9 shows a comparison of the neutrino flux from the source ($L_p = 10^{39}$ erg/s, $R = 10$ kpc) with the atmospheric ν_μ flux.

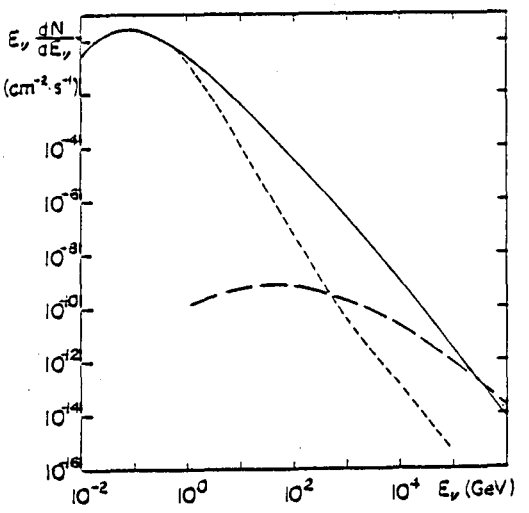

Fig. 9. Neutrino flux from Cygnus X=3 compared with the atmospheric flux (solid line). Dashed line is an estimate of the atmospheric background assuming detector resolution of 1°. For E_ν below about 1 TeV angular resolution is dominated by scattering angle in charged current neutrino interaction rather than by detector resolution.

Folded with the neutrino cross section (using two different structure functions) and muon propagation in rock the result for $\gamma = 1$ is

$$\text{Rate} = 10^{-3} \frac{L_{39}}{R_{10}^2} \text{ events/m}^2 \text{ yr}$$

and scales with the luminosity and the inverse square of the distance.

This rate is in agreement with the result of Berezinsky *et al.* for $\frac{1}{4}$ sr beaming of the proton beam and also with results of other recent calculations.[15] A remarkable consequence of the agreement between different calculations is that the expected neutrino-induced muon rate from point sources is not very sensitive to the conditions at the source. It confirms the conclusions of Ref. 16 that for target densities $< 10^{-6}$ g/cm^3 and thicknesses $\lesssim 100$ g/cm^2 the neutrino-induced muon rate varies only by factors of two or three. The new calculations also confirm the conclusions of Stenger[11] that the muon rate does not depend strongly on the muon detection threshold energy which favors large and not densely instrumented detectors such as DUMAND. The expected rates are very close to being observable by the proposed MACRO experiment [HE 6.1-4] with a sensitive area > 1000 m^2. Ten events per year in such a detector require for a source distance 10 kpc a proton luminosity $L_p > 10^{40}$ erg/s for 4π emission and correspondingly less if the emission is beamed.

In a related paper [HE 5.3-12] the MACRO collaboration has studied the detector response to point source neutrino fluxes and determined the minimum detectable neutrino flux as a function of the neutrino energy spectrum which for $\gamma = 1$ is 2.10^{-8} erg/cm^{-2} s^{-1}. The minimum detectable flux grows very rapidly with γ not only because of the importance of the production of high-energy (*i.e.* long-range) muons, but also because low-energy muons rapidly scatter out of the 1° cone, determined by the experimental resolution.

The location of the MACRO detector is suitable for observation of neutrino emission of X-ray binaries from the southern say, such as Vela X-1 and LMC X-4.

The general conclusion from the calculations of neutrino fluxes from X-ray binaries is that if the neutrino emission of these objects has a flat energy spectrum, similar to that of the observed UHE γ rays, weak signals from such objects are expected in 1000 m^2 detectors. This is especially true for faraway sources, such as LMC X-4 (estimated distance 50 kpc) whose γ-ray flux is degraded in interactions on the 3° background radiation.[17]

ACKNOWLEDGMENTS

This work was supported in part by the U. S. National Science Foundation and the U. S. Department of Energy under contract DE-AC02-76ER00881.

BRIEF NEWS

- Muon energy spectrum seems still quite steep above 1 TeV: $\gamma_{diff} \sim 4$ at Baksan [HE 5.1-15] and Artyomovsk [HE 5.1-6].
- Large surface-underground telescope is in operation at Homestake. A surface shower array will estimate shower energy, accompanying high-energy muons, and help with composition studies [HE 6.1-9].
- Muon photoproduction cross section may be a factor of 3 higher at $E_\mu \sim 10$ TeV [HE 5.4-12].
- New large liquid scintillation detector (90 tons) is operated in Mont Blanc Laboratory by INR (Moscow) and the Torino group [HE 5.3-6].
- Matter effects totally modify expectations for ν oscillations [HE 5.3-9/10].
- Testing continues at DUMAND. Important test with three detector strings (triad) is scheduled for 1986.
- No ν-induced (upward-going) air showers have been seen by the Fly's Eye above 10^{17} eV [HE 5.3-1].
- No evidence for ν oscillations from IMB data [HE 5.3-7].
- No young μ-poor showers at $\theta > 70°$ seen at Akeno—charm and heavier flavor cross section must be < 1 mb [HE 5.2-12].

REFERENCES

1. See, *e.g.*, J. Rushbrooke, talk at Inter. Europhysics Conf. on High Energy Physics, Bari, Italy, 1985, and UA5 talks at this conference.
2. T. K. Gaisser, Phys. Lett. B100, 425 (1981).
3. R. W. Clay, rapporteur talk at this conference.
4. J. Linsley, Proc. 18^{th} Inter. Cosmic Ray Conf., Bangalore, 1983, ed. by N. Durgaprasad *et al.* (Tata Institute of Fundamental Research, Bombay, 1983), vol. 12, p. 135.
5. For a description of the composition which fits data best, see G. G. Yodh *et al.*, Proc. ICOBAN '84, Park City, Utah, ed. by D. Cline (Univ. of Wisconsin, 1984).
6. J. W. Elbert, in Proc. DUMAND Summer Workshop, La Jolla, ed. by A. Roberts, (Scripps Institution of Oceanography, La Jolla, 1979), vol. 2, p. 101; T. K. Gaisser and T. Stanev, NIM, A235, 183 (1985).
7. (a) A. C. Tam and E.C.M. Young, in Proc. 11^{th} ICRC, Budapest, 1969, Acta Phys. Hung. 29, Suppl. 4, 307 (1970);

(b) E.C.M. Young, in *Cosmic Rays at Ground Level*, ed. by A. W. Wolfendale (Hilger, London, 1973), p. 105;
(c) J. L. Osborne, S. S. Said and A. W. Wolfendale, in Proc. Phys. Sco. London 86, 93 (1976);
(d) L. V. Volkova, Yad. Fiz. 31, 1510 (1980)[Sov. J. Nucl. Phys. 31, 784 (1980)];
(e) T. K. Gaisser *et al.*, Phys. Rev. Lett. 51, 223 (1983); T. K. Gaisser and T. Stanev, in Proc. SWOGU, Minneapolis, 1985, ed. by S. Rudaz and T. Walsh, in press.

8. Details of conversion from visible lepton energy are given in J. M. LoSecco *et al.*, Phys. Rev. Lett. 54, 2299 (1985).
9. B. Degrange and F. Raupach, private communication (1985).
10. For the most recent review, see A. A. Watson's rapporteur talk at this conference.
11. See, *e.g.*, D. Eichler, Nature 275, 725 (1978); V. S. Berezinsky, in Proc. DUMAND Summer Workshop, 1979, ed. by L. Learned; V. J. Stenger, Ap. J. 284, 810 (1984) and references therein.
12. T. K. Gaisser and T. Stanev, Phys. Rev. 30, 985 (1984).
13. D. W. Duke and J. J. Owens, Phys. Rev. 30, 49 (1984).
14. W. T. Vestrand and D. Eichler, Ap. J. 261, 251 (1982).
15. E. W. Kolb, M. S. Turner and D. W. Walker, Phys. Rev. 32, 1145 (1985); G. Auriemma, H. Bilokon and A. F. Grilo, in Underground Physics '85, St. Vincent, Italy, 1985.
16. T. K. Gaisser and T. Stanev, Phys. Rev. Lett. 54, 2265 (1985).
17. G. Cocconi, CERN preprint, 1985; T. K. Gaisser, in New Particles '85, Madison, ed. by V. Barger, D. Cline and F. Halzen.

GROUND-BASED VERY HIGH ENERGY GAMMA RAY ASTRONOMY - OBSERVATIONAL HIGHLIGHTS.

K E Turver
Department of Physics,
University of Durham, Durham DH1 3LE, UK.

It is now more than 20 years since the first ground based gamma ray experiments involving atmospheric Cerenkov radiation were undertaken. The present highlights in observational ground-based very high energy (VHE) gamma ray astronomy and the optimism about an interesting future for the field follow from progress in three areas:-

(i) the detection at increased levels of confidence of an enlarged number of sources so that at present claims have been made for the detection, at the 4-5 sd level of significance, of emission from 8 point sources (Cen A in 1973 [1] and more recently Crab pulsar[2], Crab nebula[3], Vela pulsar[4], Cygnus X-3[5,6,7,8], Hercules X-1[9,10,11], 4U0115+63[12], PSR 1953 (COS B source 2CG065 ?)[13],) plus three reports of diffuse emission from the galactic plane[14,15,16]

(ii) the replication of the claimed detections (e.g. Cygnus X-3[5,6,7,8], Her X-1[9,11]) with, for the first time, confirmation of the nature and detail of the emission; we are also seeing the beginnings of the detailed studies of the emission (e.g. Cygnus X-3[17], Crab pulsar[18]).

(iii) the extension of gamma ray astronomy to the ultra high energy (UHE) domain (10^{14-16}eV) with numerous reports of Cygnus X-3[19,20] and single reports of Her X-1[21], and yet to be confirmed at either VHE or UHE, Vela X-1[22] and LMC X-4[23].

At an energy around 1000 GeV (VHE) all observations employ the ground based atmospheric Cerenkov light technique[24]. The higher energy studies around 100-10000 TeV (UHE) involve air shower detecting arrays usually involving particle detectors (the Fly's Eye detector operating in the Cerenkov mode is an exception).

The pattern, if any, to emerge from the list of sources claimed so far is that X-ray binary sources (with or without a pulsar as the collapsed object) appear to be copious emitters of gamma rays over at least 4 decades of energy. Looking in more detail at these X-ray sources which behave as VHE and UHE gamma ray emitters:-

(a) CYGNUS X-3. This is a very topical object which will be mentioned frequently during this Conference. It is also the source which has been most involved in the development of the present subject in recent years. Following the radio outburst in 1972, Stepanian at hte Crimean Astrophysical Observatory reported the first of a series of detections of 1000 GeV gamma rays from the object. Initially (1973) these were detections of a DC signal[25], with the first indications at VHE gamma ray energie of the now well known X-ray periodicity at 4.8 hr following in 1975[26]. Since then similar detections at energies of 1000 GeV or thereabouts have been made by 5 groups (Tien Shan[27], FLWO/Dublin[5], FLWO/Dublin/Durham/Hawaii/Iowa/Hong Kong[7], JPL/Iowa/UCR[6], and Durham at Dugway,Utah[8]). Typical measurements made since 1980 are shown in Figure 1.

An Invited Highlight Paper Presented at
19th International Conference on Cosmic Rays
San Diego, 11-24 August 1985.

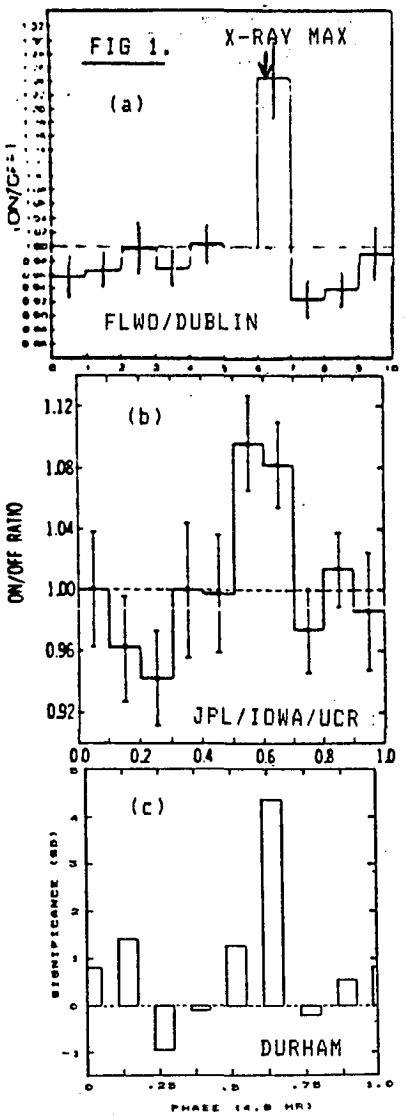

A similar story emerges from all of these observations made through the early 1980s - intermittent emission (the chance of observing during the ON state seems to be about 1 per 10-20 4.8 hr cycles ?) with a peak flux of about $10^{-10}cm^{-2}s^{-1}$ for energy > 1000 GeV always about the phase 0.62 in the 4.8 hr period corresponding to X-ray maximum, and lasting for a short time, about 10 min or so[8]. In addition there have been suggestions of time variability in the emission which is either sporadic or perhaps regular with long term periodicity involving the complete modulation of the VHE intensity (the long term period may be about 19 days - which is interpreted as possibly arising from apsidal motion according to the X-ray observations- has been mentioned in the context of radio, X- and VHE gamma rays).

At the highest energies the discovery by the Kiel group of a similar 4.8 hr modulated emission at an energy around $10^{15}eV$ [19] has been followed by other confirmatory analyses of the databases of many air shower arrays ([20], but with possible variability in the strength and a definite change in the 4.8 hr phase of the emission being suggested by later observations - see Figure 2.

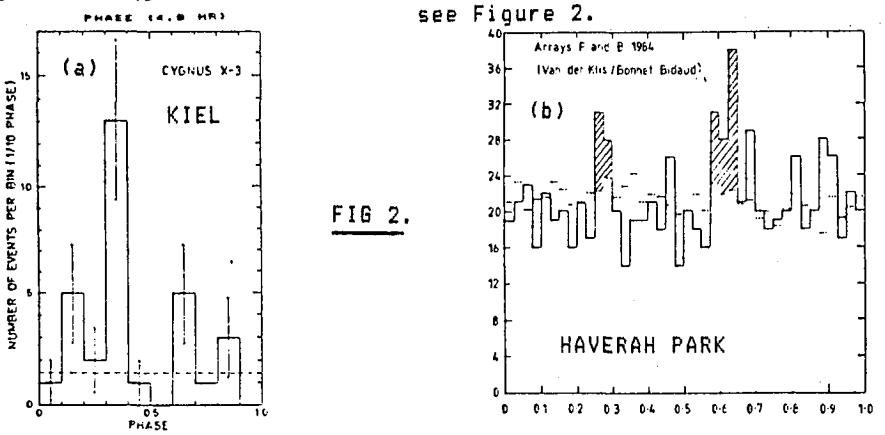

FIG 2.

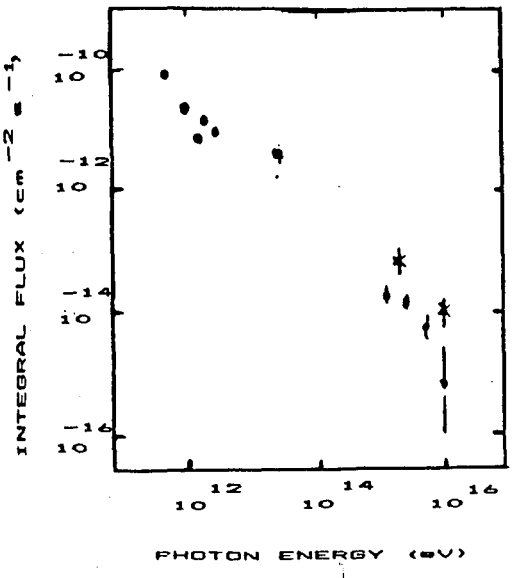

FIG 3.

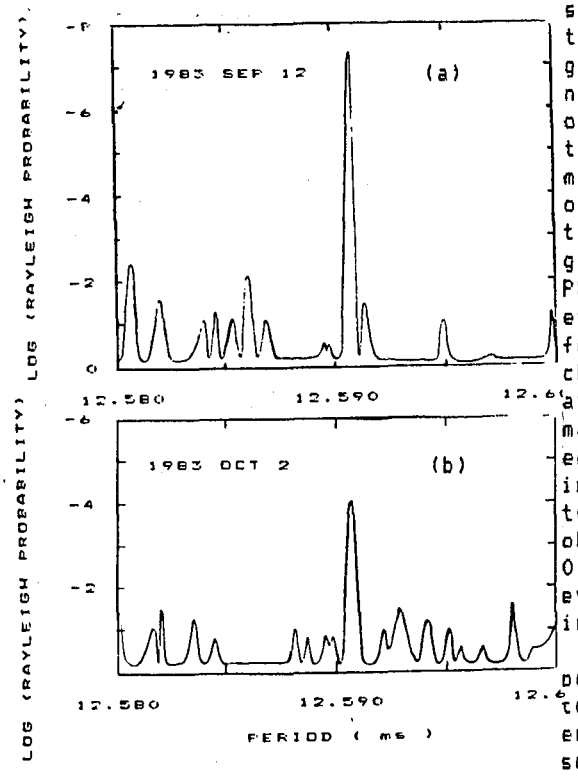

FIG 4.

The VHE and UHE gamma ray flux measurements combine to give an energy spectrum which is exceedingly flat (integral spectrum ~ 1.1) - see Figure 3.

A question which has remained unanswered at all wavelengths is whether or not Cygnus X-3 contains a pulsar as the powerhouse of the system. This has been suggested by Vladimirsky (CAO) as a consequence of a recent supernova, leading to a rotation driven process. Alternatively, it has been suggested by Brecher [28] that the mechanism is that of a unipolar inductor involving the accretion disc of a low field pulsar rotating at equilibrium when accretion is the origin of the energy. To date no suggestions have been made for the pulsar period. Recently our group in Durham [29] have analysed new data taken late in the life of the Dugway facility when our telescopes were operating with maximum sensitivity. At a level of significance which exceeds that of many of the reported VHE gamma ray detections (PSR 0532, PSR 1953, Her X-1, 4U0115 +63 etc), we find prima face evidence for ms periodicity (conservative chance prob $<3\times10^{-7}$). This occurs at those times around X-ray maximum in the 4.8 hr cycle when emission manifested as an increase in the count rate of the telescopes has been detected. The observed period is 12.5908 $\pm$ 0.0003 ms and some of the evidence for the claim is shown in Figure 4.

Confirmation of this periodicity (which may well have to be made at VHE gamma ray energies if dispersion and scattering in the coccoon or stellar wind is occurring) would represent a real highlight !!

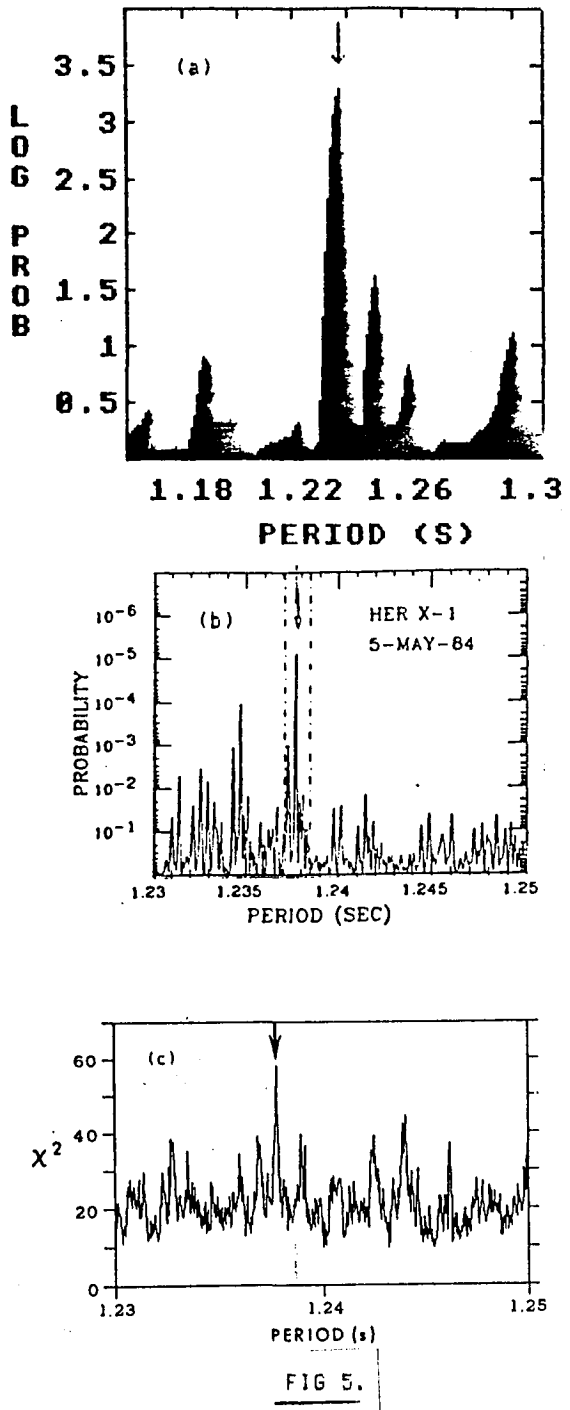

FIG 5.

(b) HERCULES X-1.

A short (3min) outburst of (1.24 s) pulsed gamma rays was detected by the Durham VHE gamma ray experiment in Utah in April 1983[9] - see Figure 5(a). The effect was at phase 0.77 in the 1.7 d orbit and , as far as we can tell, 35 d before an observed switch on of X-ray activity to the high state. The temptation to associate a burst of VHE gamma rays with X-ray switch on should perhaps be resisted - later observations only partially confirm the pattern. The VHE emission is characterized by a broad (X-ray like) light curve and a peak flux of 10^{-9} cm^{-2} s^{-1} at E > 1000 GeV. Replication of this observation, complete in many details, has been reported by the FLWO collaboration[10] - see Figure 5(b).

At energies 100-1000 times higher, the University of Utah Fly's Eye group has recently reported a July 1983 burst of <40 min duration also showing the 1.24 s periodicity of the X-ray pulsar. The light was 10% duty cycle and the observed effect was very strong - an increase of 40% above the cosmic ray background from 50 sq deg of sky - see Figure 5(c). At the same time the colocated 1000 Gev Durham Cerenkov light experiment saw no such marked effect but did observe a rather longer interval of activity (2-3 d) which included the time of the Fly's Eye outburst. This is the first example of simultaneous observations with two systems and certainly with two detectors with such dissimilar energy thresholds; it should be the first of many. If true, these two results suggesting very different origins for the gamma rays of different energies must constrain the choice of models for the Her X-1 VHE and UHE emitting system.

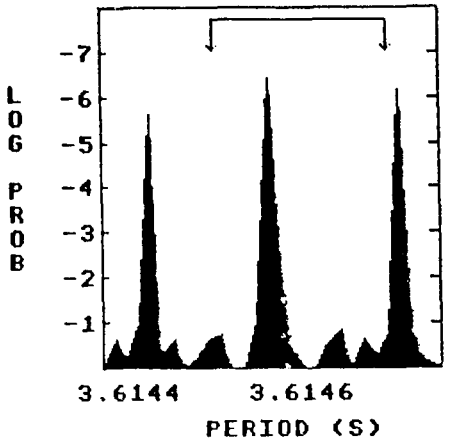

FIG 6.

(c) 4U0115+63

Following the discovery of Her X-1 as a 1000 GeV gamma ray emitter, the University of Durham project targetted 4U0115+63 as the binary system which is most similar to Her X-1 (period and X-ray luminosity) and which shares a claim to cyclotron line emission. A successful search was made in September 1984[12] and the resulting periodogram showing the 3.6 sec periodicity for the VHE gamma ray data is shown in Figure 6. This is the strongest time averaged source of 1000 GeV gamma rays detected in the Durham project (7×10^{-11} cm^{-2} s^{-1}). There is no evidence for other than a steady output over 8 or 9 days - it is certainly not the case that bursts of a few mins of intense activity provide the signal as so often seems to have been the case (e.g. Crab pulsar and Hercules X-1).

(d) VELA X-1 and LMC X-4.

At PeV energies the EAS group at Adelaide has reported evidence for an excess of showers from the directions of Vela X-1 and LMC X-4 showing, in each case, the characteristic orbital periodicity but with no indication of the (long) pulsar period in the case of Vela X-1.

	ORBIT	FLUX	CHANCE PROB	LUMINOSITY
VELA X-1	8.9 d	$9 \pm 3 \times 10^{-11}$ m^{-2} s^{-1}	10^{-4}	2×10^{34} ergs/s
LMC X-4	1.4 d	$5 \pm 2 \times 10^{-11}$ m^{-2} s^{-1}	0.009	10^{38} ergs/s

To sum up what we know about X-ray binaries as VHE and UHE gamma ray sources.

	PULSAR	ORBIT	LONGTERM
CYG X-3	12.5908 ms	4.8 hr	(19 d)
HER X-1	1.24 s	1.7 d	[35 d]
4U0115+63	3.6 s	24.3 d	[sporadic]
VELA X-1	[283 s]	8.9 d	—
LMC X-4	—	1.4 d	—
PSR 1953	6.13 ms	117.3 d	—

[Information in square brackets relates to X-ray data]

The VHE light curve of the binaries is interesting - all X-ray binaries detected so far at TeV energies have broad light curves with duty cycles 30 % or so of the cycle (rather like the X-ray light curves) - see Figure 7.

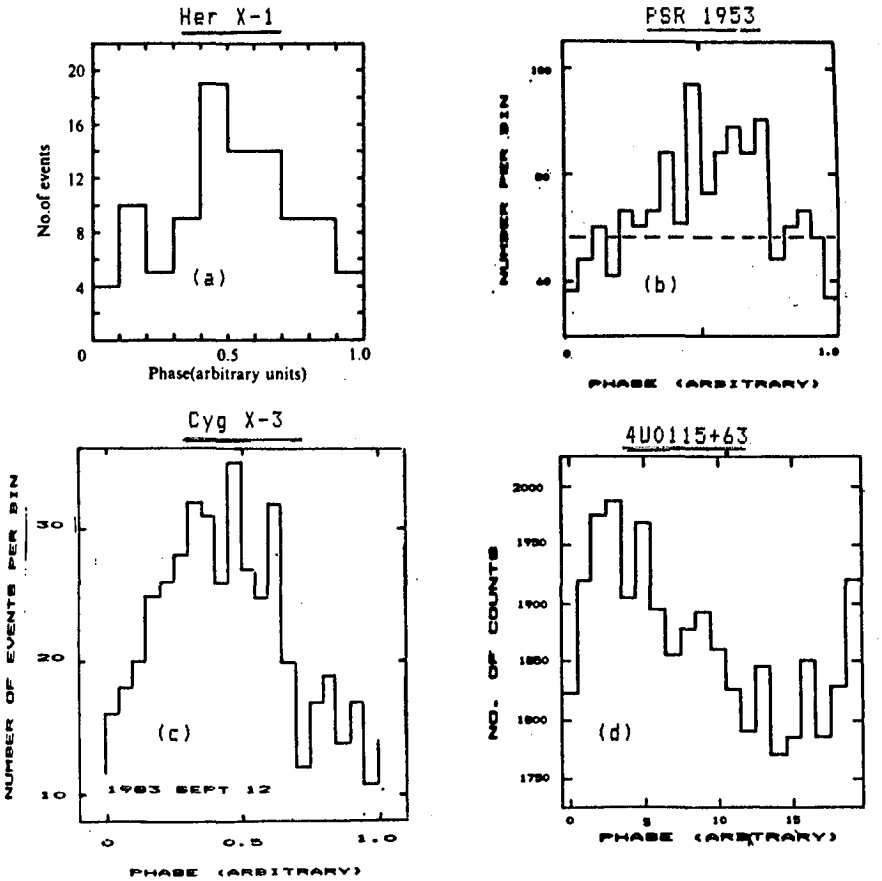

FIG 7.

As far as other VHE gamma ray sources are concerned the Vela pulsar was detected by the TATA group [8] and was found to show the double peaked light curve observed at radio wavelengths - see Figure 8. The detailed study of the VHE emission from the Crab pulsar by the Durham group [18] is an example of a new phase in gamma ray astronomy - the systematic study of the detail of the VHE emission. The width of the light curve around the radio main pulse is observed to be < 1% (<0.4 ms FWHM) - see Figure 9. This is the shortest duty cycle of emission from the Crab pulsar at any wavelength other than radio and confirms the trend first reported 12 years ago by Greisen and his collaborators [30] during gamma ray observations at energies of a few GeV. The constraints placed on models for 1000 GeV gamma ray production in pulsars by such observations are severe.

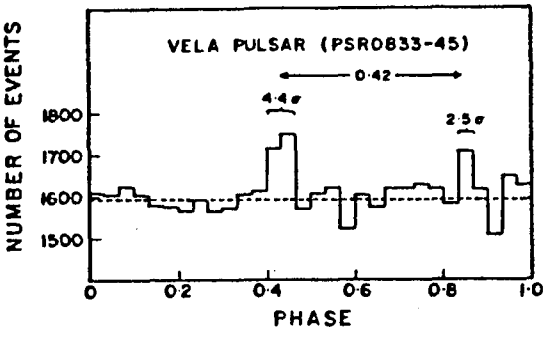

FIG 8.

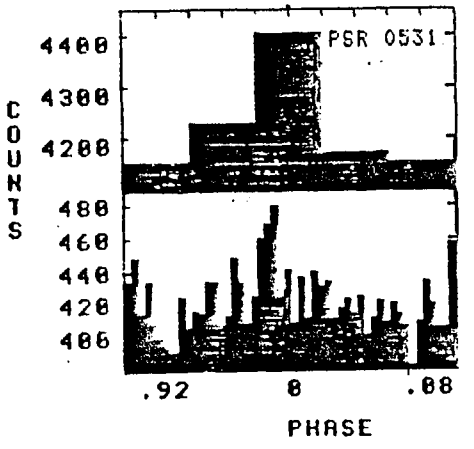

FIG 9.

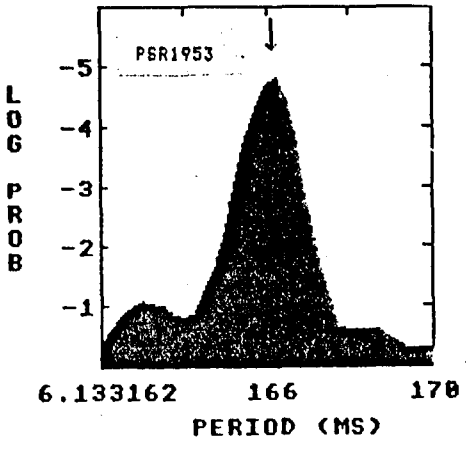

FIG 10.

The 6 ms low-field radio pulsar (PSR1953) discovered in a binary system with a 117.3 d orbit and located within the error box of the COS B source 2CG065 (but not firmly associated with it) has been seen to produce 1000 GeV gamma rays[13] - see Figure 10. Although recently the COS B collaboration has expressed doubt that some of the first quadrant point sources are genuine (and maybe the result of enhanced amounts of molecular material irradiated with cosmic rays), our VHE measurement would suggest that 2CG065 , a weak radio pulsar, is also a copious VHE gamma ray source.

The VHE data from the original 1.5 ms high-field radio pulsar has recently been analysed with the benefit of a radio ephemeris of unprecedented accuracy[31]. An indication of VHE emission in phase with the radio main pulse and significant at the 3×10^{-4} chance level has been obtained from the Durham experiment - see Figure 11.

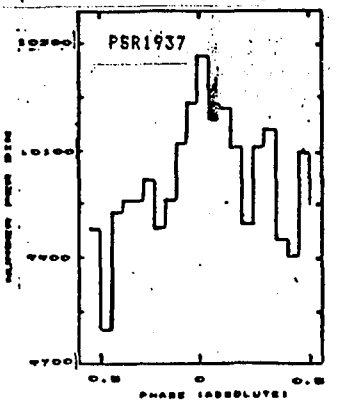

FIG 11.

References

(1) Grindlay JE et al.,(1973),Ap.J.,174,L9.
(2) Dowthwaite JC et al.,(1984),Ap J.,286,L35.
(3) Cawley MF, etal.,(1985),This Conference OG 2.3-2.
(4) Bhat PN et al.,(1980),Astron Astrophys.,81,L3.
(5) Danaher S et al.,(1981),Nature,289,568.
(6) Lamb RC et al.,(1982),Nature,296,543.
(7) Cawley M et al.,(1985),Ap J (in the press)
(8) Dowthwaite JC et al.,(1983),Astron Astrophys,126,1.
(9) Dowthwaite JC etal,(1984),Nature,309,691.
(10) Baltrusaitis RM et al.,(1985),This Conference OG 2.2-7.
(11) Cawley MF etal.,(1985),This Conference OG 2.2-9.
(12) Chadwick PM et al.,(1985),Astron Astrophys Lett (in the press)
(13) Chadwick PM et al, (1985),Astron Astrophys, (in the press)
(14) Fomin VP etal.,(1973),Proc Denver Conf 1,12.
(15) Weekes TC etal.,(1979),Proc Kyoto Conf 1,133.
(16) Dowthwaite JC et al.,(1984),Astron Astrophys,142,55.
(17) Chadwick PM et al,(1985),This Conference OG 2.1-8.
(18) Chadwick PM et al,(1985),This Conference OG 2.3-9.
(19) Stamm S and Samorski M,(1983),Ap J.,268,L17.
(20) Lloyd-Evans J et al.,(1983),Nature, 305,784.
(21) Balutaitis RM et al.,(1985),Ap J ,in the press.
(22) Protheroe RJ et al.,(1984),Ap J.,280,L47.
(23) Protheroe RJ & Clay,RW.,(1985),This Conference OG 2.6-10.
(24) Porter NA and Weekes TC,(1978), SAO Spec Report 301.
(25) Vladimirsky BM et al.,(1973),Proc Denver Conf 1,456.
(26) Vladimirsky BM et al.,(1975),Proc Munich Conf,1,118.
(27) Mukanov JB et al.,(1979),Proc Kyoto Conf,1,143.
(28) Chanmugan G & Brecher K,(1985),Nature,313,767.
(29) Chadwick PM et al,(1985),submitted to Nature.
(30) Macbreen B et al, (1973), Ap.J.184,571.
(31) Chadwick PM et al.,(1985),unpublished.

WHY IS CYGNUS X-3 (WITH "RELATED SOURCES") A HIGHLIGHT OF COSMIC-RAY ASTROPHYSICS?

A. M. Hillas
Physics Department
University of Leeds, Leeds LS2 9JT, UK.

Cygnus X-3 and some apparently related systems have sprung into remarkable prominence at this conference. I will outline the reasons for this great interest. They may be summarised as follows.

1. Gamma rays of energy up to 10^{16} eV are emitted by Cygnus X-3 (and some other sources), so, in the source, there must be charged particles that have been given energies up to $\sim 10^{17}$ eV.
2. The number of charged particles thus inferred is so great that occasional sources of such a kind could, apparently, easily maintain the Galaxy's flux of ultra high energy particles (at least in the range 10^{15} - 10^{17} eV).
3. Several of these u.h.e. gamma-ray emitters appear to be interacting neutron stars, and ultra-high-energy particle production must be a major feature of the energy budget of close binaries containing a neutron star.
4. The time scale of modulation of the output indicates that acceleration to such energies (e.g. 10^{17} eV) must take place in seconds or less.
5. A quite different reason for current excitement is that there are reports of radiations being detected deep underground apparently related to Cygnus X-3 (having a 4.8-hour repetition period) that cannot be understood in terms of known particles or interaction processes. This will be taken up in another session of highlight talks, and so will receive little attention here.

Some recent developments in the picture of these sources will now be outlined.

1. <u>How widespread is this phenomenon of u.h.e. gamma-ray emission</u>?

Searches for u.h.e. gamma-ray sources have largely focused on "interacting neutron stars" - neutron stars accreting matter from very close non-compact companion stars - normally recognised through the strong X-ray emission, which is modulated with the period of spin of the neutron star (X-ray binary pulsars). Joss and Rappaport (1) listed 8 such binary systems with well-known orbits (and masses), obtained from the observed dop-

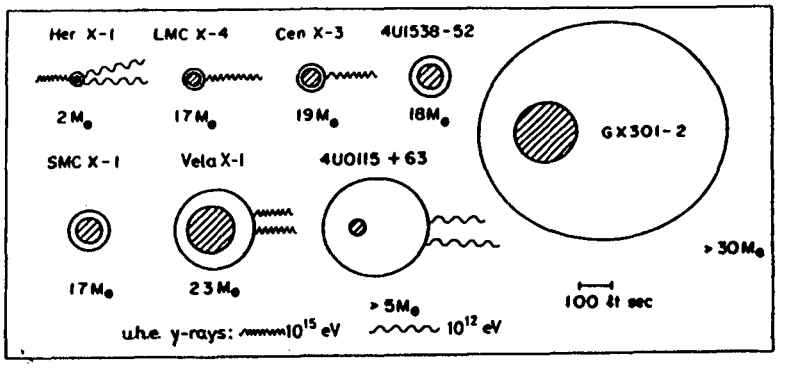

Figure 1. 8 X-ray binary pulsars with well-known orbits (to scale): those from which u.h.e. gamma-ray emission has been reported are marked.

pler shifts of the X-ray pulsation frequency, and figure 1 shows these to scale. Each wavy line attached to a diagram indicates that one research group has claimed to see emission of gamma rays in the 10^{12} or 10^{15} eV range. (The orientation of the rays has no significance.) (Refs: Her: 2,3,4; LMC: 5; Cen: 6; Vela: 7,6; 115+63: 8,9.) Thus, 5 of the 8 are already reported to emit u.h.e. gamma-rays, and although the evidence for Cen X-3 is very weak, and LMC X-4 requires confirmation, the fact that so many have already been reported leads one to guess that probably all such systems emit u.h.e. gamma rays. (The larger and the more elliptical systems probably transfer mass very spasmodically, and more extended observations may be needed to see gamma-ray emission.)

In addition to these, there is Cygnus X-3 - much more powerful (except for LMC X-4, if confirmed), and not on the list because no neutron star pulsation had been detected in X-rays, so no doppler measurement was possible. In the absence of doppler measurements and sharp eclipses there is no clear proof that Cygnus X-3 is a binary system, but the more rounded X-ray intensity curve suggests that we are for some reason getting a blurred view of an accreting close binary.

TeV gamma-ray emission from some non-interacting pulsars has already been reported by Turver's group, and the Crab pulsar is a widely observed emitter, weaker than the binaries. These "isolated" pulsars will not be discussed here.

2. The orbital signature

The vital feature identifying the source of the gamma rays has been a variation of the flux with exactly the same periodicity as the X-rays. Generally this is the binary orbital period - periods are usually of the order of days: some examples are illustrated below.

Object	*Orbital period*
Cygnus X-3	0.19968 days
Vela X-1	8.965 days
LMC X-4	1.408 days
Centaurus X-3	2.087 days

though in some cases the emission has had a short duration and the shorter X-ray periodicity attributed to the neutron star's spin has served for identification:

Object	*n-star spin period*
Hercules X-1	1.24 sec
4U 0115+63	3.61 sec.

In general, the air showers from the direction of the source do not stand out clearly from the large flux of background proton showers, without an identification by period, though the first and last sources on the list have also been seen simply as point sources.

3. Orbital phase terminology: e.g. Cygnus X-3

Phase zero corresponds to the time when the neutron star (or at least the X-ray source) is at its furthest distance, behind the companion star - in most cases in mid-eclipse. At phase 0.5 in the orbit the neutron star will be in front. In the case of Cygnus X-3, we do not know the exact furthest point of the orbit, as no sharp eclipse is seen: the X-rays instead follow a smoother rise and fall, giving the impression that there is much scattering of the X-rays and their source region is large:

and the variation is asymmetrical, with a faster fall and slower rise. Van der Klis and Bonnet-Bidaud (10), whose ephemeris is generally adopted, define phase zero as the minimum of a sine wave fitted to the intensity curves, and the true flux minimum then occurs near phase 0.96. The asymmetry is quite likely to indicate ellipticity in the orbit, but the phase is taken to change uniformly with time, from 0 to 1. Hence, for two reasons, the position of the neutron star at a given phase is not known with great accuracy.

4. Generation of gamma rays by particles (with emphasis on Cygnus X-3)

As it is hard to see how electrons could reach energies above 10^{16} eV because of rapid energy loss (30), protons (or nuclei) are at present considered much the most likely primary particles generating gamma rays in the Cygnus X-3 system, and the picture put forward by Vestrand and Eichler (11,12), in which a wide-angle hadron beam from the neutron star generates π^o mesons and hence gamma-rays, is illustrated in figure 2.

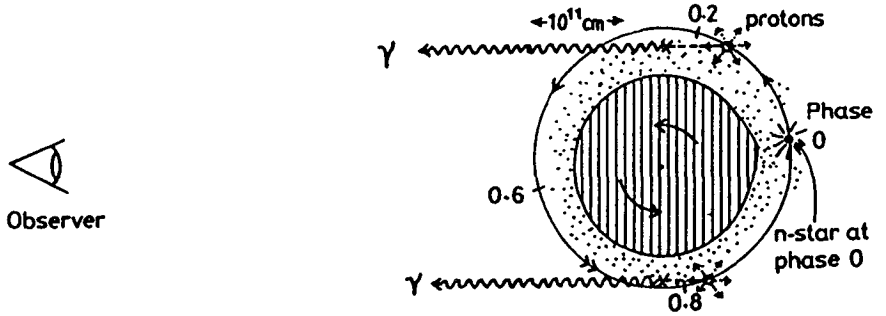

Figure 2. Schematic diagram of motion of n-star round 4.8-hour orbit. n-star emits protons in all (?) directions: at two points on orbit γ-rays will be seen as source is seen through fringe of gas surrounding companion star.

Somewhere near phases 0.2 and 0.8 of the orbit we might thus see the source through a thin layer of gas surrounding the companion.

Emission near phase 0.25 was prominent in the early 10^{15} eV signals (Samorski & Stamm, 13, Lloyd-Evans et al., 14) as published in 1983, as shown in figure 3(a); and in the early Crimean 10^{12} eV observations (15) radiation was at times detected near 0.2 and 0.8 (see figure 3c). But most of the reported detections near 10^{12} eV reported since 1979 have occurred near phase 0.6 - 0.7 (placed more precisely by the Durham group (20) at 0.63). The latest observations just below 10^{15} eV (figure 3b) also show the main emission near this latter phase of the orbit. The variation of gamma-ray signal with orbital phase is illustrated in figure 3, where the departure of the counting rate from a background rate (dashed line) is plotted on an arbitrary scale, with no attempt to assess the significance of the peaks: attention is focused on a comparison of the phases at which the signals are reported to occur. (In two cases - marked * - the time zero has been shifted from the published version, as an approximate correction to the "standard" ephemeris used by the other groups.)

The duty cycle of a "pulse" of emission has often been reported to be only ∿2% of the orbit (13,14,20: see also 7), though one gets the impression that the 0.6 pulse may wander a little.

These observations evidently call for some reconsideration of the simplest "atmospheric target" model for gamma-ray production in Cygnus X-3

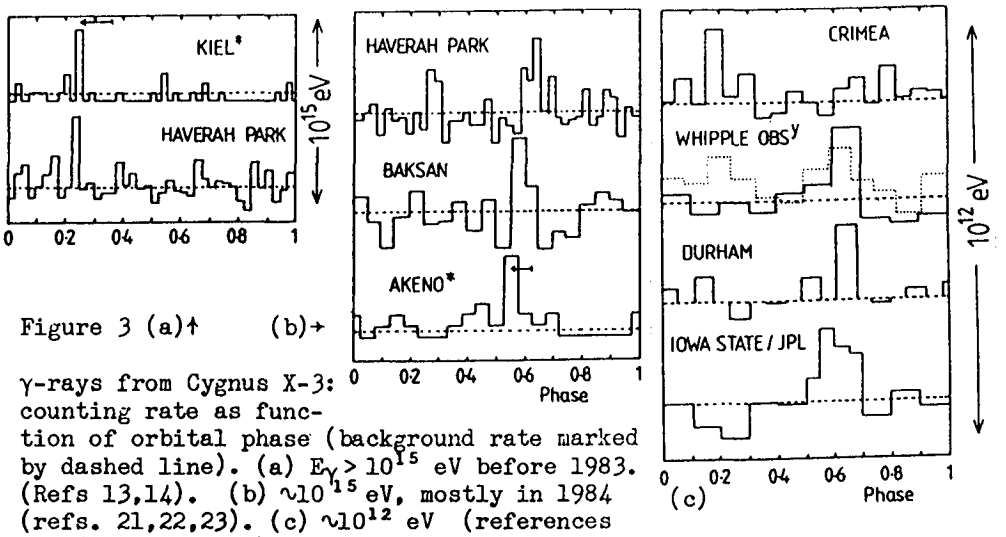

Figure 3 (a)↑ (b)→

γ-rays from Cygnus X-3: counting rate as function of orbital phase (background rate marked by dashed line). (a) $E_\gamma > 10^{15}$ eV before 1983. (Refs 13,14). (b) $\sim 10^{15}$ eV, mostly in 1984 (refs. 21,22,23). (c) $\sim 10^{12}$ eV (references 15;16 & 17; 18;19).

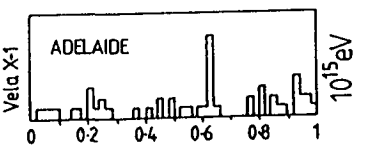

Figure 4 →
10^{15} eV gamma-rays from Vela X-1, as function of orbital phase (ref. 7).

(and also Vela X-1): they raise three questions.

(a) The most prominent emission is at the wrong phase (0.63), when the neutron star is *in front* of the companion! (The same phase is also reported in Vela X-1: figure 4.) Is there a gas target here?
(b) Since the gamma rays are emitted in a well-defined direction, the particle beam must be almost undeflected before collision, despite the fact that a 10 TeV proton's gyroradius would be $< 10^{-2}$ of the travel distance if there is a magnetic field >30 gauss. (10 TeV might be a suitable proton energy to generate 1 TeV gammas.)
(c) Are we after all wrong in supposing that the gamma-ray beam is related to the position of a gas target: is the particle beam only accelerated in a special direction?

The three queries will be considered in turn, to show that it does seem possible to retain the basic Vestrand-Eichler process.

(a) Is there a special gas target at a phase near 0.63? If accretion takes place from high-speed gas streaming from the companion, there should be an accretion wake or tail near the direction shown in figure 5, as the outflowing gas is deflected by the gravitational field of the neutron star and collects in a dense column behind it, after being shocked, and falls back onto the neutron star. The trailing angle of the tail depends on the relative velocity of the wind and the orbital motion: very reasonable wind velocities would make the neutron star lie behind the tail at phases somewhere in the range 0.55 - 0.66 (calculated for a circular orbit). In another binary, Cen X-3, X-ray absorption due to such a feature has been seen (25) at this phase (in Cyg X-3 the X-ray source is diffused), and optical absorption at the same phase is known in some other close binaries. Vela X-1 is consistent with this picture, as it is accreting

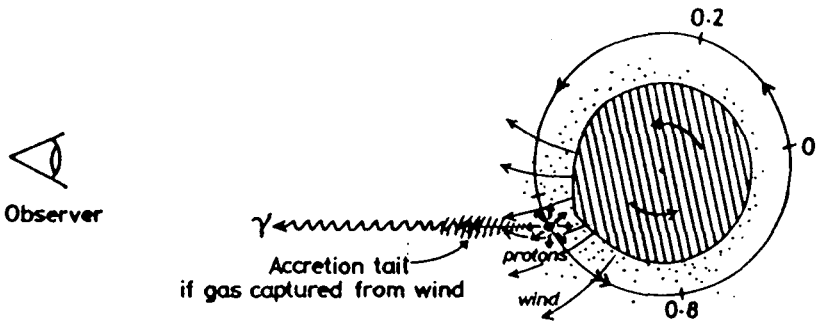

Figure 5. Accretion wake collecting behind neutron star as wind sweeps past, and forming a target for protons from n-star when it is at phase near 0.63, as seen by a distant observer.

from a wind. If the accreted mass powers the luminosity of Cygnus X-3, the column must be very massive. Some variation in wind speed due to local heating would cause the trailing angle to vary a little.

(b) Collimation of beam: 10^{17} eV protons? (or neutrons?). One way to maintain the directionality of the beam is to suppose that most of the power goes into particles near 10^{17} eV - a monoenergetic proton beam, or at least a very flat spectrum. Then the particles need not be greatly deflected before collision, where they produce gamma-rays in a forward direction, most notably around $10^{15} - 10^{16}$ eV. Provided that the gas thickness is at least about a radiation length, the gamma-rays will produce electron-positron pairs, and then a very rapid photon shower can develop by synchrotron radiation if there is a magnetic field exceeding a few tens of gauss. Surprisingly, at these high energies, synchrotron radiation is so rapid that there is no significant deflection before radiation occurs. The result (26) would be a photon spectrum very like what is observed. Enough TeV photons emerge without requiring production by, say, 10 TeV protons in the beam. (In the absence of a magnetic field, a normal electron-photon cascade could occur, but would require a greater thickness of gas.) Taking this further, one might try to explain the smaller content of TeV photons in the pulse near phase 0.25 by supposing that this signal arises in a thinner gas layer, with less cascading.

It will later be shown that Cygnus X-3 can hardly be a minor contributor to the general cosmic ray flux. Hence, if the main contribution to the proton flux is above 10^{16} eV, and one is to generate the observed steep spectrum of cosmic ray protons in the Galaxy, there are probably many more binaries that only emit protons less energetic than this.

Alternatively, Kazanas and Ellison (preprint) have proposed that particle acceleration occurs in an accretion shock near the neutron star, and many of the accelerated protons are transformed into neutrons in collisions: one then has a neutral hadron beam travelling undeflected to the gas target (any high-energy gamma-rays generated in association with the neutrons can be absorbed by the strong magnetic fields in the acceleration region).

(c) Is a gas target involved? Supporting evidence from Hercules X-1.

There is evidence from X-ray and optical work on Her X-1 that the X-rays originate near the neutron star, which is surrounded by a thick accretion disk which tilts back and forth, obscuring the neutron star for

a large part of a 35-day cycle. This precession may be connected with the way in which a gas stream is wound onto the edge of the disk. High energy gamma-rays have only been detected from this source on a few occasions (by the Durham, Fly's Eye and Whipple observatory groups: 2,3,4), and not at fixed orbital phases in this case, but just when the X-ray source was emerging from obscuration by the outer part of the disk, and at certain times when short bursts of X-ray obscuration suggested that thicker blobs of gas were running round the outer disk, presumably fed by a burst of accretion (4,27). All observers have interpreted these observations as evidence that the gamma-rays are indeed seen when a thin gas target intervenes between the neutron star and the observer. (A very thick disk stops all radiation: or with no intervening matter no π^o production occurs: only the thin edge is effective.)

Hence the production of gamma-rays by u.h.e. protons in gas streams ejected from the companion is at present a tenable model, though some special asymmetry must be introduced to suppress a pulse near phase 0.8.

5. How are particles accelerated to $10^{16} - 10^{17}$ eV?

Several acceleration processes have been considered.

Mechanism	*Authors*	*Difficulties*
v×B field of pulsar	Michel, Dessler:28,29 Eichler & Vestrand:30	Rotation too slow in Vela X-1 (but perhaps not in Cyg X-3)
v×B field of accretion disk	Chanmugam & Brecher (31)	B too high to allow fast disk? ($> 10^{12}$ G in Her X-1)
Field reconnection in accretion disk	Wang: 32	
High-speed shock in accreting gas	Kazanas & Ellison: 33 Eichler & Vestrand:34	
"Magnetospheric grindstone"	Kundt: 35	The various observed phases

Some features of the observations have an important bearing on the mechanism. Firstly, the prominence of interacting neutron stars as u.h.e. gamma-ray emitters (unless merely a consequence of the searching programme) suggests that the energy is derived from accretion. And in Cygnus X-3 at least, there is probably much more energy put into ultra high energy protons than into thermal radiation, so the infall has to be cushioned in some way to avoid thermalisation. One way of achieving this may be by a strong collisionless accretion shock, which may be able to convert most of the gas kinetic energy into high-energy particles - if they can then escape! Otherwise we want a dynamo to extract the kinetic energy near the neutron star very efficiently. It is noteworthy also that the observed particle emission is in directions close to the plane of the accretion disk (in Her X-1) or the orbit: it is not confined to the near-polar directions normally considered in dynamo models (though not in 29): so the magnetic field must be very different from a dipole form.

Quite apart from the gamma-ray evidence, neutron stars have been the most attractive sites for acceleration of the general galactic u.h.e. cosmic rays (36): this new window on an accelerator at work may revitalise the search for viable mechanisms.

6. Power emitted by Cygnus X-3 in ($\sim 10^{17}$ eV) protons

Adopting the flux of gamma-rays reported by Haverah Park (14), *(a)* the energy flux carried by the photons above 10^{15} eV, at the Earth, would be $\sim 3\times10^{-10}$ erg cm^{-2} s^{-1} (averaged over time) if one restored the losses due to interactions with the primeval microwave radiation (in 12 kpc). *(b)* The pulse was detected for about 2% of the orbital cycle; and as we take this pulse to be seen when a thin gas target intervenes, we should have seen 50 times more power had a suitable gas converter been available all round the orbit. Furthermore, *(c)*: only $\sim$10% of the energy of a 10^{17} eV proton is converted to gamma rays (1/3 of the energy radiated in collisions goes into π^os, not all above 10^{15} eV, and part is carried away by nucleons from the thin target). Finally, *(d)*: if the source is at a distance $r = 12$ kpc, we can estimate the power in the proton beam emitted in all directions:

$$\text{Total power in protons } (\sim 10^{17} \text{ eV}) \text{ accelerated in Cygnus X-3} = 3\times10^{-10} \times 50 \times 10 \times 4\pi r^2 \times (\Omega/4\pi) \quad \text{erg s}^{-1} = 3\times10^{39} \times (\Omega/4\pi) \quad \text{erg s}^{-1} ,$$

if we take the beam to appear in a solid angle Ω rather than being isotropic. The main part of these protons will escape into the Galaxy. But the rate of input of particles above 10^{16} eV needed to maintain the Galaxy's normal cosmic ray flux is probably $\sim 5\times10^{37}$ erg s^{-1} - though this is only known roughly, as the assumed trapping time of $\sim 2\times10^5$ years at such energies is only a rough estimate (26). Hence one apparently needs one Cygnus X-3 type of source to be present for only part of the time (averaged over 10^5 years) to maintain the cosmic ray flux in the 10^{16}-10^{17} eV region. (We could reduce the extravagant total energy by assuming a small solid angle Ω of proton emission - say 1% of 4π - but are then faced with another problem, as we should presumably see only 1% of all such sources, and so we could hardly suppose such a large number to be present for only a small fraction of the time.) (* See footnote at end.)

7. Are the particles from Cygnus X-3 exotic?

Of the underground proton decay detectors, three have detected fluxes of particles, deep underground, apparently related to Cygnus X-3: they show the 4.8-hour periodicity. These will be reported in a later group of highlight talks, but the difficulty in explaining these observations may be pointed out briefly, by referring to one example. The Soudan Mine experiment detects muons of about 2/3 TeV (vertical), and has reported a flux of $\sim 7\times10^{-11}$ cm^{-2} s^{-1} apparently from Cygnus X-3 (corrected to vertical threshold). Primary particles generating such muons must have energies above 1 TeV (normally well above), and much more than 1 primary above 1 TeV would be required for each secondary 2/3 TeV muon. But the reported muon flux exceeds the flux of 1 TeV primaries entering the atmosphere from that direction (or at least depositing energy in it, to generate air showers, detectable by Cerenkov radiation). The Durham group, for example, see a time averaged flux $\sim 3\times10^{-11}$ cm^{-2} s^{-1} of showers above 1 TeV from Cygnus X-3. The reported underground signals cannot be understood in terms of known primary particles and interaction processes.

The primary particles responsible for the signals seen above ground by the Cerenkov detectors (discussed in this paper) must be neutral, to maintain their alignment with distant sources, and limits can be set on their rest masses. The radiations from Her X-1 have travelled for 15000 years, but the dispersion in their travel times has not greatly smeared out the 1.24-second modulation. They are not monoenergetic: those detect-

ed have an energy spread around 1 TeV: so the rest mass must be < 10 MeV to retain considerable modulation on this time scale. If a 12-ms modulation is indeed present in the Cygnus X-3 signal (∿40,000 yr travel time), as just reported by Turver, the rest mass of these particles must be < 1 MeV. Gamma-rays meet the requirements best - certainly not hadrons.

References

1. Joss P C & S A Rappaport (1984) Ann.Rev.Astron.Astrophys. 22: 537-92
2. Dowthwaite J C et al. (1984) Nature 309: 691-3
3. Baltrusaitis R M et al. (1985) Astrophys. J. Lett. 293: L69-72
4. Cawley M F et al. (1985) 19th ICCR, La Jolla 2: 119-22
5. Protheroe R J & R W Clay (1985) Nature 315: 205-7
6. Kaneko T et al. (1985) 19th ICCR, La Jolla 2: 238-41, and private communication from K. Suga
7. Protheroe R J et al. (1984) Astrophys. J. Lett. 280: L47-50
8. Chadwick P M et al. (1985) subm. to Astron. Astrophys.
9. Stepanian A A et al. (1972) Nature 239: 40-1
10. van der Klis M & J M Bonnet-Bidaud (1981) Astron.Astrophys. 95: L5-7
11. Vestrand W T & D Eichler (1979) *Particle acceleration mechanisms in astrophysics:* 285-8. (AIP Conf. proceedings no. 56) Ed. Arons J &al.
12. Vestrand W T & D Eichler (1982) Astrophys. J. 261: 251-8
13. Samorski M & W Stamm (1983) Astrophys. J. Lett. 268: L17-21
14. Lloyd-Evans J et al. (1983) Nature 305: 784-7
15. Neshpor Yu I et al. (1979) Astrophys. Space Sci. 61: 349-55
16. Weekes T C et al. (1981) Astron. Astrophys. 104: L4-6
17. Cawley M F et al. (1985) subm. to Astrophys. J.
18. Lamb R C et al. (1982) Nature 296: 543-4
19. Chadwick P M et al. (1985) 19th ICCR, La Jolla 1: 79-82
20. Dowthwaite J C et al. (1983) Astron. Astrophys. 126: 1-6
21. Lambert A et al. (1985) 19th ICCR, La Jolla 1: 71-4
22. Alexeenko V V et al. (1985) 19th ICCR, La Jolla 1: 91-4
23. Kifune T et al. (1985) 19th ICCR, La Jolla 1: 67-70
24. Marshak M L et al. (1985) Phys. Rev. Lett. 54: 2079-82
25. Jackson J C (1975) M.N.R.A.S. 172: 483-92
26. Hillas A M (1984) Nature 312: 50-1
27. Voges W et al. (1985) MPI Garching preprint
28. Michel F C & A J Dessler (1981) 17th ICCR, Paris 2: 340-3
29. Michel F C (1985) Astrophys. J. 288: 138-41
30. Eichler D & W T Vestrand (1984) Nature 307: 613-4
31. Chanmugam G & K Brecher (1985) Nature 313: 767-8
32. Wang Y-M (1985) preprint
33. Kazanas D & D C Ellison (1985) preprint
34. Eichler D & W T Vestrand (1985) 19th ICCR, La Jolla 1: 115-8
35. Kundt W (1982) Astrophys. Space Sci. 90: 59-68
36. Hillas A M (1984) Ann. Rev. Astron. Astrophys. 22: 425-44

* Footnote: At the conference, J. Elbert mentioned a very unusual occurrence in June this year, when Cygnus X-3 was apparently emitting u.h.e. gamma-rays over a wide range of phases. This would imply that the charged particle beam was indeed not narrowly collimated. (An extensive emission of gas may have occurred.)

OBSERVATIONAL PROPERTIES OF COSMIC GAMMA-RAY BURSTS

E.P.Mazets
A.F.Ioffe Physical-Technical Institute,
Academy of Sciences of the USSR,
194021 Leningrad, USSR

1. Introduction. Intense impulsive fluxes of hard photons with an energy of ~1 keV to few tens of MeV propagate in interstellar space in our Galaxy. When such a very thin front of high photon density passes across the Solar System and meets a spacecraft with a gamma-ray detector aboard, the observer perceives what we call a gamma-ray burst. The pioneering observations of the gamma-ray bursts in the early '70s [1] were followed by their comprehensive investigation aimed at finding answers to the questions of where these very strong radiation fluxes come from, where and how they are produced. Despite the fact that much has been learned in the recent years, we still do not have full understanding of the origin of the bursts.

In their studies of the gamma-ray bursts, the astrophysicists have met with problems which are not only very intriguing but extremely complex as well.

The present paper is a brief overview of the major observational results obtained in gamma-ray burst studies. We will also discuss to what extent the thermonuclear model which appears at present to be the most plausible can account for the observed properties of the bursts. The investigation of gamma-ray bursts should cover observations of the time histories of events, of the energy spectra and of their variability, source localization and inspection of the localization regions during the active and quiescent phases of the source in other wavelengths as well as evaluation of the statistical distributions of the data obtained.

2. Time Structure of the Gamma-Ray Bursts. The bursts vary in duration over a wide range from around ten milliseconds to a few minutes. The time histories of the bursts are extremely diverse. Several attempts have been made at constructing a morphological classification of the events [2,3]. Subsequent observations confirm the existence of several types of time structures. Fig.1 shows several light curves measured in the Konus experiment on Venera 13 and 14 in the energy range 45-200 keV. Note that because of the spectral variability of radiation the time profiles observed in different energy intervals may differ slightly.

First one should point out the existence of two classes of events. Short bursts (GB811220, Fig.1), apart from their short duration, <0.5-1 s, differ strongly from long events in the short rise time, ~10-100 ms [4-6]. Among long bursts one may discriminate at least two groups of events.

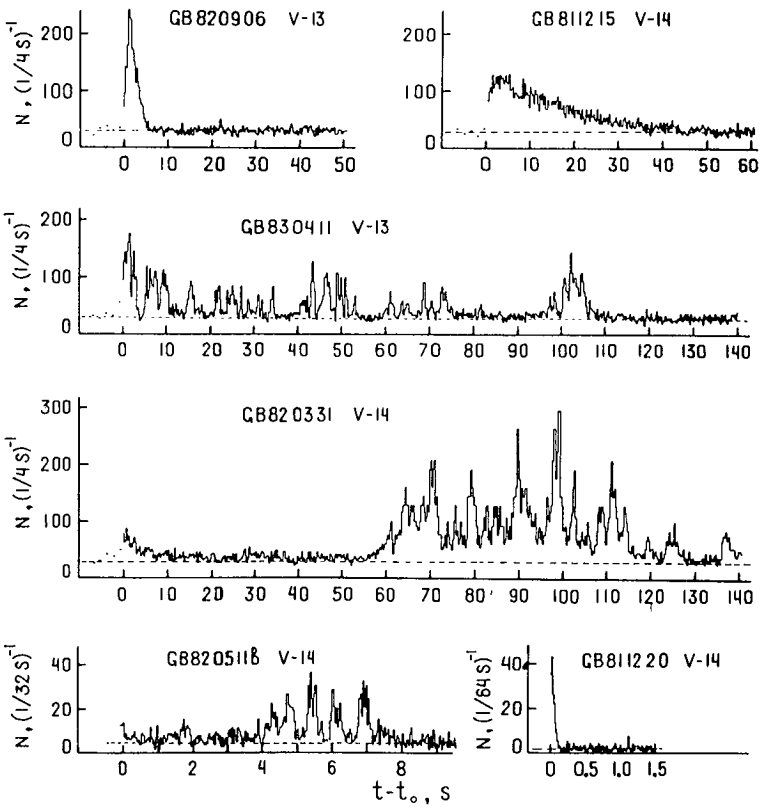

Fig.1. Typical time histories of gamma-ray bursts

Simple single-pulse bursts (GB820906) last for 5-15 s. In some cases their duration increases by a few times making them look like long structureless events (GB811215). The most numerous are bursts with a complex multipulse time structure. The number of individual peaks observed in the profile may vary reaching sometimes a few tens (GB830411). Quite frequently these peaks may form quasiperiodic trains. However barring a few exclusions, no strictly regular periodicity is observed in the burst profiles [7,8]. As a rule, the rise and decay times of individual peaks in complex bursts are shorter than those in single-pulse events. It appears that many bursts reveal a peculiar trend in their time structure. If a burst develops faster, i.e. a burst with a complex structure is shorter, then the details in its time structure are compressed accordingly (GB820511). This remarkable feature of a similarity between the time histories of various bursts analyzed on a normalized, compressed or extended, time scale was pointed out in several observations [9,10]. In many cases one observes in the pro-

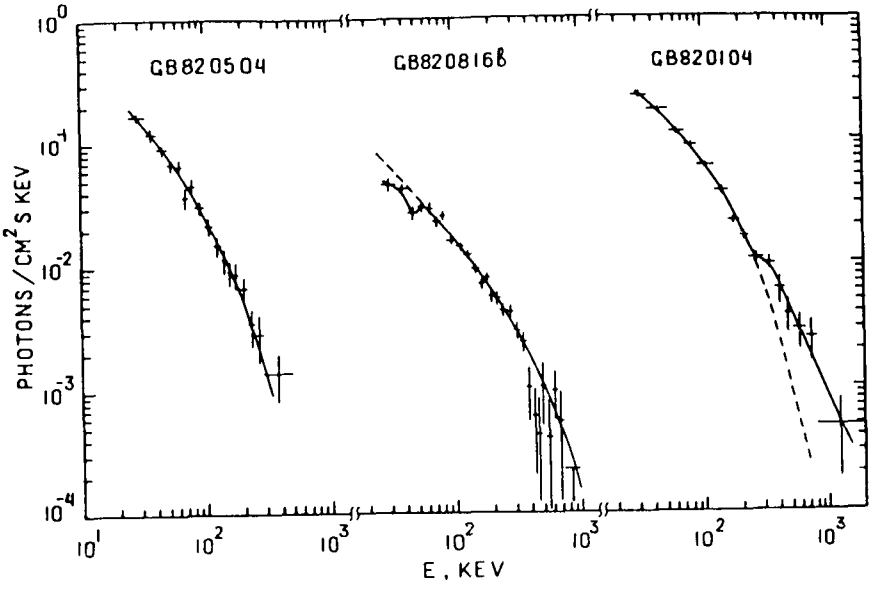

Fig.2. Typical burst energy spectra: typical continuum, spectrum with a cyclotron feature, spectrum with an annihilation feature

files precursors preceding by a few tens of seconds the main phase of the burst (GB820331). The observation of weak precursors is apparently limited by the instrument sensitivity. If the precursors are indeed a widespread feature of the bursts, then their observations should become more numerous as the sensitivity of gamma-ray burst detectors increases. The time structures of the bursts reflect obviously the inherent and most essential characteristics of the emission processes in the sources. Explanation of the time evolution of the bursts should be a major goal in the construction of any source model. Unfortunately, most of the models being developed at present focus on the energetics of the sources and on the energy spectra while paying little attention to the time structures.

3. Energy Spectra. In contrast to the time structure, the energy spectra of the bursts display a markedly uniform pattern [11]. With the present-day measurement accuracy, the smooth continua observed in the energy range 30 keV - 2 MeV (see, e.g. the spectrum of the 4 May 1982 event, Fig.2) may be fitted equally well by optically thin thermal bremsstrahlung or thermal synchrotron distributions [12,13]. The actual mechanism of emission still remains unclear [14-17]. Assuming the emission to be of thermal nature, estimates of the temperature in the sources range from 10^9 to 10^{10} K. In many cases the energy spectra were found

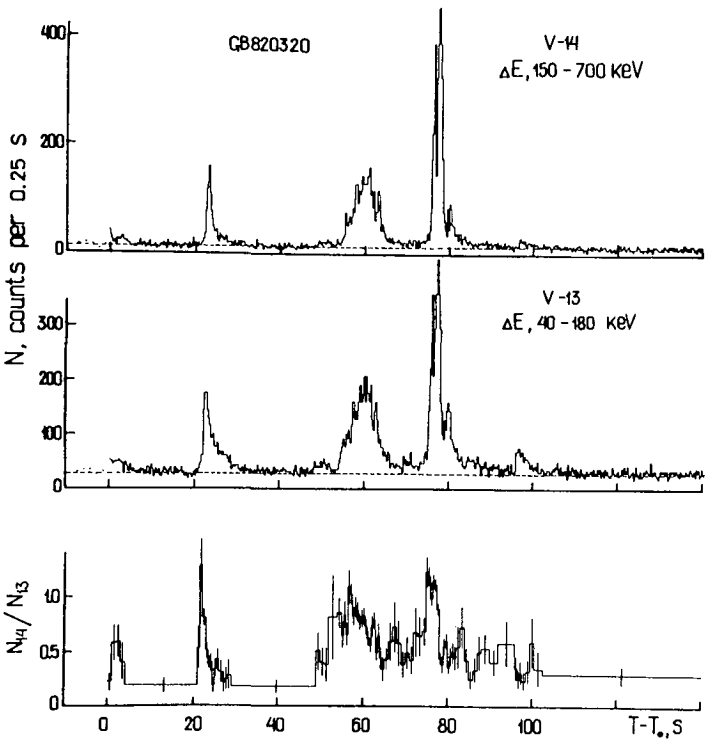

Fig.3. Gamma-ray burst time profiles in the various energy ranges. The hardness ratio indicates a fast and strong spectral variability

to reveal spectral features of two types [18]. The absorption features are observed in the energy range 30 - 100 keV (GB820816, Fig.2). They are believed to originate from cyclotron absorption at magnetic fields $B \sim (2\text{-}8)\times10^{12}$ G. The emission features peak in the range 350-450 keV (GB820104, Fig.2). These features are most probably due to gravitationally redshifted pair annihilation emission.

This interpretation has led to the presently widely accepted opinion that cosmic gamma-ray bursts are generated by strongly magnetized neutron stars.

The energy spectra are characterized by a strong and fast spectral variability [11,19,20]. The continua measured in different phases of a burst differ essentially, as a rule, in accordance with temperature variations of the emitting region. Spectral hardness may vary as fast as the emission intensity does. Fig.3 displays time profiles of GB820320 obtained in various energy intervals as well as the corresponding variations of the hardness ratio.

Spectral features also evolve rapidly. The cyclotron features are observed primarily in the initial stages of the bursts. The annihilation radiation is likewise the strongest in the beginning of a burst or is connected with the most intense peaks in the time structure.

In the recent two-three years new essential information on the burst spectra has been obtained. SMM observations have revealed a high energy component in the burst spectra (Fig.4) [21,22]. By our data, the hard tails in the

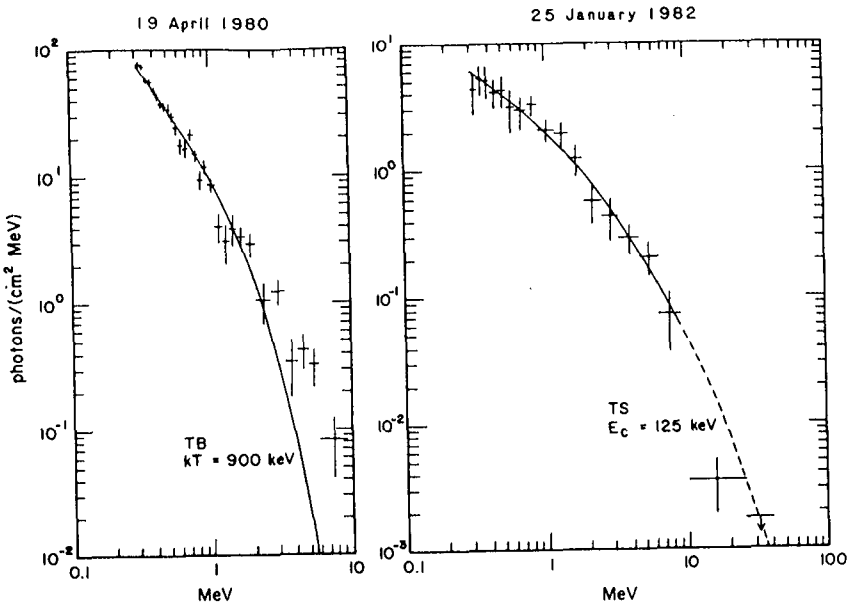

Fig.4. High energy emission in gamma-ray bursts from SMM data [22].

spectra are directly associated with the annihilation features and represent actually their extension. An investigation of a large number of spectra containing emission features has shown the spectral distribution of the annihilation radiation to be a broad line with an extended hard wing (Fig.5). This implies that the energy spectra of bursts consist of two emission components. Their angular patterns are assumed to be different [23].

The spectral shape of the softer continuum emission is affected by the absorption of hard photons involving pair formation. The angular distribution of this emission is close to isotropic.

The observed annihilation spectrum is apparently produced by superposition of in-

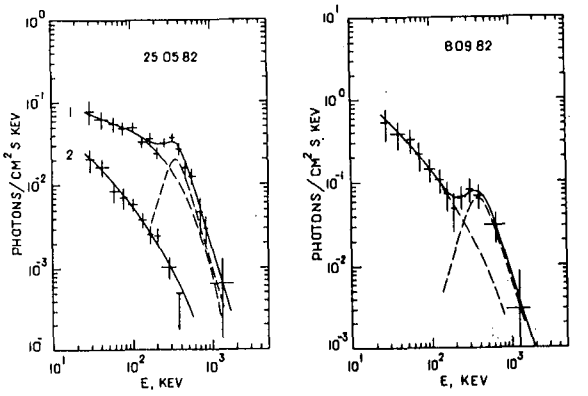

Fig.5. Two emission components in gamma-ray burst spectra. (a) Time evolution of a spectrum with annihilation feature. (b) Annihilation feature in a spectrum of a short burst of 100 ms duration.

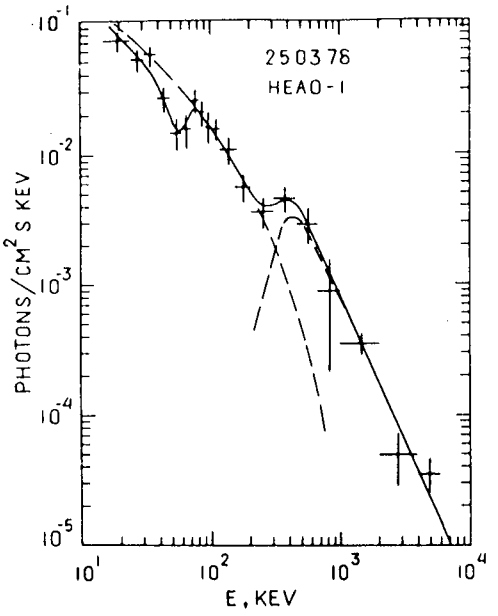

Fig.6. HEAO-1 observations of a complex spectrum [26]

stantaneous annihilation spectra [24] generated by a pair-dominated plasma with a fast and strongly varying temperature. It is also possible that this spectrum is directly related with the close-to-power law energy distribution of electrons and positrons [25] in their one-dimensional motion along the magnetic field lines. The radiation is emitted most probably from the polar region of a neutron star in a collimated beam.

A remarkable illustration of a spectrum with both a cyclotron absorption line and an intense annihilation component is provided by HEAO-1 observations of GB780325 [26] (Fig.6).

Quite recently very interesting results have been obtained in gamma-ray burst observations in an X-ray range 3-10 keV [27] (Fig.7). As shown by these observations, the X-ray luminosity of the burst sources is high, $L_X/L_\gamma \sim 0.02$, the X-ray emission is somewhat delayed compared with the time profile in gamma rays. The X-ray tail following the main phase may indicate cooling of the emitting region.

4. Optical Flashes. Operation of an international network of satellite-borne gamma-ray burst detectors has resulted in a remarkable achievement, namely, an exact localization on the celestial sphere of a number of burst sources with an error box size of $\lesssim 1$ arc minute [28, 29]. It was found that these error boxes do not contain easily

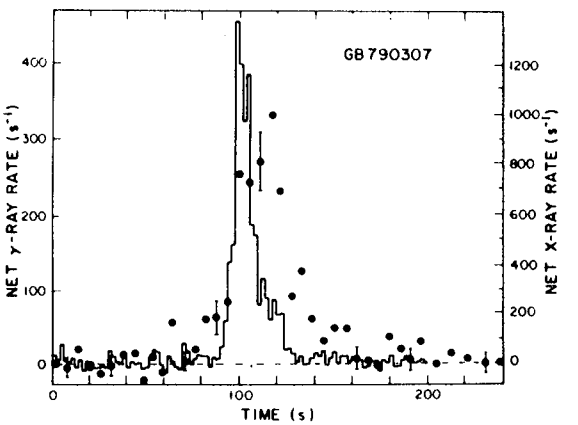

Fig.7. Simultaneous burst observations in gamma- and X-rays [27]

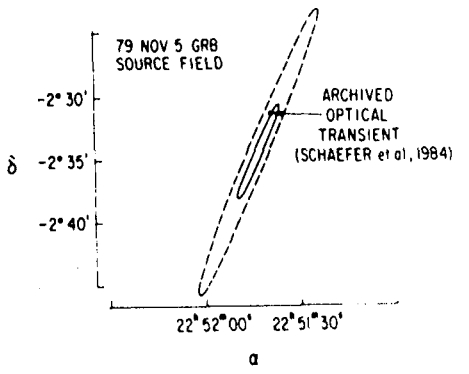

Fig.8. Error box of the 5 November 1979 event. Position of the optical flash on an archival photographic plate of 1941 [29]

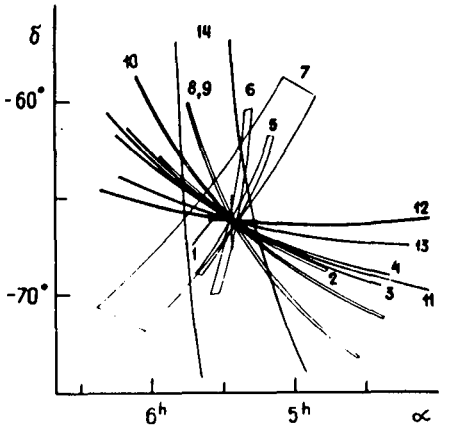

Fig.9. Error boxes for a series of recurrent bursts from GBS0526 -66

detectable radio, optical or X-ray objects. Only a deep search carried out at a very high sensitivity reveals in these regions a few weak objects. It would be very difficult to identify any of these objects as the optical counterparts of the burst sources in quiescent state [29].

All the more unexpected was the discovery on archival photographic plates of optical flashes in the error boxes of three gamma-ray burst sources [30,31] (Fig.8). The reliability of identification of these flashes with gamma-ray burst sources is apparently no more questioned at present. The ratio of the energy in the optical flash to that of the gamma-ray burst observed many years thereafter is $E_{opt}/E_{\gamma} \sim 10^{-3}$. The discovery of optical flashes will undoubtedly produce a strong impact on possible models of gamma-ray bursts.

The most remarkable feature of the famous source of the 5 March 1979 event in the subsequent years was a series of recurrent bursts observed in the Konus experiment [32]. In the period 1979-1983, 14 bursts were detected altogether with sufficiently precise localization (Fig.9). Three more bursts from this source were observed from one Venera spacecraft only when the other instrument was turned off. By the general pattern of their time profiles and energy spectra these events did not differ from the other recurrent bursts. However the directional accuracy for them was, accordingly, less precise, the corresponding source positions representing circles of $\approx 15^{\circ}$. Therefore they are not shown in Fig.9.

The persisting activity of GBS0526-66 advocated the

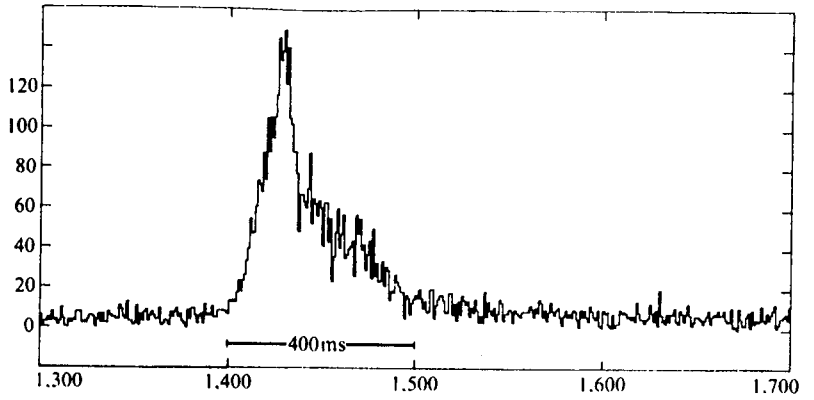

Fig.10. An optical flash presumed to originate in GB 0526-66 [34]

arrangement of optical patrolling of this source at several observatories. Of particular interest were the observations during the time period specified by Rothschild and Lingenfelter [33]. Several optical flashes from this region have been detected [34] (Fig.10). Unfortunately, the Venera 13 and 14 missions were terminated at the time, while simultaneous optical observations from different points failed. However the results of these observations appear promising and plans are under way to continue them.

5. Source Localization. A few cases of fairly precise localization of gamma-ray burst sources on the celestial sphere by triangulation are vastly outnumbered by source position measurements of modest and low accuracy. The bulk of these data were obtained in observations by Venera 11-14.

Fig.11 displays source positions of 160 gamma-ray bursts on the celestial sphere in galactic coordinates. The map does not include bursts localized as annuli-of-position and the cases where two alternative positions were obtained for a source. The sources are distributed over the sky in a random way with no noticeable clustering towards the galactic plane or the galactic center. Note, however, a certain asymmetry between the northern and southern hemispheres [35]. Fig.12 presents the source distribution in galactic latitude vs. the expected isotropic occurrence. 96 sources are found in the northern, and 64 in the southern hemisphere, the mean expected number being 80. The discrepancy is $\sim 2.5\sigma$, however it remains unclear whether it is real or originates from unaccounted for instrumental effects.

The burst distribution in intensity, i.e. in the total energy flux S (erg/cm^2), is usually presented in the log N(> S)-log S coordinates. The strong deviation of the experimental distributions from the -3/2 law is in a striking disagreement with the isotropic angular distribution obtained if one assumes a constant energy release in the

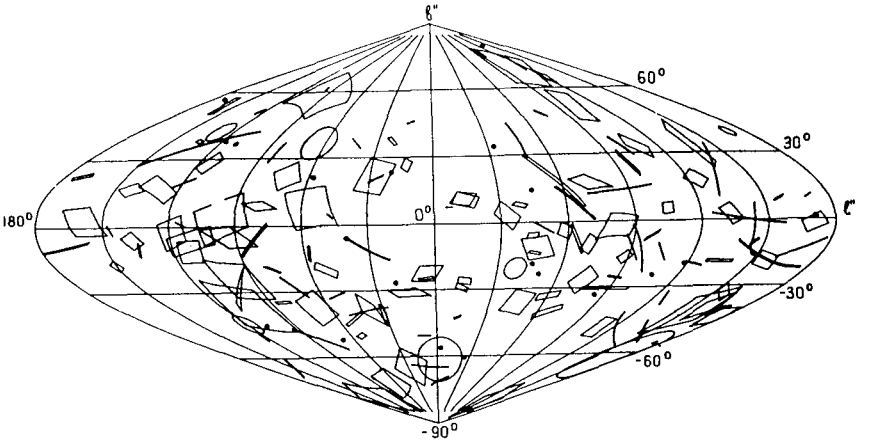

Fig.11. Sky map in galactic coordinates with positions of gamma-ray burst sources

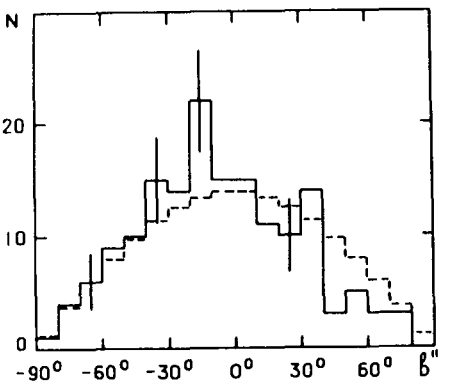

Fig.12. Source distribution in galactic latitude. Dashed line: expected relation for a random spatial distribution of the sources

sources. Several attempts were made to estimate the parameters of source spatial distribution from the observed log N - log S plots, assuming various luminosity distribution functions (Fig.13) [36,37]. However no reliable estimates of the spatial distribution of sources from the log N - log S plot can be obtained. The large extent of the measured values of S ranging from 10^{-7} to 10^{-3} erg/cm^2 does not correspond to the difference in distance scales to the closest and remotest of the observed sources. The spread in the values of S is determined predominantly by the broad distribution of gamma-ray bursts in duration and large variations between the energy spectra. Burst distributions in peak power P, erg/cm^{2}s, log N(>P) - log P, seem to be more realistic [38].

However this form of the data presentation also distorts the shape of the distribution. Gamma-ray burst detectors are not bolometric devices. In the detection and measurement of a burst they operate with count rates. Therefore the most appropriate form of data presentation is the

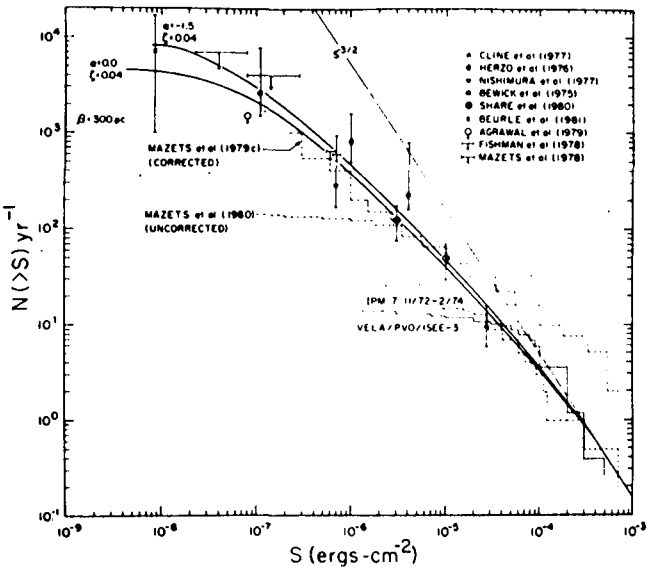

Fig.13. A comparison of some source spatial distribution models with log N - log S plots [36]

distribution of burst occurrence frequency vs. maximum count rate in the time profile, log N - log n_{max}. This approach has already been discussed as applied to the data of Venera 11 and 12 [39,40]. We have now at our disposal a sufficiently large homogeneous set of observational data from Venera 11-14. In Fig.14 these data are presented in the form of three plots: logN(>S)-log S, log N(>P)-logP, and log N(> n_{max}) - log n_{max}. Since the count rate n_{max} was determined in 1/4 s intervals, this data set does not include short bursts. As follows from the graphs, the distribution log N - log n_{max} which is the least subject to distortions shows full agreement with the -3/2 law. The deviations in the region of $n_{max} = 10^2 - 4\times10^2$ can undoubtedly be attributed to the loss of weak events near the detection threshold.

The range of n_{max} covered by observations, $\sim 10^2$-4×10^3 s^{-1}, is very narrow. It corresponds only to a factor ≈ 6 difference in distances to the closest and the remotest of the observed sources. Thus the log N - log n_{max} plot is in full agreement with an isotropic distribution of the sources over the celestial sphere. This implies that over the region of space corresponding to the sensitivity of the instrumentation used the gamma-ray burst sources are distributed uniformly. On the basis of these data alone one cannot decide between the galactic and metagalactic models of gamma-ray bursts. Evidence for the gamma-ray bursts being associated with neutron stars attests to the validity of the galactic models. Covering by observations the region of space above the galactic plane where the spatial distribution of the sources may change would apparently require a substantial increase of burst detector sensitivity by ten or

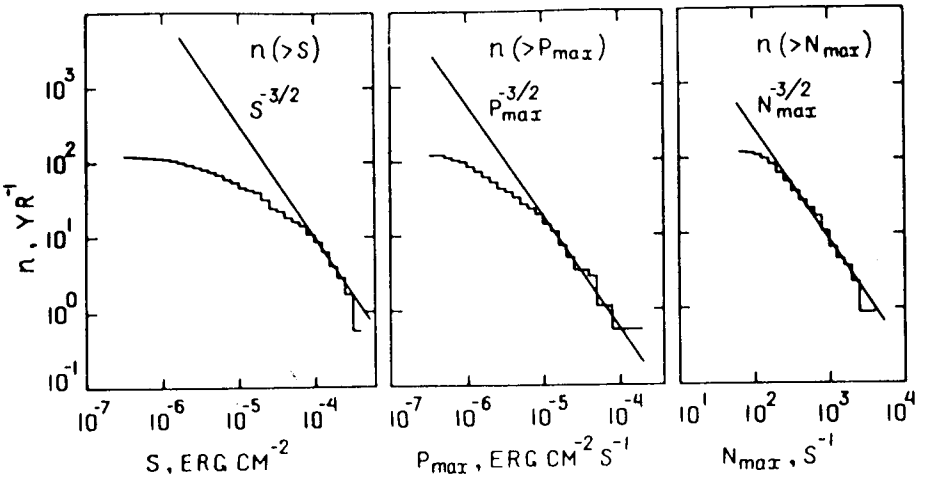

Fig.14. A comparison of three methods of data presentation. Only log $N(>n_{max})$ - log n_{max} distribution provides unequivocal interpretation

more times. Estimates of distances to the sources are at present closely connected with the existing physical models of bursts, including the sources of energy and emission mechanism. Thermonuclear models have apparently greater potential for the explanation of the origin of gamma-ray bursts [41-43].

6. Thermonuclear Scenario of a Gamma-Ray Burst. The major characteristics of gamma-ray bursts which should be taken into account in each model are as follows:

(1) By their duration the bursts are divided into two classes, namely, short (< 1 s) and long (1 s to a few minutes) ones.

(2) Long events may exhibit both a simple and very complex time structure.

(3) At least some of long bursts are preceded by weak precursors leading the bursts by 10 - 100 s.

(4) The continuum spectra of bursts evolve rapidly in time. The emission temperature correlates with emission intensity in the time profile.

(5) The burst energy spectra reveal spectral features of two types.

(6) The absorption (most probably cyclotron) features are in most cases the strongest in the initial phase of the burst.

(7) The broad annihilation lines are also the strongest in the beginning of the burst or at intense peaks of the time profile.

(8) The total energy release in a gamma-ray burst is

not constant. It grows approximately proportionately with event duration.

(9) Gamma-ray bursts may be accompanied by intense X-ray emission.

(10) The bursts may apparently be accompanied by optical flashes.

(11) When in quiescent state, the burst sources are so weak that one still has not succeeded in identifying them by emission in the X-ray and optical ranges.

The thermonuclear model of Woosley and Wallace [41] appears to account for these characteristics. It assumes that gamma-ray bursts originate in thermonuclear explosions on accreting, strongly magnetized neutron stars in binaries with a companion star of a late spectral class.

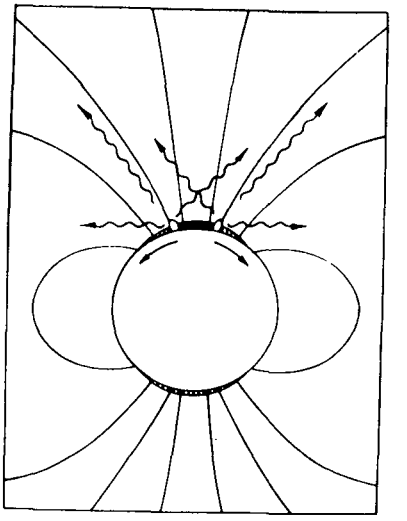

Fig.15. A thermonuclear scenario of cosmic gamma-ray burst

The suggested brief scenario of the burst is related closely to this model. However, observational data make us abandon the simplifying assumption of Woosley and Wallace that the accreting matter accumulates and is confined within a small, $\sim 10^{-3}$, polar cap region of the surface of the neutron star. The accumulated matter may apparently cover a fraction of the surface ranging from 10^{-3} to 0.1 or even greater. This may be due either to a spreading of the matter during the interval between successive bursts or directly to accretion on such a part of the surface. The distribution of matter over this spot may be extremely inhomogeneous, possibly due to the complex multipolar field structure on the neutron star surface. The thickness of the layer decreases, on the average, as one moves away from the center of the region (Fig.15). The matter in the layer undergoes preburst evolution. Stable burning of hydrogen in pycnonuclear reactions results in accumulation of helium. As soon as the helium layer density in the central part of the spot reaches a critical level, $\sim 10^{20}$ g/km^2, thermonuclear burning of helium becomes temperature-unstable. Thermonuclear runaway occurs and propagates towards the periphery of the spot.

Estimates of the lateral velocity of deflagration front are uncertain, $\sim$ 50-200 m/s [42]. This velocity apparently is not constant. It depends on density and magnetic

field. The different duration and large-scale time structure of long bursts are connected with propagation of the deflagration front across the region with an inhomogeneous distribution of fuel. The finer details in the time profile reflect apparently the front instabilities.

The energy released at the base of the layer is transported rapidly up to the surface by Alfvèn waves and dissipates there [43,44] . Hot plasma with a temperature $\gtrsim 10^9$ K is confined in the transverse direction by magnetic field while expanding vertically. On the neutron stellar surface a hot annular shell up to a few hundred meters high appears and propagates together with the annular burning region towards the periphery of the layer (Fig.15). The hot plasma pressure distorts drastically the magnetic field at the shell edge. Hence a magnetic field perturbation will propagate together with burning zone. The strong electric fields thus created accelerate electrons up to relativistic energies. Comptonization on fast electrons will produce very many hard photons. However the neutron star's magnetosphere is opaque to photons of energy >1 MeV due to magnetic pair production (γ, B) [45]. The collisions of hard photons (γ, γ) are likewise accompanied by pair creation [46]. Thus a pair plasma shell will form around the hot cloud of thermonuclear ash. The electrons and positrons lose rapidly their transverse energy by synchrotron emission. Before annihilation they move along magnetic field lines. Acceleration of particles in the radiation field may affect their longitudinal energy distribution such that the annihilation spectrum will acquire a characteristic shape of a broad line with an extended hard wing (Figs.5 and 6). This radiation can escape from the magnetosphere without appreciable attenuation only in a collimated beam at small angles to the magnetic field. The continuum emission is close to isotropic and reveals a fast falloff of intensity with increasing photon energy (Fig.2).

There is an intriguing possibility that the temperature at the trailing edge of the annular emitting region may be lower, in which case the annihilation emission will be associated predominantly with the leading edge. The cooling matter of the photosphere at the trailing edge will stream down rapidly towards the stellar surface on the free fall time scale. Radiation pressure will drive part of the matter from the photosphere away along the field lines creating a wind. Due to the negative temperature gradient in the photosphere, a cyclotron absorption line may appear in the continuum.

As the burst keeps developing, the annular burning shell passes through a layer with decreasing thickness. The energy released per unit area decreases. This results in a softening of the continuum and a reduction in intensity of the annihilation and cyclotron features.

The X-ray emission is naturally related to the cooling

of thermonuclear ash remaining after the passage of the burning shell.

There is little known about the optical flashes at present. They seem to be connected with a reprocessing of the gamma-ray burst on matter in the vicinity of the neutron star, namely, either in the accreting disc or in the plasma ejected during the burst. The suggested flash recurrence time, $\lesssim 1\ \mathrm{yr}^{-1}$ [47], is difficult to reconcile with the gamma-ray burst observations and the thermonuclear model.

The thermonuclear model permits evaluation of the distance scales to the burst sources. Single-pulse bursts 5-10 s long correspond, within our scenario, to the explosion of a region 1 to 2 km in radius. According to model I of Woosley and Wallace [41] the energy released in gamma rays in such a burst should be $\sim 5\times10^{38}$ erg. The brightest events of this type observed thus far have a total fluence $S \sim 2\times10^{-5}$ erg/cm^2. This leads to an estimate of distance to the nearest sources of ≈ 300 pc. Then, in accordance with the relation log N - log n_{max}, the farthest of the detected burst sources could be at a distance of ≈ 1.8 kpc.

For the burst recurrence time $\gtrsim 10$ yr the average accretion rate should be $\lesssim 4\times10^{-14}\ M_\odot$/yr, and the constant X-ray luminosity of the source $\sim 5\times10^{32}$ erg/s. These estimates support the assumption of the neutron star's companion in the binary being a star of the latest spectral class with low mass and luminosity. The possibility of explaining short bursts as due to detonation thermonuclear explosions by model II [41] appears very attractive. In this case, however, the corresponding distance estimates will increase ten times. Still, detonation models involving smaller energy release can apparently be also designed.

Thus the thermonuclear model developed for gamma-ray bursts appears to conform to the major observational characteristics of bursts.

The most serious difficulty for this model may come from the observation of a weak feature in the burst time profile, namely, of the precursors. These weak pulses are definitely connected with the main phase of the burst and do not exist independently of it. Otherwise one would have observed numerous weak recurrent bursts from the same source. It is difficult to account for the situation when the process of thermonuclear burning, once initiated, dropped drastically in intensity, only to flare up again a few tens of seconds later.

7. Conclusion. Cosmic gamma-ray bursts remain one of the most intriguing and complex problems in astrophysics. There is much work ahead, both experimental and theoretical,

before we may hope to come closer to the understanding of the nature of this mysterious phenomenon.

References

1. Klebesadel, R.W. et al., (1973), Astrophys.J. 182, L85.
2. Mazets, E.P., and Golenetskii, S.V., (1981), Astrophys. Space Sci. 75, 47.
3. Klebesadel, R.W. et al., (1982), in Gamma-Ray Transients and Related Astrophysical Phenomena, eds. R.E.Lingenfelter, H.S.Hudson & D.M.Worrall, AIP Conf. Proc. No 77, NY, p.1.
4. Mazets, E.P. et al., (1982), Astrophys. Space Sci. 84, 173.
5. Hurley, K., (1984), in High Energy Transients in Astrophysics, ed.S.E.Woosley, AIP Conf. Proc. No 115, NY, p.363.
6. Norris, J.P. et al., (1984), ibid., p.367.
7. Pizzichini, G., (1981), Astrophys. Space Sci. 75, 205.
8. Wood, K.S., (1984), in High Energy Transients in Astrophysics, ed. S.E.Woosley, AIP Conf. Proc. No 115, NY, p.409.
9. Desai, U.D., (1981), Astrophys. Space Sci. 75, 15.
10. Knight, F.K. et al., (1981), Astrophys. Space Sci. 75, 21.
11. Mazets, E.P. et al., (1982), Astrophys. Space Sci. 82, 261.
12. Ramaty, R. et al., (1981), Astrophys.Space Sci.75, 193.
13. Liang, E.P., (1981), Nature 299, 378.
14. Teegarden, B.J., (1984), in High Energy Transients in Astrophysics, ed.S.E.Woosley, AIP Conf. Proc. No 115, NY, p. 352.
15. Katz, J.I., (1982), Astrophys. J. 260, 371.
16. Lamb, D.Q., (1984), Ann. NY Acad. Sci. 422, 237.
17. Colgate, S.A. et al., (1984), in High Energy Transients in Astrophysics, ed. S.E.Woosley, AIP Conf. Proc. No 115, NY, p.548.
18. Mazets, E.P. et al., (1981), Nature 290, 378.
19. Golenetskii, S.V. et al., (1983), Nature 306, 451.
20. Barat, C. et al., (1984), Astrophys. J. 286, L11.
21. Share, G.H. et al., (1982), in Gamma-Ray Transients and Related Astrophysical Phenomena, eds. R.E.Lingenfelter, H.S.Hudson & D.M.Worrall, AIP Conf. Proc. No 77, NY, p.45.
22. Nolan, P.L. et al., (1984), in High Energy Transients in Astrophysics, ed. S.E.Woosley, AIP Conf. Proc. No 115, NY, p.399.
23. Aptekar, R.L. et al., (1985), these Proceedings,OG1.1-3.
24. Ramaty, R., and Mèszaros, P., (1981), Astrophys. J.250, 384.
25. Aharonyan, F.A. et al., (1983), Astrophys. Space Sci. 93, 229.
26. Hueter, G.J., (1984), in High Energy Transients in Ast-

rophysics, ed. S.E.Woosley, AIP Conf. Proc. No 115, NY, p.373.
27. Laros, J.G. et al., (1984), Astrophys. J. 286, 681.
28. Hurley, K., (1982), in Gamma-Ray Transients and Related Astrophysical Phenomena, eds. R.E.Lingenfelter, H.S.Hudson & D.M.Worrall, AIP Conf. Proc. No 77, NY, p.85.
29. Cline, T.L. et al., (1984), Astrophys. J. 286, L15.
30. Schaefer, B.E., (1981), Nature 294, 722.
31. Schaefer, B.E. et al., (1984), Astrophys. J. 286, L1.
32. Golenetskii, S.V. et al., (1984), Nature 307, 41.
33. Rothschild, R.E., and Lingenfelter, R.E., (1984), Nature 312, 737.
34. Pedersen, H. et al., (1984), Nature 312, 46.
35. Vedrenne, G., (1981), Phil. Trans. Roy. Soc. A301, 645.
36. Jennings, M.C., (1982), Astrophys. J. 258, 110.
37. Jennings, M.C., (1984), in High Energy Transients in Astrophysics, ed. S.E.Woosley, AIP Conf. Proc. No 115, NY, p.412.
38. Mazets, E.P. et al., (1980), Pis'ma v Astron. Zhurnal 6, 609.
39. Belli, B.M., (1984), in High Energy Transients in Astrophysics, ed. S.E.Woosley, AIP Conf. Proc. No 115, NY, p.426.
40. Lund, N., (1985), private communication.
41. Woosley, S.E., and Wallace, R.K., (1982), Astrophys.J. 258, 716.
42. Woosley, S.E., (1984), in High Energy Transients in Astrophysics, ed. S.E.Woosley, AIP Conf. Proc. No 115, NY, p.485.
43. Bonazzola, S. et al., (1984), Astron. Astrophys. 136, 89.
44. Mitrofanov, I.G., and Ostryakov, V.M., (1981), Astrophys. Space Sci. 77, 469.
45. Daugherty, J.K., and Harding, A.K., (1983), in Positron-Electron Pairs in Astrophysics, eds. M.L.Burns, A.K.Harding & R.Ramaty, AIP Conf. Proc. No 101, NY, p.387.
46. Burns, M.L., and Harding, A.K., (1983), ibid., p.416.
47. Schaefer, B.E., and Cline, T.L., (1985), Astrophys. J. 289, 490.

OBSERVATIONS OF SHOCK ACCELERATION PROCESSES IN THE SOLAR WIND

M. Scholer
Max-Planck-Institut für Physik und Astrophysik
Institut für extraterrestrische Physik
8046 Garching, F.R.G.

1. Introduction. Substantial evidence has been accumulated over more than two decades that ion acceleration occurs at all collisionless shocks sampled directly in our solar system. Figure 1 (after Gloeckler, 1984) shows schematically the various shock waves in the heliosphere and the associated energetic particle phenomena. Three shocks have attracted considerable attention in recent years: corotating shocks due to the interaction of fast and slow solar wind streams during solar minimum, travelling interplanetary shocks due to coronal mass ejections and planetary bow shocks. We will review briefly the signatures of these shocks and of their energetic particles, will shortly review the most prominent theoretical models for shock acceleration and discuss in more detail recent observations at the earth's bow shock and at quasi-parallel interplanetary shocks.

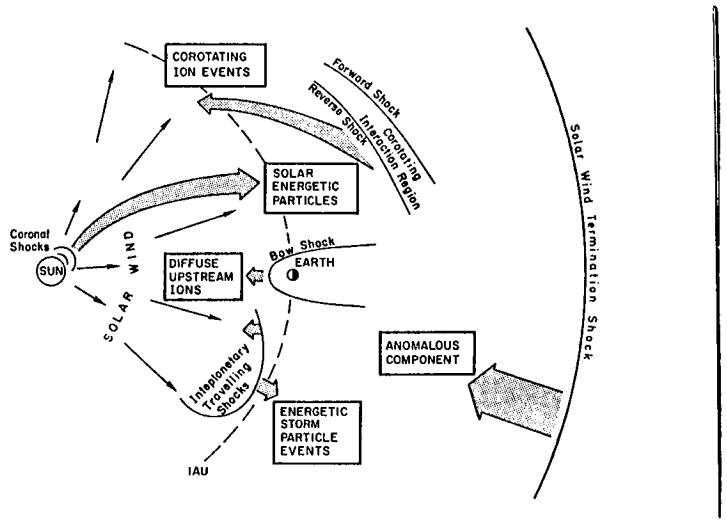

Fig. 1 Heliospheric shocks and associated particle events (after Gloeckler, 1984)

2. Corotating Interaction Regions and Associated Particle Events. During solar minimum the most prominent structures of the interplanetary medium are the high and slow velocity streams. The high velocity streams are presumably originating from polar coronal holes which extend during solar minimum at certain longitudes across the solar equator so that regions with emerging high and slow velocity solar wind are distributed at the solar equator in longitude. Due to the rotation of the sun a high velocity stream following a slow velocity stream will run into the slow velocity stream. Beyond a distance of about 1.5 AU a pair of shocks develop at the inner and

outer edges of the interaction region between high and slow velocity stream (Fig. 2). One of the shocks (running into the slow solar wind) is a foreward shock which propagates out from the sun. The other half of the shock pair is a reverse shock, so-called because it travels backward toward the sun in the solar wind frame. The position of double peaks in recurring energetic ion increases coincides more or less with the appearance of these foreward and reverse shocks (Barnes and Simpson 1976; Tsurutani et al., 1982). McDonald et al. (1976) and Van Hollebeke et al. (1978) have studied the increase of these events with increasing distance in the heliosphere. The distribution functions of protons, He, C, N, O, and Fe can all be very well represented by an exponential in velocity with nearly equal e-folding speeds for all elements in a given corotating event (Gloeckler et al., 1979). Before leaving the topic of corotating particle events we should like to mention that recently Richardson (1985) has presented evidence that in the interaction region within 1 AU, i.e. when the shocks have not developed yet, second order Fermi acceleration accelerates suprathermal solar wind ions up to ~ 300 keV.

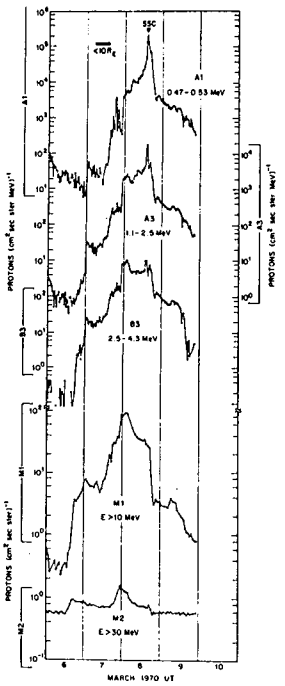

Fig. 2 Typical energetic storm particle event as observed at different energies (Lanzerotti, 1974).

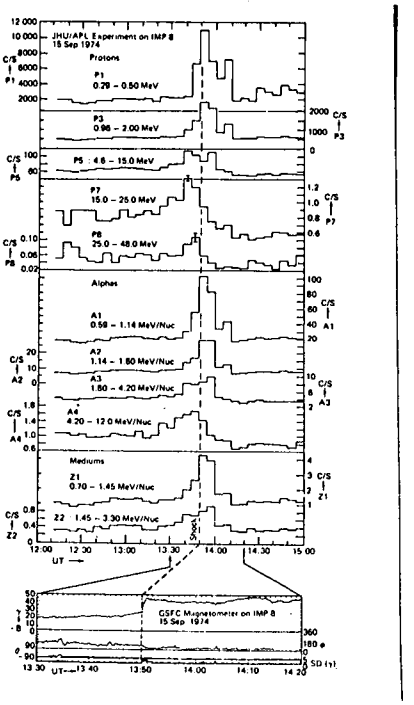

Fig. 3 Intensity vs time for a shock spike event (Sarris et al., 1976).

3. Interplanetary Travelling Shocks. Interplanetary travelling shocks are usually observed as fast mode foreward propagating (with respect to the solar wind frame of reference) shocks and are produced by coronal mass ejections. It has been known for more than two decades that the arrival of a travelling shock at the Earth is often accompanied by large enhancements of energetic solar flare particles. These events have been termed energetic storm particle (ESP) events since they often occur in connection with a sudden storm com-

mencement at Earth (SSC). The effect of the shock wave in altering the profiles of energetic particles can be seen from Figure 2 (Lanzerotti, 1974). Plotted in Figure 2 are proton fluxes measured on Explorer 34 in several different energy channels. The profile of the > 30 MeV protons indicates that two flares are responsible for the energetic particles measured during this time interval. In the lower energy range the second event deviates strongly from a simple diffusive profile and in the lowest energy channel the profile is actually dominated by the particles associated with the SSC. The duration of the ESP events is in the 1 MeV energy range typically of the order of several hours. Recently, new information on acceleration at quasi-parallel interplanetary travelling shocks in the energy range below a few hundred keV have become available from the ISEE-3 spacecraft. This is important since only for particles of this energy the acceleration time is less than (or comparable to) the shock travel time to 1 AU, so that only in this energy range detailed comparison with the predictions of the steady-state quasi-linear theory of diffusive shock acceleration can and should be made.

A different category of shock associated particle increases are the so-called shock spike events. They last typically only several minutes up to half an hour around the shock passage. Figure 3 from Sarris et al. (1976a) shows a shock spike event which extends to very high energies. Sarris and Van Allen (1974) have shown that shock spike events occur in connection with quasi-perpendicular shocks. They explained the shock spike events by an acceleration of solar flare particles in terms of a displacement along the interplanetary electric field during reflection at the shock.

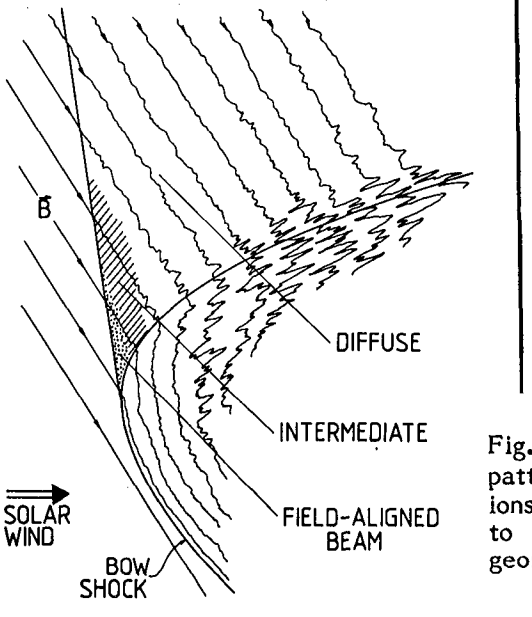

Fig. 4 Average spatial distribution pattern of diffuse ions, intermediate ions, and field-aligned beams relative to the magnetic field-bow shock geometry.

4. The Earth's Bow Shock. Since the solar wind approaches a planetary obstacle with a supersonic speed planetary bow shocks will occur in front of planets with an intrinsic dipole field or with conducting atmospheres. Along a planetary bow shock the angle θ_{Bn} between the magnetic field and the shock normal changes from 90° (at the position where the magnetic field first touches during its convection with the solar wind the bow shock) to 0° (see Figure 4). Furthermore, the region upstream of the quasi-perpendicular part

of the bow shock will be convected with the solar wind into the quasi-parallel part of the shock. Any process which depends on field line connection time, as diffusive shock acceleration, will therefore be only observed at and beyond the quasi-parallel bow shock, since here connection times are longest.

Gosling et al. (1978) have shown that in the lower energy range (below ~ 30 keV) there exist distincly different populations in the upstream region of the Earth's bow shock into which these ions can be grouped. These ions have been called reflected and diffuse bow shock ions, respectively. Reflected ions were originally identified as beams of particles travelling upstream along the interplanetary magnetic field and are found predominantly in the quasi-perpendicular bow shock regime. Diffuse ions, predominantly observed in the quasi-parallel regime, extend to much higher energies and their angular distribution is more nearly isotropic. Figure 5 shows to the left relief plots of upstream ion distributions in the v_x, v_y plane (Paschmann et al., 1981). The isolated peak in the middle is the solar wind distribution. The distribution at the top shows a beam of upstreaming ions, which is almost parallel to the magnetic field. Paschmann et al. (1981) have shown that the energy of the beams is correctly predicted by the assumption of reflection under conservation of the magnetic moment, as first proposed by Sonnerup (1969). Alternative models for upstream beams have been proposed, whereby gyrating ions in the foot of the quasi-perpendicular shock are convected downstream, are pitch-angle scattered by self-excited electromagnetic ion cyclotron waves and can escape again back upstream parallel to the magnetic field (Tanaka et al., 1983).

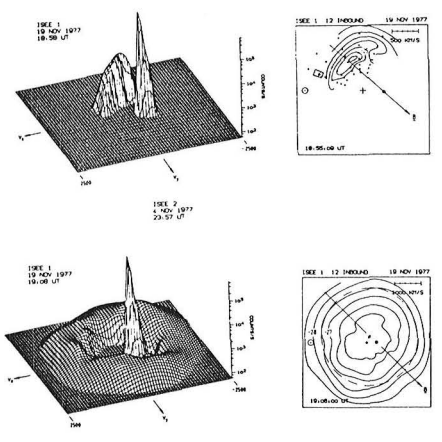

Fig .5 Left hand side: relief plots in 2-dimensional velocity space. Right hand side: contours of const. phase space density for the same events (Paschmann et al., 1981).

Figure 5 shows in the lower part a relief plot of ion distributions found upsteam of the quasi-parallel bow shock. This ion distribution is not beam-like, but is a broad ring-shaped feature or ridge, centered near the origin, with a steeper inner slope and a more gradual slope towards larger velocities. These ions are called diffuse ions since the distribution is more or less isotropic in a frame somewhere between the bow shock frame and the solar wind frame.

Spectra of diffuse ions extend into the higher energy range, i.e. up to 100 keV and higher. Ipavich et al. (1979) and Scholer et al. (1979) reported a peculiar time dependence during upstream particle events: lower energy particles reach their equilibrium intensity level earlier than higher energy particles. When the magnetic field changes from the no bow shock connection case to bow shock connection, upstream protons of 30 keV appear within a

few minutes and reach then a constant intensity level. Protons of 130 keV either do not reach a plateau profile as a function of time at all or with a delay of ~ 30-40 min. These dispersion effects have been explained in terms of a time-dependent Fermi acceleration process in the following manner: let us assume that the upstream field turns from a nonconnected situation into a nearly solar wind flow aligned situation (radial field). At the satellite position the intensities will build up in the time-dependent acceleration process with an energy dependent time constant τ. Scholer et al. (1980a) have calculated from the observed time dispersion at various energies the diffusion coefficient and its energy dependence. The mean free path at 30 keV is 4 R_E and the diffusion coefficient depends about linearly on energy. The field line connection time has therefore to be considerably larger in order to observe diffuse upstream particles at higher energies.

Discrimination between protons and alpha particles is essential in order to obtain differential intensity spectra of diffuse ions in the higher energy range. Ipavich et al. (1981) have shown that diffuse ions exhibit above ~ 15 keV spectra which can be very well represented by exponentials in energy. Figure 6 shows proton, alpha particle and heavy ion spectra averaged over the plateau phase of an upstream event (Ipavich et al., 1981) in a log versus lin representation. Note that the least squares fit to the H, He, and heavy ion spectra have the same slope, i.e. the abundance ratios are constant when evaluated at equal energy per charge.

Recently, Wibberenz et al. (1985) have performed a detailed analysis of the relation between field line connection time, the occurrence of upstream ions, and the spectral parameter (e-folding energy) of the differential intensity spectrum. They found that the hardest spectra require in general connection times above 40 min. Although the spacecraft may be magnetically connected with the bow shock all the time (positive connection time) the energetic proton intensity is nevertheless controlled by the magnitude of the connection time. This is according to Wibberenz et al. a strong argument against a magnetospheric origin of the upstream particle population during these events.

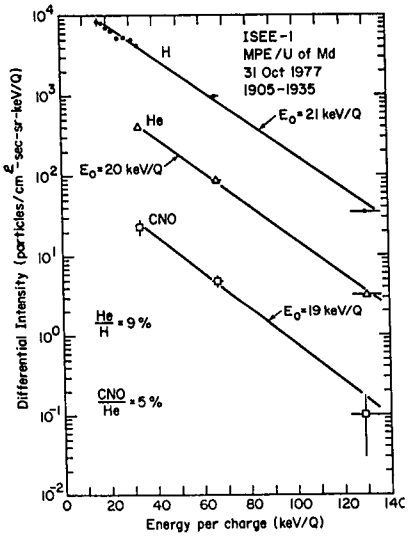

Fig. 6 Proton, alpha particle and heavy ion spectra (C, N, O) spectra during an upstream diffuse particle event (Ipavich et al., 1981).

We should like to make a few comments on the contribution of magnetospheric energetic particles to the upstream ions. The magnetosphere is known to be a large reservoir of energetic ions and electrons and these particles may escape occasionally upstream (e.g. Sarris et al., 1976b, 1978). Scholer et al. (1981) have tried to separate the magnetospheric population from the bow shock accelerated population by analyzing energetic electrons. They found two types of upstream proton events: one group is accompanied by energetic electrons and extends up to energies of 300 keV, a second group is not accompanied by energetic electrons and can be represented very well by exponential energy spectra. Scholer et al. suggested that the first group is of magnetospheric origin and the second group is due to bow shock acceleration. Recently, Anagnostopoulos et al. (1985) have questioned the interpretation of upstream ions above $\sim$ 50 keV in terms of diffusive shock acceleration. They claim that many, if not all upstream ion events above this energy are of magnetospheric origin. This has renewed interest in the topic of upstream events and a careful reevaluation of this topic appears necessary.

5. Theory of Shock Acceleration. The first analytical treatment of diffusive shock acceleration has been given by Fisk (1971) and has been developed in considerable detail by Krimsky (1977), Axford et al. (1977), Bell (1978 a, b) and Blandford and Ostriker (1978). In this model it is assumed that particles are scattered approximately elastically in the frame of the plasma. The elastic scattering is due to small-angle pitch angle scattering by hydromagnetic waves that convect approximately with the local flow speed. The particles which are scattered back toward the bow shock in the upstream medium can gain considerable energy in the shock frame. The particles are possibly reflected back from the shock front or are scattered back by downstream waves so that particles can reencounter the shock many times. This scenario does not describe how an initial reflection of a fraction of the solar wind ions incident on the shock gets the acceleration process started. In the simple case of a plane shock and monoenergetic injection at some momentum p_0 the distribution function is in the steady state at the shock given by a power law for $p > p_0$, i.e. $f \propto E^{-\gamma}$ where γ related to is the velocity difference between the upstream and downstream scattering centers. If the initial spectrum is softer than what the shock would produce for monoenergetic injection, than the spectrum near the shock is altered to the "shock" spectrum at higher energies. On the other hand, if the initial spectrum is flatter than the "shock" spectrum, the initial power law is preserved at high intensities but the intensities are shifted upward (see, e.g. Axford, 1981).

The spatial dependence of the distribution function upstream along the magnetic field is essentially given by an exponential with an e-folding distance L, $L = \kappa_{\parallel}/V_1$. Since $\kappa_{\parallel}$ in general increases with energy the e-folding distance of the phase space density depends on energy as well. Thus, the distribution function is a power law only at the shock and in the down-stream medium. Note that in the steady state and for infinite plane shocks the form and the absolute value of the distribution function is independent of the diffusion coefficient. The mean free path only determines how fast the steady state is reached. Further ahead of the shock the distribution function does depend on the form of the diffusion coefficient and tends to the peaked because the intensity of low energy particles falls off faster with distance upstream than high energy particles. As outlined in the first section, spectra of corotating events are not power laws as predicted by the steady state diffusive acceleration model at planar shocks, but close to exponentials

in velocity. Fisk and Lee (1980) have included the adiabatic deceleration term due to the radially expanding solar wind. They were able to show that upstream diffusion of the shock accelerated particles against the radially expanding solar wind leads to a steepening of the spectra with increasing energy. The leading dependence of the distribution function on particle velocity is an exponential which is independent of particle species. Furthermore their theory predicts a steeper spectrum at the forward shock than at the reverse shock, consistent with the observations (Scholer et al., 1980b).

The exponential spectral form of ion events upstream of the bow shock is also at variance with the prediction of diffusive shock acceleration at planar shocks in the steady state. Scholer et al. (1980a) have suggested that the steepening of the spectrum could be due to the limitation of the upstream wave field to some distance close to the shock and have introduced the concept of a free escape boundary. Such a free escape boundary does, of course, not really exist in nature; it is simply a means to conveniently describe the loss of particles out of the system. An analytical solution for this scenario within the limits of diffusion theory has been given by Lee et al. (1981) and Forman (1981). Ellison (1981) and Terasawa (1981) also used a free escape upstream in their numerical models.

Any process where the loss increase with energy results in a steepening of the spectra. Eichler (1981), in contrast to upstream escape, proposed as a loss process diffusive transport normal to the magnetic field and lateral free escape along field lines not connected to the bow shock. Eichler (1981) found that in addition to the spectra being close to the observed exponential form they are functions of energy per charge only, independent of the assumed mass, charge and energy dependence of the parallel diffusion coefficient.

A theory for the coupled behaviour of the hydromagnetic waves and diffuse ions that result when the magnetic field is nearly parallel to the solar wind has been presented by Lee (1982). The diffuse ions stream relative to the solar wind in the upstream direction with a velocity greater than the solar wind velocity and are therefore subject to the hydromagnetic streaming instability, the threshold of which is the Alfvén speed. This results in the growth of the hydromagnetic waves that propagate upstream, which in turn scatter the particles toward isotropy thus reducing the growth rate. At the same time waves propagating toward the shock are damped. The growth or damping rate is determined by the pitch angle anisotropy of the distribution function. Assuming an interplanetary wave activity far upstream with the waves travelling toward, the bow shock, perpendicular diffusion is required to yield other than power law spectra at the shock. For this case Lee (1982) determined uniquely the distribution function and the power spectral density as a function of distance from the shock.

A self-consistent theory for the excitation of hydromagnetic waves and the diffusive acceleration at travelling interplanetary shocks has also been given by Lee (1983). The interplanetary shock is assumed to be planar so that cross-field diffusion does not have to be considered. Since the distribution function decreases with distance upstream of the shock, the waves propagating away from the shock front in the frame of the solar wind are unstable. Interplanetary hydromagnetic waves in the spacecraft frame are observed to propagate predominantly away from the sun. Thus, the streaming anisotropy leads only to wave growth of the "background" outward travelling waves. This, together with the boundary condition at the shock and the condition that the distribution function is zero at large distances from the shock, allows the unique determination of the differential wave intensity

spectrum and of the ion omnidirectional distribution function as a function of distance upstream. A test of this quasi-linear theory has recently been performed for a specific quasi-parallel interplanetary shock by the so-called "November 11-12 shock-collaboration group" under the lead of C.F. Kennel and will be reported in section 6.

We will briefly discuss the shock drift mechanism which is presumably responsible for the shock spike events. In this so-called V x B mechanism particles gain energy in a single shock encounter by drifting in the inhomogeneous magnetic field at the shock front parallel to the V x B electric field. This mechanism was first proposed for acceleration of solar wind ions at the earth's bow shock by Sonnerup (1969). The most detailed theoretical analysis of this process has been given by Decker (1982, 1983). He calculated intensity enhancements, energy spectra, and pitch angle distributions of an initial or ambient particle distribution after a single shock encounter. The intensity enhancement and the pitch angle distribution depends strongly on the ratio of a particle's initial energy T and the energy T_o defined by the Hoffman-Teller velocity V_{HT}. (V_{HT} is the velocity of a system moving parallel to the shock front, so that the flow upstream and downstream is field aligned). Ions with $T/T_o \gtrsim 1$ stream upstream away from the shock (in the plasma frame), at $T/T_o \gg 1$ the effect of the loss cone leads to an intensity minimum parallel to the field. In the downstream medium ions with $T/T_o < 1$ stream towards the shock (in the plasma frame), ions with $T/T_o \gg 1$ exhibit a pancake-like distribution, i.e. the intensity is enhanced at 90° with respect to the magnetic field. Sanderson et al. (1984) have compared these predictions with distributions measured in shock spike events at quasi-perpendicular shocks. They found during these events large negative values of the downstream second harmonic anisotropy. This is the most recognisable feature of the drift acceleration model, and is due to the ions gyrating around the field at pitch angles of $\sim 90°$.

As pointed out by Lee (1984) the distinction between the shock drift and the diffusive acceleration rests not on basic physics but on whether one or many encounters is appropriate to a particular particle population. In general a particle gains energy by <u>both</u> compression and drift parallel to the motional electric field, although the separtion of the energy gain into compressional and drift contributions is frame-dependent (in the Hoffman-Teller frame, for example, the drift contribution vanishes). In a single encounter of a particle with an oblique shock with no scattering there is, of course, no compressional energy gain. When comparing the efficiency and the relative merits of quasi-parallel and quasi-perpendicular shocks, respectively, as particle accelerators, it should be noted that the relevant diffusion coefficient in the diffusive shock acceleration theory is that in the shock normal direction, $\varkappa_n$. Since $\varkappa_n \approx \varkappa_\parallel \cos^2 \Theta_{Bn}$, where $\varkappa_\parallel$ is the diffusion coefficient parallel to the magnetic field, it is trivial that as long as the steady state is not reached quasi-perpendicular shocks are more "efficient" accelerators. For a shock with $\Theta_{Bn} = 87.5°$ as reported by Krimigis and Sarris (SH 1.5-4), the effective diffusion coefficient is reduced by 2-3 orders of magnitude.

<u>6. Test of the Quasi-linear Theory.</u> Kennel et al. (1985) have recently performed a detailed test of the quasi-linear theory of diffusive acceleration as predicted by Lee (1983), using ISEE-3 measurements of the November 12, 1978 quasiparallel shock. The quasilinear theory makes ten specific predictions for the particle and wave signatures. We will now briefly report on the result of the Kennel et al. study.

1. The energetic ions at the shock should have a power law velocity distribution. This has been observed to be the case with the power law index, β, between 4.20 and 4.25 (Scholer et al., 1983, Van Nes et al., 1984).

2. The index is related to the upstream and downstream velocity of the scattering centers. Kennel et al. found that when correcting the upstream and downstream plasma velocities for the Alfvén velocity the predicted index is 4.2 when neglecting the Alfvén velocity an index of 4.7 is predicted (in substantial disagreement with the observations).

3. The upstream scale length (e-folding distance) should increase with energy according to a power law. The power law index α is related to the index β of the power law distribution function via $\alpha = (\beta-3)/2$. The parameter α derived from the measured scalelengths is in excellent agreement with this relation.

4. The absolute magnitude of the scalelength should depend inversely upon the partial number density of energetic protons at the shock. From the measured number density the scalelength is correctly predicted.

5. Upstream of the shock the parallel anisotropy should be positive in the solar wind frame (away from the shock) and constant. The measurements show a constant anisotropy of $\sim$ 0.3 in the upstream region and a zero anisotropy immediately downstream of the shock.

6. The phase and group velocity of the waves should be directed upstream along the magnetic field. This cannot be tested with a single spacecraft. The wave spectrum is however weakly polarized, with a roughly equal mixture of right-hand and left-hand waves, as prescribed by the quasilinear theory.

7. The scalelength of the magnetic energy density of the upstream waves should be equal to the scale length of the protons in cyclotron resonance with them. The scalelength of the trace amplitude between 0.02 and 0.06 Hz indeed corresponds to the scalelength of $\sim$ 40 keV protons.

8. The total wave magnetic energy density integrated over the spectrum of resonant waves is predicted to be proportional to the total energy density of the upstream ions. Extrapolating the measured power law of the distribution function down to 3 keV the quasilinear estimate agrees indeed with the measured normalized trace amplitude of the waves.

9. The magnetic field power spectrum of the self-excited waves should increase towards lower frequencies according to a power law with a spectral exponent $\delta = 6-\beta$. However, the observations show a flat or even peaked spectrum in the respective frequency range.

10. There should be no wave excitation at frequencies larger than the resonance frequency of a proton whose component of parallel velocity in the shock normal direction is zero in the shock frame. This frequency is about 0.1 Hz. However, the spectral density above 0.1 Hz was several hundred times larger than that in the solar wind.

This detailed investigation shows that the quasi-linear theory successfully predicts numerous observations at this particular quasi-parallel shock. The wave power spectrum is related to the protons via the resonance condition which invokes the particle's parallel velocity. Since the theory by Lee (1983) makes approximations that essentially loose the pitch-angle dependence of the particle distribution it is not unexpected that this theory gives not better agreement with the observed wave spectrum.

7. References

Anagnostopoulos, G.C., et al., (1985), submitted to J. Geophys. Res.
Axford, W.I., (1981), Proc. 17th ICRC 12, 155
Axford, W.I., et al., (1977), Proc. 15th ICRC 11, 132
Barnes, C.W., and Simpson, J.A., (1976), Ap.J. 210, L91
Bell, A.R., (1978a), MNRAS 182, 147
Bell, A.R., (1978b), MNRAS 182, 443
Blandford, R.R., and Ostriker, J.P., (1978), Ap.J. 221, L29
Decker, R.B., (1981), J. Geophys. Res. 86, 4537
Decker, R.B., (1983), J. Geophys. Res. 88, 9959
Eichler, D., (1981), Ap.J. 244, 711
Ellison, D.C., (1981), Geophys. Res. Lett. 8, 991
Fisk, L.A., (1971), J. Geophys. Res. 76, 1662
Fisk, L.A., and Lee, M.A., (1980), Ap.J. 237, 620
Forman, M.A., (1981), Proc. 17th ICRC 3, 467
Gloeckler, G., (1979), Ap.J. 230, L191
Gloeckler, G., (1984), Adv. Space Res. 4, 127
Gosling, J.T., et al., (1978), Geophys. Res. Lett. 5, 957
Ipavich, F.M., et al., (1979), Space Sci. Rev. 23, 93
Ipavich, F.M., et al., (1981), J. Geophys. Res. 86, 11153
Kennel, C.F., et al., (1985), submitted to J. Geophys. Res.
Krimsky, G.F., (1971), Dokl. Akad. Nauk 234, 1306
Lanzerotti, L.J., (1974), in Correlated Interpl. and Magnetospheric Observations, D. Reidel, 345
Lee, M.A., et al., (1981), Geophys. Res. Lett. 8, 401
Lee, M.A., (1982), J. Geophys. Res. 87, 5093
Lee, M.A., (1983), J. Geophys. Res. 88, 6109
Lee, M.A., (1984), Adv. Space Res. 4, 295
McDonald, F.B., et al., (1976), Ap.J. 203, L149
Paschmann, G., et al., (1981), J. Geophys. Res. 86, 4355
Richardson, I.G., (1985), Planet. Space Sci. 33, 557
Sarris, E.T., and Van Allen, J.A., (1974), J. Geophys. Res. 79, 4157
Sarris, E.T., et al., (1976a), Geophys. Res. Lett. 3, 133
Sarris, E.T., et al., (1976b), J. Geophys. Res. 81, 2341
Scholer, M., et al., (1979), Geophys. Res. Lett. 6, 701
Scholer, M., et al., (1980a), J. Geophys. Res. 85, 1743
Scholer, M., et al., (1980b), J. Geophys. Res. 85, 4602
Scholer, M., et al., (1981), J. Geophys. Res. 86, 9040
Scholer, M., et al., (1983), J. Geophys. Res. 88, 1977
Tanaka, M., et al., (1983), J. Geophys. Res. 88, 3046
Terasawa, T., (1981), J. Geophys. Res. 86, 7595
Tsurutani, B.T., et al., (1982), J. Geophys. Res. 87, 7389
Sonnerup, B.U.Ö., (1969), J. Geophys. Res. 74, 1301
Van Hollebeke, M.A.I., et al., (1978), J. Geophys. Res. 83, 4723
Van Nes, P., et al., (1984), J. Geophys. Res. 89, 2122
Wibberenz, G., et al., (1985), J. Geophys. Res. 90, 283

IS THE SIGNAL FROM CYG X-3, AS RECORDED IN SOME UNDERGROUND EXPERIMENTS, REAL?

(Introduction to the discussion at highlight session Aug 16, 1985)

A. E. Chudakov

On the suggestion of the oganizing committee I shall summarize briefly the results of the discussion meeting held on the evening of August 13 and try to compare evidence from different detectors.

Most of the excitement concerning the underground detection of signals from Cyg X-3 comes not from astrophysical grounds (though it could be difficult to imagine such a powerful source), but from the contradiction with surface experimental data. Believing in the Cyg X-3 signal underground and also that the main processes of muon production are well known we come to the conclusion that the signal in EAS Cherenkov or counter experiments should be remarkably high, which is not the case.

Thus, we face severe alternatives: either there is something wrong in the interpretation of the underground evidence, or a quite new Physics is involved, the structure and importance of which we can not even evaluate. This requires us to examine the experimental data very carefully.

Generally speaking, there are two approaches in a search for a point-like sources in the sky: 1) To look for an excess from a given direction (angular domain) 2) To look for the intensity variation in time from a given direction (periodic, sporadic, complex - time domain). For me the first approach is more convincing. Certainly there is a difficult question of how many "sigma's" are convincing?

Unfortunately, there is only one EAS experiment (Kiel) in which Cyg X-3 has been seen in both domains, which is so far a unique case for UHE gamma-astronomy.

It is difficult to find out what could be wrong in the phase-analysis of Cyg X-3 data. The most convincing data comes from NUSEX-experiment. The visible weak point in the analysis for this case is the choice of the acceptance solid angle. This choice is made empirically on the basis of accumulated data to have the biggest signal to noise ratio. The chosen angle is an order of magnitude greater than apriori optimal one, which forces one to assume new physical processes. But such a choice should also inevitably affect the calculated probability to obtain the result due to Poisson fluctuations.

At the Tuesday 13 discussion meeting following the presentations were made:

	A	B
1. Learned-Introduction, nondirectional data (UTAH, SOUDAH)		
2. Ayres - SOUDAN	+	-
3. D'Ettore Piazzoli - NUSEX	+	+
4. Raupach - FREJUS	-	?
5. Chudakov - BAKSAN	-	-?
6. Krishnaswami - KGF	-	-
7. Cherry - HOMESTAKE	-	-?
8. Vander Velde - IMB > 70	-	-
9. Thornton - IMB Vertical	-	-
10. Ruddick		
11. Bazer Bachi - Old M. Blanc experiment		
12. Aprile - HPV (submitted later)	-	-

In each line the speaker and then code of his experiment is indicated. At the right side of each line the result of the experiment is indicated in a following way: first column A answers the question whether Cyg X-3 is seen in this experiment (+) or not, (-), authors opinion being the main criterion. Second column B corresponds to the phase interval .7-.8 in which the most sound positive result of NUSEX - experiment is concentrated. Column B shows that there is no confirmation of NUSEX result from other experiments. It does not necessarily mean a direct contradiction because of the differences in exposure time, depth, angular window and so on. By the question mark those experiments are indicated, in which similar to NUSEX, though statistically nonsignificant result was obtained.

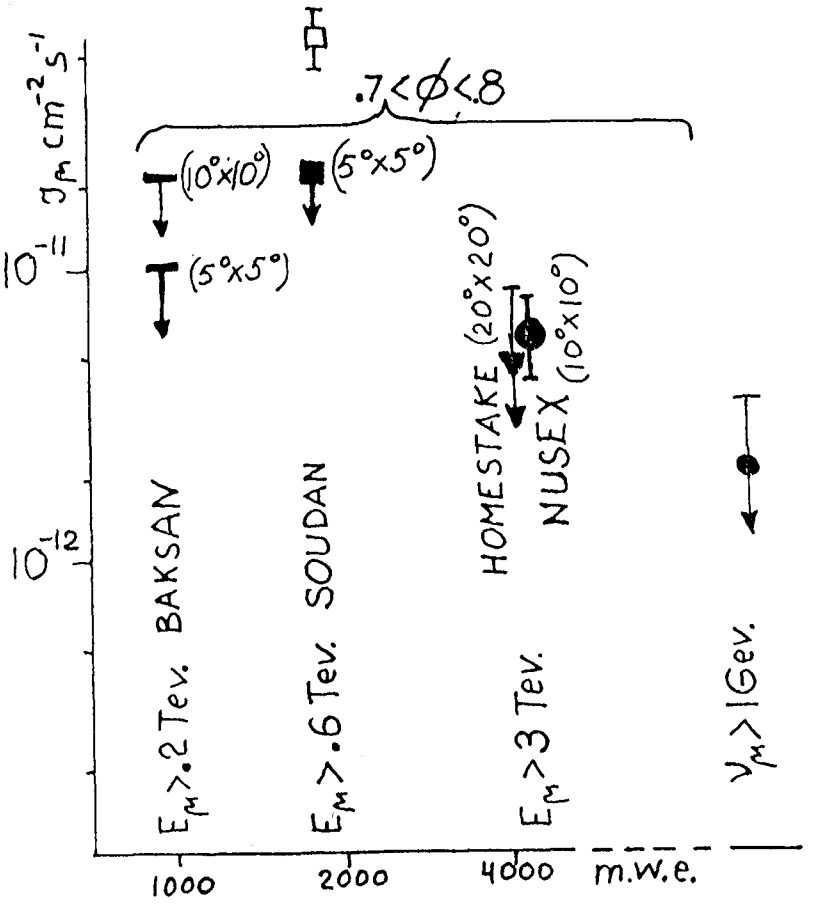

Figure 1: Cyg X-3 muon fluxes in phase internal 0.7 to 0.8 a diffeerent depths. BAKSAN data for neutrino-induced muons and Soudan data for "all phases" are also indicated.

The comparison of several experimental data in the phase interval .7-.8 is shown on the figure. One can see that there is no direct contradiction of NUSEX data with upper limits from other experiments. However, there is certainly a contradiction between NUSEX and BAKSAN for a conventional process of production of muons. In such a process muons are produced through pion decay in a hadronic cascade in the atmosphere and their energy spectrum in the range 200 - 3000 Gev should have an integral exponent no less than 1.7. Thus the flux at Baksan should be at least 15**1.7 = 100 times greater, than at NUSEX, but the experimental ratio is less than 4. Such a ratio can be explained only by nearly monochromatic muon beam, or some unknown neutral penetrating particle!? (not neutrino as is shown by NUSEX experiment itself).

To solve the puzzle new experimental data and better analysis of existing data is needed. The new FREJUS data will be most helpful as the experimental details of FREJUS and NUSEX experiments are quite

similar. Let us hope that Cyg X-3 will not stop its activity leaving us in the dark.

EVIDENCE FROM THE SOUDAN 1 EXPERIMENT FOR UNDERGROUND MUONS ASSOCIATED WITH CYGNUS X-3

D. S. Ayres
High Energy Physics Division
Argonne National Laboratory, Argonne, IL 60439

ABSTRACT

The Soudan 1 experiment has yielded evidence for an average underground muon flux of $\sim 7 \times 10^{-11}$ cm^{-2} s^{-1} which points back to the x-ray binary Cygnus X-3, and which exhibits the 4.8 h periodicity observed for other radiation from this source. Underground muon events which seem to be associated with Cygnus X-3 also show evidence for longer time variability of the flux. Such underground muons cannot be explained by conventional models of the propagation and interaction of cosmic rays.

1. Introduction. At the 1983 ICRC, the Kiel group[1] reported that extensive air showers associated with Cygnus X-3 had muon contents approximately equal to those of most other extensive air showers. At the same meeting, the Soudan group[2] showed evidence that multimuon events observed deep underground were anisotropic. One particularly active direction was centered about 20° from the x-ray binary Cygnus X-3.

In this paper, I summarize the analysis of the single-muon data[3,4] obtained from the Soudan 1 experiment during the same two-year exposure as the the multiple-muon data presented in Ref. 2. These data indicate that the muon flux from the direction of Cygnus X-3 exhibits the 4.8 h "orbital" period[5] characteristic of that source. The magnitude of the muon flux associated with Cygnus X-3 is similar to the reported flux of cosmic-ray air showers from Cygnus X-3.[1,6,7] Finally, the data suggest a longer term variability in the muon flux, in addition to the 4.8 h period. Knowledge about all levels of time variation is important for flux comparisons with surface detectors.

The reports of the Kiel,[1] Soudan,[2-4] and NUSEX[8] groups that a large muon flux is associated with Cygnus X-3 have been challenged[9] as being inconsistent with current understanding of the propagation and interaction of primary cosmic radiation. By flux arguments, the maximum primary energy that can be observed by an 8 m^2 detector like Soudan 1 in one year is $\sim 10^{16}$ eV. The primary energy associated with any statistically significant effect must be at least an order of magnitude lower. Because of the galactic magnetic fields, charged particles at energies of 10^{15} eV cannot travel more than about 1 pc without being homogenized in time and direction. Thus, any radiation associated with a source like Cygnus X-3, which is at least 10 kpc from the earth,[10] must be uncharged.

Known neutral primaries, however, cannot account for underground muon production related to Cygnus X-3. Neutrons can produce muons, but at the relevant energies, neutrons from Cygnus X-3 will decay before reaching the earth. Neutrinos also produce muons, but they interact at such a low rate that enormous fluxes would be required. Photons are very

inefficient producers of muons, because the inelastic photoproduction cross section is about 1/300 of the pair-production cross section. A secondary muon flux similar to that produced by hadron primaries is not consistent with known photon shower mechanisms.

2. The Underground Muon Data. The Soudan 1 proton-decay detector is described in detail in Ref. 11. The detector consists of an array of 3456 proportional tubes, each 2.8 cm in diameter, arranged in 48 layers of 72 tubes each. Alternate layers are rotated by 90° to provide two orthogonal views of each event. Figure 1 shows a typical cosmic-ray muon track in the detector. The experiment is located in the Soudan iron mine in northeastern Minnesota (48° N. latitude, 92° W. longitude) at a depth equivalent to 1800 m of water.

The current data sample consists of 784,456 single muon events recorded during a live time of 0.96 yr, between September 1981 and November 1983, and is the same one discussed in Refs. 3 and 4. Each event was required to consist of a single straight track, and to have a minimum of eight proportional-tube hits in each view. The most probable number of proportional-tube hits per view was sixteen, which yields an average angular resolution of ± 25 mrad. We estimate a ± 25-mrad uncertainty in the absolute orientation of the detector in the horizontal plane. We identify the observed tracks as muons both because of their depth underground and because of their passage through the detector in a straight line without substantial interaction. Tracks satisfying a 16-hit minimum (summing both views) penetrate at least 115 g cm^{-2} of material within the detector.

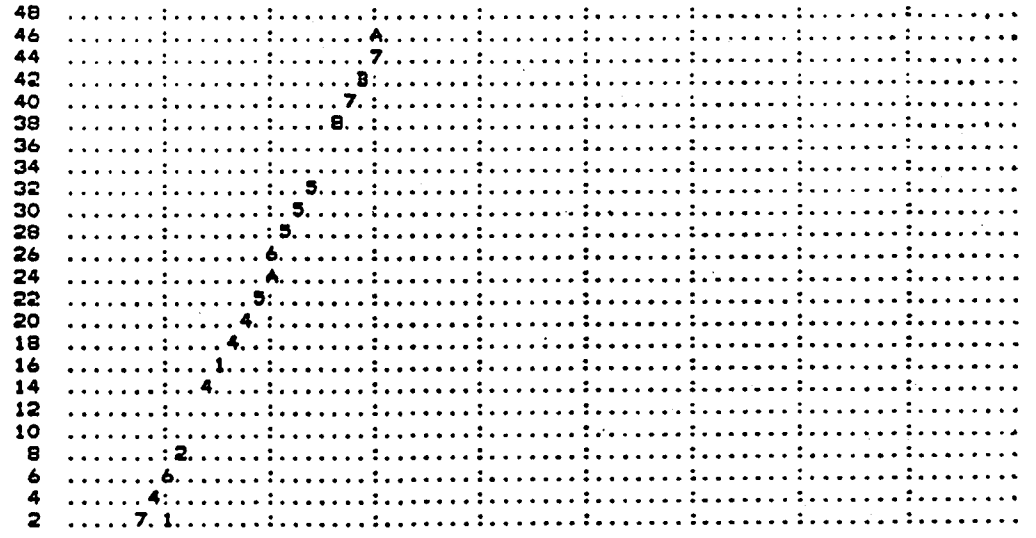

Fig. 1. One of two orthogonal views of a single-muon event in the Soudan 1 detector. Numbers and letters indicate observed pulse height, and dots show the positions of proportional tubes with no signals.

The ability of a detector to separate the signal of an x-ray binary from a random background is considerably enhanced by the source periodicity. For Cygnus X-3, both the 4.8 h period and the absolute phase are accurately known from keV x-ray data.[5] The flux modulation of Cygnus X-3 at high energies according to the same ephemeris has been observed in air showers.[7] The peak flux of TeV air showers, which may or may not produce the $\gtrsim$ 650 GeV muons that we detect, has been observed[6] since 1980 at phases in the range 0.60 to 0.73.

Using the angular resolution of the detector described above, we have selected those events whose direction of arrival points within 3° of the nominal direction (declination δ = 40.8°, right ascension α = 307.6°) of Cygnus X-3. Using the exact ephemeris of Ref. 5 (t_o = JD2440949.8986, p_o = 0.1996830 d, $\dot{p}$ = 1.18 × 10^{-9}), we calculate the Cygnus X-3 phase for each of these 1183 events. These phases are histogrammed in Fig. 2(a). The peak between phases of 0.65 and 0.90 contains 60 ± 17 events, using a background level determined from off-source directions. Figures 2(b) and 2(c) show the background distributions from nearby off-source directions, chosen at the same declination as Cygnus X-3 in order to have the same counting rate.

We have traced the dependence of the events-minus-background value for the phase plot as a function of right ascension and declination, as shown in Fig. 3. Since each point has been calculated by the use of all events within a 3° half-angle cone, nearby points are not statistically independent. The most probable right ascension is within our pointing accuracy of the nominal position of Cygnus X-3. The preferred declination is about 2.7° north of Cygnus X-3's nominal position. This discrepancy is slightly larger than our estimated pointing error, and its origin is unclear. The phase plot in Fig. 2(a) differs slightly from the similar plot in Ref. 3 because here we have selected the nominal direction of Cygnus X-3 rather than the one 2.7° from the nominal, which yields about a 30 percent higher signal.

Within statistics, the ratio of intensity within the phase peak to intensity outside the phase peak does not vary as a function of zenith angle. Thus, the local zenith-angle distribution of the events in the phase peak is similar to that of ordinary muons from hadronic interactions in the atmosphere. In particular, we can completely reject the hypothesis of an isotropic zenith-angle distribution, as would be expected if the signal muons were produced by neutrino primaries. This result is illustrated in Fig. 4, which shows the phase plot for events within the 3° half-angle cone which $\theta_z > 66°$ ($\cos\theta_z < 0.4$). Our measured flux at small slant depths predicts a signal of 18 events in the 0.65 - 0.90 phase bin if the muons are produced by neutrinos interacting in the earth, to be compared with zero events shown in Fig. 4.

3. Statistical Analysis. We have used several alternate methods[4] to estimate the statistical probability that Fig. 2(a) represents a random fluctuation of a uniform background. Ref. 3 relied principally on a χ^2 analysis. More specific tests for the presence of a Cygnus X-3 signal include a peak-over-background analysis, a Fourier coefficient analysis and a first and second moment analysis.[4] In the case of the moment (or generalized Rayleigh) analysis, a particularly powerful

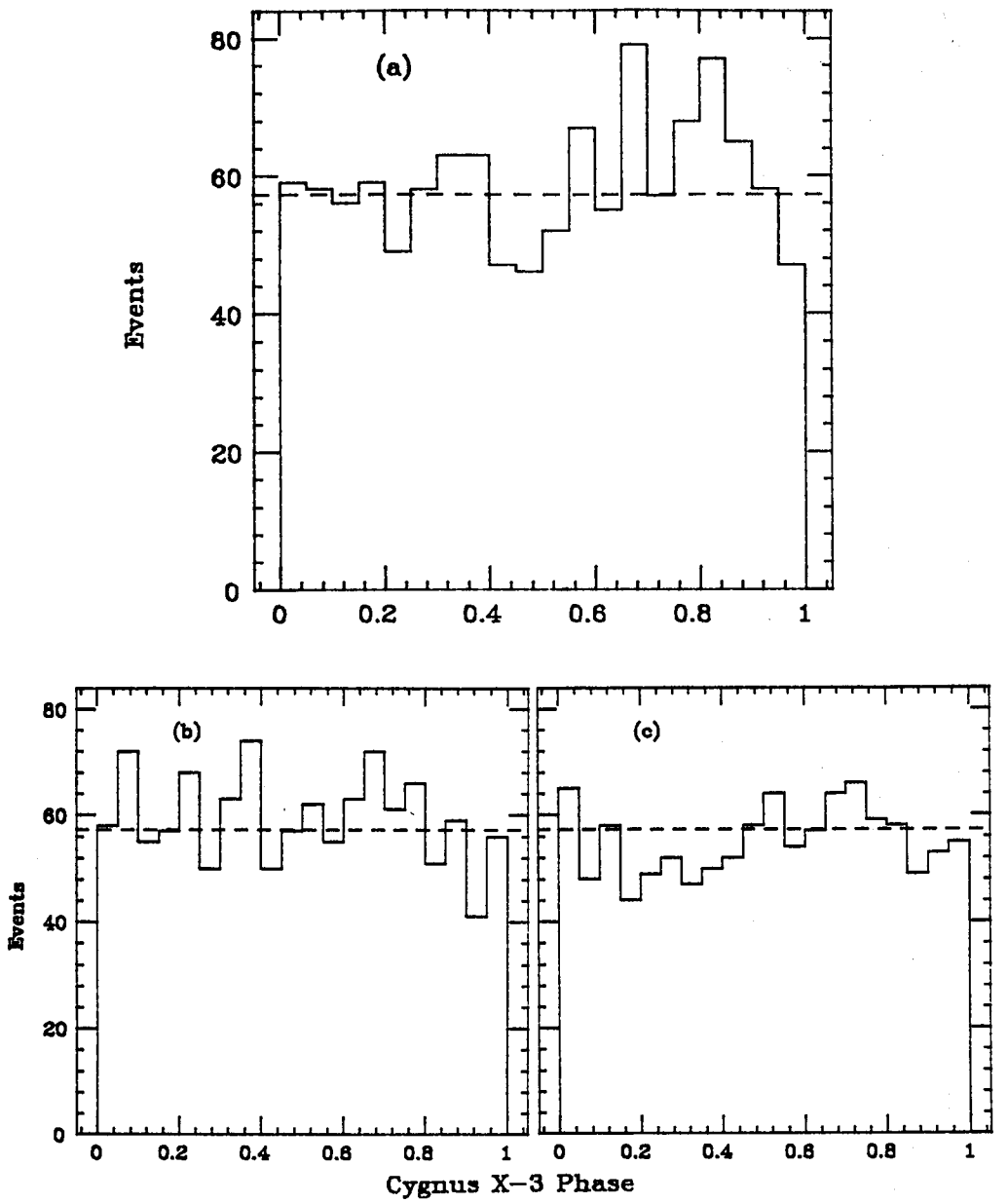

Fig. 2. (a) Cygnus X-3 phase plot for events within 3° of the nominal direction of Cygnus X-3. (b) and (c) Similar phase plots for events within a 3° half-angle cone centered at $\alpha = 297.6°$ and $\alpha = 317.6°$, respectively, and the same declination as Cygnus X-3. The dashed line shows the estimated background from a random source.

constraint can be imposed by using projections of the moments in directions specified by previous high energy data on Cygnus X-3 (such as the 0.65 phase peak direction). This method yields the phase-constrained probabilities discussed below. We have made empirical checks on the validity of these methods using both data from regions of the sky away from Cygnus X-3 and Monte Carlo generated data samples.

For Fig. 2(a), the results of our statistical analyses can be summarized as follows: A peak-over-background analysis using the 60 ± 17 event effect noted above ($3.5\ \sigma$) yields a probability of $\sim 2 \times 10^{-4}$ of it being a random background fluctuation. If the background is determined

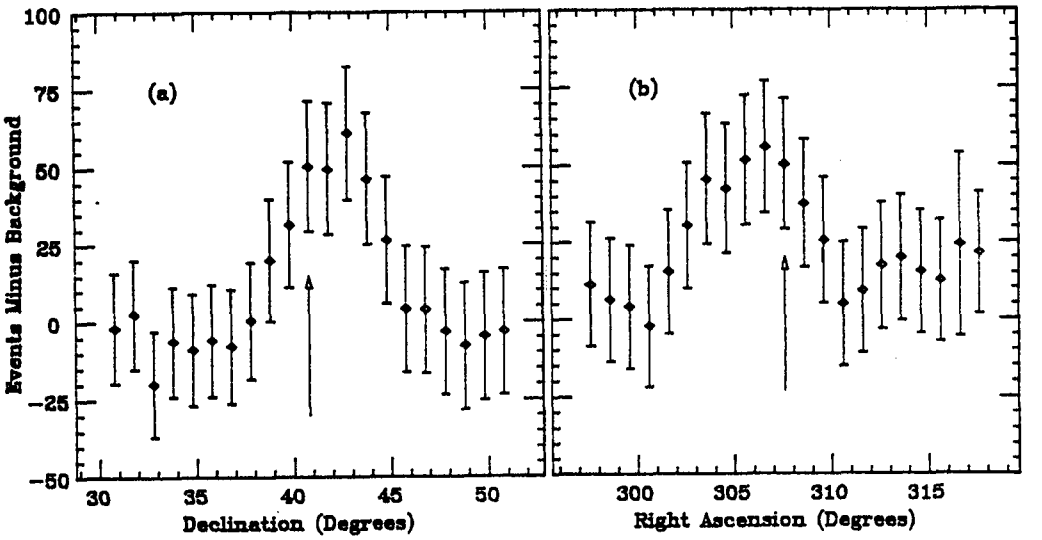

Fig. 3. Events-minus-background distribution for the phase plot as a function of (a) declination, and (b) right ascension. Note that nearby points are not statistically independent. The vertical arrows indicate the position of Cygnus X-3.

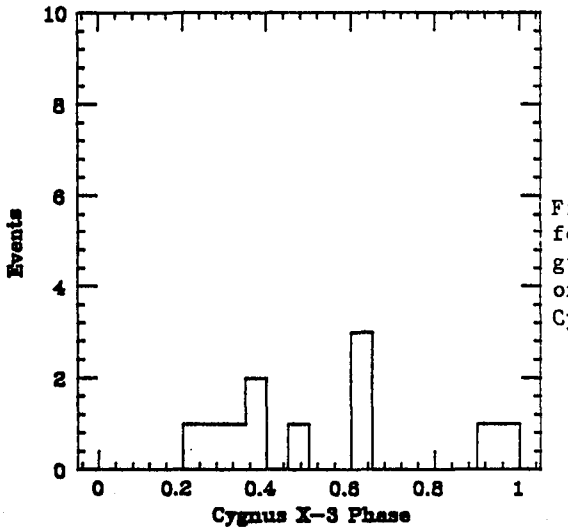

Fig. 4. Cygnus X-3 phase plot for events with zenith angles greater than 66°, and within 3° of the nominal direction of Cygnus X-3.

from all events in Fig. 2(a) (including the peak), the signal is 10 events smaller and the corresponding probability is $\sim 4 \times 10^{-3}$. These probabilities would increase by about an order of magnitude if a phase peak at any location were accepted. A moment analysis which uses neither a priori expectations nor off-source background information gives a random-fluctuation probability of ~ 0.02. Constraining the flux to be large near a phase of 0.65 and small near phases of 0.0 and 0.5, as might be expected from the air-shower data for radiation from Cygnus X-3, reduces this probability by a factor of 10 to 20.

4. Long-time Flux Variablity. The air Cerenkov data indicate that Cygnus X-3 is not a constant source.[12] Such episodic behavior suggests that the signal-to-background-ratio in Fig. 2(a) may be enhanced by plotting the phases of pairs of events which occur within a short period of time, i.e. those events associated with high-rate periods. Figure 5(a) shows such a plot where the mean phase is plotted for each pair of consecutive events which occurred within 0.5 h of each other. The signal in this plot for phases between 0.65 and 0.90 includes 29 ± 6 event pairs above background. The background for this estimate has been derived from Figs. 5(b) and 5(c), which show similar plots for nearby off-source directions. The results of a background-independent moment analysis of Fig. 5(a) indicate an unconstrained probability of a random fluctuation generating the plot as $\sim 3 \times 10^{-4}$. The constrained probability using knowledge of the absolute phase dependence of Cygnus X-3 high-energy emission is again 10 to 20 times smaller.

The larger signal-to-background ratio in Fig. 5(a) compared to that in Fig. 2(a) shows that much of the excess flux in the phase region of 0.65 to 0.90 occurs in bursts of two or more events occurring close together in time. Table 1 contains further information on this question. Listed there are the number of Cygnus X-3 cycles observed with n muons in a 1.2 hour (1/4 cycle) period. Data are shown on and off the phase peak for both on- and off-source directions.

We have fit the off-source (background) data in Table 1 with a Monte Carlo model, which uses a detection efficiency varying as $\cos^3\Theta_z$, where Θ_z is the local zenith angle. This zenith angle dependence approximates the attenuation observed for single muon events due to the higher muon threshold energy when Cygnus X-3 is not directly overhead. The model fits the background data well. The χ^2 for each of the background distributions is shown in the table. The fits are likely, except for the signal region, which has a χ^2 probability of ~ 0.01.

Our data do not uniquely determine the functional form of the source modulation. To investigate this time dependence further, we have chosen a simple model where, in addition to the background, a source may be "on" during the quarter-period with phase between 0.65 and 0.90. This "signal" is turned "on" only for a certain percentage of the Cygnus X-3 4.8 h cycles. The "signal" events are also modulated by the zenith angle dependence described earlier. The data in Table 1 are fitted well with an "on" fraction of 0.07 ± 0.04 of the active-phase quarters, a (source-overhead) signal rate when "on" of 1.3 ± 0.7 muons h^{-1} during the active quarter-period and a (source-overhead) background rate described above of 0.42 ± 0.03 muons h^{-1}.

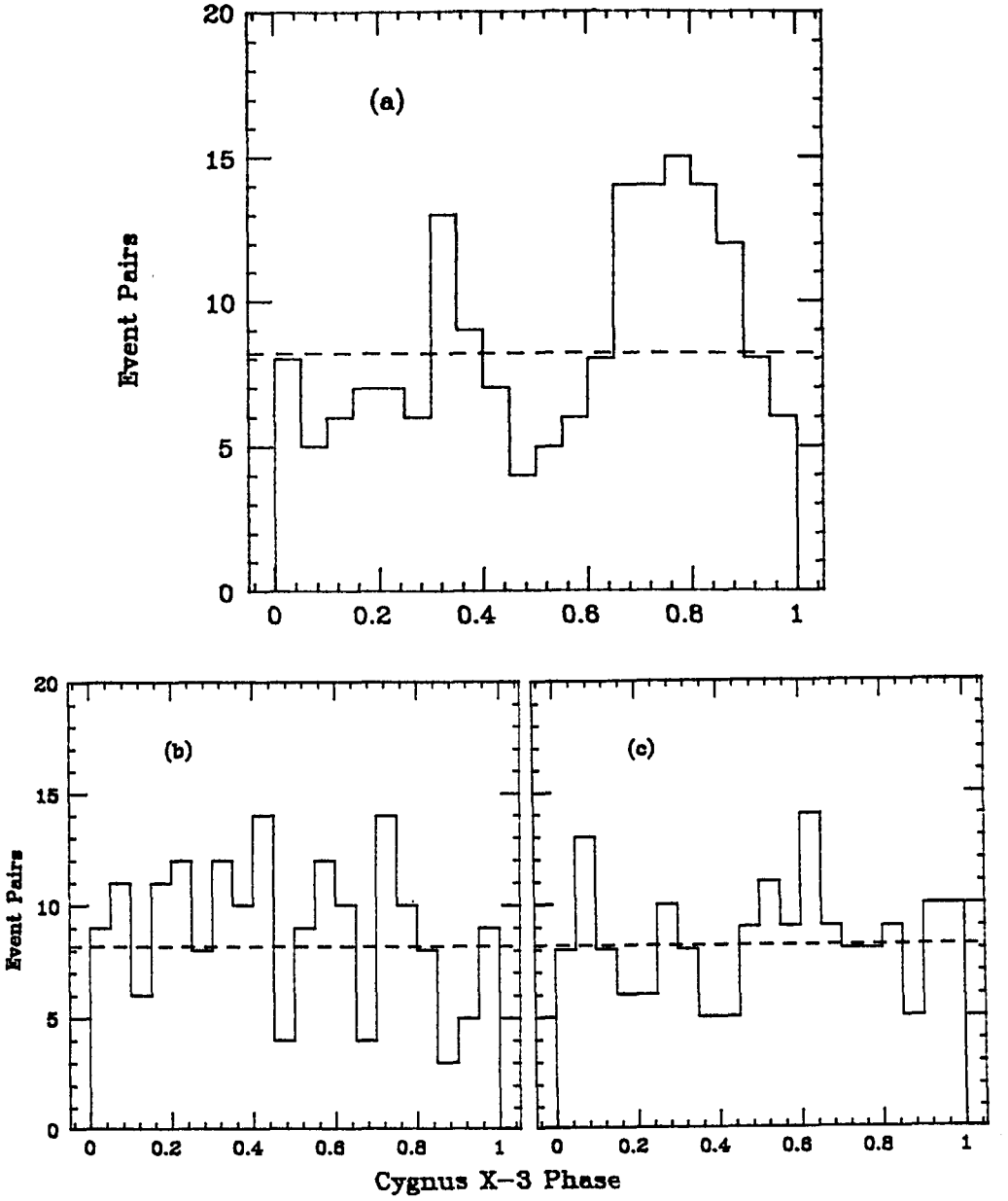

Fig. 5. (a) The Cygnus X-3 phase plot showing the mean phase for pairs of events arriving within 0.5 h, from within 3° of the nominal direction of Cygnus X-3. (b) and (c) Similar phase plots for pairs of events within a 3° half-angle cone centered at $\alpha = 297.6°$ and $\alpha = 317.6°$, respectively, and the same declination as Cygnus X-3. The dashed line shows the estimated background from a random source.

Table 1. Number of Cygnus X-3 Cycles in Which n Muons Are Observed in 1.2 h From Within 3° of On- and Off-source Directions.

Direction	Phase	n = 1	2	3	4	χ^2
on-source	0.15-0.40	206	38	2	1	2.5
	0.40-0.65	198	28	3	0	2.3
	0.65-0.90	218	49	7	2	13.6
	0.90-0.15	222	23	3	0	7.4
$\alpha = 297.6°$	0.15-0.40	203	45	5	1	3.8
	0.40-0.65	202	33	5	1	0.6
	0.65-0.90	218	36	5	1	2.3
	0.90-0.15	203	38	1	0	3.7
$\alpha = 317.6°$	0.15-0.40	166	29	6	0	7.4
	0.40-0.65	198	36	5	0	0.6
	0.65-0.90	207	32	7	1	2.2
	0.90-0.15	199	34	4	0	0.6
Fit in text		199.5	34.5	4.6	0.5	

From the ~ 8 m^2 area of the Soudan 1 detector and the 0.96-year live time, we can use the above model to estimate the following fluxes of muons from Cygnus X-3 with energy $\gtrsim$ 650 GeV:

(a) Average detected flux for the entire observation period: ~ 2.5×10^{-11} cm^{-2} s^{-1} (i.e. 60 events during 0.96 yr).

(b) Same as (a) if Cygnus X-3 were always directly overhead (assuming a $\cos^3\theta_z$ dependence): ~ 7.3×10^{-11} cm^{-2} s^{-1}.

(The following flux values are for the directly-overhead geometry.)

(c) Average flux during all potentially active times with phase between 0.65 and 0.90: ~ 2.9×10^{-10} cm^{-2} s^{-1}.

(d) Flux during "on" times with phase between 0.65 and 0.90, with 7 percent of cycles "on": ~ 4.2×10^{-9} cm^{-2} s^{-1}.

(e) Flux averaged over entire 4.8 h period during 7 percent of time source is "on": ~ 1.0×10^{-9} cm^{-2} s^{-1}.

The uncertainty in these fluxes is estimated at +50,-25 percent.

These fluxes may be compared with fluxes attributed to Cygnus X-3 by air Cerenkov experiments at similar energies. Reference 12 reports a peak pulsed flux (measured over about 0.5 h) of $(5.1 \pm 1.1) \times 10^{-10}$ cm^{-2} s^{-1} for a threshold energy of 800 ± 400 GeV. That experiment observed no significant signal a month later, indicating that this flux corresponded to a time when the source was "on." Reference 13 reports a flux averaged over the 4.8 h cycle of ~ 8×10^{-11} cm^{-2} s^{-1} at a threshold energy of 500 GeV. Our muon fluxes are apparently larger than the fluxes reported from air Cerenkov measurements at similar energies. However, deducing a primary flux from the secondary muon flux requires a knowledge of the number of muons per primary which reach the Soudan 1 depth. Because this quantity is not known, a direct flux comparison is not possible.

Our results imply that other detectors should also observe a modulation in addition to the 4.8 h period in the Cygnus X-3 flux. In particular, the times at which we observed 3 or 4 muons in the 1.2 h phase peak during one Cygnus X-3 cycle are (Universal Time) 29.82 December 1981, 30.78 January 1982, 4.39 June 1982, 19.98 October 1982, 27.94 October 1982, 23.87 December 1982, 3.86 January 1983, 17.50 April 1983 and 19.46 May 1983.

X-ray observations have suggested[14] a 34.1 d period for the flux variation of Cygnus X-3. Figure 6 shows a 34.1 d phase plot for the nine times listed above, using an arbitrary t_o of 18.04 January 1981. Note that the absolute phase has been selected using these data, and that it differs from the one in Ref. 14 by almost half a period. A Rayleigh analysis indicates a probability of about one percent that this plot is consistent with a random fluctuation of a uniform background. The plot additionally shows the phases of air shower bursts observed[15] on 20 January and 21 November 1981 and radio outbursts observed[16] on 27 September 1982 and 1 and 8 October 1983. These data are clearly anecdotal, but their near-zero phase suggests that a more systematic analysis is warranted.

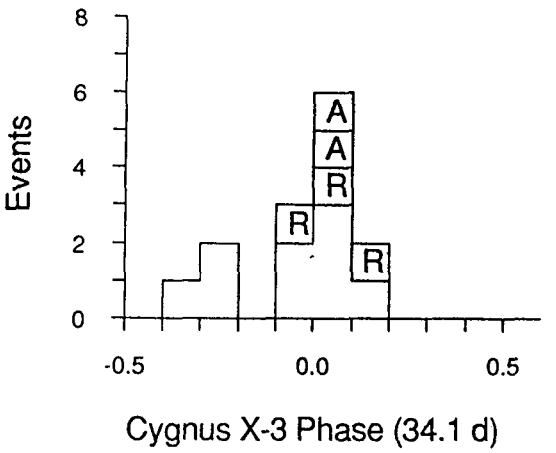

Fig. 6. The 34.1 d period phase plot for high-rate periods as defined in the text, using the ephemeris given in the text. The symbol A indicates air shower bursts described in Ref. 15. The symbol R indicates radio outbursts described in Ref. 16.

5. Conclusions. Our evidence for an underground muon flux related to Cygnus X-3 seems unlikely to be a statistical fluctuation. The data indicate that Cygnus X-3 is an episodic source, as has been previously reported from air Cerenkov measurements. Our observations support a 34.1 d variation in the flux. This result can be checked by other experiments with accumulated data. The apparent correlation in Fig. 6 of underground muon flux maxima with peaks in radio and air shower activity from Cygnus X-3 further supports the identification of muons with this particular source. This long-term episodic behavior is similar in some respects to observations we have previously reported on multimuon events in a nearby direction[2], although we have not found a connection between the two phenomena.

These data are difficult to explain in terms of conventional ideas about cosmic-ray propagation and interaction. Our results yield a muon flux several orders of magnitude larger than that expected from inelastic photoproduction by photons from Cygnus X-3. The most likely possibilities are either that high energy photons have new type of interaction that leads to direct or indirect muon production, or that the muons are produced by a new type of stable, neutral particle coming from Cygnus X-3. Further observations will be required to confirm and explore this effect.

6. Acknowledgements. The Soudan 1 experiment is the work of my colleagues J. Bartelt, H. Courant, K. Heller, S. Heppelmann, T. Joyce, M. Marshak, E. Peterson, K. Ruddick and M. Shupe at the University of Minnesota, and J. Dawson, T. Fields, E. May, L. Price and K. Sivaprasad at Argonne National Laboratory. In particular, Marvin Marshak made the initial observation of evidence for Cygnus X-3 in our data, and performed much of the analysis described here. I would also like to thank Prof. J. Learned for discussions of his preliminary results. Financial support for this work was provided by the U.S. Department of Energy and the Graduate School of the University of Minnesota. This experiment has been conducted with the cooperation of the State of Minnesota, Department of Natural Resources, particularly the staff at Tower-Soudan State Park.

References

1. M. Samorski and W. Stamm, Astrophys. J. **268**, L17 (1983).
2. J. Bartelt et al., Phys. Rev. D, in press.
3. M. Marshak et al., Phys. Rev. Lett. **54**, 2079 (1985).
4. M. Marshak et al., Phys. Rev. Lett., to be published (1985).
5. M. van der Klis and J. M. Bonnet-Bidaud, Astron. and Astrophys. **95**, L5 (1981).
6. S. Danaher et al., Nature **289**, 568 (1981).
7. J. Lloyd-Evans et al., Nature **305**, 784 (1983) and other references listed in this paper.
8. G. Battistoni et al., Phys. Lett. **155B**, 465 (1985).
9. T. Stanev, T.K. Gaisser, and F. Halzen, Phys. Rev. **D32**, 1244 (1985); T. Stanev and Ch. P. Vankov, Phys. Lett. **158B**, 75 (1985).
10. J. Dickey, Astrophys. J. **273**, L71 (1983).
11. J. Bartelt, Ph.D. thesis, University of Minnesota, 1984; J. Bartelt et al., Phys. Rev. Lett. **50**, 651 and 655 (1983).
12. M. F. Cawley et al., submitted to Astrophys. J.
13. R. C. Lamb et al., Nature **296**, 543 (1982).
14. D. Molteni et al., Astron. and Astrophys. **87**, 88 (1980).
15. G. Smith et al., Phys. Rev. Lett. **50**, 2110 (1983); T. C. Weekes, Astron. and Astrophys. **121**, 232 (1983). The first experiment does not explicitly measure directionality but Cygnus X-3 was near overhead at the time of the burst.
16. B. J. Geldzahler et al., Astrophys. J. Lett. **273**, L65 (1983); K. Johnston, private communication.

OBSERVATION OF MUONS FROM CYGNUS X-3 IN THE NUSEX EXPERIMENT

B. D'Ettorre Piazzoli
Istituto di Cosmogeofisica del CNR, Torino, Italy

INTRODUCTION

Ground based observations by means of Cerenkov light detectors and air shower arrays have established that Cygnus X-3 is a powerful source of high energy particles. The detection of a 10^{15} eV signal was first reported by the Kiel experiment. Air showers with large age parameter were accepted in order to select those generated by primary γ-rays. At variance with the expectation, the muon density associated with these events was found to be surprisingly high. This puzzling result stimulated a temporal analysis of the muons recorded in NUSEX(*) coming from the region around the source. A positive signal was found suggesting the presentation of the result at this Conference. The analysis of the data recorded during about 2.4 years of effective working time was presented at the First Symposium on Underground Physics (St. Vincent, Italy) and then published [1]. In the paper sent to this Conference a fine tuning of the period has been presented and the energy spectrum of the muons from the Cygnus X-3 direction derived assuming consistency between NUSEX and SOUDAN results [2]. Here I account for a refined and upgraded analysis of the same events.

THE APPARATUS

The NUSEX (Nucleon Stability Experiment) detector is located in the Mont-Blanc tunnel (45.9° N latitude, 6.9° E longitude) at a vertical depth of about 5000 hg/cm² of standard rock.

It consists of a cube of 150 t mass and 3.5 m side, made of 136 horizontal plates of 1 cm thickness, interleaved with planes of tubes having 1 cm x 1 cm cross section, operated in the limited streamer mode.

This paper is the written version of the talk given at the 19th ICRC, La Jolla, California (USA), 11-23 August 1985

Minimum trigger requirements are that either four contiguous planes or a pair of contiguous planes plus a group of three other contiguous ones are fired simultaneously.

Tracks are accepted for reconstruction only if the number of crossed planes is at least 10. This criterium defines a fiducial volume of well defined acceptance and detection efficiency practically equal to unity.

NUSEX was planned to search for proton decay working as a digital calorimeter with excellent tracking capability. Typical errors in reconstructing tracks satisfying the above mentioned criterium are $\sigma_\theta \sim 1$mr and $\sigma_\phi \sim 2$mr. The two track resolution is better than 2 cm.

A detailed map - contour lines at 10 m - of the rock overburden allows us to associate to each direction a slant depth with an accuray $\Delta h/h < 1\%$.

These properties make NUSEX a well suitable apparatus to perform muon physic underground in the depth range 4600 - 10.000 hg/cm ^{2}.

MUON PHYSICS

An analysis of the muon events was started to study the single muon intensity-depth distribution, multiple muon rates, stopping muons, narrow angle anisotropies. Data on single and multiple muons have been presented at this Conference [3]. The vertical muon intensity is reported in Fig. 1 together with the intensity points measured with the spark chamber apparatus located in another laboratory of the Mt. Blanc tunnel. The intensity versus depth is very well represented by the relation

$$I\mu(h) = (7.63 \pm .48) \cdot 10^{-7} \cdot \exp(-h/810.44 \pm .84) \text{ cm}^{-2}\text{s}^{-1}\text{sr}^{-1} \qquad (1)$$

The angular distribution underground is in good agreement with the expected one. (Calculations of the angular enhancement functions at different depths are given in [4]). The contribution from direct production is found to be negligible, not exceeding a 3-4 % of the total up to 8000 hg/cm^2. In conclusion, muons physics in NUSEX is well understood and predictions of muon rates in each direction can be made with high reliability.

ANALYSIS OF THE CYGNUS X-3 DATA

During the period 1 June 1982 to 31 January 1985 21,700 single muons with zenith angle up to 75° have been recorded satisfying the acceptance criterium. With this angular cut Cygnus X-3 is observed for 64% of the total time.

In a cone of 4.5° half angle aperture centered around the source [δ = 40.9 α = 307.9] we find 142 events. The time of each event is reduced to the barycenter of the solar system and then folded modulo 4.8 h using the Van der Klis and Bonnet-Bidaud quadratic ephemeris [5]. The phase diagrams for two different binnings are shown in Fig. 2. We observe 31 events in the phase interval 0.7 - 0.8 against an average off-source background of events11.32 ± .21. The associated fluctuation probability that this effect occurs by chance is less than 10^{-4}.

The quoted phase values found in TeV γ-ray observations of Cygnus X-3 occur in the range 0.6 - 0.8 [6]. This agreement with previous observations in the same energy region is not sufficient to claim a physical effect. It is not obvious that over an extended period of time no biases were introduced in data taking, so that it is necessary to verify that the probability of detecting a muon does not depend on phase or on direction, due to details of the experimental procedure. For example the Cygnus X-3 orbital period is almost exactly 1/5 of the sidereal day. If the period were an exact fraction each phase should be "seen" always in the same five directions (θ,ϕ), in such a way generating a strong correlation phase / acceptance / depth. Fortunately is not like that. A given phase precesses over the detector 2.1 times/year producing an average effect for long time measurements. This point has been checked by calculating the exposure relative to each phase bin for Cygnus X-3 and for other directions in the same declination band. 27 contiguous cones of half angle aperture 4.5° have been selected in the ± 4.5° off-Cygnus declination band, covering 321.5 degrees in right ascension around the source position. For each of the 28 cones (Cygnus X-3 + background ones) the path in the sky has been followed during the entire data taking period. At each time there is a well defined phase (for a given ephemeris), direction, acceptance area, and depth. Taking into account only the periods in which the apparatus was ON the exposure as a function of the depth for

each phase and cone has been calculated. In this way 280 very similar exposures have been generated. As an example the "Cygnus X-3 profile" for two phases is shown in Fig. 3.

To obtain the expected counting rates in each phase bin and cone the exposure has been calculated folding the acceptance with the angular distribution of conventional muons and with the intensity depth relation (1).

The measured phase distribution of the events in the 27 background cones is found in excellent agreement with expectation, no fluctuation is observed with probability less than 10^{-3}. In Fig. 4 the phase distribution of all background events is shown. It is well reproduced by the calculated one and results consistent with unformity (χ^2 = 9.78, $P(>\chi^2)$ = 36.8%). The predicted mean for each bin is 313 against an experimental value 306 ± 6. In the Cygnus cone the expected background is 11.9 events per bin, compared with 12.3 ± 1.3 observed. A χ^2 test on the phase histogram uniformity about the off-source mean yields χ^2 = 30.5 [$P(>\chi^2) = 3.6 \cdot 10^{-4}$] while the phase histogram outside the interval .7 - .8 is consistent with noise (χ^2 = 9.73, $P(>\chi^2)$ = 28.4%).

Thus we can conclude that the muon distribution in the same declination band as Cygnus X-3 follows the expected one. No non-random dependences on phase or on direction have been found in the background data, implying that there are no priviliged phases or direction. Only in the cone centered around Cygnus X-3 is a deviation from the expectation found due to an enhanced flux in the phase interval 0.7 ÷ 0.8. This excess appears to be "genuine", in that it originates either by some physical effect or by a statistical fluctuation. The χ^2 test for uniformity, the probability of fluctuation in any one of the ten bins ($6 \cdot 10^{-5}$) and the confidence level for enhanced flux (99.95%) can be considered in order to give an estimate of the statistical significance of the excess.

ANALYSIS OF THE PERIOD

The period used in the above analysis comes from a fit of the X-ray data recorded in different satellite missions [5]. We checked this period from the muon data themselves alone.

In general we expect the best period to give the narrowest peak of one or more adjacent bins according to the binning used. If a phase diagram in 10 bins is used the best period should correspond to that giving the maximum concentration of events in one bin. This search is performed moving the period and its derivative in steps of $4 \cdot 10^{-7}$ d and $2 \cdot 10^{-10}$ respectively and looking at the same time for the maximum value of χ^2 and the minimum of the probability of fluctuation.

A change in period of $4 \cdot 10^{-7}$ d gives a shift for our data recorded between June 82 and January 85, of 0.42 to 0.052. A change in the period derivative of $2 \cdot 10^{-10}$ gives a phase shift in the range 0.050 to 0.066. In the scanning over the period the derivative has been set to the ephemeris value.

The result is shown in Fig. 5 where χ^2 and fluctuation probability are plotted for both period and period derivative scannings. The best values derived from muon experimental data on the basis of these tests coincide with the x-ray ephemeris ones. The phase histogram in 20 bins shows that the excess is concentrated in a phase width of about 29'.

ANGULAR SPREAD

The previous analysis has been performed looking in a cone with half opening of 4.5° because this aperture appears necessary for full containement of the signal. This effect is shown in Fig. 6 where the signal is plotted as a function of the cone aperture. While the background "out-phase" increases as the solid angle and the counts in these phase bins follow the expectation, the count in the bin .7 - .8 shows an increasing positive excess up to about 4.5°. For larger opening angles the entries follow the expected background.

The dipersion of the signal is shown in Fig. 7. Using a gaussian distribution for point source resolution a mean angle of about 2.5° is required to get a fair agreement. It seems at variance with the expectation because the angular resolution of the apparatus is better than 1° ($\sigma_\theta \sim$ 1mr, $\sigma_\theta \sim$ 2 mr, misalignement < .3°) and the multiple scattering is estimated to contribute with a mean dispersion angle of $\sim$ .6° (Fig. 8,9).

This dispersion cannot be easily explained by transverse momentum acquired at production, 1° corresponding to about 100 GeV for energetic

muons detected in NUSEX. Thus this result remains at moment an unresolved question.

MUON SPECTRUM

The depth distribution of the 111 "off phase" events follows the one expected for atmospheric muons. Thus from the 31 "in phase" events we subtract the background events according to the depth distribution expected for atmospheric muons so obtaining the distribution for the 19 excess events given in Fig. 10. Only 1 event is found in the depth region around 7000 hg/cm^2 corresponding to the maximum of the exposure. This result rules out the hypothesis of neutrino-induced events because in such a case the muon depth distribution should follow the exposure profile. The events have been binned to obtain the intensity at four different depths. Using the calculated exposure for isotropic or conventional (according to a "secθ law"as calculated in [4]) angular distribution we find the intensity values shown in Fig. 11. A typical flux (averaged over the Cygnus X-3 period) at a depth $\sim$ 5000 hg/cm^2 (muon threshold $\sim$ 3 TeV) is $5 \cdot 10^{-12}$ cm^{-2}s^{-1}.

The depth interval covered by our data and their statistical uncertainty prevent one from obtaining the muon energy spectrum from the NUSEX events alone. This is possible if, assuming consistency between the fluxes measured in the two experiments, also the SOUDAN point at 1800 hg/cm^2 is used [7]. Folding a power spectrum with the survival probability P(E,h) [8] we obtain the muon energy differential spectrum corresponding to the measured intensities as :

$$dI/dE\ (cm^{-2}\ s^{-1}\ GeV^{-1}) = \begin{cases} (3.9 \pm .7)\ \cdot E^{-(2.3 \pm .2)} & \text{isotropic distribution} \\ (8.8 \pm 1.6)\ \cdot E^{-(2.4 \pm .2)} & \text{"sec}\theta\text{" distribution} \end{cases}$$

The muon integral spectrum is found to be

$$I(cm^{-2}s^{-1}) = \begin{cases} (3.0 \pm .6) \cdot 10^{-7}\ E^{-(1.3 \pm .2)} \\ (6.3 \pm 1.2) \cdot 10^{-7}\ E^{-(1.4 \pm .2)} \end{cases}$$

respectively. In spite of the large uncertainty in deriving this result the spectrum seems much flatter than the ordinary atmospheric muon one

($\gamma \sim 2.71$) and not far, in slope and absolute intensity, from the primary flux attributed to photons from Cygnus X-3 in the range 10^{12}-10^{15} eV. (Fig. 12).

CONCLUSIONS

The main steps of the analysis of the muon events detected in the direction of Cygnus X-3 have been reported in order to show the consistency of the data both internally and with expectation, and in particular that no biases were introduced in data taking or in the analysis procedure. From Cygnus X-3 the NUSEX experiment picked-up signals showing the precise period of this binary system and with a phase distribution consistent with the ground-based measurements. The probability that this signal was generated by chance is estimated to be 10^{-4}.

If the result is right, it is difficult to account for these data since conventional interactions of conventional particles are unable to explain in a unique consistent picture both surface air shower and muon underground fluxes [9].

Continued measurements by different detectors are requested to decide unambigously on the existence of the effect. In order to isolate a small flux of muons associated with Cygnus X-3 from background muons the dimension, angular resolution, and location of the apparatus assume a crucial importance. In fact present results seem to indicate a muon generation via prompt production, hence with flat energy spectrum and isotropic distribution, thus penalizing experiments at shallow depth or looking at high depth through large zenith angles. In this respect the continuous collection of data in the NUSEX experiment, planned at least up to the end of '86, could add decisive information to the solution of the Cygnus X-3 problem.

References

[*] G. Battistoni, E. Bellotti, C. Bloise, G. Bologna, P. Campana, C. Castagnoli, A. Castellina, V. Chiarella, A. Ciocio, D. Cundy, B. D'Ettorre Piazzoli, E. Fiorini, P. Galeotti, E. Iarocci, C. Liguori, G. Mannocchi, G. Murtas, P. Negri, G. Nicoletti, P. Picchi, M. Price, A. Pullia, S. Ragazzi, M. Rollier, O. Saavedra, L. Satta, P. Serri, S. Vernetto and L. Zanotti.

[1] B. D'Ettorre Piazzoli. Talk presented at the 1'st Symposium on Underground Physics, Saint Vincent, Italy, April (1985), to be published.

G. Battistoni et al., Phys. Lett. 155B, 465 (1985).
[2] G. Battistoni et al., Proc. of the 19th ICRC, La Jolla, Vol. 1, 62 (1985).
[3] G. Battistoni et al., Proc. of the 19th ICRC, La Jolla, Vol. 3, 158 (1985).
[4] H. Bilokon et al., Nuovo Cimento 8C, 93 (1985).
[5] M. van der Klis and J.M. Bonnet-Bidaud, Astron. Astrophys. 95, L5 (1981).
[6] J. Lloyd-Evans et al., Nature 305, 784 (1985).
[7] M.L. Marshak et al., Phys. Rev. Letters 54, 2079 (1985).
[8] L. Bergamasco et al., Nuovo Cimento 6C, 569 (1983).
[9] H. Bilokon et al., to be published on Lettere del Nuovo Cimento.

Figure Captions

Fig. 1 : Muon intensity underground at Mt. Blanc.
Fig. 2 : Phase distribution for muons arriving within 4.5° of the direction of Cygnus X-3 : a) plot in 10 bins b) plot in 20 bins.
Fig. 3 : Exposure for Cygnus X-3 integrated over the running time and averaged over the total phase (-phase 0.75, --- phase 0.005).
Fig. 4 : Phase distribution of the 3057 muon events recorded in the 27 cones used to evaluate the background. The same phase distribution as calculated by simulation is shown.
Fig. 5 : χ^2 and probability of fluctuation as a function of a trial period (a) or period derivative (b). The zero of the scale indicates the values determined from X-ray data [5].
Fig. 6 : The excess in the phase bin .7 - .8 plotted versus the cone half opening.
Fig. 7 : Scatter plot in declination and right escension for the 31 events in the phase bin .7 - .8.
Fig. 8 : Error distribution for zenith (θ) and azimuthal (ϕ) angles of tracks reconstructed in NUSEX.
Fig. 9 : Distribution of the angle between muon pairs in NUSEX: d is the distance between the tracks.
Fig. 10 : Depth distribution for the 31 "in phase" events. The distribution of the 111 "out phase" events is also shown.
Fig. 11 : Underground intensity of muons from the direction of Cygnus X-3 (NUSEX and SOUDAN results).
Fig. 12 : Integral energy spectrum of muons from the direction of Cygnus X-3 compared to the estimated flux of "γ-rays" [6].

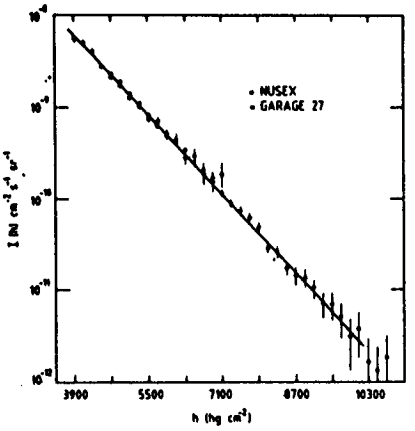

FIG. 1

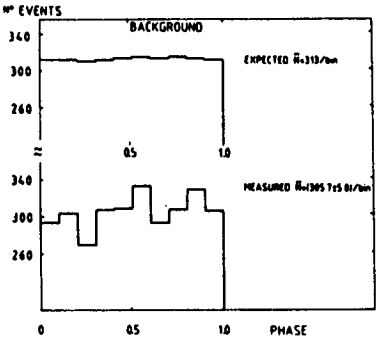

FIG 4

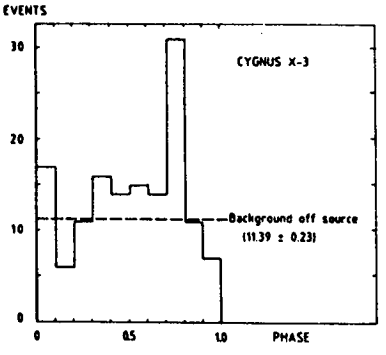

FIG. 2a

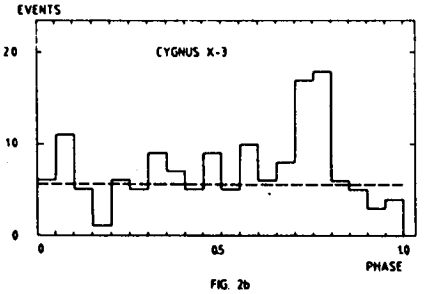

FIG. 2b

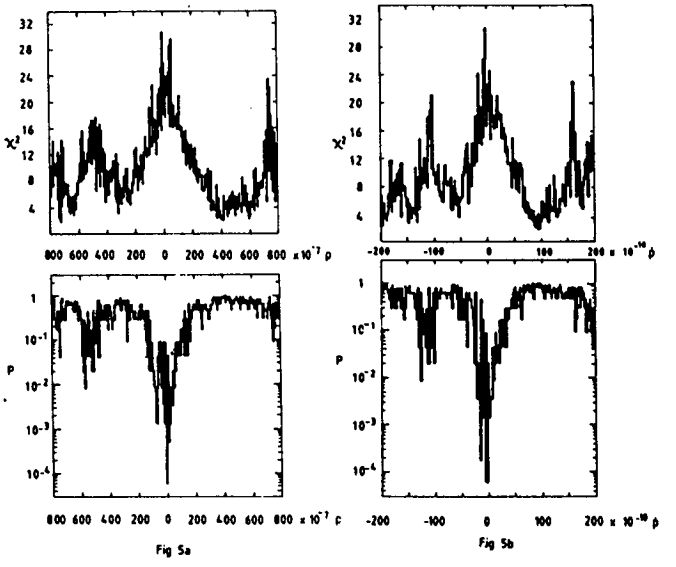

Fig 5a

Fig 5b

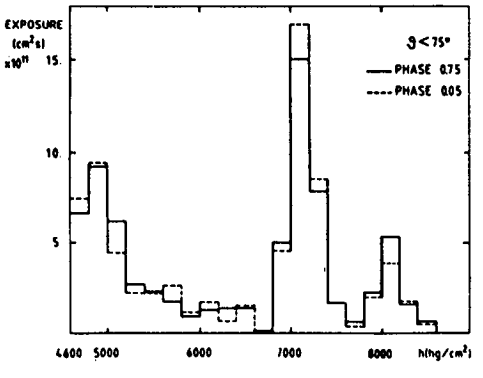

Fig 3

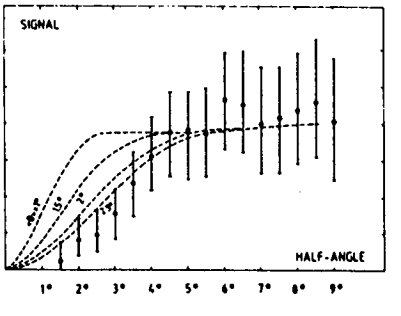

Fig 6

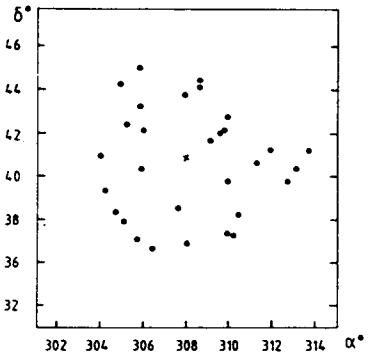

FIG. 7

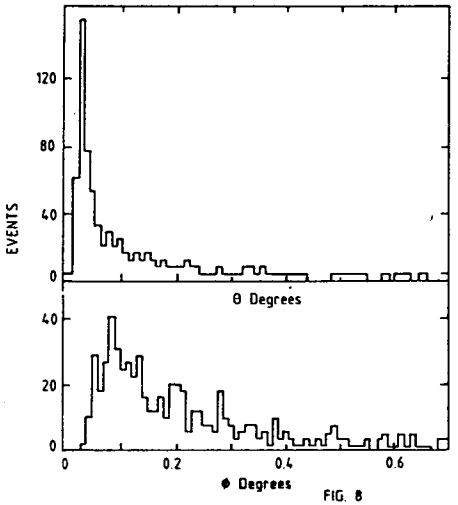

FIG. 8

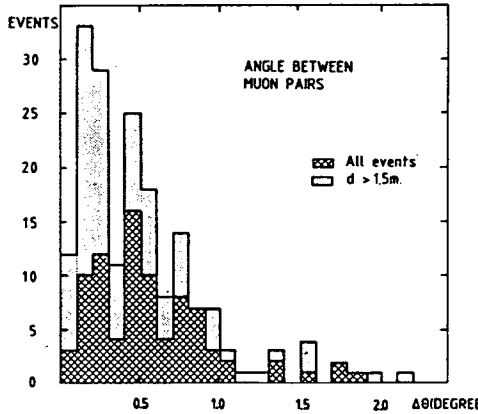

FIG. 9

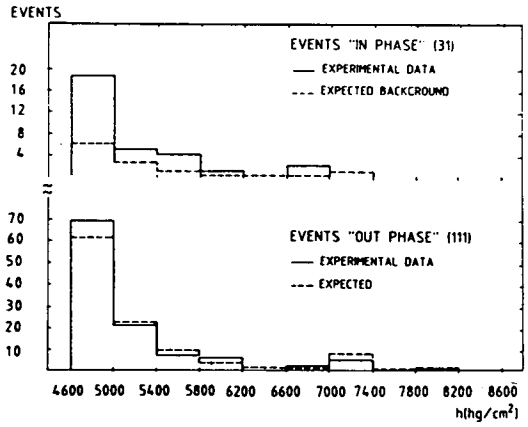

FIG. 10

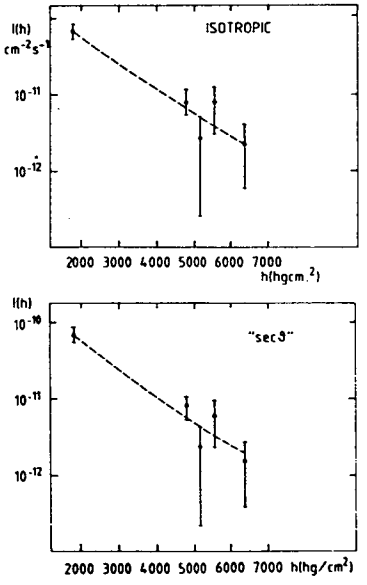

FIG. 11

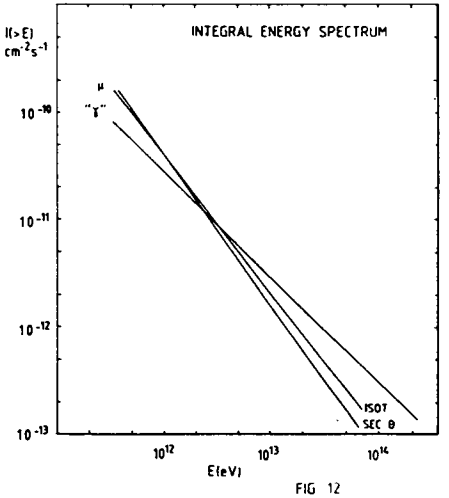

FIG 12

SEARCH FOR A PERIODIC SIGNAL FROM CYGNUS X-3 USING MUONS OBSERVED UNDERGROUND IN THE "FREJUS" DETECTOR (4800 mwe)

P. BAREYRE (4), R. BARLOUTAUD (4), K.H. BECKER (5), L. BEHR (3), C. BERGER (1), R.W. BLAND (3), G. CHARDIN (4), H.J. DAUM (5), B. DEGRANGE (3), S. DEMSKI (5), G. DEUZET (2), L. DI CIACCIO (4), B. DUDELZAK (2), P. ESCHTRUTH (2), D. EDMUNDS (4), J. ERNWEIN (4), G. GERBIER (4), R. HINNERS (5), A. HOFFMANN (1), M.A. JABIOL (4), S. JULLIAN (2), W. KOHRS (5), W. KOLTON (4), B. KUZNICK (5), D. LALANNE (2), F. LAPLANCHE (2), C. LONGUEMARE (2), R. MAYER (5), H. MEYER (5), L. MOSCA (4), L. MOSCOSO (4), U. NGUYEN-KHAC (3), D. ORTMANN (5), C. PAULOT (2), J. PETERS (5), F. RAUPACH (1), Ph. ROY (2), G. SCHMITZ (1), M. SCHUBNELL (5), P. SERRI (3), G. SZKLARZ (2), J. THIERJUNG (5), S. TISSERANT (3), J. TUTAS (1) and B. VOIGTLÄNDER (1).

(1) I. Phys. Institut der Techn. Hochschule, Aachen, Germany.
(2) Laboratoire de l'Accélérateur Linéaire, Orsay, France.
(3) Laboratoire PNHE, Ecole Polytechnique, Palaiseau, France.
(4) Département de Physique des Particules Elémentaires, Centre d'Etudes Nucléaires de Saclay, France.
(5) Universität - Gesamthochschule, Wuppertal, Germany.

1. Introduction.

Periodic signals from Cygnus X-3 in the ultra-high energy range have been recently reported by air-shower arrays [1] ; they are naturally attributed to γ-rays. Although γ-rays are expected to produce muon-poor showers [2] , the preceding observations have stimulated similar studies based on underground muons. Two groups [3,4] have claimed a significant underground signal coming from Cygnus X-3. Their results are however extremely difficult to explain in the present framework of Particle Physics, and clearly need confirmation.

We present here the preliminary results obtained from the "Fréjus" underground detector during its first 16 months of operation (March 1984-June 1985).

2. Site.

The "Fréjus" proton-decay detector is located in the "Modane underground laboratory" in the middle of the Fréjus tunnel linking France and Italy in the western Alps, about 80 km south of the Mont-Blanc. Figure 1 shows a sketch of the underground laboratory, whose main characteristics are summarized in Table 1.

TABLE 1

Longitude :	6.69° E
Latitude :	45.14° N
Average slant depth : (all muons)	4800 mwe
Average slant depth : (Cyg. X-3 direction)	5010 mwe
Average threshold for muons :	3 TeV
Muon angular deviation in the rock (average) :	1°
Muon rate :	4.2 m^{-2} day^{-1}
Primary cosmic ray energy range:	10 - 10^5 TeV
Dimensions of the main hall :	30m x 10m x 11m L ℓ h

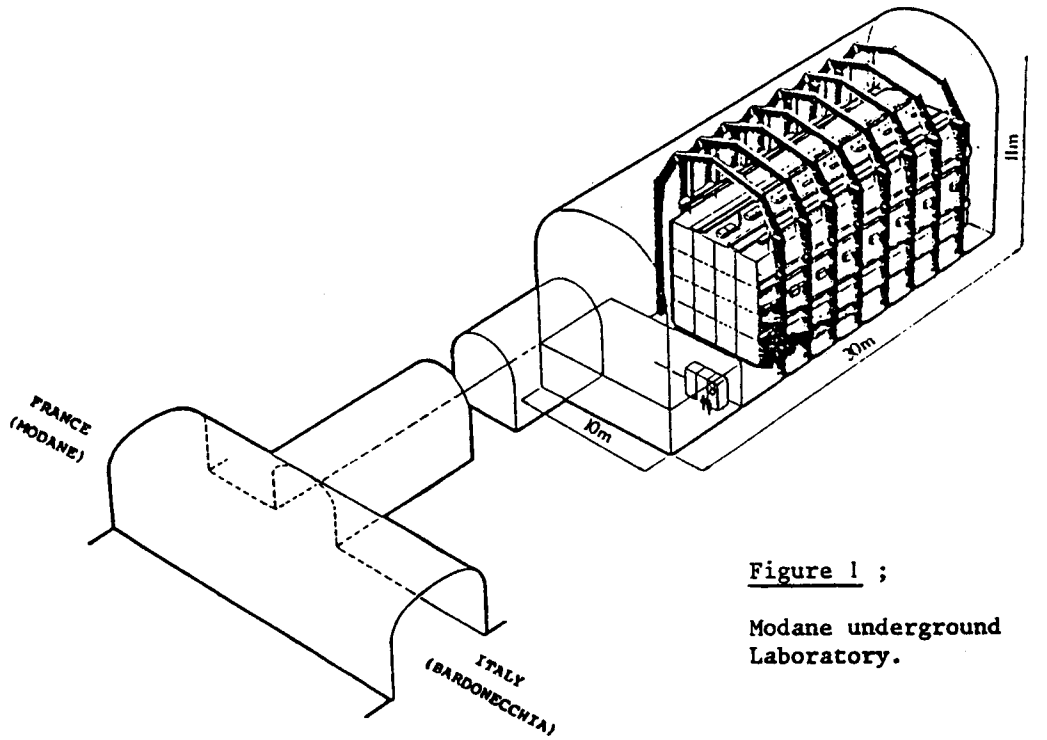

Figure 1 ;

Modane underground Laboratory.

3. The detector

The "Fréjus" proton -decay detector (12.3m x 6m x 6m) consists of a fine grain flash-tube calorimeter (0.93 10^6 flash-tubes) triggered by a set of 113 vertical Geiger planes. The trigger planes (each including 352 wires) are interspersed between flash-tube sections every 10.8cm, thus ensuring a good trigger efficiency for muons. Flash-chamber planes as well as Geiger planes are alternatively made of horizontal tubes (providing the side view of an event) and of vertical tubes (providing the top view), as is sketched in figure 2. The flash-tube section (5mm x 5mm) and the close spacing between flash-chamber planes (3mm of iron) lead to a high spatial resolution (2mm on a muon track). The projected area, averaged over all muon directions is 96 m^2. The total weight is 912 metric tons. The detector orientation is known with an accuracy of 0.2°.

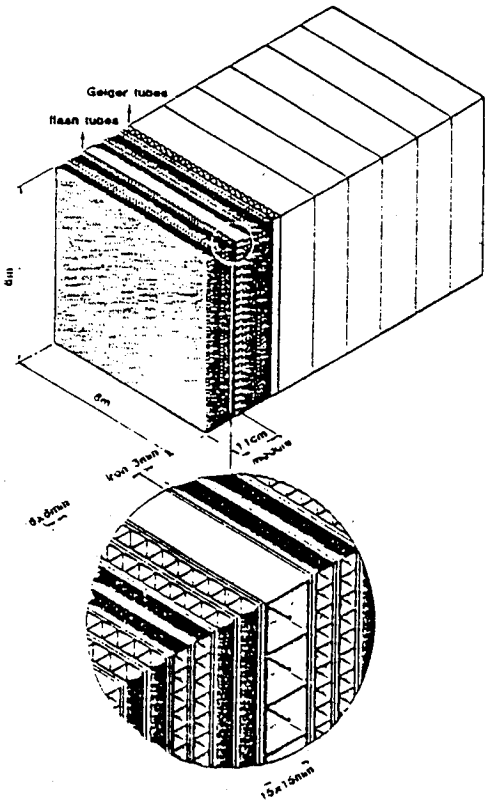

Figure 2 :
General structure of the detector.

The experiment started in March 1984 with only a part of the detector. The experimental set-up was completed at the end of June 1985. The data presented here have thus been taken in a detector with an increasing size. They mainly consist of 106 000 single muons, 3100 muon bundles (figure 3) and of 22 vertex-contained events, all of them being compatible with neutrino interactions (figure 4).

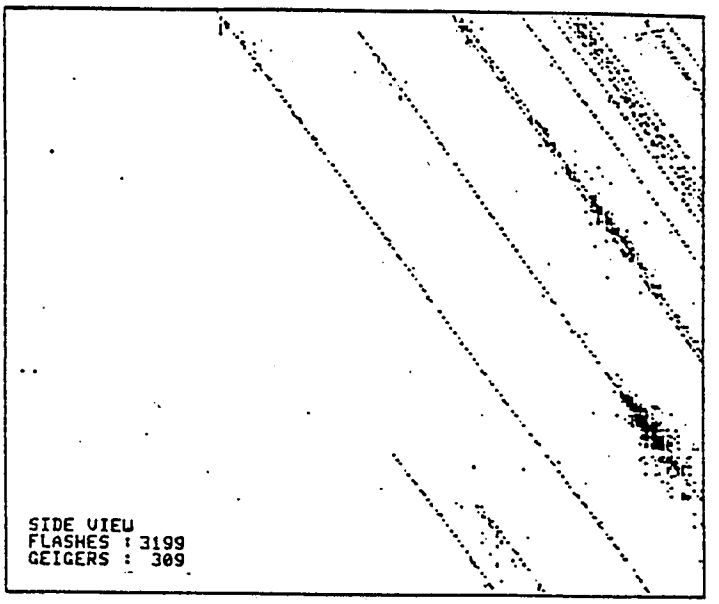

Figure 3 : A muon bundle

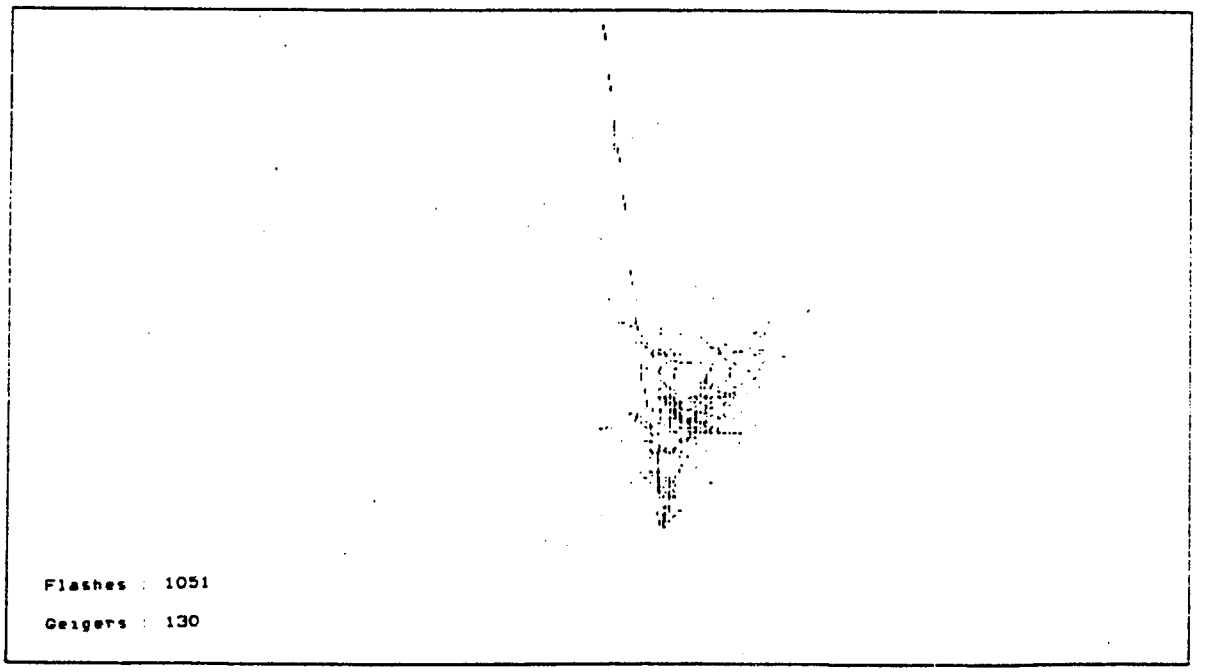

Figure 4 : A neutrino event

4. Search for a periodic signal from Cygnus X-3

In order to ensure a good direction measurement (a few milliradians), muons stopping in the detector as well as muons crossing less than 8 detection planes per view were removed from the sample of single muons. One is thus left with about 90 000 muons for which the average trigger efficiency is 96%. For such muons, the angular error on the source direction is dominated by the average angle of multiple scattering in the rock. Taking into account the small error on the arrival time of the muon (no precise clock being available to date), a conservative estimate of the angular resolution is 1.5°.

The present data are quite comparable to those of the NUSEX experiment [4] in the Mont-Blanc tunnel. Sites have nearby geographical positions and similar average slant depths; both experiments have the same angular resolution. For these reasons, we first follow the NUSEX analysis and select those muons pointing back to Cygnus X-3 within ±5° in right ascension and ± 5° in declination. This leaves us with 177 events, a statistics also comparable with that of NUSEX. No particular accumulation in the vicinity of the source is observed in figure 5. A possible signal can only be extracted by using the time structure expected from the X-ray light curve, following the ephemeris of Van der Klis and Bonnet-Bidaud [5] . The phase relative to the X-ray period was calculated taking into account its time derivative [5] and corrected for the effect of the earth orbital motion.

In order to check that no distortion of the phase histogram was induced by our apparatus or by the shape of the mountain, 6840 events within the same band in declination as the 177 selected events (Cygnus X-3 ± 5°) but with no restriction in right ascension were considered. Their phase distribution shown in figure 6 is found almost uniform, and yields an off-source background in the 10° x 10° window around Cygnus X-3 of 190 events, which is compatible with the number (177) of selected events. The phase distribution of these events is shown in figure 7. The most populated bin is the phase interval [0.6-0.7] containing 30 events, 19 being expected from a flat distribution. In the hypothesis of a uniform background, this represents a fluctuation of 2.5 σ only.

Moreover, structures of similar statistical significance can emerge if one selects an off-source window, keeping the same mean declination but shifting the mean right ascension. This is shown in figure 8 in which a shift of 30° in right ascension with respect to Cygnus X-3 has been chosen. For this reason, it is not possible to consider the structure in figure 7 as a definite signal.

Since our angular error is much smaller than the preceding window size, more restrictive conical windows have been chosen, with respective half opening angles 5° and 4°. The corresponding phase histograms are shown in figure 9. The phase interval [0.6-0.7] is still the most populated one, but the statistical significance of the excess of events with respect to background is not increased.

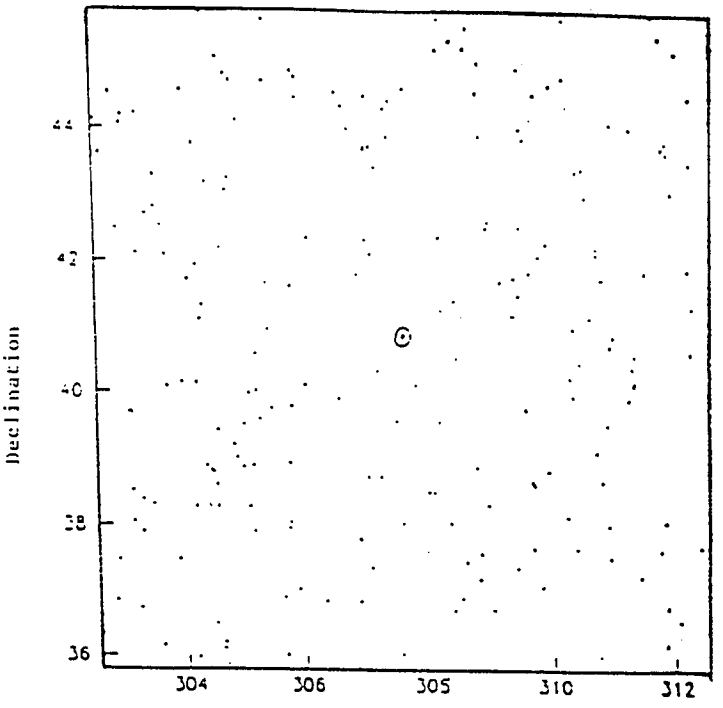

Right ascension

Figure 5

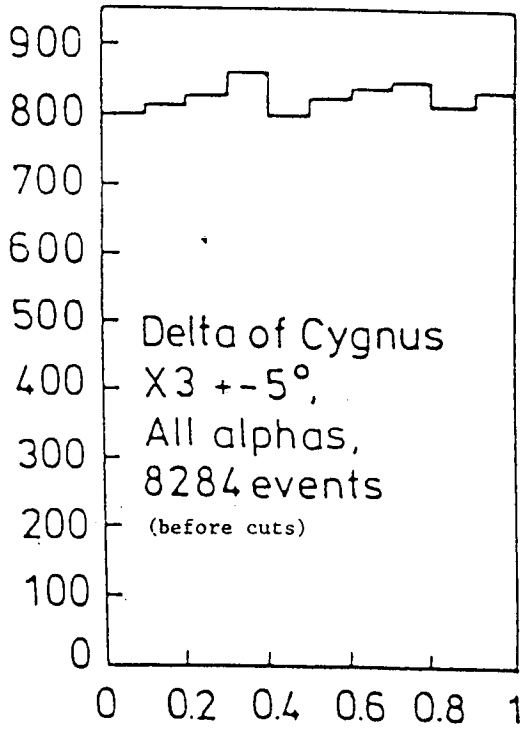

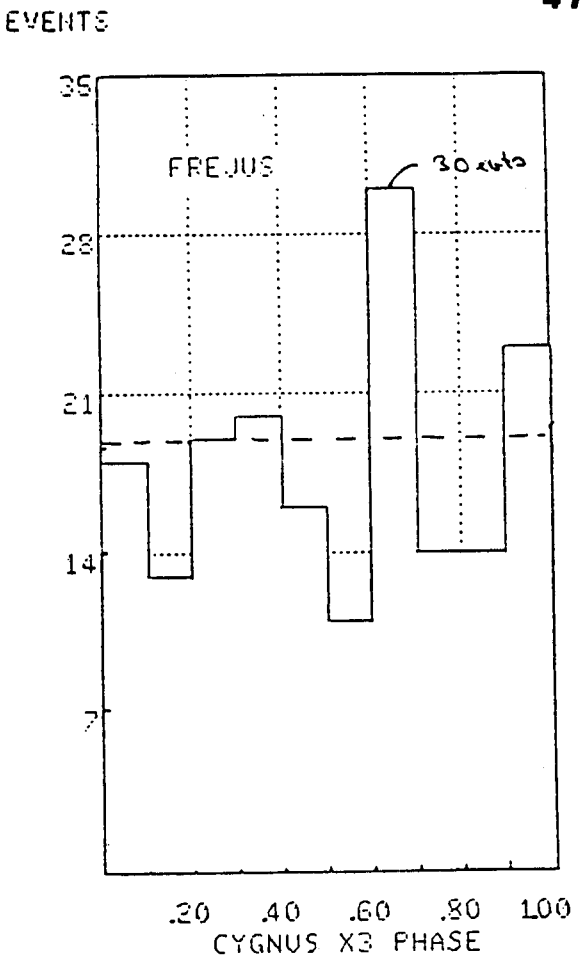
EVENTS
35
28
21
14
7
FREJUS
30 events
.20
.40
.60
.80
1.00
CYGNUS X3 PHASE

Figure 7

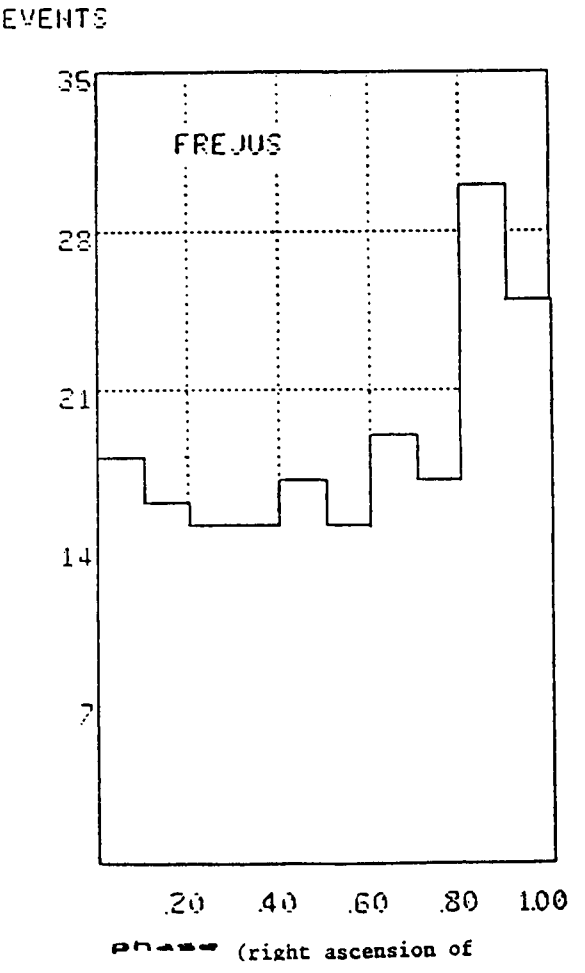
EVENTS
35
28
21
14
7
FREJUS
.20
.40
.60
.80
1.00
(right ascension of

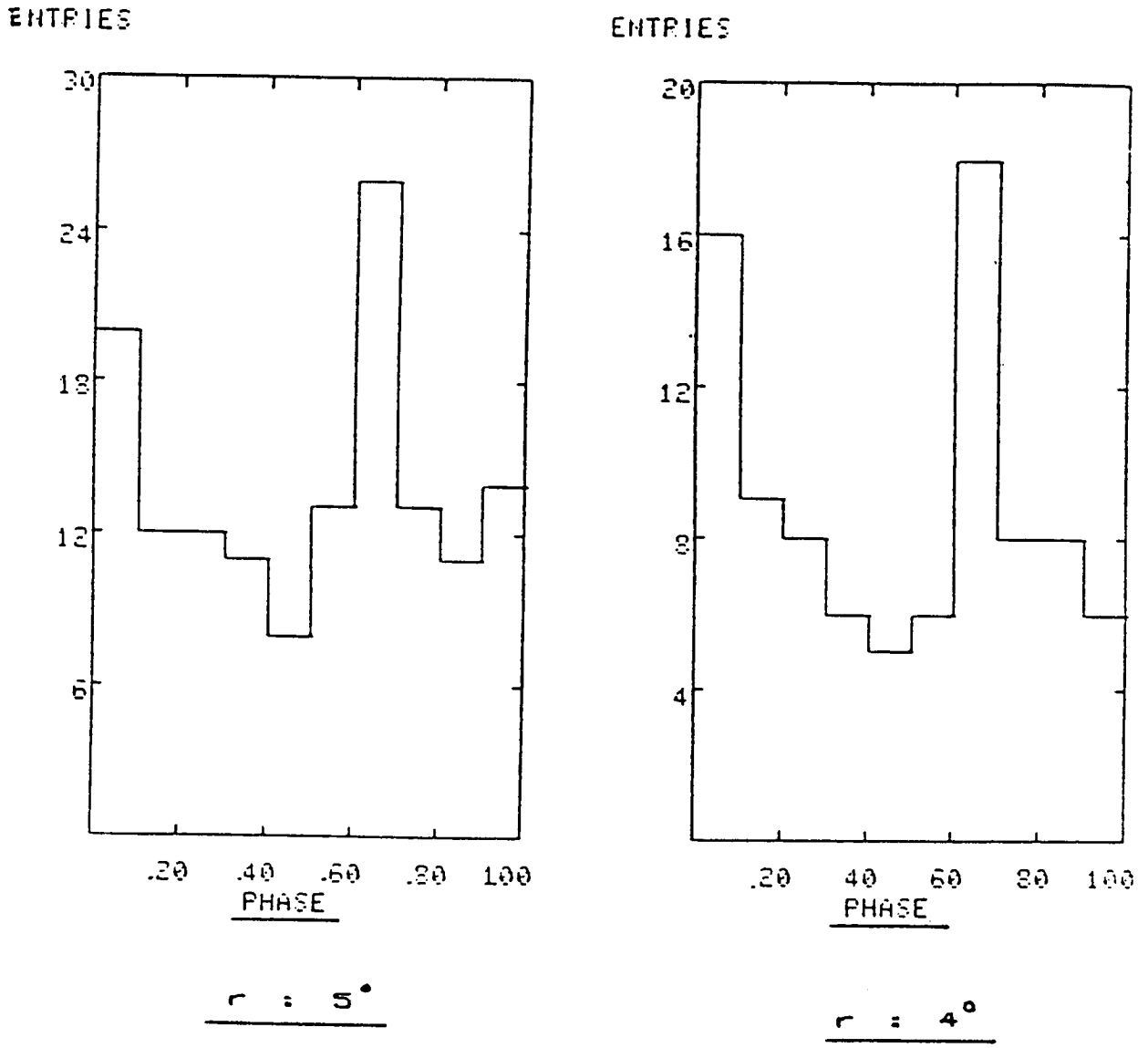

Figure 9 : Phase histograms with conical windows.

5. Conclusion

With the same window in right ascension and declination as the one chosen by the NUSEX group and a similar statistics, we find a phase histogram which is still compatible with a flat distribution, the most populated interval [0.6-0.7] being thus interpreted as a 2.5 σ fluctuation. Of course, a signal is not excluded but it should be noted that the NUSEX peak was found in the nearby phase bin [0.7-0.8] . Our statistics should be increased by a factor of 4 within 2 years. However, the source is suspected to vary with time [6] and it should be kept in mind for the comparison of the NUSEX and Fréjus data that the respective observation epochs are different.

References

1. Proceedings of the 19th ICRC, La Jolla, USA (1985), Vol. 1, P.59-127.

2. T. Stanev and Ch. Vankov, Proceedings of the 19th ICRC, La Jolla USA (1985), Vol. 7, p. 219.

3. M.L. Marshak et al., Phys. Rev. Lett. 54 (1985) 2079.

4. G. Battistoni et al., Phys. Lett. 155B (1985) 465.

5. M. Van der Klis and M. Bonnet-Bidaud, Astron. Astrophys. 95 (1981) L5.

6. A. Lambert et al., Proceedings of the 19th ICRC, La Jolla, USA (1985), Vol. 1, p. 71.

THE COSMIC RAY SPECTRUM ABOVE 10^{19} EV AT VOLCANO RANCH AND HAVERAH PARK

John Linsley
Department of Physics and Astronomy
University of New Mexico, Albuquerque, NM 87131
USA

ABSTRACT

The cosmic ray energy per particle spectrum above 10^{19} eV is measured the same way that energy spectra are measured at much lower energies, by counting all of the particles in a specified energy range that are incident per unit time with trajectories within specified geometrical limits. Difficulties with background or poorly known detection efficiency are markedly less than in some other cosmic ray measurements. The fraction of primary energy given to muons, neutrinos and slow hadrons is less than 10% in this region, so the primary energy equals the track length integral of the secondary electrons with only a small correction for the energy given to other kinds of particles.

In practice the Volcano Ranch and Haverah Park results depend for energy calibration on 'field parameters'. These quantities are accurately measured and reproducible, but relating them precisely to the primary energy without recourse to detailed models of hadron interactions has taken additional experimental work which still goes on. The field parameter S(600) (particle density measured with a scintillator at a core distance of 600 m) provides a common link between the Volcano Ranch, Haverah Park and Yakutsk experiments. There is good agreement as to the relation between this parameter and the primary energy. There is also good agreement as to the vertical intensity corresponding to a primary energy of 10^{19} eV, not only among these 3 experiments but also with the preliminary Fly's Eye results. Above 10^{20} eV there is some disagreement between the Yakutsk experiment and the others.

The first observation of the spectrum above 10^{19} eV, at Volcano Ranch, showed that the spectrum extends to 10^{20} eV without a sign of any cutoff. The spectrum appeared to be flatter in this region than in the decades just below it. These features have been confirmed by the Haverah Park and Sydney experiments, each of which has recorded more than a half dozen events with energy greater than 10^{20} eV. The Volcano Ranch array registered not only the density but also the arrival time distribution of shower particles, at widely separated locations, so it was difficult to doubt that the 10^{20} eV shower was in fact 10 times as large, and 10 times as energetic, as the showers that were assigned an energy of 10^{19} eV. The amount of density and timing information on several of the $> 10^{20}$ eV showers recorded at Haverah Park is even greater. Thus the lack of recorded events of this size from the Yakutsk array must be understood as a problem of detection efficiency, or else as an unexpectedly large statistical fluctuation. The lack of such events from the Fly's Eye is not surprising in view of the relatively small exposure to date.

1. Introduction. To explain how air showers are used to measure the primary energy spectrum, I will use examples from the history of this kind of work, beginning with a period of rapid progress following World War II. The general requirements are to measure the energy of particles incident on some target—in this case the earth's surface—and determine their directional intensity. One uses the fact that very high energy particles striking the earth invariably generate extensive air showers. The secondary particles making up these showers are concentrated in a core that lies along the path of the incident particle, and the number of these secondaries at a given distance from the start of the shower reflects the energy of the incident particle. (One now determines the primary energy more precisely from the total energy deposited in the form of ionization, making small corrections for the energy used to produce neutrinos and excite or disrupt nuclei.) Thus it was evident even before this period began that it would be possible to determine the energy spectrum at very high energies in the canonical manner, just as at much lower energies, letting air showers play the same role as individual tracks in a cloud chamber or emulsion.

2. Finding the Trajectories. The initial step in carrying out this program was taken by R.W. Williams as a member of Rossi's group at MIT. Using an array of four pulse ionization chambers set up on Mt. Evans in Colorado, he recorded the density of shower particles in each chamber for individual showers. From these densities, relying somewhat on calculations of the lateral structure function by Molière but largely just on the expected symmetry, he found estimates of the core location and the number of particles, event by event (Williams 1948).

To learn the trajectory of the primary particle one must find the direction as well as the point where the target was struck. In another MIT experiment it was shown by Bassi, Clark and Rossi (1953) that shower directions can be measured electronically, from arrival times, without using cloud chambers. Their method depends on the fact that all of the important collisions in a shower, and nearly all of the secondary particles produced in the collisions, are highly relativistic. Hence most of the secondary particles travel forward at practically the speed of light, occupying a region that is thin in the direction of motion, and nearly planar.

Within a few years these ideas had been combined in an experiment carried out in 1954-1957 at Agassiz Station of Harvard University, near Boston. Using only about a dozen 0.9 m^2 scintillators, the shower size spectrum was measured up to a size corresponding to 10^{18} eV (Clark *et al.* 1961; shower size means the number of particles in a shower). Clearly the method was so economical that it should be used on a much larger scale. In 1957 it was decided to do this, and a site was chosen at Volcano Ranch, near Albuquerque, New Mexico.

3. Finding the Energies. A weak point of the Agassiz experiment was the uncertainty in converting from shower size to primary energy. This was done using cascade calculations by Olbert, another member of Rossi's group. The calculations showed that, as expected from general arguments, there is a systematic uncertainty in this conversion, due to dependence on

some model of high energy hadron interactions. This uncertainty is substantial for relatively small showers at sea level, but it decreases at higher altitudes, becoming comparatively small at an atmospheric depth x_m corresponding to the maximum in the longitudinal development curve. Moreover, for showers registered past the maximum there are comparatively large fluctuations in size for a given primary energy. Since the energy spectrum is quite steep, these fluctuations introduce a systematic shift which must be compensated using calculated corrections (Kraushaar 1958, Clark *et al.* 1961). Difficulties associated with the location of the maximum become less at higher energies even at sea level. By choosing to locate the first giant array at Volcano Ranch, which is about a mile above sea level, these difficulties were reduced still further.

The choice of model also affects $E_{\mu\nu h}$, the amount of shower energy given to muons, neutrinos and low energy hadrons. For the comparatively small events registered in the Agassiz experiment, $E_{\mu\nu h}$ is a significant fraction of the primary energy, but this fraction decreases with increasing energy, so it was expected that $E_{\mu\nu h}$ would be relatively unimportant in the region of the spectrum the new array was intended to explore. Nevertheless, in order not to be caught unawares by unexpected behavior of the muon component, one of the Volcano Ranch detectors was provided with a lead shield.

Besides MIT, another important center of air shower research in the US was Cornell University. At the same time Williams was laying the goundwork for modern experiments, in which showers are dealt with as individuals, Greisen, with Cocconi and other collaborators, was making detailed studies both at mountain altitude and at sea level, using the statistical methods pioneered earlier by Auger and his co-workers in France. These studies encompassed the muon and low energy hadron components as well as the soft component. Combining the Cornell results with similar results in the literature of the time, Greisen (1956) made an estimate of the energy of air shower primaries along the lines of an earlier estimate by Rossi, in which Rossi tested low energy measurements of the primary intensity against data on the various secondary components throughout the atmosphere in a search for possible 'missing energy' (Rossi 1948, Puppi 1956). Applied to air showers, this kind of analysis yields a so-called 'calorimetric' evaluation of the primary energy. Greisen found the energy of primary cosmic rays having a vertical intensity (integral) of $1.7 \cdot 10^{-6}$ $m^{-2} sr^{-1} s^{-1}$ to be $(1.4 \pm 0.3) \cdot 10^{15}$ eV, remarkably near the present best value, $(1.0 \pm 0.1) \cdot 10^{15}$ eV (Linsley 1983). The calorimetric method of finding the energy of air shower primaries is regarded by all concerned to be the proper ideal for experiments up to the highest energies that have been observed.

Soon after its introduction, this method was used by Nikolskii (1962) and Zatsepin *et al.* (1963) with independent data from experiments in the Pamir mountains, including data on the atmospheric Cerenkov light produced by the showers. This light is practically not absorbed in the atmosphere. Moreover, the production efficiency can be calculated from classical electrodynamics, so there is practically no dependence on atomic or nuclear models. This makes the atmospheric Cerenkov light an especially reliable measure of the total energy deposited in the atmosphere, which is the largest term in the equation for balancing the energy. Alternatively, this term can be evaluated from N_m, the size at maximum development, and an estimate of the shower profile width.

For the Volcano Ranch experiment the latter approach had been chosen. It was important, therefore, that the altitude of the experiment be about equal to the altitude where the largest showers are expected to reach maximum development. Even at that time there were ways of determining x_m empirically, from the energy dependence of zenith angle distributions or the behavior of size spectra (Clark 1962). The conversion factor between N_m and primary energy was thought to be "about 2 GeV per particle for all models of shower development" (Clark 1962). (According to more recent evidence this figure is too high; it should be 1.3-1.4 GeV per particle; see Hillas 1972 and Linsley 1983.)

4. The Volcano Ranch Experiment. Figure 1 shows the Volcano Ranch array with the configuration it had in 1960-1963. In 1959-1960, the first year of operation, the detector spacings were half as great. The detectors were 3.26 m^2 scintillators. Nineteen of them were arranged as shown; an additional one was located in various places, usually adjacent to one of the other detectors, sometimes unshielded but usually shielded with 10 cm of lead. Two other arrays similar to the Agassiz array are also shown. The one at El Alto, just outside of La Paz, Bolivia, was an MIT-Bolivian collaboration using scintillators from the Agassiz experiment. The Cornell array was a variable density array made with the same kind of scintillators. Each of them was somewhat larger than the Agassiz array, but the Volcano Ranch array was much larger, with fifty times the area.

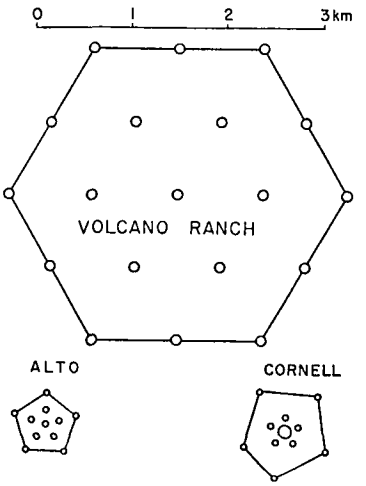

Fig. 1. Plan of the Volcano Ranch array in 1960-1963. The Cornell and El Alto arrays are shown for comparison. The large circle at the center of the Cornell array represents 5 separate 0.9 m^2 scintillators.

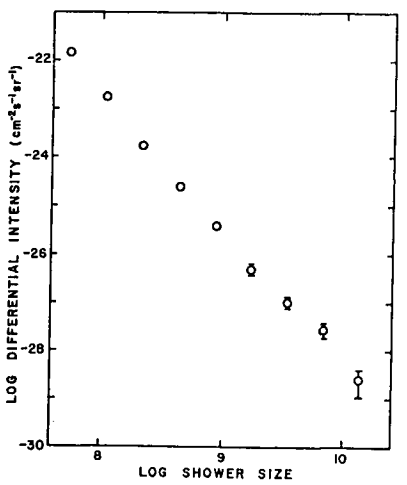

Fig. 2. Differential size spectrum at an atmospheric depth of 835 g/cm^2.

The shower size spectrum reported at the Jaipur Conference is shown in Figure 2 (Linsley 1963). The slope was unexpectedly flat compared to similar spectra at lower energies. The energy spectrum reported at that time is shown in Figure 3, superimposed on the best present spectrum. Below a few times 10^9 GeV the primary energy was considerably underestimated by assuming that the smaller showers as well as the larger ones were at maximum development when observed at 835 g/cm^2, the depth of the experiment. Above 10^{10} GeV, however, the agreement is remarkably good. Figure 4 shows a later version of the size spectrum, extending to higher energies (Linsley 1973).

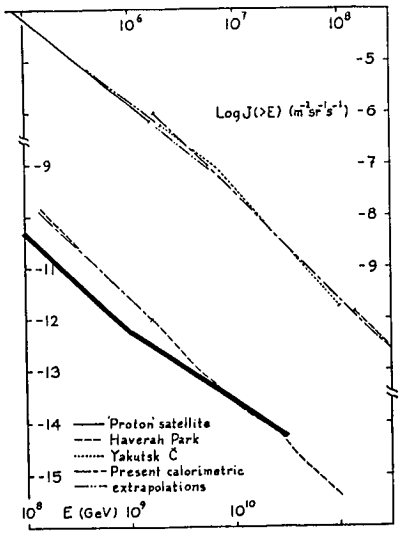

Fig. 3. *(left) Volcano Ranch integral energy spectrum (Linsley 1963, heavy line), superimposed on more recent results summarized at the Bangalore Conference (Linsley 1983).*

Fig. 4. *(below) Later version of the Volcano Ranch size spectrum.*

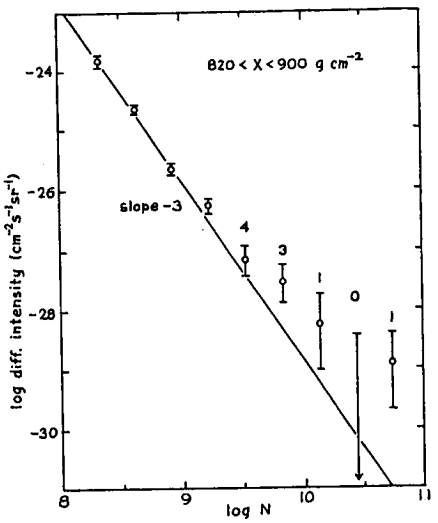

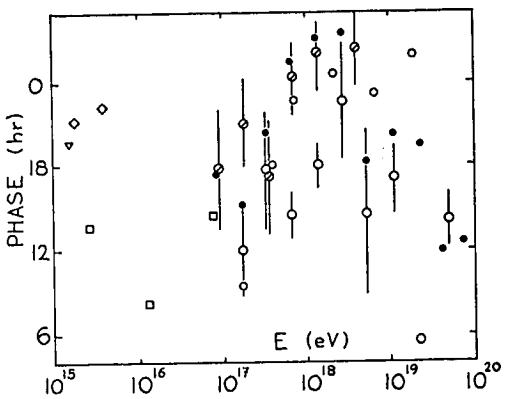

Fig. 5. *Volcano Ranch evidence for anisotropy of the highest energy cosmic rays (Linsley 1975), compared to a recent summary of similar results (Linsley 1983). The dependent variable is the phase of the first harmonic of the counting rate in sidereal time. Large circles, Volcano Ranch (points with slash are from 1959-60; without slash, from 1960-63); small filled circles, Haverah Park; small open circles, Yakutsk; squares, Cornell; diamonds, Pic du Midi; triangle, Chacaltaya.*

The Volcano Ranch experiment also contributed importantly to showing that the arrival directions of the highest energy cosmic rays are anisotropic. The pattern that stands out most clearly above statistical noise is a modulation in the direction of maximum intensity observed by arrays in the northern hemisphere, with changing energy (see reviews by Linsley, 1983, and Hillas, 1984). It was noted at the time of the Munich Conference that patterns of this kind were present in data from Volcano Ranch and Haverah Park, and that they were similar (Linsley 1975, Edge *et al.* 1975). Since then, additional confirmation has come from the Yakutsk array. Figure 5 shows these results.

5. The Haverah Park Experiment. Work on a giant air shower array to be built in England began with a meeting called by Blackett in 1958, attended by representatives of cosmic ray groups at Imperial College and the Universities of Leeds, Durham and Bristol. Later that year the site was chosen:

Haverah Park, near Leeds. For detectors it was decided to use larger versions of water-Cerenkov tanks that had been used previously by the Imperial College group in a small air shower experiment at Silwood, the site of a field station belonging to the College. A good deal of experience with large air showers had been gained earlier through a notable series of experiments at Culham airfield, using groups of Geiger tubes distributed over an area of some 0.5 km^2. (I am indebted to Harold Allan and Neil Porter for background information about early air shower work in the British Isles.)

Operation at Haverah Park began near the end of 1962 with 4 detectors, a central one with 3 other units placed symmetrically at a distance of 500 m, each detector consisting of 15 tanks with a total area of 34 m^2. In following years six clusters of similar detectors were put in service at distances of about 2 km from the central set, so that by 1968 the size of the array was about the same as Volcano Ranch. Large muon detectors had been added, and the University of Nottingham had joined the list of those using the site. At a later stage shown in Figure 6, smaller water-Cerenkov tanks were added, enabling more accurate location of shower cores and more detailed measurements of structure, within a certain portion of the array. More recently scintillators have been added, at first for the purpose of comparing their response to that of the water-Cerenkov tanks, but after the Cygnus X-3 discovery, for the purpose of improving the angular resolution in portions of the installation that now are devoted to UHE γ-ray astronomy.

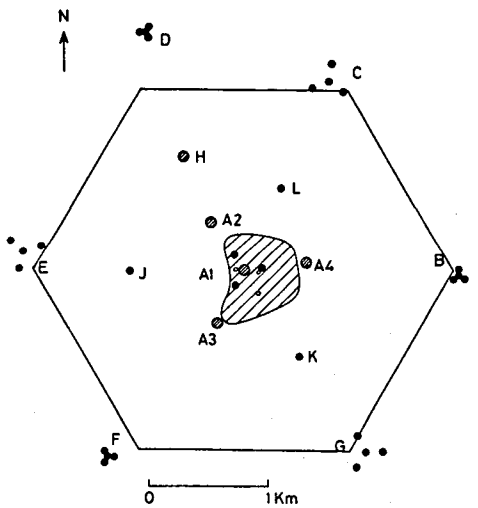

Fig. 6. The Haverah Park array. The triggering detectors A1-A4 are of area 34 m^2. The sub-arrays B-G comprise 4x13.5 m^2 detectors. At H there is 13.5 m^2, at JKL, 2.25 m^2 and at the 3 locations 150 m from A1 there is 9 m^2. Within the shaded area is a lattice (∿ 150 m spacing) of 30x1 m^2 detectors, the 'infilled' array. There are muon detectors at the positions inside the shaded area marked with open circles (Watson 1980). The hexagon shows the perimeter of the 1960-1963 Volcano Ranch array to the same scale.

By 1977, work at Haverah Park had produced results on the energy spectrum and anisotropy of > 10^{19} eV cosmic rays with substantially better statistical accuracy than any previous results. This is shown by a comparison with Volcano Ranch in Figure 7. (In deriving the Volcano Ranch points from the size spectrum shown in Fig. 4, the crude assumption used previously about x_m *vs* N at 835 g/cm^2 was replaced with a more realistic one, taking advantage of experimental and theoretical advances in the interim.) Above 10^{19} eV there is agreement, within the large statistical errors of the Volcano Ranch points. Comparison of the points below 10^{19} eV indicates that the systematic differences are within 30%. The evidence for a flattening of the spectrum above 10^{19} eV, which was only an indication in

the Volcano Ranch spectrum, is quite strong statistically in the Haverah Park result. Both spectra extend beyond 10^{20} eV with no sign of any cutoff. Figure 8 shows the Haverah Park spectrum as it was published a few years later in *The Astrophysical Journal* (Cunningham *et al.* 1980).

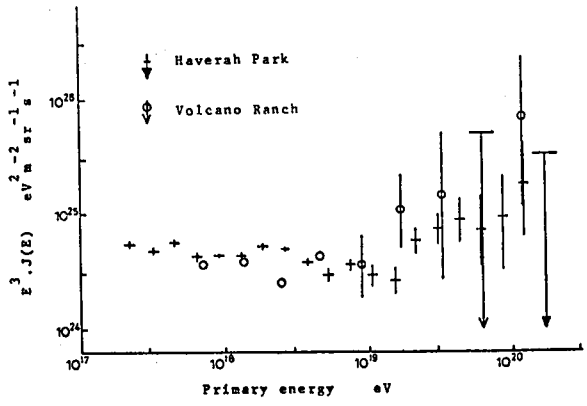

Fig. 7. Comparison of the 1977 Haverah Park energy spectrum and the Volcano Ranch spectrum (Cunningham et al. 1977).

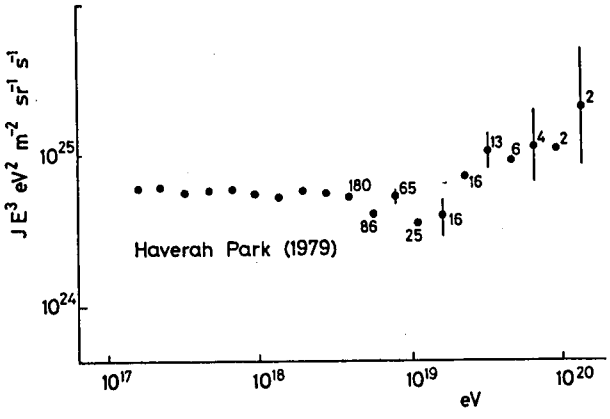

Fig. 8. Haverah Park energy spectrum (Cunningham et al. 1980).

6. Giant Arrays in Sydney and Yakutsk, and the Fly's Eye.

Planning of a giant array in Australia began in 1963. The Sydney University Giant Air-shower Recorder (SUGAR) started full operation in 1968 and continued giving data until 1979. The array had an area of some 50 km^2, giant indeed! Technical problems in the data reduction, eventually overcome, delayed publication of the final results of this experiment until recent years.

In 1965, plans for a giant array in the Soviet Union were described. Located near the Siberian city of Yakutsk, its 3 km^2 central area began operating in 1970. The full array, covering an area twice as large as the one at Volcano Ranch, began to furnish data in 1974, and it continues to run, the equipment being modernized according to a regular schedule. A special feature is the emphasis on recording the atmospheric Cerenkov light of very large showers, as well as the muon component, so that the calibration will be calorimetric to the greatest possible extent.

The notion that air fluorescence detectors might be employed for studying very large air showers seems to have occurred independently to scientists in the USA, Japan and the USSR (Greisen 1960, Delvaille *et al.* 1962, Suga 1962, Chudakov 1962). In 1965 Greisen showed in detail how such devices can be used to determine trajectories, energies and development profiles of individual showers. At that time, preliminary work at Cornell University using a relatively simple arrangement of photomultipliers had already been reported in the form of a thesis (Bunner 1964). Work on a full scale device, called a "fly's eye telescope", continued at Cornell until 1972 but then was dropped. Shortly afterward the idea was taken up by Keuffel's group at the University of Utah. Redesigned prototype units were tested successfully at Volcano Ranch in 1976. A complete fly's eye,

together with a partial eye located near it, has been operating at Dugway, Utah, for several years. The amount of fluorescent light produced in a layer of atmosphere is proportional to the amount of ionization, so when the variation of conversion efficiency with pressure is taken into account the signals from a fly's eye provide a calorimetric measurement of E_{EM}, the energy deposited by the electromagnetic component of showers. In the domain of very high energies only a small correction is required to obtain from this the energy of the primary particle.

7. On Estimating the Energy of Giant Air Shower Primaries. Although preliminary energy spectra from Yakutsk agreed with Haverah Park and Volcano Ranch as to flattening and absence of a cutoff, results given at the 8th European Cosmic Ray Symposium in 1982 showed a deficiency of very energetic events, beginning at a few times 10^{19} eV, as predicted by Greisen (1966) and Zatsepin and Kuzmin (1966) for cosmic rays with a universal origin, due to effects of the 3K background radiation. It was surmised at first that the disagreement might be due to differences in the algorithms for converting from ground parameters to primary energy. It was possible to test this hypothesis in a very direct manner, because the Yakutsk ground parameter S(600) has also been measured for some very large showers at Haverah Park, and it could be derived from Volcano Ranch data for some very large showers with slant depths corresponding closely to the altitude of Yakutsk. These tests were made, and in both cases they show good agreement (Bower *et al.* 1983). One concludes that if the Yakutsk array had detected the same showers that were detected and assigned energies $> 4 \cdot 10^{19}$ eV at Volcano Ranch and Haverah Park, these showers would likewise have been assigned energies above the Greisen-Zatsepin cutoff, energies sometimes exceeding 10^{20} eV, in agreement with the investigators at MIT and Leeds. Another conclusion that can be drawn from these tests is that, insofar as the Yakutsk energy scale is correct calorimetrically, so are the scales employed at Volcano Ranch and Haverah Park.

It should be kept in mind that some of the methods for finding the principal energy term E_{EM} are limited in the range they cover. Only with the atmospheric fluorescence method can one avoid a certain amount of extrapolation; avoid, that is, relying on approximate proportionality to energy of some ground parameter such as $\rho(600)$ at Haverah Park or S(600) at Yakutsk. The method using atmospheric Cerenkov light is limited to $E < 10^{19}$ eV by the low duty cycle of the light receivers, which can be used only on clear, moonless nights. The method using maximum size is limited at present to $E < 10^{18}$ eV by a lack of observations with sufficiently large surface arrays at sufficiently high altitudes. It is reassuring, however, that as far as they go in energy, results by this method agree with the Cerenkov method. This is shown in Figure 9, where the filled circles derive from measurements of N_m while the diamonds are from measurements of atmospheric Cerenkov light. It is notable that the filled circles agree as well as they do with the low energy portion of the Haverah Park spectrum.

Unlike the other experiments described here, the SUGAR experiment used muon size as the basis for estimating primary energy. Originally, the plan was to rely on certain cascade simulations for relating N_μ to E. It turns out, however, that these simulations disagree with direct measurements of the N_μ-E relation made in recent years at Akeno and Yakutsk. As a

result the SUGAR spectrum disagrees strongly with others described here when it is based on these simulations. In reviewing the subject for the Bangalore conference I found that by using a 2-constant parametrization of the Yakutsk N_μ-E results instead of the simulation one obtains much better agreement. The constants control the slope and intercept of the log-log energy spectrum. In case of the SUGAR spectrum, the slope is about right, indicating that one of the constants is about right, but the energies are systematically too high by 20-30%, an amount that is small in this context, indicating that the other constant is off the mark, due to residual errors in the N_μ vs E measurements at Yakutsk or to a systematic error in N_μ as measured by SUGAR.

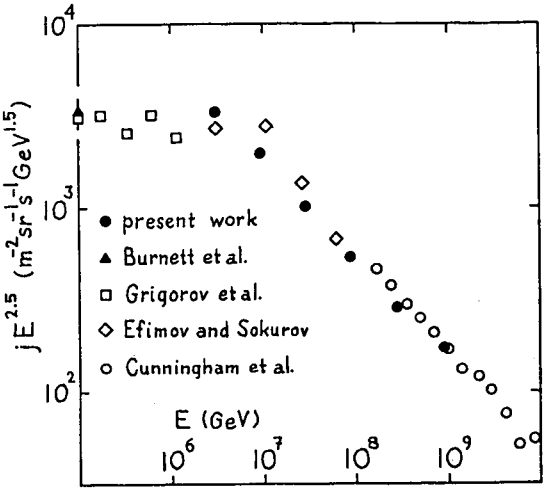

Fig. 9. All-particle energy spectrum. The filled circles are from my conference paper OG 5.1-4, "New Calorimetric All-Particle Energy Spectrum"; see also Linsley 1983, Figures 5-8 and 10.

In Figure 10 I compare the Haverah Park spectrum of Figure 8 with a preliminary Fly's Eye spectrum (Baltrusaitis *et al.* 1985) and a version of the SUGAR spectrum, where in the interest of fairness to proponents of a spectral cutoff I have adjusted the offending constant *ad hoc*, bringing *down* the energy corresponding to a given intensity so as to reach agreement with the Haverah Park spectrum at 10^{19} eV. This value was chosen because at this energy the remaining experiments (Yakutsk, Volcano Ranch and Fly's Eye) already agree rather well. The Haverah Park data base has increased significantly since 1979. A more recent spectrum is given in this conference (paper OG 5.1-3 by Brooke *et al.*)

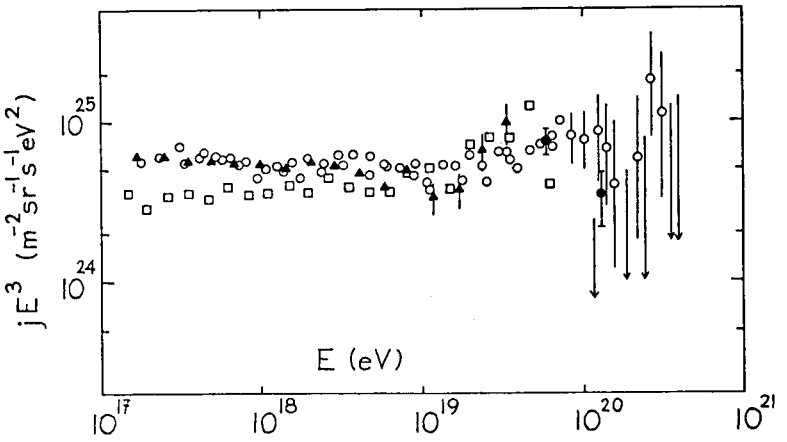

Fig. 10. Differential energy spectrum j(E) plotted as jE^3. The filled triangles are from Cunningham et al. 1980; the open squares, from Baltrusaitis et al. 1985 (with some of the error bars redrawn so as to conform with usual practice); the filled circles, from Bower et al. 1983 (converted to differential form as in Linsley 1983); the open circles and upper limit arrows, from Horton et al. 1983, with N_μ converted to E as described in the present text.

8. Statistical Fluke, or Inefficiency? Tradeoffs between quality and quantity are common in scientific work. A familiar example illustrating what I wish to say about large air shower experiments is given by the HEAO-3 Heavy Nuclei Experiment. Events selected by a loose electronic trigger were sorted into various subsets with different combinations of size (number of events) and charge resolution. For analyzing nuclei with Z = 26-46 it was appropriate to use only subsets with superior resolution, because these nuclei are relatively abundant, but in searching for actinides it was reasonable, in fact essential, to relax the selection criteria and accept the resulting loss of charge resolution in order to obtain results of greater statistical significance on these very rare but extremely important elements.

Beginning with the Agassiz experiment it has been customary to make rather severe data cuts in selecting events to use for finding the energy spectrum. The two main cuts are on the zenith angle and on the core location with respect to the array boundary. There are good reasons for cuts of this nature: the uncertainty in primary energy for a given observed size tends to increase, on the one hand with increasing zenith angle, and on the other, with increasing radial distance of the shower core from the center of an array, for showers striking outside the boundary. To a large extent these uncertainties are reflections of uncertainty about the longitudinal structure and the lateral structure, respectively, of air showers with the size in question.

In the early 1960's such uncertainties were great. They were especially great regarding the first 'giant' showers. Consequently one made severe data cuts. As late as 1973 the Volcano Ranch energy spectrum above 10^{19} eV was based on only 5 events out of 44 described as having this much energy in the *Catalogue of Highest Energy Cosmic Rays*. All but 11 of these were not sufficiently vertical (I required $\theta < 25°$!); out of the 11 that were sufficiently vertical only 5 struck inside the boundary.

In retrospect, the Volcano Ranch cuts were unnecessarily severe, even at the time, because they were imposed across the board, without taking into consideration that with a given array the direction and core location can be measured more accurately for very large showers than small ones. But at the time it didn't matter. There was no demand for better statistical accuracy; it was more important to be as certain as possible about the energy of the single largest high quality event. Anisotropy was a separate question; the selection criteria were much less strict.

Turning to present arrays, and to controversy on the question of a cutoff, I will now argue in favor of publishing the air shower spectrum results *in both of two forms*: one with optimum 'resolution' but necessarily poor statistical accuracy and the other with poorer 'resolution' but optimum statistical accuracy. I have written 'resolution' with quotes because the main rationale for data cuts is still reduction of possible systematic errors (although the cuts do tend to improve the energy resolution). I propose that one should give more recognition to the very great improvement in knowledge of shower structure from intensive experimental studies during the last decade. The effect of this improvement has been to reduce the systematic errors, so that I believe they are now smaller than the statistical errors above 10^{19} eV, even when data cuts are minimal.

Examples of the two forms are the 1979 Haverah Park spectrum ('high resolution') and the SUGAR spectrum, which was found using all of the Sydney events except for a small percentage that could not be analyzed, or when analyzed gave unphysical results (Horton *et al.* 1985). A step in the direction I advocate was taken by Bower *et al.* (1983). Integral intensities for $E > 4.10^{19}$ and $E > 10^{20}$ eV were found using all "sufficiently well measured" events from Volcano Ranch and Haverah Park combined. Quality control was assured by the fact that detailed data on many of the individual events had already been published in the *Catalogue of Highest Energy Cosmic Rays*. Examination of the detailed data for 'high resolution' and run of the mill events of this size shows that the difference in quality is small, no greater than in the analogous HEAO-3 experiment.

Following this recommendation it will be seen that the evidence against a spectral cutoff lower than a few times 10^{20} eV is strong statistically as well as in regard to energy assignment and energy calibration. This puts a heavy burden of proof on groups reporting a deficiency of events above $4\text{-}6\cdot10^{19}$ eV. At present there is no great problem with the Fly's Eye observations; up to $\sim 6\cdot10^{19}$ eV there is good agreement with the experiments showing no cutoff. The deficit above that energy has a chance probability of about 10%. There is a greater problem with the Yakutsk observations. The deficit is greater, with a chance probability of only 1 or 2%. If the groups in Yakutsk and Utah have been victims of a statistical fluke, this should be apparent within a few more years. If, on the other hand, the size of the events they register continues to be limited in this way, then I believe it will be necessary to devise some very direct, foolproof method of proving that the detection efficiency for the 'missing events' is as high as assumed. In case of the Fly's Eye this might involve tests using scattered laser light, similar to tests that have already been made but covering a wider range of distances and angles, repeated regularly during the course of the cosmic ray observations.

References. BALTRUSAITIS *et al.* 1985, Phys. Rev. Lett. 54, 1987; BASSI, CLARK and ROSSI 1953, Phys. Rev. 92, 441; BOWER *et al.* 1983, J. Phys. G: Nucl. Phys. 9, L53, and Proc. 18th ICRC (Bangalore) 9, 207; BROOKE *et al.* 1985, Proc. 19th ICRC (La Jolla) 2, 150; BUNNER 1964, MS Thesis, Cornell Univ.; *CATALOGUE OF HIGHEST ENERGY COSMIC RAYS*, ed. M. Wada (World Data Center C2 for Cosmic Rays, Inst. of Phys. Chem. Res., Tokyo) No. 1 (1980); CHUDAKOV 1962, Proc. 5th Interamerican Seminar on Cosmic Rays (La Paz, Bolivia) Vol. II, XLIX; CLARK *et al.* 1961, Phys. Rev. 122, 637; CLARK 1962, J. Phys. Soc. Japan 17, Suppl. A-III, 286; CUNNINGHAM *et al.* 1977, Proc. 15th ICRC (Plovdiv) 2, 303; 1980, Astrophys. J. 236, L71; DELVAILLE, KENDZIORSKI and GREISEN 1962, J. Phys. Soc. Japan 17, Suppl. A-III, 76; EDGE *et al.* 1975, Proc. 14th ICRC (Munich) 2, 604; EFIMOV and SOKUROV 1983, Proc. 18th ICRC (Bangalore) 2, 123; GREISEN 1956, *Progress in Cosmic Ray Physics*, ed. J.G. Wilson (Interscience, New York) III, 1; 1960, Ann. Rev. Nucl. Sci. 10, 63; 1965, Proc. 9th ICRC (London) 2, 609; 1966, Phys. Rev. Lett. 16, 748; HILLAS 1972, *Cosmic Rays* (Pergamon Press, Oxford) p. 90; 1984, Ann. Rev. Astron. Astrophs. 22, 425; HORTON *et al.* 1983, Proc. 18th ICRC (Bangalore) 6, 124; Sydney Univ. preprint "The Cosmic Ray Energy Spectrum above 10^{17} eV"; KRAUSHAAR 1958, Nuovo Cimento 8, Suppl. 2, 623; LINSLEY 1963, Proc. 8th ICRC (Jaipur) 4, 77; 1973, Proc. 13th ICRC (Denver) 5, 3207; 1975, Proc. 14th ICRC (Munich) 2, 598; 1983, Proc. 18th ICRC (Bangalore) 12, 135;

References (continued) NIKOLSKII 1962, Proc. 5th Interamerican Seminar on Cosmic Rays (La Paz, Bolivia) Vol. II, XLVIII; PUPPI 1956, *Progress in Cosmic Ray Physics*, ed. J.G. Wilson (Interscience, New York) III, 339; ROSSI 1948, Rev. Mod. Phys. 20, 537; SUGA 1962, Proc. 5th Interamerican Seminar on Cosmic Rays (La Paz, Bolivia) Vol. II, XLIX; WATSON 1980, Q. J. Roy. Astr. Soc. 21, 1; WILLIAMS 1948, Phys. Rev. 74, 1689; ZATSEPIN, NIKOLSKII and KHRISTIANSEN 1963, Proc. 8th ICRC (Jaipur) 4, 100; ZATSEPIN and KUZMIN 1966, Sov. Phys. JETP Letters 4, 78.

MEASURING THE ENERGY SPECTRUM OF PRIMARY COSMIC RAYS WITH THE YAKUTSK EAS ARRAY

G.B.Khristiansen

Institute of Nuclear Physics, Moscow State University; Moscow 119899, USSR

The Yakutsk EAS array has been designed for detecting the showers generated by the 10^{17}–10^{20}eV primary cosmic rays and consists of numerous electron, muon, and Cerenkov light detectors arranged on a 20-km^2 area terrain (see Fig. 1). The array is featured by the feasibility to detect the EAS-produced Cerenkov light, hence, as will be shown below, to find the mean energy of the primary particles generating an ensemble of EAS of given size.

The Yakutsk array detectors are on the average spaced a relatively small distance apart (compared, for example, with the Haverah Park and University of Sydney arrays), thereby permitting a comparatively high accuracy in determining the basic parameters of the EAS detected. For instance, the Monte Carlo calculations allowing for the fluctuations of t e lateral distribution function of charged particles have shown[1] that (see Table 1) the error in finding the parameter ς_{600} of individual EAS, which is the particle density at a 600-m distance from the EAS axis*), does not exceed 2% if the shower axes fall within the effective detection area of the Yakutsk array for EAS of a given size. The calculations were carried out for the various values of ς_{600} and the various zenith angles of the EAS axes. The effective detection area is determined in terms of the requirement that the probability of EAS detection within the

*) The value of ς_{600} can be determined most accurately with the Yakutsk array. Besides, ς_{600} is known to be a good measure of the primary energy.

area should be at least $\varepsilon = 0.9$, irrespectively of the possible fluctuations in the form of the lateral distribution function. Fig.2 shows the effective detection area for EAS with $E_0 \geqslant 10^{19}$eV. The primary energy spectrum is inferred from the Yakutsk array data by finding, first, the EAS $\int_{600}$ spectra for various intervals of the zenith angles of the detected EAS axes. The EAS axis direction and position and the EAS size ($\int_{600}$) are found by the maximum likelihood method described in detail in [1].

Fig.3 shows the EAS $\int_{600}$ spectra for the various zenith angles corresponding to the traversed atmospheric depths of 1046 g/cm^2, 1133 g/cm^2, and 1313 g/cm^2 [1]. The data of Fig.3 may be used to find the experimental absorption path of EAS with a given value of $\int_{600}$, $\lambda \simeq 500$ g/cm^2 which, in turn, may be used to scale the observed spectra to the vertical direction $\vartheta = 0^\circ$ (it should be noted that the same procedure is used to infer the $\int_{600}$ spectrum from the Haverah Park array data).

Fig.4 compares between the $\int_{600}$ spectra inferred from the Yakutsk data within 38000 hours and from the Haverah Park data. The Haverah Park spectrum has been obtained by scaling $\int_{600\,HP}$ from the water-tank data to the 5-cm thick scintillator readings using the formula [2]:

$$\int_{600\,sc} = (1.72 \pm 0.25) \int_{600\,HP}^{1.06 \pm 0.03}$$

on the basis of the $\int_{600\,HP}$ spectrum data from [3] and the $\int_{600}$ spectrum data of the Yakutsk array from [1]. From Fig.4 it is seen that the $\int_{600sc}$ spectra measured at Yakutsk and Haverah Park are in a good agreement with each other at $\int_{600sc} < 200$(1/m^2) and differ somewhat at higher $\int_{600sc}$. Because of a limited accuracy in measuring the particle flux densities with the Yakutsk array, the effect of its geometry (for example, at the boundary of the array) the limited accuracy in finding the axis position and direction and the parameter $\int_{600}$, the inaccuracy in calculating the effective detection areas, and the detected EAS

selection effect, the necessity arises to test the distorting role of all these factors in terms of the Monte Carlo method, that is, to find the ρ_{600} spectrum distortion function. The distortion function was calculated in [1] on the assumption of the a priori power law ρ_{600so} spectrum $F(\rho) \sim \rho^{-2}$ allowing for the real errors in determining the densities with the Yakutsk array and for the real selection of the EAS to be studied. From Fig.5 it is seen that the distortion function differs little (by not more than 10-20%) from unity at $\rho_{600} \sim 1 (1/m^2)$ and $\sim 10 (1/m^2)$. The corrections at $\rho \sim 1$ and $10 (1/m^2)$ arise from the effect of the EAS selection system on measuring the particle flux densities with scincillators if the latter are included in the system. At $\rho > 20 (1/m^2)$, the corrections are even smaller. The EAS ρ_{600} spectrum may be used to infer the energy spectrum of primary cosmic rays from the experimental time-integrated and differential Cerenkov light flux in an EAS ensemble with a given value of ρ_{600}. As was first shown in [4], the integral EAS Cerenkov light flux Q is directly related to the energy E_i lost by the shower particles for ionization and for the excitation of the medium atoms above the EAS observation level, namely, $E_i = kQ$, where, according to the calculations [5], k depends little on the position of the EAS maximum. On the other hand, the data on the time-differential Cerenkov light flux at great distances from EAS axis make it possible to find the position of the maximum of an individual EAS [6] and, hence, to judge about the extent to which E_i is close to the primary energy E_o. In the range of $\rho_{600} = 1\text{-}100 (1/m^2)$, considering the altitude of the maxima of the respective showers, we obtain that the factor k in the relation $E_i = kQ$ is 3.6×10^4 eV/photon/eV to within several per cent. At the same time, because of the high location of EAS maximum for $\rho_{600} = 1\text{-}100 (1/m^2)$, it appeared that $E_i = 0.8 E_o$; in other words, the energy scattered by a shower above the observation level makes the major contribution to the energy of the primary particle ge-

nerating an EAS ensemble with a given S_{600} [1] *). When finding the value of E_1 (which is the major component of E_0) it is absolutely necessary to allow for the EAS Cerenkov light absorption in the atmosphere due to the Rayleigh scattering and the scattering by aerosols. The value of Q measured directly may differ from the number of the generated photons involved in the relation $E_1 = kQ$.

Bearing in mind the above, we carried out the regular control of the atmospheric transparency above the Yakutsk array using the large optical detector described in [9]. The occurrence frequency of the Cerenkov light bursts in the detector exceeding a certain threshold is contingent on the atmospheric transparency at the moment of measurement and on the spectral index of the burst intensity spectrum $N(>q) \sim (q \times T)^{-\alpha}$, where T is the atmospheric transparency for the wavelengths studied by the detector; q is the burst intensity; α is the index of the burst spectrum.

Fig.6 shows the distribution of the burst occurrence frequency inferred from the 15-min observation intervals during several months of the Yakutsk array operations. The detected burst threshold is 17 photon/cm^{2}eV. The maximum value of $N = N_1 \simeq 400$. If the variations of the Cerenkov light flux are assumed to be due only to the changes of the atmospheric transparency, the distribution shown in Fig.6 may be transformed into the distribution of T with the mean value $\bar{T} = 0.71T_1$ and $\sigma(T)/\bar{T} = 0.19$, where T_1 is the maximum transparency which corresponds to the Rayleigh scattering disregarding the aerosols. Considering the angular distribution of the axes of the EAS detected with the Yakutsk array, one may calculate [9] the value of T_1

*) In [1] it has been shown that, if the mean energy of EAS muons is taken to be $\bar{E}_\mu = 9$ GeV according to the experimental data [7] and the lateral distribution of electrons near EAS axis is determined by the NKG function with $S = 1.15$ [8], the energy carried by electrons and

which proved to be 0.85. Since $\bar{T} = 0.71 T_1$, then $\bar{T} = 0.6$.

Thus, the true value of Q differs from its measured value by the factor $1/\bar{T} \simeq 1.65$. It should be noted that a a more rigorous allowance for the atmospheric transparency involves also the usage of the ratio $\sigma(T)/\bar{T}$ in making the scaling. However, the value of the ratio is sufficiently small and, to within several per cent, does not affect the results. It should also be noted that the large optical detector is a local selection system which gives an idea of photon absorption by a layer of several km thickness above the observation level [9]. The coincidence-mode functioning of the Samarkand array optical detectors spaced 120 meters apart has shown that [10] the number of coincidences in the spaced-apart detectors is in a good correlation with the number of coincidences in the local optical detectors at Samarkand ($K = 0.9$). This fact indicates that the EAS Cerenkov light absorption occures mainly within the layer immediately above the observation level, rather then uniformely throughout the atmosphere. This conclusion coincides with the present-day concepts concerning the atmospheric aerosol layer of a ~ 2-km thickness [11].

So, considering the correction for the atmospheric transparency, we may obtain [2] the following experimental relation between the value of $\int_{600}$ in EAS and the mean energy E_0 of the primary particles responsible for an EAS ensemble with a given $\int_{600}$:

$$E_0 = (5.0 \pm 1.4) \times 10^{17} \int_{600}^{0.96 \pm 0.04} \quad (\vartheta = 0^\circ).$$

The error in the numerical factor is mainly due to the error (25%) in the absolute calibration of the Cerenkov detectors.

The statistical errors, which are of importance when

---

muons below the observation level will be ≃ 15% of E_0. The rest energy belongs to neutrinos and to nuclear splittings.

deriving the above relation, can be seen in Fig.7. A given value of S_{600} is, generally, in correspondence to a distribution of E_0. However, the width of the E_0 distribution is so small ($\sqrt{D(E_0)}/E_0 \lesssim 0.2$) that the relation between $\bar{E}_0$ and S_{600} is quite sufficient to use (to within several per cent) in making the transition from the S_{600} spectrum to the primary particle energy spectrum.

Fig.8 shows the experimental differential energy spectra of primary cosmic rays inferred from the Yakutsk array data [1,2], from the Haverah Park data [3], and from the Fly's Eye data [12]. Fig.9 shows the experimental energy spectra obtained also in [1,8,12]. From Figs 8 and 9 it is seen that at energies below 10^{19}eV the Yakutsk and Haverah Park data are in a better agreement with each other than with the Fly's Eye data. The deviations of the latter are probably due to the tentative character of the results of calculating the Fly's Eye geometric factors at low primary energies, as was noted in [12]. The minor disagreement between the Yakutsk and Haverah Park data arose probably from the fact that the Hillas model used for the Haverah Park array to scale from S_{600} to E_0 is not sufficiently accurate in reflecting the true relation between S_{600} and E_0. At $E_0 > 10^{19}$eV the experimental data of different works show a significant spread. Such a spread may be caused by trivial reasons, for example, a certain inaccuracy in the absolute calibration of optical detectors for the Yakutsk array and for Fly's Eye may result in a systematic disagreement of their data even in the range of high E_0 where Fly's Eye geometric factor has been known quite accurately. For instance, a 25% variation of the absolute value of energy leads to a complete agreement between the Yakutsk and Fly's Eye data at $E_0 > 10^{19}$eV, although it results in an increased disagreement between their spectra at $E_0 < 10^{19}$eV. A more essential disagreement is observed between, on the one hand, the data obtained at Haverah Park and the Univer-

versity of Sydney [13] where no direct energy calibration was made and, on the other hand, the data obtained with the Yakutsk array and the Fly's Eye which were energy-calibrated*).

The Haverah Park and Sydney arrays give a flat spectrum in the range from $E_0 > 10^{19}$eV up to the highest detectable energies above 10^{20}eV. It is not clear what is the role played by the fluctuations of the charged particle lateral distribution function in determining the value of S_{600} for the Haverah Park array because the value of S_{600} at $E_0 > 10^{19}$eV is not determined by interpolation, but is found by specifying a fixed mean lateral distribution function. This circumstance may prove to be even more important for the Sydney array because of a great distance between its detectors. With a falling S_{600} spectrum (or the spectrum of N_μ, the total number of EAS muons, in case of the Sydney array), the great errors in determining the EAS size may flatten the measured spectrum. An additional source of errors arises also when we treat the showers whose axes fall at the array periphery.

So, we think it necessary (1) to rigorously restrict, making allowence for the lateral distribution function fluctuations, the effective detection area for EAS with $E_0 > 10^{19}$eV by the region where the accuracy in determining the EAS parameters will make sure that errors would be absent and (2) to carry out the Monte Carlo simulation of the entire process of measuring and analyzing EAS with an experimental array in order to obtain a distribution function of the type shown in Fig.5.

---

*) The energy spectrum inferred from the Sydney array data is not shown in Figs 8 and 9 because it is model-dependent. It is necessary to use the results of the Yakutsk array calibration [2] and to scale the muon number spectrum to the primary spectrum.

Thus, on examining the available Yakutsk and Fly's Eye data, one may arrive at the conclusion that they do not contradict qualitatively the Zatsepin-Greizen pattern of the cutoff of the cosmic ray energy spectrum due to the interactions with the 2.7K universal microwave radiation. Additional studies have to be carried out to demonstrate the existence of such a cutoff and to find the 'fine' spectral structure (bump).

References

1. Pravdin M.I., (1985), Thesis for Candidate Degree, Inst. Nucl. Phys., Moscow State Univ., Moscow.
2. Glushkov A.V. et al., (1985), Proc 19th ICRC, La Jolla, v.2, p.198.
3. (a) Brooke G. et al., (1985), Proc. 19th ICRC, La Jolla, v.2, p.150;
   (b) Bower A.J., (1983), Proc. 18th ICRC, Bangalore, v.9, p.207.
4. Chudakov A.E. et al., (1960), Proc. 6th ICRC, v.2, p.47.
5. Dyakonov M.I. et al., (1976), In: Parameters of Ultra-high-energy EAS, Yakutsk Div., Siberian Branch, Acad Sci. USSR, Yakutsk, p.87.
6. Fomin Yu.A. and Khristiansen G.B., (1976), Sov. Nucl. Phys., v.14, p.642.
7. Atrashkevich V.B., et al., (1983), Proc. 18th ICRC, Bangalore, v.11, p.229.
8. Nagano M. et al., (1984), J.Phys.Soc.Japan, v.53, p.1667.
9. Sokurov V.F., (1983), Cosmic Rays with Energies above 10^{17}eV, Yakutsk Div., Siber an Branch, Acad. Sci. USSR, Yakutsk, pp.61-76.
10. Alimov T.A., (1985), Thesis for Candidate Degree, M.I. Kalinin Polytechnical Institute, Leningrad.
11. McClatchey R.A. et al., (1978), Handbook of Optics, Ch.14, 1-65, Ed. Driscoll W.G., McGraw-Hill.
12. Baltrusatis R.M. et al., (1985), Phys.Rev.Lett., v.54, p.1875.
13. Horton L. et al., (1985), Preprint, School Phys., Univ. of Sydney.

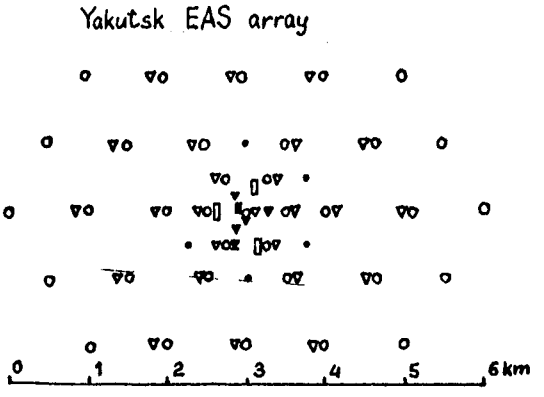

o - scintillation detector, 4 m²
• - scintillation detector, 2 m²
▽ - Cerenkov light detector, 176 cm²
⧗ - Cerenkov pulse width detector, 500 cm²
▼ - Cerenkov pulse width detector, 200 cm²
▯ - muon detector, 36 m²
▮ - muon detector, 8 m²

Fig. 1

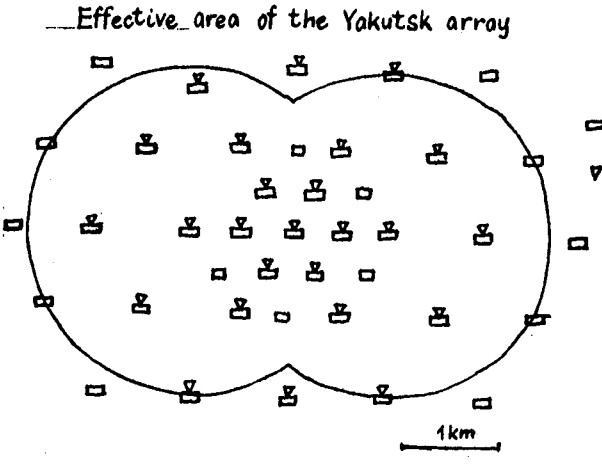

▭ - scintillation detector
▽ - Cerenkov light detector

Fig. 2

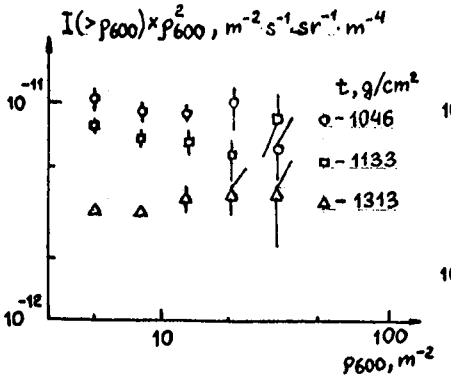

Fig. 3

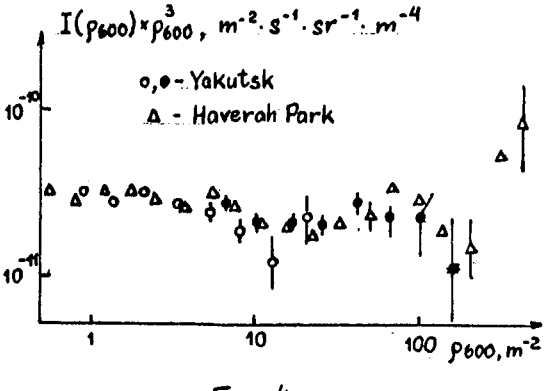

Fig. 4

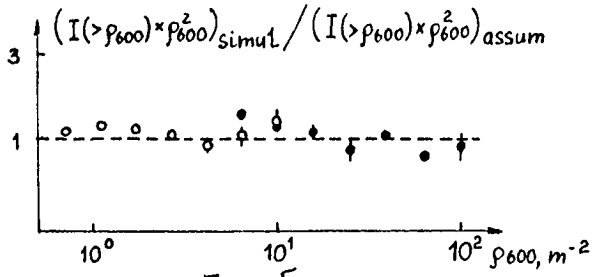

Fig. 5

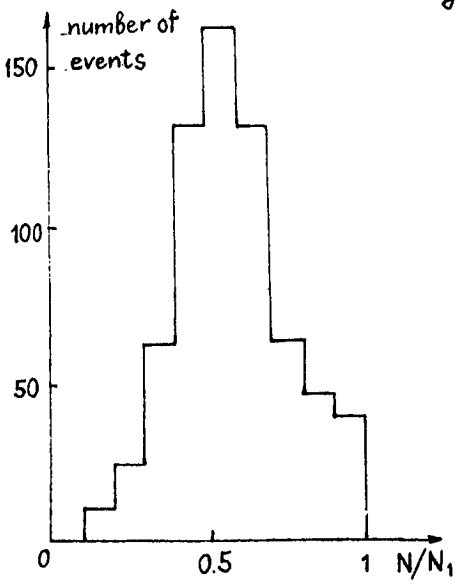

Transparancy of the atmosphere

$T = T_1 \times (N/N_1)^{1/\text{æ}}$, $T_1 = 0.85$

N is the number per 15 min of EAS with the Cerenkov light density of ≥ 17 photons/cm^2·eV.

$N_1 \equiv N_{max} \sim 400$.

$\frac{\delta(N/N_1)}{(N/N_1)} = 0.31$ $\frac{\delta(T)}{\overline{T}} = 0.19$

$\overline{T} = 0.17 \cdot T_1$

Fig. 6

$E_0 = (5.0 \pm 1.4) \cdot 10^{17} \cdot \rho_{600}^{0.96 \pm 0.04}$, eV

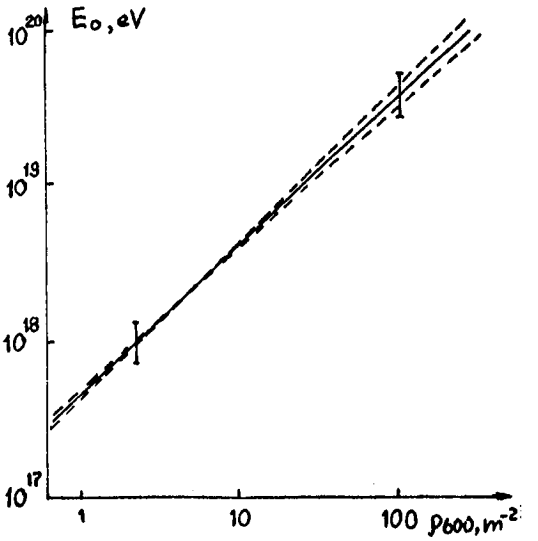

Fig. 7

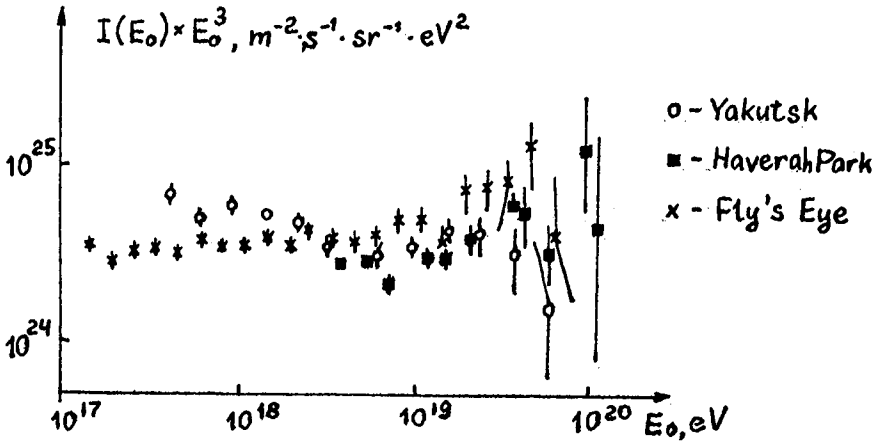

Fig. 8

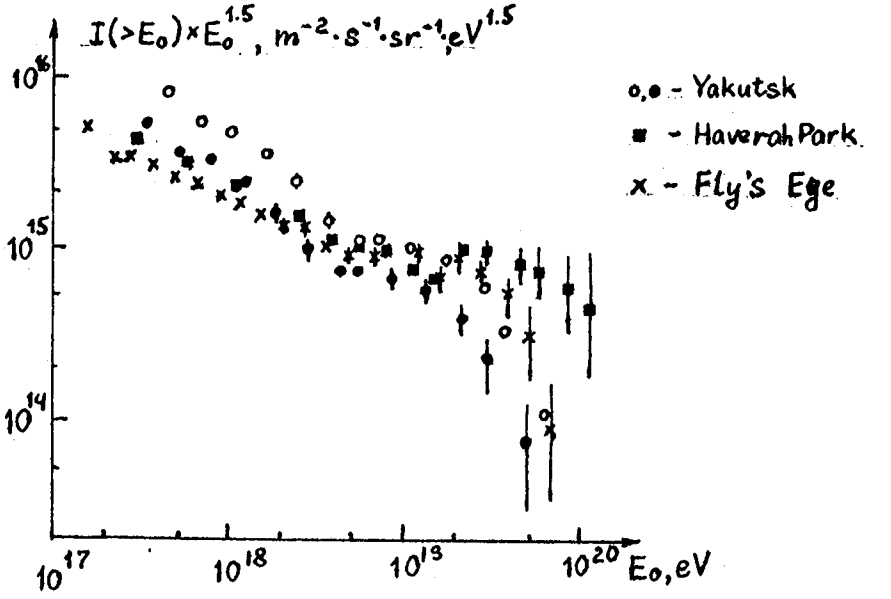

Fig. 9

ρ_{600}, m^{-2}	5	10	20	50	100	
$\frac{\delta(\rho_{600})}{\rho_{600}}, \%$	18	17	14	18	20	$\theta = 13°$
	23	17	18	21	25	$\theta = 39°$

Table 1

The Cosmic Ray Spectrum Above 10^{17} eV

M.M. Winn, J. Ulrichs, L. Horton, C.B.A. McCusker and L.S. Peak

School of Physics, University of Sydney, NSW 2006, Australia

ABSTRACT

We present the final analysis of the data obtained by the Sydney University Giant Airshower Recorder (SUGAR). The data has been reanalysed to take into account the effects of afterpulsing in the photomultiplier tubes. Event data was used to produce a spectrum of "equivalent vertical muon number" and from this, a model dependent primary energy spectrum was obtained. These spectra show good evidence for the "Ankle": a flattening at 10^{19} eV. There is no sign of the cut-off which would be expected from the effects of the universal black body radiation.

1. Introduction

The work was performed using an array which was operated at an atmospheric depth of 980 g cm^{-2} on a site a few hundred km north of Sydney (latitude 30° 32' south, longitude 149° 36' east). The array and its results are described in some detail in (1) and (2).

The geometry of the array was 54 points on a square grid where we operated autonomous "stations". At peak development, 47 of these points were occupied by operating stations. These were established on a set of nested square grids with spacings of 1600, 800 and 400 m. Each station had two liquid scintillator tanks buried 50 m apart in a north-south direction. The effective area of each scintillator was 6.0 m^2 viewed by a single EMI 9623B photomultiplier tube. The threshold energy for detected muons was 0.75 secθ GeV, where θ is the zenith angle of the incident particles. The shape of each tank was designed so that a particle traversing any part of the scintillator at a given angle would produce the same light flux on the photomultiplier tube.

The output (charge) pulse from the PM tube anode was deposited on a capacitor which then discharged with a decay time of 3.0μs. The potential difference across the capacitor was amplified and fed to a discriminator set to trigger for a signal greater than or equal to that due to three coincident vertical muons passing through the scintillator. The width of the signal above the threshold was timed using a 10 MHz clock. Ideally, the width is proportional to the logarithm of the charge deposited by the PM tube. This arrangement, known as a logarithm height to time converter, is due to Suga and his coworkers. Its advantages are that it covers a wide dynamic range of signals and the number of clock pulses provides a convenient record of pulse size. The principal deficiency of this converter is that it makes the detector system prone to errors if the photomultiplier

afterpulses. This problem is further discussed below.

The log height to time converter gave signals greater than the threshold at a rate of 30 per second; this was constantly monitored, as was the rate of pulses corresponding to more than 8 simultaneous vertical muons passing through the tank.

Identical signal processing was used on both detector channels. If both discriminators at a station fired within 350 ns, a master trigger was generated and the following information was then recorded by a local tape recorder:

(a) the time of the event as determined from the transmitted timing signal,

(b) the widths of the pulses at the output of the discriminators (recorded with 100 ns resolution).

Such "local" events occured at a rate of about 12 per hour. At regular intervals simulated "local" events were generated by injecting simultaneous electrical pulses into the PM tube anode circuits of both detectors at the station. Four different sizes of injected pulses were used in sequence, covering the dynamic range of the system.

2. Event Analysis

The taped records of the local events were collected from all the stations, transferred to a computer and compared to find coincidences, within 80 μs, between three or more stations. Such coincidences are referred to as "array" events. Events were rejected from further analysis if the participating stations were collinear or if the signal times were not consistent with the passage of an air shower (the latter being classified "unphysical"). During the eleven years of operation 15327 events were recorded; of these 1238 were collinear, 270 unphysical and 2 events were rejected on other grounds. Most of the events were registered in the minimum number of stations, namely three.

The direction of the shower axis was obtained by the method of fast timing. If three stations participated in a shower, then a straight geometrical fit of a plane front was made to the timing data. If four or more stations participated in an array event, then a weighted least squares method was used to fit a plane shower front to the data. The number of muons in the shower and the location of the shower axis was found by a maximum likelihood method taking into account the records of all stations of the array (triggered or not). The likelihood expression consisted of: a term Q giving the probability of the observed responses of the triggered stations, a term P giving the probability of zero responses from non triggered stations and a term giving the a priori probability of the occurrence of a given shower size as proportional to N_μ raised to the power -3.0.

The term Q was originally taken to be a Poissonian distribution with the mean set equal to the expected number of particles (above 100

particles this was replaced by a normal distribution with a fractional standard deviation of 10%). In the present analysis and that reported at the Bangalore Conference (3 and 4) we used a new formula for Q which was obtained after consideration of the possible effects of afterpulsing in the PM tubes of the array. Further details are given in the appendix. We feel quite confident that the new value of Q properly accounts for the effects of afterpulsing (5).

The expected densities of muons were calculated using a structure of the Greisen type (6) modified to allow for the dependence of the outer slope parameter on zenith angle.

3. The Size Spectra

The array was operated to produce a list of showers containing the following information:

Time and date of event
Zenith angle of shower axis θ
Muon number N_μ
Position of axis X,Y

In order to obtain shower spectra it is necessary to evaluate the array exposure; i.e. the effective area times the running time. We computed this using techniques substantially the same as described in Bell et al (1). A Monte Carlo method was used to simulate shower detection by our array; the probability of a station being operational was made to correspond to its average fractional on-time during an epoch. The total time of observation was divided into seven epochs during each of which the array configuration and station performance were substantially constant. The shower list and exposure information were combined to produce seven different spectra of N_μ taken at different zenith angles, these are shown in figure 1. These spectra differ from one another because the threshold energy of the muons increases with the secant of the zenith angle and because showers of different zenith angle are at different stages of development, even though their primary energy may be the same.

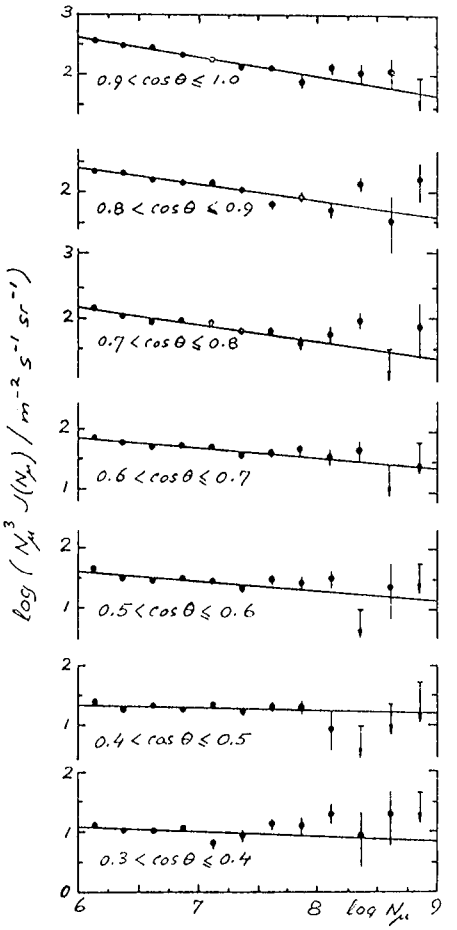

Figure 1. The differential shower size (N_μ) spectra for various zenith angle bins (θ). The ordinate is the flux multiplied by N_μ^3. The lines are fitted by maximum likelihood to the lowest seven data points in each range of θ.

For the seven lowest N_μ bins in each of the zenith angle bands,

we used the maximum likelihood method to fit a differential power law spectrum of the form

$$J[N_\mu(\theta)]\, dN_\mu = J_\theta (N_\mu / N_r)^{-\gamma_\theta}\, dN_\mu$$

where $N_r = 3.16 \times 10^6$

The five upper size bins were excluded from the fit since it appears that there may be a flattening of the primary energy spectrum for $N_\mu > 10^8$. In any case, because of the small number of events in these bins, the effect of including them in the fit is marginal. J_θ and γ_θ were found to depend on $\cos\theta$ in a linear manner allowing an analytic method (3) to be used to combine all the spectra into a single spectrum of the quantity N_v: the equivalent vertical muon number, which is the size (N_μ) the shower would have had if it had entered the atmosphere vertically. The operation above is equivalent to using the well known "equal intensity cut method" (7) to obtain a shower size at any desired atmospheric depth. The spectrum of N_v shown in figure 2 is for all showers with $\theta < 60°$.

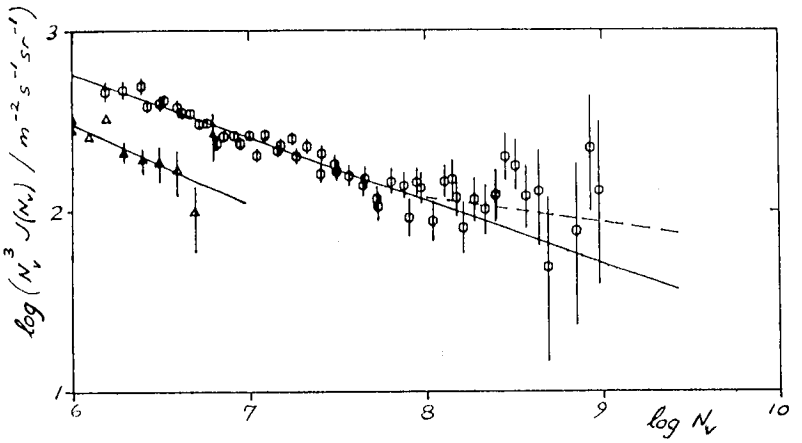

Figure 2. Differential equivalent vertical muon number (N_v) spectrum obtained by combining the various muon number spectra at different zenith angles. Line (a) is the maximum likelihood fit to showers with log $N_\mu < 7.75$ and line (b) is a similar fit for log $N_\mu > 7.75$ Each point represents the intensity in a (N_μ;θ) bin. Also shown is the result from the Akeno group ($1 < \sec\theta < 1.1$) and (c) is their fitted line.

The line (a), with a differential slope of 3.35 ± 0.01 is fitted to all events with log $N_\mu < 7.75$. (If showers with θ up to 73° are included the slope steepens to 3.36.)

It will be noticed that the equation of line (a) is effectively the same as presented by us in the 18th International Cosmic Ray Conference at Bangalore (3). Since then we have used an improved method of dealing with saturated detectors and this is the only difference between the two analyses. The effect of afterpulsing was

handled identically in the two cases.

We also show on figure 2 the N_μ spectrum from Akeno (8). We are able to explain the disagreement between our spectrum and the Akeno one by taking into account:

(a) differing altitudes of the two arrays,
(b) different threshold energies for entry of muons into the detectors,
(c) different array geometries leading to muon densities being measured at different distances from the shower core, and
(d) the use of different structure functions.

In a similar way we are able to explain the disagreement between the our spectrum and those of the Nottingham and Yakutsk groups (9) and (10).

Note the flattening of the spectrum above $\log N_\nu = 8$. A line fitted to events with $\log N_\mu > 7.75$ has a slope of 3.15 ± 0.14. One can compare the expected number of events which have $\log N_\mu > 8$ according to line (a) (namely 58) with the observed number (78). χ^2_1 gives a probability of 1% that this should arise by chance. A stronger test, with the straight line fitted to all the data gives a χ^2 probability of 3%.

4. Energy Spectra

The equivalent vertical muon size spectrum can be transformed into a primary energy spectrum using a conversion formula which is conventionally represented as a power law

$$E = E_r(N_\nu/N_r)^\alpha$$

N_r is usually chosen to be in the middle of the range of shower sizes; in our calculations we used $N_r = 10^7$.

Two different models were used to obtain this conversion: the so-called Sydney model (11) and Hillas model E (12). In what follows we use the latter because of its general acceptance by workers in the field.

The relevant relation is

$$E = 1.64 \times 10^{18} (N_\nu/10^7)^{1.075}$$

Figure 3 shows the spectrum produced.

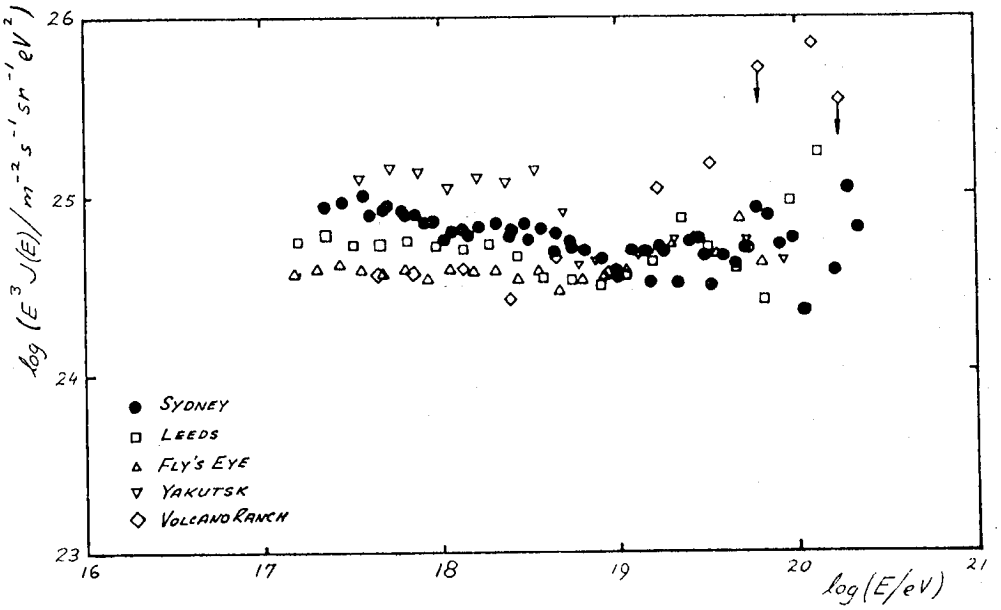

Figure 3 Comparison of energy spectra from various groups and our spectrum converted by the Hillas E model (solid circles). Each spectrum is differential with the ordinate equal to the flux multiplied by E^3.

The squares are from the Leeds group at Haverah Park (13)
The triangles are from the Utah group (14)
The diamonds are from Volcano Ranch as quoted by (15)
The inverted triangles are from the Yakutsk group (16)

As with the N_γ spectrum we have fitted two lines (which for clarity are not shown on figure 3), one below and one above $\log N_\mu = 7.75$ with differential slopes of 3.19 ± 0.01 and 2.99 ± 0.13 respectively.

On figure 3 we also show the spectra from the Leeds group (13), Utah group (14), Volcano ranch as quoted by (15) and the Yakutsk group (16). The Leeds and the Volcano ranch spectra show the ankle feature and we confirm this. Another item of interest is the possibility of a spectrum cut-off at $\sim 5 \times 10^{19}$ eV due to black body photons acting on particles from sources $\gtrsim 10$ Mpc distant. There is no sign in our own spectrum of such a cut off. As described in section 3, the spectral slope flattens above 10^{19} eV and according to the Hillas E model we have eight showers above 10^{20} eV.

5. Conclusions

We have determined the spectrum of cosmic rays for energies

$> 10^{17}$ eV using data from a site at 31° south latitude. We used Hillas model E to find the energies of our events. The differential energy spectrum has a slope of 3.19 ± 0.01 below about 10^{19} eV and the slope flattens to 2.99 ± 0.13 above this energy. The spectrum extends beyond 10^{20} eV with no sign of a cut off due to the Universal Black Body Radiation.

Appendix - Afterpulsing

An unfortunate feature of the logarithmic height to time converter is that pulses arriving late in a particular signal can keep it above threshold and hence cause the original signal height to be substantially overestimated. Ordinary random noise pulses from the PM tube are too infrequent to affect the results whereas pulses generated within a PM tube and occurring after a genuine air shower signal pulse can have serious effects. This phenomenon is known as afterpulsing.

We looked at the possibility of excluding afterpulses by using electronic gating techniques but found that the inevitable gate pedestal created more problems than it solved.

The seriousness of the effects of afterpulsing was not realised until the latter part of the experiment; even then, technology could not provide a practical solution. However we have developed a statistical method to account for the effects of afterpulsing. The technique incorporates the effects of afterpulsing and other signal enhancements into the probability distribution used in the shower fitting program. We describe below how this was done.

During the last stages of the experiment we recorded for each station a sample of pulses, each of which had its height as well as it width measured. Samples were collected from all stations as part of the local event records and for a few stations, the comparison between pulse height and width was carried out for single tanks as well (17).

From inspection of these data we chose a typical detector and removed its photomultiplier for further investigation of afterpulsing effects at larger pulse sizes. To this end we reactivated one of the original pilot arrray stations in Sydney and installed in it a PM tube with average afterpulsing. Data from this station was recorded for 8 days in a similar manner to the recordings made in the SUGAR array. To examine afterpulsing for pulses exceeding the height amplifier saturation level, the pulse height measuring system was connected to the output of the first stage of the preamplifiers rather than at the output of the final stage. We then ran the station for a further nine months in this "low gain" mode. The longer period was needed to accumulate an adequate data set at the lower rate.

We used the results from the average tube as a model for all the others in the SUGAR array. An alternative approach would have been to establish a correlation between parameters derived from the data taken in the height/width runs and calibration data collected during the normal running of each station. If this had been successful; it would have allowed us to apply retrospective corrections to each station for

any time in the array's operation. However we found no significant correlation allowing this to be done. Instead, the behaviour of the average tube was applied to all detectors of the array for the duration of the experiment. This was done by changing the probability distribution used in the shower analysis program.

The data from the average tube was analysed statistically and a new formula was produced for the quantity Q used in the maximum likelihood expression (see main text). Q was previously Poissonian (with a mean set equal to the expected number of particles) for < 100 particles and was normally distributed with a fractional standard deviation of 10% for > 100 particles. The new distribution for Q is of the gamma type. Its mean and standard deviation were fitted to the data from the average PM tube. The fit gave a constant fractional standard deviation of 30% and a mean which depended on the expected particle number n as

$$(2.3 + 0.9n + 0.004n^2)(1.25 \cos\theta)^{(0.40 - 0.45 \log n)}$$

where θ is zenith angle of the particles (taken as equal to the zenith angle of the shower).

Acknowledgements

Financial support came from the United States Air Force Office of Scientific Research in the earlier stages of the project and from the Australian Research Grants Scheme in later stages. The University of Sydney contributed directly in research grants and through the Science Foundation for Physics. The work would have been impossible without the encouragement of Professor Harry Messel, Head of the School of Physics and the excellent research facilities he has provided.

References

(1) Bell, C.J. et al 1974 J. Phys. A: Math., Gen **7** 990
(2) Winn, M.M. et al 1985 (to be submitted to J. Phys. G)
(3) Horton et al 1983 Proc 18th Int. Conf. on Cosmic Rays, Bangalore **6** 124
(4) Horton et al 1983 Proc 18th Int. Conf. on Cosmic Rays, Bangalore **2** 128
(5) Bell C.J. 1976 J.Phys. G: Nucl. Phys. **2** 857 and **ibid** p 267
(6) Greisen K. 1960 Ann. Rev. Nucl. Sci. **10** 63
(7) Clark G.W. et al 1963 Proc 8th Int. Conf. on Cosmic Rays, Jaipur **4** 65
(8) Nagano M. et al 1984 J. Phys. G. Nucl. Phys. **10** 1295
(9) Blake P.R. et al 1981 Proc 17th Int. Conf. on Cosmic Rays, Paris **6** 8
(10) Diminstein S. et al 1979 Proc 16th Int. Conf. on Cosmic Rays, Kyoto **8** 122
(11) Goorevich L. and Peak L.S. 1975 J. Phys. G: Nucl. Phys. **7** 762
(12) Hillas A.M. et al 1971 Proc 12th Int. Conf. on Cosmic Rays,

Hobart **3** 1007
(13) Bower A.J. et al 1981 Proc 17th Int. Conf. on Cosmic Rays, Paris **9** 166
(14) Cassiday G.L. 1985 (private communication) an addendum of extra data to spectrum in Proc 19th Int. Conf. on Cosmic Rays, La Jolla 2 146
(15) Cunningham G. et al 1977 Proc 15th Int. Conf. on Cosmic Rays, Plovdiv 2 303
(16) Krasilnikov D.D. et al 1983 Proc Int. Conf. on Cosmic Rays, Bangalore **9** 206, paper OG 4-19 and addendum to it
(17) Bray A.D. et al 1981 Proc 16th Int. Conf. on Cosmic Rays, Paris **12** 365

HIGH ENERGY NUCLEUS-NUCLEUS COLLISIONS

Barbara Wosiek
Institute of Nuclear Physics
Kawiory 26A
30-055 KRAKOW, POLAND

Abstract

Experimental results on high energy nucleus-nucleus interactions are presented. The data are discussed within the framework of standard superposition models and from the point-of-view of the possible formation of new states of matter in heavy ion collisions.

1. Introduction

Collisions of relativistic heavy nuclei have recently become a subject of intense investigation, both experimental and theoretical. It is expected that fundamentally important physical phenomena may occur as a result of the formation of high density and high temperature nuclear matter. Under such extreme conditions matter may transit into the deconfined quark-gluon plasma phase. These conditions existed in the early universe, just a few microseconds after the Big Bang, may be created within neutron stars, and are expected to occur in central heavy ion collisions. The latter gives us a unique opportunity to study these extreme conditions in our laboratories. However, it was soon realized that experimental data are dominated by common features which reflect the Lorentz contraction, kinematical constraints and variations in the impact parameter. Nevertheless, it is believed that new phenomena will not be completely covered by this "standard background."

This paper is organized as follows. In Section 2, I briefly describe the expectations for both conventional and new phenomena. Selected experimental results from studies of high energy nucleus-nucleus interactions are presented in Section 3. In the last Section, I summarize the present stage of investigation of nucleus-nucleus collisions and say a few words about future perspectives.

2. Expectations

2.1. Conventional phenomena

Our predictions for conventional phenomena follow from the study of high energy hadron-nucleus collisions [1]. The main outcome of these studies was the observation of a moderate increase in the number of particles produced in nuclear targets in comparison to the multiplicity of particles produced in a hydrogen target. This 'nuclear transparency' is surprising, at first sight, since in a collision of a hadron with a heavy nucleus, the hadron must penetrate

several mean free paths of nuclear matter. Therefore, we would expect that both the incident hadron and the produced secondaries would undergo multiple scatterings, developing a hadronic shower inside the target nucleus (see Figure 1). The absence of such a shower can be explained by formation zone arguments [2], namely the production of a secondary particle is not an instantaneous process but requires a certain creation time in its rest frame (1 fm/c). Due to the time dilation in the laboratory frame, the fast particles are produced outside the nucleus and, therefore, only the incident hadron and the slow secondaries can undergo rescattering inside the target nucleus, as illustrated schematically in Fig. 1.

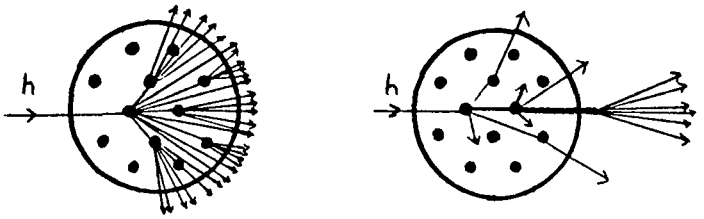

FIGURE 1. Particle production in hadron-nucleus interactions.

The nuclear transparency, along with the additional assumptions that (a) slow particles modify only slightly the observed final state, and (b) the incident hadron (or hadron constituent) undergoes independent collisions inside the nucleus, represent the basic principles of the so called Superposition Models [3], which satisfactorily describe the hadron-nucleus data. All of these models can be extended in a straightforward way to nucleus-nucleus interactions at high energies [4], and we expect that the majority of nucleus-nucleus experimental data may be explained by these conventional models.

2.2. New phenomena

Comprehensive reviews of the expectations of new phenomena which may occur in central nucleus-nucleus collisions have been published [5]. In the limited space available only a very general coverage of this topic is possible.

When two large nuclei collide centrally at high energies, they pass through one another and in the central region between the two, now receding, nuclei dense nuclear matter may be formed. If the density exceeds some critical value, the nuclear matter may transit into the deconfined phase of quarks and gluons (see Fig. 2). Different theories and models (e.g. relativistic hydrodynamics, transport theory, QCD Monte Carlo calculations on the lattice, etc.) have been applied to describe the phenomena occuring in the head-on collision of two such compound objects as heavy nuclei. All of them agree that at energy densities exceeding 2 GeV/fm^3 a transition to the quark-gluon plasma is likely to occur. There still remain many theoretically unresolved problems, mainly connected with the

stability of the solutions, but it is believed that the transition will effect the spectra and the composition of final state particles. However, bearing in mind the unresolved problems, one has to be cautious in considering the experimental observables and signatures.

Now I proceed further with the discussion of diagnostic tools to study the quark-gluon plasma. Among the possible hadronic signals, we expect high multiplicities of produced particles, an enhanced ratio of strange to nonstrange particles, high average transverse momenta and unusual event structure, e.g. rapidity fluctuations. The leptonic signals, such as direct photons emitted as plasma electromagnetic radiation and direct dileptons produced in quark-antiquark anihilation, will provide information about the early stage of plasma formation, particularly the plasma temperature. Additionally, one can expect that any correlations between hadronic and leptonic signals may be considered as experimental triggers for a quark-gluon plasma.

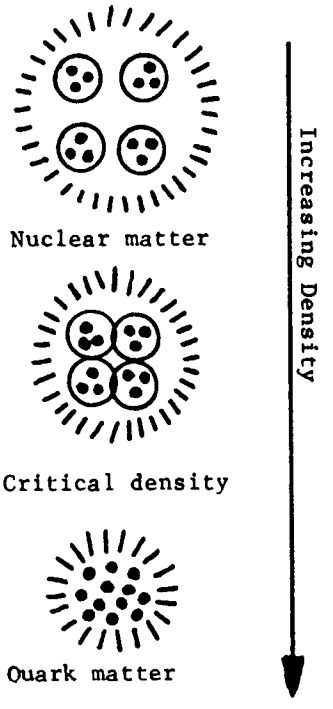

Figure 2. Transition to the quark matter phase.

3. Experiment

The systematic study of nucleus-nucleus collisions are presently limited to laboratory energies of about 4 GeV/nucleon at accelerators. The data on cosmic ray nuclei with energies 20 - 65 GeV/nucleon have been reported recently from a hybrid electronic counter-emulsion chamber experiment [6]. A systematic analysis of cosmic ray interactions with mean energy of 20 GeV/nucleon averaged over the rapidly falling energy spectrum, are also available [7]. At energies above 100 GeV/nucleon one can analyze only single cosmic ray events recorded in emulsion chambers. For these highest energies, I will present data obtained in a series of balloon flights by the JACEE collaboration.

3.1. Inclusive data

As I said at the beginning, we expect that inclusive nucleus-nucleus data can be explained within the framework of superposition models. I show only one example as an illustration that these models do describe the experimental inclusive data. It is expected that in nucleus-nucleus collisions the distribution of the number of produced particles will be very wide due to the large range of variation of the impact parameters. Different superposition models [4] predict

that the ratio of the dispersion, D, to the average multiplicity $\bar{N}$ will be about twice as large as the same ratio for proton-nucleus interactions. In Figure 3, the dependence of D on the average multiplicity $\bar{N}$, is displayed. The shaded area represents the predicition of superposition models ($D/\bar{N}$ = 0.8 - 1.3 depending upon the model), and points with error bars are the experimental data for

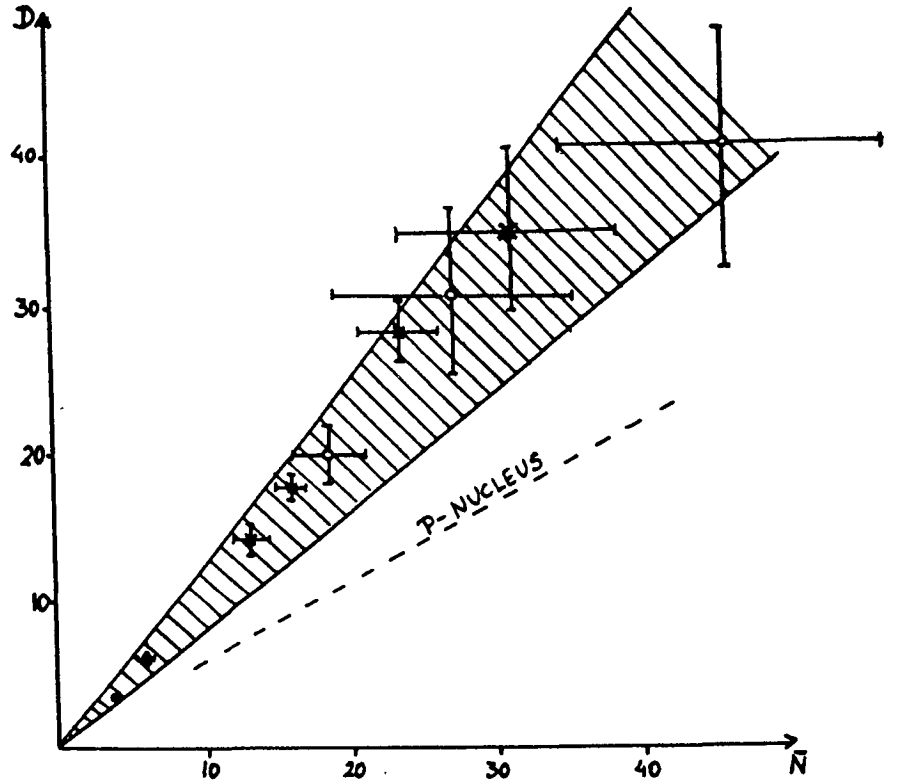

Figure 3. Dependence of the dispersion of the multiplicity distribution on its average value. Points are • - 3.7 GeV/n ^{22}Ne interactions in emulsion [9], o - 35 GeV/n ^{56}Fe interactions in C, emulsion and Pb [6], and x - <20 GeV/n> cosmic ray (^{4}He - ^{56}Fe) interactions in emulsion [7].

different projectile and target nuclei and for different primary energies [6,7,9]. The universality of the $D/\bar{N}$ ratio, which depends neither on the energy nor on the target and projectile masses, can be observed in Figure 3. A similar universality was reported for proton-nucleus collisions [10]. The consistency between the experimental data and superposition model predictions is evident in Fig. 3.

However, the inclusive data are dominated by peripheral interactions and we expect that inclusive spectra taken over many events may smear out any information on quark-gluon plasma which may be created only in central collision events.

3.2. Central nucleus-nucleus collisions

The JACEE collaboration has observed several high energy (above 500 GeV/nucleon) nucleus-nucleus interactions, which demonstrate characteristics not expected from what we consider as "standard background." For a better understanding of the data, let me start with a brief description of the procedure for data recording and analysis used in the JACEE experiments. The high energy interactions were recorded in emulsion chambers exposed to the primary cosmic rays in a series of balloon flights [8]. The emulsion chamber is a multilayered detector which serves simultaneously as both target and coordinate/ionization recorder. The vertical configuration of the typical JACEE emulsion chamber is shown in Figure 4. Incident particles are identified in the primary section by means of ionization measurements in the emulsion layers as well as by pit measurements in CR-39 etchable plastics. Charge resolution is typically 1.0 charge unit. The target section contains thin emulsion plates interleaved with acrylic and/or iron sheets. Thick emulsion and CR-39 plates are inserted in the target section to permit the identification of projectile fragments. The following spacer section, used in some chambers, allows photons from π^o decays to diverge before reaching the calorimeter section, so that individual photon cascades can be observed. The calorimeter contains Pb plates interleaved with emulsion plates and x-ray films. The total thickness of the calorimeter is 5-7 radiation lengths.

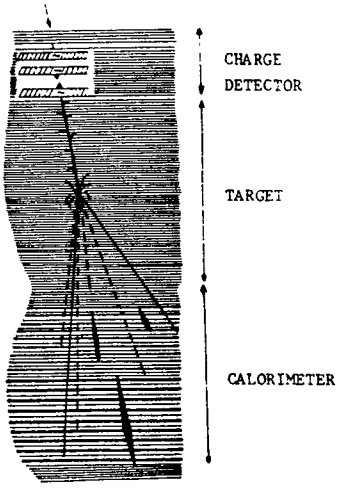

Figure 4. Schematic diagram of a typical JACEE chamber.

Thanks to the high spatial resolution of the emulsion, the hundreds of particles emerging from an interaction vertex can be unambiguously detected. Multiplicities N_{ch} and emission angles of all secondaries are measured in consecutive emulsion plates downstream of the interaction vertex, with a typical error in relative angle measurements of 0.1 - 0.2 pseudorapidity units. In the calorimeter section the emission angles and energies of individual photons are measured, so information on the transverse momenta of photons, with accuracy of $\Delta p_t/p_t = 0.25$, is obtained. The average value of the transverse momentum ($< p_t >_\gamma$) for an individual event is estimated by an exponential fit to either the differential or integral distribution of $p_{t,\gamma}$, and it can be related to the average transverse momentum of π^o meson via: $< p_t >_\pi = 2 < p_t >_\gamma$. For events with overlapping individual photon showers (interactions in the calorimeter section and the highest energy collisions) $< p_t >_{\pi^o}$ is obtained by comparing the three dimensional cascade development with Monte Carlo simulations which use as input the measured pseudorapidity distribution of

charged particles and assume isospin symmetry for pions and an invariant p_t distribution.

For each event the energy densities (ε) have been evaluated at the time of 1 fm/c after the collision from the formula proposed by Bjorken [11]:

$$\varepsilon = \frac{3}{2} \sqrt{\langle p_t \rangle_\pi^2 + m_\pi^2} * \frac{dN}{d\eta} * \frac{1}{2\pi A_{min}} \quad 2/3 \ , \qquad (1)$$

where A_{min} = Min ($A_{projectile}$, A_{target}), $\langle p_t \rangle_\pi$ is the determined transverse momentum of π^o and $dN/d\eta$ is the measured density of charged particles in the CM pseudorapidity central region ($|\eta|<1$).

3.2.1 Multiplicities, average transverse momenta & energy densities

In Table 1, the heavy ion interactions with charged particle multiplicities exceeding 400, which may be considered as central collisions, are listed. The observed large multiplicities for these events are consistent with the calculations of the Multi-chain Model [4c] for collisions with impact parameter b=0. The average transverse momenta exhibit high values compared to the values interpolated from CERN ISR and SPS collider experiments [12]. For the events listed, the energy densities are above 2 GeV/fm^3.

Table I. High multiplicity events ($N_{ch} \geq 400$) in JACEE.

Event Type	E_0 (TeV/n)	N_{ch}	$\langle p_t \rangle_{\pi^o}$ (GeV/c)	$dN/d\eta$	ε (GeV/fm^3)
Ca+Pb	1.5	1050^{+300}_{-50}	0.55±0.10	258±12	3.0
Si+AgBr	4.1	1010±30	0.55±0.10	183±10	2.7
Ca+C	100.0	760±30	0.53±0.04	81±10	2.0
Ca+Pb	0.5	670±40	(1.03)	142±8	(3.0)
Ca+Pb	1.8	457	(2.1±0.1)	100±16	(4.3)
Ar+Pb	1.0	416	1.2±0.2	134±8	3.3

*Values in ( ) require further experimental checking.

3.2.2. Rapidity fluctuations

Figure 5 shows the CM pseudorapidity distribution of the high multiplicity Si+AgBr event. This large multiplicity is consistent with the predictions of the Multi-Chain Model, but we observe a rich structure in the pseudorapidity spectrum and the question we want to answer is "Are the observed fluctuations purely statistical, i.e. due to the fine binning of the data, or are they of physical origin and, for example, may be related to the expected violent cooling of a quark-gluon plasma?"

It is not a simple task to answer this question, since we do not know in advance the distribution of the real event. Various methods have been applied to identify nonstatistical fluctuations in the psuedorapidity and azimuthal angle distributions [13]. In a recently published paper [14], the dependence of factorial moments of the rapidity distribution on the size $\delta\eta$ of the η resolution was studied. Figure 6 shows the scaled factorial moment $\langle F_5 \rangle$

versus $\delta\eta$ on a logarithmic scale. The moments, computed from the measured pseudorapidity distribution of the event on Figure 5, in the interval $-3.55 < \eta < 3.65$ are marked by dots in Fig. 6. A general tendency for $\langle F_5 \rangle$ to increase with decreasing $\delta\eta$ is

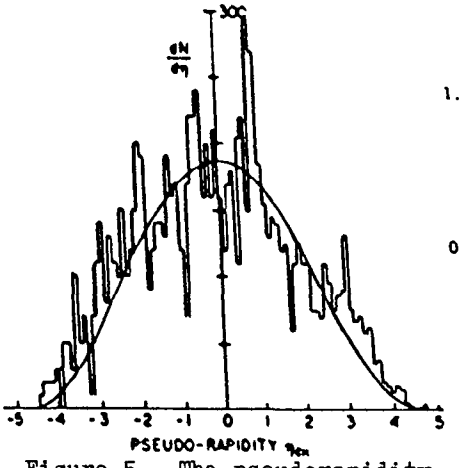

Figure 5. The pseudorapidity distribution for the Si+AgBr event.

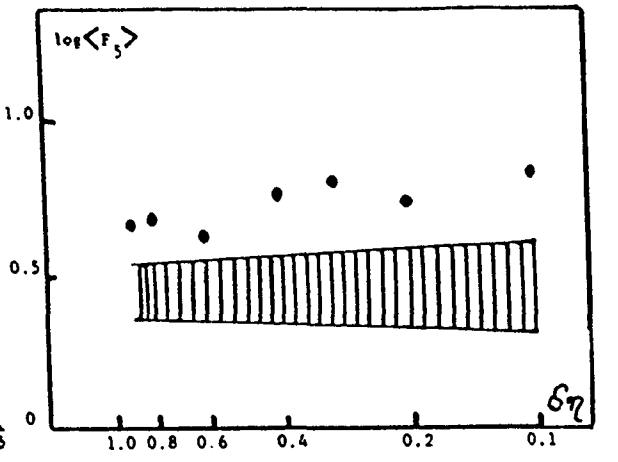

Figure 6. Log $\langle F_5 \rangle$ [14] for the event Si+AgBr.

observed. For comparison the moments simulated from a smooth pseudorapidity distribution with purely statistical fluctuations are shown in Fig. 6 as the shaded area. One sees clearly that the data lie well above the predictions for a smooth pseudorapidity distribution.

Other methods have also been used to study the fluctuations, for example, Takagi [15] applied power spectrum analysis or Chebyshef expansions to three of the high multiplicity nucleus-nucleus events observed by JACEE. He concluded that there was fairly strong evidence in favor of non-statistical fluctuations in the analysed events.

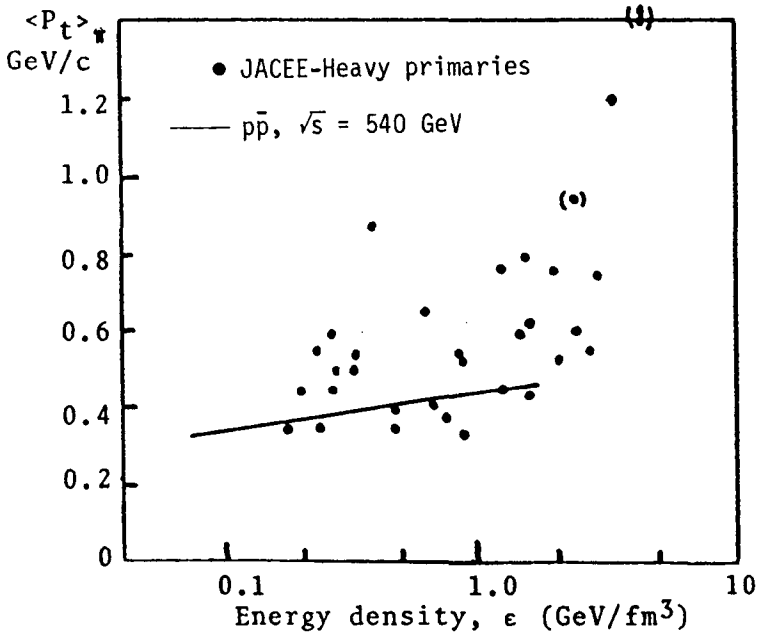

Figure 7. Correlation between transverse momentum and energy density.

3.2.3. Correlation of $\langle p_t \rangle$ with the energy density

In Figure 7 the correlation between $\langle p_t \rangle_\pi$ and the energy density for individual nucleus-nucleus interactions is displayed. For comparison the data from the $p\bar{p}$ collider at 150 TeV from the UA1 group are shown [12]. The $p\bar{p}$ rapidity density data were converted to an energy density by taking $A_{min} = 1$ in Eq. (1). As seen on Figure 7, the $p\bar{p}$ data do not show energy densities higher than 2 GeV/fm^3. The increase of $\langle p_t \rangle_\pi$ with energy density for the $p\bar{p}$ data can be satisfactorily explained by the contribution of low p_t (< 5 GeV/c) QCD jets and is not related to quark-gluon plasma formation. The JACEE nucleus-nucleus data are widely dispersed on Figure 7, but it appears that the growth of $\langle p_t \rangle$ with increasing energy density is faster than in $p\bar{p}$ data. In addition, above 2 GeV/fm^3 the slope changes even more rapidly. This increase cannot be explained by any conventional considerations, for example multiple scattering or contributions from QCD mini-jets. On the other hand, the statistics for the events of the greatest interest ($\varepsilon > 2$ GeV/fm^3) are still low, and any interpretation of the observed increase in $\langle p_t \rangle$ as the formation of new states of matter can only be regarded as speculative at the present stage.

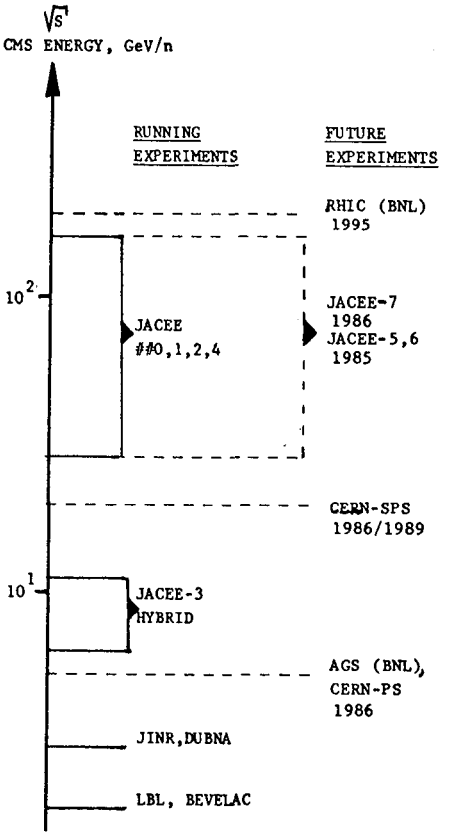

Figure 8. Current and Future Experiments.

4. Summary

Experimental results on nucleus-nucleus interactions show that the inclusive data, as well as the large multiplicities of produced particles in central collisions, are consistent with conventional superposition models. On the other hand, there are data such as the observations of high $\langle p_t \rangle$, nonstatistical pseudorapidity fluctuations, and the growth of $\langle p_t \rangle$ with energy density which cannot be described in the framework of standard superposition models. Although these results cannot be definitely interpreted as quark-gluon plasma formation, they encourage us to continue the search for new states of matter in nucleus-nucleus collisions.

There are still problems which need further exploration both theoretically

and experimentally. Theoretically a better understanding of the stability of solutions and more precise predictions for both conventional and new physics are needed. On the experimental side we need to increase the primary energy, extend the range of available masses of colliding nuclei and enlarge the event statistics. The development of new heavy ion accelerators at Brookhaven and CERN together with the proposed experiments searching for specific quark-gluon plasma signatures will be extremely interesting. In Figure 8, I schematically display the energy range covered by presently working accelerators/experiments as well as future possibilities.

I would like to end my talk concluding that although the present situation is still not clear, we can expect that in the future we shall learn a lot about fundamentally important problems of hadron physics.

Acknowledgements

The author thanks Dr. R. Holynski for valuable discussions and many helpful comments in the preparation of the talk and Dr. J. P. Wefel for a critical reading of this manuscript. This work is supported, in part, at LSU by NSF grant PHY-8304003.

References

1. J. E. Ellias et al., Phys. Rev. D22, 13 (1980); J. Babecki et al., Phys. Lett. 52B, 274 (1974); I. Otterlund, Nucl. Phys. A418, 87c (1984).

2. E. L. Feinberg, Sov. Phys. JETP 23, 132 (1966); K. Gottfried, Phys. Rev. Lett. 32, 957 (1974).

3. V. V. Anisovich, Yu. M. Shabelsky and V. M. Shekhter, Nucl. Phys. B135, 477 (1978); A. Bialas, W. Czyz and W. Furmanski, Acta Phys. Pol. B8, 585 (1977); N. N. Nikolaev, Phys. Lett. B70, 95 (1977); A. Capella and J. Tran Thanh Van, Phys. Lett. 93B, 946 (1980); W. Q. Chao, C. Chiu, Z. He and D. M. Tow, Phys. Rev. Lett. 44, 518 (1980); K. Kinoshita, A. Minaka and H. Sumiyoshi, Prog. Theor. Phys. 61, 165 (1979).

4. a) A. Bialas, M. Bleszynski and W. Czyz, Nucl. Phys. B111, 461 (1976);
   b) A. Capella, C. Pajares and A. V. Ramallo, CERN preprint TH3700;
   c) K. Kinoshita, A. Monaka and H. Sumiyoshi, Z. Phys. C8, 205 (1981).

5. E. V. Shuryak, Phys. Reports 115, 151 (1984);
   Recent reviews: M. Jacob and H. Satz (Eds.), Quark Matter Formation and Heavy Ion Collisions, World Scientific Publ., Singapore, 1982; T. Ludlam and E. Wegner (Eds.), Proceedings of the "Quark Matter 83", Nucl. Phys. A418, 1c (1984); B. Muller, Lecture Notes in Physics, Vol. 225 (1985).

6. JACEE Collaboration, T. J. Burnett, et al., 19th ICRC Conference Papers, 6, p. 152-163 (1985).

7. B. Wosiek, Acta Phys. Pol., B9, 191 (1978); T. W. Atwater, P. S. Freier and M. P. Kertzman, 19th ICRC Conference Papers 6,184 (1985).

8. JACEE Collaboration, T. H. Burnett et al., Phys. Rev. Lett. 51, 1010 (1983) and ibid 50, 2062 (1983) and 19th ICRC Conference Papers, 6, 164 (1985).

9. Alma-Ata, Bucharest, Dubna, Dushanbe, Erevan, Gatchina, Kosice, Krakow, Leningrad, Moscow, Tashkent, Tbilisi, Ulan-Bator Collaboration, 19th ICRC Conference Papers, 6, 176 (1985).

10. A. Bialas et al., Nucl. Phys. B100, 103 (1975).

11. J. D. Bjorken, Phys. Rev. D27, 140 (1983).

12. UA1 Collaboration, G. Arnison et al., Phys. Lett. 118B, 173 (1982); Ames-Bologna-CERN-Dortmund-Heidelberg-Warsaw Collaboration, A. Breakstone et al., Phys. Lett. 132B, 463 (1983).

13. F. Takagi, Phys. Rev. Lett. 53, 427 (1984).

14. A. Bialas and R. Peschanski, Saclay preprint/SPhT/85/101.

15. F. Takagi, Tohoku Univ. preprint TU/85/284.

STUDIES OF AIR SHOWERS PRODUCED BY PRIMARIES > 10^{16} eV USING A COMBINED SCINTILLATION AND WATER-CERENKOV ARRAY

G Brooke, J C Perrett and A A Watson
Department of Physics, University of Leeds, LEEDS 2, UK.

ABSTRACT

An array of 8 x 1.0 m^2 plastic scintillation counters and 13 water-Cerenkov detectors (1 to 13.5 m^2) has been operated at the centre of the Haverah Park array to study some features of air showers produced by 10^{16} eV primaries. Measurements of the scintillator lateral distribution function, the water-Cerenkov lateral distribution function and of the distance dependence of the Cerenkov/scintillator ratio are described.

1. Introduction. An array of 8 x 1.0 m^2 scintillation detectors and 13 water-Cerenkov detectors were operated at the centre of the Haverah Park array from September 1982 - December 1983. The arrangement of the array is described in Brooke et al (1983). The output from each detector is digitized locally and transmitted to a central controlling computer (Astley et al 1983). This configuration of detectors has given us the opportunity to make a number of measurements in showers with primary energy $10^{16} - 10^{17}$ eV. In addition a sample of showers with very precise core locations have been obtained for use in searches for muon-poor showers.

2. The scintillator lateral distribution function for $E > 10^{16}$ eV. In a three month period from October 1983 1531 events were recorded with $\theta < 50^{o}$ and with mean energy 3.5×10^{16} eV. The trigger for this run was supplied by a three-fold coincidence between 4 x 9 m^2 water-Cerenkov detectors spaced at 150 m. The scintillator lateral distribution function (LDF) was measured with the 8 scintillators using shower cores derived from water-Cerenkov data fitted to the average water-Cerenkov LDF obtained by Coy (1984). Various trial scintillator LDFs were fitted to the data (Perrett 1985). The best fit was obtained using the modified NKG lateral distribution adopted by the Akeno group (Hara et al 1979), namely

$$S(r) = \frac{NC}{r_o^2}\left(\frac{r}{r_o}\right)^{(s-2)}\left(1+\frac{r}{r_o}\right)^{(s-4.5)}\left(1+0.2\left(\frac{r}{r_o}\right)^{1.6}\right),$$

where S(r) is the scintillator density at a distance r, $s = 1.07 \pm 0.01$, $r_o = 79$ m, $\log(NC/r_o^2) = 2.02$ and $C = 1/\{B(s, 4.5-s) + 0.2\, B(s+1.6, 4.5-1.6-2s)\}$ where B(z,w) is the beta function. The data and fit are shown in Figure 1 which is based on 108 showers with $\theta < 30^{o}$. Figure 2(a) and (b) show the measured variation of s with primary energy and zenith angle for a larger data set of 1531 showers with $\theta < 50^{o}$. The zenith angle variation of s in the range $1.0 < \sec\theta < 1.2$ was found to be $(5.1 \pm 0.6) \times 10^{-4}$ g^{-1} cm^2. This value of $ds/d\sec\theta$ accounts for the different values of S, 1.07 and 1.02, measured at Haverah Park and Akeno respectively.

3. The water-Cerenkov lateral distribution for $E > 10^{16}$ eV. Using the

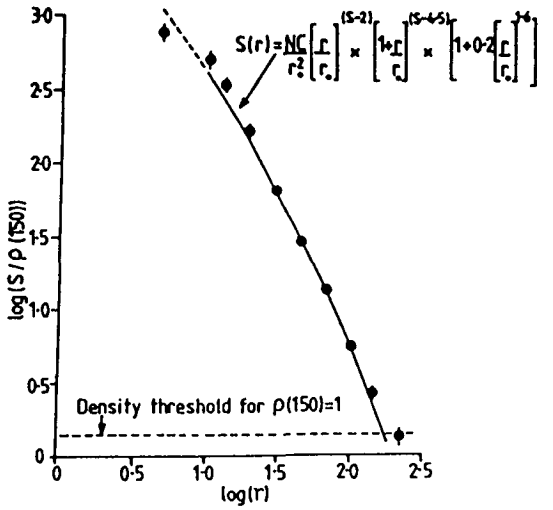

Figure 1: The modified NKG LDF fitted to 108 events with $\theta < 30^{o}$. Core location was provided by the water-Cerenkov detectors. A value of 1.07 ± 0.01 was obtained for the age parameter s.

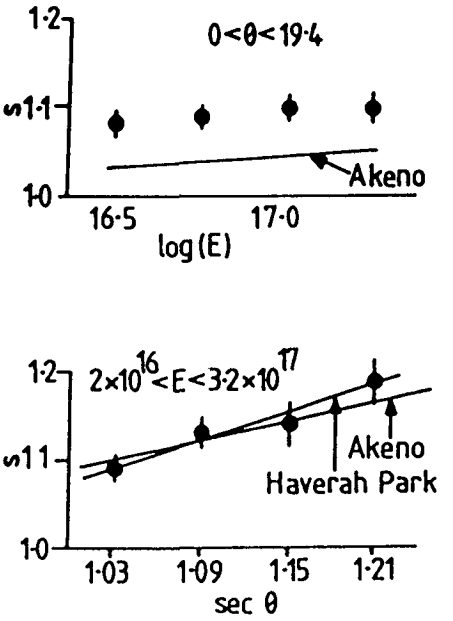

Figure 2a: The variation of s as a function of energy in the theta range $0^{o} < \theta < 19.4^{o}$.
Figure 2b: The variation of s as a function of $\sec\theta$ in the energy range $2 \times 10^{16} < E < 3.2 \times 10^{17}$. A value of $(5.1 \pm 0.6) \times 10^{-4}\ g^{-1}\ cm^{2}$ was obtained.

same 1531 events discussed above the water-Cerenkov LDF (described by $\rho(r) = k\ r^{-(\eta + r/4000)}$) was investigated above 10^{16} eV with the scintillator data being used to locate the shower core. These data are shown for $\theta < 30^{o}$ in Figure 3. The LDF is found to be a good fit to the data in the distance range $20 < r < 300$ m. It is quite remarkable that this form of function (with an energy and θ-dependent η) fits water-Cerenkov data from $10^{16} - 10^{20}$ eV. To measure the variation of η with energy and zenith angle a subset of 924 events which satisfied a strict acceptance criteria (Perrett 1985) was used. A multi-parameter weighted least squares fit was carried out on the values of η derived in individual showers in the energy range $2 \times 10^{16} < E < 2 \times 10^{17}$ eV and compared with that found by Coy (1984) for $E > 2 \times 10^{17}$ eV. The results are:-

$$2 \times 10^{16} < E < 2 \times 10^{17}\ \text{eV}: \quad \eta = (2.261 \pm 0.018) - (1.146 \pm 0.092)\ (\sec\theta - 1) + (0.192 \pm 0.035)\ \log(E/10^{17}),\ \text{and}$$

$$\text{for } E > 10^{17}\ \text{eV}: \quad \eta = (2.198 \pm 0.014) - (1.275 \pm 0.051)\ (\sec\theta - 1) + (0.160 \pm 0.022)\ \log(E/10^{17}).$$

At $\theta = 0^{o}$, $E = 10^{17}$ eV the values of η determined in the two independent

experiments differ by 0.063 ± 0.023. We consider this good agreement in view of the well-known difficulty of avoiding systematic errors in this type of work. The regression coefficients have been used to calculate the elongation rate (Linsley 1977) in each energy range. The derived values are (99 ± 20) gcm^{-2}/decade for $10^{16} < E < 10^{17}$ eV and (81 ± 12) gcm^{-2}/decade above 10^{17} eV. There is no evidence for any change of elongation rate with energy from 10^{16} to 3×10^{18} eV (the effective upper range of the data obtained by Coy (1984)).

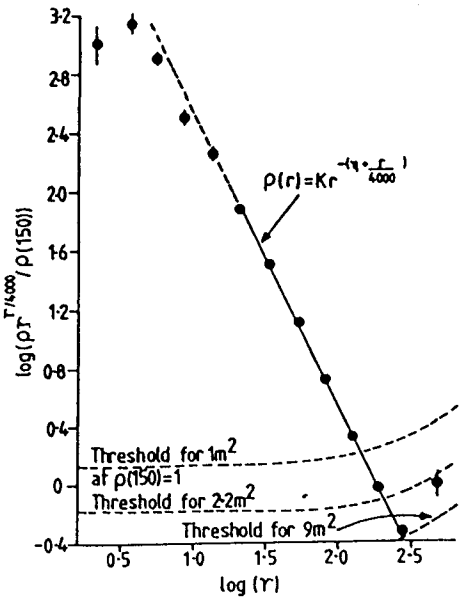

Figure 3: The water-Cerenkov data fitted to the Cerenkov LDF for $\theta < 30^{o}$. Core location was provided by the scintillation detectors.

Fluctuations between the values of η found for individual showers are considerably larger than can be accounted for by measurement error alone.

4. The Cerenkov/Scintillator density ratio. The ratio of the density measured in the water-Cerenkov detectors (C) to that observed in the scintillator detectors (S) (both in units of vertical equivalent muons) is a function of the energy of the primary initiating the shower and of the distance of the detectors from the shower core. It is a useful quantity both for comparison with model calculations and for use in cross-calibration checks between arrays. In the present experiment the ratio C/S has been measured directly for showers in the distance range $10 < r < 200$ m for showers of mean energy 5×10^{16} eV. The data shown in Figure 4 are for a mean zenith angle 19°. The expected rise of the C/S ratio at small core distance is observed.

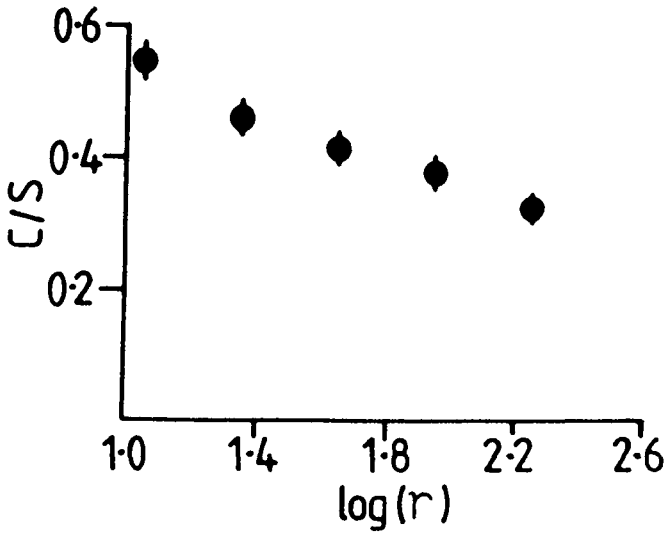

Figure 4: The variation of the Cerenkov (C) to Scintillator (S) ratio as a function of for $\bar{\theta} < 19^{o}$ and $\bar{E} = 3.5 \times 10^{16}$ eV.

Acknowledgements. We thank D Pearce and P Ogden for their help in running the array and the Science and Engineering Research Council (UK) for their continued support of work at Haverah Park.

References

S M Astley et al 1983 Nuclear Inst. and Methods 205, 465.
A J Bower et al 1981 Proc. 17th ICRC (Paris) 9, 166.
A J Bower et al 1983 J Phys G 9, 15969.
G Brooke et al 1983 Proc. 18th ICRC (Bangalore) 11, 185.
R N Coy 1984 PhD Thesis, University of Leeds.
T Hara et al 1979 Proc. 16th ICRC (Kyoto) 13, 148.
J Linsley 1977 Proc. 12th ICRC (Plovdiv) 12, 89.
J C Perrett 1985 PhD Thesis, University of Leeds.

THE HOMESTAKE SURFACE-UNDERGROUND SCINTILLATORS -- INITIAL RESULTS

M.L. Cherry*, S. Corbato*, T. Daily*, E.J. Fenyves+, D. Kieda*, K. Lande*, and C.K. Lee

* Depts. of Physics and Astronomy, Univ. of Penna, Philadelphia, PA 19104
+ Dept. of Physics, Univ. of Texas, Dallas, TX 75080

The first 70 tons of the 140-ton Large Area Scintillation Detector have been operating since Jan. 1985 at a depth of 4850 ft. (4200 m.w.e.) in the Homestake Gold Mine, Lead, S.D. A total of 4 x 10^4 high-energy muons ($E_\mu \gtrsim 2.7$ TeV at the surface) have been detected. The remainder of the detector is scheduled to be in operation by the Fall of 1985. In addition, a surface air shower array is under construction. The first 27 surface counters, spaced out over an area of 270' x 500', began running in June, 1985. We describe the LASD performance, discuss the potential of the combined shower array and underground muon experiment for detecting point sources, and present the initial results of a search for periodic emission from Cygnus X-3.

I. Detector Status

Underground, the Large Area Scintillation Detector will be used to detect high-energy muons, slow monopoles, and neutrinos[1]. The detector consists of 140 tons of liquid scintillator housed in 200 PVC boxes, each 30 cm x 30 cm x 8 m, placed around the outside of the ^{37}Cl solar neutrino detector of Davis et al.[2] at a depth of 4850 ft. in the Homestake Gold Mine (Fig. 1). The surface array currently consists of twenty-seven 3 m^2 x 4" thick liquid scintillation detectors, spaced by 15 - 25 m over an area of 80 x 150 m^2. The surface and underground detectors are currently being operated both independently and in coincidence in order to study the cosmic ray composition near 10^{15} eV and to search for high energy sources. The detectors have been described elsewhere in these Proceedings[1]. Here we discuss the potential of the surface-underground telescope to see point sources with high angular resolution, and illustrate the initial

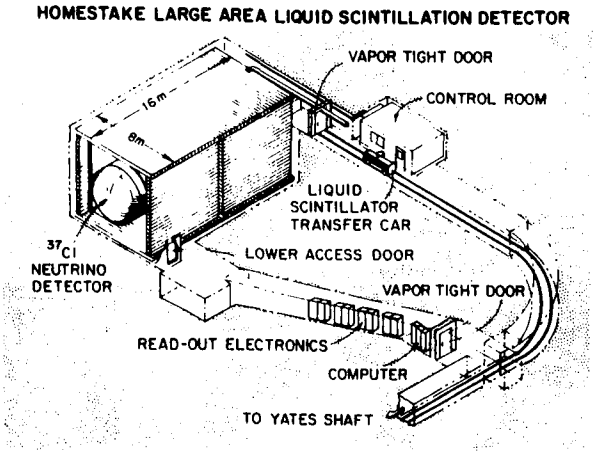

Fig. 1

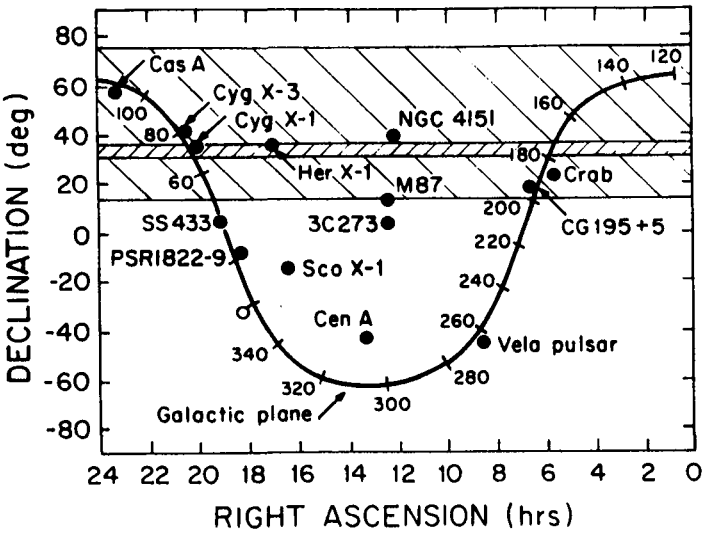

Fig. 2

performance of the system. In addition, we present the first results of a search with the LASD for a periodic muon signal from Cygnus X-3.

II. The Surface-Underground Telescope

The latitude of the detectors is $44^{\circ}21'$ N. Since the surface array operated independently has high efficiency for showers inclined at angles up to 30° from the zenith, a $\pm 30^{\circ}$ band in the sky is shown in Fig. 2. Several interesting x-ray, γ-ray, and radio point sources are shown, together with the Galactic plane. A line connecting the underground LASD and the current 270' (north-south) by 500' (east-to-west) surface array is at an angle of 11° south of vertical. The band from 31° to 35° subtended by the surface array

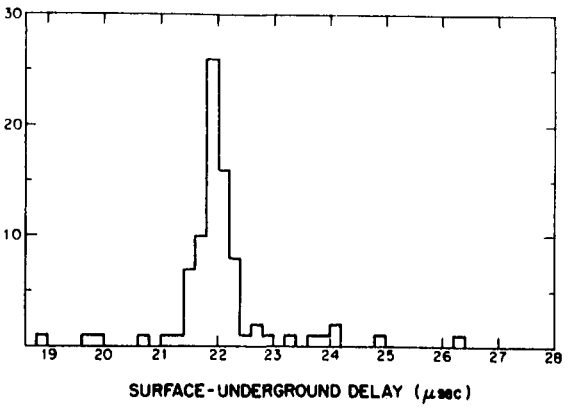

Fig. 3

is also shown in Fig. 2. The sources Cyg X-1 and Her X-1 lie within this band; Cyg X-3 and NGC 4151 lie less than 6° to the north, and will be covered by the next expansion of the surface array.

It should be noted that the existing surface array is comparable in size to the Kiel[3] and Haverah Park[4] arrays used to detect 10^{15} eV showers from Cyg X-3, and the LASD is significantly larger than the Soudan I[5] and NUSEX[6] underground detectors which have also reported small flux excesses from near Cyg X-3.

The angular resolution of the combined surface and underground detectors is 3-10 mrad.

With the full area of the underground LASD in operation, we detect 5 surface-underground coincidences day^{-1}. In Fig. 3, we show the measured time delay between surface and underground for the first 83 detected coincidence events. The distribution is peaked at 21.8μs (corresponding to a 5μs muon travel time and 17μs cable delays), with a FWHM of 0.6μs (due largely to the spread in flight times for showers passing through different parts of the surface array). The delay time distribution shows very little background -- based on the independent surface and underground counting rates, we expect an accidental coincidence rate of $1/30\mu s^{-1}\,day^{-1}$, in good agreement with the data. In Fig. 4, we show the observed shower size distributions (plotted as the number of surface counters above threshold) for events with multiple underground muons (top) and single underground muons (bottom).

III. Search for Underground Events From Cygnus X-3

We have searched our data for the period 5/24/85 - 7/23/85 for events with a characteristic period of 4.8 hours from the direction of the binary pulsar Cygnus X-3. In order to minimize detector biases, the detector ran nearly uninterrupted during this interval, with a fractional live time of 98%. We analyzed the data by imposing fiducial cuts, by requiring that the measured flight time corresponded to a velocity $\beta = 1$, by requiring that the events arrived from within 36° of the vertical, and by requiring that the events came from within 10° of the known Cygnus X-3 position. We performed a phase analysis by folding the data using the x-ray ephemeris of van der Klis and Bonnet-Bidaut[7]. The result is shown in Fig. 5, where the solid line is the phase plot for potential source events, and the dashed line is the background distribution (where the background comes from the same declination band but from all right ascensions except those within 30° of the source). We see a 1σ excess in the phase bin 0.7 - 0.8 (the same bin where the NUSEX excess was seen) and a 3σ excess in the region $\psi = 0 - 0.2$. The arrival directions of the individual events in the 3σ peak are plotted in Fig. 6; there is no noticeable enhancement at the position of Cygnus X-3. With a sample of 1.2×10^4 events (half the size of the NUSEX sample), we feel that we have no evidence for significant positive excesses in our phase plot.

Funding for the Homestake scintillator experiments is provided by the U.S. Department of Energy. The assistance and generous cooperation of the Homestake Mining Company are deeply appreciated. We are especially indebted to A. Gilles and J. Dunn. In addition, we appreciate the advice, assistance, and participation of T. Ashworth, K. Brown, B. Cleveland, R. Davis, I. Davidson, J. Lloyd-Evans, E. Marshall, R. Reid, R. Steinberg, and A. Watson.

References

1) M.L. Cherry, S. Corbato, D. Kieda, K. Lande, C.K. Lee, and R.I. Steinberg, in Solar Neutrinos and Neutrino Astronomy, ed. by M.L. Cherry, K. Lande, and W.A. Fowler, AIP Conf. Proceedings No. 126, AIP, New York (1985); and 19th ICRC, La Jolla, paper HE 6.1-9 (1985).
2) J.K. Rowley, B.T. Cleveland, and R. Davis, Jr., in Solar Neutrinos and Neutrino Astronomy, ed. by M.L. Cherry, K. Lande, and W.A. Fowler, AIP Conf. Proceedings No. 126, AIP, New York (1985).
3) M. Samorski and W. Stamm, Ap. J. 268, L17 (1983).
4) J. Lloyd-Evans et al., Proc. 18th Intl. Cosmic Ray Conf., Bangalore 9, 65 (1983).
5) M.L. Marshak et al., Argonne preprint ANL-HEP-PR-85-19 (1985).
6) B. D'Ettorre Piazzoli, UP85 (1st Symposium on Underground Physics), Saint-Vincent, April (1985).
7) M. van der Klis and M. Bonnet-Bidaud, Astron. Astrophys. 95, L5 (1981).

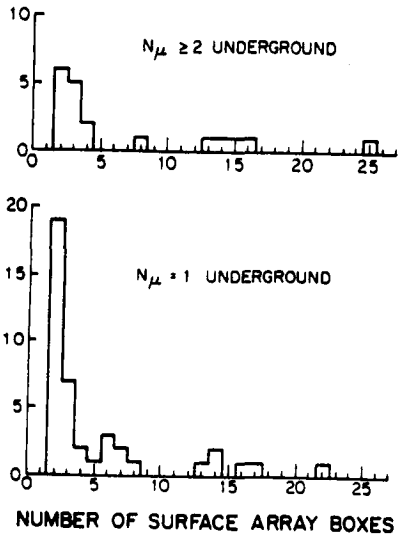

Fig. 4

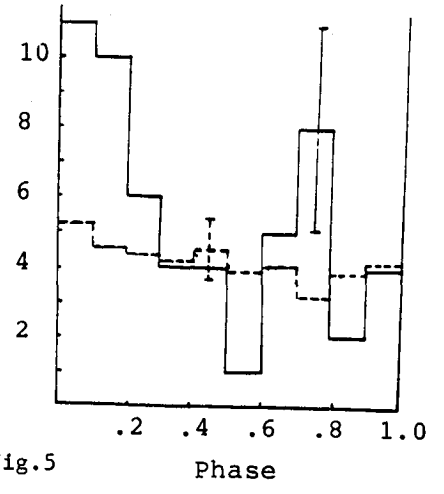

Fig.5

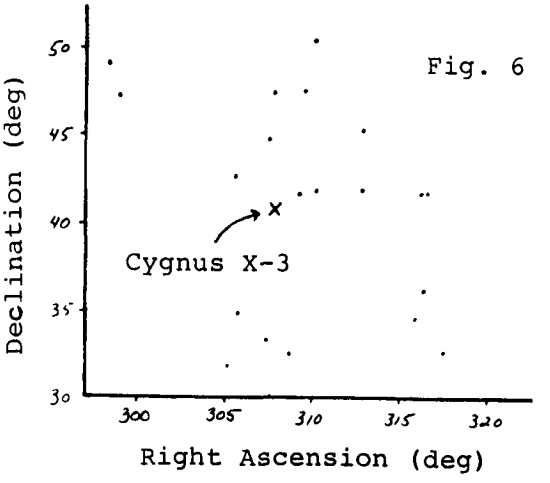

Fig. 6

LEAD, PLATINUM, AND OTHER HEAVY ELEMENTS IN THE PRIMARY COSMIC RADIATION--HEAO-3 RESULTS

C.J. Waddington,[1] W.R. Binns,[2] N.R. Brewster,[1] D.J. Fixsen,[1]
T.L. Garrard,[3] M.H. Israel,[2] J. Klarmann,[2] B.J. Newport,[3] E.C. Stone [3]

[1]School of Physics and Astronomy, University of Minnesota, Minneapolis, MN 55455
[2]Department of Physics and the McDonnell Center for the Space Sciences, Washington University, St. Louis, MO 63130
[3]George W. Downs Laboratory, California Institute of Technology, Pasadena, CA 91125

1. Introduction. This paper reports an observation of the abundances of cosmic-ray lead and platinum-group nuclei using data from the HEAO-3 Heavy Nuclei Experiment (HNE) which consisted of ion chambers mounted on both sides of a plastic Cherenkov counter (Binns et al., 1981). Previously we have reported on a search for actinide nuclei, $Z > 88$ (Binns, et al. 1982a). Further analysis with more stringent selections, inclusion of additional data, and a calibration at the LBL Bevalac, have allowed us to obtain the abundance ratio of lead and the platinum group of elements for particles that had a cutoff rigidity $R_c > 5$ GV.

2. Analysis. We have analyzed 580 days of exposure and considered selected data for those events where the Cherenkov detector and at least two of the ion chambers were triggered. These selection criteria will be described elsewhere, Binns et al. (1985).

Two sets of events satisfying the selections were formed--one for which $Z > 49.5$; the other, a "normalization" set, with 1/400 of all events with $Z > 19.5$, chosen at random.

The events were separated into two groups, 67% with $R_c > 7$ GV and 33% with $5 < R_c < 7$ GV. The charge scale and resolution for each group were determined independently by examining the iron peak in the corresponding normalization set. In both groups, the nuclear charge of each event was inferred from the Cherenkov signal, assuming that the signal was simply proportional to Z^2, Garrard et al. (1983).

Fig. 1 shows the observed charge spectrum. This data set demonstrates an odd-even abundance effect for $50 \leq Z \leq 56$ and a sharp falloff in abundances between 56 and 60, similar to that found previously in a data subset having higher charge resolution (Binns et al. 1983). The 322 nuclei with $Z \geq 50$ used in this analysis correspond to $(9.6 \pm 0.5)10^6$ iron nuclei which satisfy the same selection criteria and are observed within

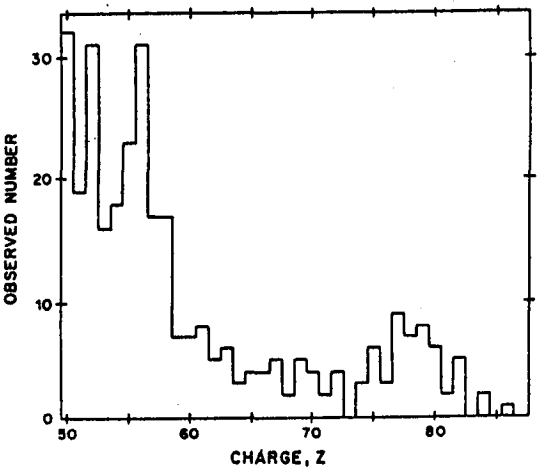

Fig. 1. Observed charge spectrum with charges assigned assuming a Z^2 dependence of the Cherenkov signal.

the instrument, not in free space. The quoted uncertainty is predominately due to the uncertainty in resolving $_{25}Mn$ from $_{26}Fe$.

3. Comparison with Other Data. Results that cover this charge range have been reported from the Ariel-6 UH-nuclei detector which was exposed in a 55° inclination orbit (Fowler et al. 1984), and hence extends to appreciably lower energies than our data. In order to analyze the Ariel data, Fowler et al. had to deconvolve their data using an extrapolation of the resolution function found for Fe and lighter nuclei. We have not attempted a deconvolution of our charge spectrum, since the results of such a process are quite sensitive to the form of the assumed resolution function, particularly when individual element peaks are not apparent in the data. Due to our limited charge resolution we have considered only the following physically significant groups of charges:

Name	Abbreviation	Range	Number observed
"Lead"	Pb	81≤Z≤86	10
"Platinum"	Pt	74≤Z≤80	42

The ratio of the abundance of lead to platinum will be compared with other data and with model predictions. The secondary ratios will be discussed elsewhere, see Klarmann et al. (1985; OG 4.4-6).

The value of 0.24±0.08 for the Pb/Pt ratio derived from our observations differs from that outside the detector because of nuclear interactions during entry and penetration of the detector and the instrumental resolution, which smears the charge distribution. For each of eight plausible models we calculated abundances expected near earth, as described below. Entry into the detector was then simulated by propagation through various slabs of hydrogen approximating the amount of aluminum in the various paths into and through the detector. The resulting element distribution inside the detector was then convolved with the instrument resolution to derive the distribution we would expect to observe. Although the eight models gave very different values for the ratio at the outside of the instrument, the factor by which the ratio changed after propagation into the instrument and convolution with the resolution was nearly the same for all the models. Therefore, we have used a single correction factor of 1.06±0.02 for the ratio.

Our resulting ratio of 0.25±0.09, outside the detector, can be compared with the corresponding result reported by the Ariel experiment of 0.40±0.10. If this result is combined with those on the secondary ratios, there does seem to be a systematic difference between the two sets of results, although of marginal statistical significance on any individual ratio.

4. Comparison with Models. Our observed charge spectrum, Fig. 1, can be compared with those predicted by various models. A series of predictions were made using the solar system abundances of Anders and Ebihara (1982) and the derived s- and r-process contributions to these abundances. These abundances, taken as calculated, or adjusted for the effects of an exponential dependence on first ionization potential (FIP) fractionation, were used as source abundances. An alternative dependence on FIP, with a step at 9 eV or above, Cook et al. (1979); Meyer (1981), would lead to abundances essentially independent of FIP. These various source abundances were then propagated through the

interstellar medium, assuming a leaky-box model, and using the revised code of Brewster et al. (1983 , 1985) with a rigidity dependent escape length (Ormes and Protheroe 1983) that is 6.21 g/cm^2 of hydrogen at 7 GV. We have used the cross-sections calculated from the formalism of Silberberg and Tsao (1983). The predictions of this program are in good agreement with the latest predictions obtained by Margolis and Blake (1983), at least for the solar system source abundances.

In Fig. 2, we have shown the calculated values of this ratio for solar system abundances and for r-process abundances; s-process abundances are not given because they show little relation to the observed values with Pb/Pt ratios of $\sim$ 1.0.

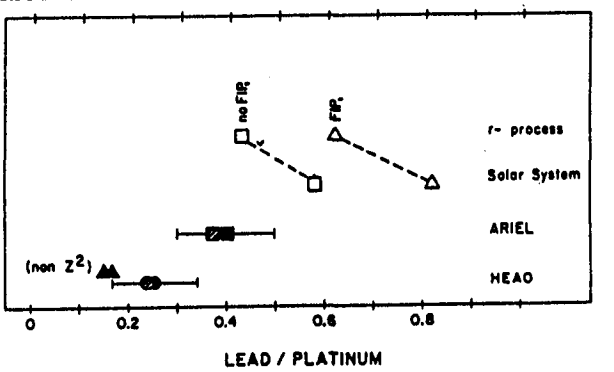

Fig. 2. The "lead to platinum" ratio as observed and predicted. Observed values are shown shaded, while in space values are shown solid and with error bars. The shaded and solid triangles indicate the ratios when a non Z^2 correction to our charge assignments is included.

Our observed ratio for Pb/Pt (Fig. 2) is distinctly lower than that predicted from solar system source abundances in any of the four models considered. In particular, even considering the models without exponential FIP fractionation, we find an observed ratio that is distinctly lower than that predicted for either a solar-system or an r-process source. This result might suggest that, unlike the cosmic rays with Z < 60 (Binns et al. 1982b, 1983), the cosmic rays with Z around 80 come from a source with a distinctly different nucleosynthesis history than do the solar system elements. However, two alternatives to this conclusion must also be considered. First, the Pb abundance in the cosmic ray source may be suppressed by some form of source fractionation which depends upon a different parameter than FIP. Second, it could be that the Pb abundances assumed in our model calculations are not really representative of the solar system or of the r- or s- process contributions to the solar system.

We have noted (Israel et al. 1983) that the cosmic ray abundance of Ge relative to Fe is down by a factor of about two compared to the solar system. Ge, like Pb, is one of the few volatile elements with moderate to low FIP. The factor-of-two underabundance of Ge lends support to the suggestion (Cesarsky and Bibring 1980; Epstein 1980) that it is volatile elements, rather than elements with high FIP, which are underabundant in the cosmic rays. Such a source fractionation dependent on volatility could produce our observed low Pb abundance even with a cosmic ray source whose composition is essentially the same as that of the solar system.

Alternatively, there are reasons for believing that the source abundances of Pb used in our models may not be representative of the solar system values. Our observed Pb/Pt ratio could be consistent with

that expected from a "Pb-poor r-process", either with or without FIP fractionation.

It is possible that the assumed solar system Pb abundance itself is too high. If the Anders and Ebihara Pb abundance were twice that of typical solar system matter, then a solar system source abundance, either with or without FIP fractionation, would agree with our data.

Finally, we note that Ge and Pb, like most elements with higher FIP, have abundances in C2 chondritic meteorites about a factor of two lower than abundances in the C1 chondrites which are the basis for the Anders and Ebihara solar system abundances. If the C2 rather than the C1 chondrites were more nearly representative of the composition of the heavier elements in the solar system, then our low Pb/Pt ratio would again be consistent with a cosmic ray source of composition similar to that of the solar system.

Thus, while our Pb/Pt ratio is distinctly lower than that predicted by any of the standard models for cosmic ray sources, it is possible that the difference is not an indication that the cosmic ray source composition is greatly different from that of the solar system, but rather that there is less Pb in the solar system and in the r-process than is assumed in the standard model.

5. Acknowledgements. The research was supported in part by NASA under grants NAG 8-498, 500, 502, and NGR 05-002-160, 24-005-050, and 26-008-001.

References

Anders, E., and Ebihara, M. (1982), Geochimoca et Cosmochimica Acta, 46, 2363.
Binns, W. R., et al. (1981), Nucl. Inst. Meth., 185, 415.
Binns, W. R., et al. (1982a), Ap.J. (Letters), 261, L117.
_____. (1982b), Ap.J. (Letters), 247, L115.
Binns, W. R., et al. (1983), Ap.J. (Letters), 267, L93.
Binns, W. R., et al. (1984), Adv. Space Res., 4, 25.
Binns, W. R., et al. (1985), to be published in Ap.J., Oct. 1.
Brewster, N. R., Freier, P. S., and Waddington, C. J. (1983), Ap.J., 264, 324.
_____. (1985), to be published in Ap.J., July 1.
Cesarsky, C. J., and Bibring, J. P. (1980), IAU Symposium, 94, 361.
Cook, W. R., et al. (1979), 16th ICRC, Vol. 12, 265.
Epstein, R. I. (1980), MNRAS, 193, 723.
Fowler, P. H., et al. (1984), 9th European Cosmic Ray Symposium.
Garrard, T. L., et al. (1983), 18th ICRC, Vol. 9, 367.
Israel, M. H., et al. (1983), 18th ICRC, Vol. 9, 305.
Klarmann, J., et al. (1985), this conf., OG 4.4-6.
Margolis, S. H., and Blake, J. B. (1983), 18th ICRC, Vol 9, 283.
Meyer, J. P. (1981), 17th ICRC, Vol. 2, 281.
Silberberg, R., and Tsao, C. H. (1983), Ap.J. Supp. 25, 315, 335.

AUTOMATED SCANNING OF PLASTIC NUCLEAR TRACK DETECTORS USING THE MINNESOTA STAR SCANNER

P. J. Fink and C. J. Waddington

School of Physics and Astronomy, University of Minnesota
Minneapolis, Minnesota 55455

1. Introduction. This report describes the problems found in an attempt to adapt an automated scanner of astronomical plates, the Minnesota Automated Dual Plate Scanner (APS), Landau and Humphreys (1982), to locating and measuring the etch pits produced by ionizing particles in plastic nuclear track detectors, CR-39. A visual study of these pits was made to determine the errors introduced in determining positions and shapes, by comparing measurements made under a low power microscope with those from the APS.

2. The Apparatus. The scanner was designed to detect the boundaries of the images on astronomical photographic plates by scanning them with a swept 12 μm diameter laser beam. This beam sweeps over a 12 mm wide stripe during each scan. The location of coordinates where the intensity of the beam is abruptly changed by an image on the plate is recorded with a nominal accuracy of 3/8 μm. These coordinates are then organized into images by an online computer. The resulting data consist of images defined by a series of strips. At its maximum rate the system can scan at a rate of 1300 cm^2/hour. As a consequence it would be able to scan in a reasonable time the very large areas of plastic that might be expected to result from the exposures that have been planned to study the UH-nuclei in the cosmic radiation, such as those on LDEF I and II. Obviously, such scanning is only worthwhile if the detection efficiency is high and if the images obtained adequately represent those of the etch pits in the plastic.

In operation there are three parameters that can be selected by the user: the scan line spacing, trigger level or "gate", and the frequency cutoff of a low pass filter. The spacing between scans may be set at either 5 or 10 μm. The change in intensity needed to trigger the recording of an image, the gate level, may be selected as a percentage of the incident light, so that the higher the gate level selected the more images will be recorded. Finally, the analog stream of data from the scanner is put through a low pass filter which removes small transitions, or noise, typical of a fogged background on a photographic plate. The range of this filter can be set by the user and generally must be selected by trial and error for each exposure. The images obtained can then be examined at any desired degree of magnification by software selection. The depth of focus is sufficient that pits in nominally 600 μm CR-39 plates can be scanned with equal efficiency on both surfaces.

3. Experimental Material. Three different set of CR-39 plastics, exposed to different types of particles and etched under different conditions, were scanned in order to evaluate the capabilities of the system.

a) Plates that had been exposed at the LBL Bevalac to a beam of 1.0 Gev/n gold nuclei. These plates were deliberately overetched, in an

attempt to look at the lighter charged fragments, so that the majority of the pits had etched through and produced large images some 500 μm long and 200 μm across.

b) Plates exposed to a beam of 1.7 Gev/n manganese nuclei, also from the Bevalac. These plates contained well defined etch pits of both the primary nuclei and their secondary fragments. The data from these plates has been reported elsewhere by Atwater et al. (1984) and shown to be capable of yielding a charge resolution characterized by a standard deviation of 0.14 charge units.

c) Plates exposed to the cosmic radiation during a balloon flight from South Dakota and made available to us by B. Price. These plates show widely scattered pits of all sizes below about 100 μm due to the isotropically distributed cosmic ray particles. Furthermore, due to the incidence of both slow and fast particles, the shapes of the pits vary considerably. These plates represent the most severe test of the system, since the additional degrees of freedom introduced by the isotropy and energy spread makes the detection of true events much more difficult.

4. Scans. As a first assay of the system capabilities the Au plates were scanned with a 10 μm scan separation using a 50 kHz filter and a 35% gate. Typical high and low magnification views are presented in Fig. 1. The low magnification view shows large images and it was found that the detection efficiency was essentially 100%. The high magnification view shows the images of two etched through pits produced by Au-nuclei, (a) and (b), and the images of a secondary fragment of lesser charge which has a separate pit on each surface, (c1) and (c2). It can be seen that the images are somewhat deformed by occasional scan lines continuing past the envelope of the optical image. We estimate that the average systematic error on the true length of an individual scan line is of the order of 10 μm. This result would appear to preclude the use of the system to make accurate measurements of individual pits, but still leaves the possibility that it would be capable of being used as a rapid scanning device.

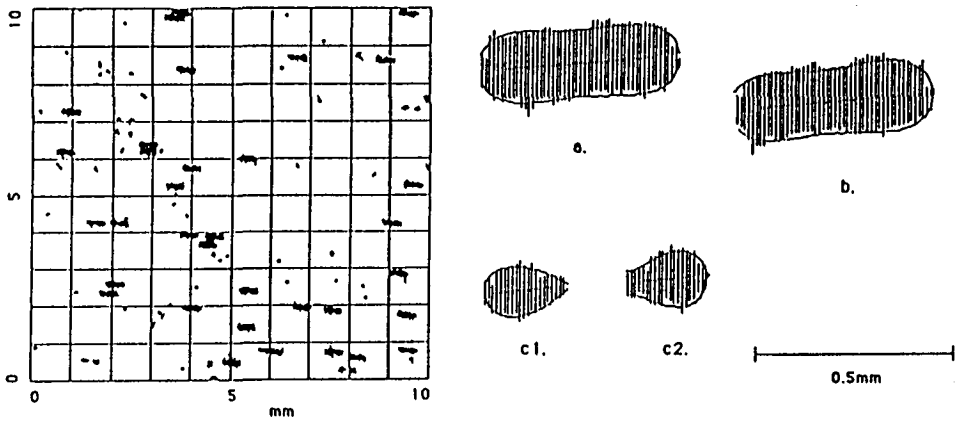

Fig. 1. Scans of Au plates. (a) Under low magnification. (b) Under high magnification. Envelopes shown are computer best fits to the images.

The two manganese plates were scanned with a 5 μm scan separation over the same area that had been visually studied by Atwater et al. (1984), using various settings on filter and gate. The Table shows, for various scans, the signal-to-noise ratio, i.e., the ratio of the number

Table

	Plate 1		Plate 2	
settings	S/N	Eff.	S/N	Eff.
90 kHz filter 50% gate	0.36±0.07	0.83±0.18	0.13±0.02	1.00±0.24
90 kHz filter 40% gate	0.33±0.09	0.44±0.12	0.27±0.07	0.49±0.14
60 kHz filter 50% gate	0.32±0.08	0.44±0.12	0.29±0.07	0.57±0.16
60 kHz filter 40% gate	0.13±0.08	0.07±0.04	0.19±0.04	0.17±0.08

of located pits to the number of recorded images; and the efficiency, the number of located pits to the number of pits identified visually as true pits. Although the statistics are poor it appears that the efficiences are sensitive to the settings chosen and that in order to obtain a high efficiency it is necessary to accept a poor signal to noise ratio. Figure 2 shows medium magnification views of scans made under two different settings. It can be seen that not only does the signal to noise ratio change, but so do the sizes of the individual images and the detection efficiency. It should also be noted that the identification of pits in this scan depends on the predetermined knowledge of the direction and angle of incidence, thus requiring a matched pair of pits. Individual pits are not uniquely distinguished from the background images.

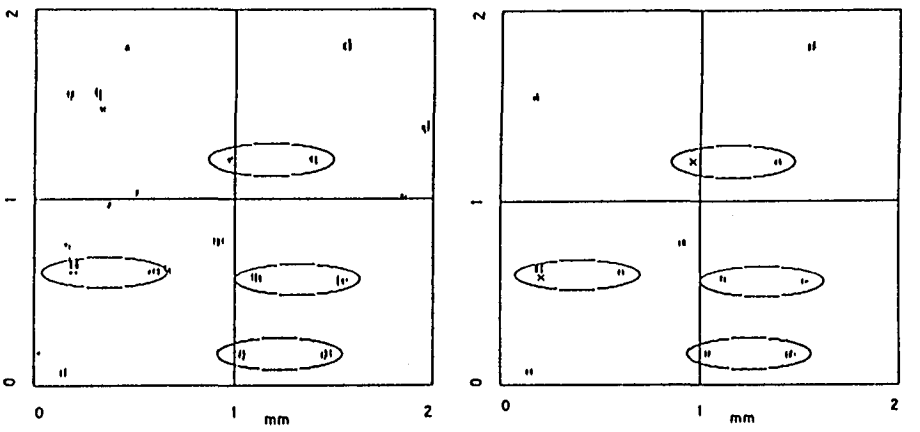

Fig. 2. Moderate magnification scans of Mn plates. (a) 90 kHz filter, 50% gates; (b) 90 kHz filter, 40% gate. Crosses denote positions of missing images of real pits.

Finally, the cosmic ray plates were scanned with a scan width of 5 μm, 90 kHz filter and gate settings of 40 and 60%. In order to distinguish genuine pits from noise it was necessary to develop a technique of "blinking" the images in two adjacent plates against each other. This greatly improved the signal-to-noise ratio but at the cost of a reduced efficiency and increased scanning time.

We conclude that this system is not suitable for the tasks described above, having neither the detection efficiency nor the spatial resolution needed for the low contrast, non-circular images involved in this application.

5. Acknowledgements. We are grateful to R. Landau for help and advice in assessing this system and to R. Humphreys for permission to divert its use from the prime purpose. This work was partially supported by NASA under Grant NGR 24-005-050.

References

Atwater, T. W., Freier, P. S., and Waddington, C. J. (1984), Nucl. Tracks 9, 107.
Landau, R. and Humphreys, R. (1981), SPSE Conf., Tucson.

COSMIC RAY ANISOTROPIES AT HIGH ENERGIES

N. J. Martinic, A. Alarcon, F. Teran
Chacaltaya Cosmic Ray Laboratory
University of La Paz

ABSTRACT
The directional anisotropies of the energetic cosmic ray gas due to the relative motion between the observers frame and the one where the relativistic gas can be assumed isotropic is analyzed. The radiation fluxes formula in the former frame must follow as the Lorentz invariance of $d\underline{p}/E$, where $\underline{p}$, E are the 4-vector momentum-energy components; $d\underline{p}$ is the 3-volume element in the momentum space. The anisotropic flux shows in such a case an amplitude, in a rotating earth, smaller than the experimental measurements from say, EAS-arrays for primary particle energies larger than 1.E(14) eV. Further, it is shown that two consecutive Lorentz transformations among three inertial frames exhibit the violation of $d\underline{p}/E$ invariance between the first and the third systems of reference, due to the Wigner rotation. A discussion of this result in the context of the experimental anisotropic fluxes and its current interpretation is given.

1. Introduction

Using the inertial frames S, S'; the so-called Compton Getting anisotropies can be deducted as follows. (Cf' for instance Gerantos and Martinic, 1977). The Lorentz transformation is written:

$$p_1 = p\sqrt{A}, \quad E_1 = \gamma pc\,(\zeta-\beta\mu), \quad \mu_1 = \gamma(\mu-\beta\zeta)/\sqrt{A}; \tag{1}$$

with $A = 1+\gamma^2(\beta^2\zeta^2+\beta^2\mu^2-2\beta\zeta\mu)$, γ the Lorentz factor and β the relative speed between the frames, in c-units; $\zeta=E/pc$, and μ (or μ_1) the cosine of the inclination angle of the $\underline{p}$ (or $\underline{p}_1$) momentum with respect to the x-axes of both frames. In Eq. (1) the velocity $\underline{\beta}$ was taken parallel to the x-axes of both systems of reference; E_1(or E) is the total energy of the particle. Notice that $d\underline{p} = p^2dp\,d\mu 2\pi$, and that it can be checked that $d\underline{p}/E = d\underline{p}_1/E_1$.

$$d\phi_\alpha = f(\underline{p},E(p),\underline{r},t)\,p_\alpha d\underline{p}/E \tag{2}$$

where f is the scalar distribution function in the 8-dimensional space. Further, (see for instance Fisk et al., 1973) it can be shown the $fp^2=J$, where $J(p,E(p)...)$ is the cosmic ray intensity, i.e. the number of particles per unit of time, solid angle, per unit of surface (normal to the flux direction) and per energy window: E, E+dE. Notice in Eq. (2) that f and $d\underline{p}/E$ are

scalars; and that $d\phi_\alpha$ can be written as $(d\underline{\Phi}, d\Phi_4)$ and parallel to $(\underline{p},E)$. The Lorentz transformation can be applied to $d\Phi = |d\underline{\Phi}|$:

$$d\Phi_1 = d\Phi \sqrt{A} \tag{3}$$

between S and S' frames. Moreover, in polar coordinates, $d\underline{p}/E = p\, dE\, d\mu\, 2\pi$ and, as mentioned, is invariant. Replacing in Eq. (2)

$$f_1 p_1 p_1 dE_1 d\mu_1 = fp\sqrt{A}\; p\; dE\; d\mu \tag{4}$$

and, for $fp^2 = J$

$$J_1 dE_1 d\mu_1 = J\sqrt{A}\; dE d\mu \tag{5}$$

From Eqs. (1) it can be calculated the Jacobian: $dE_1 d\mu_1 = dE d\mu/\sqrt{A}$ and

$$J_1/A = J \tag{6}$$

which can be found in the references as $J_1/p_1^2 = J/p^2$.

From Eq. (6), assuming that J_1 is isotropic one can obtain the cosmic ray anisotropic intensity J, $J = J_1\,(p,E(p))\,\{1+(2+\nu)\beta\zeta\cos\theta + O(\beta^2\zeta^2)\}$, where ν is the exponent of the isotropic power law intensity of the energy. The drawback of expression (6), for energies such that $\zeta=1$ ($pc \simeq E$), $\nu = O(3)$, and relative speeds of 300 km/s (typical figure for the peculiar velocity of the solar system with respect to distant cosmic ray sources) is that one obtains values of less than 1% for the amplitude of the anisotropy; this value is small compared to experimental measurements for energies larger than 1.E(14) eV. At these energies the amplitude of the anisotropy exhibit a law proportional to $\sqrt{E}$, reaching about 100% for energies of the order of 1.E(20) eV. (cf Linsley, 1983). In consequence, either it should be looked for dynamical sources for the measured anisotropies and discard formula (6), or make a critical appraisal of the conditions of validity of the deductions which led to Eq. (6).

2. The Wigner Effect

Now we use three inertial frames: S, S' and S" which exhibit parallel axes: The S with S' and the S' with S"; one should not be tempted to extrapolate the transitivity property and assume the parallelism among all the former frames. The relative velocity $\underline{\beta}_1$ between S and S' is take parallel to the x-axes of both frames; and $\underline{\beta}_2$ the one between S' and S" has an inclination angle α with respect to the x-axes of the latter frames. Say, S sees S' with the velocity $\underline{\beta}_1$ towards the right side; S' sees S" towards the right and upwards with the speed β_2. Any frame that sees another one to its left shall

see it with reverse sense i.e. the S" sees the S' with a left-downward motion and with speed β_2.

Our aim is to use the Lorentz transformations between S and S" in order to check the invariance of $d\underline{p}/E$ between these frames. It can be expressed that S" shall move with a velocity $\underline{\beta}$ and inclination angles (as seen from S") measured with respect to its x-axis. The ε angle shall be ambigously defined in the S frame due to the Wigner rotation. The latter frame shall rotate an angle $\delta = (\gamma_1-1)\ |\underline{\beta}_1 x \underline{\beta}_2|/\beta^2 - O(\beta_2^2)$ as seen from S"; the axis of rotation is perpendicular to the $\underline{\beta}_1,\underline{\beta}_2$ plane, at least for small β_2. Let us calculate two successive Lorentz transformations: we call $\underline{p}_i$, E_i (i=0, 1, 2) the four-vector momentum-energy in every frame S, S', and S" respectively. The two transformations are (i=0, 1):

$$p_{i+1} = p_i/A_i,\ E_{i+1} = \gamma_{i+1}p_i c(\zeta_i-\beta_{i+1}\mu_i),\ \mu_{i+1} = \gamma_{i+1}(\mu_i-\beta_{i+1}\zeta_i)/A_i \qquad (7)$$

In the set of Eq. (7), $A_i = 1+\gamma_{i+1}^2(\beta_{i+1}^2\zeta_i^2+\beta_{i+1}\mu_i^2-2\beta_{i+1}\zeta_i\mu_i)$, where $\mu_0 = \cos\theta$ and $\mu_1 = \cos\theta_1$ for i=0; and $\mu_1 = \cos(\theta_1-\alpha)$ and $\mu_2 = \cos(\theta_{2-\alpha})$ for i = 1. In this two sets of transformations θ_1 is the angle measured with respect to the x-axis of its frame, $\zeta_i = E_i/p_i c$. The first equation of Eqs. (7) is the relativistic cosine theroem of vector addition of momenta $\underline{p}_i$ and $\underline{\beta}_{i+1}mc^2$ (m is the rest mass of the particle). Non relativistically, when $\gamma_i = 1$ and $\gamma_i^2\beta_i^2 = 0$, we obtain the cosine formula for vector addition. From the sets of Eqs. (7) one obtains (we drop the 0-subscripts):

$$p_2 = p/\{1+\gamma^2(\beta^2\zeta^2+(\underline{\beta}\underline{p}/p)^2-2(\underline{\beta}\underline{p}/p)\zeta)\} = p/A \qquad (8)$$

and

$$E_2 = \gamma pc\{\zeta-\underline{\beta}\underline{p}/p\}, \qquad (9)$$

where $\gamma = \gamma_1\gamma_2(1+\underline{\beta}_1\underline{\beta}_2)$, and

$$\underline{\beta} = \{\underline{\beta}_2+\underline{\beta}_1/\beta_1\{\gamma_1\beta_1+(\gamma_1-1)\underline{\beta}_2\underline{\beta}_1/\beta_1\}\}/\{\gamma_1(1+\underline{\beta}_1\underline{\beta}_2)\} \qquad (10)$$

that is the relativistic addition of velocities $\underline{\beta}_1$ and $\underline{\beta}_2$. So far the Wigner effect is absent, specially if the angle relations were

$$\cos(\theta_2-\varepsilon) = \gamma\{\cos(\theta-\varepsilon)-\beta\zeta\}/A = \gamma\{\cos\theta\cos\varepsilon+\sin\theta\sin\varepsilon-\beta\zeta\}/A \qquad (11)$$

however one obtains

$$\cos(\theta_2-\alpha) = \gamma\{\frac{\cos\alpha+\beta_1\beta_2}{1+\beta_1\beta_2\cos\alpha}\cos\theta + \frac{\gamma_1^{-1}\sin\alpha\sin\theta}{1+\beta_1\beta_2\cos\alpha} - \frac{\beta_2+\beta_1\cos\alpha}{1+\beta_1\beta_2\cos\alpha}\zeta\}/A \qquad (12)$$

if one writes

$\cos\alpha_1 = (\cos\alpha+\beta_1\beta_2)/(1-\beta_1\beta_2\cos\alpha)$, one recognizes a similar expression as the aberration angle formulae for photon transformation. Using the α_1 angle Eq. (12) transforms into (we call α, α_2)

$$\cos(\theta_2-\alpha_2) = \gamma\ \{\cos\alpha_1\cos\theta+\frac{\sqrt{(1-\beta_1^2)}\ \sin\alpha_1\sin\theta}{\sqrt{(1-\beta_1^2\beta_2^2)}}\ -\underline{\beta}^*\underline{\beta}_2/\beta_2\ \zeta\}/\sqrt{A} \qquad (13)$$

where $\underline{\beta}^*$ is obtained from Eq. (10) except that the 1, 2 - subscripts of the velocities has been interchanged. It can be seen that $\underline{\beta}$ and $\underline{\beta}^*$ have the same mudulus but they are not parallel: their difference of inclinations is the Wigner rotation. Notice that Eqs. (11) and (13) are the same equation when $\underline{\beta}_1$ and $\underline{\beta}_2$ are parallel: The Wigner rotation as well as the non-communtativity of the addition of velocities disappear. Although Eqs. (8) and (9) assures the invariance of $E^2-p^2c^2$, between the S and S" frames, one cannot guarantee the invariance of dp/E: to do that one needs the Eq. (11) in addition of Eqs. (8) and (9).

3. Discussion

In order to investigate the effects of the Wigner rotation we have introduced three inertial frames. The physical picture can be seen as follows: The S; frame is the one where the cosmic ray is isotropic. The S" frame is the observers one, say, the terrestrial EAS detectors. The introduction of the S frame seems to be necessary in order to put up a scenario to allow in S' cosmic ray isotropic fluxes; further, the relative velocity between the former frames can be considered as relativistic i.e. $\beta_1\simeq 1$. The future (as shall be detected in S" later on) cosmic ray gas, in S can be thought as (may be) non-relativistic and anisotropic. The velocity dispersion in S is a consequence of the acceleration mechanisms of these particles and cannot be pin-pointed to a point source in a given $\underline{\beta}_1$ direction. Besides, at every region of the sky, as seen by S', we have equivalent S frames to guarantee the isotropic fluxes.

We need flux transformations between frames such as the S and S" that takes into account the Wigner effect.

References

Geranios, A., Martinic, J. N., 1977, 15th ICRC, Plovidiv, 11, 192.
Fisk, L. A., Forman, M. A., Axford, W. I., J. Geophys. Res. 78, 995, 1973.
Lindsley, J., 1983, 18th ICRC, Bangalore, Rapporteur paper.

HIGH ENERGY ELECTRONS BEYOND 100 GEV OBSERVED BY EMULSION CHAMBER

J.Nishimura*, M.Fujii*, A.Yoshida*, T.Taira**, H.Aizu***, Y.Nomura***, T.Kobayashi****, M.Kazuno#, A.Nishio##, R.L.Golden###, T.A.Koss####, J.J.Lord#### and R.J.Wilkes####

* Institute of Space and Astronautical Science
** Kanagawa University
*** Kanagawa Prefectual College
**** Aoyama Gakuin University
\# Toho University
\#\# Kyoto University
\#\#\# New Mexico State University
\#\#\#\# University of Washington

ABSTRACT

Much efforts have been expended to observe the spectrum of electrons in high energy region with large area emulsion chambers exposed at balloon altitudes, and we have now observed 15 electrons beyond 1 TeV. The observed integral flux at 1 TeV is $(3.24\pm0.87)\times10^{-5}/m^2$ sec sr. The statistics of the data around a few hundred GeV are also improving by using new shower detecting films of high sensitivity. The astrophysical significance of observed spectrum are discussed for the propagation of electrons based on the leaky box and the nested leaky box model.

1. INTRODUCTION

Observations of high energy electrons beyond a few hundred GeV is important for the studies of propagation and acceleration of cosmic rays. Since higher energy electrons have shorter life time by synchrotron and the inverse Compton losses, those electrons observed should be produced nearby sources from the solar system, having a possibility to draw a new clue for the sources of cosmic ray electrons. (J.Nishimura et al.: 1979)

The measurments of electrons in such high energy region, however, are limited by an instrumental capabilities. One needs to identify the electron initiated showers from relatively high background showers due to other hadronic or gamma-ray origins.
Chicago group used a large area transition detectors to identify the electrons from protons, but are limited to the energy up to 300 GeV. (D.Muller and J. Tang: 1983)
Emulsion chambers are the unique detectors with large acceptance solid angles and have capability of identifying the electron initiated showers from other showers even in

TeV energy region. After the exposures of about 7 m^2.dy.sr., we have now observed 15 electrons beyond 1 TeV. The integral flux at 1 TeV is $(3.24\pm0.87)\times10^{-5}$ /m^2.s.sr. To improve the statistics of the data in the energy range of a few hundred GeV, we are now analyzing the chambers with shower detecting films of high sensitivity.

Observed electron spectrum from 30 GeV to 2 TeV are compared with those calculated by using leaky box model and nested leaky box model with various parameters. Astrophysical significance of those parameters after fitting the observed spectrum is discussed.

2. Experiment

The emulsion chamber is the pile of photographic materials and lead plates. When an electron is incident on the chamber, an electron shower starts inside the chamber. By using the high sensitive X-ray films, we can locate the shower as a dark spot by naked eye scanning. The shower is identified in the nuclear emulsions in the same layer, and we can trace back in the plates in the adjacent layers. Then inspecting the starting point of the shower, we can clearly identify the shower whether this is an electron, gamma-ray and hadronic origin. The energy of the electron is determined by counting the shower tracks within a circle of 100 microns. The errors of this energy determination is typically 10%, which is calibrated by the electron beam of FNAL. More detailes of our instrument is described in the reference. (J.Nishimura et al.: 1980)
A series of long exposure have been performed at balloon altitudes since 1975, and the total exposure achieved is 7 m^2.dy.sr.

For the medium energy range around a few hundred GeV, statistics of our observed data is limited due to the microscope scannings. We now find Fuji G8-RXO screen type X-ray films and imaging plates are quite sensitive to detect the showers by naked eye scanning down to around 200 GeV. (T.Taira et al.: 1985). We then performed a series of exposures of the chambers with these films at balloon altitudes from Sanriku Balloon Center since 1984, and are now improving the statistics of the data in this energy range.

3. RESULTS AND DISCUSSIONS

Analysing the electron showers exposed at balloon altitude, we find 15 electrons, giving the integral flux of electrons as $(3.24\pm0.87)\times10^{-5}/cm^2$.s.sr. The observed spectrum covering 30 GeV to 2 TeV is shown in Fig.1. The spectral index beyond 100 GeV is well replesented by $\gamma = 3.3\pm0.2$, which agrees with those obtained in our earlier observations.

(J.Nishimura et al.: 1981)
Expected spectrum from the leaky box model was discussed at the time of Paris conference (J.Nishimura et al.: 1981), and it was shown good agreement is obtained, assuming $\tau = \tau 0 (E/5)^{-\delta}$ for the parameters of:

$\gamma = 2.3$, $\tau 0 = 2 \times 10^7$ yr at 5 GeV, $\delta = 0.4$.

The situation is unchanged even if we take our new spectrum. It is difficult to reconcil with the observed spectrum in this model. If we assume $\delta = 0.6$ referring to the recent HEAO-3 data for heavy primaries in the energy around 10 GeV (L.Koch-Miramond et al.: 1983)

When electrons are accelerated in their sources, those electrons may lose their energy in the relatively strong magnetic field in the source region. Then the nested leaky box model seems to be more realistic to model the propagation of cosmic ray electrons. If super nova remnants (SNR) are really the sources of those electrons as widely accepted view, radio emission from SNR is just correspond to the energy loss in the source here we assumed.
Electron propagation in the nested leaky box have been discussed by several authors. (for recent work, see Mugarer and Ormes :1983) Here we consider the cases $\tau 0$ and δ may change in each place, denoting δ as $\delta 1$ and $\delta 2$ by putting suffix 1 and 2 in the source and the Galaxy. The same suffix are used for b and τ as b1, $\tau 1$ and b2, $\tau 2$. The relative importance of the energy loss is defined as $f = b1\tau 1 / b2\tau 2$ in source region and the Galactic space. Then we have for the spectrum of electron as :

low energy side : $E^{-\gamma-\delta_2}$
medium energy region : $E^{-\gamma-1}$
high energy side : $E^{-\gamma-2+\delta_1}$

Numerical integrations to obtain electron spectrum with various parameters in this model are performed, and results are shown in Fig.1. An example of parameters giving good agreement with our observed spectrum is shown in Table 1.

Table 1

Relationships between γ, f, $\delta 1$ giving good agreements with observed spectrum

$f \backslash \gamma$	2.0	2.2
0.01	/	0
0.1	0.1	0.3
1.0	0.4	0.6

Here we assume :
$b2 = 10^{-16} (GeV.s)^{-1}$, $\tau 2 = 2 \times 10^7$ yr at 5 GeV,
$\delta 2$ is assumed to be 0.6 referring to HEAO-3 data.

We believe more definitive parameter fitting are possible by increasing the statistics in the medium energy region.

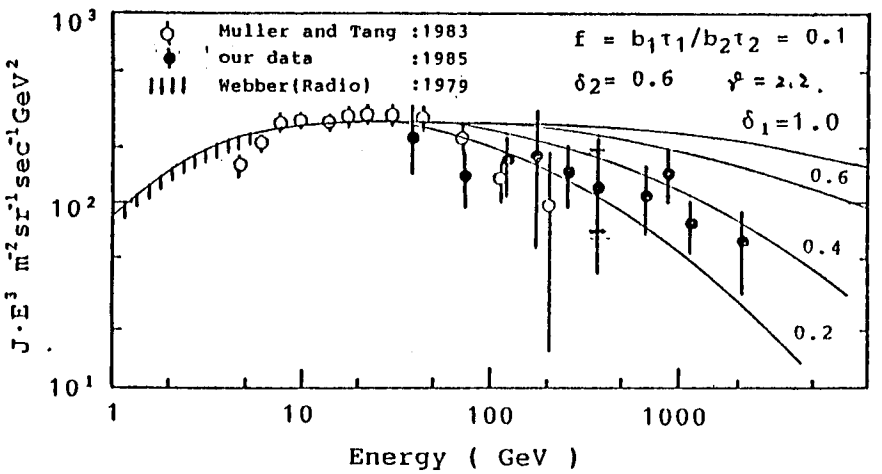

Fig.1 Observed electron spectrum and an example of the expected spectrum from Nested Leaky Box Model. Description of the parameters are shown in the paper.

Then the conclusion are :
1) The existence of electrons beyond 2 TeV indicates that they should have been produced within past 10 years or less, and their source locations are expected to be within a few hundreds of pc. This gives us a possibility to identify the sources of these electrons if they have been produced in SNR.
2) If we take the leaky box model, $\delta 2 = 0.6$ is too large to reconcil to the observed spectrum. $\delta 2$ should be smaller at high energy region beyond 100 GeV.
3) In the nested leaky box model, it seems natural that δ holds the same value in the source region and the Galactic space. If this is the case, the argument shown in 2) still hold except to the case that loss of energy in the source is larger than a few tens of % of that in the Galactic space. The condition is a little bit relaxed if we take a larger value of b2 as discussed by Mugaer and Ormes.

REFERENCES

Kock-Muramond,L at al. : 1983 Proc. 18th ICRC Vol. 2, 219
Mugaer,B.G. and Ormes,J.F. : 1983 Proc. 18th ICRC Vol. 2, 6
Nishimura,J., Fujii,M., and Taira,T. :
1979 Proc. 16th ICRC Vol. 1, 488
Nishimura,J. et al. : 1980 APJ 238, 394
1981 Proc. 17th ICRC, Vol. 2, 94
Taira,T. et al. : 1985 in this Proc.

DIFFUSIVE ELECTRON ACCELERATION AT SNR SHOCK FRONTS AND THE OBSERVED SNR RADIO SPECTRAL INDICES

T. J. Bogdan
High Altitude Observatory, National Center for Atmospheric Research
P.O. Box 3000, Boulder, CO 80307

M. A. Lee
Space Science Center, University of New Hampshire
Durham, NH 03824

I. Lerche
University of South Carolina
Columbia, SC 29208

G. M. Webb
Lunar and Planetary Laboratory, University of Arizona
Tucson, AZ 85721

1. Introduction. The radio synchrotron emission from relativistic electrons in shell supernova remnants (SNRs) provides a unique opportunity to probe the energy distribution of energetic electrons at their acceleration site (SNR shock fronts). This information provides insight into the acceleration mechanism(s). Here we discuss the implications of these observations for the diffusive (first-order Fermi) acceleration of electrons at the SNR shock fronts.

2. Observations. In Figs. 1 and 2, the diameter, D, and radio spectral index, α (defined by the relation, $S_\nu \sim \nu^\alpha$, where S_ν is the radio flux density, and ν is the observing frequency) are plotted for SNRs in our Galaxy [8, 12] and in the Large Magellanic Cloud (LMC) [14]. In Fig. 1, the filled circles and diamonds are taken from Clark and Caswell's [8] Tables I and II respectively, and the open triangles are from Göbel et al. [12]. We have omitted the 20 SNRs Weiler [16] classifies as plerions (Class P) or Class C objects, so our sample is representative of shell (Class S) SNRs. For the LMC SNRs, this distinction is not easily made. The open circles in Fig. 2 represent SNRs with optical diameters significantly in excess of their radio diameters. These objects may not be Class S objects. The uncertainties in α ($\approx \pm 0.05$), and especially D ($\approx \pm 10$ pc), are considerably larger than the extent of the points used in Fig. 1. Perhaps the open triangles are the most reliable galactic data since their α's are determined from at least three flux measurements (408 MHz, 1, 5 GHz), and they function as distance calibrators (via the Σ–D relation) for the filled points [5]. On the other hand, the relative D values in Fig. 2 should be quite realistic, although their overall scaling depends upon the assumed distance to the LMC (≈ 55 kpc).

As noted previously [8, 13] there is a complete lack of correlation of α with D. Rather, $<\alpha> \approx -.5$ with a spread $\Delta\alpha \approx \pm 0.15$ in **both** Fig. 1 and 2. The range of estimated diameters is comparable in both plots.

3. Interpretation. There have been a number of attempts to obtain constraints on and insight into acceleration mechanisms via the data presented in Fig. 1 and 2 [6, 10, 13]. In the remainder of this paper we will attempt to interpret this data in terms of the diffusive (first-order Fermi) acceleration mechanism at the SNR shock front [1, 2, 11, 15].

In its most naive form, this theory predicts a definite relationship between α and the effective compression ratio, $\bar{r}$, which the 0.1 - 10 GeV electrons responsible for the radio emission (assuming $10^{-4} < B < 10^{-6}$ gauss) sample in their scattering across the shock front:

$\alpha = -1.5/(\bar{r}-1)$. Now the gyro-radii of these same electrons are certainly $<10^{-5}D$, so it is plausible that the spatial extent of the scattering centers about the subshock (e.g. the region where the flow velocity decreases continuously from its upstream to its downstream value) reduces $\bar{r}$ from the net compression through the entire shock, r [4, 15]. If the electron scattering mean free path increases rapidly with a characteristic length that is comparable to the spatial extent of the subshock, and is a monotone increasing function of the electron momentum, then the shock-accelerated electron energy spectrum need not even exhibit a power-law behavior [15]. The spatial extent of the subshock and the scattering zone need not, however, be equal (though they may be weakly correlated), in which case $\bar{r}$ is simply the compression across the scattering zone and not r [4]. While r is likely to correlate with D, [2,7] $\bar{r}$, which is determined by the spatial character of the turbulence and hydromagnetic waves generated by the shock, must be rather sensitive to the detailed nature of the surrounding interstellar medium (ISM) (e.g., the strength, orientation and fluctuations in the galactic magnetic field; the clumpiness of a multicomponenet ISM, etc.). Thus a distribution of α's below some upper bound $-1.5/(r-1)$ may result from the variations in the position and extent of the scattering zone relative to the subshock from SNR to SNR. This would suggest that the SNRs in Figs. 1 and 2 should lie to the right of some bounding curve, say $\alpha = \alpha_c\ (D)$, that is itself less sensitive to the detailed structure of the ISM, but related more to the average properties of the ISM, and the energy release in the initial SNR explosion.

The net compression r must also depend upon the radiative/conductive cooling flux $\dot{Q}$ [10, 13]. Cooling fluxes [3, 7] on the order of $\approx uP$ (u-shock velocity, P-post shock pressure) are required to produce the observed spectral indices as flat as -0.25 in a $\gamma = 5/3$ gas. Certainly the conductive flux will be influenced by the local structure of the magnetic field in the ISM, as well as the presence of dense clouds [9], and may well vary significantly from SNR to SNR. If the bounding curve $\alpha = \alpha_c\ (D)$ incorporates the maximal $\dot{Q}$, then the spread in α for a given D follows naturally in terms of variations in $\dot{Q}$ and the structure of the electron scattering zone from one SNR to the next.

4. Conclusions. While we argue (as does Drury [10]) that diffusive electron acceleration at SNR shock fronts can qualitatively account for the data in Figs. 1 and 2, this speculation does *not* address the key trend in the data: $<\alpha> \approx -0.5$ and $\Delta\alpha \approx \pm\ 0.15$. Nor have we touched upon the temporal evolution of α observed in several SNRs (see e.g. [2]), and the implications this may have for the acceleration mechanism. It is clear, however, that the similarities between Figs. 1 and 2 give us an important clue as to the ultimate source of energetic particles and perhaps, indirectly, the nature of the ISM.

Quantitative progress hinges upon a study of the self-consistent evolution of the hydromagnetic wave intensity and particle distibution across a shock with structure. If such a program can be carried out, then via $<\alpha>$, $\Delta\alpha$ and the location of the $\alpha_c\ (D)$ boundary, the radio SNRs may eventually become a most valuable probe of the detailed nature of the ISM in our Galaxy and perhaps other galaxies as well.

Acknowledgments. The National Center for Atmospheric Research is sponsored by the National Science Foundation.

References.

1. Axford, W. I., E. Leer, and G. Skadron, (1977), *Proc. 15th ICRC*, **11**, 132.
2. Beck, R., L. O'C., Drury, H. J. Völk, and T. J. Bogdan, (1985), *Proc. 19th ICRC*, OG 8.1-10.
3. Blandford, R. D. and L. L. Cowie, (1982), *Ap. J.*, **260**, 625.
4. Bogdan, T. J. and I. Lerche, (1985), *MNRAS*, **212**, 413.
5. Caswell, J. L. and I. Lerche, (1979), *MNRAS*, **187**, 201.

6. Caswell, J. L. and I. Lerche, (1979), *Proc. ASA*, **3**, (5), 343.
7. Chevalier, R. A., (1977), *Ann. Rev. Astr. Ap.*, **15**, 175.
8. Clark, D. H. and J. L. Caswell, (1976), *MNRAS*, **174**, 267.
9. Cowie, L. L. and C. F. McKee, (1977), *Ap. J.*, **211**, 135.
10. Drury, L. O'C., (1983), *Sp. Sci. Rev.*, **36**, 57.
11. Drury, L. O'C., (1983), *Rep. Prog. Phys.*, **46**, 973.
12. Göbel, W., W. Hirth, and E. Fürst, (1981), *Astr. Ap*, **93**, 43.
13. Lerche, I., (1980), *Astr. Ap.*, **85**, 141.
14. Mills, B. Y., A.J. Turtle, A.G. Little, and J.M. Durdin, (1984), *Aust. J. Phys.*, **37**, 321.
15. Webb, G. M., T. J. Bogdan, M. A. Lee, and I. Lerche, (1985), *MNRAS*, (in press).
16. Weiler, K. W., (1983), in *Supernova Remnants and Their X-Ray Emission*, ed.: J. Danziger and P. Gorenstein, (Dordrecht: Reidel), p. 299.

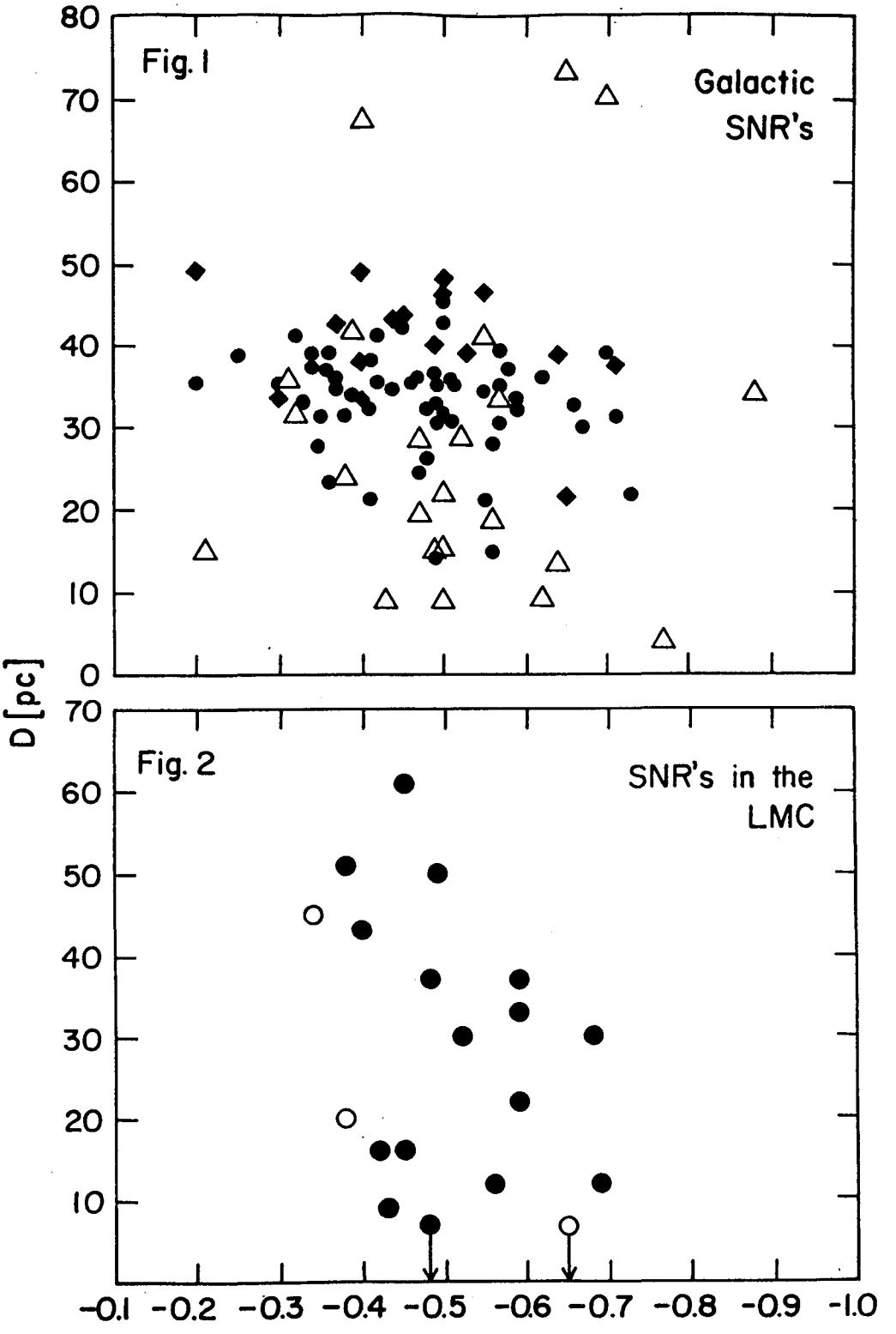
Fig. 1
Galactic
SNR's
Fig. 2
SNR's in the
LMC
D [pc]
80
70
60
50
40
30
20
10
0
-0.1
-0.2
-0.3
-0.4
-0.5
-0.6
-0.7
-0.8
-0.9
-1.0

ELEMENTAL ABUNDANCES IN COROTATING EVENTS

T. T. von Rosenvinge and R. E. McGuire*
NASA/Goddard Space Flight Center, Greenbelt, MD 20771, U.S.A.

1. Introduction. Large, persistent solar-wind streams in 1973 and 1974 produced corotating interaction regions which accelerated particles to energies of a few MeV/nucleon. The proton to helium ratio (H/He) reported in reference (1) was remarkably constant at a value (22 ± 5) equal to that in the solar wind (21 ± 3), suggesting that particles were being accelerated directly out of the solar wind. In this paper we report on preliminary results from a similar study approximately 11 years (i.e., one solar cycle) later. Corotating events have been identified by surveying the solar wind data, energetic particle time-histories and anisotropies. This data was all obtained from the ISEE-3/ICE spacecraft. These events also show H/He ratios similar to that in the solar wind. In addition, we have examined other corotating events at times when solar flare events could have injected particles into the corresponding corotating interaction regions. We find that in these cases there is evidence for H/He ratios which are significantly different from that of the solar wind but which are consistent with the range of values found in solar flare events.

2. Results. In Figure 1 we present a 27-day recurrence plot of the solar wind speed obtained from the Los Alamos National Laboratory Solar Wind Experiment on the ISEE-3 spacecraft (now renamed ICE); this data was processed by a simplified algorithm adequate for this purpose and is not to be considered definitive. ICE at this time was near 1 AU, leading the Earth in its orbit. Figure 1 shows the formation of two recurrent solar wind streams. A similar plot for the interplanetary magnetic field direction shows that these two streams are in opposite portions of a two sector magnetic field pattern. Using Figure 1 and particle time-history plots, we identified eight different time intervals as candidate corotating events. Low energy electron rates and high energy proton rates were scanned for any evidence of impulsive (solar) origin. In addition, anisotropy data was examined for apparent flow from the east. (Corotating events typically have particle flow from the east. This results from the vector sum of the radial Compton-Getting anisotropy due to the outward flow of the solar wind and the backward flow along the interplanetary magnetic field lines from the presumed acceleration region at several AU from the Sun.) The H/He ratio was evaluated for each interval in the energy range 4.5-6.5 MeV/nucleon. Also the C/O ratio was evaluated in the energy range 1.8-2.8 MeV/nucleon. Averaged over all eight intervals we find H/He = 20 ± 8 and C/O = .8 ± .2 (to be compared with H/He = 22 ± 5 and C/O = .8 ± .2 in reference (1)).

Other time periods since the launch of ISEE-3 in 1978 have been examined in a similar manner. A long-lived high-speed stream gave rise to a brief but apparently clean corotating event August 1-4, 1979. The

* Also Department of Physics and Astronomy, University of Maryland College Park, MD 20742, U.S.A.

anisotropy data shows clear evidence of backwards flow into the inner solar system. The previous two appearances of this stream were associated with large solar flares. Evaluating the H/He ratio for August 1-2 we find H/He = 67 + -4, distinctly different from the ratios found in 1984. On the other hand, this value is well within the range found for solar flares (e.g., 20 to 156 cited in reference (1)).

Conclusions. Corotating events associated with two recurrent high-speed streams in 1984 show evidence that their source population is the solar wind, as was also found in reference (1) for streams existing approximately 11 years earlier. Evidence has been presented however that other corotating events are dominated by particles injected by solar flares.

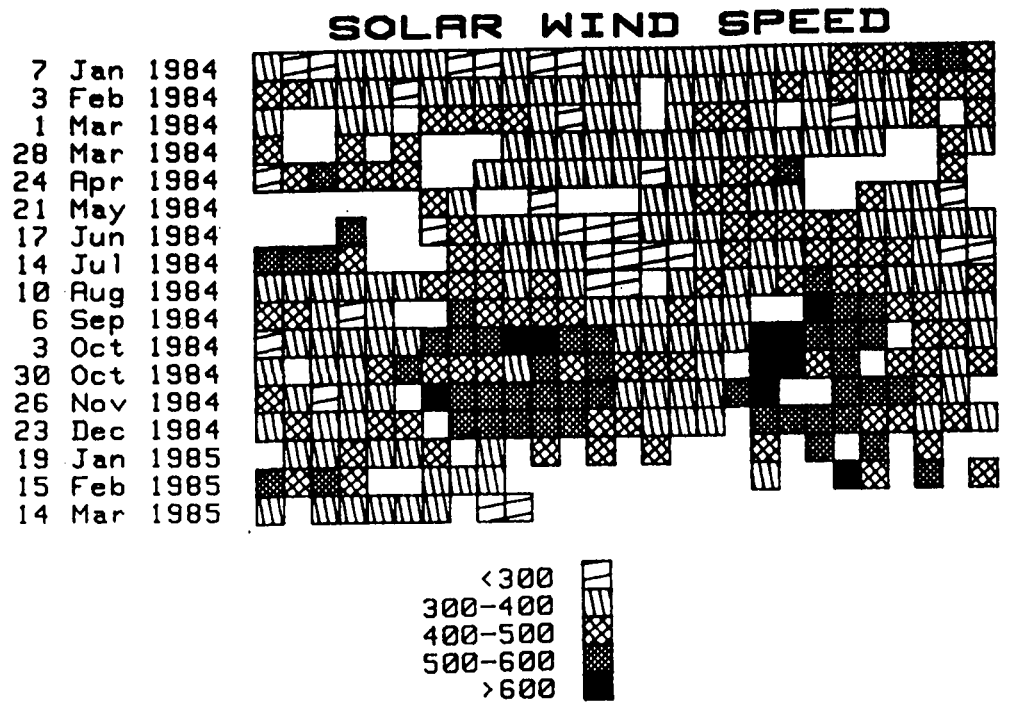

Figure 1

References

1. McGuire, R. E., T. T. von Rosenvinge, and F. B. McDonald, Ap. J., 224, L87, 1978.

Standard Bibliographic Page

1. Report No.	2. Government Accession No.	3. Recipient's Catalog No.
NASA CP-2376		

4. Title and Subtitle	5. Report Date
19th International Cosmic Ray Conference Papers - Volume 9	July 1986
	6. Performing Organization Code
7. Author(s)	8. Performing Organization Report No.
Frank C. Jones, Compiler	
9. Performing Organization Name and Address	10. Work Unit No.
Laboratory for High Energy Astrophysics Goddard Space Flight Center Greenbelt, MD 20771	11. Contract or Grant No.
12. Sponsoring Agency Name and Address	13. Type of Report and Period Covered
National Aeronautics and Space Administration Washington, DC 20546-0001	Conference Publication
	14. Sponsoring Agency Code

15. Supplementary Notes

16. Abstract

These volumes contain papers submitted for presentation at the 19th International Cosmic Ray Conference held on the campus of the University of California, San Diego, in La Jolla, CA, Aug. 11-23, 1985. This conference is held every other year. The present volume contains all of the Rapporteur talks and most of the Invited and Highlight talks given at the conference as well as a few papers of a miscellaneous nature.

17. Key Words (Suggested by Authors(s))	18. Distribution Statement
Author index Participants Cosmic Ray Conference	Unclassified - Unlimited Subject Category 93

19. Security Classif.(of this report)	20. Security Classif.(of this page)	21. No. of Pages	22. Price
Unclassified	Unclassified	576	$200/set

For sale by the National Technical Information Service, Springfield, Virginia 22161

NASA Langley Form 63 (June 1985)

U.S. GOVERNMENT PRINTING OFFICE: 1986-627-232/40044

National Aeronautics and
Space Administration

Goddard Space Flight Center
Greenbelt, Maryland 20771